AD-A202 879

UNITED STATES AIR FORCE

GRADUATE STUDENT SUMMER SUPPORT PROGRAM 1986

PROGRAM TECHNICAL REPORT

UNIVERSAL ENERGY SYSTEMS, INC

VOLUME 2 of 2

PROGRAM DIRECTOR, UES — PROGRAM MANAGER, AFOSR
RODNEY C. DARRAH — MAJOR RICHARD KOPKA
PROGRAM ADMINISTRATOR, UES

JAN 28 1989

SUBMITTED TO
AIR FORCE OFFICE OF SCIENTIFIC RESEARCH
WASHINGTON DC

BEST AVAILABLE COPY

89 1 23 0

DISCLAIMER NOTICE

THIS DOCUMENT IS BEST QUALITY PRACTICABLE. THE COPY FURNISHED TO DTIC CONTAINED A SIGNIFICANT NUMBER OF PAGES WHICH DO NOT REPRODUCE LEGIBLY.

DISCLAIMER NOTICE

SECURITY CLASSIFICATION OF THIS PAGE

REPORT DOCUMENTATION PAGE

1a. REPORT SECURITY CLASSIFICATION: UNCLASSIFIED

1b. RESTRICTIVE MARKINGS:

2a. SECURITY CLASSIFICATION AUTHORITY:

2b. DECLASSIFICATION/DOWNGRADING SCHEDULE:

3. DISTRIBUTION/AVAILABILITY OF REPORT: APPROVED FOR PUBLIC RELEASE; Distribution Unlimited.

4. PERFORMING ORGANIZATION REPORT NUMBER(S):

5. MONITORING ORGANIZATION REPORT NUMBER(S): AFOSR-TR- 87-0305

6a. NAME OF PERFORMING ORGANIZATION: Universal Energy Systems, Inc

6b. OFFICE SYMBOL (If applicable):

7a. NAME OF MONITORING ORGANIZATION: AFOSR/XOT

6c. ADDRESS (City, State and ZIP Code): 4401 Dayton-Xenia Road, Dayton, OH 45432

7b. ADDRESS (City, State and ZIP Code): Building 410, Bolling AFB, DC 20332-6448

8a. NAME OF FUNDING/SPONSORING ORGANIZATION: AFOSR

8b. OFFICE SYMBOL (If applicable): XOT

9. PROCUREMENT INSTRUMENT IDENTIFICATION NUMBER: F49620-85-C-0013

8c. ADDRESS (City, State and ZIP Code): Building 410, Bolling AFB, DC 20332

10. SOURCE OF FUNDING NOS.

PROGRAM ELEMENT NO.	PROJECT NO.	TASK NO.	WORK UNIT NO.
61102F	3396	D5	

11. TITLE (Include Security Classification): USAF Graduate Student Summer Support Program ~~- Volume 2~~ - 1986 Program Technical Report

12. PERSONAL AUTHOR(S): Rodney C. Darrah, Susan K. Espy

13a. TYPE OF REPORT: Annual

13b. TIME COVERED: FROM ______ TO ______

14. DATE OF REPORT (Yr., Mo., Day): December 1986

15. PAGE COUNT:

16. SUPPLEMENTARY NOTATION:

17. COSATI CODES

FIELD	GROUP	SUB. GR.

18. SUBJECT TERMS (Continue on reverse if necessary and identify by block number)

19. ABSTRACT (Continue on reverse if necessary and identify by block number)

See Attached

DTIC ELECTE JAN 23 1989 S D

CD

20. DISTRIBUTION/AVAILABILITY OF ABSTRACT: UNCLASSIFIED/UNLIMITED ☒ SAME AS RPT. ☐ DTIC USERS ☐

21. ABSTRACT SECURITY CLASSIFICATION: UNCLASSIFIED

22a. NAME OF RESPONSIBLE INDIVIDUAL: Major Richard W. Kopka, Program Manager

22b. TELEPHONE NUMBER (Include Area Code): 202-767-4970

22c. OFFICE SYMBOL: XOT

DD FORM 1473, 83 APR EDITION OF 1 JAN 73 IS OBSOLETE.

89 1 23 003

SECURITY CLASSIFICATION OF THIS PAGE

I. INTRODUCTION

Universal Energy Systems, Inc. (UES) was awarded the United States Air Force Summer Faculty Research Program on August 15, 1984. The contract is funded under the Air Force Systems Command by the Air Force Office of Scientific Research.

The program has been in existance since 1978 and has been conducted by several different contractors. The success of the program is evident from its history of expansion since 1978.

The Summer Faculty Research Program (SFRP) provides opportunities for research in the physical sciences, engineering, life sciences, business, and administrative sciences. The program has been effective in providing basic research opportunities to the faculty of universities, colleges, and technical institutions throughout the United States.

The program is available to faculty members in all academic grades: instructor, assistant professor, professor, department chairman, and research facility directors. It has proven especially beneficial to young faculty members who are starting their academic research programs and to senior faculty members who have spent time in university administration and are desirous of returning to scholarly research programs.

Beginning with the 1982 program, research opportunities were provided for 17 graduate students. The 1982 pilot student program was highly successful and was expanded in 1983 to 53 students; there were 84 graduate students in the 1984 program.

In the previous programs, the graduate students were selected along with their professors to work on the program. Starting with the 1985 program, the graduate students were selected on their own merits. They were assigned to be supervised by either a professor on the program or by an engineer at the Air Force Laboratories participating in the program. There were 92 graduate students selected for the 1985 program.

Again in the 1986 program, the graduate students were selected on their own merits, and assigned to be supervised by either a professor on the program or by an engineer at the participating Air Force Laboratory. There were 100 graduate students selected for the 1986 program.

Follow-on research opportunities have been developed for a large percentage of the participants in the Summer Faculty Research Program in 1979-1983 period through an AFOSR Minigrant Program.

On 1 September 1983, AFOSR replaced the Minigrant Program with a new Research Initiation Program. The Research Initiation Program provides follow-on research awards to home institutions of SFRP participants. Awards were made to approximately 50 researchers in 1983. The awards were for a maximum of $12,000 and a duration of one year or less. Substantial cost sharing by the schools contributes significantly to the value of the Research Initiation Program. In 1984 there were approximately 80 Research Initiation awards.

AFOSR-TR- 87-0~~307~~
0305

UNITED STATES AIR FORCE

GRADUATE STUDENT SUMMER SUPPORT PROGRAM

1986

PROGRAM TECHNICAL REPORT

UNIVERSAL ENERGY SYSTEMS, INC.

VOLUME II of II

Program Director, UES
Rodney C. Darrah

Program Manager, AFOSR
Major Richard Kopka

Program Administrator, UES
Susan K. Espy

Submitted to

Air Force Office of Scientific Research

Bolling Air Force Base

Washington, DC

December 1986

TABLE OF CONTENTS

Section	Page
Preface	i
List of 1986 Graduate Student Participants	ii
Participant Laboratory Assignment	xix
Research Reports	xxii

PREFACE

The United States Air Force Graduate Student Summer Support Program (USAF-GSSSP) is conducted under the United States Air Force Summer Faculty Research Program. The program provides funds for selected graduate students to work at an appropriate Air Force Facility with a supervising professor who holds a concurrent Summer Faculty Research Program appointment or with a supervising Air Force Engineer. This is accomplished by the students being selected on a nationally advertised competitive basis for a ten-week assignment during the summer intersession period to perform research at Air Force laboratories/centers. Each assignment is in a subject area and at an Air Force facility mutually agreed upon by the students and the Air Force. In addition to compensation, travel and cost of living allowances are also paid. The USAF-GSSSP is sponsored by the Air Force Office of Scientific Research, Air Force Systems Command, United States Air Force, and is conducted by Universal Energy Systems, Inc.

The specific objectives of the 1986 USAF-GSSSP are:

(1) To provide a productive means for the graduate students to participate in research at the Air Force Weapons Laboratory;

(2) To stimulate continuing professional association among the Scholars and their professional peers in the Air Force;

(3) To further the research objectives of the United States Air Force;

(4) To enhance the research productivity and capabilities of the graduate students especially as these relate to Air Force technical interests.

During the summer of 1986, 100 graduate students participated. These researchers were assigned to 25 USAF laboratories/centers across the country. This two volume document is a compilation of the final reports written by the assigned students members about their summer research efforts.

LIST OF 1986 GRADUATE STUDENT PARTICIPANTS

NAME/ADDRESS	DEGREE, SPECIALTY, LABORATORY ASSIGNED
Susan M. Abrams University of Illinois Dept. of Bioengineering Chicago, IL 60680 (312) 996-8661	Degree: B.S., Human Factors Engineering, 1984 Specialty: Zoology Assigned: HRL/OT
William H. Acton University of New Mexico Dept. of Psychology Albuquerque, NM 87131 (505) 277-4121	Degree: M.A., Applied Behavioral Science, 1984 Specialty: Psychology Assigned: AAMRL
Julie A. Albertson Washington State University Dept. of Mechanical Engineering Pullman, WA 99164-2920 (509) 335-8654	Degree: B.S., Mechanical Engineering, 1985 Specialty: Mechanical Engineering Assigned: FJSRL
Jay H. Ambrose University of Kentucky Dept. of Mechanical Engineering Lexington, KY 40506 (606) 257-2663	Degree: M.S., Mechanical Engineering, 1985 Specialty: Mechanical Engineering Assigned: APL
Mark R. Anderson Purdue University School of Aeronautics and Astronautics Grissom Hall W. Lafayette, IN 47907 (317) 494-5154	Degree: M.S., Engineering, Aeronautics and Astronautics, 1984 Specialty: Engr. Aeronautics and Astronautics Assigned: FDL
Stanley F. Anton Rutgers-The State University of New Jersey Psychology Department Psychology Bldg. Busch Campus New Brunswick, NJ 08903 (201) 932-4036	Degree: M.S., Cognitive Psychology, 1986 Specialty: Cognitive Psychology Assigned: AAMRL

Christopher P. Antworth
Florida State University
Department of Chemistry
Box 13
Tallahassee, FL 32306
(904) 644-1274

Degree: B.S., Chemistry, 1980
Specialty: Chemistry
Assigned: ESC

Sherif A. Aziz
Wright State University
Systems Engineering
School of Engineering
130 Eng. and Math Bldg.
Dayton, OH 45435
(513) 873-2403

Degree: B.S., Systems and Biomedical Eng., 1984
Specialty: Biomedical Engineering
Assigned: AAMRL

Alan H. Baginski
University of Lowell
Electrical Engineering
Lowell, MA 01854
(617) 452-5000

Degree: B.S., Electrical Engineering, 1983
Specialty: Electrical Engineering
Assigned: RADC

Joseph M. Boroughs
University of New Mexico
Psychology Department
Albuquerque, NM 87131
(505) 277-4121

Degree: M.A., Psychology, 1981
Specialty: Psychology
Assigned: AAMRL

Dale T. Bracken
University of Georgia
Dept. of Psychology
302 Morris Hall
Athens, GA 30602
(404) 542-8362

Degree: B.S., Psychology, 1985
Specialty: Psychology
Assigned: HRL/ID

Angela M. Braun
Trinity University
Biology Department
715 Stadium Drive
San Antonio, TX 78212
(512) 736-7011

Degree: B.A., Biology, 1986
Specialty: Biology
Assigned: SAM

David A. Bridenstine
Arizona State University
Mechanical & Aerospace Engineering
Tempe, AZ 85287
(602) 965-3291

Degree: M.S., Engineering, 1985
Specialty: Engineering
Assigned: ML

Paul E. Bussey
University of Colorado at
Colorado Springs
Austin Bluffs Parkway
Colorado Springs, CO 80933-7150
(303) 593-3351

Degree: B.S., Electrical Engineering, 1986
Specialty: Electrical Engineering
Assigned: FJSRL

Timothy T. Clark
University of New Mexico
Mechanical Engineering
Albuquerque, NM 87131
(505) 277-2761

Degree: BSME, Fluid Dynamics, 1983
Specialty: Mechanical Engineering
Assigned: WL

Otis Cosby, Jr.
Meharry Medical College
School of Medicine
1005 D. B. Todd Jr. Blvd.
Nashville, TN 37208
(615) 327-6223

Degree: BS, Natural Science, 1983
Specialty: Natural Science
Assigned: SAM

Jennifer L. Davidson
Department of Mathematics
University of Florida
201 Walker Hall
Gainesville, FL 32611
(904) 392-0268

Degree: M.S, Mathematics, 1986
Specialty: Mathematics
Assigned: AD

Douglas W. DeHart
University of Wisconsin-Madison
Dept. of Engineering Mechanics
1415 Johnson Drive
Madison, WI 53706
(608) 262-3990

Degree: B.S., Engineering Mechanics, 1985
Specialty: Engineering Mechanics
Assigned: RPL

Brian J. Doherty
Duke University
Biomedical Engineering Dept.
Durham, NC 27706
(919) 684-6185

Degree: B.S.E., Bioenginnering, 1984
Specialty: Bioengineering
Assigned: AAMRL

Franklin J. Dunmore
Howard University
Dept. of Physics and Astronomy
2355 Sixth Street, N.W.
Washington, D.C. 20059
(202) 636-6241

Degree: B.S., Physics, 1982
Specialty: Physics
Assigned: ML

Michael P. Farr
Pennsylvania State University
312 Steidle Building
University Park, PA 16802
(814) 863-0154

Degree: M.S., Polymer Science, 1984
Specialty: Polymer Science
Assigned: ML

Christopher A. Feild
Dickinson College
Box 914
Carlisle, PA 17013
(717) 245-1533

Degree: B.S., Chemistry, 1986
Specialty: Chemistry
Assigned: ML

Michelle J. Ferry
Wright State University
Dayton, OH 45435
(513) 873-2855

Degree: B.S., Chemistry, 1984
Specialty: Chemistry
Assigned: AAMRL

Carl V. Frank
Univ. of Southern Mississippi
Computer Science Dept.
Southern Station, Box 9157
Hattiesburg, MS 39406-9157
(601) 266-3216

Degree: B.S., Computer Science, 1985
Specialty: Computer Science
Assigned: SAM

Beverley A. Gable
Ohio University
Psychology Dept.
1222 Carriage Hill
Athens, OH 45701
(614) 594-7167

Degree: B.S., Psychology, 1984
Specialty: Psychology
Assigned: AAMRL

Michael D. Garner
University of North Carolina at Greensboro
Physics Dept.
Greensboro, NC 27412
(919) 379-5844

Degree: B.S., Physics, 1984
Specialty: Physics
Assigned: RADC

Maurice B. Gilbert Meharry Medical College Medicine Department 1005 Dr. D.B. Todd Blvd. Nashville, TN 37208 (615) 327-6111	Degree: Specialty: Assigned:	B.S., Biology, 1982 Biology SAM
Beverly E. Girten Ohio State University Exercise Physiology and Physiological Chemistry Dept. College of Medicine 333 W. 10th Avenue Columbus, OH 43210 (614) 422-1462	Degree: Specialty: Assigned:	M.S., Exercise Physiology, 1983 Physiology, AAMRL
Ellen S. Goldey Miami University Zoology Dept. 210 N. Main #4 Oxford, OH 45056 (513) 529-3451	Degree: Specialty: Assigned:	B.S., Biology, 1984 Biology AAMRL
Alfred W. Gordon Atlanta University Dept. of Biology 360 Westview Drive, S.W. Atlanta, GA 30314 (404) 681-0251	Degree: Specialty: Assigned:	B.A., Biology, 1976 Biology SAM
Nadia C. Greenidge New York University Dept. of Anthropology 25 Waverly Place New York City, NY (212) 598-3258	Degree: Specialty: Assigned:	M.S., Physical Anthropology Physical Anthropology AAMRL
Peggy J. Grigsby Wright State University Physics Department Dayton, OH (513) 873-2950	Degree: Specialty: Assigned:	M.S., Mathematics, 1978 Mathematics ML

Brad L. Halverson
Washington State University
Dept. of Civil and Environmental Engineering
Sloan Hall 102
Structures Section
Pullman, WA 99164-2914
(509) 335-4921

Degree: B.S., Civil Engineering, 1985
Specialty: Civil Engineering
Assigned: WL

Charles R. Hammond
Vanderbilt University
Dept. of Mechanical and Materials Engineering
P O Box 1592, Station B
Nashville, TN 37235
(615) 322-0892

Degree: M.S., Mechanical Engineering, 1983
Specialty: Mechanical Engineering
Assigned: AEDC

Darren E. Hart
Texas A&M University
Dept. of Psychology
College Station, TX 77843
(409) 845-2581

Degree: B.A., Psychology, 1984
Specialty: Psychology
Assigned: HRL/MO

Peter V. Hlinomaz
University of Michigan-Dearborn
4901 Evergreen Road
Dearborn, MI 48128
(313) 593-5420

Degree: B.S., Electrical Engineering, 1985
Specialty: Electrical Engineering
Assigned: RADC

Stephen Hom
Massachusetts Institute of Technology
Mechanical Engineering Dept.
77 Massachusetts Avenue
Cambridge, MA 02139
(617) 253-5028

Degree: M.S., Structural Engineering, 1977
Specialty: Structural Engineering
Assigned: ML

Jamal A. Hussein
University of Toledo
Mechanical Engineering Dept.
2801 W. Bancroft
Toledo, OH 43606
(419) 537-2620

Degree: M.S., Mechanical Engineering, 1986
Specialty: Mechanical Engineering
Assigned: APL

David W. Jansen
Dept. of Zoology
Washington State University
Pullman, WA 99164-4220
(509) 336-3564

Degree: M.S., Zoology, 1980
Specialty: Zoology
Assigned: AAMRL

Karl K. Klett, Jr.
University of Wyoming
P O Box 3905
University Station
Laramie, WY 82071
(307) 766-6150

Degree: B.S., 1979
Specialty: Astrophysics
Assigned: AFGL

Raymond M. Kolonay
Ohio State University
Dept. of Civil Engineering
2070 Niel Avenue
Hitchcock Hall, Room 470
Columbus, OH 43210
(614) 422-2771

Degree: B.S., Civil Engineering, 1985
Specialty: Civil Engineering
Assigned: FDL

Craig A. Langenfeld
Ohio State University
Mechanical Engineering Dept.
305 Stonemill Road
Dayton, OH 45409
(513) 299-3218

Degree: B.S., Mechanical Engineering, 1986
Specialty: Mechanical Engineering
Assigned: APL

Tieu-Binh Le
Wright State University
Chemistry Dept.
Dayton, OH 45435
(513) 873-2855

Degree: B.S., Chemistry, 1985
Specialty: Chemistry
Assigned: ML

Mark W. Lisee
University of Lowell
Dept. of Electrical Engineering
Box 2615
North Campus
1 University Avenue
Lowell, MA 01854
(617) 452-5000

Degree: B.S.E.E., expected 1988
Specialty: Electrical Engineering
Assigned: AFGL

Robert K. Littleton
University of Colorado
Physics Department
Austin Bluffs Parkway
Colorado Springs, CO 80903
(303) 593-3000

Degree: B.S., Chemistry, 1975
Specialty: Chemistry
Assigned: FJSRL

George A. Liu
Meharry Medical College
Dept. of Physiology
1005 18th Avenue, North
Nashville, TN
(615) 327-6413

Degree: B.A., Chemistry, 1986
Specialty: Chemistry
Assigned: SAM

Isabel Lopez
Wright State University
Dept. of Chemistry
Dayton, OH 45435
(513) 873-2855

Degree: M.S., Chemistry, 1985
Specialty: Chemistry
Assigned: AAMRL

Michael M. Lukes
Florida State University
Meteorology Dept.
Tallahassee, FL 32306
(904) 644-6205

Degree: B.S., Meteorology, 1973
Specialty: Meteorology
Assigned: ESC

Wayne R. Lundberg
Wright State University
Dept. of Physics and Mechanical Engineering
3640 Col. Glenn Hiway
Dayton, OH 45435
(513) 873-2954

Degree: B.S., Physics, 1985
Specialty: Physics
Assigned: ML

William A. Marty
University of Oklahoma
Electrical Engineering and Computer Science
202 West Boyd, Room 219
Norman, OK 73069
(405) 325-4721

Degree: B.S., Electrical Engineering, 1985
Specialty: Electrical Engineering
Assigned: AL

Mary R. McGill
Eastern Kentucky University
Dept. of Chemistry
1661 Foxhaven #3
Richmond, KY 40475
(606) 624-9772

Degree: B.S., Chemistry, 1985
Specialty: Chemistry
Assigned: ESC

Jennifer McGovern-Weidner University of Florida Dept. of Psychology 114 Psychology Bldg. Gainesville, FL 32611 (904) 392-0605	Degree: Specialty: Assigned:	M.A., Gifted Education, 1983 Psychology SAM
Dara C. Merenski University of Dayton Computer Science Dept. 300 College Park Drive Dayton, OH 45469 (513) 229-2343	Degree: Specialty: Assigned:	B.S., Systems Analysis, 1986 Systems Analyst HRL/LR
Peter D. Meyer University of Montana Physics Department Missoula, MT 59801 (406) 243-6535	Degree: Specialty: Assigned:	B.A., Chemistry, 1984 Chemistry AD
Douglas R. Moore Univ. of Southern Mississippi Dept. of Polymer Science Southern Station Box 10076 Hattiesburg, MS 39406-0076 (601) 266-4868	Degree: Specialty: Assigned:	B.S., Chemistry, 1977 Chemistry ML
Eric V. Morris Meharry Medical School 1005 18th Street, N. Nashville, TN 37208 (615) 327-6000	Degree: Specialty: Assigned:	B.S., Biological Sciences, 1984 Pharmacology SAM
Russell Moy Dept. of Chemical Engineering The University of Michigan 2135 Dow Building Ann Arbor, MI 48109-2136 (313) 764-3379	Degree: Specialty: Assigned:	MSE, Chemical Engineering, 1982 Chemical Engineering FJSRL
Glenn D. Munkvold University of Texas at Austin Dept. of Chemical Engineering Austin, TX 78712 (512) 471-1046	Degree: Specialty: Assigned:	B.S., Chemical Engineering, 1984 Chemical Engineering SAM

Conrad R. Murray Meharry Medical College 1005 D.B. Todd Blvd. Nashville, TN 37208 (615) 327-6111	Degree: Specialty: Assigned:	B.S., Pre-Medicine, 1983 Medicine SAM
Victoria T. Nasman Northwestern University Psychology Department CRESAP Laboratory 633 Clark Street Evanson, IL 60201 (312) 492-7643	Degree: Specialty: Assigned:	B.A., Psychology, 1983 Psychology SAM
Sharon E. Navard Univ. of Southwestern Louisiana Dept. of Statistics USL Box 44187 Lafayette, LA 70504 (318) 231-6772	Degree: Specialty: Assigned:	M.S., Statistics, 1984 Statistics AD
Bernadette P. Njoku Meharry Medical College School of Medicine 1005 D.B. Todd Blvd. Nashville, TN 37208 (615) 327-4098	Degree: Specialty: Assigned:	B.A., Chemistry, 1982 Chemistry SAM
David P. Norton Louisiana State University Dept. of Electrical and Computer Engineering Baton Rouge, LA 70803 (504) 388-5488	Degree: Specialty: Assigned:	M.S., Electrical Engineering, 1986 Electrical Engineering RADC
Roland L. Palmer The University of Alabama- Tuscaloosa Psychology Department Box 2968 University, AL 35486 (205) 348-5083	Degree: Specialty: Assigned:	M.A., Psychology, 1985 Psychology HRL/MO
Daniel S. Park Univ. of Southern California Aerospace Engineering University Park Los Angeles, CA 90089-0126 (213) 743-7177	Degree: Specialty: Assigned:	MSAE, Aerospace Engineering, 1985 Aerospace Engineering FDL

April G. Parker
The Ohio State University
Dept. of Ceramic Engineering
177 Watts 2041 College Road
Columbus, OH 43202
(614) 422-2960

Degree: B.S., Ceramic Engineering, 1985
Specialty: Ceramic Engineering
Assigned: ML

Deborah L. Parker
Tulane University
Psychology Department
2007 Percival Stern Hall
New Orleans, LA 70118
(504) 865-5331

Degree: M.A., Experimental Psychology, 1985
Specialty: Psychology
Assigned: HRL/LR

Werner K. Perry
University of Florida
Computer and Info. Sciences
3117 S.W. 29 Avenue
Gainesville, FL 33312
(904) 374-8971

Degree: B.S., BEG-CIS, 1986
Specialty: Engineering
Assigned: AD

Frank M. Pitman
Clemson University
Mechanical Engineering Dept.
Clemson, SC 29631
(803) 654-5140

Degree: B.S., Mechanical Engineering, 1985
Specialty: Mechanical Engineering
Assigned: FDL

Amy B. Powell
Texas A&M University
Psychology Department
College Station, TX 77843
(409) 845-0377

Degree: B.S., Psychology, 1984
Specialty: Psychology
Assigned: HRL/MO

Surya Raghu
Yale University
Dept. of Mechanical Engineering
Mason Laboratories
Box 2159
New Haven, CT 06520
(203) 436-8676

Degree: M.S., Engineering, 1980
M.S., M. Philosophy, 1986
Specialty: Aeronautical Engineering
Assigned: APL

Mark L. Ratcliff University of Tennessee Space Institute Dept. of Mathematics U.T.S.I. Upper E Tullahoma, TN 37388 (615) 455-0631	Degree: Specialty: Assigned:	B.A., Math, 1984 Mathematics AEDC
Christopher Reed University of Florida Dept. of Engineering Sciences Gainesville, FL 32611 (904) 392-0961	Degree: Specialty: Assigned:	M.S., Engineering Science, 1984 Aerodynamics AD
Gregg A. Reger Univ. of Texas - San Antonio Life Sciences Dept. 6900 Loop 1604 W. San Antonio, TX 78285 (512) 691-4458	Degree: Specialty: Assigned:	B.S., Dietics, 1981 Dietics SAM
Anthony E. Restaino State Univiversity of New York- at Albany Dept. of Atmospheric Science 1400 Washington Avenue Albany, NY 12222 (518) 457-3987	Degree: Specialty: Assigned:	B.S., Meteorology, 1984 Meteorology AFGL
Dennis W. Richardson Pennsylvania State University Dept. of Electrical Engineering 322 Atherton Hall University Park, PA 16802 (814) 862-7595	Degree: Specialty: Assigned:	B.S., Electrical Engineering, 1983 Electrical Engineering AL
Kyle W. Ross University of New Mexico Dept. of Mechanical Engineering Albuquerque, NM 87131 (505) 277-2761	Degree: Specialty:	B.S., Mechanical Engineering, 1982 Mechanical Engineering

Susan E. Sadofsky
Boston Universtiy
Math Department
111 Cummington Street
Boston, MA 02215
(617) 353-2560

Degree: M.A., Mathematics, 1986
Specialty: Mathematics
Assigned: AFGL

Yolman J. Salinas
Meharry Medical College
School of Medicine
1005 Dr. D.B. Todd Blvd.
Nashville, TN 37208
(615) 327-6308

Degree: M.S., Biochemistry, 1984
Specialty: Biochemistry
Assigned: SAM

William D. Schmidt
Indiana Univ. of Pennsylvania
Physics Department
Indiana, PA 15705
(412) 357-2100

Degree: B.S., Physics, 1983
Specialty: Physics
Assigned: AL

James P. Seaba
The University of Iowa
Mechanical Engineering Dept.
2228 Engineering Bldg.
Iowa City, IA 52242
(319) 353-6045

Degree: B.S., Mechanical Engineering, 1984
Specialty: Mechanical Engineering
Assigned: APL

Laura Sewall
Brown University
Psychology Department
Box 1853
Providence, RI 02912
(401) 863-2727

Degree: B.S., Psychology, 1985
Specialty: Psychology
Assigned: HRL/OT

Loren T. Simpson
Davidson College
Mathematics Department
P O Box 2964
Davidson, NC 28036
(704) 892-8226

Degree: B.S., Mathematics, 1986
Specialty: Mathematics
Assigned: AFGL

Jim S. Sirkis University of Florida Dept. of Engineering Sciences 321 Aerospace Building Gainesville, FL 32611 (904) 392-0961	Degree: Specialty: Assigned:	M.S., Engineering Mechanics, 1985 Engineering Mechanics AD
Michael J. Slifker Cornell University Dept. of Computer Science 304 Kimball Ithaca, NY 14850 (607) 255-5577	Degree: Specialty: Assigned:	B.S., Computer Science, 1985 Computer Science WL
Barry J. Stagg Louisiana State University Mechanical Engineering Dept. Baton Rouge, LA 70803-6413 (504) 388-5792	Degree: Specialty: Assigned:	B.S., Mechanical Engineering, 1986 Mechanical Engineering RPL
Martin A.P. Strnat University of Dayton Dept. of Biology 300 College Park Drive Dayton, OH 45469 (513) 229-2135	Degree: Specialty: Assigned:	B.S., Biology, 1984 Biology AAMRL
John E. Swift University of Oklahoma School of Electrical Eng. and Computer Science 202 West Boyd Norman, OK 73069 (405) 325-4721	Degree: Specialty: Assigned:	B.S., Electrical Engineering, 1986 Electrical Engineering AL
Moussa P. Tamer Meharry Medical College School of Medicine 1005 18th St. Nashville, TN 37208 (615) 356-8756	Degree: Specialty: Assigned:	B.S., Chemistry, 1983 Chemistry SAM
Donald E. Tilton University of Kentucky Dept. of Mechanical Engineering Lexington, KY 40506 (606) 257-2662	Degree: Specialty: Assigned:	B.S., Mechanical Engineering, 1985 Mechanical Engineering APL

Shun P. Tschen
University of Iowa
Mechanical Engineering Dept.
Iowa City, IA 52242
(319) 353-5638

<u>Degree</u>: B.S., Mechanical Engineering, 1985
<u>Specialty</u>: Mechanical Engineering
<u>Assigned</u>: APL

Cheryl A. Ulmer
Wright State University
Dayton, OH 45435
(513) 873-2210

<u>Degree</u>: B.S., Psychology, 1980
<u>Specialty</u>: Psychology
<u>Assigned</u>: HRL/LR

Joseph C. Varga
Kent State University
Dept. of Physics
Kent, OH 44242
(216) 672-2246

<u>Degree</u>: M.S., Physics, 1978
<u>Specialty</u>: Physics
<u>Assigned</u>: ML

Gregory L. Walker
University of Wisconsin-Madison
Engineering Mechanics Dept.
Engineering Building
1415 Johnson Drive
Madison, WI 53706
(608) 262-3990

<u>Degree</u>: B.S., Engineering Mechanics, 1985
<u>Specialty</u>: Engineering Mechanics
<u>Assigned</u>: RPL

Mark M. Weislogel
Washington State University
Dept. of Mechanical Engineering
Pullman, WA 99164-2920
(509) 335-2727

<u>Degree</u>: B.S., Mechanical Engineering, 1986
<u>Specialty</u>: Mechanical Engineering
<u>Assigned</u>: APL

Steven P. Wicelinski
Louisiana State University
Dept. of Chemistry
LSU Box 22023
Baton Rouge, LA 70893
(504) 388-5811

<u>Degree</u>: B.S., Chemistry, 1981
<u>Specialty</u>: Chemistry
<u>Assigned</u>: FJSRL

Celeste B. Williams
Auburn University
Dept. of Electrical Engineering
Broun Hall
Auburn, AL 36830
(205) 887-1843

<u>Degree</u>: B.S., Physics, 1984
<u>Specialty</u>: Physics
<u>Assigned</u>: RADC

Cornell L. Wooten Texas Southern University Math Department 3201 Wheeler Houston, TX 77004 (713) 527-7011	Degree: Specialty: Assigned:	B.S., Math and Mechanical Engineering, 1985 Mathematics AFGL
John S. Wroblewski Univ. Southwestern Louisiana Chemistry Department P O Box 44370 Lafayette, LA 70504 (318) 231-6734	Degree: Specialty: Assigned:	B.S., Chemistry, 1984 Chemistry RPL
Jon D. Zobel, Jr. University of Colorado at Colorado Springs Dept. of Electrical Engineering Austin Bluffs Parkway Colorado Springs, CO 80907 (303) 593-3351	Degree: Specialty: Assigned:	B.S., Electrical Engineering, 1986 Electrical Engineering FJSRL

PARTICIPANT LABORATORY ASSIGNMENT

C. PARTICIPANT LABORATORY ASSIGNMENT (Page 1)

1986 USAF/UES GRADUATE STUDENT SUMMER SUPPORT PROGRAM

AERO PROPULSION LABORATORY (AFWAL/APL)
(Wright-Patterson Air Force Base)

1. Jay H. Ambrose
2. Jamal Ali Hussein
3. Craig Anthony Langenfeld
4. Surya Raghu
5. James Phillip Seaba
6. Donald E. Tilton
7. Shun Peter Tschen
8. Mark Milton Weislogel

ARMAMENT LABORATORY (AD)
(Eglin Air Force Base)

1. Jennifer Lee Davidson
2. Peter David Meyer
3. Sharon Elizabeth Navard
4. Christopher William Perry
5. Christopher William Reed
6. James Sanford Sirkis

ARMSTRONG AEROSPACE MEDICAL RESEARCH LABORATORY (AAMRL)
(Wright-Patterson Air Force Base)

1. William Howard Acton
2. Stanley Francis Anton
3. Sherif Adel Aziz
4. Joseph Marshall Boroughs
5. Brian John Doherty
6. Michelle Joanne Ferry
7. Beverley Ann Gable
8. Beverly Elaine Girten
9. Ellen Sue Goldey
10. Nadia C. Greenidge
11. David W. Jansen
12. Isabel Lopez
13. Martin A.P. Strnat

ARNOLD ENGINEERING DEVELOPMENT CENTER (AEDC)
(Arnold Air Force Station)

1. Charles Reif Hammond
2. Mark Lindsay Ratcliff

AVIONICS LABORATORY (AFWAL/AL)
(Wright-Patterson Air Force Base)

1. William Albert Marty
2. Dennis William Richardson
3. William David Schmidt
4. John Edward Swift

ENGINEERING SERVICE CENTER (ESC)
(Tyndall Air Force Base)

1. Christopher Paul Antworth
2. Michael Miles Lukes
3. Mary Ruth McGill

C. PARTICIPANT LABORATORY ASSIGNMENT (Page 2)

FLIGHT DYNAMICS LABORATORY (AFWAL/FDL)
(Wright-Patterson Air Force Base)

1. Mark Ronald Anderson
2. Raymond Michael Kolonay
3. Daniel Suwhan Park
4. Frank Mark Pitman
5. Kyle W. Ross

FRANK J. SEILER RESEARCH LABORATORY (FJSRL)
(USAF Academy)

1. Julie Ann Albertson
2. Paul Eugene Bussey
3. Robert K. Littleton
4. Russell Moy
5. Steven Paul Wicelinski
6. Jon D. Zobel, Jr.

GEOPHYSICS LABORATORY (AFGL)
(Hanscom Air Force Base)

1. Karl Kennedy Klett, Jr.
2. Mark Welson Lisee
3. Anthony Edward Restaino
4. Susan Ellen-Ann Sadofsky
5. Loren Taylor Simpson
6. Cornell Leroy Wooten

HUMAN RESOURCES LABORATORY/ID (HRL/ID)
(Lowry Air Force Base)

1. Dale Thomas Bracken

HUMAN RESOURCES LABORATORY/LR (HRL/LR)
(Wright-Patterson Air Force Base)

1. Dora C. Merenski
2. Deborah Lynn Parker
3. Cheryl Ann Ulmer

HUMAN RESOURCES LABORATORY/MO (HRL/MO)
(Brooks Air Force Base)

1. Daren Edward Hart
2. Roland Lavelle Palmer
3. Amy Beth Powell

HUMAN RESOURCES LABORATORY/OT (HRL/OT)
(Williams Air Force Base)

1. Susan Marci Abrams
2. Laura Sewall

MATERIALS LABORATORY (AFWAL/ML)
(Wright-Patterson Air Force Base)

1. David Allen Bridenstine
2. Franklin John Dunmore
3. Michael Patrick Farr
4. Christopher Adam Field
5. Peggy Jo Grigsby
6. Stephen Hom
7. Tieu-Binh Le
8. Wayne Randolph Lundberg
9. Douglas Roger Moore
10. April Gayle Parker
11. Joseph Charles Varga

C. PARTICIPANT LABORATORY ASSIGNMENT (Page 3)

ROCKET PROPULSION LABORATORY (RPL)
(Edwards Air Force Base)
1. Douglas Wayne DeHart
2. Barry James Stagg
3. Gregory Lane Walker
4. John Stephen Wroblewski

ROME AIR DEVELOPMENT CENTER (RADC)
(Griffiss Air Force Base)
1. Alan Henry Baginski
2. Michael Dean Garner
3. Peter Vladimir Hlinomaz
4. David Paul Morton
5. Celeste Benay Williams

SCHOOL OF AEROSPACE MEDICINE (SAM)
(Brooks Air Force Base)
1. Angela Marie Braun
2. Otis Cosby, Jr.
3. Carl Von Frank
4. Maurice B. Gilbert
5. Alfred Wendell Gordon
6. George Albert Liu
7. Jennifer McGovern Weidner
8. Eric Van Morris
9. Glenn D. Munkvold
10. Conrad Robert Murray
11. Victoria Nasman
12. Bernadette Patricia Njoku
13. Gregg Allen Reger
14. Yolman John Salinas
15. Moussa Pierre Tamer

WEAPONS LABORATORY (WL)
(Kirtland Air Force Base)
1. Timothy Truman Clark
2. Bradlee Halverson
3. Michael Jude Slifker

RESEARCH REPORTS

1986 GRADUATE STUDENT SUMMER SUPPORT PROGRAM

Technical Report Number	Title	Graduate Researcher
Volume I		
1	The Effects of Fourier Limited Targets Upon Peripheral Perception	Susan M. Abrams
2	Studies of the Dimensionality of Subjective Workload and Standard Loading Levels in a Continuous Recall Task	William H. Acton
3	An Investigation of Unsteady Vorticity Production by a Pitching Airfoil	Julie A. Albertson
4	An Apparatus for Transient Saturation Measurements in a Heat Pipe	Jay H. Ambrose
5	Flight Control Synthesis with Practical Design Constraints	Mark R. Anderson
6	The Effects of Flow Rate and Edge Rate on the Perception of Self Speed	Stanley F. Anton
7	A Dispersion-Corrected HPLC/FACP Method for Measuring Sorption Isotherms of Substituted Aromatics on Soil Organic Matter	Christopher P. Antworth
8	Computer Simulation of the Cardio-vascular System Under $+G_z$ Stress	Sherif A. Aziz
9	Inefficiencies of High Transmission Delays on Computer Protocols and their Applications	Alan H. Baginski
10	Cognitive Resources and Multi-Task Cost	Joseph M. Boroughs
11	Job/Task Difficulty and Job/Task Experience: A Literature Review	Dale T. Bracken, Jr.
12	Chlamydomonas Phototaxis as a Simple System for Testing the Effect of Drugs on Vision	Angela M. Braun
13	Research for the Development of an Executive System Prototype for Unified Life Cycle Engineering	David A. Bridenstine

14	Development of a High Speed Infrared Detection and Recording System with Resident Image Processing and Graphic Data Display for Support of Remote Defense Nuclear Agency High-Powered Pulsed Microwave Source Measurements	Paul E. Bussey
15	Modification of a Finite-Difference, 2-Dimensional Boundary Layer Code for Application to the Free Shear Layer of an Axisymmetric Jet	Timothy T. Clark
16	Mesopic Visual Function in Aircrew	Otis Cosby, Jr.
17	A Mathematical Classification of a Family of Edge Detectors	Jennifer L. Davidson
18	Design and Analysis of Models of Large Space Structures	Douglas W. DeHart
19	A Biomechanical Study of Anthropomorphic Head-Neck Systems	Brian J. Doherty
20	Materials Evaluation and Failure Analysis of Various Electronic Circuitry Components of Air Force Aircraft	Franklin J. Dunmore
21	Thermal Characterization of New Thermally Stable Matrix Materials	Michael P. Farr
22	Synthesis of Intermediates and Monomer of Polybenzothiazole	Christopher Feild
23	The Metabolism of t-Butylcyclohexane in Male Fischer 344 Rats	Michelle J. Ferry
24	Data Management Within the School of Aerospace Medicine	Carl V. Frank
25	The Effects of High Noise Levels and Obstruction to Articulation on the Acoustic-Phonetic Structure of Speech: A Preliminary Investigation	Beverley A. Gable
26	A Study of the Probability Distributions of the Long Term Variations of Acoustical Noise Over Time of Various Military Environments	Michael D. Garner
27	Exposure of Polycarbonate Lens to Natural Elements	Maurice B. Gilbert

28	Effects of Dobutamine Administration on Suspension Hypokinesia/Hypodynamia Deconditioning in Rats	Beverly Girten
29	Experimental Evidence Supporting a Pharmacokinetic Model of Uptake and Metabolism of Trichloroethylene in the Pregnant and Lactating Rat	Ellen S. Goldey
30	Effects of Acceleration Stress Upon Blood Lipid Levels	Alfred W. Gordon
31	Microfracture Patterns in the Lumbar Vertebrae of Macaca mulatta	Nadia C. Greenidge
32	Effects of Coherent Scattering on IR Absorption in Doped Semiconductors	Peggy J. Grigsby
33	A Modification of the ACSYS Preprocessor Code for use with the SAMSON2 Finite - Element Program	Brad L. Halverson
34	Automation of the Method of Optimal Design	Charles R. Hammond
35	Empirical Confidence Intervals for a Validity Coefficient Under Range Restriction: An Application of the Bootstrap	Daren E. Hart
36	An Analysis of Residual Output Noise from the R.A.D.C. Speech Enhancement Unit	Peter V. Hlinomaz
37	Knowledge for the ULCE Expert System	Stephen Hom
38	An Analytical Investigation for Designing an Energy Storage Container for Storing Lithium Hydride Between 300K and 1200K	Jamal A. Hussein
39	Modeling of Human Body Movement	David W. Jansen
40	Noise Analysis and Reduction for the AFGL Infrared Focal Plane Array Spectrometer	Karl K. Klett, Jr.
41	Structural Optimization Using Bending Elements	Raymond Kolonay
42	Swirling Flows in Dump Combustors	Craig A. Langenfeld

43	Thermal Stability Studies of Structure-Property Relationship of Various Silahydrocarbon Lubricants	Tieu-Binh Le
44	Computer Software Development in a Study of Executable Image Efficiency	Mark W. Lisee
45	Optimization of a Material to be used to detect Incident Microwave Radiation by IR Imaging	Robert K. Littleton
46	Synergistic Effects of Antimalarial Drugs and Hyperoxia on the Growth of Malaria Parasites in Culture	George A. Liu
47	The Metabolism of Isopropylcyclohexane in Male Fisher 344 Rats	Isabel Lopez
48	A Comparative Study and Evaluation of Four Atmospheric Dispersion Models with Present or Potential Utility in Air Force Operations	Michael M. Lukes
49	A Load-Balancing Modification to A. George's Incomplete Nested Dissection Algorithm for Mapping a Compact Irregular Quadrilateral Finite-Element Mesh onto the Hypercube Parallel Processing Architecture	Wayne R. Lundberg
50	Guide to ISPX: The Interactive Signal Processing Executive	William A. Marty
Volume II		
51	Polynuclear Aromatic Hydrocarbons in Particulate Turbine Engine Exhaust and From Combustion of Single Compound Fuels	Mary R. McGill
52	Electroencephalography and Online Analysis: An Evaluation of Some Available Choices	Jennifer McGovern-Weidner
53	Program Code: Style and Conventions	Dara C. Merenski
54	Synthesis and Time to Explosion Studies of Some Potential High Explosives	Peter D. Meyer
55	Polybenzimidazoles: Solubilization, Modification and Synthesis	Douglas R. Moore

56	MBTI Psychometric Study of United States Air Force Aircrew Personnel	Eric V. Morris
57	Chemical and Electrochemical Behavior of Aluminum Electrodes in Acidic 1-Methyl-3-Ethylimidazolium Chloride/Aluminum Chloride Room Temperature Molten Salt Electroyltes	Russell Moy
58	OBOGS Studies	Glenn D. Munkvold
59	Effects of Acceleration Stress Upon Blood Lipid Levels	Conrad R. Murray
60	Heart Rate Self-Regulation: The Effects of Increasing Cognitive Demands	Victoria Nasman
61	Modernization of Statistical Software	Sharon E. Navard
62	Visual Characteristics in Pilots with Central Serous Retinopathy	Bernadette P. Njoku
63	Residual Carrier Concentration Dependence on the Arsine Pressure for Gallium Arsenide Grown by Hydride-Based VPE	David P. Norton
64	Frequency and Temporal Information Processing	Roland L. Palmer
65	Parametric Numerical Simulation for Hypersonic Flow Over a Compression Ramp	Daniel S. Park
66	Characterization of Alkoxide Derived Zirconia Toughened Fused Silica	April G. Parker
67	On the Measurement of Variables Impacting the Performance of Flightline Maintenance Crews	Deborah Parker
68	Image Algebra Preprocessor and Image Algebra Executive	Werner K. Perry
69	Decentralized Control of Large Flexible Space Structures	Frank M. Pitman
70	Empirical Confidence Intervals for a Validity Coefficient Under Range Restriction: An Application of the Bootstrap	Amy B. Powell

71	Study and Control of Organ Pipe Type Oscillations in a Horizontal Combustion Tunnel	Surya Raghu
72	A Locally Implicit Numerical Method	Mark L. Ratcliff
73	Adaptive Grid Generation for Viscous Flow Problems	Christopher W. Reed
74	An Ultrastructural Study of Mossy Fiber Terminals Isolated from the Mamalian Brain	Gregg A. Reger
75	Response of Downslope and Florida Mesoscale Wind Systems to Physiographic Features	Anthony E. Restaino
76	Atmospheric Modeling for Operational Tactical Decision Aid	Dennis W. Richardson
77	An Experiment to Characterize the Turbulent Flow of a Circular Free Jet of Helium	Kyle Ross
78	Weather Attenuation	Susan E. Sadofsky
79	MBTI Psychometric Study of United States Air Force Aircrew Personnel	Yolman J. Salinas
80	Analytical Computer Modeling of the NPN BICFET Device	William D. Schmidt
81	Jet Diffusion Flame	James P. Seaba
82	Mechanisms of Chromatic Contrast	Laura Sewall
83	Computer Simulation of Physical Phenomena	Loren T. Simpson
84	A Discussion of Boundary Element Methods	Jim S. Sirkis
85	Automatic Program Generation from Specifications	Michael J. Slifker
86	A Study of the Use of Optical Combustion Diagnostics on Premixed Flames and Solid Rocket Propellant Flames	Barry J. Stagg
87	Expansion of USAF AAMRL/THT Electron Microscopy Division Capabilities with Respect to Specimen Preparation and Analysis	Martin A.P. Strnat

88	Translation of TRW's ADAPT-II to a Perkin-Elmer OS-32 Environment	John E. Swift
89	MBTI Psychometric Study of United States Air Force Aircrew Personnel	Moussa P. Tamer
90	High Power Density Evaporative Cooling	Donald E. Tilton
91	Visualization of Jet Diffusion Flames	Shun P. Tschen
92	The Effects of Stress and Crisis Conditions on Decision Making	Cheryl A. Ulmer
93	Numerical Calculations of Thermal and Dopant Diffusion in Ion-Implanted Laser-Annealed Silicon	Joseph C. Varga
94	Void and Boundary Layer Effect on the Stress Distribution Near Cylindrical Inclusions	Gregory L. Walker
95	Experimental Studies on Heat Pipe Coupling and Condensation Rates in Packed Beds of Spheres	Mark M. Weislogel
96	An Investigation of Prospective Media for Thin Film Fabrication of III-V Semiconductors	Steven Wicelinski
97	Study of Oxygen-Related Defects in Electron-Irradiated, Boron-Doped Silicon	Celeste B. Williams
98	A Study of the Finite Element Method in Limited Area Weather Prediction Modeling	Cornell L. Wooten
99	Synthesis and Polymerization of Dinitropropyl Vinyl Ether	John S. Wroblewski
100	Development of a High Speed Infrared Detection and Recording System with Resident Image Processing and Graphic Data Display for Support of Remote Defense Nuclear Agency High-Powered Pulsed Microwave Source Measurements	Jon D. Zobel, Jr.

1986 USAF-UES SUMMER FACULTY RESEARCH PROGRAM/
GRADUATE STUDENT SUMMER SUPPORT PROGRAM

Sponsored by the
AIR FORCE OFFICE OF SCIENTIFIC RESEARCH
Conducted by the
UNIVERSAL ENERGY SYSTEMS, INC.
FINAL REPORT

POLYNUCLEAR AROMATIC HYDROCARBONS IN PARTICULATE TURBINE ENGINE EXHAUST AND FROM COMBUSTION OF SINGLE COMPOUND FUELS

Prepared by:	William D. Schulz and Mary R. McGill
Academic Rank:	Professor of Chemistry; M.S. degree Candidate
Department and University:	Department of Chemistry Eastern Kentucky University

Research Location:	Headquarters Air Force Engineering Services Center, Engineering Research Directorate, Environics Division, Tyndall Air Force Base, Florida
USAF Research:	Mr. Surendra B. Joshi, Captain, Paul E. Kerch
Date:	September 30, 1986
Contract No.:	F49620-85-C-0013

Polynuclear Aromatic Hydrocarbons
in Particulate Turbine Engine Exhaust
and From Combustion of Single Compound
Fuels

By

Dr. William D. Schulz and Miss Mary R. McGill

ABSTRACT

Particulate exhaust samples of turbine engines and a combustor rig were sequentially extracted with methylene chloride, benzene-methanol and toluene. No solvent was found superior to methylene chloride for the entire range of polynuclear aromatic hydrocarbons (PNAs) in these samples.

Turbine engine exhaust samples from three engines at four different power settings were extracted, concentrated and analyzed. Analysis was by G.C. (F.I.D.) and GC/MS. Blanks and samples contained large amounts of plasticizers and filter loadings were too low for reliable quantitation or identification by GC/MS. G.C. (F.I.D.) analysis and identification by retention times indicated that PNA concentration was highest at the "idle" power setting and that it was also higher for the one afterburning sample.

Samples of exhaust particulates from a bluff body combustor, burning pure acetylene, propane, propene, butane, 1-butene and isobutene were extracted, concentrated and analyzed. Soot yield of the fuels was not determined. Higher concentration of higher molecular weight PNAs were found for the aliphatic compounds with unsaturation and for isobutene, with unsaturation and branching.

Acknowledgments

We wish to thank the Air Force Systems Command and the Air Force Office of Scientific Research for sponsorship of this research. We also thank the entire Environics Division of the Air Force Engineering Services Center for their friendliness, helpfulness, and for allowing total access to their fine laboratory equipment. The civilian and military laboratory personnel worked beyond the call of duty to make room for, and cooperate with, a number of visiting scientists equal to their own number, in limited space.

We thank Lt. Cols. Brocato, Bramlett and Olfenbeutel for doing everything that made the summer very convenient and enjoyable. Doctoral candidate Abdulraluman Touati and Capt. Paul Kerch supplied total cooperation in supplying combustor laboratory samples, information and reference material. We thank Mr. Surrendra Joshi, Dr. Howard Mayfield, Lieutenant Glen Seitchek, Mr. Mike Henly and M/Sgt. Dan Stork for help and guidance that extended even to nights and weekends if needed.

I. Introduction

One area of interest to the Environics Division at Tyndall Air Force Base is the mechanism of soot formation. This interest is evidenced by the Combustor Laboratory, with equipment for precise conditions of combustion in a centerbody burner (or "bluff body combustor") and laser light scattering equipment for particle size and density measurements. Information gathered in soot formation studies is of fundamental importance in a number of areas: Air Quality (as measured by visibility), Health Effects (the concentration of hazardous materials adsorbed on air particulates formed by combustion) and Tactical Concern (possible abatement of turbine engine soot trails). Applications of such studies can range from waste incineration particulate formation to particulates emitted from tactical fighter aircraft turbine engines.

Another area of interest to the A.F.E.S.C. Environics Division is the total characterization (and Photoreactivity) of turbine engine exhaust. This area is primarily with concern for environmental and health effects of jet engine exhaust. Study of this area of concern has been contracted to Dynamac Corporation[1] for literature review and to Battelle Corporation[2-4] (Columbus) for actual implementation. The area not covered by the Battelle contract is the concentration of hazardous substances on turbine emitted particulates. Although this area is covered, at the present, in a recent contract with Battelle Corporation, particulate samples would become available from May or early June 1986 sampling that would not be analyzed by Battelle, and these samples could not only be analyzed for hazardous materials (principally polynuclear aromatic hydrocarbons-"PNAs"), but could also be used for experiments to determine the optimum methods and conditions for extraction, concentra-

tion and analysis of particulate turbine exhaust samples.

I have had intensive experience in sampling, extraction and high resolution gas chromatography-mass spectrometry analysis of air particulate samples over an academic year and two summers under NSF grant ATM-801 4191, with Kent J. Voorhees, at the Colorado School of Mines in 1981-82. Because of this experience, Mr. S. B. Joshi of the Environics Division and Dr. C. W. Spicer of the Battelle Institute thought it desirable for me to experiment with extraction and concentration techniques and to attempt to analyze turbine exhaust samples preliminary to a contract effort by Battelle to analyze particulate samples collected in the late summer or fall. It was thought that this effort, at a minimum, would provide data necessary for successful turbine exhaust particulate collection and analysis in the Battelle contract work.

Miss Mary R. McGill is a Masters Degree candidate at Eastern Kentucky University who had recently completed my Analytical Separation Methods course. She expressed an interest in working on this problem as a part of her thesis research, under my direction, and was awarded the A.F.O.S.R. Graduate Fellowship by Universal Energy Systems upon approval by the Environics Division at Tyndall Air Force Base.

II. Objectives of the Research Effort

The initial objective of this research effort was to be evaluation of extraction techniques, solvents and extract concentration methods for analysis of samples from aircraft turbine engine exhaust particulates. Samples collected at Tinker A.F.B., Oklahoma, by the Battelle Corporation in May or early June were to be analyzed for polynuclear aromatic hydrocarbons (PNA). The analyses and method development both require gas chromatography-mass spectrometry for positive identification of analytes.

Upon arrival at Tyndall A.F.B., a serendipitous decision was made to begin extraction experiments with soot from the combustor laboratory, where pure aliphatic hydrocarbons (acetylene, propane, propene, 1-butene and isobutylene) were being burned in soot formation studies. Analysis of extracts of soot formed by these fuels indicated that the nature of the PNA content of the soot varied with the nature of the fuel.

A literature search indicated that, while soot formation had been studied for several pure compounds, essentially no research had ever been done involving qualitative and quantitative analysis of the PNAs formed from combustion of pure, simple aliphatic compounds. With this finding, extraction and analysis of soot samples from the combustion of pure fuels from the combustion laboratory because of at least equal importance to analysis of the turbine engine exhaust particulates.

The major objectives of this effort then became:

1. Method development and analysis of authentic particulate exhaust samples from aircraft turbine engines with the goal of at least identifying problem areas and advising Battelle personnel on optimum conditions for their own subsequent sampling and analysis.

2. Extraction and analysis of particulates formed by the combustion of pure aliphatic hydrocarbons in the combustor laboratory.
3. Establishing a pattern from the PNA content of pure fuel particulates and attempting to understand the significance of the pattern.
4. Attempting to devise a sampling procedure for the combustor laboratory that would give samples with "real world" combustion product implications.

III. Background

A. Extraction and Analysis

Particulate matter associated with incomplete combustion of organic materials (soot) is of environmental concern for several reasons, including esthetic, but the paramount concern is for the health-related aspects. Chief among the health related concerns is the association of polynuclear aromatic hydrocarbons ("PNAs") with soot. Many of the PNAs (also known as "PAHs" or "PACs", for polycyclic aromatic compounds) are proven carcinogens. The literature of analysis of PNAs in combustion products is voluminous. A 1981 review of chemical analysis of particulate carbon by Lee and Bartle(5) contains 127 references. The 1986 literature survey by Dynamac Corporation(1) for the A.F.E.S.C. Evironics Division contains 282 references.

Examination of the literature shows that there is no general agreement on the method of extraction of PNAs from particulate carbon. In the reviews cited above, there are references citing the comparison of soxhlet extraction vs. ultrasonication and recently supercritical fluid extraction(6) has been claimed to be more efficient for extraction. Solvents for Soxhlet extraction include cyclohexane, dichloromethane,

benzene-methanol, toluene, di and trichlorobenzenes and even napthalene at reduced pressure. All of these have been preferred by various groups. In a very recent study by Junk and Richard[7], pyridine, benzene, dichloromethane, dimethylsulfoxide, dimethylformamide and n-methylpyrrolidone were compared, both by Soxhlet extraction and ultrasonication, for extraction of PNAs from urban air, diesel and stack particulate samples. The results were ambiguous. The researchers conclude that "there is neither a single extraction technique nor a solvent that is effective for the efficient extraction of all organic compounds from all types of solid matrices". This is not surprising if one considers that the extractable compounds are formed with, and in a matrix of, the graphitic, insoluble portion of the particulate matter. The nature of a soot sample then, depends upon a number of combustion parameters and extraction efficiency can not be absolutely determined. This is in contrast to an adsorbtion model, in which extraction efficiency could be simply determined by "spiking" a known amount of deutero, or other "tagged" compounds into a known amount of sample. The conclusion would seem to be that, for an uninvestigated matrix, the analyst should, at the very least, sequentially extract his samples with known efficient solvents until satisfied with the recovery is maximized.

Analysis of extracts of exhaust particulates is indeed the analysis of complex mixtures. Capillary gas chromatography of such extracts typically gives dozens to a few hundred peaks. Samples are usually expensive and difficult to collect, so it is usually undesirable to apply clean up procedures that would remove all but one class of compounds. Analysis of extracts under these conditions requires high resolution gas chromatography-mass spectrometry. The mass spectra of isomeric PNAs are

essentially identical and identification must be made on the basis of retention time but the mass spectrum is necessary to assure a peak is due to a PNA for example, and not a nitro-PNA. In spite of recent publication of relative retention indices[8,9] it is essential to have authentic compounds for identification standards since relative retention can change with cross-linking of the stationary phase or with nominally identical stationary phases from different suppliers. In spite of earlier problems with the separation of isomeric PNAs (such as triphenylene and chrysene or benzo [a] and [e] pyrene) and even synthesis of stationary phases as exotic as bonded phase liquid crystals[10], common modern, bonded phase capillary columns essentially separate PNAs, up to a molecular weight of about 400 Daltons. Quantitation can only be done at high levels of precision by the use of standards due to the vastly different detector response for different PNAs. Ideally, quantitation would be with per-deutero internal standards for each compound of interest, by GC/MS.

B. Soot Formation and PNA Identity

The mechanism(s) of particulate carbon and PNA formation by combustion are certainly complex and are certainly far from being well elucidated. It is, however, generally accepted that soot formation involves two distinctly different mechanism steps; pyrolysis and pyrosynthesis. Organic molecules are partially cracked (pyrolysis) to give smaller, highly reactive species. These species, mostly radicals, recombine to give larger relatively stable aromatic compounds (pyrosynthesis). The literature of formation of PNA in combustion has been reviewed by Crittenden and Long[11]. It is generally accepted that aromatic rings in fuels accelerate soot formation and that both chain branching and un-

saturation result in increased soot and PNA formation. It is known that soot and PNA yields, as well as the identity of the PNA formed, can vary widely depending on temperature, residence time in a combustion zone and the nature of the organic fuel being burned. It is assumed that chemical characterization of PNA products of combustion can lead to valuable information for the understanding of the mechanisms of formation in combustion. Whether or not this is true, it is rapidly becoming apparent that there may be immediate and practical applications for the identification and quantification of PNA's from combustion. In 1982 Spitzer and Dannecher[12] found substantial amounts of three PNAs in the exhaust of Pratt and Whitney JT3D3 turbine engines on a Boeing 707 aircraft that are absent, or present in trace quantities, in urban air samples. Such findings obviously have health implications for personnel such as flight line and test cell mechanics.

A very recent report by National Bureau of Standards personnel suggests that the identities of PNAs in soot from arson can be used to identify the accelerant[13] or even to prove arson through the detection of an accelerant.

Findings such as these indicate that, as more information on the identity and relative quantity of different PNAs from different fuels and flame conditions become known, there are immediate and practical uses, as well as the theoretical possibilities for such information. One very exciting prospect is that of source apportionment of particulate pollution and another is that of proving that all soot producing process are not equally health-threatening per gram of soot produced.

IV. Experimental Materials and Methods

A. Reagents

High purity analytical standards were obtained from a variety of

sources, chiefly Chem Service, Inc., and the U.S.E.P.A. and were checked by G.C./M.S. for 70 eV spectra and retention indices. Solvents were HPLC grade (Fischer Chemical and Burdick and Jackson) and were blanked by FID-G.C. analyses.

B. Sample Extraction and Concentration

Samples were Soxhlet extracted employing Whatman 33x80 mm single thickness cellulose thimbles with a light glass wool plug at the top. The glass wool and thimbles were always pre-extracted with the extraction solvent, dried at 50°C/3 torr and tared. Solvent volume was approximately 250 mL and the cycle time for the extraction was approximately 6 minutes. Samples were extracted for 24 hours, replenishing solvent if necessary. After extraction, samples were concentrated to 5.0 mL in a Kudena-Danish apparatus, at 98°C in a water bath. Samples for GC/MS analysis were further concentrated by "blowing down" with dry nitrogen to a final volume of 0.20 mL.

"Free" soot samples, scraped from the combustor rig burner face, of between 0.090 and 0.10 grams were placed directly in the thimbles, weighed to 0.1 mg. and extracted. Variable weights of soot collected on various filter media were extracted by placing the folded filter into the soxhlet thimble. In all cases the samples were contained by a pre-weighed light plug of glass fiber. Solvent from pre-extractions of the thimbles and glass fiber plugs was routinely concentrated and analyzed by FID gas chromatography.

C. Sample Collection

Soot samples were collected from the combustor rig (center body combustor) located at the Tyndall A.F.B. Combustion Laboratory. The combustor has been described elsewhere[14]. In all cases, the soot col-

lection was secondary to light scattering studies of particle size and rate of formation. Samples were simply scraped off the face of the burner after any run in which a pure hydrocarbon fuel was burned. The samples were scraped onto a glassine weighing paper, weighed, the weighing paper folded around the sample, then placed in a small paper envelope and stored in at $0^{o}C$ in a glass container in a freezer until they were extracted.

Other samples were obtained on 47 mm. teflon coated "Millipore" filters, using a pumped probe set at fixed distances behind the burner head. Later, a filter holder was designed which fit into the stainless steel exhaust system, in order to obtain soot samples at room temperature. The filter holder was a 12 inch diameter aluminum plate with a centered 4 1/2"x 7 1/2" rectangular aperture, fitted with a frame and wing nuts to hold one half of a Schleicher and Schull binder-free quartz micro fiber 8x10 inch filter. The filters were conditioned in an oven at $400^{o}C$ for four hours, cooled, weighed and stored in a dessicator prior to use. Samples were collected, using this system, for burns of each pure hydrocarbon fuel, weighed, protected by $400^{o}C$ fired aluminum foil and stored with samples collected from the burner head, from the same burn, in a covered cake pan in a freezer at $0^{o}C$.

Exhaust particulate samples from 3 different engines at 4 different power settings were collected by personnel from Battelle Institute, Columbus, Ohio at Tinker AFB on 6/6 to 6/10, 1986. The filters were Pallflex Corporation 2500 QAST 6 inch diameter quartz fiber filters. The sampling rake and collection procedure are described elsewhere(2). The filters were preweighed in a controlled humidity chamber and held at $150^{o}C$ for the duration of sampling. They were again equilibrated in

the humidity chamber and reweighed after sampling. The filters were stored in glassine envelopes enclosed by "zip lock" plastic bags. The samples were delivered to Tyndall A.F.E.S.C. in ordinary packaging by common carrier.

D. Analytical Conditions and Instruments

The gas chromatographic analysis were carried out using a J and W Scientific 30 M. x 0.25mM x 0.1 μM bonded film of DB-5 (J and W Scientific) in a Perkin-Elmer Sigma 2000 instrument using the flame ionization detector (FID). The injection mode was a 30:1 split ratio (because of lack of a splitless injection port liner) and the linear velocity of helium through the column was 35 cm/sec at $100^{\circ}C$. The injection port and detector were maintained at $300^{\circ}C$. The oven temperature program was 2 minutes at initial temperature of $50^{\circ}C$, then increased to $125^{\circ}C$ at $5^{\circ}C$/min. and then increased to $300^{\circ}C$ at $8^{\circ}C$/min., with a 10 minute final temperature hold. One or 2 μL samples were injected. The initial gas chromatography-mass spectrometry (GC/MS) analyses were performed on a Hewlett-Packard (H-P) 5987 mass spectrometer with capillary-direct sample introduction from an H-P 5880 gas chromatograph with control and data collection by an H-P RTE-6 data system. The chromatography was with the splitless injection mode, system purge on at 0.5 minutes with a 50M by 0.20 mM by 0.10 μM bonded phase "HP-5Ultra" column (Hewlett Packard Corporation). The linear He velocity was 2.5 cm/sec., at $200^{\circ}C$. The same temperature programs used in the G.C. FID analysis were used. The mass spectrometer was programmed to scan from 50 to 400 amu and operated in the 70 eV electron impact mode.

Later analysis were carried out using an identical capillary column with an H-P 5890 GC/5970 "MSD" system employing essentially identical G.C. and M.S. conditions. Except that the 5970 analyzer was operated at above five times the source pressure ($2\text{-}3 \times 10^{-5}$ torr) as the 5987 instrument ($4\text{-}5 \times 10^{-6}$ torr).

V. Results and Discussion

A. Combustor Soot Formation: Initial data from the analysis of PNAs formed in the combustion of the different pure compounds is summarized in Table I. Representative chromatograms from these analyses are shown in Figure I. The elution order in these chromatograms is essentially the same order as increase in boiling point. Many unidentified peaks are due to methylated PNAs for which standards were not available. The difference in PNA composition patterns is quite dramatic in the chromatograms. The 1-butene and isobutene soot extracts, particularly, are much richer in five and six ring components. The flame temperatures and fuel/air ratios are, unfortunately, not known for these samples.

The lower set of two chromatograms in Figure I is a comparison of sequential (1. methylene chloride, and 2. benzene/methanol) extracts of the same sample. The results are representative; in no case was more than 10% of a given PNA found in a second extraction, when solvents were benzene/methanol, toluene or dichloro benzenes. This observation, coupled with increased difficulty in solvent removal made methylene chloride the obvious choice for sample extraction with these samples. The same results were observed for the same experiments with turbine engine exhaust particulates. (Lack of space prevents presentation of more chromatograms).

Table II is a representation of the PNA content of soot collected for three fuels, (a) from the burner head, and (b) from a filter at essentially ambient temperature about 10 ft. down the 75 $ft.^3$ min^{-1} exhaust stream. Soot samples from the other three fuels are currently being analyzed. Representative chromatograms are not presented due to the

page constraint. The quantitation is relative. Quantitation was to have been done with internal standards by SIM mode GC/MS. Instrument problems made this impossible in the 10 week period.

These soot extracts do not show the dramatically higher concentration of higher molecular weight PNAs for 1-butene. The data are consistent in the absence of lower PNAs in soot collected at low temperature, with high air dilution. This could either be attributed to loss of volitiles from the sample or to quenching of the pyrosynthesis mechanisms at the burner face. We believe that it is the latter. We believe very strongly that this work needs to be repeated with known flame conditions, collection temperatures and for a statistically significant number of samples.

B. Turbine Engine Exhaust Particulates: Table III represents FID data from turbine engine particulate exhaust analysis. Quantatative data is given only for benzo (a) and benzo (e) pyrene. These data were generated from external standards run several days before the samples. Detector response could not remain constant over the time interval and the data should be considered semi-quantitative at best. Samples of these extracts were run by GC/MS but due to a very high noise level, with numerous large noise spikes the PNAs were essentially below the limits of detection. Filter blanks of these samples were not subjected to the 150^{o}C collection temperature or airflow, but were otherwise handled the same, including installation in filter holders. The "blanks" all contained two different phthalates at more than 100 times the concentration of any analyte. Only comparative amounts of phthalate were found in actual samples. Several of these extracts were run on an HP 5970B instrument about six weeks after extraction. Compounds were well above limits of detection but there was some indication of sample

degradation/oxidation. This, coupled with the initial gross imprecision of sample mass leads to the conclusion that, although possible, reanalysis of these samples would be largely a waste of time. A ratio of benzo (a) and/or (e) pyrene to total particulate would be significant for comparison to other combustion sources.

Several hundred G.C. and several dozen GC/MS runs were done in the course of this investigation. Some of the data is still being organized and some analyses are still being done. Significant results and a report addendum will be presented to our Environics Division colleagues in a short time.

VI. Recommendations

A. Turbine Exhaust Samples: (1) A decision on the type of information required must be made before particulate sampling and the sampling technique can then either be biased toward; (a) real contribution of hazardous compounds to particulate pollution, or (b) precursor compound formation, by turbine engine exhaust. (2) If the goal is (a, above) then samples should be collected by air dilution cooling and sufficient residence time to duplicate the atmospheric equilibrium products. We believe that there is a definite quenching effect on PNA formation in combustion processes and that this should be avoided unless kinetic/mechanistic studies of soot formation are planned. (3) Sampling must be conducted in a way to obtain sufficient particulate loading (without vapor condensation) on filters to give sufficient concentrations for reliable analysis. We suggest 100 mg. as a reasonable lower limit. (4) Sample blanks should be handled in exactly the same manner, including heated air flow, as sample filters. (5) The method must give a reasonable degree of precision for the total particulate load on filters. (i.e., blanks should indicate no load to 0.1 mg. if samples are

in the 100 mg range). (6) If there is to be a high volume of this type of work done, or if it should become routine, research should be done on automated supercritical fluid extraction/S.F. Chromatography/Mass Spectrometry for analysis of large numbers of samples. We believe that these rather new techniques could be automated to very high efficiency and precision if they seem economically attractive. (7) If small volumes of very light samples are done, unusual methods of concentration such as a "solid injector" or on column cyro trapping should be used.

We have been supplied (Capt. Paul Kerch) with a large number of filters (over 70) collected from J-79-GE-15A engines at various power settings, with and without ferrocene additive. The filter set contains duplicates for each collection conditions and each set has a very good sample mass correlation. The filters all have over 100 mg load and seem to have been subject to reasonable preservation. We recommend that these samples are worth funding for extraction and analysis. We have adequate facilities for extraction and concentration, appropriate standards and we can essentially dedicate a GC/MS system to analysis of extracts for as long as is required.

B. Combustor Laboratory Samples: We feel that our summer results from analysis of the particulate combustion products of pure hydrocarbons are very exciting, but that a great deal more experimentation is necessary for truly significant results. We believe that the difference in PNA contents of "burner face" and "downstream filter" samples is due to reaction quenching at the burner face. This could be tested and "quenched" products could be analyzed from a sampling probe that would give very rapid cooling at or in the sooting flame. In addition, the particulate products collected at essentially ambient conditions should be repetitively collected and analyzed. The collection should be done for precis-

ely determined combustion and collection conditions. The combustor laboratory at Tyndall A.F.B. has the capability for this sample production and collection. We will propose to extract, concentrate and analyze such samples and to attempt interpretation of the results in terms of soot formation mechanism.

Figure I
Chromatograms of Soot Extracts
from Pure Fuels

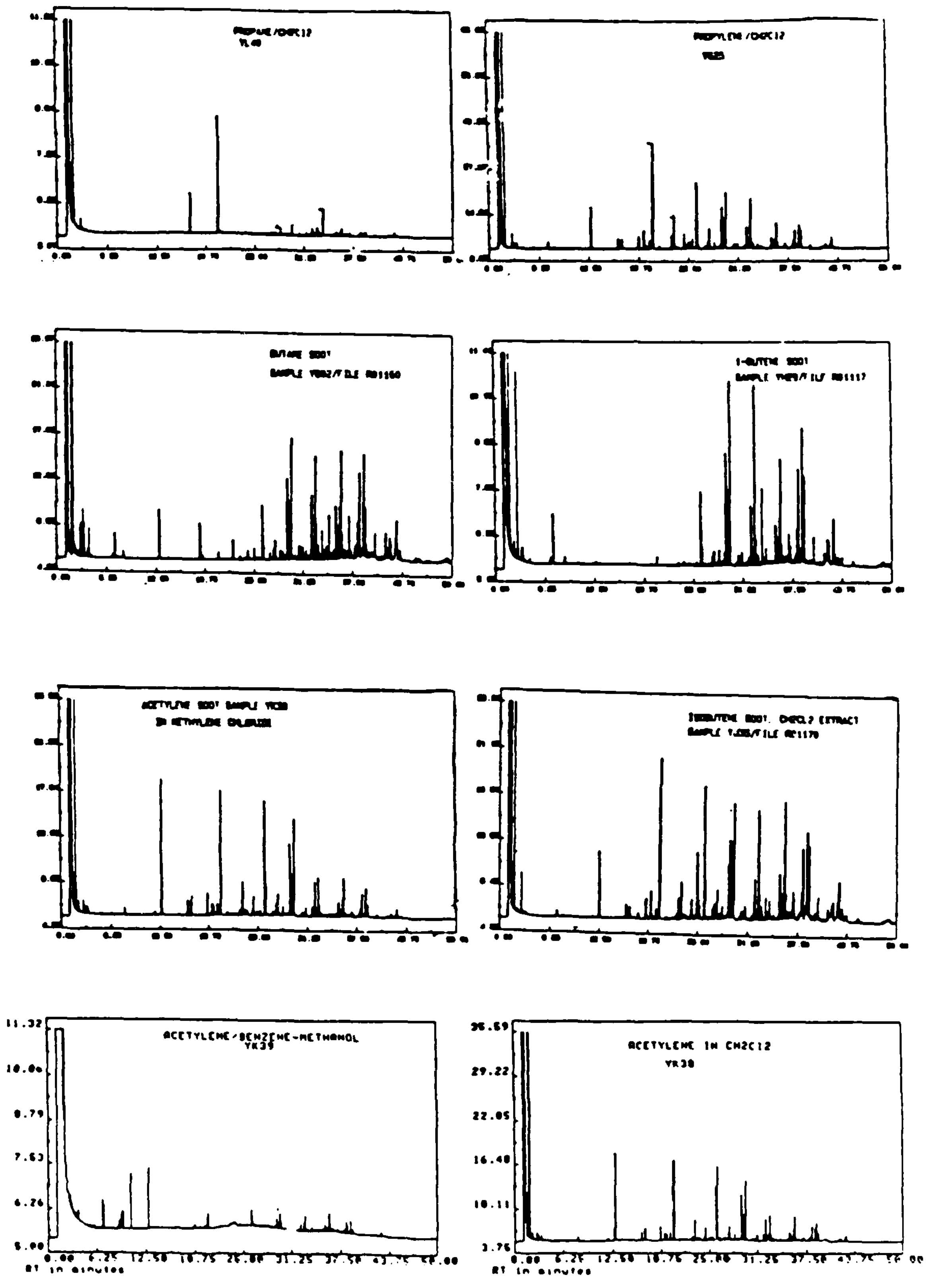

(a) No quantitative information is implied by these chromatograms.

Figure 11

Chromotograms of Turbine Engine Exhaust Particulate Extracts

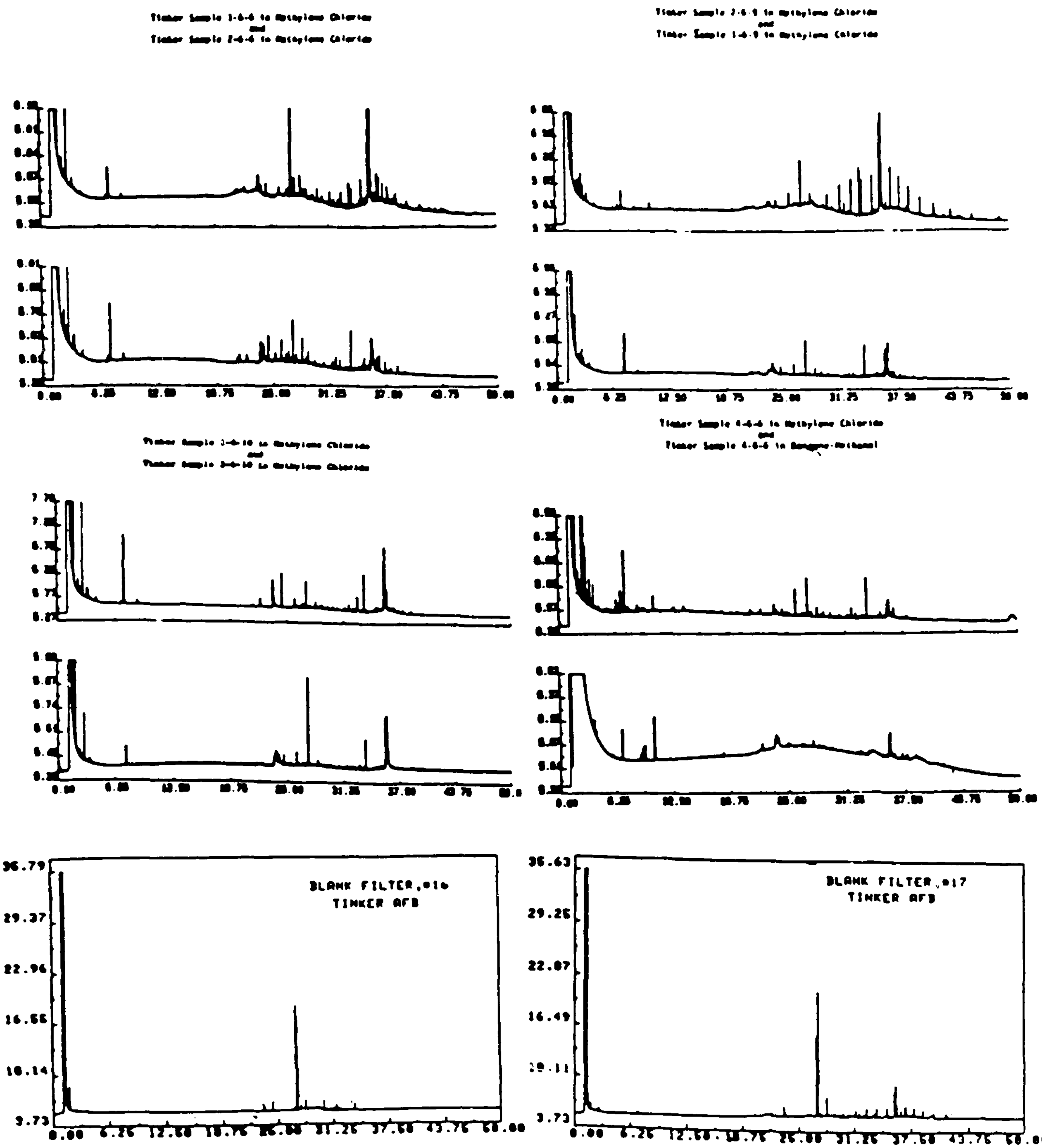

Table I

PAH's Identified by
Retention Times in Combustor
Soot Samples

Fuel	Area	PAH Identified
Propane	5516	Azulene
	1604	Benzo(ghi) Perylene
(Peaks Present- 22; Peaks Identified -2)		
Propene	33406	Napthalene
	5831	Azulene
	166825	1-4 Dimethylnapthalene
	2237	Phenanthrene
	1222	Benzo(b) Fluorene
	4370	Triphenylene
	1339	Benzo(a) anthracene
	8580	Benzo(b) fluoranthene
	21364	Benzo(e) pyrene
	2700	Benzo(a) pyrene
	29038	Benzo(ghi) perylene
	10459	Coronene
(Peaks Present- 42; Peaks Identified -12)		
Butane	25369	Napthalene
	2570	Benzo(b) fluorene
	9385	Triphenylene
	25372	Benzo(e) pyrene
	64560	Indeno (1,2,3,cd) perylene
	1704	Benzo(ghi) perylene
	8776	Coronene
(Peaks Present- 45; Peaks Identified -7)		
1-Butene	1033	1-5 Dimethylnapthalene
	7084	Fluroantnene
	2650	Triphenylene
	5578	Benzo(b) fluoranthene
	13090	Benzo(e) pyrene
	22253	Benzo(ghi) perylene
	20848	Coronene
(Peaks Present- 40; Peaks Identified -7)		
Acetylene	79830	Napthalene
	81201	1-5 Dimethylnapthalene
	15641	Fluoranthene
	18630	Benzo(e) pyrene
	1499	Benzo(a) pyrene
	5320	Triphenylene
	7695	Coronene
(Peaks Present -49; Peaks Identified -7)		

Fuel	Area	PAH Identified
Isobutylene	33598	Napthalene
	114843	1-5 Dimethylnapthalene
	2237	Fluorene
	18125	Fluoranthene
	23.07	Benz (b) fluroanthene
	8309	Chrysene
	16197	Benzo(a) anthracene
	20946	Benzo(k) fluoranthene
	3483	Benzo(e) pyrene
	79693	Benzo(ghi) perylene
	61115	Coronene
(Peaks Present-42; Peaks Identified -11)		

Table II

Relative Amounts of Major Polycyclic Aromatic Compounds formed from Different Fuels at the Combustor Head and Found in Exhaust at Ambient Temperature(a)

PAH's	Fuels: Propane Filter	Propane Burner Face	Propene Filter	Propene Burner Face	1-Butene Filter	1-Butene Burner Face
Napthalene	- -	$1.26\times10^{7*}$	- -	$4.86\times10^{4*}$	- -	$2.21\times10^{6*}$
Azulene	- -	8.74×10^{5}	- -	- -	- -	3.01×10^{5}
1-5 Dimethylnapthalene	4.45×10^{3}	- -	- -	3.09×10^{5}	- -	5.50×10^{6}
Anthracene	- -	- -	- -	- -	$4.59\times10^{3*}$	- -
Fluoranthene	- -	- -	- -	- -	- -	$8.59\times10^{5*}$
Pyrene	$3.59\times10^{3*}$	- -	- -	- -	$3.22\times10^{3*}$	- -
Benzo [b] Fluorene	$3.04\times10^{4*}$	$1.83\times10^{5*}$	$1.13\times10^{5*}$	2.92×10^{4}	2.02×10^{4}	8.06×10^{4}
Triphenylene	6.33×10^{4}	$9.60\times10^{6*}$	5.56×10^{5}	6.54×10^{5}	3.62×10^{4}	$4.00\times10^{5*}$
Chrysene	1.16×10^{4}	- -	- -	- -	- -	- -
Benzo [a] Anthracene	1.42×10^{4}	$2.92\times10^{5*}$	8.24×10^{4}	1.83×10^{4}	- -	- -
Benzo [b] Fluoranthene	- -	$1.67\times10^{6*}$	- -	- -	$6.02\times10^{4*}$	6.41×10^{5}
Benzo [k] Fluoranthene	$2.29\times10^{5*}$	- -	- -	1.26×10^{5}	- -	- -
Benzo [e] Pyrene	- -	- -	1.59×10^{6}	1.25×10^{5}	$1.6\times10^{6*}$	$1.74\times10^{7*}$
Benzo [a] Pyrene	$3.10\times10^{5*}$	$3.45\times10^{6*}$	2.50×10^{5}	$1.62\times10^{4*}$	2.68×10^{4}	9.82×10^{4}
Indeno [1,2,3,cd] Pyrene	$1.51\times10^{5*}$	$2.73\times10^{6*}$	- -	- -	- -	- -
Benzo [ghi] Perylene	- -	- -	1.31×10^{6}	$2.21\times10^{5*}$	$3.61\times10^{3*}$	$3.84\times10^{4*}$

(a) Numbers are Simply Integrator Areas per Gram Sample.

(*) Identify confirmed by Mass Spectrometry

Table III
Analysis of Turbine Engine Exhaust Samples

Run #	Engine	Powersetting	$\mu g/ft^3$ of Benzo (e) Pyrene	ft^3 @ 150^oC	Sample Mass Wt/Mg	Benzo Pyrenes: Benzo(a)pyrene µgPAH	Benzo(a)pyrene ppmEOM(a)	Benzo(e)pyrene µg PAH	Benzo(e)pyrene ppm EOM(a)
1-6-6	TF-41	Idle	36.03	35.15	0.12	. . .	. . .	915.0	1600.0
2-6-6	TF-41	30%	0.0763	43.20	-3.5	. . .	. . .	3.30	6.925
3-6-6	TF-41	75%	5.57	45.75	15.30	. . .	. . .	25.50	402.50
4-6-6	TF-41	Normal Rated	0.436	52.25	41.25	. . .	. . .	22.80	300.00
1-6-9	TF-30-103	30%	. . .	34.80	-0.85	3.30	214.25	. . .	. . .
2-6-9	TF-30-103	75%	1.499	58.50	10.40	3.15	?	86.50	?
3-6-9	TF-30-103	Normal Rated	0.0028	58.90	8.00	6.65	175.5	36.00	950.00
4-6-9	TF-30-103	Idle	1.132	32.70	-1.85	. . .	. . .	37.00	2435.00
1-6-10	TF-30-109	Idle	2.88	40.43	-3.95	2.15	390.00	116.75	21225
2-6-10	TF-30-109	30%	1.667	17.40	-0.60	. . .	. . .	29.00	1895
3-6-10	TF-30-109	75%	1.715	14.23	0.80	. . .	. . .	24.42	4200
4-6-10	TF-30-109	Normal Rated	. . .	51.30	0.90	0.53	27.50	. . .	. . .
5-6-10	TF-30-109	Normal Rated (roof top)	2.038	26.13	0.93	6.00	91.00	53.10	807.5
6-6-10	TF-30-109	After/burning	1.225	26.13	0.90	247.25	24725	32.0	3200

(a) Figures in ppm of extractable organic material. Data is not reliable due to very low filter loadings and difficulty equilibrating temperature/humidity conditions for weighing.

. . . not detected

References

(1) Drake, R. L. Characterization of Chemicals on Engine Exhaust Particles (final report) Dynamac Corporation, Rockville, MD. Sept. 1985.

(2) Berry, D. A., Holdren, M. W., Lyon, T. F., Riggin, R. M., and Spicer, C. W., Turbine Engine Exhaust Hydrocarbon Analysis, Tasks 1 and 2, Interim Report No. ESL-82-43, June, 1983.

(3) Spicer, C. W., Holdren, M. W., Lyon, T. F., and Riggin, R. M., Composition and Photochemical Reactivity of Turbine Engine Exhaust, Final Report No. ESL-TR-84-28, 1984.

(4) Spicer, C. W., Holdren, M. W., Lyon, T. F., and Riggin, R. M., Composition and Photochemical Reactivity of Turbine Engine Exhaust, Final Report No. ESL-TR-84-61, June 1985.

(5) Lee, M. L., and Bartle, K. D., "The Chemical Analysis of Particulate Carbon" Particulate Carbon, Formation During Combustion, Siegla, D. C. and Smith, G. W., Editors, Plenum Press, New York, N.Y., 1981.

(6) Hawthorne, S. B. and Miller, D. J., "Analytical Extractions of PAH From Environmental Solids Using Supercritical Fluids". Presentation at 192nd National Meeting of the American Chemical Society (Anaheim, CA., September 7-12, 1986) Paper #90, Division of Analytical Chemistry.

(7) Junk, G. A., and Richard, J. J., Analytical Chemistry, 1986, 58, 962-965.

(8) Lee, M. L., Vassilaros, D. L., White, C. M., and Novotny, M., Analytical Chemistry 1979, 51, 768-773.

(9) Rostad, C. E., and Pereira, W. E., Journal of High Resolution Chromatography and Chromatography Communications, 1986, 9, 328-334.

(10) Markides, K. E., Chang, H-C. Schregenberger, C. M., Tarbet, B. J., Bradshaw, J. S., and Lee, M. L., Journal of High Resolution Chromatography and Chromatography Communications, 1985, 8, 516-520.

(11) Crittenden, B. D., and Long, R., "Carcinogenesis-a Comprehensive Survey: Polynuclear Aromatic Hydrocarbons", R. Freudenthal and P. W. Jones (eds.) Raven Press, New York, (1976) p. 209.

(12) Spitzer, T., and Dannecker, W., Journal of High Resolution Chromatography and Chromatography Communications, 1982, 5, 98-99.

(13) Chesler, S. N., News Item in Chemical and Engineering News, Sept. 1, 1986, p. 25 and personal communication.

(14) Proctor, Charles and Touati, Abderrahmane, Survey of Soot Formation, I. Soot Precursor Mechanism, Contract No. F08635-83-C-0136, October, 1983.

1986 USAF-UES SUMMER FACULTY RESEARCH PROGRAM/

GRADUATE STUDENT SUMMER SUPPORT PROGRAM

Sponsored by the

AIR FORCE OFFICE OF SCIENTIFIC RESEARCH

Conducted by the

Universal Energy Systems, Inc.

FINAL REPORT

Electroencephalography and Online Analysis: An Evaluation of Some Available Choices

Prepared by:	Jennifer McGovern-Weidner
Academic Rank:	M. A.
Department and	Department of Psychology
University:	University of Florida
Research Location:	USAF School of Aerospace Medicine
	Crew Technology Division
	Crew Performance Laboratory
USAF Researcher:	Dr. Nita L. Lewis

Date:	22 August, 1986
Contract No:	F49620-85-C-0013

Electroencephalography and Online Analysis:

An Evaluation of Some Available Choices

by

Jennifer McGovern-Weidner

Abstract

Online analysis of electroencephalographic data is a desirable product. There are a number of analysis methods for EEG data and for data collected over time. Six analyses were evaluated and some were tested for effective use in online realtime analysis. Recommendations for future use were made. This project is ongoing and no final conclusions were made.

ACKNOWLEDGMENTS

I would like to acknowledge the Air Force Systems Command and the Air Force Office of Scientific Research for their sponsorship of this summer opportunity. I would also like to thank the people of the School of Aerospace Medicine, especially those in the Crew Technology Division and the Crew Performance Lab. Special thanks to those people outside of Division who help make experience so positive. Merci mille fois to the following: Dr. Bill Storm, Dr. Doug Eddy, Dr. Jay Miller, and Col John Bomar for their answers and their respective humors (and bad puns). But first and foremost my greatest thanks and appreciation to Dr. Nita L. Lewis for her insight, enthusiasm, scientific merit, inspirational talkings to and most especially, her time.

I. Introduction

I am working toward my Ph. D. at the University of Florida studying cognitive psychology. Within cognitive psychology I have done research in the general areas of Event Related Potentials (ERPs) and performance. The event related potential is an electroencephalogram which is time locked to an event in the environment such as a flash of light or a tone or the presentation of a meaningful word or sentence. Background in this very specialized version of EEG analysis as well as experience in performance measurement allowed me to work effectively on some of the questions being asked at the USAF School of Aerospace Medicine.

The research problems posed at the Crew Performance Laboratory included such questions as determining the state of the observer (subject) from the EEG collected from him during a task, the effects of certain mechanically simulated environments on the EEG and performance of the subject, and the best methods for the analysis of the EEG and performance data collectec.

The questions being asked in the CPL are akin to those [illegible] in the U. F. ERP lab. Algorithms for on-line real-time data [illegible] are being sought in many labs around the country. [illegible] uses for a real-time data system. The number of analysis [illegible] available is large. The problems reside in locating effective [illegible] form other fields often not read by psychologists and [illegible] the most appropriate, most effective and efficient [illegible]. [illegible] has been used in a [illegible] number of years [illegible]

anomalies of the brain, and some mental disorders. It has also been used to confirm sleep stages and levels of anesthesia. These clinical records are usually scored by hand by highly trained observers [illegible] later than the records are recorded. More recently, the EEG has been used in a variety of laboratory situations to assess variables such as workload and attention.

The question posed to me by CPL was utilize the data available to begin generation of a prototype on-line real-time EEG data analysis system. This system required capability for expansion and generalization.

II. Objectives of the Research Effort

The major objective of the CPL effort is monitoring of physiological variables in flight. One of these variables is EEG. The minor objectives included:

1. a review of the literatures on EEG collection, EEG analysis, and collection of physiological data inflight.

2. evaluation of the analysis methods as they related to [illegible] environmental and resource constraints.

3. use of the analysis methods on some previously collected [illegible] data.

III. The Candidate Analyses

All the analyses chosen for final evaluation utilize [illegible] information from the EEG signal to determine when a change in the EEG pattern has occurred. The EEG is an oscillating signal which is assumed to be random with respect to events in the environment.

Changes in the basic characteristics of the waveform of the EEG signal reflect a sometimes visible change in the state of the subject. The data on the EEG of sleep is a good example. As a subject sleeps the EEG waveform shifts from its active, 13-20 Hz frequency, low amplitude waveform through a series of frequency slowings and amplitude suppressions down to a low of 2 to 4 Hz (delta activity) with very small amplitude. There are periods during sleep which consist of high frequency high amplitude activity as well.

These shifts in activity are the result of an "interface" between states. At the "interfaces" the variance in the signal spans with respect to its previous level. By detecting the large activity changes or variance shifts from the EEG signal, we may be able to determine state of the subject. There are a variety of mathematico-statistical methods for finding these variance shifts and determining if they are of any import to the experimenter.

A. EEG Spectral Moment Estimation

The spectral moment estimation procedure is computationally economical because it avoids calculation of a Fourier [illegible] and instead uses a moment based on the autocorrelation function. This allows for a test of significance that is based on a [illegible] (Saltzberg, 1968).

B. Wavelength-Amplitude Profile Analysis

This computer program simulates the human electroencephalographer by attempting to determine the dominant frequency at a [illegible]. It also determines the degree of variability by detecting [illegible]

dominant frequency changes. Finally it notes the number of waves in a period that are not of the dominant frequency. These are the three attributes an electroencephalographer determines when reading an EEG trace. The effectiveness of this system has been shown to good with a high degree of correlation (Carrie and Frost, 1971)

C. V-Mask Control Schemes

Because errors are assumed to be normally distributed, the V-mask calculated a standard deviation of the errors and uses that to determine the goal which is the mean. The V-mask procedure is used most often in manufacturing for product output quality control (Lucas, 1976).

D. Unknown Time Point Variance Shift Tests

Hsu (1977) reviewed two tests for variance shift given independent normal values and a known level of variance. The two tests presented are the T statistic, which is a weighted ratio of X^2 and the G statistic, which is a cusum of the X^2 values. This procedure is useful in economic modeling.

E. Time Domain Analysis

The time domain analysis (Hjorth, 1970) attempts to describe the EEG trace in a few quantitative terms. It is derived from the statistical properties of the spectrum but are based solely on the time dimension. Because they are grounded on variance (as are all the techniques discussed here) the characteristics of the time domain analysis are cumulative.

F. Complex Demodulation for Trend and Rhythm Analysis

Because much time series data is collected over a vast time (with respect to the sampling rate) the cycles can obliterate the seasonal information. With complex demodulation the trend, or season, can be removed to look at the cycle (Sing, Thorne, Hegge, and Babkoff, 1985).

G. Variance Index

Byford (1963) uses a variance index or ratio of the variances of the EEG signal as it moves over time. The slope of variance of the EEG waveform is calculated and then the ratio of two adjacent slopes is calculated. The ratio, for statistical reasons, can be tested for significance with an F ratio table. The utility of the variance index is in the simplification of the EEG signal to a series of linear relationships between the various frequencies over time.

IV. Evaluation of the Analyses

A. EEG Spectral Moment Estimation

This analysis is very good for online realtime possibilities. It is easily calculated, computationally and resourcefully efficient and reaches conclusion from a convergent operation. It does assume that sampling fast enough will make the EEG signal stationary, but that is an acceptable assumption.

B. Wavelength-Amplitude Profile Analysis

The major flaw of this method results from its major strength. Because it simulates a human electroencephalographer it is as slow or slower in interpretation and is as inaccurate if not more so.

C. V-Mask Control Schemes

The assumption that error is normally distributed cannot be upheld. Because the entire V-mask scheme rests on this assumption, it is not appropriate for our use at this time. Because it is an iterative process, the V-mask is also too slow for online analysis.

D. Unknown Time Point Variance Shift Tests

This analysis would not stand alone. The statistics are easily calculated and would be useful in concert with other methods.

E. Time Domain Analysis

This analysis is quite good because it is quantitative and describes the data in a useful fashion. It uses both the frequency domain which is most often referred to in this work and the time domain which is more obvious intuitively. It is on-line and efficient.

F. Complex Demodulation for Trend and Rhythm Analysis

Complex demodulation is a strong analysis. It will be useful in the future when a great deal of data is collected over a long time (more than 8 hours). But it is too long term oriented for the problem at hand.

G. Variance Index

The variance index is an easily calculated, intuitive measure. It is operational on-line and is dynamic in the same range as the EEG signal (over short periods of time). It is easy to interpret and useful in its final form.

V. Recommendations

1. Online data analysis is not within our reach at this time. however, the analyses used now should reflect the desire to move to online analysis of the EEG and other physiological data. By streamlining the procedures now less adaptation of the methods will be required when the shift to online is made.

2. At this time the Byford (1963, 1965, Adams and Byford, 1973) variance index is the most acceptable analysis for our current offline and future online EEG analyses. It affords the most benefit with the most minimal cost. Time domain analysis will continue to be a viable alternative or concurrent analysis for the time being. With further testing of the previously collected data one may shine forth as the better. If time domain analysis and variance indices are equally effective the more efficient in terms of required resources should be used.

References

1. Adams, E. R. and Byford, G. H., "A Dynamic Evolutionery Spectral Analysis for the EEG," Reference unavailable.

2. Byford, G. H., "A Technique for Measuring Changes in EEG Activity," Proceedings of the Physiological Society, 1963, pp. 62 64.

3. Byford, G. H., "Signal Variance and its Application to Continuous Measurements of EEG Activity," 1965.

4. Carrie, J. R. G. and Frost, J. D., "A Small Computer System for EEG Wavelength Amplitude Analysis," Bio Medical Computing, (2), 1971.

5. Hjorth, B., "EEG Analysis on the Time Domain Properties," and Clinical Neurophysiology, 29, 1970.

6. Hsu, D. A., "Tests for Variance Shift at an Unknown Time Point," Applied Statistics, 26, 1977.

7. Lucas, J. M., "The Design and Use of V Mask Control Schemes," Journal of Quality Technology, 8, 1976.

8. Saltzberg, B., "EEG Spectral Moment Estimation," Personal Communication, 4 January, 1985.

9. Sing, H. C., Thorne, D. R., Hegge, F. W., and Babkoff, H., "Trend and Rhthym Analysis of Time Series Data Using Complex Demodulation," Behavior Research Methods, Instruments, and Computers, 17, 1985.

1986 USAF-UES SUMMER FACULTY RESEARCH PROGRAM/

GRADUATE STUDENT SUMMBER SUPPORT PROGRAM

Sponsored by the

AIR FORCE OFFICE OF SCIENTIFIC RESEARCH

Conducted by the

Universal Energy Systems, Inc.

FINAL REPORT

Program Code: Style and Conventions

Prepared by:	Dara Merenski
Academic Rank:	Graduate
Department and	Computer Science
University:	University of Dayton
Research location:	Air Force Human Resources Lab Logistics and Human Factors Division Combat Logistics Branch Wright Patterson Air Force Base Dayton Ohio
USAF Researcher:	Tim Hansell

Date:	July 22, 1986
Contract no:	F49620-85-C-0013

Program code: Style and conventions

by

Dara Merenski

ABSTRACT

This report contains guideline and conventions concerning programming style and documentation for the in-house software development at the Air Force Human Resources Lab Logistics and Human Factors Division Combat Logistics Branch in Dayton. The conventions include how to's for commenting, structuring, and documenting code so that readability, understanding, and maintainability is enhanced. The first section gives general conventions to be universally followed for all programming languages. The following sections contain guidelines applicable to specific programming languages. Some of the guidelines were left inspecific so as to allow the programmer creativity in the programming process. The purpose of this report was not to stifle the programmer but to standardize much of the coding so that programs and packages can be easily read, understood, and maintained. Programmers can easily check the programs available to see if they fit a given problem and thereby reduce duplicate and redundant code.

Acknowledgement

I would like to thank the Air Force Office of Scientific Research and Universal Energy Systems for sponsoring my research. I would also like to thank Human Resources Lab Logistics and Human Factors Division Combat Logistics Branch for the opportunity to work at the lab. Thanks also to Branch Chief Robert Johnson and Professor Raghava Gowda for their help and guidence. Special thanks goes to Tim Hansell. Without his help this project would never have been completed. I would also like to thank Gail Hudson for her assistance and for her help in finding the necessary items for my research.

Finally, I would like to thank my family for their support and faith in my work.

I. INTRODUCTION:

A Bachelors of Science in Systems Analysis at the University of Dayton and work experience involving much research and programmming led to familiarity with the many aspects of library research and with programming.

This background in research and programming supported the research for the Air Force Human Resources Lab Logistics and Human Factors Division Combat Logistics Branch. At the time of this report, just completed the research and development of programming standards and conventions for the lab.

The research delved into the programming conventions, style, and documentation and led to the formulation of program coding and documentation procedures for in-house software development at the lab.

II. Objectives of the Research Effort

The project objective was the creation of procedures and standards for the Air Force Human Resources Lab Logistics and Human Factors Division Combat Logistics Baranch. These standards were necessary so that programmers can understand programs at a glance and be able to maintian the library with more ease and efficiency.

Personal Objectives:

1. Research in the areas of coding, software engineering, and structured programming.
2. Creation of coding and commenting techniques for general use and for the fortran programming language.
3. Review of the current standards, and conventions for coding and commenting for areas of improvement.
4. Compilation of a programmer's guide to programming at the Air Force Human Resources Lab Logistics and Human Factors Division Combat Logistics Branch.

III. Programming Conventions

Software developed for the In–house effort shall adhere to the following coding conventions. Coding conventions shall be broken down into conventions which shall be universal to any language used, and conventions that shall be specific to a particular programming language.

IV. Universal Conventions

univ–1.

Module source code shall be stored one per file, with the file name being the same as the module it contains as the file name conventions of the computer allow.

univ–2.

Modules shall be created with the intent that they be separately compiled producing object code. Include files containing declarations common to modules shall be used to reduce duplication of code.

univ–3.

Modules shall contain relevent documentation in a preamble of the format defined for the particular language, as well as additional comments that make the code clearer. Any fields in the preamble which are not applicable to a particular module shall be marked "N/A". As the module is updated, the preamble and any affected comments shall be updated.

univ–4.

Programmers should set apart major blocks of code with header comments that describe the function of a major block.

univ–5.

Modules should be limited to a size of 100 lines of executable code. Comments shall be considered executable code if they are required to make code readable. In general modules should take no more the two printed pages of text.

univ–6.

Modules should have a specific distinct function to perform. Avoid multiple function modules.

univ–7.

Indentation and "white space" should be used to make code more readable. The number of spaces to indent subordinate levels shall be defined for each language so that language capabilites can be taken into account. If a module requires more than 5 levels of subordination consider breaking it into multiple modules.

univ–8.

Naming conventions are important to any programming effort, but any attempt to generate a general purpose set of naming conventions is really beyond the scope of this document. Each programming project must to set down naming conventions based upon its own requirements. Project naming conventions shall be an authority for the project, and must be followed as would these conventions.

univ–9.

Modules should contain only one entry and only one exit point.

V. Conventions for C programming.

c–1. The following macros shall be defined and shall be contained in the file "/usr/in–house/include/general.h". These macros shall be used in modules to make the code more readable and clearer.

```
#define TRUE 1
#define FALSE 0
#define Begin {
#define End }
```

c–2. Subordinate blocks shall be indented 3 spaces beyond the previous level.

c–3. While the C language has many wonderfully elegant ways of expressing things the following examples of valid C code shall be avoided and replaced the the suggested replacement.

Instead Of This	Use this
x+ = 2 ;	x = x + 2 ;
goto "label" ;	some other control structure
max = (x > y) ? x : y ;	if x > y then max = x else max = y ;

for (i=0;i<=10;i++;j++) Begin
<some code >
End
(where j is no the loop counter)
	for (i=0 ; i <= 10; i++) Begin
	j++ ;
	<some code >
	End ;

c–4. The Begin-End pair which delineates the executable code of a module shall appear in column 1 with code between them indented to the next level of indenture, as is shown in the following example:

```
Col 1
|
V
module_name() ;
  <some module declarations>
Begin
  <executable code of module>
End
```

c–5. A Begin-End pair which is part of a looping control structure shall appear with the Begin on the same line as the loop control, and the end indented to the same level of indenture as the code in the block, as is shown in the example for the convention c–6.

c–6. Any time a block is ended there should be a comment reflecting what the block is that is ending. See the following example :

```
for (i=0 ; i <= 10 ; i++) Begin
  <some code ...>
  End /* for */
```

c–7. Whenever possible user register variables in inner blocks for iterative variables.

c–8. The preamble for C language modules is contained in the file "/usr/in-house/preamble/preamble.c". Copy this file and modify it for the particular modules being written.

c–9. Semicolons ";" shall be separated from surrounding code by at least one blank space. Example :

```
Pay_Amount = Time_Worked * Hourly_Rate ; /* compute weekly pay */
```

c–10. Arithmetic, boolean, and assigment operators shall be separated by one space from the surrounding code as in the following examples. An exception to this rule is the case of a binary operator (requiring only one operand) such as the not operator (!), as shown in the examples below.

```
assignment operator ( = )
  left_hand_side = right_hand_side ;

arithmetic operators ( +, -, *, /, etc.)
  i = i + 1 ;

boolean operators
  while (( !eof ) && ( !searchdone )) begin
```

c–11. Parenthesis, commas and any other symbol which serves as a delimiter should be followed by at least one space, except when these symbols are part of a text string or comment. In general use spaces and blank lines in the code to enhance readability.

VI. Conventions for FORTRAN programming.

fortran–1.

The preamble for FORTRAN language modules is contained in the file "/usr/in–house/preamble/preamble.f". Copy this file and modify it for the particular modules being written.

fortran–2.

Follow the preamble with the following comment block for program header:

```
C
C *****   Module header   *****
C
```

Put the program header statement after the module header comment block.

fortran–3.

Commas shall be followed by at least one space except in character strings and where the logical function of the program is altered by the addition of a space.

fortran–4.

Spaces shall come before and after keywords and the equal sign "=" in assignment statements, except where the logical function of the program is altered by the addition of a space.

fortran–5.

Place the following comment block directly after the program header statement:

```
C
C *****   Variable declaration   *****
C
```

Place the variable declarations directly following the variable declaration comment block.

fortran–6.

Always declare all variables used. Do Not assume any defaults.

fortran–7.

Use the following order for grouping of variable declarations.

```
INTEGER*2 (or INTEGER)
INTEGER*4
REAL*4 (or REAL)
REAL*8 (or DOUBLE PRECISION)
LOGICAL*2
LOGICAL*4 (or LOGICAL)
COMPLEX
DOUBLE COMPLEX
CHARACTER (or CHARACTER*#)
```

fortran–8.

Use Alphabetical order for variables within each group . For example:

```
REAL AVAR, BVAR, CVAR,...
```

fortran–9.

Variable declarations can be grouped on one line separated by a comma and a space (not to

exceed 72 columns) or they can be placed one to a line, as long as they are grouped according to the order given in convention nine. Do not continue declarations (if they exceed 72 columns). If a line needs to be continued, start a new declaration in column 7 with the type name and continue with the list. For example:

Instead of This	Do This
REAL A1, A2,...,AN, +AN+1,...	REAL A1,A2,...,AN REAL AN+1

fortran-10.

The comment block for subroutine/function declarations follows the data declarations. Use this form:

```
C
C *****   Subroutine/function declarations   *****
C
```

fortran-11.

Code is not to extend beyond column 72. Avoid the use of continuation except where absolutely necessary. When continuation is necessary, use an asterisk '*' in column 6 and indent three spaces from the first line of the continued statement..

fortran-12.

The initialization comment block follows the subroutine/function declarations. Use this form:

```
C
C *****   Initialization   *****
C
```

Place the DATA statements first in the initialization section, follow with the the parameter statements, and follow finally by the initialization code.

fortran–13.

The comment block for the main body follows all declarations and initializations. Use this form:

```
C
C *****   Main body   *****
C
```

fortran–14.

Only have one RETURN statement in a subroutine/function.This means no alternate returns statments.

fortran–15.

Do loops shall follow this form:

```
      DO line# varname = lobound, upperbound, stepvalue
         code for do loop; indented three spaces from do statement position.
line# CONTINUE
```

Always place the continue statement on a separate line and allign with the DO in the do statement.

fortran–16.

Do not use GOTO, except in valid DO WHILE or DO UNTIL constructs.

fortran–17.

DO WHILE loops shall be coded in this way:

```
C       DO WHILE (while condition)
line#     IF (while condition) THEN
             code for while loop; indented three spaces from if statment.
             GOTO line#
          ENDIF
C       ENDWHILE
```

fortran–18.

DO UNTIL loops whall be coded in this way:

```
C      DO UNTIL (until condition)
line#    code for until loop; indented three spaces from DO UNTIL in Comment.
         IF (until condition) line#2
         GOTO line#
C      END UNTIL
line#2 code continues here...
```

fortran–19.

The line numbers shall follow logical numerical order in placement.

fortran–20.

The CASE statement shall be implemented using the IF-ELSEIF-ELSE-ENDIF construct.

Do not use Computed GOTO. Use the following form:

```
IF (condition 1) THEN
   code for condition 1; indented three spaces from IF
ELSEIF (condition 2) THEN
   code for condition 2; indented three spaces from ELSEIF
   .
   .elseifs continue in this manner for other cases
   .
ELSE
   code for other condition; indented three spaces from ELSE
ENDIF
```

fortran–21.

The IF-THEN-ELSE construct follows this form:

```
IF (condition for true) THEN
   code for true state; indented three spaces
ELSE
   code for false state; indented three spaces
ENDIF
```

fortran–22.

The comment block for the format statement section shall follow this form:

```
C
C *****   format statements   ***
C
```

fortran–23.

Comments shall be inserted in the code to make it more readable. A blank comment line shall be inserted before and after all comment lines.

For example:

```
C
C *****   this is a comment for a major section   *****
C
```

fortran-24.

The end of the program includes the RETURN statement of functions and subroutines in addition to the END statement. The end of program shall be indicated by a comment block using the following form.

```
C
C *****   End of program   *****
C
```

VII. Reccomendations

1. The Conventions given should be followed during software development at the Human Resources Lab Logistics and Human Factors Division Combat Logistics Branch.

2. Convetions for LISP, Pascal, and Assembly language are needed. The Conventions above can be used as a guide for further convention development.

REFERENCES

1. Abbott, Russel J., "Program Design by Informal English Descriptions," Communications of the ACM, vol. 26, no. 11, November 1983, pp. 882-894

2. Aron, Joel D., The Program Development Process: The Individual Programmer, Addison-Wesley Publishing Company, Reading, Massachusetts, 1974.

3. Basili, Victor R. and Harlan D. Mill, "Understanding and Documenting Programs," IEEE Transactions on Software Engineering, vol. SE-8, no. 3, May 1982, pp. 270-283.

4. Baxter, Patricia, "Bring Your Computer Training Manuals Down to Earth," Training and Development Journal, vol. 38, no. 8, September 1984, pp. 55-59.

5. Bersoff, Edward H., Villa D. Henderson, and Stanley G. Siege, Software Configuration Management: an investment in product integrity, Prentice-Hall Inc., Englewood Cliffs, N.J., 1980.

6. Birns, Peter, Patrick Brown, and John C.C. Muster, Unix for People, Prentice-Hall Inc., Englewood Cliffs, N.J., 1985.

7. Birrel, N. D. and M. A. Ould, A Practical Handbook for Software Development, Cambridge University Press, New York, 1985.

8. Boyd, Warren A. and John R. Eldridge , "Beyond User Friendly," Training and Development Journal, vol. 38, no. 12, pp. 36-38.

9. Brooks, Frederick P., The Mythical Man-Month: Essays on Software Engineering, Addison-Wesley Publishing Company, Reading, Massachusetts, 1979.

10. Davis, Gordon B. and Margrethe H. Olsen, Management Information Systems: Conceptual Foundations, Structure, and Development, McGraw-Hill Book Co., New York, 1985.

11. Department of Defense, "Department of Defense System Software Development Draft," DOD-STD-2167, January 30, 1984, pp. 50-52, 67-69.

12. Depledge, P. ed., Software Engineering for Microprocessor Systems, Peter Peregrinus Ltd., London, UK, 1984.

13. Dijkstra, E., "GOTO Statement Considered Harmful," Communications of the ACM, vol. 11, no. 3, March 1968, pp. 147-8.

14. Emmerichs, Jack, How to Build a Program, Dilithium Press, Beaverton, Oregon, 1983.

15. Feather, Martin S., "Program Specification Applied to a Text Formatter," IEEE Transactions on Software Engineering, vol. SE-8, no. 5, September 1982, pp. 490-498.

16. Jackson, Michael, "Mnemonics," Datamation,vol. April 1967, pp. 26-28.

17. Kammins, Scot and Mitchel Waite, Apple Backpack: Humanized Programming in Basic, BYTE Books, Peterborough, N.H., 1982.

18. Kernighan, Brian and P. J. Plauger, Software Tools, Addison-Wesley Publishing Company, Reading, Mass., 1976.

19. Kernighan, Brian and P. J. Plauger, The Elements of Programming Style, McGraw-Hill Book Company, New York, 1974.

20. Koffman, Elliot B. and Frank Friedman, Problem Solving and Structured Programming in Basic, Addison-Wesley Publishing Company, Reading, Mass., 1979.

21. Kreitzberg, Charles B. and Ben Shneiderman, The Elements of Fortran Style, Harcourt Brace Javanovich, New York, New York, 1972.

22. Ledgard, Henry F., Programming Proverbs, Hayden Book Company, Inc., Rochelle Park, 1975.

23. Ledin, George and Victor Ledin, The Programmer's Book of Rules, Wadsworth Inc., Belmont, California, 1979.

24. McCracken, Daniel D. and Gerald M. Weinberg, "How to Write a Readable FORTRAN Program," Datamation, vol. 18, no. 10, October 1972, pp. 73-77.

25. McGilton, Henry and Rachel Morgan, Introducing the UNIX System, McGraw-Hill Book Company, New York, 1983.

26. Meek, Brian and Patricia Heath, eds., A Guide to Good Programming Practice, Halsted Press, New York, New York, 1980.

27. Metzger, Philip W., Managing a Programming Project, Prentice-Hall Inc., Englewood Cliffs, N.J., 1973.

28. Miara, Richard J., Joyce A. Musselman, Juan A. Navarro, and Ben Shneiderman, "Program Indentation and Comprehensibility," Communications of the ACM, vol. 26, no. 11, November 1983, pp. 861-867.

29. More, John B and Leo J. Makela, Structured Fortran with WATFIV, Reston Publishing Company, Inc., Reston, Virginia, 1978.

30. Purdum, Jack J., C Programming Guide Second Edition, Que Corporation, Indianapolis, Indiana, 1985.

31. Senn, James A., Analysis and Design of Information Systems, McGraw-Hill Book Co., New York, 1984.

32. Shannon, Terry, "How to WRite User-friendly Documentation," The DEC Professional, vol. 3, no. 6, November 1984, pp. 50-60.

33. Shooman, Martin L., Software Engineering: Design, Reliability, and Management, McGraw-Hill Inc., New York, New York, 1983.

34. Sippl, Charles and Roger Sippl, Computer Dictionary and Handbook, Howard W. Sams and Company, Inc., Indianapolis, Indiana, 1980.

35. Sohr, Dana, "Better Software Manuals," Byte, vol. 8, no. 5, May 1983, pp. 286-294.

36 Tassel, Dennie Van, Program Style, Design, Efficiency, Debugging, and Testing, Prentice-Hall Inc., Englewood Cliffs, N.J., 1974.

37. Thomas, Richard A., "Using Comments to Aid Program Maintenance," Byte, vol. 9, no. 5, May 1982, pp. 415-422.

38. Utter, D. F., "Properties of System Design Through Documentation (SDTD) Methodology," IEEE 1984 International Conference on Computers and Applications, IEEE Computer Press, January 20-22, 1984, pp. 809-814.

39. Walsh, Dorothy, A Guide For Software Documentation, Advanced Computer Techniques Corporation, New York, N.Y., 1969.

40. Wile, David S., "Program Development: formal explanations of implementations," Communications of the ACM, vol. 26, no. 11, November 1983, pp. 902-911.

41. Yourdon, Edwared Nash ed., Classics in Software Engineering, Yourdon Press, New York, New York, 1979.

42. Yourdon, Edward and Larry Constantine, Structured Design, Prentice-Hall Inc., Englewood Cliffs, N.J., 1979.

43. Yourdon, Edward, Structured Walkthroughs, Yourdon Inc., New York, New York, 1977.

1986 USAF-UES SUMMER FACULTY RESEARCH PROGRAM/

GRADUATE STUDENT SUMMER SUPPORT PROGRAM

Sponsored by the

AIR FORCE OFFICE OF SCIENTIFIC RESEARCH

Conducted by

UNIVERSAL ENERGY SYSTEMS, INC.

FINAL REPORT

Synthesis and Time to Explosion Studies of Some Potential High Explosives

Prepared by:	Peter D. Meyer
Academic Rank:	Graduate Student
Department and University:	Physics and Astronomy Department University of Montana, Missoula, MT 59801
Research Location:	High Explosives Research & Development Facility Armament Division, Eglin AFB FL 32542-5434
USAF Researcher:	Dr Robert L. McKenney, Jr

Date:	28 August 1986
Contract No:	F49620-85-C-0013

Synthesis and Time to Explosion Studies of Some Potential High Explosives

by

PETER D. MEYER

A B S T R A C T

EAK (a mixture of 1,2-Ethanediammonium Dinitrate, Ammonium Nitrate (AN) and Potassium Nitrate (KN)) was dropped as an Air Force insensitive high explosive (IHE) several years ago. It is hoped that by doing time to explosion studies on other alkyldiammonium dinitrate systems that insight will be gained as to the reasons why EAK failed several of the required tests before becoming an IHE.

Acknowledgements

Research was sponsored by the Air Force Office of Scientific Research/AFSC, United States Air Force, under contract F49620-85-C-0013.

I would like to thank the Air Force Systems Command, Universal Energy Systems, Air Force Office of Scientific Research, the AFATL Energetic Materials Branch at Eglin Air Force Base, Dr McKenney and Dr Bolduc and all others who contributed their time and energy toward the research mentioned in this paper.

INTRODUCTION

An explosive system's response to heat is a balance of chemical decomposition and heat dissipation. Physical processes control heat dissipation in a detonation of an explosive system. Our work concerned the characterization and, if possible, mechanistic explanations of thermally induced explosive decomposition.

The Frank-Kamenetskii equation relating critical temperature to the activation energy of the process is often used.

$$\frac{Eact}{T_c} = R \log \left\{ \frac{a^2 QZ\ Eact}{T_c 2 \rho \lambda R \alpha} \right\}$$

(Frank-Kamenetskii, 1969)

where:

E_{act} = Thermal activation energy

T_c = Critical temperature

Z = Pre-exponential

Q = Heat of the self-heating reaction

a = Arbitrary dimension

ρ = Density

R = Ideal gas constant

λ = Thermal conductivity

α = Shape factor

For a given specific size and shape of an explosive system, the lowest temperature at which catastrophic self-heating occurs is called its critical

temperature, T_c (Rogers, Janney and Loverro, 1984). This does not mean that the energetic system will not decompose at temperatures below T_c. Indeed, decomposition may occur at lower temperatures. This may result in pressure bursts in time to explosion experiments that may be misconstrued as bursts due to self-heating and thus imply that the T_c has not yet been reached. Since these bursts are inconsistent, they are readily detectable by data analysis.

The T_c for BAK and EAK systems was extracted directly from the raw time to explosion data. These data were then reduced to yield activation energies that approximate those for the mechanisms controlling T_c.

From the overall thermal study of BDD (1,4-Butanediammonium Dinitrate) and its mixtures (BAKs) with varying amounts of Potassium Nitrate (KN) and Ammonium Nitrate (AN), and the study of other selected energetic organodi- and polyammonium nitrate salts, we may soon be able to infer some possible mechanistic routes for the decomposition of the BAK system. It is anticipated that this study will give some insight as to the EAK (1,2-Ethanediammonium Dinitrate, AN, KN mix) decomposition scheme as well as into any other mix of the XAK (X-diammonium Dinitrate, AN, KN: X=alkyl) format (McKenney, Fryling, Neveu and Meyer, 1985). If any of these systems are to be considered as military explosives, it is mandatory that their thermal degradation properties be completely understood.

The BAK system under study had an AN/KN weight percent ratio of 85:15. KN was added to AN to suppress a phase change that was also accompanied by a volume change. The latter could not be tolerated. Any differences in thermal behavior can be related to the corresponding concentrations of the components of the BAK mix. EAK systems were also tested in a similar fashion.

Deuterated EAK and BAK systems were also tested to see if there was any type of deuterium isotope effect present.

PROCEDURE

Material Processing: All of the energetic material samples were prepared as follows:

An α,ω-alkyldiamine is dissolved in a minimal amount of ethanol and cooled in an ice bath with stirring. HNO_3 (density 1.4 g/cc) is added dropwise in a mole ratio in slight excess of 2:1. After all the HNO_3 has been added, the mixture is stirred well with continual cooling in an ice bath. The crystals, if not formed after 30 minutes, can usually be precipitated by scratching the sides of the reaction vessel. The resulting crystals are then vacuum filtered, washed twice with cold ethanol, recrystallized from ethanol and/or water and then dried.

Table 1 lists all of the alkyldiamine dinitrate compounds that were prepared for experimental use.

TABLE 1

NAME	ACRONYM	RECRYSTALLIZED FROM	MP(^{o}C)
1,2-Ethanediammonium Dinitrate	EDD	EtOH/H_2O	188.3
1,3-Propanediammonium Dinitrate	PDD	EtOH/H_2O	126.1
1,4-Butanediammonium Dinitrate	BDD	EtOH/H_2O	140.1
1,6-Hexanediammonium Dinitrate	HDD	EtOH/H_2O	108.2
1,1-Dimethylethylenediammonium Dinitrate	ISBDD	EtOH	230.0

N-Methylethylenediammonium Dinitrate	MEDD	EtOH/H_2O	78.[illegible]
N-Ethylethylenediammonium Dinitrate	EEDD	EtOH/H_2O	85.7
N-Isopropylethylenediammonium Dinitrate	IPEDD	Not done	93.4
N,N'-Dimethylethylene-diammonium Dinitrate	DMEDD	EtOH/H_2O	130.0
N,N'-Diethylethylenediammonium Dinitrate	DEEDD	EtOH/H_2O	193.1
N,N'-Isopropylethylene diammonium Dinitrate	DIPEDD	not done	98.2
N,N,N'-Trimethylethylene-diammonium Dinitrate	TRMEDD	EtOH	92.8
N,N,N'-Triethylethylene-diammonium Dinitrate	TREEDD	EtOH	86.1
N,N-Dimethyl-N'-ethylethylene-diammonium Dinitrate	DMEEDD	EtOH	101.2
N,N,N',N'-Tetraethylethyl-enediammonium Dinitrate	TMEDD	EtOH/H_2O	222.8
N,N,N',N'-Tetraethylethyl-enediammonium Dinitrate	TEEDD	EtOH	140.1
Piperazinium Dinitrate	PIPZD	EtOH/H_2O	224.2
1,4-Diazo-bicyclo[2,2,2]octane Dinitrate	DABCODN	EtOH/H_2O	174.1

Attempts at preparing the 1,5-Pentanediammonium Dinitrate (PeDD) salt were initiated. Previously this compound was not isolable. However, by using acetone to remove water, a brownish product was formed. It was previously thought that PeDD may be cyclizing to piperadinium nitrate and thus a pure PeDD isolation was impossible. GC/MS analysis showed that the yellowish product could not be the cyclized PeDD but may indeed be the PeDD sought.

The α,ω-alkyldiammonium dinitrate is then mixed with a AN/KN mixture (AN:KN,85:15 m/m) to form the mixtures listed in Table 2.

TABLE 2

Mixture Name	XDD	AN	KN
	Weight of Component Used/100g		
EAK (eutectic)	45.70	46.20	8.10
EAK (74%)	74.80	21.40	3.80
EAK (89%)	88.70	9.58	1.72
BAK (eutectic)	77.76	18.19	4.05
BAK(CO_2)	39.23	51.65	9.11
BAK (60%)	60.36	33.66	5.98
BAK (94%)	94.15	4.5	1.35

Currently, no work has yet been started on mixing the N-substituted EDD based salts with AN and KN.

These mixtures were deuterated in order to see if a kinetic isotope effect (KIE) exists. Deuteration is done by dissolving 10 grams of the dinitrate salt in 10 grams of D_2O twice and each time rotovapping off the liquid. Although complete deuteration of all ammonium functional groups is not possible in our laboratory set-up, we were able to perform at least an 80% deuteration (99.9% is possible theoretically).

Test Preparation. The time to explosion experiments use a pure aluminum blasting-cap shell of dimensions 6.5 mm inside diameter and 4 cm in length. A 40 mg sample is placed in the tube, covered with an aluminium plug and compacted in an appropriate die. The aluminium plug is then flared outward in the pressing operation to provide a consistent seal. This is shown in the accompanying diagram (Fig 1).

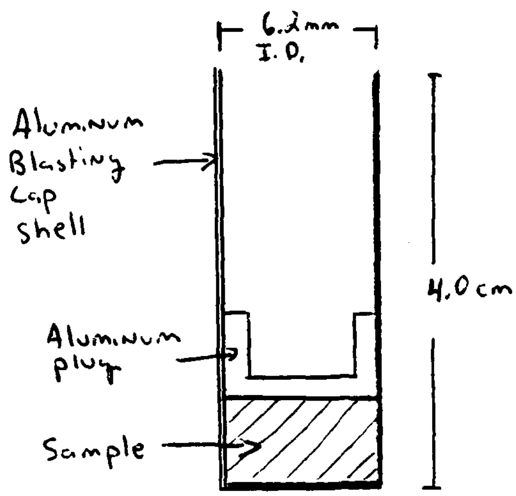

Figure 1 - Henkin Sample Holder

In order to measure the time to explosion, the sample tube is placed in a sample holder, and an explosion indicator is placed through the holder and down into the reaction tube. The tube is then inserted into a heated metal bath. The time until explosion is then measured at a preset temperature for each experiment.

Time to explosion experiments were carried out on the XDD compounds and on their aforementioned mixtures. The N,N,N,N',N',N'- deuterated counterparts of the parent compounds were also used. None of the EDD derivatives were tested at this time.

Results and Discussion

Time to explosion experiments carried out on the various combinations of XAK and XAK-d_x; EDD, BDD, AN and their corresponding deutero-counterparts, yielded data that are listed in Table 3 below. All data were plotted as log time vs 1/T which allowed obviously spurious data to be detected and removed prior to the calculation of the approximate E_{act}. E_{act} in Table 3 is calculated using the previously mentioned Frank-Kamenetskii equation.

TABLE 3

Mixtures*	T_c (°C)	Approximate E_{act} (Kcal/mole)
EDD	231	43.1 ± 2.4
EDD-d_x	231	33.7 ± 3.4
EAK (eutectic)	239	43.1 ± 0.9
EAK-d_x (eutectic)	244	38.9 ± 4.7
74% - EAK	239	42.7 ± 1.7
74% - EAK - d_x	230	40.8 ± 2.1
89% - EAK	239	44.8 ± 3.3
89% - EAK - d_x	230	41.0 ± 1.4
BDD	222	20.5 ± 1.5
BDD - d_x	244	25.9 ± 2.0
BAK (eutectic)	230	35.4 ± 2.1
BAK (CO_2 balanced)	279	50.5 ± 3.4
BAK - d_x (CO_2 balanced)	267	46.7 ± 4.6
60% - BAK	264	64.6 ± 5.8
60% - BAK - d_x	253	52.0 ± 3.75
94% - BAK	239	56.9 ± 5.8
94% - BAK - d_x	230	62.3 ± 12.7
AN	324	***
AN - d_x	**	***

* Percent value indicated weight percent of XDD in the mixture

** Not measurable by our machine as the T_c is above 390°C

*** Not calculated

It is noteworthy to see that the deuterated XAK samples had lower critical temperatures than their protonated counterparts. ΔT_c is the difference between the T_c values of the protonated and deuterated samples. This is shown in Table 4:

TABLE 4

Mixture	ΔT_c (°C)
EDD	0
EAK (eutectic)	5
74% - EAK	9
89% - EAK	9
BDD	0
BAK (eutectic)	14
BAK (CO_2 balanced)	12
60% - BAK	11
94% - BAK	9
AN	*

* Not possible to measure due to instrumental limitations.

The EAK systems have a ΔT_c in the 5-9° range and BAK systems have T_c values in the range of 9-14°C. This may indicate that a similar thermal decomposition mechanism is operating in each of the mixes and that the nearly constant ΔT_c for each system may be a function of the rate determining step. This rate determining step may control the T_c and could possibly be independent of the AN concentrations.

During the time to explosion analyses, it was noted that the EAK systems reacted more violently than the BAK systems. Likewise, the violence of the reaction of a particular XAK group increased with increasing concentration of AN/KN. Violence in this case is noted as the celerity with which the indicator was expelled and the intensity of sound produced upon explosion.

Analysis of the results of the time to explosion study yielded differences between the times to explosion of the protonated and deuterated EDD, BDD, XAK and AN.

The EDD and BDD pairs exhibited little or no difference in T_c, whereas, in AN the protonated sample had a lower T_c than the deuterated sample. In the XAK systems, however, the difference between the protonated mixture and the deuterated mixture is very noticeable. This faster reaction rate of the deuterated XAK samples indicated an inverse KIE.

As mentioned by McKenney, et al., the rate determining step that controls the critical temperature may not involve N-H bond breaking, but possibly C-N bonds (Ref 3).

Recommendations

This type of research is quite valuable in the study of thermal characteristics of any explosive system. However, one must realize that a great deal of time is required for all of the necessary work to be completed to a high degree of confidence. Therefore, I make the following recommendations for follow-on research.

There needs to be more time spent on the time to explosion studies of the XAK systems. In order to observe any trends and see that they are not merely coincidental, the study involving the parent hydrocarbon chain length should be continued. There were interesting trends involving the transition from the ethyl to the butyl chain. If one were to continue experimentation on the other further polycarbon chains, one might see a continuation of these effects.

More testing needs to be performed by using further concentrations of XDD and AN/KN. Again, interesting trends with the varying concentrations of the components of each mixture have been noticed.

Additionally, research into the effects of substituted systems and the overall reaction rates needs to be studied further. This could possibly lead to confirmation that the initial reaction involves C-N bond cleavage.

References

1. Frank-Kameneskii, D. A., *Diffusion and Heat Transfer in Chemical Kinetics*, Plenum Press, N.Y., N.Y., 1969.

2. Rogers, R.N., Janney, J.L., and Loverro, N.P., *J. Ener. Mat.*, *2*, (1984) 293.

3. McKenney, R.L., Fryling, J.A., Neveu M. C. and Meyer, P.D., "The Chemistry and Preliminary Kinetics of the Thermal Decomposition of 1,4-Butanediammonium Dinitrate." *Minutes of JTCG/WPE meeting*, 1985.

1986 USAF-UES Summer Faculty Research Program/

Graduate Student Summer Support Program

Sponsored by the

Air Force Office of Scientific Research

Conducted by the

Universal Energy Systems, Inc.

Final Report

Polybenzimidazoles: Solubilization, Modification, and Synthesis

Prepared by:	D. Roger Moore
Academic Rank:	PhD Candidate
Department and University:	Polymer Science University of Southern Mississippi
Research Location:	Materials Laboratory, AFWAL, Wright-Patterson Air Force Base
USAF Researcher:	Dr. Robert C. Evers
Date:	September, 1986
Contract No.:	F49620-85-C-0013

Polybenzimidazoles: Solubilization, Modification, and Synthesis

by

D. Roger Moore

Abstract

Rigid rod polybenzimidazoles (PBIs) were solubilized in non-polar aprotic solvents using a strong base proton abstraction technique previously found to be effective for poly(p-phenyleneterephthalamide). The soluble PBI anion could be grafted with acrylamide to form PBI-g-Nylon 3 copolymers which also showed improved solubility over unmodified PBIs. The synthesis of N-phenyl substituted PBIs using orthoester monomers and active ester solvent systems was found to be uneffective. High purity hexamethyl-orthoterephthalate could be produced by sublimation of crude material, which was heretofore not reported in the literature. This monomer could prove useful in synthesizing other types of PBI polymers.

Acknowledgements

I would like to thank the Air Force Systems Command and the Air Force Office of Scientific Research for their sponsorship of this research. I would like to thank the members of the staff of the Materials Laboratory for their help and guidance in my research, specifically Drs. Bob Evers, Ted Helminiak, and particularly Prof. Thuy Dang, my labmate, who was most helpful in equipment and material procurement, in the design and execution of my experiments, and in providing excellent Vietnamese cuisine.

I. Introduction

In my dissertation research at the University of Southern Mississippi, we have been involved with studying the behavior of rigid chain aromatic polyamide polymers combined with flexible coil matrix polymers to produce a new kind of composite material known as the molecular composite. This concept was originated at the AFWAL/MLPB, and I wished to gain background in these materials to enhance my understanding of this new concept.

The MLPB has been in the business of producing rigid rod aromatic heterocyclic polymers for some thirty years. Techniques which yield high molecular weight polymers of this type have been developed for polybenzthiazole and polybenzoxazole polymers but not polybenzimidazoles (PBIs). The MLPB is also interested in obtaining polymers of the rigid rod variety with improved solubility in non-polar aprotic solvents. To this end, they have been re-studying the syntheis of PBIs in hopes of obtaining more soluble polymers.

My work then, was to investigate new synthesis and solubilization techniques for PBIs.

II. Objectives of the Research Effort

The overall objective of the MLPB is the production of new polymers which have high modulus and strength, environmental resistance, and are able to be used as primary components for aircraft part fabrication. Polymers of this type with less stringent processing constraints than those currently available are of major interest.

The objectives of this research were:

1. Investigate the solubilization of rigid rod PBIs in polar aprotic solvents using strong base abstraction techniques to produce the polyanion.

2. Study the anionically initiated grafting reaction of the soluble PBI polyanion with acrylamide to produce PBI-g-Nylon 3 and measure the properties of the resulting copolymers.

3. Prepare bisorthoesters, specifically hexamethyl-orthoterephthalate (HMOT) in >99.5% purity to be used as a monomer in synthesizing N-phenyl substituted PBIs.

4. Investigate the use of a triphenylphosphine /pyridine/hexachloroethane activating solvent system in the preparation of PBIs from terephthalic acid and N,N-diphenyl substituted tetraamines.

III. PBI Solubilization

In 1964, Marvel reported the use of a sodium hydride/dimethyl sulfoxide (DMSO) activation/solvent system to prepare the polyanion of poly-2,2'-(m-phenylene)-5,5'-bibenzimidazole.[1] This polymer has limited solubility in DMSO in its normal protonated form, so the system was designed to produce activated PBIs which could be reacted with halogenated derivatives to give N-substituted PBIs. Marvel produced methyl and carboxymethyl PBIs by reacting the polyanion with methyl iodide and methyl chloroformate, respectively.

In 1981, Takayanagi reported the use of a similar sodium hydride/DMSO solvent system for the dissolution of poly-(p-phenyleneterephthalamide) (PPTA).[2] PPTA is inherently

insoluble in all solvents except for concentrated sulfuric acid, so this technique represented a method for preparing a soluble polyanion from an initially insoluble polymer. Takayanagi also reported nuclephilic substitution[2] and grafting[3] reactions using the PPTA polyanion as the substrate.

The procedure of Takayanagi was used to solubilize PBIs of the rigid rod type. This process is shown below in Figure 1.

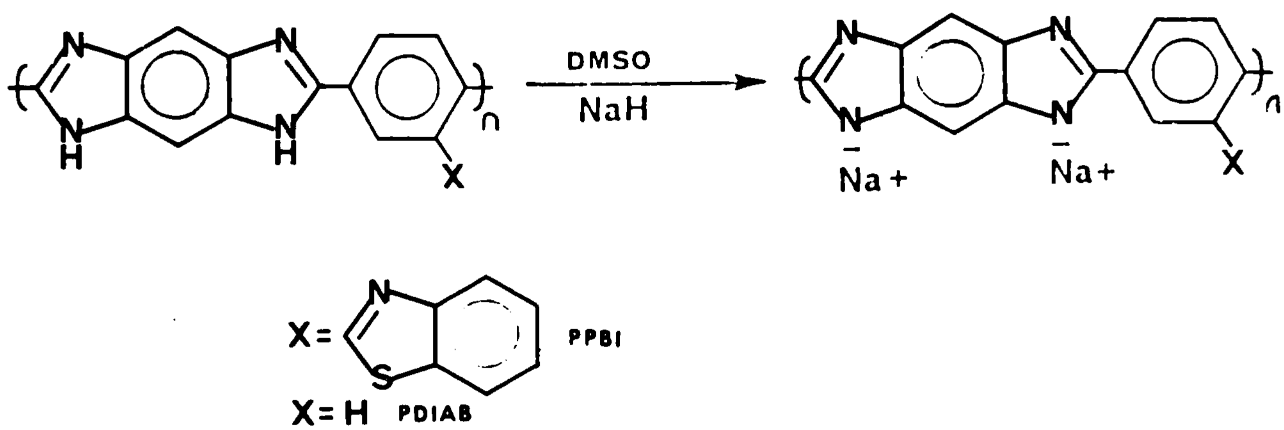

Figure 1. Reaction Scheme for Solubilizing PBI in DMSO/Sodium Hydride

The first step of the process involves the production of methyl sulfinyl carbanion from the reaction of DMSO with sodium hydride. This methyl sulfinyl carbanion is soluble in DMSO and acts as the base in the proton abstraction reaction.

Four PBIs were tested for solubilization in this solvent system. Of the four, only the polymer with the pendant

benzthiazole moiety (PPBI) was found to dissolve. This polymer showed immediate reaction with the solvent and would eventually dissolve completely after several hours of reaction at $40^{\circ}C$. The other three polymers, all containing mostly para oriented polybenzimidazo linkages, exhibited poor interaction with the solvent and showed no tendency to dissolve. It should be pointed out that these polymers were approximately fifteen to twenty years old and had experienced a variety of treatments prior to these dissolution studies. The PPBI polymers were of more recent vintage, and the polymer used for the majority of these studies was prepared fresh. It is well-known that PBIs have a tendency to absorb moisture which is difficult to completely remove by vacuum drying. It is possible that the older samples contained significant levels of water which may have reacted with the methyl sulfinyl carbanion, resulting in neutralization of the base.

In addition to dissolution in DMSO, the use of cosolvents was briefly investigated. The solvent combination of dimethylacetamide (DMAc) combined with lithium chloride (LiCl) has been extensively investigated as a solvent for difficult to dissolve polymers such as cellulose and its derivatives and aromatic and aliphatic polyamides. It was found that the PPBI anion solutions could tolerate the addition of significant amounts of this solvent, which appeared to help solubilize one high molecular weight sample which initially exhibited incomplete dissolution in 100% DMSO. It was also found that mixing a solution of

DMSO/methyl sulfinyl carbanion with DMAc/LiCl resulted in the formation of an insoluble precipitate whose identity was not investigated. The use of 18-crown-6 as a possible activator for the base was also investigated for the solubilization of the para oriented polybenzimidazoles, but was found to be ineffective.

IV. Polybenzimidazole Modification

Following reports of the grafting of PPTA by Takayanagi, Moore and Mathias reported the use of similar chemistry to prepare molecular composites by an in situ polymerization process which utilized the PPTA anion as both the initiator and reinforcing component.[4] This process involved the anionic polymerization of acrylamide to form Nylon 3. The polymerization reaction resulted in the formation of both graft and homopolymer Nylon 3. It was therefore of interest to determine if this type of chemistry could be used with the PPBI anion to produce PPBI-g-Nylon 3.

The reaction of acrylamide with PPBI anion was carried out with three different mole ratios of monomer/polymer. As was the case with PPTA anion/acrylamide polymerization, heating the initially homogeneous solutions to the polymerization temperature of 110-115°C resulted in the solutions becoming viscous and ultimately precipitating as the Nylon 3 was formed. The results of these polymerizations are given below in Table I.

Table I. PPBI Anion-Nylon 3 Polymerization Results

Monomer Compositon wt/wt Acrylamide/PPBI mole/mole	91.7/9.3 50/1	91.7/9.3 50/1	82.93/17.07 25/1	59.7/40.3 7.6/1
Solvent	50/50 DMSO DMAc-LiCl	DMSO	DMSO	DMSO
% Yield	46.7	64.9	64.2	65.0
% Conversion of Acrylamide	41.2	61.3	56.8	41.3
Polymer Composition wt/wt Nylon 3/PPBI	80/20	85.6/14.4	73.4/26.6	37.9/62.1
Polymer Solubility				
97% Formic Acid	+	+	+	+
DMAc-LiCl	±	NT	NT	NT
Specific Viscosity (0.5 g/dl in 97% Formic Acid)	0.506	0.404	0.665	2.45

One interesting result of these polymerizations is the improved solubility of the graft copolymers as compared to PPTA/Nylon 3 graft copolymers. PPTA/Nylon 3 graft copolymers were insoluble in Nylon 3 solvents such as 98% formic acid, trifluoroethanol, hexafluoroisopropanol, and DMAc/LiCl. PPBI/Nylon 3 graft copolymers were soluble in 97% formic acid and DMAc/LiCl, which were the only Nylon 3 solvents available for testing. Unfortunately, this does not allow the Nylon 3 homopolymer to be easily separated from the graft copolymer, which makes it impossible to determine the true composition of the graft copolymers. Figure 2 shows an FTIR spectrum of a thin film cast from formic acid solution of the 80/20 Nylon 3/PPBI copolymer together with a spectrum of a thin film PPBI homopolymer which was cast from DMSO solution.

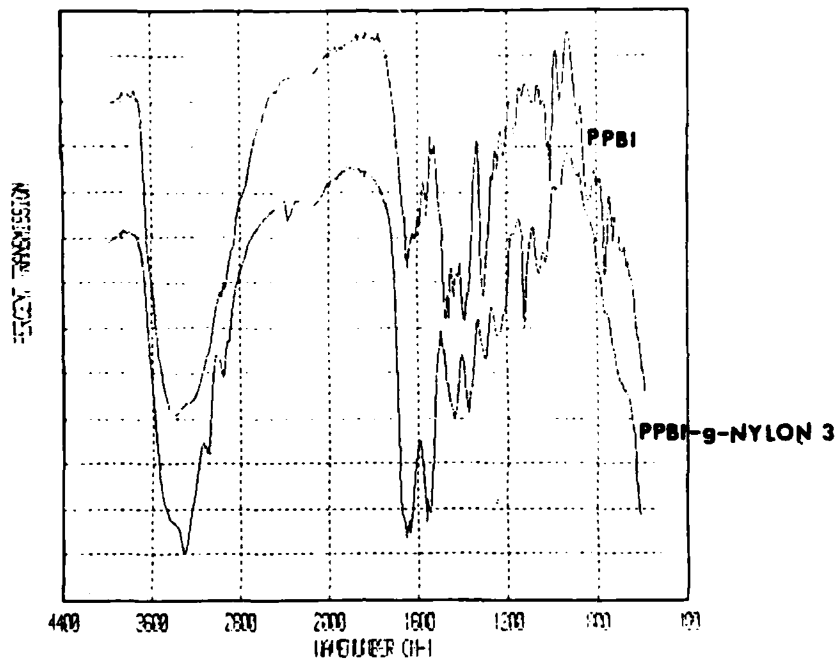

Figure 2. FTIR Spectra of PPBI and PPBI-g-Nylon 3.

The graft copolymer spectrum shows structural bands due to Nylon 3 at 3300, 2950-2900, 1675, and 1580 cm^{-1} which are due to N-H, C-H, C-O, and N-C-O, respectively. These spectra also show the overlap of the PPBI main structural bands at 3400 and 1675 cm^{-1} with the Nylon 3 bands, which makes quantitation of the copolymer composition by FTIR spectroscopy impossible.

V. <u>HMOT Synthesis and Attempted Polymerization</u>

In 1978, Vogl reported the synthesis of PBIs by the direct condensation of bisorthoesters with tetraamines.[5] This reaction was carried out in a DMSO/pyridine solvent combination, and high yields of moderate molecular weight polymers were obtained. It was theorized that N-phenyl PBIs could be made by this type of process which would have

improved solubility in non-polar aprotic solvents and would exhibit high molecular weights.

HMOT was synthesized from hexachloro-p-xylene and sodium methoxide in methanol following the procedure of Vogl.[6] Following recrystallization from hexanes, this monomer was found to be 98.5% pure by GC analysis. Vogl reported that the hexapropylorthoterephthalate derivative could be prepared by molecular sieve mediated ester exchange of HMOT with propanol, and this derivative could be distilled to obtain monomer with >99.5% purity. The attempted synthesis of this derivative from HMOT resulted in the production of a high melting compound which appeared to be a partially exchanged product. This was probably due to the use of extremely old molecular seives in the exchange reaction, whose efficency had been used up in storage. It was found that the HMOT could be easily sublimed at temperatures of 125-130^{o}C and vacuum of 0.5-0.1 mm Hg. Two sublimations gave material with purity of 99.3% by GC.

Polymerization of HMOT with 1,3-dianilino-4,6-diaminobenzene was carried out at using the standard procedure of Vogl. The solution failed to become viscous after 18 hours of reaction, and took on a very dark brown color. Precipitation of the solution in excess methanol was unsucsseful, and the solution was finally precipitated into a large excess of water. The precipitate was identified by FTIR as the starting tetraamine. No evidence of polymer was found from this reaction. As noted by Vogl, the use of 1,2,4,5-tetraaminobenzene in reaction with bisorthoesters

resulted in low yields of very low viscosity (0.08 dl/g) polymers. Tetraaminobenzene type monomers have a long history of poor reactivity in PBI polymerizations, and the use of N,N-diphenyl substitution would be expected to reduce the reactivity even further. The problem with this polymerization would therefore seem to lie in the amine monomer and not in the HMOT or the process itself.

VI. Synthesis of PBIs by Reaction in Activating Media

Since the discovery that high strength, high modulus fibers can be produced from para-catenated aromatic polyamides, a great deal of work has gone into exploring new procedures to prepare high molecular weight polymers of this type. One such process has been reported by Ogata, who utilized an activating solvent system composed of triphenylphosphine/pyridine/hexachloroethane to make poly(p-benzamide) with viscosites as high as 3.5 dl/g.[7] Ahmed and Mathias utilized this same chemistry to make hydroxy substituted polyamides which were then thermally cyclized to produce polybenzoxazoles.[8] It was theorized that 1,3-dianilino-4,6-diaminobenzene could be utilized in similar fashion to prepare amino substituted polyamides which could then be cyclized to produce PBIs.

Several attempts were made to react terephthalic acid and 1,3-dianilino-4,6-diaminobenzene in the activating solvent system to prepare polymers. It was found that mixing the diacid with the tetraamine in pyridine solution produced an instantaneous change from the initially clear solution to a green-purple colored solution from which a precipitate

gradually separated on stirring. Various ingredient mixing orders and temperatures failed to alter this tendency. The precipitate could be isolated by stirring the reaction mixture into water followed by filtration, and the precipitate was found to be soluble in organic solvents such as methanol and acetone, which indicated that it was non-polymeric. Spectroscopic studies were inconclusive as to determing the nature of the material.

VI. Recommendations

The solubilization of PPBIs in polar aprotic solvents should continue to be investigated, especially with high molecular weight polymers. Other copolymers of PPBI units with PBO or PBT units should also be investigated to determine the limits of this solubilization procedure.

Reactions of the PPBI anion with halo derivatives and monomers capable of anionic polymerization should be explored as a method for producing soluble rigid rod type polymers.

The use of HMOT as a monomer with other possibly more reactive tetraamines should be explored as a method for preparing soluble PBIs

Activating solvent systems represent a totally new and wide-open area for research into preparing aromatic heterocyclic polymers. This type of research should be contintued on an exploratory basis to determine if it is possible to make these polymers in solvents other than polyphosphoric acid.

VII. Experimental

Materials

DMSO was distilled twice over calcium hydride and stored in a tightly sealed jar. Sodium hydride was used as a 60% dispersion in oil (Aldrich). Acrylamide was electrophoresis grade (99+%) from Aldrich and was used as received. 2-benzothiazole terephthalic acid was recrystallized from acetic acid and vacuum dried. 1,2,4,5-tetraaminobenzene tetrahydrochloride was recrystallized from water/HCl and vacuum dried. Polyphosphoric acid was prepared by reacting commercial 85% phosphoric acid with P_2O_5 (Baker). All other solvents and reagents were used as received from commercial sources.

Synthesis of Pendant Polybenzimidazole

A 100 ml resin kettle equipped with a mechanical stirrer, nitrogen inlet, and vacuum outlet was charged with 4.2845 grams of 1,2,4,5 tetraaminobenzene, 4.5147 grams of 2-benzothiazole terephthalic acid, and 8.34 grams of 77% polyphosphoric acid. The mixture was heated with nitrogen purge under vacuum to $80^{o}C$ for three hours, and then heated to $100^{0}C$ for 16 hours. After the addition of 10.1 grams of P_2O_5 to come to 83% polyphosphoric acid, the dark-colored mixture was heated to $175^{o}C$, during which time stir opalesecence became evident. After 24 hours at $175^{o}C$, the reaction was heated to $190-195^{o}C$ for 6 hours, then cooled and poured into water. The polymer was washed several times with water and placed in a blender and stirred with water until it was completely broken up. The polymer was then washed with dilute ammonium hydroxide, filtered, extracted in a soxhlet with water for 48 hours, and dried in vacuo at $100^{o}C$ in a

drying pistol for 24 hours. The relative viscosity determined at 0.2 g/dl concentration was 1.27 dl/g.

Polymer Dissolution

A 250 ml three-necked round-bottom flask equipped with a mechanical stirrer, thermometer, and nitrogen inlet and outlet was charged with 50 grams of DMSO. The DMSO was stirred under nitrogen for 30 minutes, after which time 0.22 grams of sodium hydride was added. The solution was heated to 75^{o}C for a period of one hour, during which time the sodium hydride dissolved and the solution took on a greenish tint. The solution was then cooled to 40^{o}C, and 1.00 grams of PPBI added. The solution was stirred for 16 hours at 40^{o}C, and became homogeneous during this period. The solution was heated to 60^{o}C for 2 hours to insure complete solubilization. The cooled solution was poured into 800 ml of a dilute hydrochloric acid solution in water, and the polymer collected and dried. The polymer exhibited a relative viscosity of 1.21 dl/g in methanesulfonic acid solution.

Graft Polymerization of PPBI with Acrylamide

A 250 ml three-necked round-bottom flask equipped with a mechanical stirrer, thermometer, and nitrogen inlet and outlet was charged with 25 grams of PPBI solution in DMSO, 4.86 grams of acrylamide, and 25 grams of DMSO. The flask was placed in a constant temperature bath at 115^{o}C for a period of 16 hours, during which time the solution became hazy and finally precipitated the polymer. The cooled solution was poured into 1000 ml of water and allowed to stir

until all the polymer was broken up into a fine suspension. The polymer was filtered and washed with several aliquots of acetone. The polymer was carefully collected and dried in vacuo for 24 hours. Yield was 3.48 grams, 64.9% of theoretical. The conversion and the polymer composition were calculated as follows:

$$\% \text{ Conversion} = \frac{\text{Yield Wt} - \text{Starting Wt PPBI}}{\text{Starting Wt Acrylamide}}$$

$$\text{Wt \% PPBI} = \frac{\text{Starting Wt PPBI}}{\text{Yield Wt}}$$

References

1. Marvel, C. S., ML-TDR 64-39 pp 36-40 (1964).

2. Takayanagi, M. and Katayose, T., J. Poly. Sci., Poly. Chem. Ed., 19, (1983) 1133-1145

3. Takayanagi, M. and Katayose, T., J. Poly. Sci., Poly. Chem. Ed., 21, (1983) 31-39.

4. Moore, D. R. and Mathias, L. J., J. Appl. Poly. Sci., in press.

5. Dudgeon, C. D. and Vogl, O., J. Poly. Sci., Poly. Chem. Ed., 16, (1978) 1815-1830.

6. Dudgeon, C. D. and Vogl, O., J. Poly. Sci., Poly. Chem. Ed., 16, (1978) 1831-1852.

7. G-C. Wu, H. Tanaka, K. Sanui, and N. Ogata, J. Poly. Sci., Poly. Lett. Ed., 19, (1981) 343-346.

8. Mathias, L. J., Ahmed, S. U., and Livant, P. D., Macromolecules, 18, (1985) 616-622.

1986 USAF-UES SUMMER FACULTY RESEARCH /
GRADUATE STUDENT SUMMER SUPPORT PROGRAM

Sponsored by the

AIR FORCE OFFICE OF SCIENTIFIC RESEARCH

Conducted by the

UNIVERSAL ENERGY SYSTEMS , INC.

FINAL REPORT

MBTI PSYCHOMETRIC STUDY OF UNITED STATES AIR FORCE AIRCREW PERSONNEL

Prepared by	:	John Yolman Salinas Eric V. Morris Moussa Pierre Tamer
Academic Rank	:	M.D. Students
Department and University	:	Meharry Medical College School of Medicine
Research Location	:	Department of NeuroPsychiatry School of Aerospace Medicine Brookes Air Force Base
USAF Research	:	Dr. Timothy Strongin
Date	:	August 18th , 1986
Contract No.	:	F49620-85-C-0013

MBTI Psychometric Study of United States
Air Force Aircrew Personnel

Eric V. Morris

ABSTRACT

A retrospective study of MBTI scores of thirty-four aircrewmen from Air Force files were analyzed and integrated to yield information of personality structure and patterns among the group. Comparisons with other sample populations were made, as well as with a previous study from the School of Aerospace Medicine.

ACKNOWLEDGEMENTS

The writers would like to thank the Department of Neuropsychiatry in the School of Aerospace Medicine for their valuable support , assistance , and guidance throughout this project. It was a pleasure to be able to contribute to this ongoing study.

We would also like to acnowledge our appreciation to Dr. Timothy Strongin , Capt. , for his generous guidance and indispensible collaboration in allowing us to contribute with this project.

The writers would also like to acknowledge our appreciation to Dr. Bryce Hartman , Dr. D.R. Jones , and Dr. J.C. Patterson for their valuable presence and feedback during our stay at the School of Aerospace Medicine.

Thanks are also due to Air Force personnel Gary Schofield , Skip Holden , Janet Ross , and Tom Eckhoff for their assistance with all the details.

We would like to acnowledge sponsorship of the Air Force Systems Command , Air Force Office of Scientific Research , and the Schoool of Aerospace Medicine who made all this possible.

OBJECTIVES OF THE RESEARCH

U.S Air Force Aircrew members are a unique population. The present research describes personality traits in an elaboration and update of work initiated by Fine and Hartman (1967). Specifically MBTI scores were analyzed from samples of Air Force Pilots, Navigators, and finalists for MSE (space shuttle) duties . Parametric statistics were applied to a retrospective analysis of these MBTI (Myers Brigg Type Inventory) scores obtained from Air Force Aircrew members. This study will explore the possible existence of a type model as established by Fine and Hartman for this population with regards to the MBTI. It is hoped that these findings will contribute to an empirical understanding of psychometric norms or patterns which might be useful in balanced clinical evaluations and organizational consultations regarding Air Force Aircrew members.

INTRODUCTION

The MBTI (Myers-Briggs Type Indicator) is a test that uses the concept of psychological types, described by C.G. Jung (1921), and attempts to specify random variation in behavior as actually being quite orderly and consistent, being due to basic differences in the way individuals prefer to use their perception and judgement. It is a self-report inventory developed to measure personality preferences. The merit of the theory underlying the MBTI is that it enables us to expect specific differences in specific people and to use this information to more constructively understand human behavior. Specifically in this instance, the theory of the MBTI is to be implemented and tested on U.S. Air Force flyers to possibly delineate them as being a unique population. Their unique responses on standard personality tests as revealed by Fine and Hartman (1967) will be further tested with regards to the MBTI, which was not previously examined in the original battery of tests.

Military pilots represent a specific segment of of modern American society. They have enough personality characteristics in common to justify model analysis. It was found that there is a personality pattern common to successful professional flyers, with strengths and weaknesses so balanced that they adapted well to their particular lifestyle. In particular , emotional life, coping skills, current life adjustment, personal information, physical findings, career, and childhood were found to bias the personality types most common among the group, as stated by Hartman. The study allowed construction of a model personality picture since results were both reliable and internally consistent. What deviance existed, particularly on the projective tests, was discussed as a trend in personality balance. For the most part , however, these men had a personality pattern in common. The typical personality is characterized by an alloplastic approach to the world, matter of fact, terse direct ways of coping, strong needs for personal achievement, and high regard for responsibilities and family life. This conceptualization was arrived through formulation established by White and his theories regarding motivation as applied by Hartman.

The typical personality pattern described by Hartman suits these men to adapt to military flying insomuch as the pilots seemed to fit a Piagin model, a continuous series of assimilation-accomodation transactions with the environment in which previous experiences structure the individual's relationship to and incorporation of a new experience. Furthermore, flying is consistent with these men's typical identification with a lower middle class blue collar worker father and with a background emphasis on orderliness, respect, sports, and health as was also discovered by Hartman. With this general personality pattern that was described by Hartman , it was the intention of this research project to incorporate and evaluate the use of the Myers-Briggs Type Indicator to further understand the military flyer's typical , common personality traits , and adaptations which can hopefully be applied by psychiatrists toward evaluation of individual prognosis, management, and suitability for special tasks . In support of this goal, it was found that psychiatric problems of pilots seen at aerospace referral centers were consistent with the modal pattern described by Hartman.

The value of implementing the Myers-Briggs Type Indicator is in its particular efficiency as a potential

screening tool. Also it offers a new method to analyze personality patterns with a basic underlying theory that stresses dichotomies. The MBTI contains four separate dichotomous indices - extroversion/introversion , sensing/intuition , thinking/feeling , judgement/perception . As stated , each index reflects one of four basic preferences which under Jung's theory , direct the use of perception and judgement. The preferences affect what people attend to and also how they draw conclusions about what they perceive. By design, each of the four indices expresses one dominant pole , so that the four indices yield sixteen possible combinations called personality types. The intent of the theory is to reflect a habitual choice between rival alternatives within each index. Each type , therefore, is a reflection of an acquired personality pattern with its unique approaches to handling the environment. The MBTI is concerned with individual differences in basic functions and attitudes. It is this quality that proves useful in such areas as career guidance and counseling where use of a preferred mode of perception and judgement can provide valuable information to the type of functioning of an individual. The MBTI , therefore can provide information about individuals and about trends within individuals in certain professions where specific modes of functioning are preferred. Studies have been

performed crossexamining such unique patterns within as well as between certain professions.

With regards to Air Force Aircrew members, it was found that not only were certain personality patterns more common but that there were certain similarities and differences between other professions which further helped to define and compare the model proposed by Hartman. Specifically comparisons were made with models described by Korchin and Ruff of Mercury astronauts as discussed by Hartman. On a more general basis, studies using the MBTI have indicated a difference between the personality type interactions of scales of those samples versus this study. Such studies include those by Thomas , Hicks, and Kerin and Slocum. which will be presented later. The value of the MBTI in allowing psychometric analysis of the various type indices for interaction permits cross-comparison between similar studies of other sample populations.

CHARACTERISTICS FREQUENTLY ASSOCIATED WITH EACH TYPE

		SENSING TYPES: WITH THINKING	SENSING TYPES: WITH FEELING	INTUITIVES: WITH FEELING	INTUITIVES: WITH THINKING
INTROVERTS	JUDGING	**ISTJ** Serious, quiet, earn success by concentration and thoroughness. Practical, orderly, matter-of-fact, logical, realistic, and dependable. See to it that everything is well organized. Take responsibility. Make up their own minds as to what should be accomplished and work toward it steadily, regardless of protests or distractions. Live their outer life more with thinking, inner more with sensing.	**ISFJ** Quiet, friendly, responsible and conscientious. Work devotedly to meet their obligations. Lend stability to any project or group. Thorough, painstaking, accurate. May need time to master technical subjects, as their interests are not often technical. Patient with detail and routine. Loyal, considerate, concerned with how other people feel. Live their outer life more with feeling, inner more with sensing.	**INFJ** Succeed by perseverance, originality and desire to do whatever is needed or wanted. Put their best efforts into their work. Quietly forceful, conscientious, concerned for others. Respected for their firm principles. Likely to be honored and followed for their clear convictions as to how best to serve the common good. Live their outer life more with feeling, inner more with intuition.	**INTJ** Have original minds and great drive which they use only for their own purposes. In fields that appeal to them they have a fine power to organize a job and carry it through with or without help. Skeptical, critical, independent, determined, often stubborn. Must learn to yield less important points in order to win the most important. Live their outer life more with thinking, inner more with intuition.
INTROVERTS	PERCEPTIVE	**ISTP** Cool onlookers, quiet, reserved, observing and analyzing life with detached curiosity and unexpected flashes of original humor. Usually interested in impersonal principles, cause and effect, or how and why mechanical things work. Exert themselves no more than they think necessary, because any waste of energy would be inefficient. Live their outer life more with sensing, inner more with thinking.	**ISFP** Retiring, quietly friendly, sensitive, modest about their abilities. Shun disagreements, do not force their opinions or values on others. Usually do not care to lead but are often loyal followers. May be rather relaxed about assignments or getting things done, because they enjoy the present moment and do not want to spoil it by undue haste or exertion. Live their outer life more with sensing, inner more with feeling.	**INFP** Full of enthusiasms and loyalties, but seldom talk of these until they know you well. Care about learning, ideas, language, and independent projects of their own. Apt to be on yearbook staff, perhaps as editor. Tend to undertake too much, then somehow get it done. Friendly, but often too absorbed in what they are doing to be sociable or notice much. Live their outer life more with intuition, inner more with feeling.	**INTP** Quiet, reserved, impersonal. Enjoy especially theoretical or scientific subjects. Logical to the point of hair splitting. Interested mainly in ideas, with little liking for parties or small talk. Tend to have very sharply defined interests. Need to choose careers where some strong interest of theirs can be used and useful. Live their outer life more with intuition, inner more with thinking.
EXTRAVERTS	PERCEPTIVE	**ESTP** Matter of fact, do not worry or hurry, enjoy whatever comes along. Tend to like mechanical things and sports, with friends on the side. May be a bit blunt or insensitive. Adaptable, tolerant, generally conservative in values. Dislike long explanations. Are best with real things that can be worked, handled, taken apart or put back together. Live their outer life more with sensing, inner more with thinking.	**ESFP** Outgoing, easygoing, accepting, friendly, fond of a good time. Like sports and making things. Know what's going on and join in eagerly. Find remembering facts easier than mastering theories. Are best in situations that need sound common sense and practical ability with people as well as with things. Live their outer life more with sensing, inner more with feeling.	**ENFP** Warmly enthusiastic, high-spirited, ingenious, imaginative. Able to do almost anything that interests them. Quick with a solution for any difficulty and ready to help anyone with a problem. Often rely on their ability to improvise instead of preparing in advance. Can always find compelling reasons for whatever they want. Live their outer life more with intuition, inner more with feeling.	**ENTP** Quick, ingenious, good at many things. Stimulating company, alert and outspoken, argue for fun on either side of a question. Resourceful in solving new and challenging problems, but may neglect routine assignments. Turn to one new interest after another. Can always find logical reasons for whatever they want. Live their outer life more with intuition, inner more with thinking.
EXTRAVERTS	JUDGING	**ESTJ** Practical realists, matter of fact, with a natural head for business or mechanics. Not interested in subjects they see no use for, but can apply themselves when necessary. Like to organize and run activities. Tend to run things well, especially if they remember to consider other people's feelings and points of view when making their decisions. Live their outer life more with thinking, inner more with sensing.	**ESFJ** Warm hearted, talkative, popular, conscientious, born cooperators, active committee members. Always doing something nice for someone. Work best with plenty of encouragement and praise. Little interest in abstract thinking or technical subjects. Main interest is in things that directly and visibly affect people's lives. Live their outer life more with feeling, inner more with sensing.	**ENFJ** Responsive and responsible. Feel real concern for what others think and want, and try to handle things with due regard for other people's feelings. Can present a proposal or lead a group discussion with ease and tact. Sociable, popular, sympathetic. Responsive to praise and criticism. Live their outer life more with feeling, inner more with intuition.	**ENTJ** Hearty, frank, decisive, leaders in activities. Usually good in anything that requires reasoning and intelligent talk, such as public speaking. Are well informed and keep adding to their fund of knowledge. May sometimes be more positive and confident than their experience in an area warrants. Live their outer life more with thinking, inner more with intuition.

METHODS

A retrospective analysis of Myers-Briggs Type Inventory scores for 34 Aircrew personnel will be performed from information derived from United States Air Force files. The data will be graphically analyzed in this study. Parametric statistical studies will be performed in an upcoming study. The study was conducted at the USAF School of Aerospace Medicine, a consultation service for Air Force operations. The 34 Aircrew members selected for this study represent a cross-section of Air Force flying officers. These men were in residence at the school when the test was administered. A tabulation of their MBTI scores and status is shown below in figure one. The sample included 33 male and one female ranging in age from 20 - 41. Their Air Personnel position varied from MSE (Manned Space Engineer) to Pilot to Navigator.

The study being reported here was designed to explore the hypothesis of whether a specific personality type pattern predominated with regards to the MBTI , and whether specific interactions among the various scales were apparent for comparison with other studies of different populations.

[illegible]	[illegible]	PERSONALITY TYPE (1)	AIR PER. POS. (2)	ALIST 08	ALIST1 08	TRAITS (3)	AGE	SEX (4)	STATUS (5)	RACE (6)
[illegible]	[illegible]	1000	11	030070	107109	030140	25	1	1	0
[illegible]	[illegible]	0000	10	107109	107109	107109	25	1	0	1
[illegible]	[illegible]	1101	10	107109	107109	107109	31	1	0	0
[illegible]	[illegible]	0110	10	030000	106110	107109	29	1	2	0
[illegible]	[illegible]	1000	13	030700	107109	107109	23	1	0	0
[illegible]	[illegible]	1000	12	107109	107109	107109	41	1	1	0
[illegible]	[illegible]	0001	10	107109	107109	107109	39	1	1	0
[illegible]	[illegible]	0000	10	107109	107109	107109	24	1	1	0
[illegible]	[illegible]	1010	14	031600	107109	030181	25	1	0	0
[illegible]	[illegible]	0000	12	107109	107109	107109	34	1	2	0
[illegible]	[illegible]	0001	10	107109	107109	107109	24	1	0	0
[illegible]	[illegible]	1000	12	107109	107109	107109	39	1	1	0
[illegible]	[illegible]	0000	12	031600	107109	030140	39	1	1	0
[illegible]	[illegible]	0000	10	107109	107109	107109	20	1	0	0
[illegible]	[illegible]	1111	11	107109	107109	107109	32	1	1	0
[illegible]	[illegible]	1100	00	107109	107109	107109	31	1	0	0
[illegible]	[illegible]	1000	00	107109	107109	107109	29	1	1	0
[illegible]	[illegible]	0000	00	107109	107109	107109	29	1	1	0
[illegible]	[illegible]	1100	00	107109	107109	107109	28	1	0	0
[illegible]	[illegible]	0100	00	107109	107109	107109	29	1	1	0
[illegible]	[illegible]	0100	00	107109	107109	107109	30	1	0	0
[illegible]	[illegible]	0100	00	107109	107109	107109	29	1	1	0
[illegible]	[illegible]	0110	00	107109	107109	107109	27	1	1	0
[illegible]	[illegible]	0100	00	107109	107109	107109	31	1	0	0
[illegible]	[illegible]	1000	00	107109	107109	107109	31	1	1	0
[illegible]	[illegible]	1110	00	107109	107109	107109	31	1	1	0
[illegible]	[illegible]	0100	00	107109	107109	107109	30	1	1	0
[illegible]	[illegible]	0101	00	107109	107109	107109	29	1	1	0
[illegible]	[illegible]	0000	00	107109	107109	107109	31	1	1	0
[illegible]	[illegible]	0100	00	107109	107109	107109	29	1	1	0
[illegible]	[illegible]	0000	00	107109	107109	107109	31	1	1	0
[illegible]	[illegible]	1000	00	107109	107109	107109	30	1	1	0
[illegible]	[illegible]	1000	00	107109	107109	107109	25	0	0	0
[illegible]	[illegible]	0100	00	107109	107109	107109	30	1	1	0

NOTES:
(1) PERSONALITY TYPES:
E=0 I=1
S=0 N=1
T=0 F=1
J=0 P=1
EXAMPLE: 1000 = ISTJ
(2) AIR PERSONNEL POSITION
00 = N/A
10 = STUDENT PILOT
11 = INSTRUCTOR PILOT
12 = COMMANDER
13 = CO-PILOT
14 = NAVIGATOR
(3) TRAITS:
1 = NO TRAIT
0 = TRAIT
(4) SEX:
0 = FEMALE
1 = MALE
(5) MARITAL STATUS:
0 = SINGLE
1 = MARRIED
2 = DIVORCED
(6) RACE:
0 = WHITE
1 = BLACK

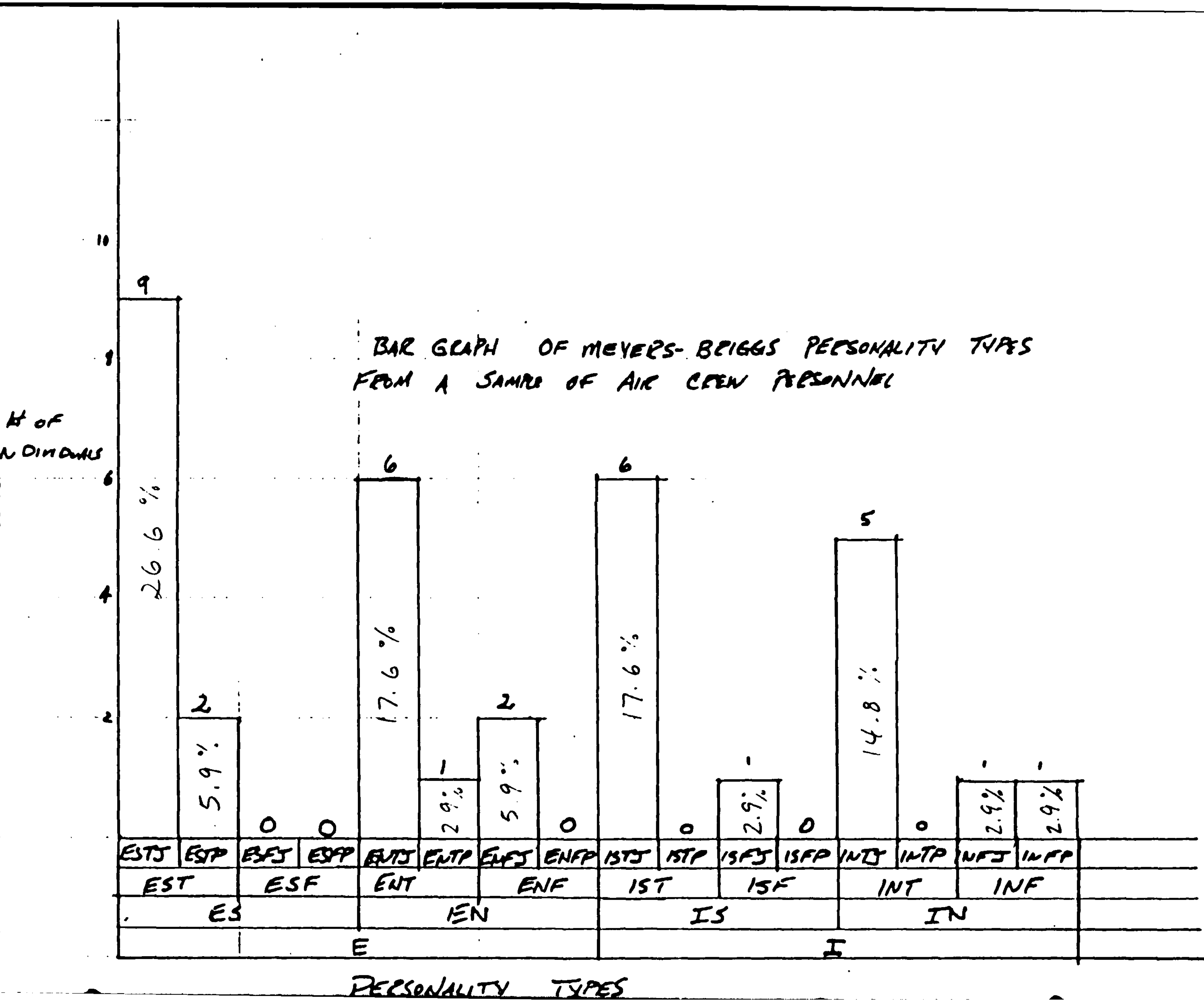

BAR GRAPH OF MEYERS-BRIGGS PERSONALITY TYPES
FROM A SAMPLE OF AIR CREW PERSONNEL
# of INDIVIDUALS
10
8
6
4
2
9
26.6 %
2
5.9 %
0
0
6
17.6 %
1
2.9 %
2
5.9 %
0
6
17.6 %
0
1
2.9 %
0
5
14.8 %
0
1
2.9 %
1
2.9 %
ESTJ ESTP ESFJ ESFP ENTJ ENTP ENFJ ENFP ISTJ ISTP ISFJ ISFP INTJ INTP INFJ INFP
EST ESF ENT ENF IST ISF INT INF
ES EN IS IN
E I
PERSONALITY TYPES

BAR GRAPH OF MEYERS-BRIGGS PERSONALITY TYPES FROM A SAMPLE OF EMPLOYEES OF A RURAL PUBLIC SCHOOL SYSTEM

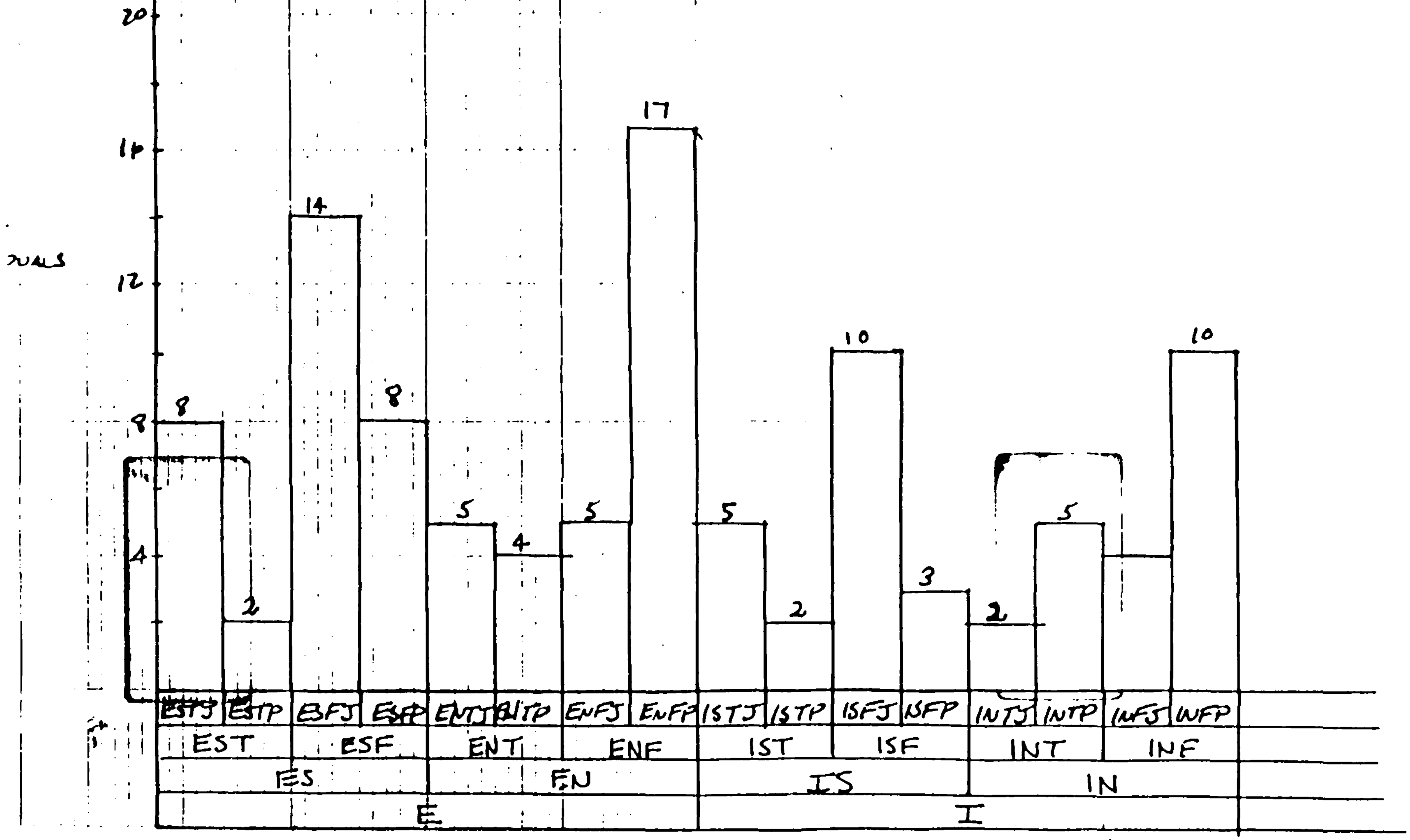

FREQUENCY GRAPH OF FLYERS

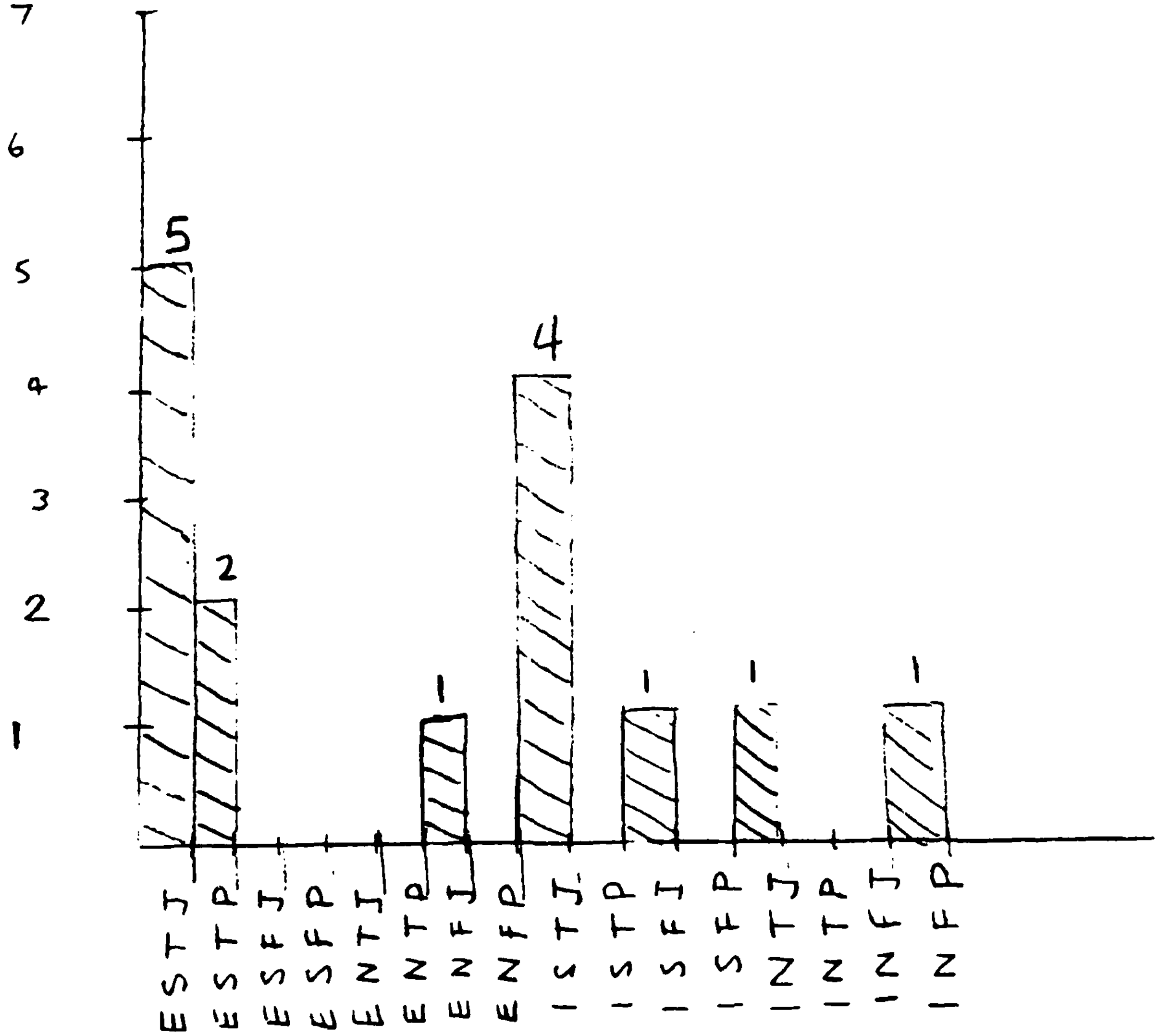

FREQUENCY GRAPH
OF
MSEs

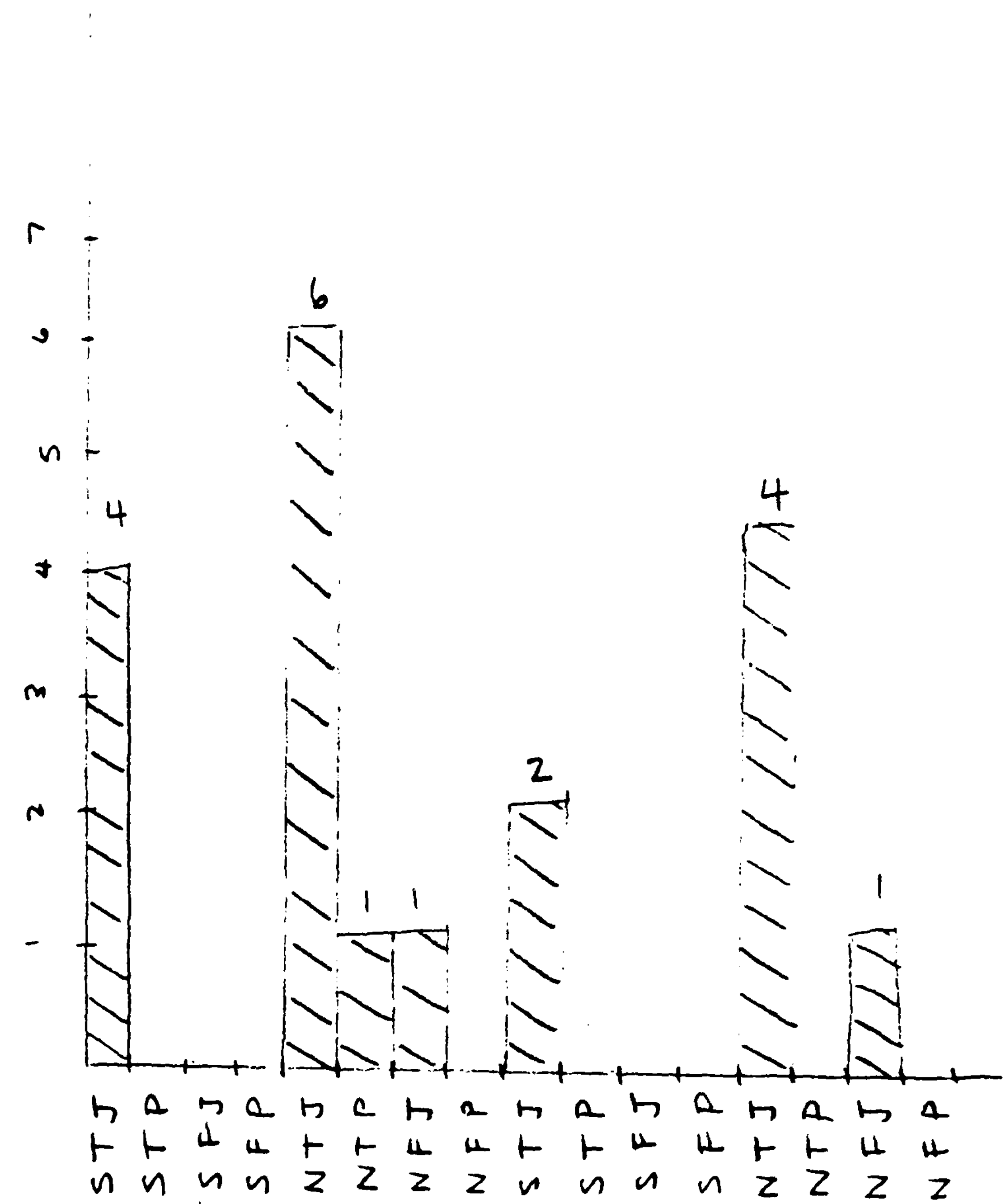

RESULTS and DISCUSSION

Upon initial collection of the data, an effort to categorize the 34 Aircrew members according to MBTI types was graphed, figure 2. This data can be further analyzed and compared. When figure 2 is compared to figure 3 , different sample's distribution,(Hicks 1984) , the raw data seems to be quite distinct with some minor overlaps. Although sample number might be significant, the data was percentage-wise quite unique in many ways lending support to the belief that different professions would tend to reflect differently with regards to the MBTI of personality.

Nevertheless, when aircrew members are analyzed as a group, they can be further broken down by position. Representation of the type breakdown for each is shown in figures 4 and 5 for MSE (Manned Space Engineers) and Flyers respectively. Even before this data is analyzed, it might be more useful and worthwhile to note that not so initially obvious, a pattern was uncovered .n figure 2. Specifically, there was an unusually large population of aircrew personnel who shared to particular scales, namely T-J , Thinking and Judgement versus Feeling and

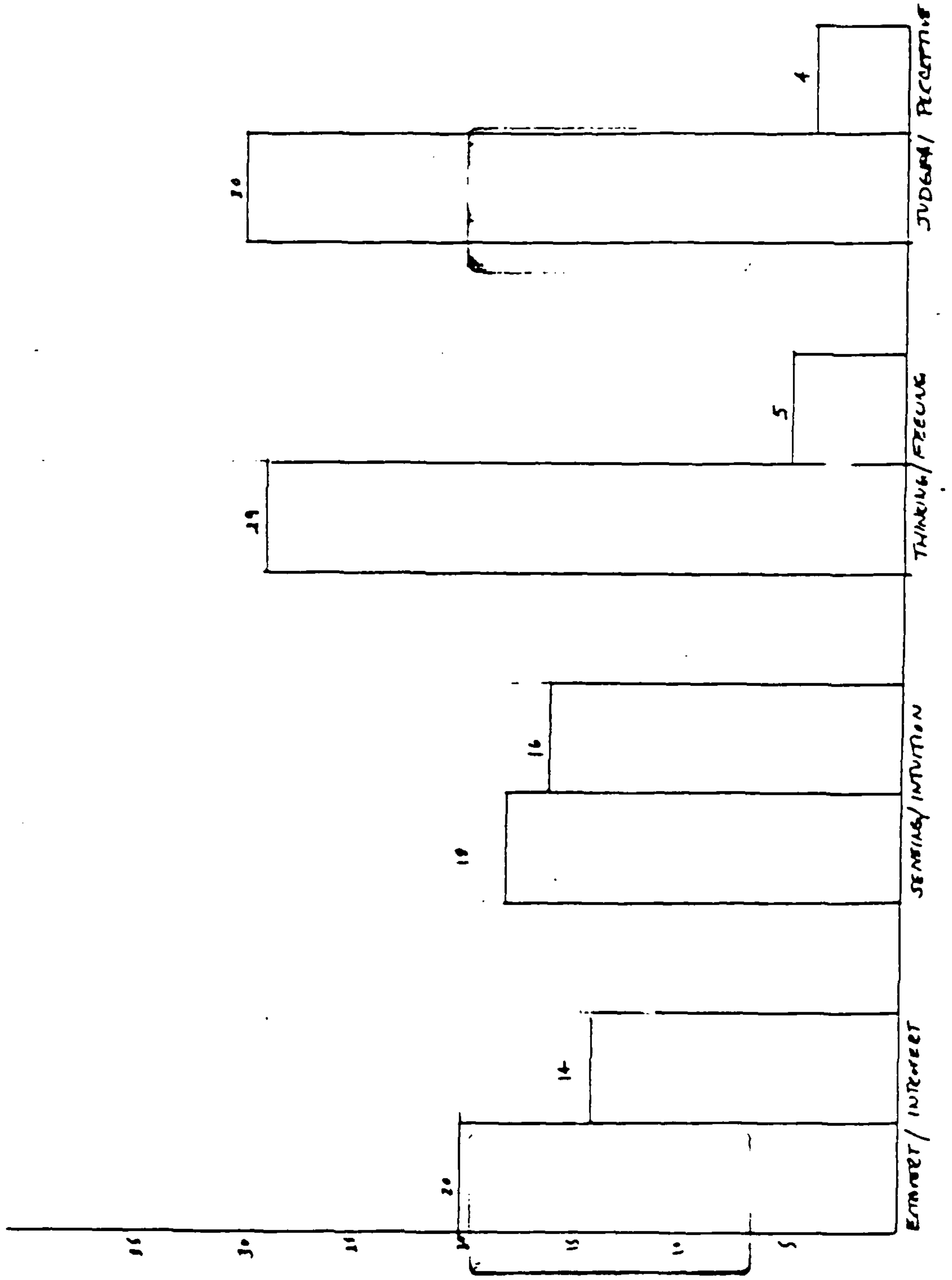

SENSING/INTUITION
THINKING/FEELING
20
14
19
16
29
5
30
4

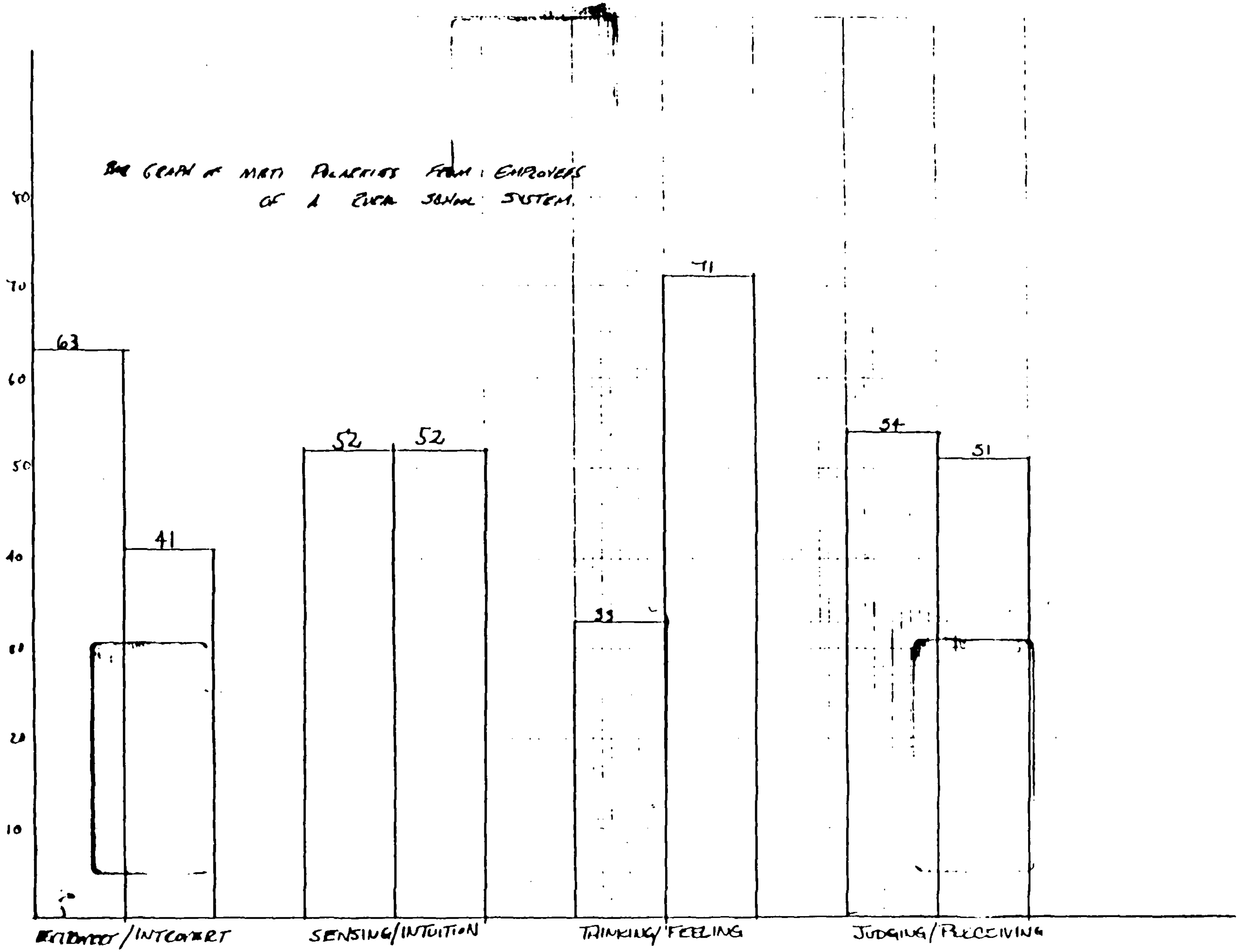
SENSING/INTUITION
THINKING/FEELING
JUDGING/PERCEIVING
63
41
52
52
71
54
51
10
40
50
60
70

Perception. Of the 34 Aircrew, 26 demonstrated this similarity 76.6%. This topic of interaction between scales was not so dramatically evident between any other two scales, something which could be statistically testable. Even after breaking this sample of Aircrew to determine whether there was some underlying factor regarding position, it was noticed that all of the ENTJ were MSEs. The MSEs also dominated the INTJ type, but the flyers retaliated by dominating the ISTJ to account for the overall predominant TJ subclass. The ESTJ nevertheless prevailed in both Flyers and MSEs.

When the data was further broken down into individual scales, to detect further patterns, figure 6 , of polar dominance among the scales, it was again apparent that the T & J , Thinking and Judgement dominated their respective scale. This was not the case in the study by Hicks , figure 7 . In this instance, the employees of a rural public school system showed completely different results with regards to the thinking/ feeling and judgement/perception scales. This again provided some distinction among the Aircrew members when compared to another profession , school administrators.

A more detailed analysis of a particular scale with regards to its score breakdown, continuous data, yielded

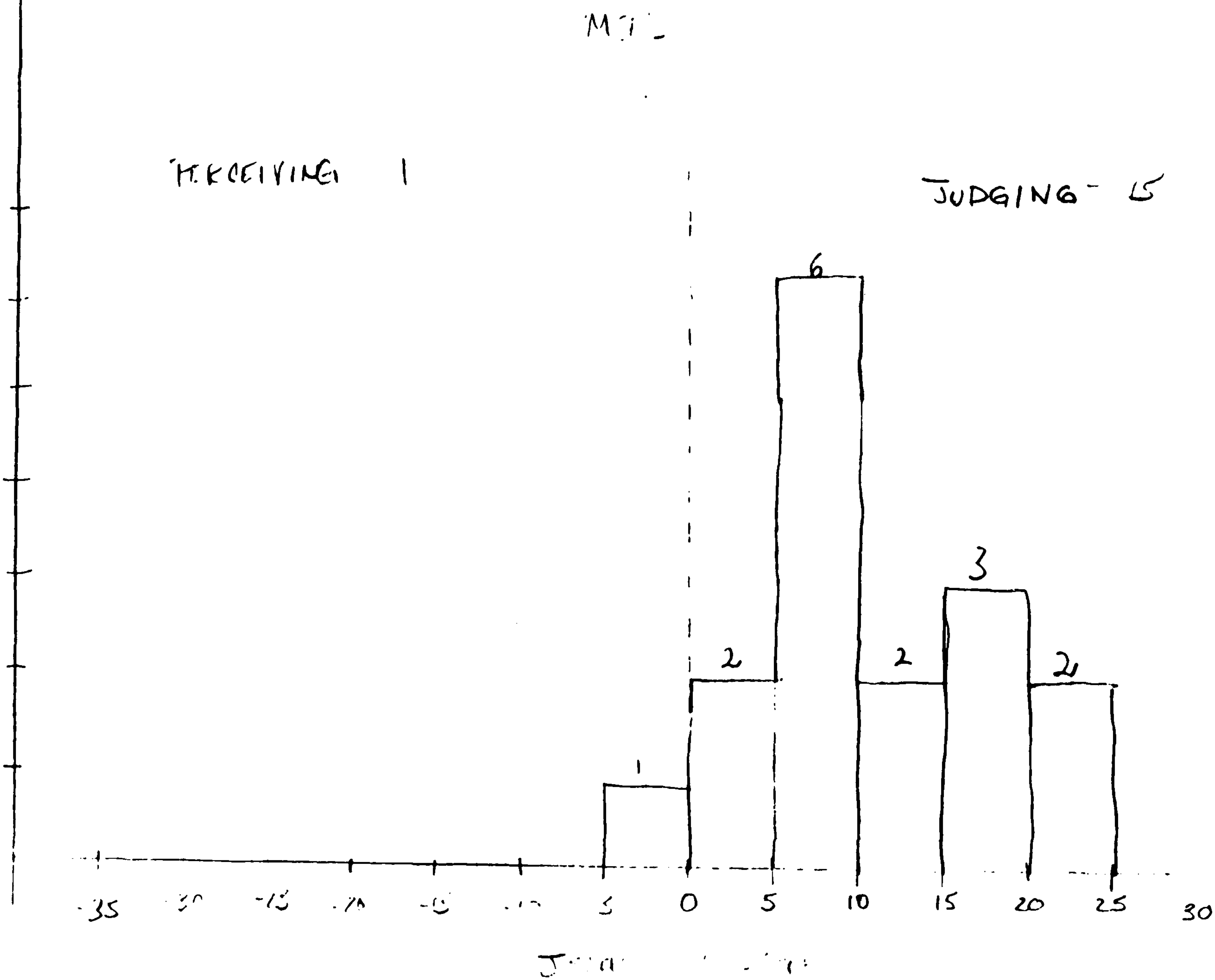

PERCEIVING 1
JUDGING 15
6
2
2
3
2
1
-35
0
5
10
15
20
25
30

+6	
+10	-1
	-3
+10	-8
+26	-4
+5	-12
+10	-21
	-16
+15	-11

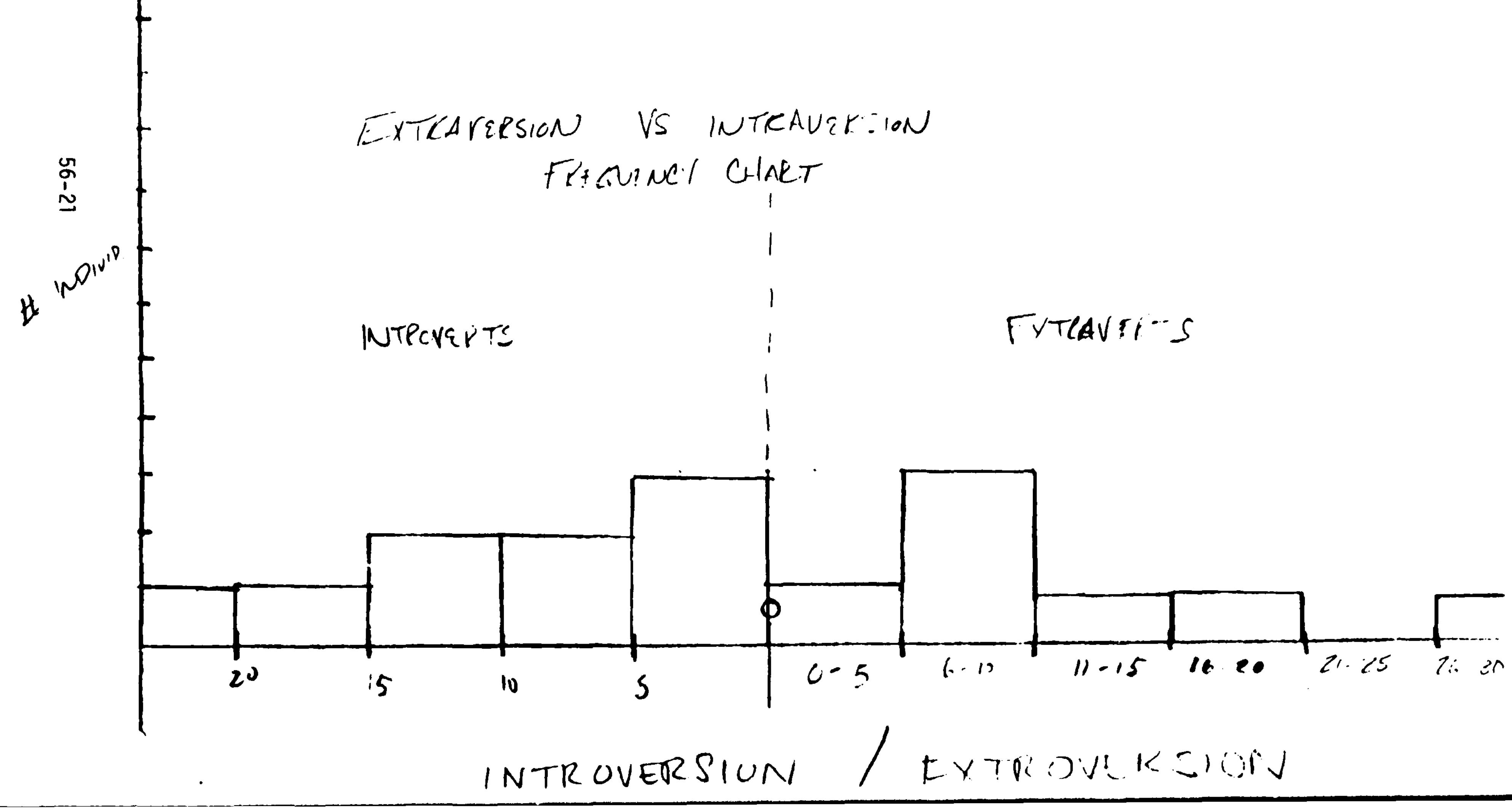

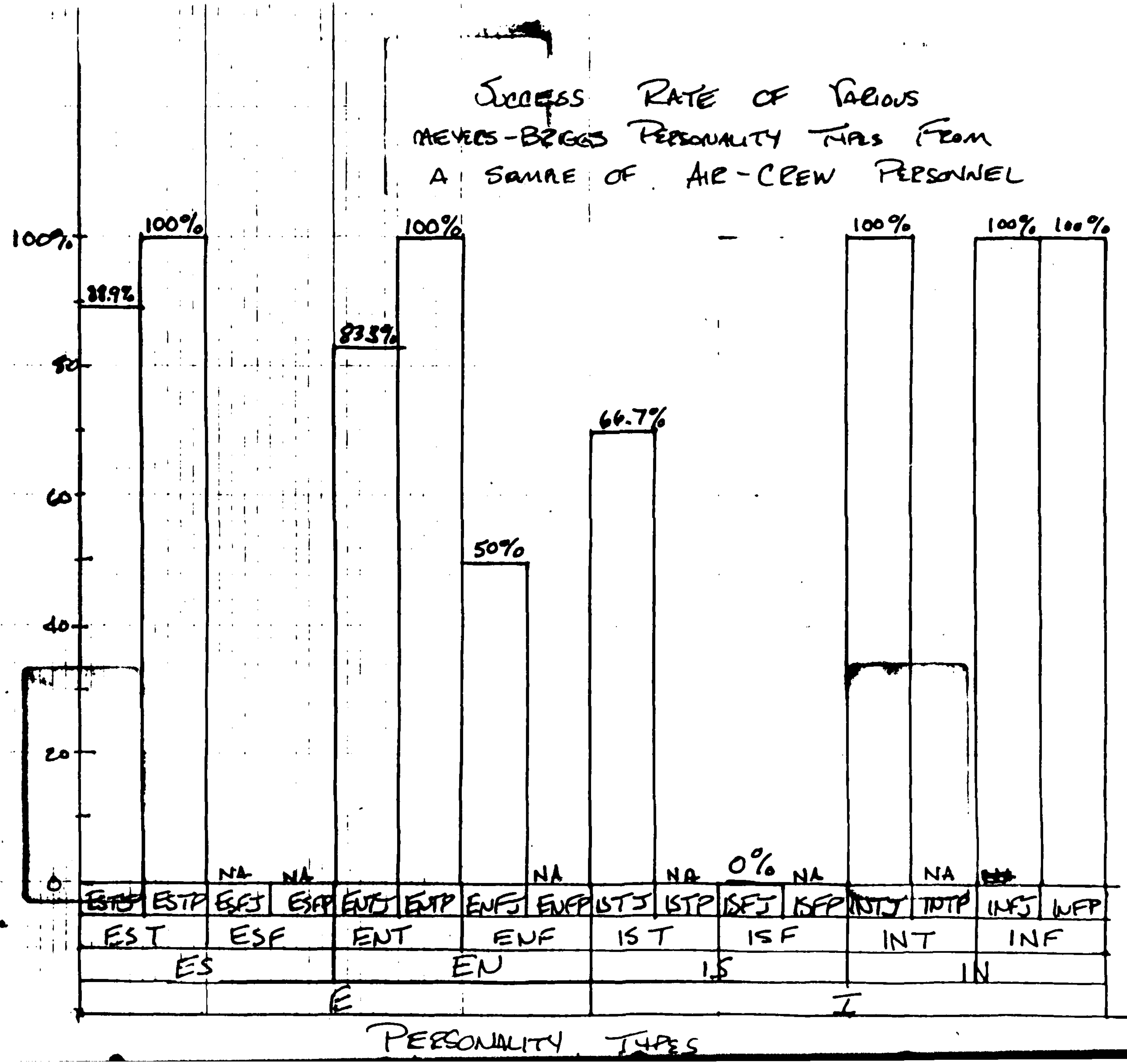
SUCCESS RATE OF VARIOUS
MEYERS-BRIGGS PERSONALITY TYPES FROM
A SAMPLE OF AIR-CREW PERSONNEL
100%
80
60
40
20
0
88.9%
100%
NA
NA
83.3%
100%
50%
NA
66.7%
NA
0%
NA
100%
NA
100%
100%
ESTJ
ESTP
ESFJ
ESFP
ENTJ
ENTP
ENFJ
ENFP
ISTJ
ISTP
ISFJ
ISFP
INTJ
INTP
INFJ
INFP
EST
ESF
ENT
ENF
IST
ISF
INT
INF
ES
EN
IS
IN
E
I
PERSONALITY TYPES

other interesting results. Specifically, the judgement/ perception scale was chosen, which happens to be the central scale in Jungian theory. When the scores of the MSEs was distributed, not only was the polar dominance of the (Figure 8) judging index evident, but a particular modal score dominated as well for 6 of the 16 MSEs. This particular statistic could be useful if the continuous data was statistically analyzed parametrically, which will be done in an upcoming study. The same chart was performed for a more evenly distributed scale for MSEs, the (Figure 9) extroversion/introversion scale. Upon observing the data, no apparent pattern was evident, something which could be statistically verified.

The value of analyzing the data in this retrospective study, is that performance could be tracked according to the personality type on file for the Aircrew member to determine any patterns. It is possible that certain personality types might be more successful than others at handling the demands of the job. On the other hand, this might not necessarily be true, but nonetheless the data is open for scrutiny. In Figure 10, just this representation was made, where success rate of a sample of Aircrew personnel was categorized against MBTI type. It was found that success rate greater than 80% was pretty evenly distributed among types with the exception of 3 types , ENFJ , ISFJ , ISTJ .

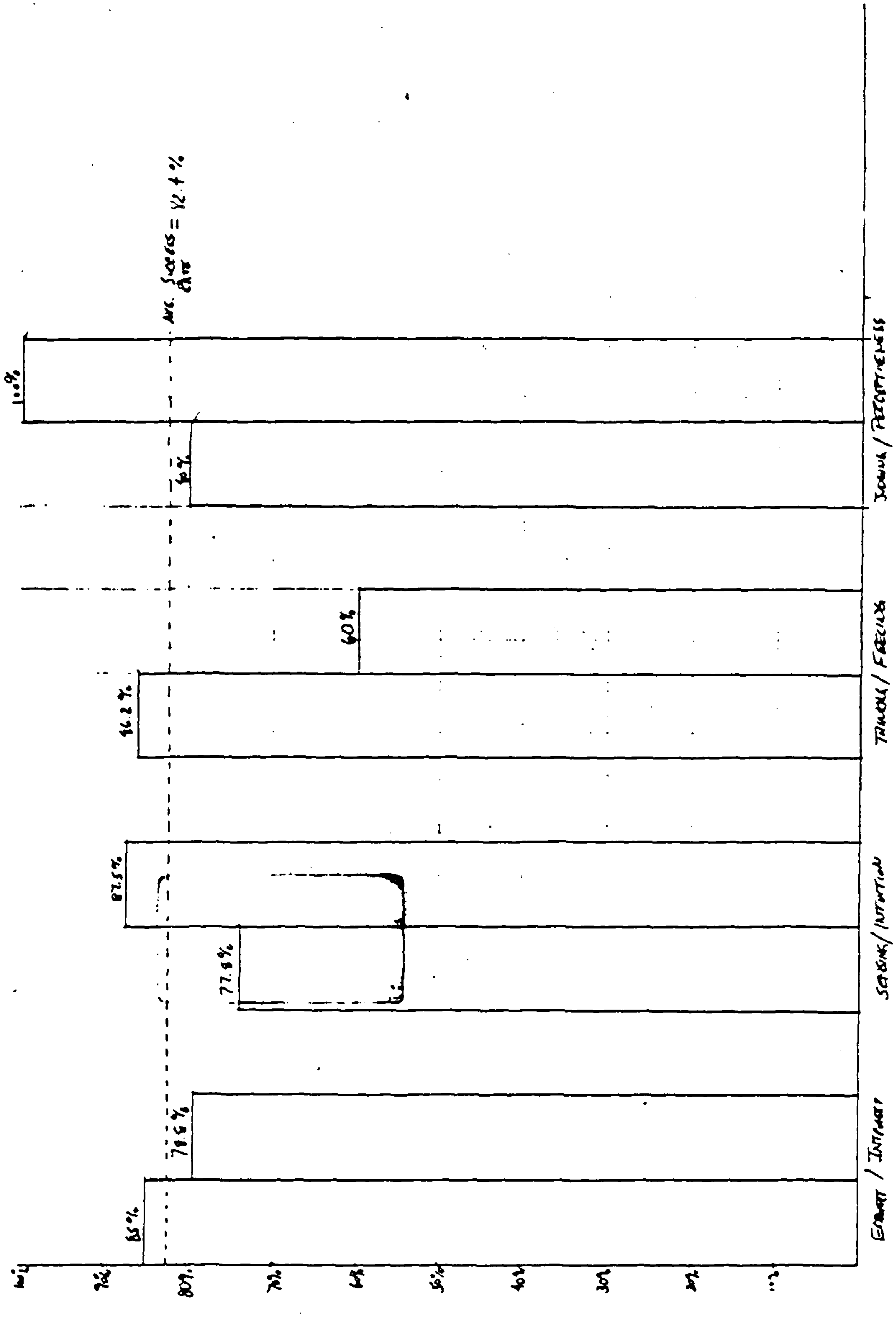
85%
78.5%
77.8%
87.5%
86.2%
60%
80%
100%

At first glance this statistic might be misleading, if one fails to look at specific sample and group N number, which would make this finding statistically invalid until a larger sample number was available. Another interesting representation, Figure 11, analyzes success rate with respect to particular scale. If one remembers that the T/F scale , Thinking/Feeling was dominated by Thinkers overwhelmingly, then the low Feeling percentage would also have to be said to be statistically not reliable until a larger sample pool was available. Nevertheless, the possibilities of uses of the MBTI are worthwhile, if one considers the relative efficiency of the test. Studies involving the use of the MBTI for assessing occupational choice, performance , and the like have been done, with particular citation of a study by Carlyn (1977).

When comparisons are made with other studies , the results displayed for the aircrew members tends to seem unique to this population. Specifically, in a study by Thomas (1984) of mechanical engineer students , it was found a correlation between the the J/P dimension and the S/N and T/F dimensions. In our case , a correlation was only evident between the J/P and T/F. In a study by Kerin and Slocum (1981) of graduate marketing subjects with one year experience of business it was found that NFs differed

with NTs in their preference for more objective , quantitative data. This was something which was found in the original Hartman paper for the prototype aircrew member, and which could lead the MBTI as a valuable tool in informational data retrieval from the different personality types of aircrew. Another different study by Bruhn , Bunce and Greaser tested physician assistants and nurse practitioners with the hopes of finding correlations among the scales of the MBTI and also to determine predictors of success from personality characteristics, something very similar to this study. Correlations were indeed found between the SN and JP scales, which was once again quite distinct from our study observations. A TF and JP interaction similar to ours was found but only for a sub-sample of their population and it was inversely related to ours in any case with an FP rather than Tj dominance.

Significantly the Myers Briggs Type Indicator has found many uses in vocational counseling, in screening and selecting applicants, and in predicting academic success. In our case , it is hoped that the Indicator has served a purpose in further typifying the personality patterns of existing successful Aircrew, which can subsequently be used in the capacities mentioned above.

REFERENCES

1. Fine , Paul M. , Hartman , Bryce O. , " Psychiatric Strengths and Weaknesses of Typical Air Force Pilots ", Air Force Publication SAM TR 68 121 , USAF School of Aerospace Medicine Texas , November 1968

2. Hicks , Lou E. , " Conceptual and Empirical Analysis of Some Assumptions of an Explicitely Typological Theory " Journal of Personality and Social Psychology , 1984 Vol 46, No. 5 , 1118-1131

3. Bruhne, J.G. , Bunce, H. , Greaser, R.C. , " Correlations of the Myers-Briggs Type Indicator with Other Personality and Achievement Variables ", Psychological Reports 1978 Vol 43 , 771-776

4. Kerin, R.A. , Slocum, J.W. , " Decision-Making Style and Acquisition of Information : Further Exploration of the Myers Briggs Type Indicator " , Psychological Reports 1981 , Vol. 49 , 132-134

5. Thomas, Charles R.," Regression of Myers Briggs Type Scales " Psychological Reports , 1984 , 55,568

6. Carlyn, M. , " An Assessment of the Myers Briggs Type Indicator ", Journal of Personality Assessment , 1977 Vol 41 , 3

7. Myers, I.B. , The Myers Briggs Type Indicator Manual , Princeton , New Jersey , Consulting Psychologists Press , 1985

8. Lynch , Anne Q., " The Myer Briggs Type Indicator : A Tool for Appreciating Employee and Client Diversity ", Journal of Employment Counseling , September 1985 , 105

9. Pinkney, J.W. , " The Myers-Briggs Type Indicator as an Alternative in Career Counseling ", The Personnel and Guidance Journal , November 1983 , 173

10. Carlson, J.G. , " Recent Assessments of the Myers Briggs Type Indicator ", Journal of Personality Assessment 1985 , Vol. 49 , 356

11. Carskadon , T.G. , " Test-Retest Reliabilities of Continuous Scores on the Myers Briggs Type Indicator " Psychological Reports , 1977 Vol 41, 1011-1012

1986 USAF-UES SUMMER FACULTY RESEARCH PROGRAM/

GRADUATE STUDENT SUMMER SUPPORT PROGRAM

Sponsored by the

AIR FORCE OFFICE OF SCIENTIFIC RESEARCH

Conducted by the

UNIVERSAL ENERGY SYSTEMS, INC.

FINAL REPORT

CHEMICAL AND ELECTROCHEMICAL BEHAVIOR OF ALUMINUM ELECTRODES IN ACIDIC 1-METHYL-3-ETHYLIMIDAZOLIUM CHLORIDE/ALUMINUM CHLORIDE ROOM TEMPERATURE MOLTEN SALT ELECTROLYTES

Prepared by:	Russell Moy
Academic Rank:	Graduate Student
Department and University:	Department of Chemical Engineering The University of Michigan
Research Location:	The Frank J. Seiler Research Laboratory FJSRL/NC Colorado Springs, CO 80840
USAF Researcher:	Dr. John S. Wilkes

Date:	August 22, 1986
Contract No.:	F49620-85-0013

CHEMICAL AND ELECTROCHEMICAL BEHAVIOR OF ALUMINUM ELECTRODES IN ACIDIC 1-METHYL-3-ETHYLIMIDAZOLIUM CHLORIDE/ALUMINUM CHLORIDE ROOM TEMPERATURE MOLTEN SALT ELECTROLYTES

by

Russell Moy

ABSTRACT

Rotating cylinder aluminum electrodes were used to study the deposition and dissolution of aluminum from slightly acidic 1-methyl-3-ethylimidazolium chloride/aluminum chloride room temperature molten salt electrolytes. A steady state current response could not be obtained for the oxidation or reduction of $X_{AlCl3} = 0.510$ electrolytes. Steady state cathodic current response was observed when $X_{AlCl3} = 0.505$, but the Tafel region was poorly defined. Cathodic polarizations of the working electrode resulted in the deposition of aluminum. However, current response was peak limited during anodic and some cathodic cyclic voltammograms of the rotating electrode. This type of behavior is indicative of the formation of a passive film.

ACKNOWLEDGEMENTS

The author thanks The Air Force Systems Command, Air Force Office of Scientific Research, and The Frank J. Seiler Research Laboratory for financial and technical support of this research.

I. Introduction

Aluminum is an attractive anode candidate for electrochemical energy conversion devices. It has the highest volumetric energy density of any metal, and is more easily handled than lithium and sodium. However, development of high energy density aluminum batteries has been hampered because a suitable electrolyte has not been identified.

Preliminary studies found that an electrolyte consisting of a mixture of 1-methyl-3-ethylimidazolium chloride (MEIC) and aluminum chloride ($AlCl_3$) could be used for the reversible deposition of aluminum (1,2,3). These investigators examined the Faradaic efficiency of aluminum deposition/dissolution, and deposition morphology. Unfortunately, no attempt was made to identify the kinetic parameters (Tafel slopes, exchange current density and reaction orders) of these processes. Moreov r, mass transfer data of the electroactive heptachloroaluminate anion is of questionable reliability. Consequently, insufficient information exists to suggest a mechanism for aluminum deposition and dissolution from the MEIC/$AlCl_3$ electrolytes. Such a mechanism would be useful for secondary battery development, optimization of electrolyte composition, as well as in the design of aluminum refining and plating systems.

II. OBJECTIVES OF THE RESEARCH EFFORT

The primary objective of this research is to measure the cathodic and anodic Tafel slopes and exchange current density of the aluminum electrode in the MEIC/$AlCl_3$ molten salt. Tafel slopes can be used to identify some of the microscopic electrode processes that may occur (e.g. adsorption and reaction scenarios). The exchange current density is used to estimate rate constants for electrochemical reactions. These measurements are to be made in several electrolyte compositions because different mechanisms may prevail for various MEIC/$AlCl_3$ ratios.

The second object of this research is to determine the limiting current for aluminum deposition and dissolution in the above molten salt electrolyte. Limiting currents can be used to estimate the diffusion coefficient of the electroactive species in solution, which is useful in characterizing the maximum rate of mass transfer of electroactive species to the electrode.

III. Experimental

1-Methyl-3-ethylimidazolium chloride was prepared according to Wilkes (4). Aluminum chloride was purified by sublimation in the presence of aluminum wire and sodium chloride. Early batches of melt were prepared at The University of Michigan and were purified by exhaustive electrolysis between two high purity aluminum electrodes at less than 1 mA/cm^2. Subsequent batches of electrolyte were

prepared at FJSRL, but were found to be contaminated by an electroactive impurity that could not be removed.

Electrochemical measrrements made in forced convection cells were obtained at high purity (m5N) 6.35 mm aluminum rotating cylinder electrodes that were fabricated in- house. The rotation rate of this electrode was 500 RPM. The working and counter electrodes were abraded with 400 grit SiC paper and rinsed with acetonitrile in the dry box to remove surface oxides. Quiescent cyclic voltammograms were obtained at 5 mm platinum disk electrodes (Pine Instrument Company) or 3 mm glassy carbon electrodes (5). Counter electrodes were fabricated from high purity (m5N) aluminum wire coils, or 7 mm aluminum rod. Reference electrodes were either aluminum plated on platinum in an $X_{AlCl3} = 0.505$ melt (Al/Al^{+3}), or aluminum wire immersed directly in the working electrolyte (Al^{0}). When the $Al/X_{AlCl3} = 0.505$ reference electrode was used, the reference electrolyte was separated from the test electrolyte by an ultra fine glass frit. Due to the hygroscopic nature of aluminum chloride and 1-methyl-3-ethylimidazolium chloride, all experiments were conducted in a helium filled glove box with continuous moisture and oxygen removal.

III. RESULTS AND DISCUSSION

Steady state cathodic or anodic current responses could not be obtained for potentiostatic polarizations of the aluminum RCE in an X_{AlCl3} = 0.510 melt at room temperature. Slow cyclic voltammograms (1 mV/s) of the RCE found that the current response increased with subsequent scans when the cathodic switching potential was more negative than -40 mV vs. Al/Al^{+3}. The return scans also exhibited a higher current response than the forward scans. At higher scan rates (50 to 500 mV/s) a cathodic current peak was observed for cyclic voltammograms at the rotating cylinder electrode. The current response for the return scan was insensitive to changes in applied potential. A current response maximum was also observed for an anodic cyclic voltammogram of the RCE at 1 mV/s. A dark film could be seen forming on the working electrode during some of the polarizations.

Current maxima, observed in forced convection systems, is indicative of passive film formation. Similar results have been reported in more acidic MEIC/$AlCl_3$ melts (6), and for NaCl/LiCl/$AlCl_3$ molten salt electrolytes (7). Holleck and Giner (7) have suggested that the compositional changes at the electrode/electrolyte interface, caused by electrolysis of the chloroaluminate melts, drive the electrolyte into the solid region of the phase diagram at the electrode surface. The potential independent current response for the return portion of the cyclic voltammogram

is therefore the limiting current caused by the dissolution of the passive film.

Steady state cathodic polarizations were obtained at the aluminum RCE in $X_{AlCl3} = 0.505$ melts, with a measured cathodic Tafel slope of 100 mV/decade, and an exchange current density of 0.105 mA/cm^2. However, the Tafel region was not well defined, and extended only over approximately 35 mV (-65 mV to -100 mV vs. Al/Al^{+3}).

Repeated attempts to duplicate this experiment were unsuccessful. Several batches of $X_{AlCl3} = 0.505$ prepared at FJSRL were found to be contaminated by an electroactive redox couple. These impurities were detected by cyclic voltammetry at platinum disc electrodes as reduction peaks at +1000 and +600 mV and oxidation peaks at +1200 and +550 mV vs Al^0. These peaks were not detected by cyclic voltammetry at glassy carbon disc electrodes-- it is well known that platinum electrodes are exceptionally sensitive to adsorbed species (8). Corrosion of the unpolarized aluminum rotating cylinder could be observed visually.

Haloaluminate electrolyte purification techniques such as exhaustive electrolysis (9), stirring over aluminum powder (10), and contact with aluminum amalgams (10,11) were unsuccessful in removing these impurities. Vacuum treatment was also used in an attempt to purify the electrolyte because it was suspected that volatile protonic impurities such as HCl may be responsible for the anomalous redox peaks. In fact, vacuum treatment increased the reduction

current, but did decrease the oxidation current. This response is undoubtedly caused by a contaminant to the dry box atmosphere that is being absorbed by the electrolyte. Aluminum chloride and tetrachloroaluminate salts are known to form complexes with a number of species (12)-- the vapors of organic solvents have been found to contaminate $SO_2/LiAlCl_4$ electrolytes that were stored in the same dry box (13). The obvious remedy for this problem would be to remove all unnecessary materials from the dry box, and to purge the dry box with an inert gas such as dry helium.

IV. Recommendations

Because of the passivation phenomenon that was observed during the electrolysis of the MEIC/$AlCl_3$ molten salt, future experiments should be developed that will minimize interfacial salt precipitation. One technique that was investigated by Holleck and Giner (7) was to increase the operating temperature of the cell. Higher temperature cells had increased current plateaus, indicating that there is a more rapid dissolution of the passive film. Variable temperature experiments may allow for the characterization of the passive film dissolution.

A more promising alternative would be to study the aluminum deposition and dissolution from electrolytes consisting of the molten salt mixed with a suitable organic cosolvent. The use of a cosolvent may help to solubilize the films that are formed on the electrode surface, and

would decrease the viscosity of the electrolyte, thereby increasing the specific conductivity.

Fannin and coworkers (14) found that MEIC/$AlCl_3$ was soluble with a number of nitrile and aromatic cosolvents. They observed significant increases in the specific conductivity of the electrolyte, but they did not investigate the electrochemistry of these ternary mixtures. Robinson and Osteryoung (15) found the addition of benzene to butylpyridinium chloride/aluminum chloride molten salts had no effect on the electrochemical behavior of aluminum. One obvious disadvantage of these cosolvents is the increased vapor pressure of the electrolyte. This factor however, is not insurmountable-- extremely volatile sulfur dioxide (BP -10 $^{\circ}$C) is used commercially as a battery electrolyte. Suitable cosolvents for use with MEIC/$AlCl_3$ molten salts are acetonitrile and toluene.

One powerful technique that has not been used for the evaluation of chloroaluminate electrolyte involves the measurement of the complex impedance of an electrode/electrolyte interface. In this technique, a small amplitude sinusoidal potentiostatic perturbation is applied to an electrode, and the phase shift of current response is measured as a function of frequency. This type of experiment is well suited for the MEIC/$AlCl_3$ system because the perturbations are made near the equilibrium potential of the electrode, so the mean polarization of the electrode is zero, minimizing passivation problems that have been

experienced with DC techniques. The exchange current density (and rate constants) of an electrochemical reaction can be obtained by AC impedance experiments. AC impedance can also be used to characterize films (e.g. porosity, thickness, ionic conductivity, etc.) that may form on the electrode surface, as well as corrosion processes that may occur (16).

<u>References</u>

1. Wilkes, J.S., and Auborn, J.J., Abstract 242, Electrochemical Society Fall Meeting, Washington, DC, (1983).

2. Auborn, J.J., and Schregengerger, Y.L., Abstract A4-13, International Society of Electrochemistry 35th Meeting, Berkeley, CA, (1984).

3. Auborn, J.J., and Barberio, Y.L., <u>J. Electrochem. Soc.</u>, <u>132</u>, 598-601, (1985).

4. Wilkes, J.S., Levisky, J.A., Wilson, R.A., and, and Hussey, C.L., <u>Inorg. Chem.</u>, <u>21</u>, 1263-1264, (1982).

5. Moy, R., accepted for publication in <u>The Analyst</u>.

6. Moy, R., Simonsen, L.R., and Donahue, F.M., Electrochemical Society Fall Meeting, San Diego, CA, (1986).

7. Holleck, G.L., and Giner, J., <u>J. Electrochem. Soc.</u>, <u>119</u>, 1161-1166, (1972).

8. Bard, A.J., and Faulkner, L.R., <u>Electrochemical Methods</u> pp. 539-40, John Wiley β Sons, New York, (1980).

9. Gale, R.J., and Osteryoung, R.A., <u>J. Electrochem. Soc.</u>, <u>121</u>, 983-987, (1974).

10. Giner, J., and Turchan, M., Second Quarterly Report, NASA Contract NAS 12-688, Tyco Laboratories, Inc., (1968).

11. Peled, E., Mitavski, A., and Gileadi, E., Z. Physik. Chem. (N.F.), 98, 111-122, (1975).

12. Bedfer, Y., Corset, J., Dhamelincourt, M.C., Wallart, F., and Barbier, P., J. Power Sources, 9, 267-272, (1983).

13. Moy, R., unpublished results.

14. Fannin, A.A., Floreani, D.A., King, L.A., Landers, J.S., Piersma, B.J., Stech, D.J., Vaughn, R.L., Wilkes, J.S., and Williams, J.L., FJSRL-TR-82-0006, (1982).

15. Robinson, J., and Osteryoung, R.A., J. Electrochem. Soc., 127, 122-128, (1980).

16. Radman, D.M., Abstract 125, Electrochemical Society Fall Meeting, New Orleans, LA, (1984).

1986 USAF-UES SUMMER FACULTY RESEARCH PROGRAM/

GRADUATE STUDENT SUMMER SUPPORT PROGRAM

Sponsored by the

AIR FORCE OFFICE OF SCIENTIFIC RESEARCH

Conducted by the

Universal Energy Systems, Inc.

FINAL REPORT

OBOGS STUDIES

Prepared by:	Glenn Munkvold
Academic Rank:	Graduate Research Assistant
Department and University:	Department of Chemical Engineering University of Texas at Austin
Research Location:	USAF School of Aerospace Medicine, Crew Systems Branch, Crew Technology Division
USAF Researcher:	Dr. Kenneth G. Ikels
Date:	September 23, 1986
Contract No.:	F49620-85-C-0013

OBOGS STUDIES

By

Glenn Munkvold

ABSTRACT

Studies were done in three areas of on board oxygen generation system (OBOGS) research. First, a temperature correlated computer model of the F-16 type OBOGS was implemented, and computer codes were written to facilitate use of ReGis graphics on Dec VT terminals. Work was also begun on data formats to be used on an improved model being developed. Second, experiments were done concerning the possibility of reducing the required bed size for an OBOGS unit through the use of oxygen enriched feed. Such feeds may be available as exhaust from on board inert gas generators. While not conclusive, these experiments indicate that any bed size reduction achievable with these feeds may be small, especially as compared to required overdesign of the beds for safety reasons. Third, a chromatographic technique for determination of adsorption isotherms was attempted. The results from these experiments were not physically reasonable. Reasons for the failure of this experiment are being explored.

ACKNOWLEDGMENTS

I would like to thank the Air Force Systems Command and the Air Force Office of Scientific Research for sponsorship of my research. I would also like to thank the people at USAF SAM/VNL for providing me with support for my work, especially Ken Ikels and Colonel John Bomar.

I. Introduction

I received my bachelor's degree from the University of Illinois at Urbana-Champaign in chemical engineering. Currently, I am enrolled at the University of Texas in pursuit of my PhD in chemical engineering. I spent my first year at Texas studying underground coal gasification before switching to modeling pressure swing adsorption (PSA) under Dr. J. J. Beaman in the mechanical engineering department (however, I am still in the chemical engineering department). Previous work in the area had been done by students in the mechanical engineering department who did not have the benefit of formal instruction in chemical processes. I was taken on the project because I have this background.

PSA is of interest to the Air Force because the process can be used to generate oxygen from a compressed air stream. Thus it is possible to remove the liquid gas systems currently in use in most aircraft. This has many logistical advantages: liquified oxygen is expensive, difficult to transport, and represents a significant fire/explosion hazard. PSA on board oxygen generation systems (OBOGS) draw a compressed air stream from an intermediate compression stage in the engine(s). In a simple two bed system, this stream is fed to one of the beds, which are packed with zeolites that preferentially adsorb nitrogen. Therefore, a stream enriched in oxygen is produced. The product stream is used by the crew and as a purge to regenerate the bed that is not connected to the supply pressure. As the producing bed becomes saturated, the supply is switched so that the second bed produces oxygen while the first is purged. Research has been active in this area for several years, and OBOGS are currently flying in some aircraft. The systems have generally performed well, but performance and design questions remain.

Because of the availbility of equipment and OBOGS expertise at USAF SAM, I was assigned there to continue my studies on OBOGS.

II. Objectives of the Research Effort

The summer's work was in three main areas:

1. Development of a library of ReGis graphics routines for use on Dec VT terminals, implementation of a temperature correlated model of the F-16 OBOGS, and preliminary work on structure of a new OBOGS/PSA model being developed.

2. A study on integration of an OBOGS with an on board inert gas generation system (OBIGGS).

3. Use of a chromatographic techinque to characterize a zeolite suitable for use in an OBIGGS.

III. Computer Work

The current model is relatively inflexible. While it performs well for the oxygen - nitrogen system, expansion to include a third component will require an extensive revision of the program. As part of this restructuring, I spent approximately three weeks developing a graphics library and data structure to allow for maximum flexibility in the new program.

The graphics library was developed to make the implementation of the ReGis graphics on the Dec VT terminals easier. ReGis uses strings of control characters typed to the screen (in graphics mode) to position the cursor and draw. The method becomes clumsy when complex graphics are sent to the screen. Also, line after line of cryptic combinations of control codes are extremely difficult to debug if something needs to be changed. Therefore, fifteen subroutines were written to execute ReGis commands. The control characters are supplied by the subroutines; the call to the subroutine supplies appropriate screen coordinates. Complex figures can be drawn without repeated construction of command sequences.

To further exploit the advantage of a graphics library, I developed a "finite state machine" to actually draw the graphics on the screen. Essentially, this is a generic program

that reads a data file of commands and executes instructions based on those commands. Thus, the single program can be used to construct any screen graphics without recompilation of the program.

Ths ability to use a generic program (subroutine) to generate graphics is important because it allows us to simplify the simulator by removing bed design from its functions. Instead, the user will choose a bed design and enter the appropriate dimensions in a utility program which will generate a data file for input to the simulator. The user will be able to run and compare different designs easily, without ever needing to edit the source code.

Work on the utility program was begun, but was stopped as equipment for experiments became available.

IV. OBOGS/OBIGGS Integration

Inert gas (nitrogen) is used in fuel tanks to supress fire by excluding oxygen from the environment. Inert gas streams can be produced either by PSA (as oxygen is generated in an OBOGS, except that a different zeolite is used) or by selective permeation through polymer membranes. One can expect to obtain a stream enriched in oxygen as an exhaust from OBIGGS. How much can the size of an OBOGS be reduced, without a loss of performance, if it uses an oxygen enriched gas as a feed from an OBIGGS?

In an effort to answer this question, as well as to gain a familiarity with experimental technique, experiments were done with the Small Oxygen Concentrator (SOC, see Figure 1) at different feed compositions (1). Four inlet pressures (10,20, 30, 40 psig), four product flowrates (0.25, 0.5, 1.0, and 1.5 STD lpm), four bed activities (Fully active bed, 75%, 50%, and 25% active), and three inlet compositions (30%, 40%, and 50 mole % oxygen) were investigated. A cycle time of 8 seconds was used; all experiments were done at room temperature. The bed packing was Linde molecular sieve 5A that had been activated by drying approximately 20 hours at 350° C with a nitrogen purge. The bed was partially deactivated by the substitution of water deactivated sieve for active sieve in the

bed. Inlet mass flowrate and outlet gas compositions were measured. Outlet gas composition was determined using a Perkin-Elmer Medical Gas Analyzer (MGA), which is a mass spectrometer.

On the basis of these experiments, OBOGS size reduction through integration with OBIGGS does not seem promising. First, the level of oxygen enrichment possible in the exhaust stream of an OBIGGS is limited. PSA OBIGGS are almost as inefficient as OBOGS; a two to four percent enrichment is the most that can be expected. Membrane OBIGGS are more efficient, but the maximum oxygen concentration possible in the exhaust stream is still only about 30%.

Second, unit performance is relatively insensitive to active zeolite mass until a critical value is reached. Then performance degrades rapidly (see Figure 2). This is the same behavior found by Beaman (2), with air as the feed. If OBOGS performance were a smooth function of zeolite mass, then one could expect to be able to safely reduce the mass of the bed if an enriched feed were used. However, because performance degrades so rapidly at a critical mass, it is important, from a safety standpoint, to overdesign the bed to stay away from this dangerous operating region. It does not appear that the reduction in bed mass possible through the use of an enriched feed will be significant compared to this "safety factor" that will be necessary in design. However, more work remains to be done. Little has been done concerning variation of purge orifice diameter. Simulations indicate that this dimension is critical to system performance.

V. <u>Isotherm Experiments</u>

The isotherm experiments were done using a chromatographic technique outlined by van der Vlist and van der Meijden (3), who extended work done by Haydel and Kobayashi (4). In chromatographic analysis, one can determine the "partition coefficient" of a packing material from the time taken by a pulse of gas to travel the length of a column filled with the material (retention time) and the flowrate of the carrier gas. The partition coefficient is

actually the slope of the isotherm for the pulsed component at the composition of the carrier gas. In van der Vlist and van der Meijden's treatment, the retention time for the pulses was fitted to a cubic polynomial as a function of the partial pressure of the pulsed component. This expression was then integrated to yield an expression for the isotherm (moles adsorbed per gram of molecular sieve as a function of partial pressure, at constant total pressure). The supposed advantages of the chromatographic technique are that it is faster and easier to obtain isotherms at constant total pressure than conventional volumetric and gravimetric means.

It was planned to duplicate the work done by van der Vlist, et al, on Linde molecular sieve 5A before continuing to characterize a 4A zeolite which may be used in inert gas generation. Due to the fact that no vacuum was available for exhaust, I had to do my experiments at 3 psig instead of at atmospheric pressure, where van der Vlist, et al, did their work. Unfortunately, only the 5A work was attempted due to lack of time. Figures 3 through 5 show the isotherm apparatus.

Data analysis is continuing on the isotherm experiments. Because the detector (the MGA) could not be used on streams with a helium concentration in excess of 20 mole %, the oxygen and nitrogen pure component isotherms could not be determined. This represented a problem because the endpoints of the pure component isotherms (i.e., moles adsorbed when the partial pressure of a component is equal to the total pressure) were required in order to determine the coefficients in the oxygen - nitrogen binary isotherms. It was decided to proceed with the binary experiments and use endpoint values from (3), extrapolated from 0 psig to 3 psig. However, comparison of the values obtained in this manner with values found in Miller (5) showed significant differences. Miller's value for nitrogen adsorption was nearly twice that of van der Vlist, et al. Miller's oxygen value was about 80% greater than van der Vlist. Further investigation revealed an error in the mathematical analysis in van der Vlist and van der Meijden's paper. Unfortunately, they do

not supply enough information to recalculate the isotherm coefficients, so the quality of the values presented in their paper is unknown. Therefore, Miller's values for the pure component isotherm end points were used in my integrations.

In the van der Vlist paper, several pulse volumes were run and the value for the retention time extrapolated to zero sample size. This was done because the governing equations hold only for "small" perturbations, or pulses. Due to lack of time, I only ran two pulse volumes this summer. I have analyzed all of my isotherm data and have obtained non-physical results in all cases. Therefore, either the method is completely without merit, or I have committed an error in analysis. This latter possibility is presently being investigated.

VI. Recommendations

1. The "temperature correlated" model now in place at USAF SAM should be used with discretion at extreme temperatures (especially low temperatures ≈ -40° C and below). The power law correlation implemented for isotherm parameters has no theoretical basis, but has been used because it improves model performance over the case with no temperature correlation of parameters.

2. OBOGS size reduction through integration with OBIGGS still needs further study. The purge orifice in these units has a critical bearing on performance, but was not considered in these experiments. These studies may be done with the existing computer model (2); however, changes need to be made to simulate the solonoids in the SOC (the model is based on a rotary valve used in the F-16 OBOGS).

3. Water deactivated sieve should not be used in future bed deactivation experiments. During some of the 25% active bed runs, the outside of the "deactivated" portion of the bed became extremely cold. It was postulated that the water is not as strongly bound as was originally believed and that this phenomenon was due to desorption of water from the

zeolite. Water has a high heat of adsorption; desorption would therefore require energy and, consequently, cool the bed.

4. The isotherm experiments are under review to try to resolve the non-physical results. The method is relatively simple to implement, but data reduction was time consuming because all measurements had to be made by hand from chart paper. Digitizing data collection would make the process easier, faster, and less prone to error.

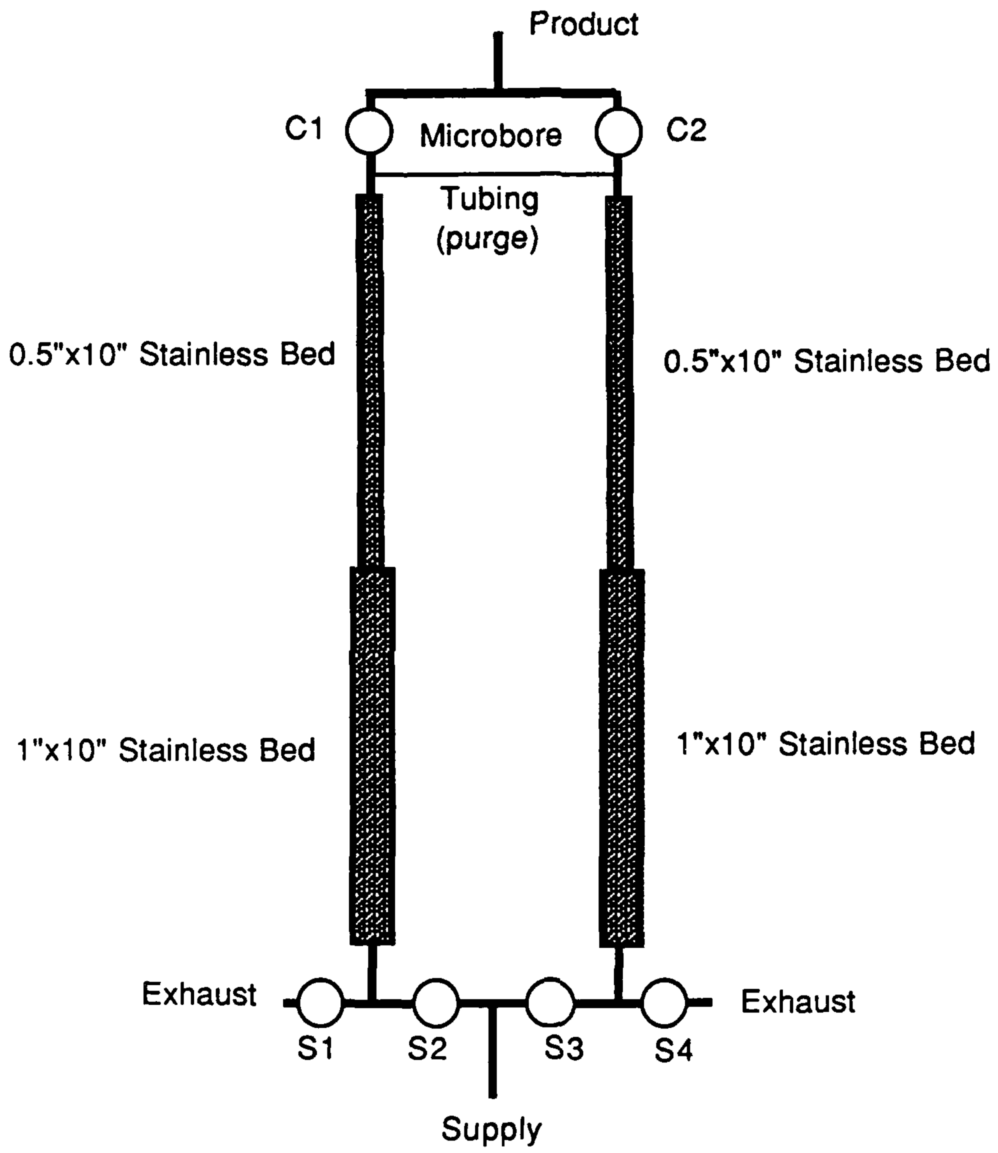

Figure 1. SOC Apparatus-Overview. S1, S2, S3, S4 are on-off solonoids. C1 and C2 are one way check valves. Purge is through the microbore tubing. The beds are packed with zeolite.

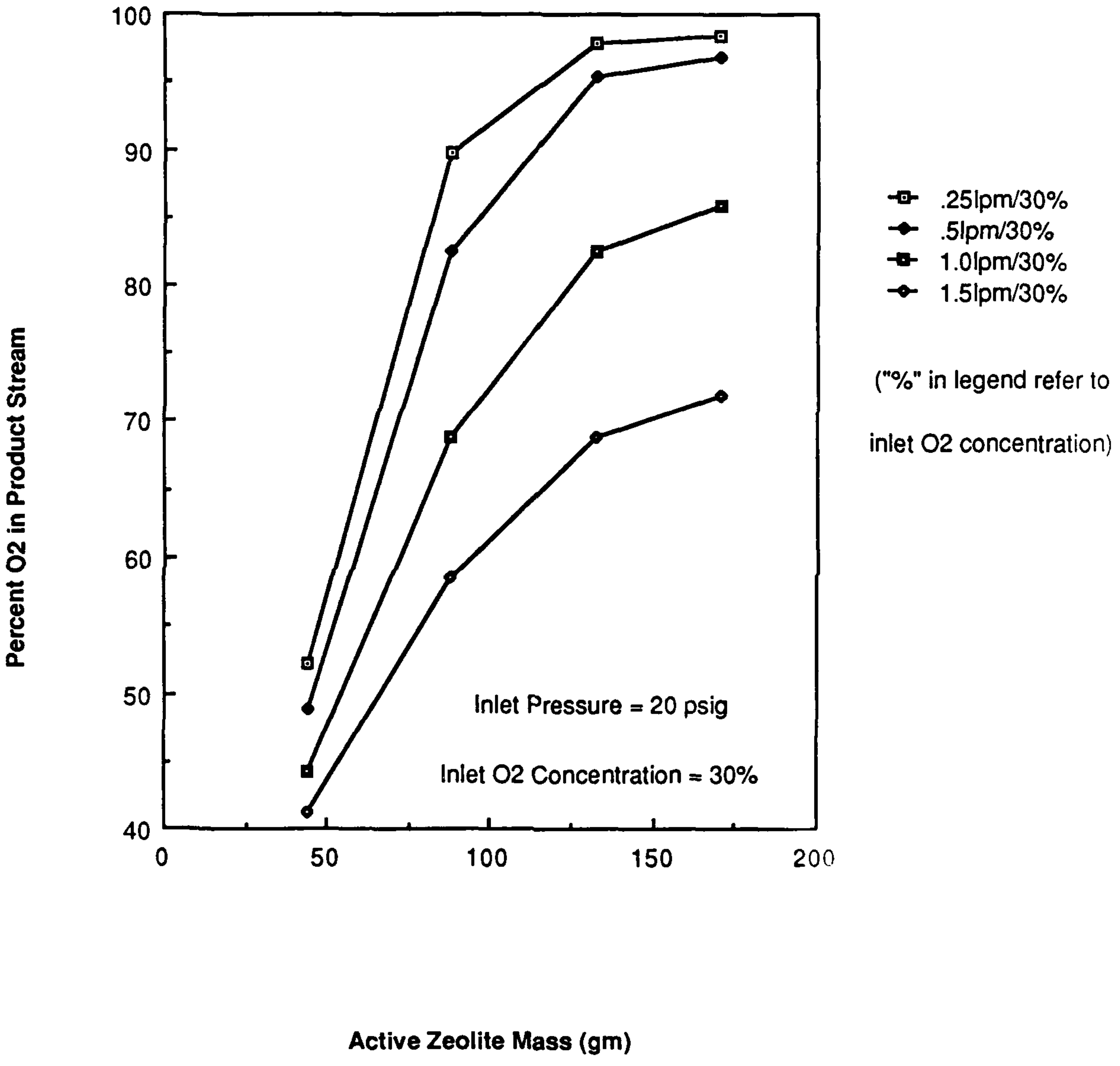

Figure 2. Note rapid performance loss between 130 and 85 gm active zeolite mass.

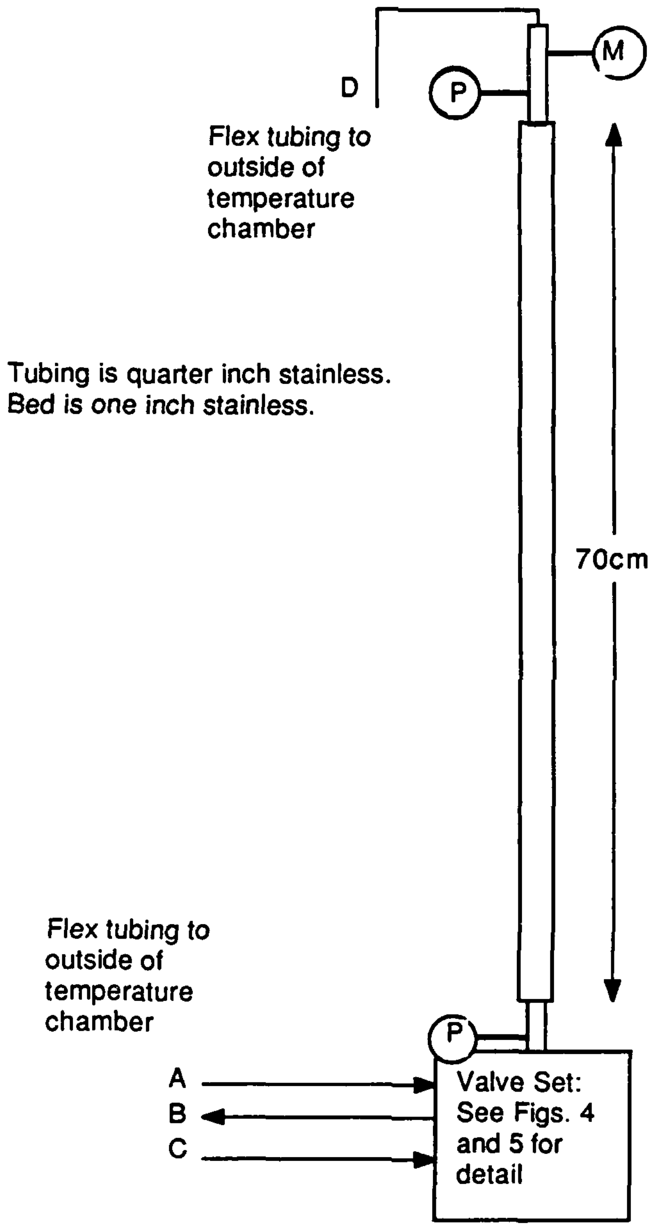

Figure 3. Isotherm Experiment Apparatus-Overview
A is carrier gas inlet, B is pulse charge loop exhaust, C is pulse charge loop inlet, D is column exhaust.

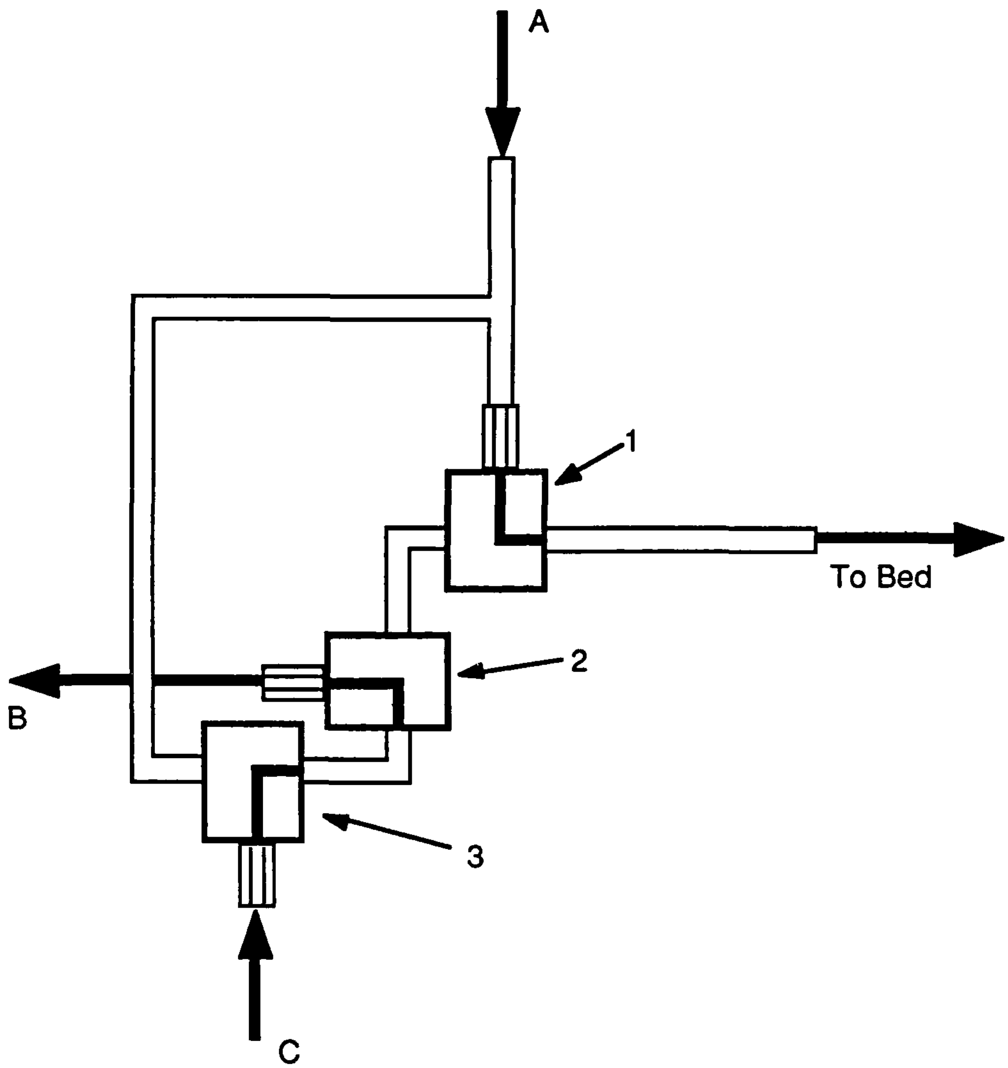

Figure 4. Isotherm Apparatus-Valve detail, normal position
A is carrier gas inlet, B is pulse charge loop exhaust,
C is pulse charge loop inlet. Valves 1, 2, and 3 are
three way solonoid operated valves.

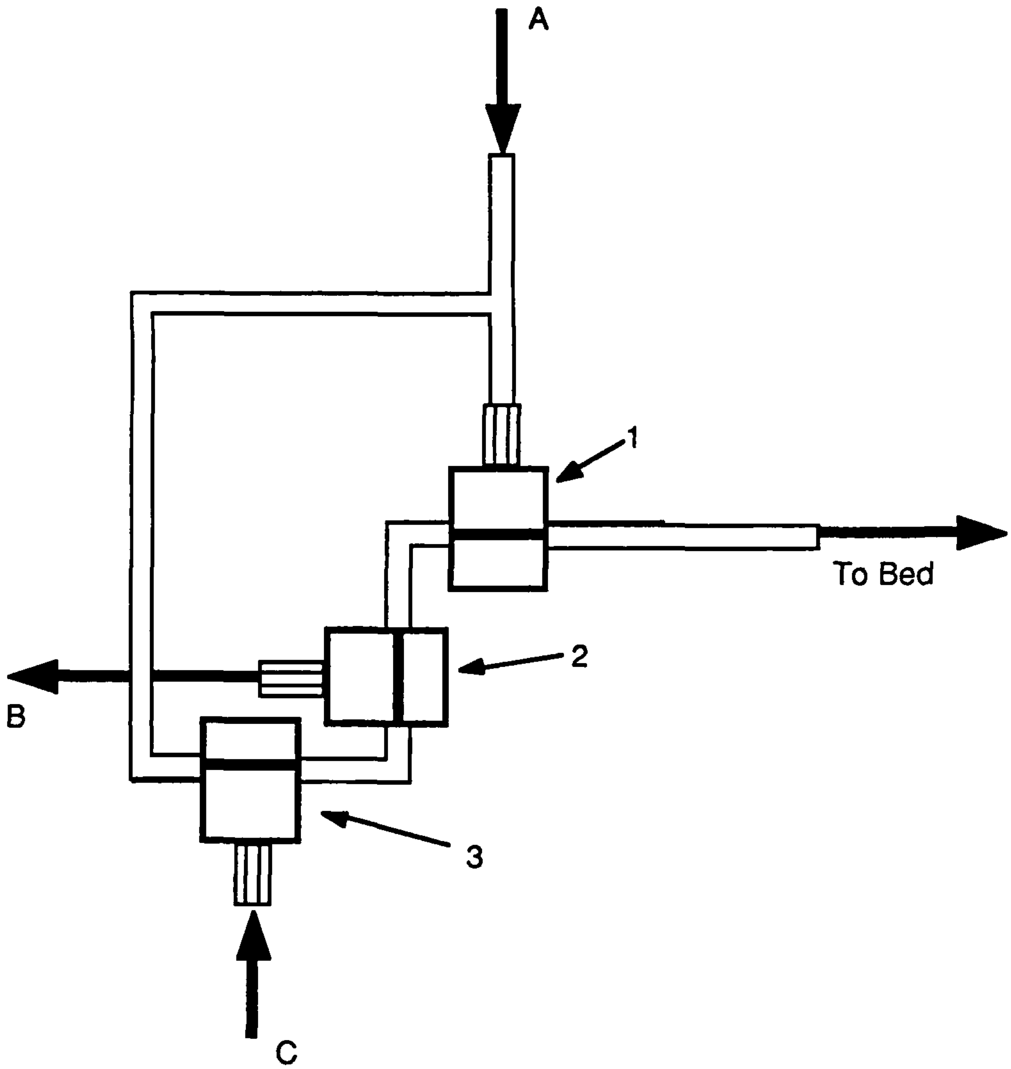

Figure 5. Isotherm Apparatus-Valve detail, pulse position
A is carrier gas inlet, B is pulse charge loop exhaust, C is pulse charge loop inlet. Valves 1, 2, and 3 are three way solonoid operated valves.

REFERENCES

1. Theis, C. F., K. G. Ikels, and R. G. Dornes, A Small Oxygen Concentrator, USAFSAM-TR-85-18, December 1985.

2. Beaman, J. J., "A Dynamic Model of a Pressure Swing Oxygen Generation System," Trans. of ASME J. Dynamic Systems, Measurement, and Control, 107 (1985), pp. 111-116.

3. Vlist, E. van der, and J. van der Meijden, "Determination of Adsorption Isotherms of the Components of Binary Gas Mixtures by Gas Chromatography," J. of Chromatography, 79 (1973), pp. 1-13.

4. Haydel, J. J., and R. Kobayashi, "Adsorption Equilibria in the Methane-Propane-Silica System at High Pressures," Ind. Eng. Chem. Fund., 6 (1967), pp. 546-554.

5. Miller, G. W., Adsorption Equilibria and Performance of a Pressure Swing Adsorption Air Separation Unit, M.S. Thesis, Ohio State University, 1984.

1986 USAF-UES SUMMER FACULTY RESEARCH PROGRAM/

GRADUATE STUDENT SUMMER SUPPORT PROGRAM

Sponsored by the

AIR FORCE OFFICE OF SCIENTIFIC RESEARCH

Conducted by the

UNIVERSAL ENERGY SYSTEMS, INC.

FINAL REPORT

EFFECTS OF ACCELERATION STRESS UPON BLOOD LIPID LEVELS

Prepared by:	Conrad R. Murray
Academic Rank:	Medical Student
Department and University:	Department of Medicine MeHarry Medical College
Research Location:	USAF School of Aerospace Medicine, Brooks AFB, TX, Clinical Sciences Division, Clinical Pathology Branch
USAF Researcher:	Dr. Harvey A. Schwertner
Date:	August 7, 1986
Contract No:	F49620-85-C-0013

EFFECTS OF ACCELERATION STRESS UPON BLOOD LIPID LEVELS

BY

CONRAD R. MURRAY

ABSTRACT

Serum total cholesterol and triglyceride concentrations of two individuals were measured after daily exposures to high gravitational forces (+Gz) simulating aerial combat maneuvers. The post-acceleration cholesterol levels were significantly higher (40-95%) than the normal resting levels. Serum cortisol levels were higher than the resting levels. This agrees with previous studies which have shown significant increases in serum cortisol levels after acceleration stress. Cortisol and total cholesterol values were significantly correlated ($r = 0.614$, $p < 0.05$) in one of the individuals of this study. Since cortisol is a hormone which influences lipid metabolism, there may be a causal relationship between the increased cortisol levels produced by acceleration stress and increased lipid levels. The lipid levels in the two subjects after acceleration exceeded the 90th percentile for the population as a whole. As such, they could be at high risk for subsequent coronary heart disease if they are exposed to high G-forces on a frequent basis.

An ancillary study was conducted to develop an electrophoretic method to rapidly separate and quantitate serum high density lipoprotein (HDL) subfractions HDL_2 and HDL_3. Serum levels of one of these subfractions may be a better predictor of coronary heart disease than total cholesterol. Serum α-lipoproteins isolated by affinity chromatography were separated into a number of subfractions by polyacrylamide gel electrophoresis. These subfractions were marked by the usual lipoprotein stains, and by filipin, a fluorescent, naturally occurring antibiotic which, reportedly, binds specifically to cholesterol. Identification and quantification of these HDL subfractions remain to be accomplished.

ACKNOWLEDGMENTS

I would like to thank the Air Force Systems Command and the Air Force Office of Scientific Research for sponsorship of this research. Special thanks to Dr. Harvey Schwertner, my Effort Focal Point, for his generous assistance and guidance. I would like to also thank personnel of the Acceleration Effects Laboratory, Crew Technology Division, the Clinical Radioassay Function, Epidemiology Division, and the Lipids Evaluation Function, Clinical Sciences Division for their support in this research.

I. INTRODUCTION.

I received my earliest training from St. Joseph College, Trinidad West Indies. Between 1976-1979, I successfully graduated from the division of biological science at the University of London; following which I taught school at Port of Spain, Trinidad. (1980-83) I attended Texas Southern University, Houston, Texas, where I graduated with high honors ("Magna Cum Laude") in the spring of '83. As an academist, I accomplished several commendable milestones inclusive of: Who is Who among American College Students (1981), Member of the National Deans List (1981, 1982, 1983). President of Alpha Kappa Mu Honor Society Epsilon Chapter (1983). Membership to Beta, Beta, Beta Biological Honor Society; Member of the American Medical Student Association (AMSA) 1983 to present time. My first participation in research was attempted under supervision of Dr. Watkins, professor and veterinarian of Texas Southern University, Houston, Texas. I am a motivated and dedicated 3rd year Medical Student of Meharry Medical College, Nashville, Tennessee.

II. OBJECTIVES OF THE RESEARCH EFFORT.

Pilots flying high-performance aircraft are repeatedly exposed to high sustained G-forces during aerial combat maneuvers. Since both cortisol and physical stress are elevated during high G-forces, and since both cortisol and physical stress have been shown to be associated with elevated lipids levels (1), we sought to determine if lipid levels are elevated in subjects exposed to high G-forces. In addition, we measured serum cortisol concentrations in order to determine if the cholesterol increases are related to the increases in this particular stress hormone.

A complementary goal of this research was to develop an electrophoretic method to rapidly separate serum high density lipoproteins (HDL) into HDL_2 and HDL_3 subfractions, and to rapidly quantitate HDL_2 and HDL_3 cholesterol in these subfractions. The measurement of serum HDL_2 cholesterol may be a better indicator of coronary heart disease than total HDL (2).

To accomplish these goals, the following objectives were established:

1. Obtain serum samples from individuals prior to and after their exposure to an established protocol of daily +Gz accelerations simulating aerial combat maneuvers.
2. Determine serum cortisol and total serum cholesterol in these serum samples and determine whether the cholesterol levels are related to the cortisol levels. Also, determine whether they increase with increase in G-force.
3. Separate serum high density lipoproteins (HDL) from other serum lipoproteins, and develop an electrophoretic technique to separate the HDL into subfractions HDL_2 and HDL_3. Identify the HDL subfractions with lipid stains or with fluorescent filipin which has been reported to bind specifically to cholesterol (3).

III. +Gz ACCELERATION PROTOCOL AND ANALYTICAL METHODOLOGY.

As part of an ongoing, independent study, two military volunteers were subjected to daily +Gz acceleration on the human centrifuge for a one week training period and for a two week test period. The acceleration protocol included the drawing of a pre-acceleration fasting blood sample on Monday morning prior to acceleration exposure. On Monday, Wednesday, and Friday,

volunteers were exposed, unprotected, to rapid and gradual onset of +Gz acceleration to the maximum tolerable +Gz level (4.5-9G). On Tuesday and Thursday, they were exposed, but protected, to more exhaustive aerial combat maneuvers (SCAM, 4.5-9G) and were required to perform specific tracking tasks.

A post-acceleration blood sample was withdrawn from each subject about 15 minutes after each acceleration period. Serum samples were stored at -20°C (about 3 weeks) until analyzed for total cholesterol, triglyceride, and cortisol concentrations. Serum cortisol concentrations were determined by radioimmunoassay. Cholesterol and triglyceride levels were determined by enzymatic methods.

IV. SERUM CORTISOL, CHOLESTEROL, AND TRIGLYCERIDE LEVELS AFTER EXPOSURE TO +Gz ACCELERATION.

In the first subject, a 40-year-old male, serum cholesterol levels increased from a normal 158 mg/dl to 281 mg/dl (approximately 78%) after exposure to +Gz acceleration. The cholesterol remained elevated for the duration of the experiment (Table 1, Fig.1). These elevations are the likely result of the chronic daily exposure to +Gz forces, and are the first reported observations of a rise in serum cholesterol associated with +Gz acceleration. The cortisol levels also appear to be elevated in the first subject, however, cortisol baseline levels were not taken prior to G-force exposure. Previous studies (4, 5) however, have shown that increases in cortisol levels do occur as a result of +Gz acceleration. More importantly, a statistically significant correlation ($r = 0.614$, $n = 11$, $p < 0.05$) was found to exist between cortisol and cholesterol concentrations (Fig. 3). Triglyceride concentrations were also elevated, but varied widely.

The second subject also had elevated cholesterol levels, however, the increases were less pronounced than for the first subject. With this subject, the cholesterol concentration increased from a baseline value of 148 mg/dl to 186 mg/dl after the first acceleration test. The cholesterol values remained elevated through the completion of the experiment, but were less variable than the values for the first subject (Table 1, Fig. 2). The cortisol levels were also lower than for the first subject. Even though the cortisol and cholesterol levels were elevated after exposure to +Gz forces, there was no significant correlation between them. The differences in absolute cholesterol values between the two subjects could be due to age differences (40 versus 21). Some of the differences could also be due to the fact that some individuals can tolerate stress and others cannot. In other words, some individuals can be classified as responders and others respond to a lesser extent.

V. ELECTROPHORETIC DETERMINATION OF SERUM HIGH DENSITY LIPOPROTEIN (HDL) SUBFRACTIONS HDL_2 AND HDL_3.

Electrophoretic methods were examined for the purpose of developing a rapid clinical method for the analysis of HDL subfractions. Serum samples were fractionated into α-lipoprotein (HDL) and β-lipoprotein (LDL) components with commercially prepared heparin-agarose affinity chromatography columns (Isolab, Inc.). The HDL component was subjected to a number of electrophoretic techniques to separate, identify, and quantitate its subfractions.

A. Agarose Gel Electrophoresis.

Agarose gel electrophoresis has been used to separate serum lipoproteins into patterns showing two lipoprotein bands in the "α zone" of the electrophoretogram (10). The bands were not identified as HDL subfractions.

However, we conducted a number of agarose gel electrophoretic analyses of total serum samples and HDL and LDL components isolated by affinity chromatography. Various slab agarose gel plates (0.3 to 2% agarose in Tris barbital buffer, pH 8-9) abcut 3 mm thick were prepared. Before electrophoresis, serum or lipoprotein samples were mixed with lipid pre-stains or the fluorescent, natural product filipin, which supposedly binds specifically to cholesterol-containing lipoproteins. The electrophoresis was conducted in closed horizontal chambers in the Tris buffer for 1-2 hours at a constant voltage of 5-6 V/cm. Lipid stained and filipin-treated electrophoretic patterns of α-lipoproteins gave only a single broad band in the HDL region, and even a broad band in the LDL region, which indicates that affinity columns only partially purified the α fraction. We checked the effects of pH between 7.2 and 8.6. In general, the lower pH resulted in slower lipoprotein migration.

B. Polyacrylamide Gel Electrophoresis.

In the polyacrylamide gel studies, a wide range of parameters were modified. The concentration of the acrylamide as well as the degree of cross-linking has been found to be critical. In general, the higher the degree of cross-linking the greater the number of HDL subfractions. A polyacrylamide concentration of 5% with 0.04% cross-linking, and 0.1M sodium phosphate buffer (pH 7.2) gave best resolution of HDL bands. Filipin-treated serum samples were also electrophoresed in slab and tube polyacrylamide gels. However, filipin has not proven to be specific for cholesterol-containing lipoproteins, since fluorescence has appeared in the zone where albumin is expected.

C. Lipid and Lipoprotein Stains.

We have evaluated a number of lipid staining reagents for specificity and sensitivity. Those studied were Sudan Black, Oil Red-O, and filipin. Filipin has been used in anatomical pathology as a fluorescent, cholesterol specific

stain. This is the first time it has been used for quantification of lipoprotein cholesterol levels. In these studies, Sudan Black was found to be more specific than Oil-Red-O in that it did not bind to albumin. Filipin appeared to have sensitivities equal to that of Sudan Black. Some tests were also made to use cholesterol oxidase reagents to specifically stain the lipoprotein cholesterol. This is perhaps the most specific stain.

VI. RECOMMENDATIONS.

In this study, we have shown that exposure to high G-force results in significant increases in cholesterol and triglyceride. In addition, we have provided some evidence that the lipid increases could be the result of increased cortisol levels which accompany the intense physical stress of acceleration. The cholesterol levels of the two subjects studied here had cholesterol levels which exceeded the 90th percentile for their age bracket. With such levels, they are in the high risk group for developing coronary disease.

Since this study involved only two subjects, we feel that further studies should be performed in order to determine whether other individuals exposed to G-forces also experience elevated levels of serum cortisol and cholesterol, and whether there is significant correlation between the two levels.

Since the human centrifuge is capable of producing exact quantifiable levels of G-force, we recommend that further studies be conducted which more closely show the association between G-force, stress intensity, cholesterol concentration, and cortisol concentration. The study would not only have important health implications for pilots of high performance aircraft, but would also be of importance to the population as a whole. Studies identifying

changes in individual lipoproteins would also be important, as would studies of other lipid fractions such as the free fatty acids. Other endocrine hormones besides cortisol should also be examined.

It is also recommended that serum high density lipoprotein (HDL), and subfractions HDL_2 and HDL_3 concentrations be determined before and after subjects are exposed to +Gz acceleration. It should be of interest to determine which lipoprotein component is responsible for the observed increases in total serum cholesterol. Studies have suggested that cholesterol associated with these lipoproteins are better indices of the risk of coronary heart disease than total cholesterol (6-9).

Efforts to separate and identify serum high density lipoproteins into subfractions HDL_2 and HDL_3 should continue. Various electrophoretic techniques have been employed, but results have not been consistent. Cellulose acetate electrophoresis on pre- or post-stained slides did not prove promising. Polyacrylamide gel electrophoresis (slabs or tubes) of chromatographically prepared α-lipoproteins produced a number of lipoprotein fractions. Results varied with pH, concentration and degree of cross-linking of the gel. The effect of higher pH (above pH 8) upon resolution of HDL subfractions should be explored. There should also be an examination of the effect of pre-staining upon the separation of HDL into subfractions. Pre-staining may alter migration rates of lipoproteins and, thus, impede their resolution. Finally, an attempt should be made to resolve the α-lipoprotein fraction (isolated on an affinity column) by high performance liquid chromatography (HPLC). This method would permit the evaluation of several parameters in the effectiveness of resolving HDL subfractions.

REFERENCES

1. Schwertner, H.A. and Torres, Linda, et. al., Clinical Sciences Division, USAF School of Aerospace Medicine, Brooks AFB, Texas 78235-5000.

2. Miller, N.E. and Hammett, F., "Relation of Angiographically Defined Coronary Artery Disease to Plasma Lipoprotein Subfractions and Apolipoproteins," British Medical Journal, 282 (1981) 1741-44.

3. Howard, S.K., "Platelet-Mediated Cholesterol Accumulation in Cultured Aortic Smooth Muscle Cells," Science, 227 (1985) 1243-45.

4. Mills, F.J. and Marks, V., "Human Endocrine Responses to Acceleration Stress," Aviation, Space, and Environmental Medicine, 53 (1982) 537-40.

5. Vernikos-Danellis, J. and Dallman, M.F., "Hormonal Indices of Tolerance to +Gz Acceleration in Female Subjects," Aviation, Space, and Environmental Medicine, 49 (1978) 886-89.

6. Gordon, T., Castelli, et. al., "High Density Lipoprotein as a Protective Factor Against Coronary Heart Disease," American Journal of Medicine, 62 (1977) 707-14.

7. Kannel, W.B., et. al., "Cholesterol in the Prediction of Atherosclerotic Disease. New Perspectives Based on the Framingham Study," Ann. Intern. Med., 90 (1979) 85-91.

8. Tan, M.H., et. al., "Serum High Density Lipoprotein Cholesterol in Patients with Abnormal Coronary Arteries," Atherosclerosis, 37 (1980) 187-8.

9. Miller, N.E., et. al., "Relation of Angiographically Defined Coronary Artery Disease to Plasma Lipoprotein Subfractions and Apolipoproteins," Clinical Chemistry, 282 (1981) 1741-43.

10. Papadopoulos, N.M. and Kintzios, J.A., "Determination of Human Serum Lipoprotein Patterns by Agarose Gel Electrophoresis," Annl. Biochem, 30, (1969) 421-26.

TABLE 1. SERUM CORTISOL, CHOLESTEROL, AND TRIGLYCERIDE LEVELS OF SUBJECTS EXPOSED TO +Gz ACCELERATION

NO.	DATE	DAY	IDENTIFICATION	TOTAL CHOLESTEROL	CORTISOL	TRIGLYCERIDE
0	---	---	Pre-G Baseline	158	---	---
1	5-5-86	Monday	PGB-1G-11 Baseline	281	23.3	206
2	5-5-86	Monday	PGB-1G-11 Post G	294	22.3	223
3	5-7-86	Wednesday	PBG-1G-13 Post G	274	16.7	156
4	5-8-86	Thursday	PBG-1G-14 Post G	241	16.2	307
5	5-9-86	Friday	PBG-1G-15 Post G	252	12.3	117
6	5-12-86	Monday	PBG-1G-21 Baseline	281	17.8	332
7	5-12-86	Monday	PBG-1G-21 Post G	294	19.4	208
8	5-13-86	Tuesday	PBG-1G-22 Post G	277	22.2	238
9	5-14-86	Wednesday	PBG-1G-23 Post G	229	12.5	226
10	5-15-86	Thursday	PBG-1G-24 Post G	234	15.6	163
11	5-16-86	Friday	PBG-1G-25 Post G	273	10.3	273
00	---	---	Pre-G Baseline	148	---	62
12	6-2-86	Monday	PBG-2G-31 Baseline	186	12.3	102
13	6-2-86	Monday	PBG-2G-31 Post G	195	16.6	301
14	6-3-86	Tuesday	PBG-2G-32 Post G	194	6.8	113
15	6-4-86	Wednesday	PBG-2G-33 Post G	195	8.7	198
16	6-5-86	Thursday	PBG-2G-34 Post G	185	-	160
17	6-6-86	Friday	PBG-2G-35 Post G	180	9.4	159
18	6-9-86	Monday	PBG-2G-41 Post G	199	11.0	108
19	6-10-86	Tuesday	PBG-2G-42 Post G	205	13.8	240
20	6-12-86	Thursday	PBG-2G-43 Post G	185	-	95
21	6-13-86	Friday	PBG-2G-44 Post G	175	-	296
22	6-13-86	Friday	PBG-2G-45 Post G	170	12.3	179

a See test for +Gz acceleration protocol. Statistical comparison between serum cortisol and total cholesterol: First subject, $n = 11$, $r = 0.6138$, $p \angle 0.05$; Second subject, $n = 8$, $r = 0.103$, insignificant.

b mg/dl.

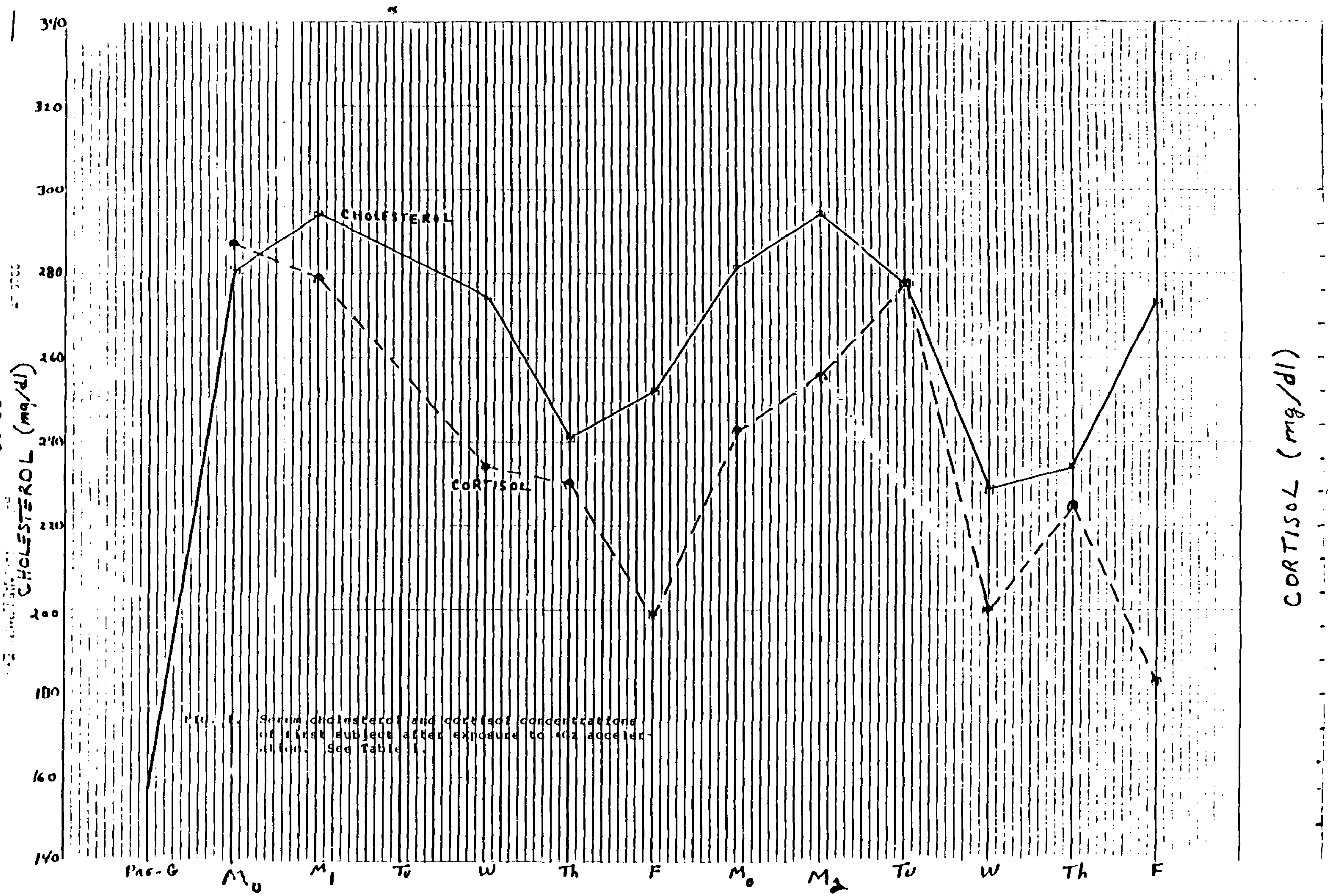

FIG. 1. Serum cholesterol and cortisol concentrations of first subject after exposure to +Gz acceleration. See Table 1.

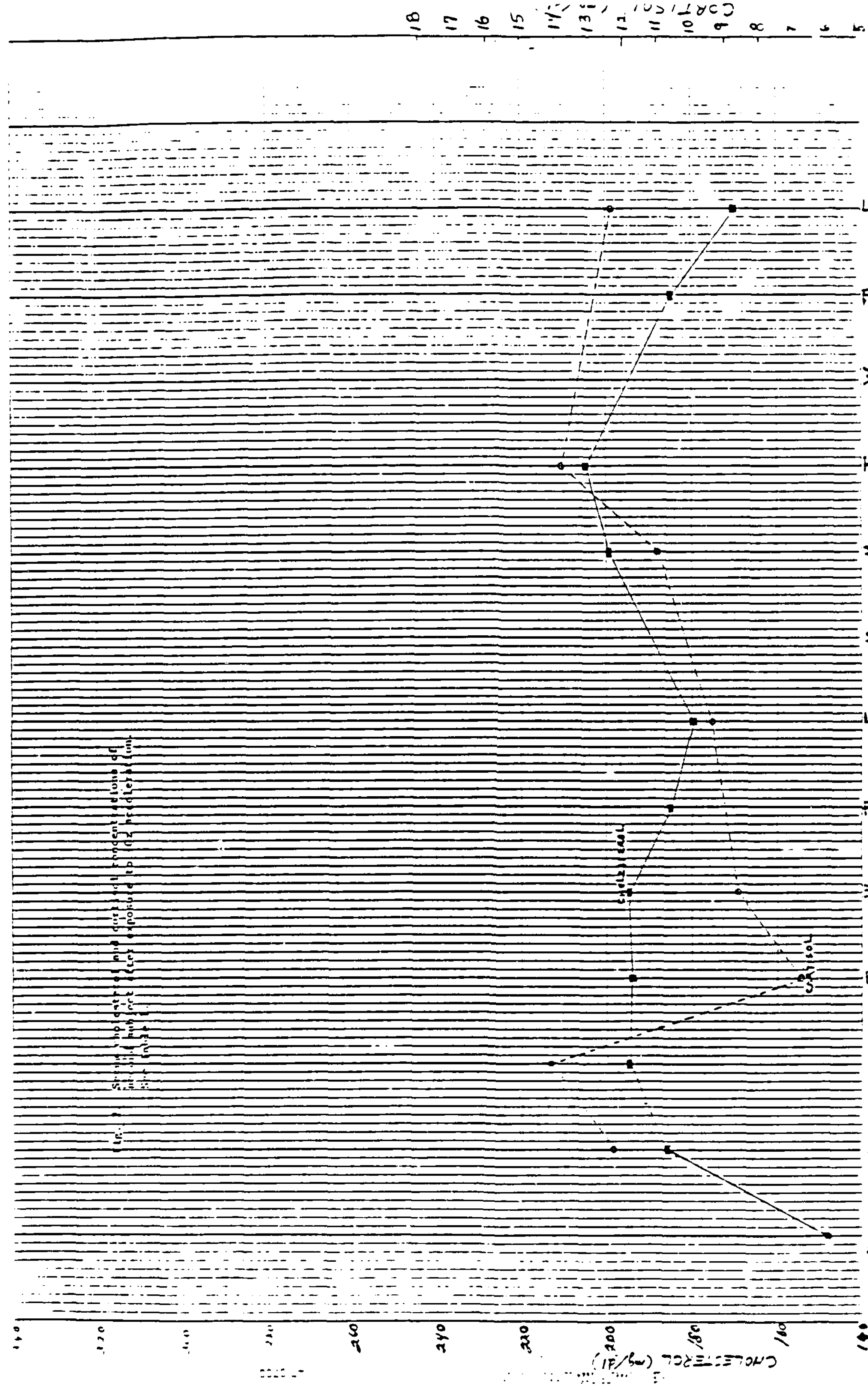

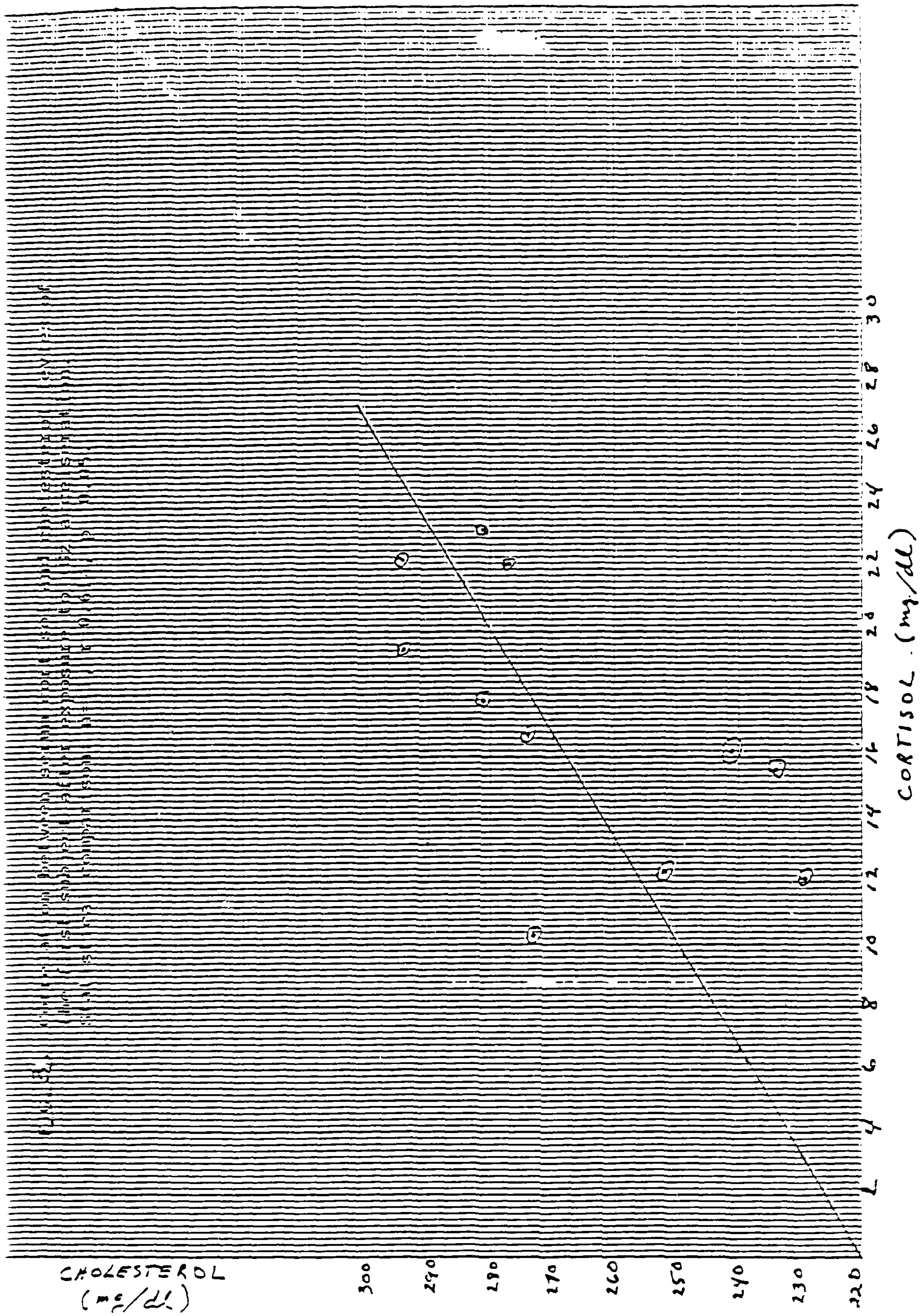
CHOLESTEROL (mg/dl)
300
290
280
270
260
250
240
230
220
CORTISOL (mg/dl)
2
4
6
8
10
12
14
16
18
20
22
24
26
28
30

1986 USAF-UES SUMMER FACULTY

RESEARCH PROGRAM/GRADUATE STUDENT

SUMMER SUPPORT PROGRAM

Sponsored by the

AIR FORCE OFFICE OF SCIENTIFIC RESEARCH

Conducted by the

Universal Energy Systems, Inc.

FINAL REPORT

Heart Rate Self-regulation: The Effects of Increasing Cognitive Demands

Prepared by: Victoria Tepe Nasman

Academic Rank: Graduate Student

Department and University: Department of Psychology, Northwestern University

Research Location: Air Force School of Aerospace Medicine
Brooks Air Force Base
Crew Performance Laboratory

USAF Researcher: Frederick J. Bremner

Date: September 3, 1986

Contract No.: F49620-85-C-0013

ACKNOWLEDGMENTS

The author, April G. Parker, would like to thank the Air Force Systems Command and the Air Force Office of Scientific Research for sponsoring the research conducted at the Air Force Wright Aeronautical Labs (AFWAL). The assistance provided by Mr. K. S. Mazdiyasni and his sincere interest and hospitality were greatly appreciated. The guidance provided by Mr. Ed Hermes and Mr. Mark Battison is also acknowledged. In addition, a special thanks is given to all the staff at AFWAL/MLLM for their helpfulness.

I. Introduction

The need for high temperature and high strength materials has led to increased research in the area of composite ceramics. These materials are used by the Air Force for defense applications and by United States industries for structural as well as non-structural applications.

Composite materials are made by adding a second phase in the form of particulates, whiskers, chopped fibers, or continuous fibers to a variety of ceramic matrices. It has been shown that the resulting composite material exhibits improved room and high temperature mechanical properties over the monolithic materials. Theoretically, the introduction of a second phase is perceived to increase the strength by blocking or deflecting cracks that are propagating through the material. Development of these materials should include a study of the role of the interface and thermostability of the matrix and the reinforcement.

Zirconia has been used for increasing the toughness, resistance to crack propagation, and the strength of ceramic materials. Mathematical models and explanations are still being developed to explain the toughening that results in these materials due to the presence of zirconia. The toughening mechanism involves the stress induced tetragonal to monoclinic phase transformation of dispersed zirconia particles or poly-crystals. Associated with this martensitic phase transformation is a volume change of three

to five percent which causes a compressive stress to be placed on the advancing crack, effectively reducing the energy of the crack and, thereby, toughening the material. Microcracking, another possible mechanism, involves the nucleation and extension of microcracks. Because the zirconia particles are constrained within the matrix, upon transformation, the matrix must deform due to the increase in volume of the transformed particles. This deformation is in the form of microcracks, which,as with the previous mechanism causes compressive stresses to develop and the energy of the crack to be reduced.(2)

The microstructures of zirconia toughened materials are outlined by Claussen (3). The most common microstructures are those that are partially stabilized by the addition of MgO, CaO, and Y_2O_3. CaO, MgO, and Y_2O_3 cause zirconia to transform almost completely from a cubic phase to a tetragonal phase upon cooling. However, according to Claussen (3) the effective grain size of the tetragonal zirconia particles, as far as toughening is concerned, must be less than 10 um. Materials developed using these toughening mechanisms have shown an increase in damage tolerance and strength. It is therefore, feasible that a fine grained tetragonal zirconia glass or glass ceramic should exhibit similar properties.

Generally, powders derived from metal alkoxides allow for high purity, a well dispersed zirconia phase, low fabrication temperatures, and control over grain size .

Depending on the method of preparation, the resulting powders may vary in degree of flocculation, particle size, particle morphology, and degree of agglomeration . The parameters that must be controlled to obtain a fine powder are the pH of hydrolysis, drying, and the process variable associated with drying and calcining procedures.

Mazdiyasni et. al.(4) has prepared several oxide powders from alkoxide precursors. In the zirconia system, a powder was prepared by alkoxide vapor decomposition and heat treated from 140°C to 1000°C. Mazdiyasni et. al. (4) concluded that submicron metastable cubic zirconia powder can be prepared by vapor decomposition of zirconium tertiary butoxide and that the transition from cubic to tetragonal phase occurs between 300 and 305°C for an approximately 5 nm particle size and from 250 to 270°C for a 8-10 nm particle size. The monoclinic transformation occurs gradually over the temperature range of 305 to 400°C in a 5 nm size powder.

Gels of zirconia have also be utilized to produce tetragonal zirconia powder. In the sol-gel method, an amorphous zirconia gel is allowed to form and then is heated until it transforms to tetragonal phase at 300°C.(5) Mazdiyasni (6) has also shown that zirconia prepared by the metal organic route requires a decreased amount of stabilizer when compared to classical processing. Mazdiyasni's (6) results show that 6m/o yittria heated for 1/2 hour at 800°C produces a stabilized zirconia comparable to that produced using the traditional method of 12% yittria heated 24 hours at 1800°C.

Klein and Garvey (7) have studied the preparation of silica gels produced by the alkoxide route. Silicon alkoxides do not hydrolize as readily as other alkoxides and thus, require an acidic or basic solution to form the sol. Silica gels can be dried to form a glass that shows optical transparency and no crystallinity. The reaction involved in forming these gels is a polymerization condensation reaction.

The zirconia-silica system has been studied by Nogami (8). The compositions studied contained up to 50 mole percent zirconia and were prepared by heating gels made by mixing solutions of zirconium isopropoxide, $Zr(OC_3H_7)_4$, and partially hydrolized silicon ethoxide, $Si(OC_2H_5)_4$. Porous gels resulted and, after removing the physically and chemically absorbed water, were converted into non-porous impervious glasses by low temperature sintering processes. The Zr^{4+} ions took up interstitial positions in the silica network, and subsequently, the density, refractive index, and hardness increased with an increase in the percentage of zirconia. In another study, Nogami and Tomozawa (9) prepared a composition of $3ZrO_2$ $2SiO_2$ and found that tetragonal zirconia was precipitated by heat treatments between 1000 and 1200^oC. The fracture toughness of the glass-ceramics increased with increasing crystallite size of the tetragonal zirconia and peaked at 50 $MN/m^{3/2}$.

The method utilized by the author of this summer project involves three steps. In the first step, the alkoxide liquids were thoroughly mixed. In the second step,

the mixture was acid hydrolized and in the final step, the mixture was neutralized to its hydroxide form. The hydroxides were vacuum dried to powders and vacuum hot pressed to obtain high density and finer grain sizes at relatively low temperatures.

The silica zirconia system was chosen because fused silica is a relatively high melting material, with a melting point of 1723°C. The simplicity of the system should enhance the study of the toughening and strengthening mechanisms.

II. Objectives

As previously indicated, the purpose of this research was to develop a SiO_2-ZrO_2 system that exhibits an increase in both toughness and strength. The procedure is unique because the materials were to be synthesized using alkoxide precursors. Powders were to be synthesized and the effect of changes in pH, drying and calcining treatments, and the mole percentages of zirconia were to be observed. Powders synthesized by the alkoxide method were to be characterized by x-ray diffraction, microscopy, and DTA/TGA studies. These powders were to be processed by vacuum hot pressing for varying times and temperatures and observations made on any improvements in the strength and the toughness. The pressed samples were to be characterized using x-ray diffraction and ceramographic studies. The information generated will hopefully assist in determining the

toughening mechanism.

III. Powder Synthesis

The alkoxide materials used for this study were purchased from the Alfa chemical company. The materials used were tetraethylorthosilicate (TEOS), and zirconium n-propoxide. In general the synthesis method used to produce the metal alkoxide in the laboratory is either from a base metal or metal chlorides and an alcohol. The general reaction is written as follows:

$$M + nROH \xrightarrow{\text{Catalyst}} M(OR)_n + (n/2)H_2 \qquad (1)$$

For a specific example, Zr n-propoxide could be synthesized from anhydrous metal chloride and an alcohol. The reaction is as follows:

$$ZrCl_4 + 4C_3H_7OH + 4NH_3 \xrightarrow{5^\circ C} Zr(OC_3H_7)_4 + 4NH_4Cl \qquad (2)$$

It is to be noted, that due to the moisture sensitivity of metal alkoxides, the anhydrous condition for preparation must be maintained prior to their decomposition. Any moisture present in the reaction causes premature hydrolysis and, subsequently, stops the reaction.

The alkoxide solutions were then hydrolized using a 10% solution of water and nitric acid. The solution was continuously stirred while the hydrolysis was completed. The general reaction for hydrolysis is:

$$M(OR)_n + H_2O \rightarrow MO(OR)_{n-2} + 2ROH \qquad (3)$$

Initially, the hydrolized materials were allowed to stand overnight, but these solutions gelled and so it was necessary to redisperse them with a blender before

neutralization. The procedure was modified by immediately neutralizing the acid solution with NH_4OH to a pH of approximately 8.5. Also, small samples were made with a pH of 4 and 7. The powder samples processed with lower pH's tend to gel more easily and produce larger, more agglomerated powders. Microscopy and BET analysis will be done later to confirm these results.

The materials were then rotovapped to remove liquids, vacuum dried at 125°C for 6 hours, calcined at 300°C, ground, and re-calcined at 600°C. Since silica has a tendency to hold water at high temperature, it was necessary to calcine the powders at 300°C to produce a crisp powder that did not stick together during grinding. The effect of varying the calcining temperature was not investigated.

The as prepared and calcined at 600°C powders were amorphous as indicated by x-ray diffraction. A TGA showed a 31% weight loss from the dried powder as a result of the removal of chemically and physically absorbed water. The DTA did not show any transformations on heating or cooling within the temperature range of 25 to 1400°C.

V. Vacuum Hot Pressed Materials

A major part of this research project concerned vacuum hot pressing. Five grams of material were loaded into a one inch graphite die and pressed at 24.13 MPa and varying temperatures. Initially all the samples consistently cracked into quarters and it was necessary to determine a method of processing to avoid cracking. The ramp and

cooling rates, the processing temperatures and pressures, and the soak time were all varied to determine the processing variable most likely to be causing the cracking. Thermal shocking was eliminated as the cause of the cracking by heating a sample in a molybdemum furnace and rapidly cooling. The processing used to produce solid samples was a rapid heating rate and high pressure. It is believed that the cracking was a result of a rapid sintering process that occurs between 1100 and 1200°C, but further research was not done to verify this theory.

Several samples were then pressed at varying temperatures to examine the effect of temperature on crystallinity. The samples varied in color, amount and type of crystallization. These results are summarized in Table I.

Table I. Crystalline Phases Present

Temperature °C	Sample Color	Phases Present	Peak Description
1100	White	-	Amorphous
1350	Translucent	T	Broad
1375	Transparent	T SiO_2 $ZrSiO_4$	Sharp Moderate Intensity Strong
1450	Translucent	$ZrSiO_4$ T	Sharp and Strong Moderate and Broad
1550	Translucent	$ZrSiO_4$ T SiO_2	Very Strong Strong Moderate

T-Tetragonal Zirconia

These samples varied slightly in composition which may account for some of the changes in the phases present.

Tetragonal zirconia was present from 1350 - 1450°C but as temperature was increased zircon becomes the predominant phase.

After polishing the samples to 3 um to remove the graphoil, indentation toughness tests were performed on a limited number of samples. However, these indentations were badly chipped so toughness calculations could not be made accurately. In order to alleviate the problem, the samples were then annealed at 1000°C to relieve surface stresses. A Vicker's indentation tester was used with a load of 1.5Kg. Toughness calculations were done using the formula developed by Evans (10) and is as follows:

$$K_{IC} = 0.055a^{1/2}(1/a)^{-1/2} \qquad (4)$$

The toughness tends to decrease with processing temperatures, but this trend is still being verified because of the limited number of samples that could be prepared and tested before the ten week period allotted for research ended. The average toughness and hardness values are found in Table II along with densities.

After polishing the surface, the monoclinic phase did not appear in x-ray diffraction patterns and so, the toughness of these materials may not be a result of the zirconia phase transformation. An electron microscopy study is needed to determine the zirconia particle size in these glasses. If the particle sizes are too small, then it may be necessary to heat treat the samples to induce grain growth to allow for phase transformation to occur. The

densities of the 1350 to 1550^{o}C disks averages at 93% of theoretical density (2.37g/cc).

Table II. Average Density, Toughness, and Hardness Values

Temperature ^{o}C	Density g/cc	Hardness GN/m^{2}	Toughness MN/m$^{3/2}$
1100	1.27	-	-
1350	2.26	11.71	2.33
1450	2.17	8.29	1.79
1550	2.20	5.55	1.46

Samples were also prepared with 1%, 5%, 10%, and 15% zirconia. These were all processed at 1550^{o}C and 24.13 MPa. The samples changed in color from white to almost transparent to translucent with an increase in the amount of zirconia present. The major zirconia phases present also changed with the tetragonal zirconia phase being the most predominant in the 5% samples. Based on the preliminary results obtained, it is reasonable to assume that at lower concentrations of zirconia, the zirconia is incorporated into the silica network and at 5% there is enough zirconia present to form tetragonal zirconia, at high percentages of zirconia there is excess zirconia present and it again forms zircon. However it must be emphasized that, the hot pressing conditions do not allow the system to achieve equilibrium so the phases present are not consistent with the phase diagram. Indentations were not completed on these samples.

Finally, microscopy of these materials needs to be done

as was indicated previously. These materials have shown promise, but much more work is required before conclusive results can be obtained. The bulk of the unfinished work will be completed by the author at the Ohio State University and presented in a master's thesis.

VI. Conclusions

Although work on this material is incomplete the following has been demonstrated.

1. The alkoxide route allows for the production of materials that contain a tetragonal zirconia phase without the addition of a stabilizer.

2. The crystalline phases present have been identified as zircon, zirconia, and minor amounts of alpha cristobalite.

3. These materials can be vacuum hot pressed to near theoretical densities.

4. The amount and type of crystallinity in the samples can be controlled by varying the processing parameters and the amount of zirconia.

VII. Recommendations

1. Further study is needed to characterize the starting powders.

2. Indentations and four point bend tests need to be performed on these materials to determine strength and toughness.

3. Microscopy of the crystalline phases, indentations and fractography needs to be completed.

4. A sintering study should be done between 1000 and 1200°C.

VIII. References

1. Morey, G., Properties of Glass, Reinhold Publishing Corp., pp.224-225 (1954).

2. Claussen, N., "Strengthening Strategies for ZrO_2-toughened Ceramic at High Temperatures," Materials Science and Engineering, 71, pp. 23-38 (1985).

3. Claussen, N., "Microstructural Design of Zirconia Toughened Ceramics (ZTC)," Advances in Zirconia Technology, J. Am. Ceramic Soc., pp. 325-351 (1983).

4. Mazdiyasni, K. S., Lynch, C., and Smith, J., "Metastable Transitions of Zirconium Oxide Obtained from Decomposition of Alkoxides," J. Am. Ceramic Soc., 49, pp. 286-287 (1966).

5. Osendi, M., Moya, J., Serna, C., and Soria, J., "Metastability of Tetragonal Zirconia Powders," J. Am. Ceram. Soc., 68, pp. 135-139 (1985).

6. Mazdiyasni, K. S., "Chemical Synthesis of Single and Mixed Phase Oxide Ceramics," Mat. Res. Soc. Symp. Proc., 32, pp. 175-186 (1984).

7. Klein, L., and Garvey, G., "Monolithic Dried Gels," J. Non-Crystalline Solids, (1982).

8. Nogami, M., "Glass Preparation of the ZrO_2 SiO_2 System by the Sol Gel Process from Metal Alkoxides, J. Non-Cryst. Solids, 69, pp. 415-423 (1985).

9. Nogami, M., and Tomozawa, M., "ZrO_2-Transformation-Toughened Glass-Ceramic Prepared by the Sol-Gel Process From Metal Alkoxides", J. Am. Ceram. Soc., 69, pp. 99-102 (1983).

10. Evans, A. G., and Charles E. A., "Fracture Toughness Determination by Indentation," Discussions and Notes, J. Am. Ceram. Soc., pp. 371-372 (1976).

1986 USAF-UES Summer Faculty Research Program/

Graduate Student Summer Support Program

Sponsored by the

Air Force Office of Scientific Research

Conducted by the

Universal Energy Systems, Inc.

Final Report

On the Measurement of Variables Impacting the Performance of Flightline Maintenance Crews

Prepared by:	Deborah L. Parker
Academic Rank:	Graduate Assistant
Department and University:	Department of Psychology Tulane University
Research Location:	Air Force Human Resources Laboratory, Combat Logistics Branch, Wright-Patterson AFB
USAF Research:	Cheryl Batchelor
Date:	August 25, 1986
Contract No.:	F49620-85-C-0013

On the Measurement of Variables Impacting the Performance of Flightline Maintenance Crews

by

Deborah L. Parker

ABSTRACT

Background research was conducted related to an ongoing project concerned with variables that potentially will impact the performance of flightline maintenance crews. A literature review was conducted in order to determine whether appropriate methods exist for the measurement of variables that are determinants of performance on the flightline. Literature on vigilance, information processing, individual differences, performance, and behavioral measures was reviewed for this purpose. The review indicated that certain personality variables and group characteristics are undoubtedly related to effectiveness and should be considered in relation to the performance of flightline maintenance crews.

Acknowledgments

I would like to thank the Air Force Systems Command and the Air Force Office of Scientific Research for sponsorship of my research. I would also like to express to AFHRL/LRC my appreciation for the provision of an appropriate and enjoyable environment in which to do my work.

I would like to thank Colonel Donald C. Tetmeyer, Bertram W. Cream, and Robert C. Johnson for giving me the opportunity to gain important experience in conducting research with the United States Air Force. I extend a special thanks to Cheryl Batchelor for her continuous provision of valuable guidance, support and encouragement throughout the summer.

I. Introduction

I received my M.A. from Wake Forest University, studying general experimental psychology. I am currently pursuing a Ph.D. at Tulane University, studying industrial/organizational psychology. Recently, I have been studying psychological measurement, as part of my curriculum. My research has focused on variables that potentially modify work performance, for example, workload variability.

Robert C. Johnson and Cheryl Batchelor are currently initiating a research project directed toward the performance of flightline maintenance crews. Little, if any, research has been directed at personnel other than those directly confronted with combat. It is now necessary to attend to the needs of Air Force support personnel, who may, in future conflicts, be faced with more direct combat conditions than has been the case in the past.

Because of the particular research I was conducting at Tulane and my experience with measurement in psychology I was assigned to this project. The objective was for me to do research in support of the overall project by conducting a review of potential methods of measurement of variables of interest, and to provide an organizational perspective on an appropriate approach to the research.

II. Objectives of the Research Effort

The overall objective of the research project on flightline maintenance crews is to provide for effective performance on the part of support personnel faced with difficult combat conditions. The role of the present researcher was to provide project personnel with a subset of necessary background information relevant to psychological and criterion assessment.

The researcher's individual objectives were:

1. The general investigation of factors that may impact manpower planning in the flightline maintenance environment.

2. To conduct a literature review, looking at relevant measurement techniques in areas of individual differences such as cognitive ability, processing, and personality. A review of potential criterion measures and the assessment of extraneous variables was also relevant to the project for the provision of effective flightline maintenance and sortie generation rates.

3. To provide for project personnel recommendations for completing background research, and approaching the research problem at an appropriate level of analysis from an organizational perspective.

III. The Flightline Maintenance Environment

In order to focus on relevant areas for the literature review, it was necessary, first, to take the time to learn about the basic structure and environment of flightline maintenance crews. The first two weeks of the assignment was spent interviewing with former maintenance officers, who explained how each wing is structured, and separated into a Component Repair Squadron, an Equipment Maintenance Squadron, and an Aircraft Generation Squadron. The aircraft generation squadron structure was examined in detail because these units perform most of the work directly at the flightline.

An aircraft generation squadron is further divided into three aircraft maintenance units (AMU's), each of which is supposed to be a self-contained unit with the ability to keep as .gned aircraft fully maintained and operational. Eacl. AMU includes a number of personnel who are repair specialists, weapon specialists, or crew chiefs, all of whom are supervised by an officer in charge.

Each type of specialist in an AMU has specific duties in relation to weapons, repair, or inspections. Daily routine activities were described and examples given of typical communication and environmental characteristics on the flightline. Most importantly, the possibility was explained that

much more severe conditions could arise for these particular personnel in future conflicts than has occurred in past conflicts wherein maintenance personnel operated from very stable bases.

This background information provided for the determination of the types of variables that potentially could impact manpower planning, including personnel selection, and crew performance in the flightline maintenance environment. At this point, attention was directed to the study of paradigms used and measurement techniques available for assessing the many different variables that operate in this complex organizational structure.

Methods of personnel selection, individual characteristics, environmental and combat conditions, and training all can have a major influence upon the final performance of an aircraft maintenance unit. Hence, the coverage of material was limited to psychological literature and other literature specifically related to the combat environment.

IV. Literature Review: Approach and Conclusions

To list all books and articles covered and to give a detailed account of this literature review would carry this report well beyond its limitations. Thus, the approach to the area, will be briefly explained, with a description of the areas in which material was

covered. Conclusions as to whether or not such information is relevant to the task at hand are included.

Initially, the researcher reviewed some material covering the combat environment and leadership structure so as to become familiar with psychological issues related to military operations. An extensive search was made for research that had been conducted specifically on support and maintenance personnel.

Almost no research has been directed specifically at military support personnel. Most psychological research has focused on those who are most active in combat. The performance of pilots, marine and army ground forces and other personnel who actually work on the battle front has been studied extensively. However, this left no exemplary paradigms or assessment techniques for research on support personnel.

At this point, following examples of literature on aircrew and pilot performance, the literature on individual differences was reviewed to determine whether or not relevant paradigms and measures had been used in these areas. Many of the studies with pilots had used vigilance tasks as dependent measures. These tasks were used to indicate mental workload, reactions to overload, the durability of attentional processes,

quality of decision-making and other hypothesized cognitive processes (Broadbent, 1958).

In as much as flightline maintenance crews need to troubleshoot, perform inspections, and notice tiny flaws in equipment, their activities are similar to a vigilance task. Since this was a potential approach to performance measurement, or possibly prediction, a considerable amount of time was spent reviewing vigilance and information processing literature.

Tracking tasks, signal detection tasks, matching signals to response, and the measurement of mental workload by secondary or combined tasks were used to assess the effects of an enormous range of independent variables. (Williges & Wierwille, 1979; Ogden, Levine, & Eisner, 1979). Mental workload was discussed repeatedly. The effects of extraneous variables such as noise, heat and time of day were also measured using vigilance tasks. However, the nature of the paradigms, and the physical aspects of the experimental scenarios are not at all practical for highly mobile people. The researcher was led to conclude that perhaps a vigilance task could be included in an assessment battery for personnel selection as indicative of a certain level of information processing ability. However, such vigilance tasks are not really appropriate for researchers to employ while examining behavior and performance on the flightline.

Throughout the literature on combat performance. several authors make mention of individual or personality characteristics that appear to be related to performance. The literature that was reviewed implied that there are several characteristics of individuals and group dynamics that can contribute to effective performance in the combat environment. The most consistent reported result indicated that those individuals with an internal as opposed to an external locus of control were likely to adapt to group functioning during combat (Batlis, 1980).

Other variables that could provide useful information if measured are organizational commitment, social conformity vs. rebelliousness, emotional stability vs. neuroticism, trust vs. defensiveness, and possibly activity vs. lack of energy. These variables are indicative of some of the psychological variables that many experts in the area of combat effectiveness have determined can be even more important than physical ability in terms of the effectiveness of a unit. (Sarkesian, 1980; Kanungo, 1979; Bandura, 1977).

Group cohesion and morale are undeniably a most important factor in developing an effective work unit(Sarkesian,1980; Moos,1974; Kobasa,1983). Hence, the measurement of such variables with scales that are valid at an acceptable level could be helpful in researching flightline maintenance crews, especially

when one considers the fact that the emphasis is on the performance of the group.

During the remainder of the literature review, attention was turned to other behavioral measurement techniques that are not specifically related to vigilance or information processing theory. One possible method of assessment in the area of flightline maintenance performance is the use of Behaviorally Anchored Rating Scales based on the critical incidents technique (Schwab & Heneman, 1975). This technique, although subjective, is fairly well standardized and could be efficient given trained observers.

Another possibility would be to use a different form of behavioral observation with trained observers, in order to assess the effectiveness of a given AMU. Scott (1967) discusses the development of semantic differential scales as measures of morale, which is another possibility as part of an assessment battery. However, reliability and validity are likely constraints when such methods are employed. Some other more direct performance measures do exist, which, given some development specifically for this project, could be useful.

Interviews, questionnaires and subjective performance appraisal by superiors are frequently considered in the literature. However, these techniques have notoriously low validity and reliability

(Guion ,1965; Bouchard, 1976). Some more objective measures of performance are latency to detection of a given stimulus, the ratio of actual output to criterion levels of output, and the quantity or quality of production. The latter could possibly apply to sortie production rates. Other performance criteria that may be of use are the number and type of movements unrelated to task, variability in cycle time, misses, "blocks", or fumbles in long cycle times, and reaction time to a secondary task (Sharit & Salvendy, 1982).

Of the performance measures listed above, reaction time, or some measure of the rate of sortie generation would be the most convenient measure of performance on the flightline. The measurement of sortie generation rate in response to manipulations of different independent variables would be an index of efficiency to some degree. It would also, however, be beneficial to try to develop some other indices of the quality of performance through a detailed behavioral analysis of the work that is done on the flightline.

V. Recommendations

1. At this point, the literature review that was initiated cannot be considered complete. USAF personnel will be provided with a complete list of all books and articles covered and those noted but not thoroughly reviewed. It is also suggested that the Psychological

Abstracts be reviewed carefully from 1982 through 1986 in order to assure that all recent material that could be of use is available for review. More relevant or important material appearing in the extensive bibliography that has been compiled will be marked so that it can be obtained by project personnel. The full bibliography is not included in this report because it alone would exceed space limitations.

2. Concerning an appropriate approach to research regarding the performance of flightline maintenance crews, it is suggested that individual psychological characteristics and measures related to group dynamics be seriously considered as indices of potential effectiveness. Several authors repeatedly stress the importance of group cohesion, involvement and morale as essential to combat effectiveness. It would be most prudent to attempt to develop some valid indices of these characteristics specifically for this project. Measures of performance, or lack of it, without indices of potential causal factors would yield little information that would be relevant to the development of a solid training program.

7. Kobasa, S.C., and M.C. Puccetti, " Personality and Social Resources in Stress Resistance," Journal of Personality and Social Psychology, 45, 1983, pp. 839-850.

8. Moos, R.H., " Psychological Techniques in the Assessment of Adaptive Behavior," In G.V. Coelho, D.A. Hamburg, and J.E. Adams, (Eds.), Coping and Adaptation, New York: Basic Books, 1974.

9. Ogden, G.D., J.M. Levine, and E.J. Eisner, " Measurement of Workload by Secondary Tasks," Human Factors, 21, 1979, pp. 529-548.

10. Sarkesian, S.C., Combat Effectiveness: Cohesion, Stress, and the Volunteer Military, Beverly Hills, CA: SAGE Publications, 1980.

11. Schwab, D.P., and H.G. Heneman, III, " Behaviorally Anchored Rating Scales: A Review of the Literature," Personnel Psychology, 28, 1975, pp. 549-562.

12. Scott, W.E., Jr., " The Development of Semantic Differential Scales as Measures of 'Morale'," Personnel Psychology, 20, 1967, pp. 179-198.

References

1. Bandura, A., "Self-efficacy: Toward a Unifying Theory of Behavioral Change," Psychological Review, 84, 1977, pp.191-215.

2. Batlis, N.C., "Job Involvement and Locus of Control as Moderators of Role-Perception/Individual-Outcome Relationships," Psychological Reports, 46, 1980, pp. 111-119.

3. Bouchard, T.J., Jr., "Field Research Methods: Interviewing, Questionnaires, Participant Observation, Systematic Observation, Unobtrusive Measures," In M.D. Dunnette, (Ed.), Handbook of Industrial and Organizational Psychology, Chicago: Rand McNally, 1976.

4. Broadbent, D.E., "Noise, Paced Performance, and Vigilance Tasks," British Journal of Psychology, 44, 1953, pp. 295-303.

5. Guion, R.M., Personnel Testing, New York: McGraw-Hill, 1965.

6. Kanungo, R.N., " The Concepts of Alienation and Involvement Revisited," Psychological Bulletin, 86, 1979, pp. 119-138.

13. Sharit, J., and G. Salvendy, " Occupational Stress: Review and Reappraisal," Human Factors, 24, 1982, pp. 129-162.

14. Williges, R.C., and W.W. Wierwille, " Behavioral Measures of Aircrew Mental Workload," Human Factors, 21, 1979, pp. 549-574.

1986 USAF-UES Summer Faculty Research Program/

Graduate Student Summer Support Program

Sponsored by the

Air Force Office of Scientific Research

Conducted by the

Universal Energy Systems, Inc.

Final Report

Image Algebra Preprocessor and Image Algebra Executive

Prepared by: Werner Kurt Perry

Academic Rank : Bachelor of Science in Engineering

Department and

University : Computer and Information Science Department, 512 Weil Hall, University of Florida

Research Location: AFATL/ASE, Armament Division,

Eglin Air Force Base.

USAF Researcher: Henry Neal Urquhart

Date: August 1, 1986

Contract No: F49620-85-C-0013

Image Algebra Preprocessor and Image Algebra Executive

by

Werner Kurt Perry

ABSTRACT

The image processing field is characterized by very complex algorithms that do not translate well into any conventional programming language. It is for this reason that Dr. Gerhard X. Ritter of the University of Florida has been researching the feasibility of an Image Algebra. Dr. Ritter has isolated a heterogeneous Image Algebra consisting of several different types of operands as well as different operations among those operands. The Image Algebra Preprocessor incorporates these operands and operations to create a image processing environment that allows the user to create efficient algorithms rapidly. The Image Algebra Preprocessor was written in FORTRAN and produces FORTRAN-77 from a FORTRAN-like code. The Image Algebra Executive software allows user to implement Image Algebra Preprocessor algorithms on groups of images without having to constantly interact with the software.

ACKNOWLEDGMENTS

This work was supported by the United States Air Force Armament Division and the Air Force Office of Scientific Research. I would like to thank them for this unique opportunity to do research in such a supportive atmosphere. I would also like to thank Dr. Sam Lambert and Mr. Neal Urquhart of the Air Force Armament Laboratory for their continued support and encouragement.

I. Introduction

I am presently working on my M.S. in Engineering at the University of Florida in the area of image processing and computer languages. I received my B.S. in Engineering from the University of Florida. As an undergraduate I worked on an autonomous bridge detection algroithm that was developed for the Armament Laboratory at Eglin AFB. As a graduate I have been working on an Image Processing Language based on the Image Algebra (IA) as defined by Dr. Gerhard X. Ritter of the University of Florida.

The Armament Laboratory has an Image Processing Laboratory where seeker research is carried out. Because of my background in image processing and the research into an IA Preprocessor I was assigned to the Armament Laboratory at Eglin AFB to continue my research into the IA Preprocessor.

II. Objectives of research effort.

The overall objective of the IA Preprocessor research was to create an algorithm developement environment that would facilitate image processing development. Another goal was the design of an Image Algebra Executive software system to facilitate the implementation of the algorithms developed with the IA Preprocessor.

My individual goals were:

1. Finish coding the IA Preprocessor.
2. Remove any bugs in the IA Preprocessor.
3. Create an Image Algebra Executive (IAX) system.
4. Integrate the IA Preprocessor and the IAX.

III. Image Algebra (IA) Preprocessor (VAX/VMS Version)

The program F85.FOR and the command file F85.COM together make up the IA Preprocessor. This preprocessor maps FORTRAN like code into FORTRAN-77. This FORTRAN like code includes most of the IA operations as defined Dr. Gerhard X. Ritter of the University of Florida. Because of the lack of special characters on most terminals, IA operation symbols were chosen from the ASCII character set. A list of the IA operations and their preprocessor counterparts is listed in section IV. You will notice that the preprocessor does not implement the template & template operations, this is the next major addition that should be considered for the IA preprocessor. For the definition of each operation represented below and for a full explanation of the IA see [1], for a full explanation of the IA preprocessor see [2].

IV. Image Algebra Preprocessor Operations

Given: Images A,B , Template T, and Scalar k.

	Image & Scalar	Image & Image
ADDITION	A + k	A + B
SUBTRACTION	A - k	A - B
MULTIPLICATION	A * k	A * B
DIVISION	A / k	A / B
EXPONENTIATION	A ** k	A ** B
DOT PRODUCT	A # k	A # B
PSEUDO-INVERSE	A ~ k	A ~ B
CHARACTERISTIC	A <= k	A <= B

	Image & Template
CIRCLE PLUS	A + T
CIRCLE MAXIMUM	A # T
CIRCLE MINIMUM	A % T
SQUARE MAXIMUM	A ! T
SQUARE MINIMUM	A ^ T

V. Example of an Image Transformation Expressed in Terms of the Image Algebra

The Sobel edge detection is a good example to introduce the reader to the use of the IA preprocessor and the capabilities of the IA. The Sobel edge detection algorithm is as described herin. Given an image, to use the Sobel to highlight the edges, one can convolve the image with two 3x3 arrays (Fig 1 and Fig 2). The result of convolving the image with these two arrays is two new images which must be combined to form the final image. These are the types of convolutions that the IA was designed to handle efficiently. In the IA the images remain images and the 3x3 arrays, or any other configuration for that matter, become what are known as variant or invariant templates. The IA equation for the Sobel edge detection follows:

$$\left((\text{IMAGE circleplus T})^{2} + (\text{IMAGE circleplus S})^{2} \right)^{1/2}$$

-1	0	1
-2	0	2
-1	0	1

Fig 1.

-1	-2	-1
0	0	0
1	2	1

Fig 2.

VI. Image Algebra Preprocessor Code

Coding an image transformation that has been expressed in terms of the IA into code the preprocessor understands is analogous to coding an algebraic formula into code that FORTRAN understands. The following will be a step by step example of how to code IA expressions into preprocessor code. This example will be continued with the Sobel edge detection image transformation.

The first thing to be done is to inform the preprocessor of the storage locations that you wish to reserve. To reserve space for an image, you tell the preprocessor the type, size and name of the image. There are four basic FORTRAN types (Integer, Real, Complex, Double Precision). The size must be a two dimensional array of arbitrary size (i.e. 512x512, 120x360, etc). The name is any valid FORTRAN name (i.e. Six or less characters and numbers, and must start with a letter). An example of image declarations follow:

```
INTEGER IMAGE(100,100), BARRAY(512,512)
REAL    X(100,100), Y(100,100)
```

Notice these declarations are exactly the same as two-dimensional FORTRAN array declarations.

Templates are the only new data structures defined by the Image Algebra, since these are not of an existing FORTRAN data type you must inform the preprocessor of your desire to use templates. Temlates have two characteristics you must inform the preprocssor of: first, you need to tell the preprocessor the type (Integer, Real, Complex, Double Precision), and second you must tell the preprocessor if the template is configuration

variant or invariant. Variant or invariant is decided on the basis as to whether the template configuration and template weights remain constant or not over the entire image. The following are examples of declarations of a real invariant template invar1 and integer variant var1 and var2.

```
REAL INVARIANT INVAR1
INTEGER VARIANT VAR1, VAR2
```

These declarations are very similir to scalar variable declarations in FORTRAN, the only difference is the keywords [IN]VARIANT. The generic template declaration follows:

```
[TYPE]  [IN]VARIANT  NAME1 [ {,NAME#} ]
```

This simply states that type type is optional [TYPE] (if omitted, FORTRAN default type is assumed (Real A-H:O-Z, Integer I-N) and the configuration is either variant or invariant, and it is followed by one or more names separated by commas. An example follows:

```
REAL VARIANT FIRST, SECOND
COMPLEX INVARIANT CMPLXX
```

Up to now we have only informed the preprocessor of our intentions, at this point the preprocessor has a symbol table containing the image and template names and their respective sizes and types. After informing the preprocessor of all the declarations we are now ready to write statements, the core of the IA preprocessor. Any valid FORTRAN statement is allowed by the preprocessor, with a few exceptions.

FIRST, you must never use continuation lines on any IA statements.

SECOND, when passing an array to a funcition you should pass

the first element and not the entire array. This arises from the fact that the preprocessor will try to apply the function pointwise to the entire array.

Example:

```
SUM = MYFUNC(ARRAY)
```

sould be

```
SUM = MYFUNC(ARRAY(1,1))
```

If you wanted to apply MYFUNC to the entire image (array) pointwise you would use the former, if you wished to pass the array you would use the latter.

THIRD, only one Image & Template operation per line.

Example:

The IA equation

$$ARRAY2 = (ARRAY1 \text{ circleplus } T)^2 + (ARRAY1 \text{ circleplus } S)^2$$

would be coded into the preprocessor code as folows:

```
TEMP1 = ARRAY1 + T
TEMP2 = ARRAY1 + S
ARRAY2 = TEMP1 ** 2 + TEMP2 ** 2
```

Notice Image & Image operations may be arbitrarily complex, also notice that the preprocessor takes care of all looping conventions so that the user is relieved of the burden of loops and loop variables.

The last thing you need to know is how to define teplates. The template definition is much the same as a FORTRAN function or subroutine declaration, in fact the templates are implemented as FORTRAN subroutines. The first line in a template definition is the template header. Its generic form is as follows:

```
[TYPE]  [IN]VARIANT  TEMPLATE NAME[(PARM1 {,PARM#})]
```

This means it, a template definition, has a FORTRAN type, is either configuration variant or invariant, the name is any valid FORTRAN name, and the name is followed by zero or more parameters separated by commas and enclosed by parenthesis. Next you have your standard FORTRAN declaration block followed by the code to implement the template. This is the section where the template configuration and values are assigned. Available to the user is the image points X, Y which hold the following relation to the image.

X-1, Y-1	X-1, Y	X-1, Y+1
X , Y-1	X, Y	X , Y+1
X+1, Y-1	X+1, Y	X+1, Y+1

Fig 3.

Templates can have as many elements as you wish and their configuration can be as arbitrary as you like. When you reach the physical end of a template definition you signal the termination with the 'END' statement.

VII. Example of Coding the Sobel Edge Detection

Step 1. Translate the IA expression into code for the IA preprocessor.

IA expression:

$$[\ (\text{IMAGE circleplus } T)^{2} + (\text{IMAGE circleplus } S)^{2}\ ]^{1/2}$$

IA preprocessor code:

```
TEMP1 = IMAGE + T
TEMP2 = IMAGE + S
RESULT = (TEMP1 ** 2 + TEMP2 ** 2) ** 0.5
```

Notice that the few temporary images were used, this happens

because the preprocessor can only handle one Image & Template operation per line. You must remember to declare any temporary images (arrays) that you use.

Step 2. Go back and declare all the images (arrays) that are used in your program. Assume for the time that the images are 100x100 integer images, and that the resultant image is real. The following declarations inform the preprocessor so.

```
INTEGER IMAGE(100,100), TEMP1(100,100), TEMP2(100,100)
REAL    RESULT(100,100)
```

Step 3. Declare any templates you use in the program. Remember, in the Sobel edge detection transform the templates are integer valued and invariant configuration as in Fig 1 and Fig 2. The following code informs the preprocessor so.

```
INTEGER INVARIANT S, T
```

Step 4. Define any templates that you used in the program. For this example see Fig 1 and Fig 2 for the configuration and weights. The definition for template T follows:

```
INTEGER INVARIANT TEMPLATE T

T(X-1, Y-1) = -1
T(X-1, Y 1) =  0
T(X-1, Y+1) =  1
T(X  , Y-1) = -2
T(X  , Y  ) =  0
T(X  , Y+1) =  2
T(X+1, Y-1) = -1
T(X+1, Y  ) =  0
T(X+1, Y+1) =  1

END
```

and the template definition for template S:

```
INTGER INVARIANT TEMPLATE S

S(X-1, Y-1) = -1
S(X-1, Y  ) = -2
S(X-1, Y+1) = -1
S(X  , Y-1) =  0
S(X  , Y  ) =  0
S(X  , Y+1) =  0
S(X+1, Y-1) =  1
S(X+1, Y  ) =  2
S(X+1, Y+1) =  1

END
```

Step 5. Enter the above steps (1-4) into a file using an editor. This is done the same way you would edit a FORTRAN file. Remember the order: image declarations, template declarations, code, and template definitions. The following is the preprocessor code for the Sobel image transformation.

```
C**
C**  EXAMPLE OF SOBEL EDGE DETECTION ALGORITHM
C**
        INTEGER IMAGE(100,100), TEMP1(100,100), TEMP2(100,100)
        REAL    RESULT(100,100)
        INTEGER INVARIANT S, T
C**
C**  USER SUPPLIED INPUT GOES HERE
C**
        CALL INPUT(IMAGE)
C**
C**  IMAGE ALGEBRA FORUMLA:
C**                           2                        2  1/2
C**     ((IMAGE circleplus T)  +  (IMAGE circleplus S)  )
C**
        TEMP1 = IMAGE + S
        TEMP2 = IMAGE + T
        RESULT = (TEMP1 ** 2 + TEMP2 ** 2) ** 0.5
C**
C**  USER SUPPLIED OUTPUT GOES HERE
C**
        CALL OUTPUT(RESULT)

        STOP
        END
```

```
C**
C**     PREPROCESSOR CODE FOR INTEGER INVARIANT TEMPLATE T
C**
        INTEGER INVARIANT TEMPLATE T

        T(X-1, Y-1) = -1
        T(X-1, Y 1) =  0
        T(X-1, Y+1) =  1
        T(X  , Y-1) = -2
        T(X  , Y  ) =  0
        T(X  , Y+1) =  2
        T(X+1, Y-1) = -1
        T(X+1, Y  ) =  0
        T(X+1, Y+1) =  1

        END
C**
C**     PREPROCESSOR CODE FOR INTEGER INVARIANT TEMPLATE S
C**
        INTEGER INVARIANT TEMPLATE S

        S(X-1, Y-1) = -1
        S(X-1, Y  ) = -2
        S(X-1, Y+1) = -1
        S(X  , Y-1) =  0
        S(X  , Y  ) =  0
        S(X  , Y+1) =  0
        S(X+1, Y-1) =  1
        S(X+1, Y  ) =  2
        S(X+1, Y+1) =  1

        END
```

Step 6. The last thing you need to do is to run this file through the preprocessor to create the equivalent FORTRAN source file to be compiled under the FORTRAN compiler.

VIII. Image Algebra Executive Software System

The Image Algebra Executive is a package of software routines that allow the user to create batch modules that can be used to verify IA preprocessor algorithms on a large set of data and/or images. The Image Algebra Executive is a menu driven system, which makes its use almost entirely self documenting. The system is configured so at any point

in any menu the user may request HELP or may execute a Digital Command Language (DCL) command. The Image Algebra Executive was written entirely in Digital Command Language (DCL) and will be compatible with any VAX system running under the VAX/VMS operating system.

The basic idea behind the Image Algebra Executive is to allow the user to choose a set of image processing transforms and a set of images on which the transforms will perform. This is accomplished in a menu driven environment where the user interacts with the system to choose the appropriate algorithms and images. The Image Algebra Executive employs an on-line help facility to allow the user to query the the system as to the proper use of a menu option or the proper sequence of steps in creating a batch module. The system also allows the user to execute a DCL command from within the system, this is more of a convenience than a necessity.

The Image Algebra Executive system is a valuable tool for the image processing environment created by the Image Algebra Preprocessor.

IX. Recommendations

1. The coding of the IA preprocessor is finished for the time being. The preprocessor could be extended and enhanced, but the benifits of this are questionable since the preprocessor is written entirely in FORTRAN. To be a more versatile peice of software the preprocessor should be recoded in a language that supports abstract data types.

2. The Image Algebra Executive is in its final state. It is a extremely useful tool for the Image Algebra environment and can save the user time and effort in developing image processing algorithms.

3. The IA preprocessor provided valuable insight into the IA itself. Much was learned about the very essence of the IA while the coding of the IA preprocessor, in fact several changes were to the IA were initiated through discoveries made while coding the IA preprocessor.

4. The one major recommendation that I would make is to undertake a feasiblity study of an Image Algebra Compiler project. Through the IA preprocessor the IA has proved to be a valuable image processing tool and an Image Algebra Complier would be a valuable asset to any image processing laboratory.

References

[1] G. X. Ritter and et. al., "Image Algebra Tutorial, Version I," unpublished TR, Image Algebra Project, F08635-84-C-0295, Eglin AFB, FL (1985).

[2] J. N. Wilson and W. K. Perry, "A Fortran Preprocessor Implementation of the Image Algebra," unpublished TR, Image Algebra Project, F08635-84-C-0295, Eglin AFB, FL (1986).

1986 USAF-UES SUMMER FACULTY RESEARCH PROGRAM/

GRADUATE STUDENT SUMMER SUPPORT PROGRAM

Sponsored by the

Air Force Office of Scientific Research

Conducted by the

Universal Energy Systems, Inc.

Final Report

Decentralized Control of Large Flexible Space Structures

Prepared by:	Frank Mark Pitman
Academic Rank:	Graduate Assistant
Department and University:	Mechanical Engineering Clemson University
Research Location:	Wright-Patterson Air Force Base, Flight Dynamics Laboratory

Date:	September 20, 1986
Contract Number:	F49620-85-C-0013

Decentralized Control of Large Flexible Space Structures

by

Frank Mark Pitman

ABSTRACT

Decentralized control is considered as an alternative to centralized control techniques such as pole placement, state feedback, and optimal control as a tool for controlling undesirable vibrations in large flexible space structures (LFSS). The method presented here allows one to determine the decentralized system equations directly from the centralized system equations. Furthermore, this formulation neither requires a coordinate transformation nor ignores any coupling between the subsystems. This makes the method both computationally attractive and reliable. The idea of optimal control is applied to the decentralized subsystems in an attempt to determine the optimal controller for the total system. The necessary equations are developed in the paper, however, the method still needs to be programmed and tested on various cases to ensure the validity of the results. This work should be extended to include provisions for both variations in the system parameters and external disturbances.

Acknowledgments

I would like to express my gratitude to the Air Force Systems Command and the Air Force Office of Scientific Research for sponsorship of this research project. I would also like to thank my major advisor, Dr. Mehdi Ahmadian, for giving me the necessary help and guidance throughout the research period.

I. Introduction

I received my B.S. Degree in Mechanical Engineering from Clemson University in May, 1985. I am currently working towards my Master's Degree in Mechanical Engineering at Clemson, specializing in mechanical systems design and more specifically controls. The topic of my Master's Thesis is "Decentralized Control of Large Flexible Space Structures."

My major advisor, Dr. Mehdi Ahmadian, was awarded an AFOSR Summer Faculty Fellowship to perform research pertaining to decentralized control of large flexible space structures at the Flight Dynamics Laboratory (FDL) of Wright-Patterson AFB. For this reason I submitted an application for an AFOSR fellowship in hopes of providing myself with an opportunity to work closely with Dr. Ahmadian while at Wright-Patterson AFB.

II. Objectives

The overall objective of my research is to determine the answer to the following question: Given a large flexible space structure (LFSS), is it possible to find a robust decentralized controller for the system that allows the closed-loop stability to occur independent of modeling inaccuracies and system disturbances?

My individual objectives for the ten-week research period are listed below.

1. Familiarize myself with research that has been done in the areas of decentralized control and large space structures in the past.

2. Develop a systematic method for obtaining a decentralized system directly from a centralized system model, without the loss of pertinent information (i.e., without making any assumptions regarding model interactions, etc.).

3. Apply the idea of optimal control to the decentralized system mentioned above.

III. Decentralized Control

Centralized control techniques such as pole placement, state feedback, and optimal control have commonly been used in the past in an attempt to control undesirable vibrations in large flexible space structures (LFSS). However, these techniques have often resulted in various computational difficulties due to the fact that a large number of degrees-of-freedom are required to effectively model LFSS. Therefore, it is desirable to reduce the order of the system (if possible).

There are a number of model reduction techniques available to reduce the order of a given system, many of which have been used in the past in an attempt to facilitate the control of large scale systems. Model reduction techniques such as decomposition techniques, model reduction by aggregation, model reduction by perturbation, and hierarchical control have all been used. However, techniques such as these sometimes result in accuracy problems since preliminary assumptions are often required. For example, decomposition techniques assume weak interconnections between modes, and certain dynamic interactions are ignored in perturbation methods. Another problem that arises is the fact that the "reduced" system may still be too large for the use of existing control algorithms. These inadequacies have motivated research in the area of decentralized control.

The basic idea behind decentralized control is to break the system down into a number of "manageable" subsystems and control

each subsystem individually, keeping in mind that the subsystems are interconnected [1-4]. It is desirable to develop a decentralized control technique that makes no assumptions regarding model interactions, etc., so that no error will be introduced as the system is broken down.

IV. System Development

Consider a centralized system governed by the following set of equations:

$$\dot{x} = Ax + Bu \tag{1}$$

$$y = Cx \tag{2}$$

where x is the state vector, u is the control vector, y is the output vector, A, B, and C are matrices of appropriate dimensions, and C is assumed to be in block diagonal form.

Rewriting the above system in its decentralized form as p subsystems yields:

$$\dot{x}_i = A_i x_i + B_i v_i \tag{3a}$$

$$y_i = C_i x_i \qquad ; \ i = 1, 2, 3, \ldots, p \tag{3b}$$

where x_i is the state vector, v_i is the control vector, and y_i is the output vector of the i^{th} subsystem. Here, the control vector for the i^{th} subsystem includes both an external control input to the subsystem and the effects of coupling between the subsystems, and is formulated as:

$$v_i = u_i + \sum_{\substack{j=1 \\ j \neq i}}^{p} G_{ij} z_{ij} \tag{3c}$$

$$z_{ij} = y_j + D_{ij} u_j \quad (\text{for } j \neq i) \tag{3d}$$

where u_i is the external control input to the i^{th} subsystem, z_{ij} is the coupling state between subsystems i and j, and G_{ij} and D_{ij} are weighting matrices (to be calculated).

The governing equations for the decentralized system can be found by combining equations (3a), (3b), (3c), and (3d) to form the state equation and leaving the output equation unchanged:

$$\dot{x}_i = A_i x_i + B_i[u_i + \sum_{\substack{j=1 \\ j\neq i}}^{p} G_{ij}(C_j x_j + D_{ij} u_j)] \tag{4a}$$

$$y_i = C_i x_i \qquad ; i = 1, 2, 3, \ldots, p \tag{4b}$$

Now, the matrices A_i, B_i, C_i, G_{ij}, and D_{ij} need to be determined in terms of the submatrices of A, B, and C in equation (1) as they are partitioned according to the dimensions of the subsystems, i.e.

$$A = [A_{ij}]$$

$$B = [B_{ij}]$$

$$C = [C_{ij}] \quad , i = 1, 2, \ldots, p$$

$$j = 1, 2, \ldots, p$$

It is possible to show that in order for the systems (1) and (3) to be equal, the following must hold:

$$A_i = A_{ii} \tag{5a}$$

$$B_i = B_{ii} \tag{5b}$$

$$C_i = C_{ii} \tag{5c}$$

$$G_{ij} = (B_{ii})^{-1} A_{ij} (C_{jj})^{-1} \tag{5d}$$

$$D_{ij} = (B_{ii} G_{ij})^{-1} B_{ij} \tag{5e}$$

In some cases the matrices B_{ii}, C_{jj} and the product $(B_{ii}G_{ij})$ in equations (5d) and (5e) above will not be square matrices. In these cases the pseudo-inverse must be used in place of the inverse

of the matrix in question [5]. *Note that the form that the pseudo-inverse* of a matrix takes depends on the dimensionality of the matrix (i.e., whether the number of rows is greater than the number of columns, or vice versa). For example, consider an nxm matrix F:

$$F^{-1} = (F^T F)^{-1} F^T \text{ ; if } n > m \tag{6a}$$

$$F^{-1} = F^T (F F^T)^{-1} \text{ ; if } n < m \tag{6b}$$

Note that B_{ii} will be an $n_i x m_i$ matrix, C_{jj} will be a $k_j x n_j$ matrix, and the product $(B_{ii} G_{ij})$ will be an $n_i x k_j$ matrix:
where n_i is the order of subsystem i, m_i is the number of external inputs to subsystem i, and k_i is the number of outputs from subsystem i.

The order of the matrices is purely a matter of choice, and depends only on the desired dimensions of the subsystems. However, the following must hold:

$$\sum_{i=1}^{p} n_i = N \tag{7a}$$

$$\sum_{i=1}^{p} m_i = M \tag{7b}$$

$$\sum_{i=1}^{p} k_i = K \tag{7c}$$

where N, M, and K are the order of the centralized system, the number of inputs to the centralized system, and the number of outputs from the centralized system respectively.

It is worthwhile noting that the decentralized system is determined directly from a centralized model. Furthermore, this formulation neither requires a coordinate transformation nor

ignores any coupling between subsystems. This makes the method both computationally attractive and reliable.

V. Optimal Control

Reference [6] is used extensively in the formulation of this section. Choosing a performance index that penalizes the error of each subsystem at some terminal time (t_f), the error over the period from 0 to t_f, and the control power used over the period from 0 to t_f yields the following performance index:

$$J = \sum_{i=1}^{p} J_i \tag{8a}$$

where $J_i = (\tfrac{1}{2})e_i^T(t_f)Q_i(t_f)e_i(t_f)$

$$+ (\tfrac{1}{2}) \int_0^{t_f} [e_i^T(t)Q_ie_i(t) + u_i^T(t)R_iu_i(t)]dt \tag{8b}$$

and $\quad e_i(t) = y_i^{ref} - y_i(t) \quad ; \quad i = 1, 2, \ldots, p \qquad (8c)$

R_i is a positive definite weighting matrix while Q_i and $Q_i(t_f)$ are positive semidefinite weighting matrices. And y_i^{ref} is some reference input to the i^{th} subsystem.

The basic idea is to minimize equation (8b) for each subsystem (i.e., suboptimal control) instead of minimizing the performance index of the composite system. The Hamiltonian for each subsystem is given by [7]:

$$H_i = (\tfrac{1}{2})[e_i^T(t)Q_ie_i(t) + u_i^T(t)R_iu_i(t)]$$

$$+ \lambda_i^T[A_ix_i + B_iu_i + B_i \sum_{\substack{j=1 \\ j\neq i}}^{p} G_{ij}z_{ij}] \tag{9}$$

where $z_{ij} = y_j + D_{ij}u_j$ and λ_i is a vector of Lagrange Multipliers for the i^{th} subsystem.

The following equations are found by applying the well known minimum principle [8].

$$\dot{x}_i(t) = A_i x_i(t) - B_i R_i^{-1} B_i^T \lambda_i(t) + B_i \sum_{\substack{j=1 \\ j \neq i}}^{p} G_{ij} z_{ij} \qquad (10a)$$

$$\dot{\lambda}_i(t) = -C_i^T Q_i C_i x_i(t) - A_i^T \lambda_i(t) + C_i^T Q_i y_i^{ref} \qquad (10b)$$

$$u_i(t) = -R_i^{-1} B_i^T \lambda_i(t) \qquad (10c)$$

The boundary conditions are given by [8]:

$$x_i(0) = x_{io}$$

$$\lambda_i(t_f) = C_i^T Q_i(t_f) C_i x_i(t_f) - C_i^T Q_i(t_f) y_i^{ref}(t_f)$$

The two point boundary value problem specified by these boundary conditions and equations (10a), (10b), and (10c) can be represented as a Ricatti Matrix Problem by letting [6]:

$$\lambda_i(t) = P_{i(t)} x_i(t) - g_i(t) \qquad (11a)$$

$$\dot{\lambda}_i(t) = \dot{P}_i(t) x_i(t) - P_i(t) \dot{x}_i(t) - \dot{g}_i(t) \qquad (11b)$$

where P_i is an $n_i x n_i$ matrix and g_i is an n_i dimensional vector.

Equating (11b) to (10b) and substituting the expressions for x_i from (10a) and λ_i from (11a), the following equations can be realized:

$$\dot{P}_i(t) = (-P_i A_i - A_i^T P_i + P_i B_i R_i^{-1} B_i^T P_i - C_i^T Q_i C_i) \qquad (12a)$$

$$\dot{g}_i(t) = -(A_i - B_i R_i^{-1} B_i^T P_i)^T g_i(t) - C_i^T Q_i Y_i^{ref}$$

$$+ P_i B_i \sum_{\substack{j=1 \\ j \neq i}}^{p} G_{ij} z_{ij}) \qquad (12b)$$

The boundary conditions become:

$$P_i(t_f) = C_i^T Q_i(t_f) C_i \tag{12c}$$

$$g_i(t_f) = C_i^T Q_i(t_f) y_i^{ref}(t_f) \tag{12d}$$

In the steady state case, equation (12a) reduces to the Algebraic Ricatti Matrix Equation and equation (12b) can be easily solved, thus P_i and g_i are readily attainable. Theoretically, the optimal controller for each subsystem can now be determined using an optimization routine.

VI. Recommendations

1. The existing equations must now be solved to yield the optimal controller (u_i) for each subsystem. Both the decentralization method and the suboptimal control algorithm should be programmed and tested on various cases to ensure that the methods are computationally feasible.

2. Once a controller has been selected, the idea of robustness needs to be resolved by applying the controller to a perturbed system and reevaluating its effectiveness (i.e., allow the state matrix to be perturbed from A_i to $A_i + \Delta A_i$). The controller is termed "robust" if the resulting closed-loop system is both asymptotically stable and regulated.

3. The controller should also be evaluated in terms of its ability to regulate a system that is subjected to external system disturbances. For example, for the case of a constant disturbance to the i^{th} subsystem, equation (3c) should be altered to include the disturbance (D_i) as follows:

$$v_i = u_i + \sum_{\substack{j=1 \\ j\neq i}}^{p} G_{ij} z_{ij} + D_i$$

The performance index should then be reevaluated for the problem with external disturbances (as given above).

References

1. Sandell, N. R. Jr., P. Varaiya, M. Athens, and M. G. Safonov, "Survey of Decentralized Control Methods for Large Scale Systems," IEEE Transactions on Automatic Control, vol. AC-23, no. 2, April 1978, pp. 108-128.

2. Siljak, D. D. and M. B. Vukcevic, "Decentralization, Stabilization, and Estimation of Large-Scale Linear Systems," IEEE Transactions on Automatic Control, June 1976, pp. 363-366.

3. Jamshidi, Mohammad, Large-Scale Systems Modeling and Control, New York, Elsevier Science Publishing Co., Inc., 1983.

4. Siljak, D. D., Large-Scale Dynamic Systems Stability and Structure, New York, Elsevier North-Holland Publishers, Inc., 1978.

5. Ahmadian, M. and D. J. Inman, "Closed-Loop Stability of Large Space Structures with Reduced-Order Controllers," Proceedings of the Fifth VPI&SU/AIAA Symposium on Dynamics and Control of Large Structures, June 12-14, 1985, Blacksburg, Va., pp. 275-289.

6. Guanguan, L. I. and Gordon K.F. Lee, "Decentralized Control of Large Scale Systems with Dynamic Interconnected Subsystems," International Journal of Controls, vol. 37, no. 4, 1983, pp. 775-786.

7. Kirk, Donald E., Optimal Control Theory an Introduction, Englewood Cliffs, N.J., Prentice-Hall Inc., 1970.

8. Denn, Morton M., Optimization by Variational Methods, New York, McGraw-Hill Book Company, 1969.

1986 USAF-UES SUMMER FACULTY RESEARCH PROGRAM/

GRADUATE STUDENT SUMMER SUPPORT PROGRAM

Sponsered by the

AIR FORCE OFFICE OF SCIENTIFIC RESEARCH

Conducted by the

Universal Energy Systems, Inc.

FINAL REPORT

Empirical Confidence Intervals for a Validity Coefficient Under Range Restriction: An Application of the Bootstrap

Prepared by:	Amy B. Powell
Academic Rank:	Doctoral Student
Department and	Department of Psychology
University:	Texas A&M University
Research Location:	Air Force Human Resources Laboratory/MOAE
	Brooks Air Force Base, TX
USAF Researcher:	Malcolm Ree

Date:	August 11, 1986
Contract No.:	F49620-85-C-0013

EMPIRICAL CONFIDENCE INTERVALS FOR A VALIDITY COEFFICIENT UNDER RANGE RESTRICTION: AN APPLICATION OF THE BOOTSTRAP

by

Jorge L. Mendoza

with the assistance of

Darren E. Hart and Amy B.Powell

ABSTRACT

Efron's bootstrap procedure was utilized to develop two computer intensive techniques for constructing confidence intervals on the unrestricted correlation parameter under explicit predictor restriction. One procedure bootstrapped the corrected correlation coefficient to obtain the interval, while the other one relied on the frequency distribution of the applicant test scores to generate the bootstrap confidence interval. The techniques were evaluated using a Monte Carlo procedure. The study assessed the techniques under a number of hypothetical selection situations. The results showed that boostrapping the corrected correlation coefficient is a reliable technique for obtaining confidence intervals for the population correlation under most selection situations.

ACKNOWLEDGEMENTS

We would like to thank the Air Force Human Resource Laboratory at Brooks AFB for sponsoring our research. All laboratory personnel associated with this project went out of their way to accomodate us. The atmosphere at the HRL not only facilitated our research efforts, but also made this summer an enjoyable one. We would also like to thank Malcolm Ree, Toni Wegner, John Welsh, Lonnie Valentine, and Jim Earles for their support and guidance.

I. Introduction

I received a B.S. in psychology from Southwestern Oklahoma State University in 1984. I am currently in the doctoral program in Industrial/Organizational Psychology at Texas A&M University, and will receive my M.S. in August, 1986. My research interests include cognitive aspects of performance appraisal, occupational stress, social influence, and many areas of personnel selection, including test validation. This interest in selection validation prompted me to apply for the summer research position at AFHRL, in order to work with Dr. Jorge Mendoza in developing a statistical solution to a common problem in selection test validation.

II. Background

One of the oldest and most common problems in test validation is that of range restriction on the predictor due to explicit selection. Range restriction occurs when predictor and criterion data are available only for the selected group. This is a group that is systematically different from the applicant group mainly because of the organization's selection policy. The restricted variable for which data are missing has generally a restricted variance. Hence, the correlation between the predictor and the criterion in this group underestimates the validity of the test.

Investigators have been concerned with this attenuation problem for some time. Karl Pearson (1903) was the first to provide a procedure to correct for the bias inherent in the selection process. Lawley (1943) relaxed the assumptions necessary for the correction, and Thorndike (1947) is accredited with bringing the procedure to the attention of psychologists. The Pearson correction formula for

explicit selection is

$$r_c = \frac{Sr}{Sr^2 + S'^2(1 - r)}$$

The " ' " indicates that the test variance and the correlation were computed in the selected group.

The correction procedure makes two assumptions: a) linearity of the regression of the criterion y on the test x, and b) homoscedasticity of the residual variances. Linn (1968) and Lord & Novick (1968) have pointed out that these assumptions are usually not met in practical settings. In general, departures from linearity tend to deflate the corrected correlation, while lack of homoscedasticity tends to inflate it. The correction is robust to lack of homogeneity of variances, but very sensitive to lack of linearity (Greener and Osburn, 1979). Nevertheless, some (Campbell, 1979; Linn, 1968) have suggested that it may be disadvantageous to adjust the correlation under such conditions.

Greener and Osburn (1979) found that while corrected correlations, for moderate to large unrestricted population correlations, are more accurate than uncorrected ones, they become less accurate as the proportion of selected individuals decreases. Using a Monte Carlo procedure, Brewer and Hill (1969) examined the correction under varying degrees of predictor skewness. They found that correction becomes less accurate as skewness and selectivity increase.

Others have investigated the correction under more general conditions. Alexander, et al (1984) have examined the robustness of the correction procedure when both the predictor and the criterion are truncated, and found that the procedure undercorrected in most

circumstances. Gross and Fleishman (1983) found that when the selection process is incorrectly assumed to be based solely on the predictor, the corrected correlation is highly positively biased, and it is less accurate than the uncorrected correlation.

Olson and Becker (1983) claimed that the correction has the additional assumption of complete truncation, which is generally not met in applied settings. Complete truncation occurs when all of the observations falling above or below a certain point are lost from the applicant sample. Incomplete truncation or attrition, on the other hand, occurs when "it is possible to observe an individual at any point on the test or job performance distribution, but the probability that an observation is lost from the sample is related to test or job performance itself" (Olson & Becker, 1983, p137). It is likely that incomplete truncation more realistically represents practical situations. Incomplete truncation can appear in situations where there is no strict adherence to a cut off score, and/or when the selection is not based solely on the test score.

Although we know much about the performance of r_c, we know little about its standard error and its sampling distribution. Not knowing the sampling distribution has impeded researchers from testing hypotheses or constructing confidence intervals. The traditional sampling theory for the Pearson product moment coefficient is not appropriate for r_c (Forsyth, 1971).

Given the state of the art, it would be desirable to find either a procedure for obtaining confidence intervals on the unrestricted population correlation ρ based on r_c, for situations where we know that r_c does a reasonable job and/or establish a procedure for

obtaining an estimator of ρ that does not make the assumptions of r_c. Until now, the mathematics necessary for doing such a procedure have been prohibitive. But it can now be attempted using Efron's (1979) bootstrap procedure. In this paper we suggest two bootstrap procedures for setting confidence intervals on ρ and evaluate their effectiveness using a Monte Carlo simulation.

Efron's bootstrap procedure is a computer assisted nonparametric method to evaluate the precision of a statistic. The bootstrap procedure is implemented when parametric assumptions cannot be made regarding the population where the observations were drawn. The central feature of the procedure is the repeated generation of bootstrap samples. A bootstrap sample of size n is obtained by sampling at random and with replacement from one's original sample of size n. Each bootstrap sample is used to estimate the statistic of interest. Efron & Gong (1983) suggest that 200 bootstrap replications are sufficient for most applications. These bootstrap values are then used to estimate population parameters or set confidence interval. Excellent descriptions of the method can be found in Efron & Tibshirani (1984) and Lunneborg (1985). The bootstrap works because the sample data resembles the population from which they were obtained. Its use, of course, requires some degree of confidence in the sample.

III. Objectives

The purpose of the paper is two fold: a) to suggest and evaluate a procedure for constructing confidence intervals on ρ based on r_c and, b) to suggest and evaluate a parametric free procedure for

estimating ρ which does not depends on r_c.

IV. Bootstrap confidence intervals

Two bootstrap procedures are presented.. The first is a procedure for obtaining a confidence interval on p using the r_c. The procedure requires two bootstrap samples for each repetition, one from the applicant sample and one from the selected group. The second procedure does not rely on r_c, but instead relies on the applicant frequencies.

Bootstrapping the corrected r

The procedure can be summarized as follows:

1) Obtain a bootstrap sample of the applicant sample and compute the test variance S^2.

2) Obtain a bootstrap sample of the selected group and compute the correlation r' between the test and the criterion. Also compute the variance S'^2 of the test.

3) Using equation (1) correct r' for range restriction using S and S' to obtain the bootstrap value r_c^*.

4) Repeat 1-3 two hundred times to obtain $r_c^*(1)$, $r_c^*(2)$, . . . , $r_c^*(200)$.

5) Rank order $r_c^*(1)$, ... ,$r_c^*(200)$ and count 5 from the top and 5 from the bottom to establish a 95% confidence interval. Efron (1981) calls this method of constructing confidence interval the percentile method.

Bootstrapping using the applicant frequencies

The procedure is summarized below:

1) Obtain the frequency distribution of the test scores for the n applicants. Then, divide the range of test scores the into k equal intervals (e.g., 0-10, 11-20, 21-30, ... ,91-100) and count the number of individuals in each interval.

2) Obtain a bootstrap sample of the selected group using the applicant frequencies divided by n. For example, if there are 100 applicants in interval I(3) and 500 in the total sample, then we would sample interval I(3) with probability .20. Once I(3) is selected then each individual in the interval has an equal probability of being selected. For I(3), it would be 1/100. This is similar to obtaining a quota sample.

3) Compute the correlation r_c^* in the bootstrap sample.

4) Repeat 1-3 two hundred times, rank order $r_c^*(1)$, $r_c^*(2)$, ... , $r_c^*(200)$ and construct the confidence interval.

V. THE MONTE CARLO

Under the assumption that the applicant sample resembles a random sample, we wrote a computer program which simulates the hiring process in an organization, to allow us to evaluate the general applicability of the bootstrap procedure to the attenuation problem in the selection paradigm. Given the paradigm, the bootstrap can be applied in a variety of ways. We developed two, both of which utilized information from the applicant sample. (See the section on bootstrap.)

The Monte Carlo study investigated the behavior of the bootstrap corrected coefficient r_c^* for a number of bivariate distributions that

represented the joint distribution of the criterion and predictor in the unrestricted population. The computer program sampled from the bivariate normal distribution, the contaminated bivariate normal (this distribution is symmetric but not normal) and from the bivariate gamma distribution, a skewed distribution.

The program started the simulation by drawing a random sample of size n (200) from a given bivariate distribution with correlation ρ. This random sample represented the sample of applicants. Each applicant had a test score and y (criterion) score. If the individual was selected later by the selection routine, the y score became the criterion score. If, on the other hand, the individual was not selected, the y score for that individual was discarded, resembling the situation where one has only criterion scores for those hired.

The selection routine selected "ns" individuals from the applicant sample according a set of attrition (conditional) probabilities. Table 1 contains the four sets of probabilities used in the study. Note that each set is composed of ten conditional probabilities. These probabilities were chosen to reflect four situations ranging from low-to-high selection and from low-to-high attrition. Next, ten equal intervals were obtained and each interval was then sampled according to its attrition probability. Individuals in the same interval had the same probability of being selected. However, individuals in high-scoring intervals had a higher chance of being selected than those in low-scoring intervals.

After the individuals were selected, the program began the bootstrapping. The program, first, generated a bootstrap sample from the applicant sample and another one from the selected group. Then, it computed the bootstrap corrected correlation r_c^*. This process was

repeated 200 times to generate $r_c^*(1)$, $r_c^*(2)$, ... ,$r_c^*(200)$. By rank ordering the correlations and counting 5 from the top and 5 from the bottom, we identified the lower and upper 95% confidence bounds.

The second bootstrap correlation was obtained utilizing the frequency distribution of the applicant sample. The bootstrap sample was drawn so that it resembled the distribution of the test scores in the applicant sample. This was accomplished by creating ten intervals in both samples and counting the number of applicants that fell into each interval. This process yielded ten intervals in the applicant sample and ten corresponding intervals in the selected group. The sampling proceeded as follows. Suppose that out of 200 applicants, interval I(2) in the applicant sample had 20. Then, we would sample from interval I(2) in the selected group with probability .10. We repeated the procedure 200 times and used the median of $r_c^*(1)$, ... ,$r_c^*(200)$ as the bootstrap estimate of ρ.

VI. Data Generation

One standard normal and one standard gamma random deviate generator from the Institute of Mathematical Statistical Library (IMSL) were used in the study. The normal routine was used to generate bivariate normal distributions and contaminated normals. We obtained the contaminated normal by mixing two normal distributions with weights .7 and .3. A total of two bivariate normal and two contaminated distributions were utilized in the study. The standard gamma routine was use to generate three standard gamma variables, x_0, x_1, and x_2. By forming the variables $x_0 + x_1$, and $x_0 + x_2$, we obtained the bivariate gamma distribution. This distribution has a linear regression of y on x, but the homoscedasticity assumption does not

hold. Two gamma distributions were used in the study. By reversing the attrition probabilities when we sample from the bivariate gamma, we simulated the effects of a negatively skewed distribution. Two sets of distributions were used, one set had ρ = .50 and the other had p = .33. We sampled 500 times from each distribution for each situation.

VII. Results

Tables 2 and 3 contain the Monte Carlo results. Each table displays in columns 2, 3, and 4 the average correlation for the restricted correlation, the bootstrap correlation (median r_c^*), and the corrected correlation, respectively. The number within the parentheses in columns 3 and 4 indicate percentage time that the confidence interval included the unrestricted population correlation. Furthermore, each table displays in column 1 the ratio of the average restricted variance over the average unrestricted variance. The average selection ratio is given in column 5. Table 3 shows the results for ρ = .33, and Table 3 gives the results for .50.

Tables 2 and 3 show that overall the corrected correlation r_c estimated the unrestricted population correlation accurately. The r_c tended to overestimate, however, under high-truncation/low-acceptance, and when the samples were drawn from a skewed distribution, corroborating the results of Brewer and Hill (1969).

The r -bootstrap confidence interval on ρ performed remarkably well. Even in the worst of the situations, it still included the correlation 89% of the time, rather than 95%. It was somewhat

affected by skewness, but overall it was quite robust.

The median r_c^* generally underestimated the correlation, especially when the correlation was .33. Overall, it performed better than the restricted correlation. The confidence interval based on the r_c^*'s unfortunately did not perform well.

Selectivity did not seem to play much of a role in the estimation of ρ or the accuracy of the confidence intervals. Both estimators r_c and median r_c^* performed reasonably well under highly selective situations as can be seen from Tables 2 & 3. This is somewhat contrary to what Greener and Osburn (1979) observe, but they had complete truncation and we did not. It is possible that the r_c is more robust under incomplete truncation than under complete truncation, since under incomplete truncation it utilizes more information.

VIII. Recommendations

The r_c -bootstrap interval was shown to be robust to incomplete truncation, lack of normality, and lack of homoscedasticity. The study did not investigate, however, the effects of nonlinearity and/or the effects of incorrectly assuming that the selection process is solely based on the predictor. Future studies will have to assess the effects of these conditions on the r_c-bootstrap interval, since these conditions may negatively impact on the stability of the confidence interval. For situations in which these two conditions are not a factor, however, we feel comfortable in recommending the use of the r_c-bootstrap interval. Hence, we recommend that personnel researchers in the U. S. Air Force and other institutions correct their validity coefficients for range restriction, and obtain a confidence interval on the unrestricted population correlation using the r -bootstrap

method proposed here.

References

Alexander, R.A., Carson, K.P., Alliger, G.M., & Barrett, G.V. (1984). Correction for restriction of range when both X and Y are truncated. Applied Psychological Measurement, 8, 231-241.

Brewer, J.K., & Hills, J. R. (1969). Univariate selection: The effects of size of correlation, degree of skew, and degree of restriction. Psychometrika, 34, 347-361.

Campbell, J.P. (1976). Psychometric theory. In M. Dunnette (Ed.), Handbook of industrial and organizational psychology. Chicago: Rand McNally.

Efron, B. (1979). Bootstrap method: Another look at the jackknife. The Annals of Statistics, 7, 1-26.

Efron, B., & Gong, G. (1983). A leisurely look at the bootstrap, the jackknife, and cross-validation. The American Statistician, 37, 36-48.

Efron, B., & Tibshirani, R. (1986). Bootstrap methods for standard errors, confidence intervals, and other measures of statistical accuracy. Statistical Science, 1, 54-77.

Greener, J.M., & Osburn, H.G. (1979). An empirical study of the accuracy of corrections for restriction in range due to explicit selection. Applied Psychological Measurement, 3, 31-41.

Lawley, D. (1943). A note on Karl Pearson's selection formulae. Royal society of Edinburgh, Proceedings, Section A, 62, 28-30.

Linn, R.L. (1968). Range restriction problems in the use of self-selected groups for test validation. Psychological Bulletin, 69, 795-801.

Lord, F.M., & Novick, M.R. (1968). Statistical theories of mental test scores. Reading, MA: Addison-Wesley.

Lunneborg, C.E. (1985). Estimating the correlation coefficient: The bootstrap approach. Psychological Bulletin, 98, 209-215.

Olson, C.A., & Becker, B.E. (1983). A proposed technique for the treatment of restriction of range in selection validation. Psychological Bulletin, 93, 137-148.

Pearson, K. (1903). Mathematical contributions to the theory of evolution XI. On the influence of natural selection on the variability and correlation of organs. Philosophical transactions of the Royal Society, London, Series A, 200, 1-66.

Thorndike, R.L. (1950). The problem of classification of personnel. Psychometrika, 15, 215-235.

Table 1

Attrition Probabilities by Test Intervals

	Test Intervals									
	1	2	3	4	5	6	7	8	9	10
	Low-truncation					Low-acceptance				
p1:	.05*	.10	.15	.20	.25	.30	.40	.40	.40	.35
	Moderate-truncation					Moderate-acceptance				
p2:	.01	.01	.01	.01	.05	.10	.30	.60	.60	.55
	High-truncation					Low-acceptance				
p3:	.001	.001	.001	.001	.001	.003	.28	.39	.39	.39
	Low-truncation					High-acceptance				
p4:	.05	.06	.10	.12	.20	.30	.90	.95	.95	.95

* The probability of being selected (and accepting) given that an individual falls within the test range

Table 2

Monte Carlo Results for the Bootstrap when ρ = .33

The table displays the average correlation and the percent time that the C.I. contains p, in parentheses.

Distribution	Mean S / Mean S	Restricted Correlation	Bootstrap Correlation	Corrected Correlation	Average Selection Ratio
	p1:	Low-truncation, Low-acceptance			
Normal	.88	.32	.33 (88)	.34 (93)	.28
Mixed	.86	.31	.32 (90)	.34 (94)	.28
- skewed	.67	.29	.30 (89)	.34 (93)	.36
+ skewed	1.23	.33	.31 (93)	.32 (95)	.19
	p2:	Moderate-truncation, Moderate acceptance			
Normal	.65	.26	.27 (79)	.33 (93)	.06
Mixed	.73	.27	.29 (85)	.35 (91)	.15
- skewed	.32	.20	.24 (67)	.35 (95)	.38
+ skewed	1.87	.32	.32 (83)	.35 (89)	.05
	p3:	High-truncation, Low-acceptance			
Normal	.32	.19	.19 (86)	.41 (90)	.09
Mixed	.35	.19	.20 (82)	.44 (90)	.09
- skewed	.25	.19	.20 (83)	.36 (93)	.26
+ skewed	.65	.16	.19 (86)	.48 (88)	.05
	p4:	Low-truncation, High-acceptance			
Normal	.79	.29	.31 (83)	.33 (94)	.40
Mixed	.82	.29	.31 (84)	.32 (91)	.39
- skewed	.45	.24	.29 (77)	.35 (93)	.73
+ skewed	1.76	.30	.34 (92)	.30 (95)	.18

Table 3

Monte Carlo Results for the Bootstrap when ρ = .50

The table displays the average correlation and the percent time that the C.I. contained p, in parentheses.

Distribution	Mean S / Mean S	Restricted Correlation	Bootstrap Correlation	Corrected Correlation	Average Selection Ratio
		p1: Low-truncation, Low-acceptance			
Normal	.87	.46	.46 (89)	.48 (93)	.28
Mixed	.88	.47	.47 (89)	.50 (92)	.28
- skewed	.70	.43	.46 (87)	.50 (94)	.34
+ skewed	1.12	.48	.47 (94)	.47 (92)	.20
		p2: Moderate-truncation, Moderate-acceptance			
Normal	.69	.37	.41 (93)	.49 (93)	.15
Mixed	.83	.39	.44 (86)	.49 (93)	.13
- skewed	.37	.35	.40 (69)	.52 (91)	.32
+ skewed	1.48	.46	.45 (85)	.47 (89)	.06
		p3: High-truncation, Low-acceptance			
Normal	.33	.29	.30 (75)	.50 (90)	.09
Mixed	.39	.30	.30 (84)	.52 (89)	.09
- skewed	.28	.32	.33 (72)	.53 (93)	.23
+ skewed	.64	.36	.34 (92)	.53 (95)	.06
		p4: Low-truncation, High-acceptance			
Normal	.76	.45	.47 (83)	.50 (92)	.39
Mixed	.84	.45	.47 (84)	.49 (94)	.40
- skewed	.49	.40	.46 (73)	.53 (91)	.68
+ skewed	1.49	.51	.49 (90)	.45 (92)	.21

1986 USAF-UES SUMMER FACULTY RESEARCH PROGRAM/

GRADUATE STUDENT SUMMER SUPPORT PROGRAM

Sponsored by the

AIR FORCE OFFICE OF SCIENTIFIC RESEARCH

Conducted by the

Universal Energy Systems, Inc.

FINAL REPORT

STUDY AND CONTROL OF ORGAN PIPE TYPE OSCILLATIONS IN A HORIZONTAL COMBUSTION TUNNEL

Prepared By: Surya Raghu

Academic Rank: Graduate Student

Department and University: Department of Mechanical Engineering, Yale University

Research Location: Aero Propulsion Laboratory, Wright-Patterson AFB OH

USAF Researcher: Dr W. M. Roquemore

Date: 5 September 1986

Contract No: F49620-85-C-0013

STUDY AND CONTROL OF ORGAN-TYPE OSCILLATIONS

IN A HORIZONTAL COMBUSTION TUNNEL

by

Surya Raghu

ABSTRACT

Organ-pipe type oscillations are a common occurrence in combustion systems. These oscillations are important because of the noise and unsteady combustion that is associated with the instability. In this report, the efforts undertaken towards control of such instabilities and some properties of the flame in such a combustion system are discussed. Considerable reduction in the noise (10-20 dB) was achieved by means of positioned screens and heat addition. Luminosity measurements indicate a strong coupling between the pressure and the heat release rate fluctuations in agreement with the Rayleigh criterion.

ACKNOWLEDGMENTS

I gratefully acknowledge the sponsorship of this research by the Air Force Systems Command, the Air Force Office of Scientific Research and the Aero Propulsion Laboratory.

I would like to thank Dr W. M. Roquemore for his support, guidance and encouragement during this research. I would also like to thank Mr Royce Bradley for this invaluable help and suggestions in the running and modification of the tunnel.

My thanks are also due to Messrs Ronald Britton, Melvin Russell and Richard Homer for their help during the course of the experiments.

Finally, I thank the staff of the Aero Propulsion Laboratory (Fuels and Lubrication) for making my stay a very pleasant one.

I. INTRODUCTION:

I am currently a graduate student at Yale University in the Department of Mechanical Engineering. My dissertation research is in the area of control of combustion and fluid dynamic instabilities.

The above mentioned type of instabilities involves interaction of a number of processes--fluid dynamic, as well as the combustion phenomenon itself. The vortex roll up and shedding, the propagation of the pressure waves, etc., constitute the fluid mechanical aspect while the heat/release rate and the structure of the flame constitute the combustion aspect of the instabilities. Since the Aero Propulsion Laboratory (APL) had the facilities to conduct an inter-disciplinary research activity in this area, I was assigned this Laboratory to work on the research problem mentioned above. Interestingly, the organ-pipe 'rumbling' of the APL Combustion Tunnel was very similar to the systems I had studied at Yale.

II. OBJECTIVES OF THE RESEARCH EFFORT:

The overall objective is to understand the mechanism of instability and devise methods of control for the same. In particular, it was decided to undertake the following work.

a. Control combustion driven oscillations (Rumble) in the horizontal Combustion Tunnel.

b. Conduct experiments on the Rijke tube to understand the interaction of the flame and the pressure oscillations.

III. THE APL COMBUSTION FACILITY:

The Combustion Tunnel Facility was designed to study the characteristics of bluff body combustors and the evaluation of theoretical models. During the course of testing, it was found that it exhibited

organ-pipe type resonance. This instability was observed to occur over a wide range of fuel and air flow rates that are of interest in the combustion studies. Although the exact source of this instability cannot in many instances be identified, it has been recently established (Ref 1) that such oscillations could be suppressed by means of periodic heat, body force or mass addition. In brief, this method of control is based upon the principle that the interaction of an energy source and a disturbance could result in either enhancement or decay of energy in the disturbance, depending upon the phase of relationship between them.

This report describes the efforts undertaken to control the oscillations in the combustion tunnel using the methods established earlier (Ref 1, 2 and 3). Also, included is a brief note on the experiments conducted with the Rijke tube apparatus.

The details of the facility are reported elsewhere (Ref 4). A schematic of the facility is shown in Figure 1. A 2.5 gal/hr, 60° spray angle nozzle was used to inject the liquid JP-4 fuel into a swirling, recirculating airflow. The primary swirl air which was maintained constant throughout the experiments. The acoustic characteristics of the tunnel are governed by the length of the tunnel beginning from the burner to the end of the tail pipe. This length is about 5.3 m and has several resonance frequencies, as shown in Figure 2. To obtain the resonance frequencies and the mode shapes, the tunnel was excited by means of a 10-inch loudspeaker at the open end (downstream end), and a traversing microphone was used to measure the acoustic amplitudes. Note that these measurements were all made when the tunnel was not running.

Appropriate corrections had to be made for the increased temperature during the tunnel run. The dominant frequency during the cold conditions was 85 Hz which translated to a frequency of about 100 Hz at combusting conditions. No change in the mode shape was assumed and this was later verified (see Figure 3) by traversing the microphone during the running conditions.

IV. METHOD OF CONTROL:

After identification of the resonance frequency and the corresponding mode shape, two 80 mesh screens were positioned at the pressure nodes (where the velocity fluctuations are are maximum). Such screens were earlier used to suppress oscillations in a whistler nozzle (Ref 3). In addition, four heating coils (8 inch diameter and 2300 watt) were positioned at x = 305 cm. The method of heat addition is discussed in detail in Ref 2. A thin steel wire screen of 45 mesh was sandwiched between each pair of heating coils to improve the heat release characteristics of the heaters.

V. INSTRUMENTATION:

A Bruel and Kjar sound pressure level (SPL) meter was used to measure the SPL of the tunnel noise. The instrument was placed at x = 356 cm and approximately 70 cm from the center line of the tunnel. All measurements were made in the linear scale setting. Two Kistler pressure transducers (Type 211B5), mounted at x = 18 cm and x = 127 cm on the walls of the tunnel, were used to obtain the pressure fluctuations inside the tunnel. The output from the above instruments was also connected to a Nicolet Spectrum Analyser and an x-y recorder.

The light intensity fluctuations were measured by means of a photo-multiplier tube in conjunction with an optical lens system. Two points, one at the tip of the burner and the other at 14 cm downstream, were chosen for the local intensity fluctuation measurement. Later, a different optical arrangement enabled us to measure the whole-field intensity fluctuations.

VI. RESULTS:

Typical power spectrum plots of the pressure signals for the cases of resonance and quiet running of the tunnel are shown in Figures 4 and 5, respectively. Note that there is a strong peak at the resonance frequency and that several harmonics are also present. The SPL meter recorded a value of 116 dB during strong oscillations while the background noise was about 96 dB. Figure 6 shows the regions of instability with and without control. The instability has been suppressed for a large region below a fuel flow rate of 4.5 kg/hr and air flow rates greater then 0.6 kg/s. The maximum conditions were chosen from the possible operating range of the tunnel. Even in the regions where oscillations occurred, the SPL was reduced by a significant amount ranging from 10 to 20 dB, as can be seen in Figure 7. Measurements of the pressure levels inside the tunnel also show similar results (Figure 8).

Point measurements of the light intensity fluctuations in the flame show strong periodicity similar to the pressure fluctuations. The power spectrum of the light intensity and the pressure fluctuations for a typical case are shown in Figure 9. The cross-spectrum (Figure 10) also shows a strong phase coherence between the signals. Measurements of the phase relationship between the total heat release rate (entire

flame area) and the pressure fluctuations show that the conditions for resonance indeed follow the Rayleigh criterion; i.e., the heat release rate and the pressure are in phase (within experimental error) for most of the cases of oscillation. The strong interaction of the pressure and the flame could also be seen in the high speed movie pictures--the vortex shedding being strong and periodic in nature.

VII. CONCLUSIONS:

a. The noise due to the organ pipe type resonance in the combustion tunnel was significantly reduced (about 10 to 20 dB); and in some cases, the oscillations were completely suppressed.

b. The luminosity measurements agree well with the theoretically arrived Rayleigh criterion--the heat release rate and the pressure fluctuations are in phase. This is a very significant measurement in the understanding of the combustion instabilities and hence their control.

c. The above results show great promise for the control of combustion instabilities in ramjet, afterburners and several other combustion systems where such oscillations are found to occur.

VIII. RECOMMENDATIONS:

The method of control demonstrated in this work could be used to control combustion noise in similar systems. With the design of better heat addition devices and feedback systems, the author is confident of suppressing the oscillations completely. Time was a major factor in not implementing the above suggestions.

IX. RIJKE TUBE EXPERIMENTS:

The Rijke tube is a simple apparatus to demonstrate the thermoacoustic instability. It consists of a long tube (5 feet long and

4 inches in diameter) open at both ends and held vertically. A burner is introduced in the lower half of the tube and, depending upon certain conditions of the fuel and air mixtures, a loud singing sound is produced. Since this represents the simplest case of combustion instability, it was decided to study the flame structure and the flow field in the configuration.

The instrumentation is similar to that used in the combustion tunnel. The phase between the pressure and the luminosity fluctuations ranged from -30 to -50 degrees and satisfies the Raylight's criterion. High speed movies were taken with both the flame and the annular flow seeded with $TiCl_4$ vapor and illuminated by a sheet of laser through the cross section of the flame. The light scattering from the TiO_2 particles and the observation of the flame, indicate a periodic flame structure coupled with an organized vortex motion in the tube. A systematic study is required to understand the exact response of the flame at various positions of the burner in the Rijke tube.

REFERENCES

1. B. T. Chu, K. R. Sreenivasan and S. Raghu - "On the Control of Combustion Instability," to Appear in Progress in Aerospace Sciences
2. K. R. Sreenivasan, S. Raghu and B. T. Chu, "The Control of Pressure Oscillations in Combustion and Fluid Dynamical Systems," AIAA Shear Flow Control Conference, Boulder, Colorado, March 1985, Paper AIAA-85-0540
3. S. Raghu, "Control of Pressure Oscillations in a Whistler Nozzle Using Body Forces," Departmental Report, Yale University, 1986
4. W. M. Roquemore, et.al., "Utilization of Laser Diagnostics to Evaluate Combustor Models," AGARD Conference, Turkey, October 1983

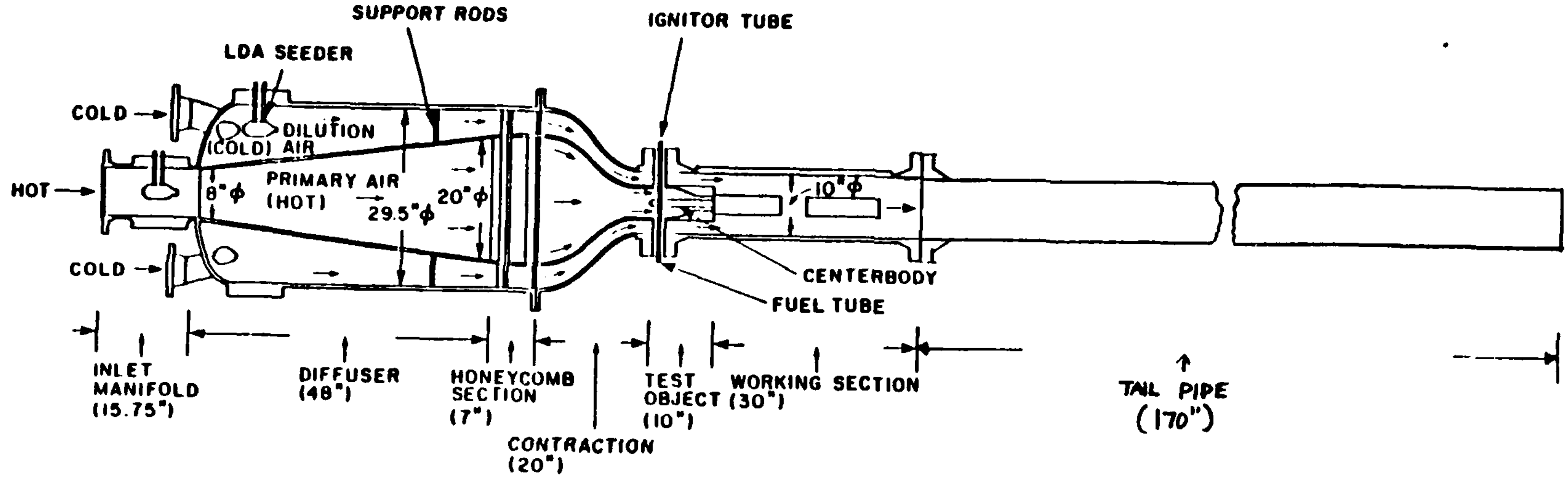

Figure 1. Schematic of the APL Combustion Tunnel

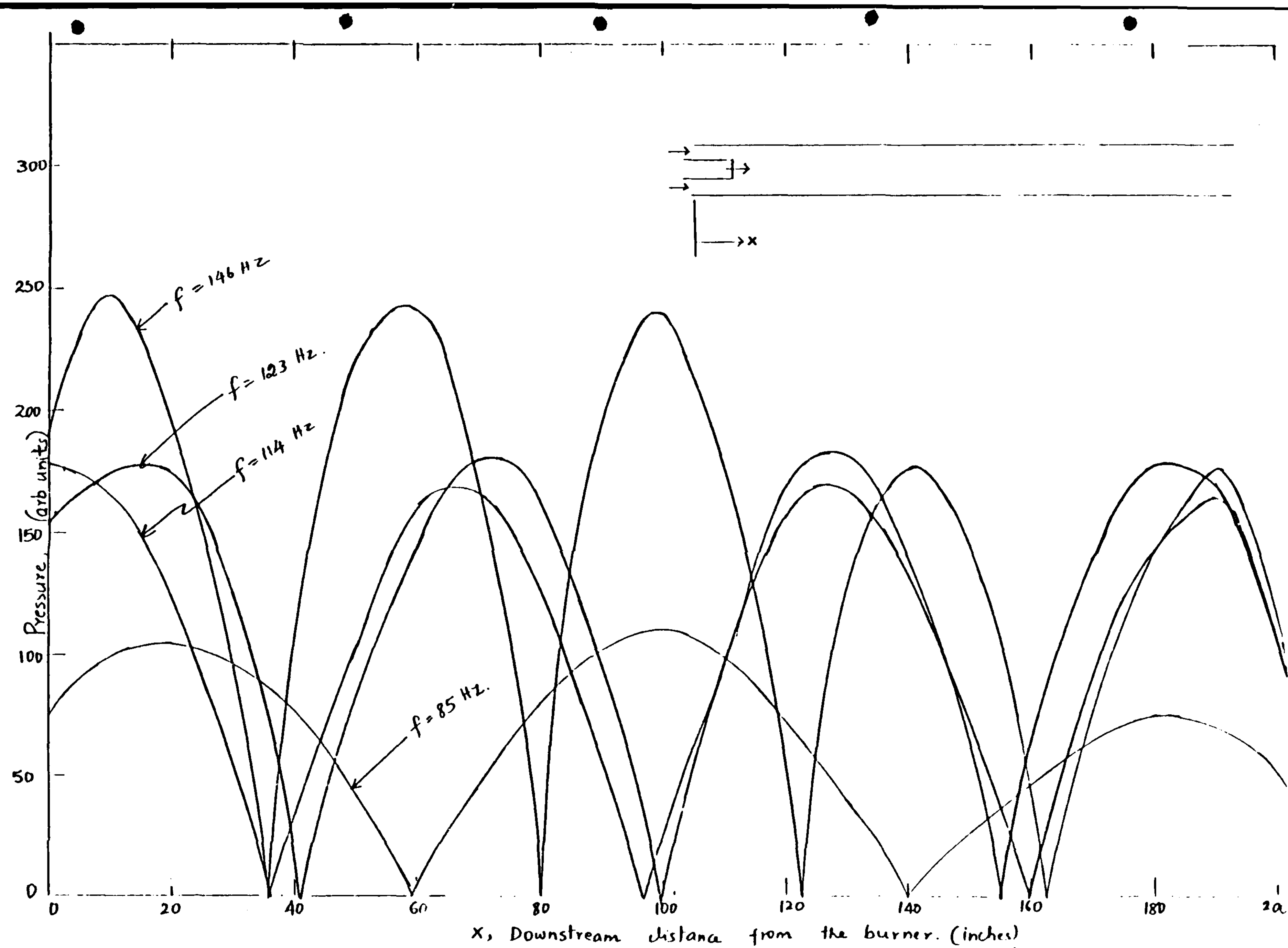

Figure 2. Mode Shapes in the Tunnel excited by a Loudspeaker

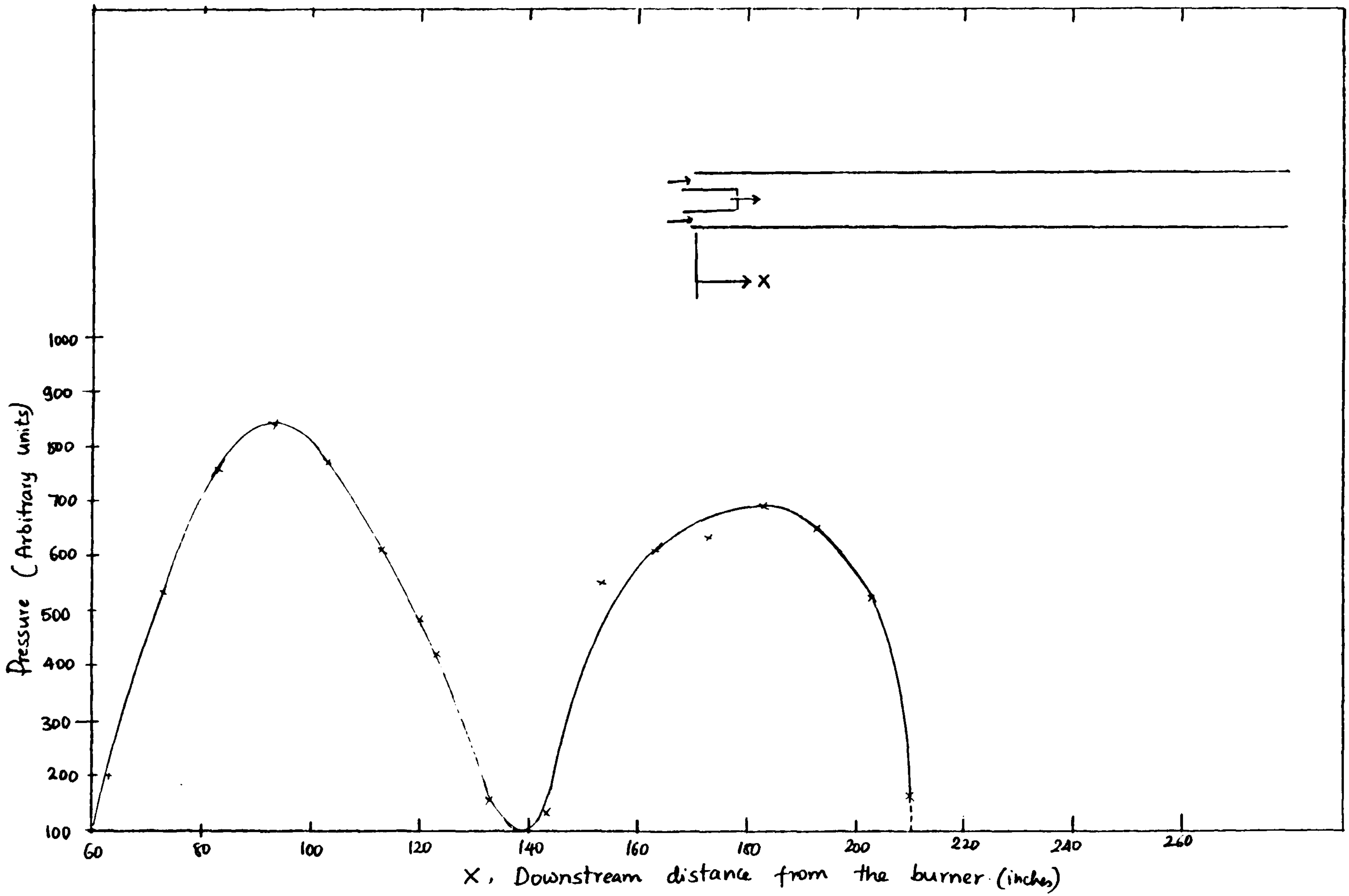

Figure 3. Acoustic Mode Shape during Combusting Conditions

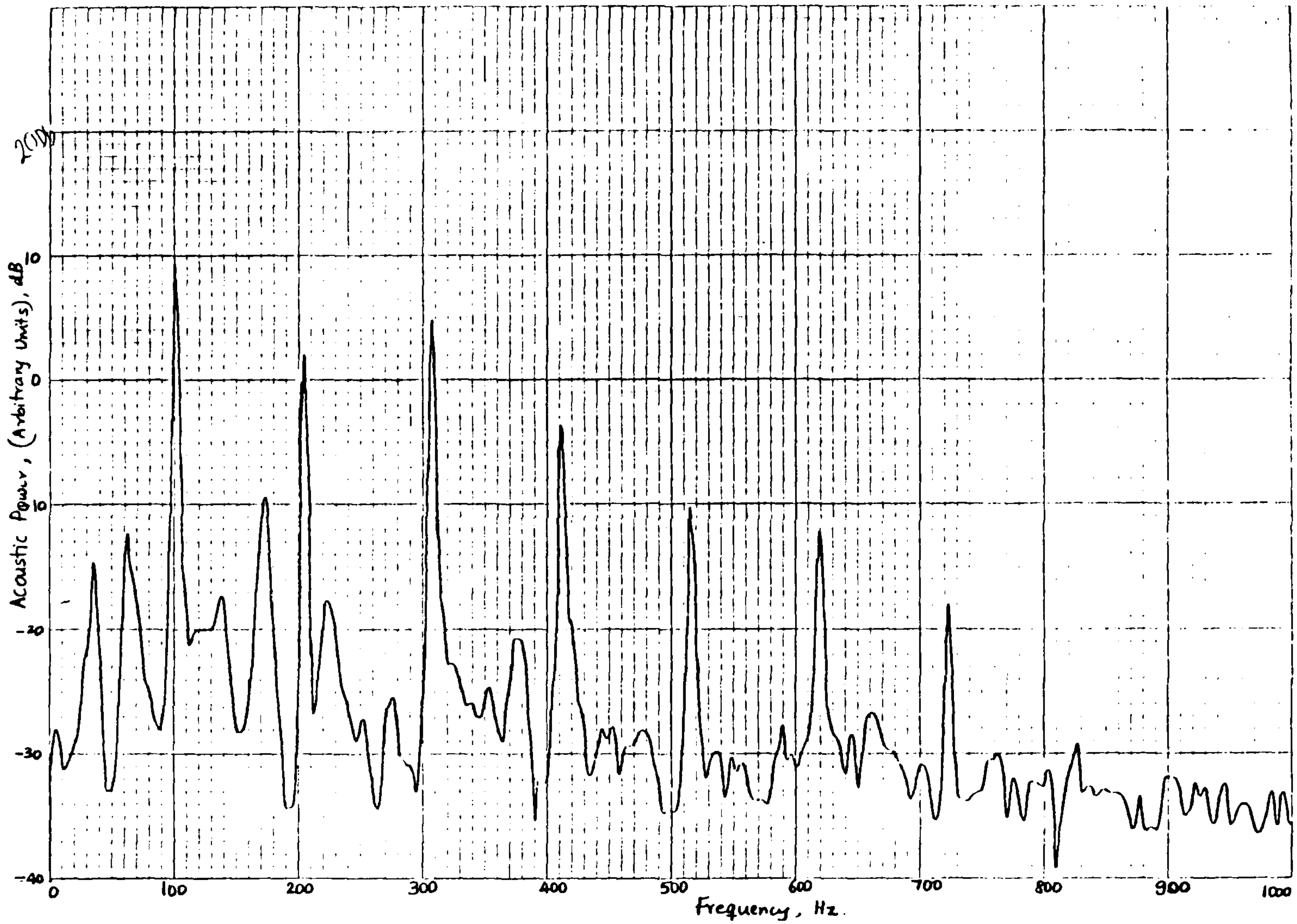

Figure 4. Power Spectrum of the Pressure Signals in the Tunnel during Combustion with Oscillations.

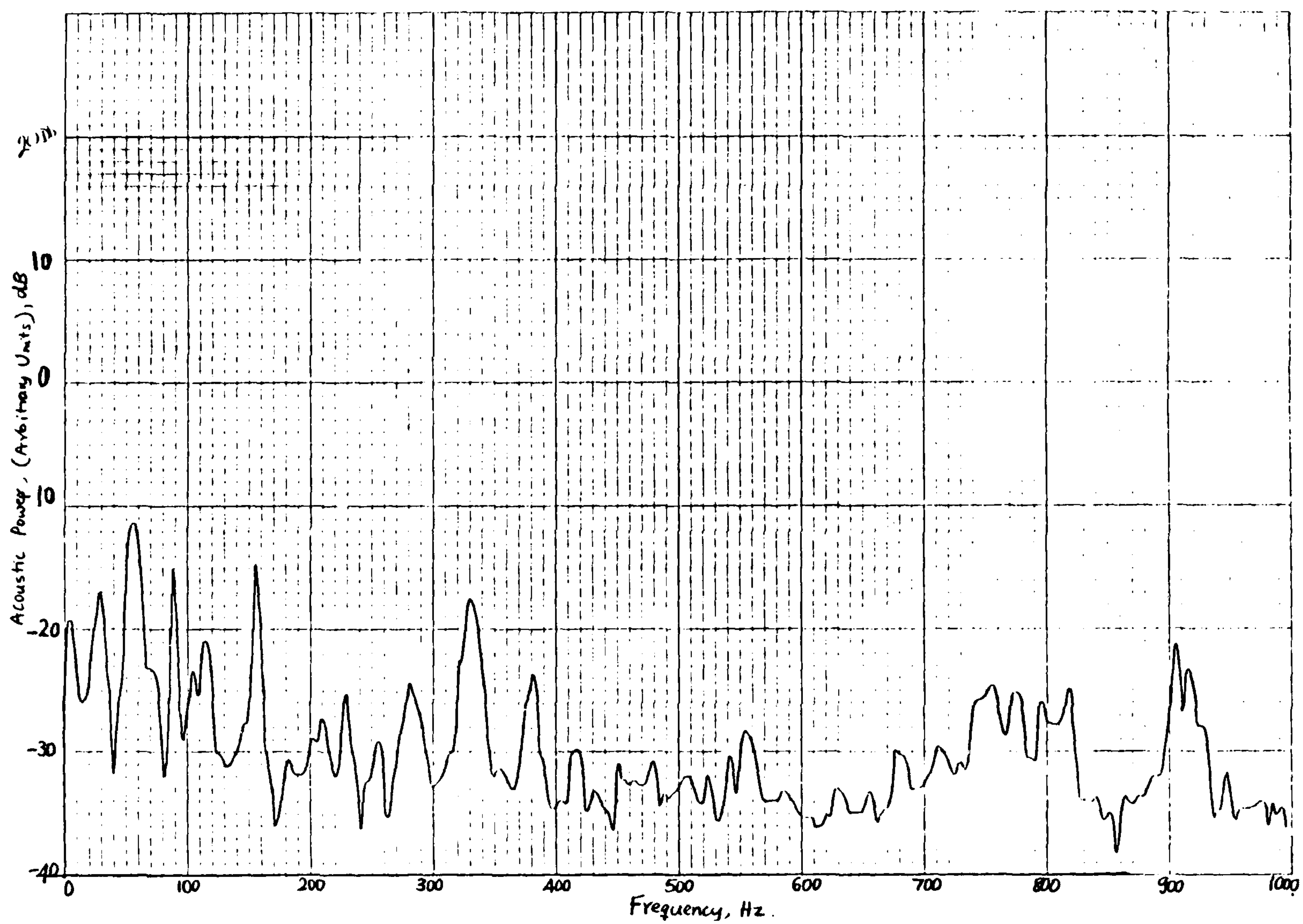

Figure 5 Power Spectrum of Pressure Signals in the Tunnel during Combustion without Oscillations.

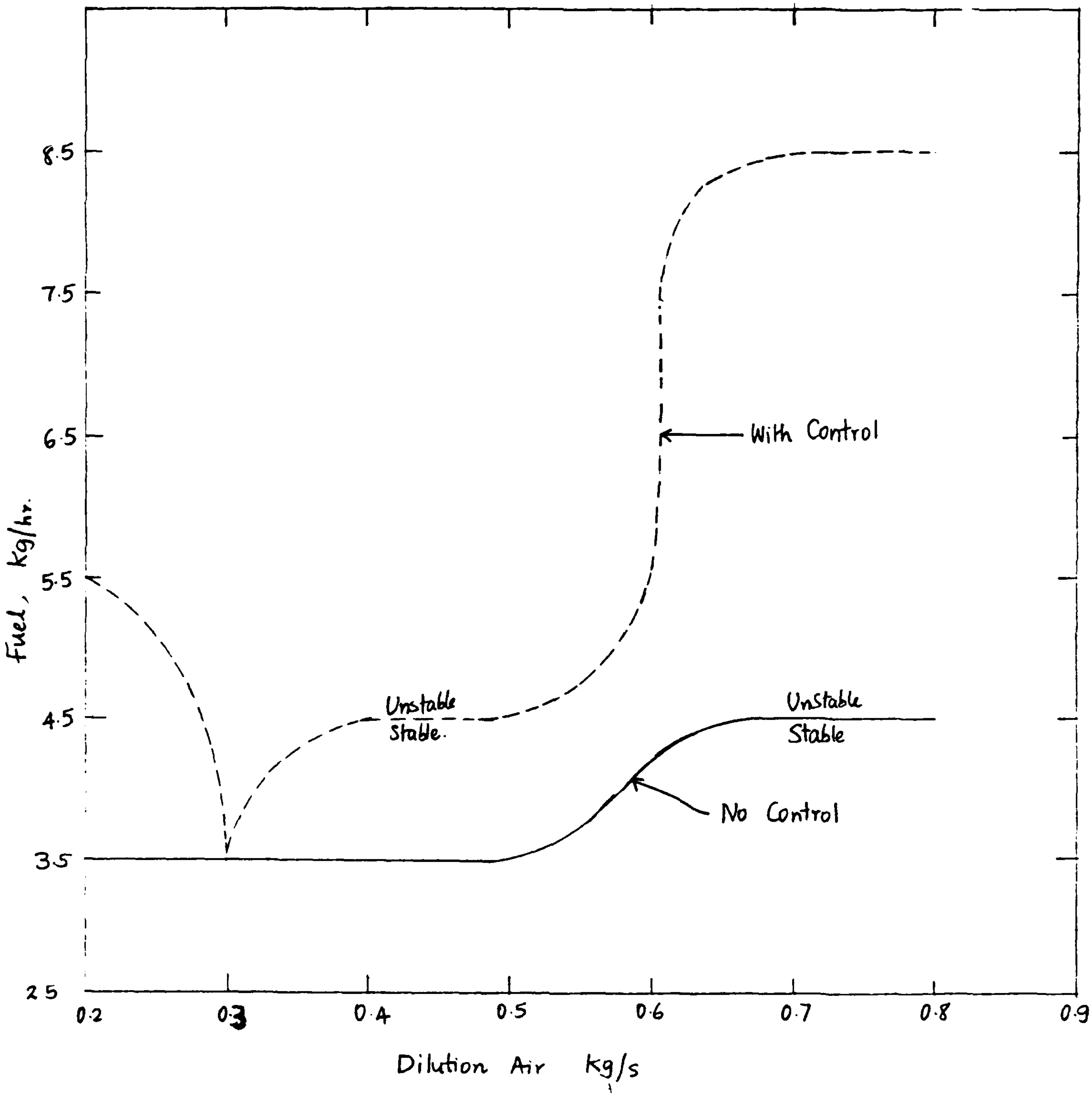

Figure 6. Regions of Stable and Unstable Combustion

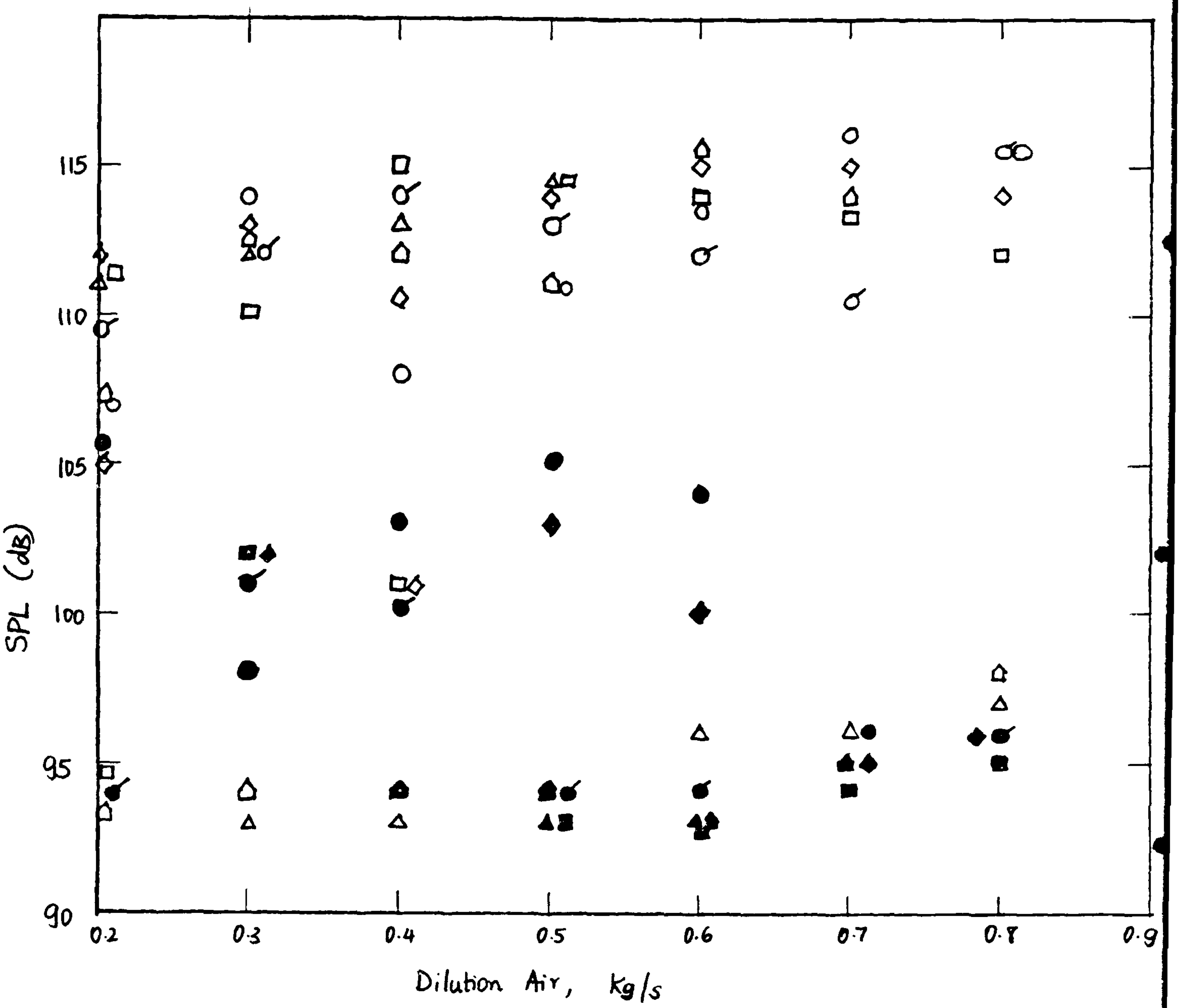

Figure 7. Sound Pressure Level (SPL) with and without Control. Open Symbols are without control at different fuel flow rates Closed symbols are with Control.

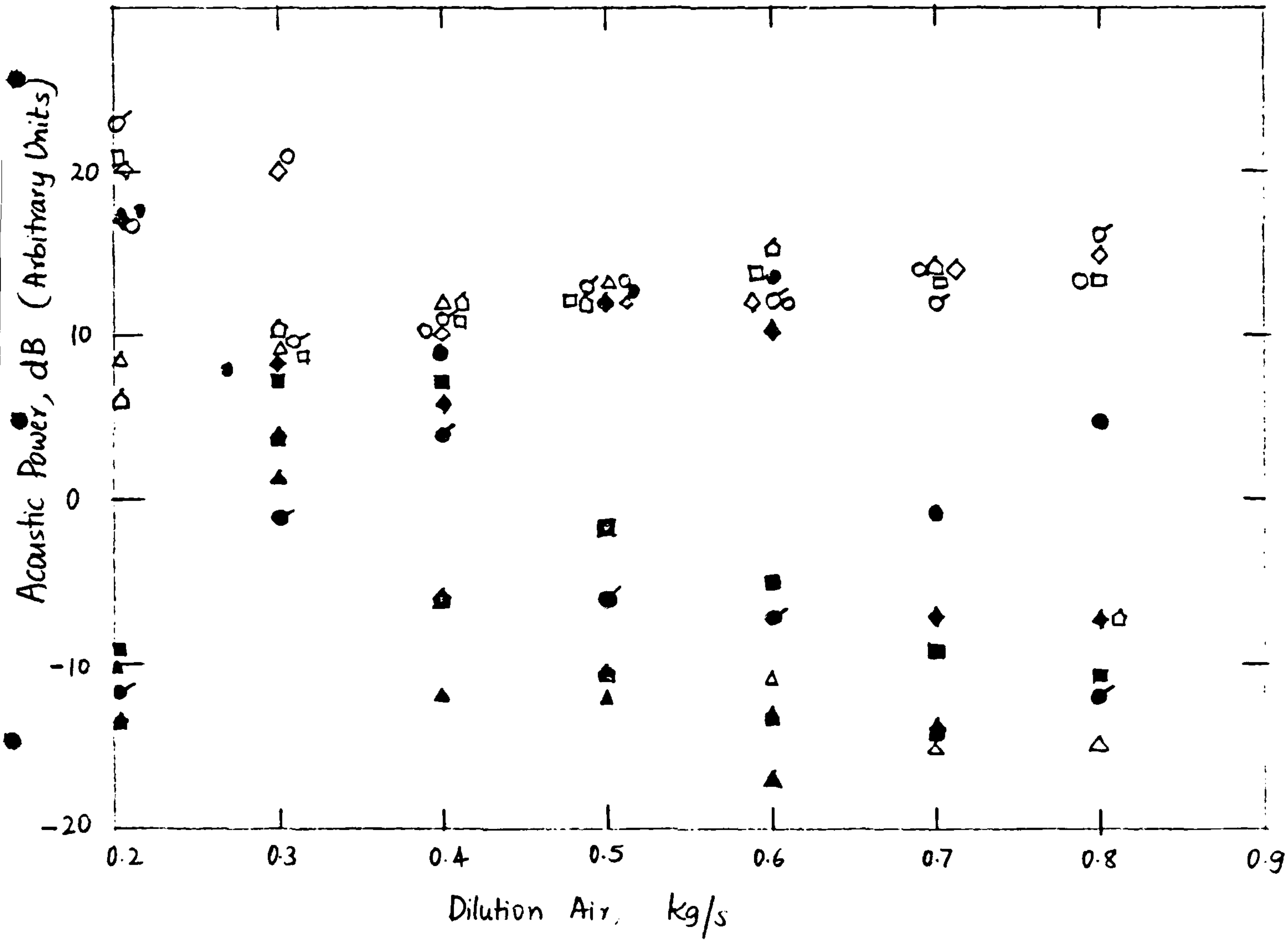

Figure 8. Acoustic power inside the tunnel with and without Control. Open symbols are without Control at different fuel flow rates. Closed symbols are with Control.

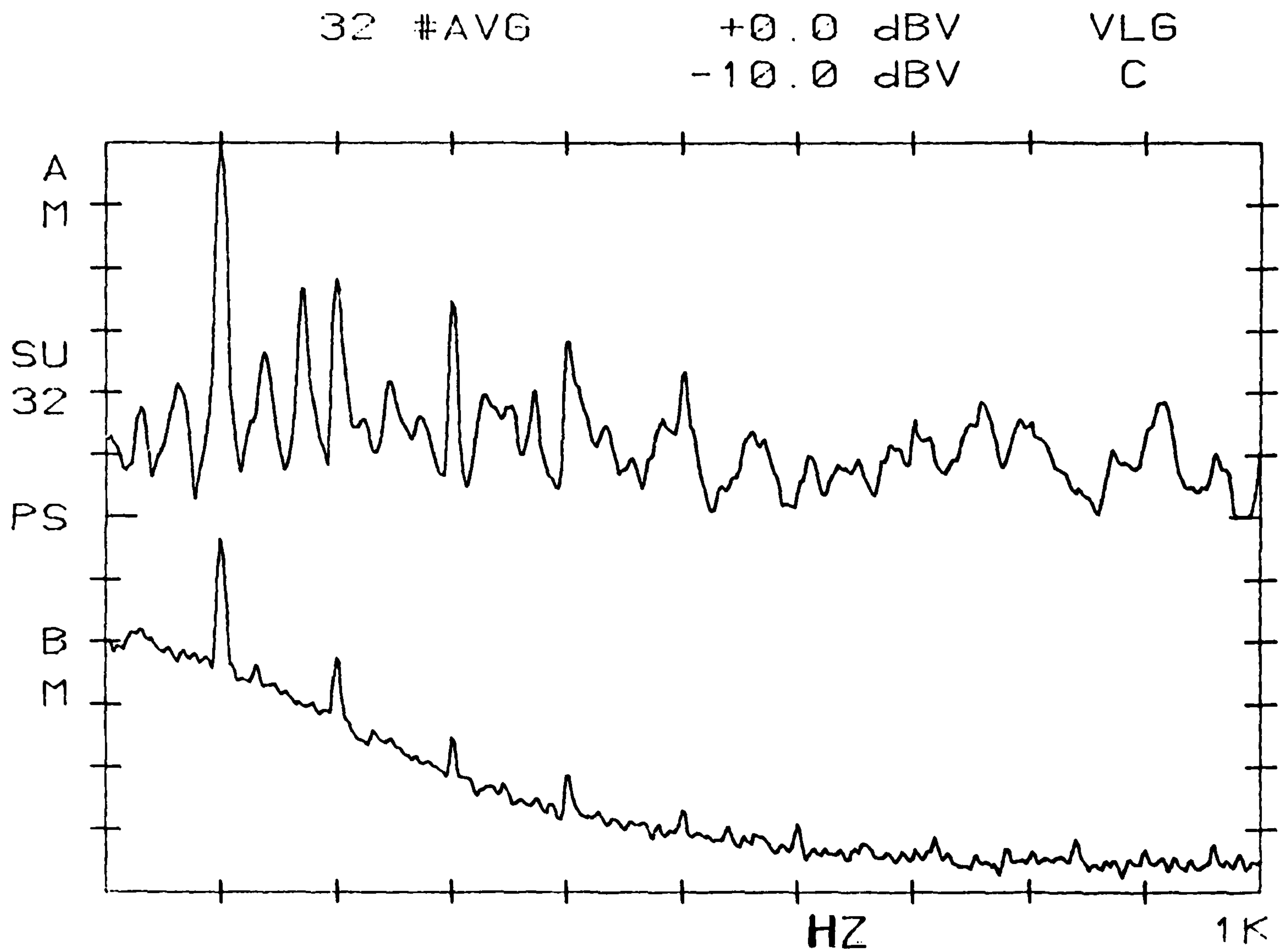

Figure 9. Power-spectrum of light and pressure signals during Oscillations.

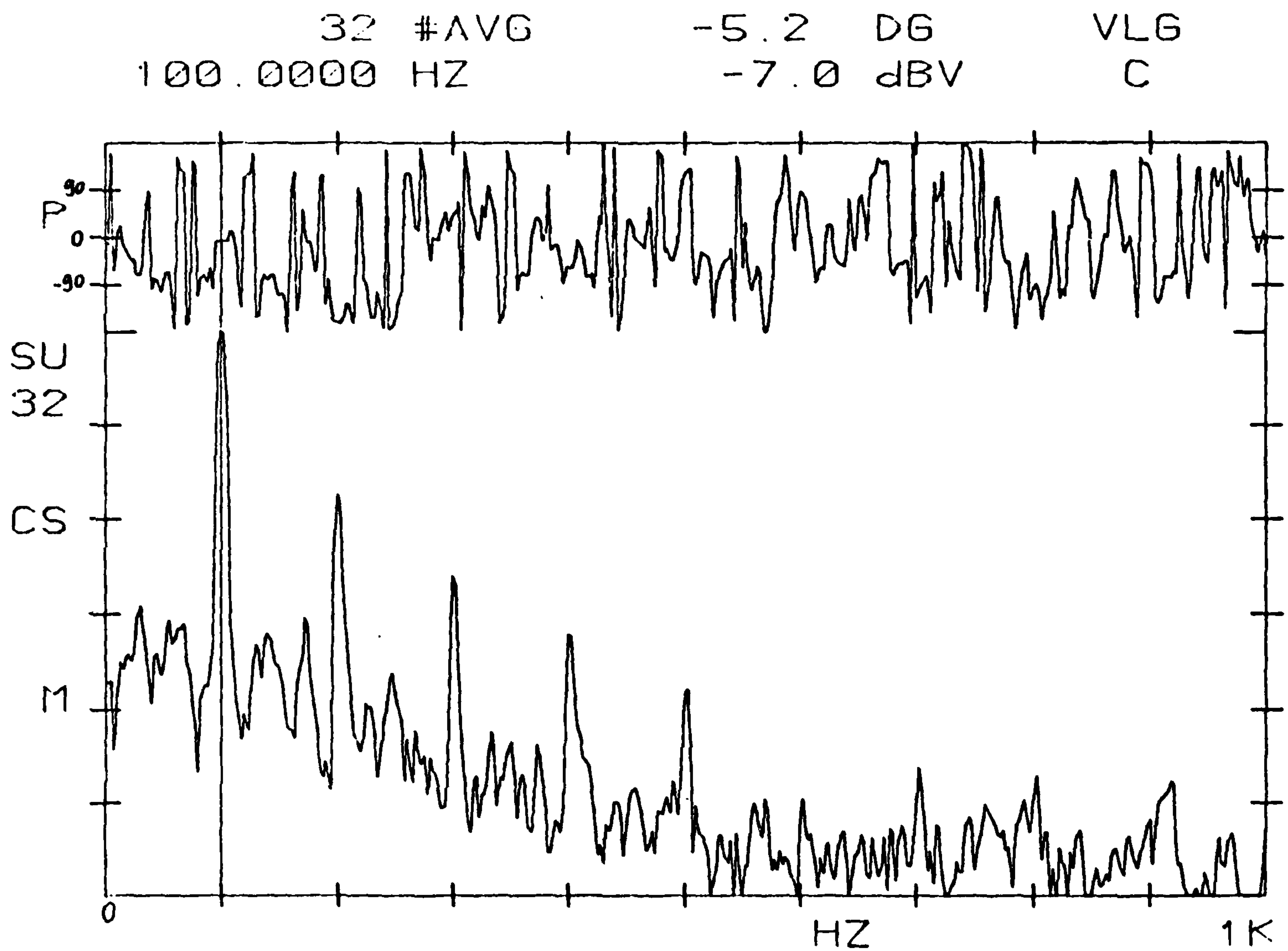

Figure 10. Cross-spectrum of light and pressure signals during Oscillations.

1986 USAF-UES SUMMER FACULTY RESEARCH PROGRAM

GRADUATE STUDENT SUMMER SUPPORT PROGRAM

Sponsored by the

AIR FORCE OFFICE OF SCIENTIFIC RESEARCH

Conducted by the Universal Energy Systems, Inc.

FINAL REPORT

A LOCALLY IMPLICIT NUMERICAL METHOD

Prepared by:	Mark L. Ratcliff
Academic Rank:	Graduate Student
Department and	Mathematics,
University:	The University of Tennessee Space Institute
Research Location:	Arnold Engineering and Development Center, Propulsion Wind Tunnel, Computational Fluid Dynamics Group.
USAF Researcher:	Dr. K. C. Reddy
Date:	September 30, 1986
Contract Number:	F49620-85-C-0013

A Locally Implicit Numerical Method

by

MARK L. RATCLIFF

ABSTRACT

The stability and application of a locally implicit numerical method were investigated. The method was analyzed for two particular cases. First, difference equations were written at two grid points in the spatial direction. Second, the difference equation was written at one spatial node. Both cases proved the scheme stable after some modifications. Certain Courant Number restrictions and parameter ranges were discovered. Work is continuing for negative Courant Numbers in both cases.

ACKNOWLEDGEMENTS

The author would like to thank the Air Force Office of Scientific Research and the Air Force Systems Command for the opportunity to carry on this research. He would also like to extend his gratitude to Marshall Kingery, who served as his Laboratory Focal point.

A special thanks is also extended to Jim Jacocks, Head of the Computational Fluid Dynamics group in the Propulsion Wind Tunnel Facility at the Arnold Engineering Development Center and to K. C. Reddy, Professor at The University of Tennessee Space Institute, and Peter Hoffman, Professor at the University of Colorado at Denver.

The assistance, cooperation, and contributions from the members of the CFD group in the Propulsion Wind Tunnel Facility at AEDC are invaluable and greatly appreciated.

I. Introduction Many of the CFD codes currently used are based on time integration or some relaxation procedure to obtain asymptotic steady state solutions. These procedures are either explicit or implicit in updating the flow field from one state to the next. Explicit procedures are bound by stability restrictions and can take thousands of time steps to reach convergence. Implicit methods involve large systems of non-linear algebraic equations and typically utilize iterative approximate factorization procedures. Convergence to steady state solution by the factorization method can be extremely slow for 3-D problems.

The goal is to reduce the time required to obtain steady state solutions. The central difference spatial approximation with implicit Euler time stepping would be sufficient if cost were no object. However, locally implicit methods avoid the cost of implicit solutions by time-lagging the point in the direction of the march.

II. Objective The object of this research was to analyze both a two-point and one-point locally implicit method. In particular, we sought to determine stability regions for both schemes with artificial viscosity imposed. If inadequacies were found in these methods, modifications would be sought to improve the basic schemes. In any case, the goal of faster convergence to steady state solutions governed the definition of what was considered to be a sufficient method. Finally, the practical application of these methods to aerodynamic problems was to be examined.

III. Two-Point Scheme

Consider the one-dimensional wave equation

$$U_t + aU_x + \mu \Delta X^3 U_{xxxx} = 0. \tag{1}$$

Backward differencing in time and central differencing in space yields the Euler implicit scheme:

$$\frac{U_j^{n+1} - U_j^n}{\Delta t} + a\frac{U_{j+1}^{n+1} - U_{j-1}^{n+1}}{2\Delta x} + a\mu\frac{U_{j-2}^{n+1} - 4U_{j-1}^{n+1} + 6U_j^{n+1} - 4U_{j+1}^{n+1} + U_{j+2}^{n+1}}{\Delta x} = 0 \tag{2}$$

We approximate the difference equations at the j and $j+1$ nodes in the following locally implicit form:

$$U_j^{n+1}(1+6D) + U_{j+1}^{n+1}(C-4D) = U_j^n + U_{j-1}^{n+1}(C+4D) - U_{j-2}^{n-1}D - U_{j-2}^n D \quad (3)\text{a}$$

$$-U_j^{n+1}(C+4D) + U_{j-1}^{n+1}(1+6D) = U_{j+1}^n - U_{j-1}^{n+1}D - U_{j-2}^N(C-4D) - U_{j-3}^n D, \quad (3)\text{b}$$

where $C = a\frac{\Delta t}{2\Delta x}$ $D = \mu\frac{\Delta t}{\Delta x}$ a

Now let $j = 2\ell$, $j-1 = 2\ell-1$ and perform a local stability analysis.

We look for a solution in the form.

$$U_{2\ell}^n = A^n e^{i\alpha j\Delta x} \quad (4)\text{a}$$

$$U_{2\ell-1}^n = B^n e^{i\alpha(j+1)\Delta x}. \quad (4)\text{b}$$

Substituting (4) into (3) and letting $\alpha\Delta x = \varsigma$ we have.

$$A^{n+1}\left\{1-6D-De^{-2i\varsigma}\right\} + B^{n+1}\left\{e^{i\varsigma}(C-4D) - e^{-i\varsigma}(C-4D)\right\} =$$

$$A^n\left\{1-De^{2i\varsigma}\right\} \quad (5)\text{a}$$

$$A^{n+1}\left\{-(C-4D)\right\} - B^{n+1}\left\{e^{i\varsigma}(1-6D) - e^{-i\varsigma}D\right\} =$$

$$A^n\left\{-e^{2i\varsigma}(C-4D)\right\} - B^n\left\{e^{i\varsigma} - De^{3i\varsigma}\right\} \quad (5)\text{b}$$

Writing this system in matrix form.

$$\left[L\right]_{2\times 2}\begin{bmatrix}A\\B\end{bmatrix}^{n+1} = \left[R\right]_{2\times 2}\begin{bmatrix}A\\B\end{bmatrix}^{n} \quad (6)\text{a}$$

the solution set at the $n+1$ time step is

$$\begin{bmatrix}A\\B\end{bmatrix}^{n+1} = \left[L^{-1}R\right]\begin{bmatrix}A\\B\end{bmatrix}^{n} \quad (6)\text{b}$$

Now we let λ be the eigenvalue of $G = L^{-1}R$, the amplification matrix, satisfying,

$$|R - \lambda L| = 0. \quad (7)$$

For stability $|\lambda| \leq 1$ for $0 \leq \varsigma \leq \pi$.

Solving (7) for λ and evaluating λ for $D = 1/32$ at $C = 5$, 10, and 20 we find that $|\lambda| \not\leq 1$ for some ς on $[0, \pi]$. Consider now the implementation of a relaxation factor into our scheme.

To simplify things let $w = \begin{bmatrix} A \\ B \end{bmatrix}$.

$$L\, w^{n+1} = R\, w^n$$

$$L\,(w^{n+1} - w^n) = (R - L) w^n$$

$$L \Delta w^n = (R - L) w^n$$

define $\overline{w}^{\,n+1} = w^n - \phi \Delta w^n$, ϕ is relaxation factor.

$$L\overline{w}^{\,n+1} = Lw^n - \phi L \Delta w^n$$

$$= [L(1 - \phi) + \phi R]\, w^n$$

The amplification matrix for the scheme with ralaxation then becomes.

$$\overline{G} = L^{-1}\{[L(1 - \phi) + \phi R]\}$$

Now λ are the eigenvalues of $\overline{G}$ satisfying

$$|L(1 - \phi) + \phi R - \lambda L| = 0. \qquad (8)$$

Solving (8) for λ and evaluating λ for $D = 1/32$ at $C = 5$, 10, and 20 we find that $|\lambda| \leq 1$ for all ς on $[0, \pi]$ if $\phi \leq .91$. So from this analysis it would appear that an under relaxation would stabilize our two-point scheme.

IV. One-Point Scheme

We can also write a one-point locally implicit scheme at the node j as follows:

$$U_j^{n+1} - U_j^n + C/2\left(U_{j+1}^n - U_{j-1}^{n+1}\right)$$

$$+ C\mu\left(U_{j+2}^n - 4U_{j+1}^n + 6U_j^{n+1} - 4U_{j-1}^{n+1} + U_{j-2}^{n+1}\right) = 0. \tag{9}$$

where $C = a\dfrac{\Delta t}{\Delta x}$.

Performing stability analysis on (9) we seek solutions in the form,

$$U_j^n = A^n e^{i\alpha j\Delta x} = A^n e^{ij\xi} \tag{10}$$

Substituting (10) into (9) gives us,

$$A^{n+1} = gA^n, \tag{11}$$

where

$$g_+ = \frac{1 - C\left\{(1/2)e^{i\xi} - \mu\left(e^{2i\xi} - 4e^{i\xi}\right)\right\}}{1 - C\left\{(1/2)e^{-i\xi} - \mu\left(6 - 4e^{-i\xi} - e^{-2i\xi}\right)\right\}} \tag{12a}$$

for waves with positive velocity and

$$g_- = \frac{1 - C\left\{(-1/2)e^{i\xi} - \mu\left(e^{2i\xi} - 4e^{i\xi}\right)\right\}}{1 - C\left\{(-1/2)e^{-i\xi} - \mu\left(6 - 4e^{-i\xi} - e^{-2i\xi}\right)\right\}} \tag{12b}$$

for waves with negative velocity.

For stabilty $|g| \leq 1$ for $0 \leq \xi \leq \pi$.

Evaluating (12) for $\mu = 1/32$ and $C = .5, 10,$ and 20 shows certain instabilty regions for g_+ while g_- is stable for all ξ on $[0, \pi]$.

The cause of this instability associated with g_+ can be seen by expanding each term in (9) by a Taylor series about U_j^n.

Performing this operation and substituting for terms in (9) yields,

$$\Delta t\,\partial u/\partial t\Big|_j^n (1-C/2+3C/\mu) - \Delta x\,\partial u/\partial x\Big|_j^n (C) - \Delta t^2\partial^2 u/\partial t^2\Big|_j^n \left(1/2 - C/4 - C/\mu - \frac{C/\mu}{2}\right)$$

$$-\Delta x^2\partial^2 u/\partial x^2\Big|_j^n (C/2) - \Delta x\Delta t\,\partial^2 u/\partial t\partial x\Big|_j^n (C/2 - 2C/\mu) = 0. \qquad (13)$$

Thus, dividing through by Δt and writing the last three terms of (13) as truncation error ε we see that we are actually approximating the modified equation.

$$(1 - C/2 - 3C/\mu)U_t + aU_x - \varepsilon = 0. \qquad (14)$$

To obtain the desired form we rewrite equation (9) by placing the coeffieient $(1-\alpha)$ on the discritization in time.

$$(1-\alpha)\left(U_j^{n+1} - U_j^n\right) - C/2\left(U_{j-1}^n - U_{j+1}^{n+1}\right)$$

$$- C/\mu\left(U_{j-2}^n - 4U_{j-1}^n - 6U_j^{n+1} - 4U_{j+1}^{n+1} - U_{j+2}^{n+1}\right) = 0 \qquad (15)$$

where $\alpha = C/2 - 3C/\mu$.

Again expanding each term by Taylor series and substituting into (15) we arrive at the desired approximation.

$$U_t + aU_x = -\varepsilon \qquad (16)$$

We perform stability analysis on (15) in the same manner as for (9). After substituting (10) into (15) and collecting terms we find.

$$A^{n+1}\left[(1-\alpha) - (C/2)e^{i\theta} - D\,(6 - 4e^{i\theta} - e^{2i\theta})\right]$$

$$- A^n\left[(1-\alpha) - (C/2)e^{i\theta} - D\,(e^{2i\theta} - 4e^{i\theta})\right] = 0. \qquad (17)$$

So now our solution is written

$$A^{n+1} = gA^n$$

where

$$g = \frac{(1-\alpha) - (C/2)e^{i\theta} - D\,(e^{2i\theta} - 4e^{i\theta})}{1-\alpha - (C/2)e^{i\theta} - D\,(6 - 4e^{i\theta} - e^{2i\theta})}.$$

Note that for right traveling waves $C > 0$ and for left traveling waves $C < 0$.

For stability we need $g^2 \leq 1$. So we solve for C in the following way.

$$\{1 + \alpha - (C/2 - 4D)\cos\zeta - D\cos 2\zeta\}^2 + \{(C/2 - 4D)\sin\zeta - D\sin 2\zeta\}^2$$

$$\leq \{1 + \alpha + 6D - (C/2 + 4D)\cos\zeta + D\cos 2\zeta\}^2 + \{(C/2 + 4D)\sin\zeta + D\sin 2\zeta\}^2$$

$$0 \leq D(1 + \alpha + 3D)\cos^2\zeta - \cos\zeta\{2D(1 + \alpha + 3D) + CD\} + D(1 + \alpha + 3D) + CD$$

$$0 \leq (1 - \cos\zeta)\,(1 + \alpha + 3D) - \cos\zeta(1 + \alpha + 3D) + C\,D.$$

$$D = C\mu > 0 \text{ and } (1 - \cos\zeta) \geq 0 \text{ for all } \zeta \text{ on } [0, \pi].$$

Hence to insure stability,

$$(1 + \alpha + 3D) - \cos\zeta(1 + \alpha + 3D) + C \geq 0$$

$$C \geq -(1 + \alpha + 3D) + \cos\zeta(1 + \alpha + 3D)$$

$$C \geq (\cos\zeta - 1)\,(1 + \alpha + 3D)$$

$$C \geq 0\,.$$

So, from this analysis it appears that our modified equation scheme is restricted to $C \geq 0$. Hoffman [1], has suggested that reversing the direction of our sweep will control problems with $C < 0$ and provide stability for all C.

V. Application to Burgers' Equation

In order to better understand the properties of our scheme we applied it to the nonlinear conservation law, Burgers' equation without viscosity:

$$U_t + (U^2/2)_x = 0. \tag{18}$$

This will simplify matters by avoiding complicating factors such as boundary conditions and complex geometries. Setting the boundary conditions at

$$U(0,t) = 1.0, \quad U(1,t) = -1.0.$$

can provide us with a steady entropy satisfying solution with a shock wave at a location depending on the initial conditions, if we have a dissipative numerical scheme.

The first case we will consider is the two-point scheme. This scheme allows for the solution to be solved simultaneously at the j and $j-1$ spatial nodes. The numerical discretization has the form

$$\frac{\left(U_j^{n+1} - U_j^n\right)}{\Delta t} + a_j \frac{U_{j+1}^{n+1} - U_{j-1}^{n+1}}{2\Delta x} - D_j^{n+1} = 0 \qquad (19)$$

where $D_j^{n+1} = (d_{j+1/2} - d_{j-1/2})$ is the dissipative flux and we set $a_j = U_j$ for the nonlinear case. The dissipation term is added to eliminate the expassion shock solution.

Several forms of the dissipation terms were tested. The numerical experiments suggest that the form, suggested by Jameson [2],

$$d_{j+1/2}^{n+1} = \frac{\Delta x}{\Delta t}\Big\{ \epsilon_{j+1/2}^{(2)}\,\alpha_{j+1/2}\left(U_{j+1}^{n+1} - U_j^{n+1}\right) \qquad (20)$$
$$- \epsilon_{j+1/2}^{(4)}\,\alpha_{j+1/2}\left(U_{j+2}^{n} - 3U_{j+1}^{n+1} + 3U_j^{n+1} - U_{j-1}^{n+1}\right)\Big\}$$

where

$$\alpha_{j+1/2} = 1/4\,|U_{j+1} - U_j| + 0.5, \qquad (21)$$

gives good results. (i.e., acceptable solutions and fast convergence to steady state) The $\epsilon_{j+1/2}^{(2)}$ and $\epsilon_{j+1/2}^{(4)}$ coeffients are determined by

$$\nu_j = \frac{|U_{j+1} - 2U_j + U_{j-1}|}{|U_{j+1}| + 2|U_j| + |U_{j-1}|} \qquad (22)$$

which essentially recognizes discontinuties.

Set

$$\nu_{j+1/2} = \max(\nu_{j-2}, \nu_{j-1}, \nu_j, \nu_{j+1}).$$

then

$$\epsilon^{(2)}_{j+1/2} = \min\left(k^{(2)}, \bar{\nu}_{j+1/2}\right) \tag{23a}$$

and

$$\epsilon^{(4)}_{j+1/2} = \max\left(0, k^{(4)} - \bar{\nu}_{j+1/2}\right). \tag{23b}$$

Reasonable values for $k^{(2)}$ and $k^{(4)}$ were found to be

$$k^{(2)} = 1 \quad \text{and} \quad k^{(4)} = 1/32.$$

Defining $\nu_{j+1/2}$ in this manner and determining $\epsilon^{(2)}_{j+1/2}$ and $\epsilon^{(4)}_{j+1/2}$ by $\nu_{j+1/2}$ controls the effective dissipation in regions of smooth flow in such a way that $\epsilon^{(2)}_{j+1/2}$ is proportional to the square of the mesh width, while $\epsilon^{(4)}_{j+1/2}$ is of order one, and the dissipative flux is of third order compared to the convective flux. Near a shock wave ν_j is of order one, effecting the behavior of the scheme such that it becomes locally a first order scheme. Subtracting $\bar{\nu}_{j+1/2}$ for $k^{(4)}$ eliminates the fourth differences, which otherwise cause oscillations near the shock wave. 2

VI. Two-Point Scheme Application

Write the difference equation at j and $j+1$.

Denote $P_1 = \frac{\Delta x}{\Delta t}$

$$P_1\left(U_j^{n+1} - U_j^n\right) + a/2\left(U_{j+1}^{n+1} - U_{j-1}^{n+1}\right) - \left(d_{j+1/2}^{n+1} - d_{j-1/2}^{n+1}\right) = 0 \tag{24}$$

The Δ-form of the difference equations denotes

$$\Delta U_j^n = U_j^{n+1} - U_j^n.$$

Using this form the equations at j and $j+1$ are

$$B_j \Delta U_j^n + C_j \Delta U_{j+1}^n = RHS_j^n - D_j \Delta U_{j-2}^n - A_j \Delta U_{j-1}^n - G_j U_{j+2}^n \tag{25}$$

$$A_{j+1} \Delta U_j^n + B_{j+1} \Delta U_{j+1}^n = RHS_{j+1}^n - D_j \Delta U_{j-1}^n - C_j \Delta U_{j+2}^n. \tag{26}$$

For simplicity let $\epsilon^{(2)}_{j+1/2} \equiv \epsilon^{(2)}_{j+1/2}\,\alpha_{j+1/2}$, $\epsilon^{(4)}_{j+1/2} \equiv \epsilon^{(4)}_{j-1/2}\,\alpha_{j-1/2}$.

$$A_j = \left(-a_{j-1}/2 - P_2\left(\epsilon^{(4)}_{j+1/2} + \epsilon^{(2)}_{j-1/2} - 3\,\epsilon^{(4)}_{j-1/2}\right)\right) \tag{27a}$$

$$B_j = \left(P_1 - P_2\left(\epsilon^{(2)}_{j-1/2} - 3\,\epsilon^{(4)}_{j+1/2} + \epsilon^{(2)}_{j-1/2} + 3\,\epsilon^{(4)}_{j-1/2}\right)\right) \tag{27b}$$

$$C_j = \left(a_{j+1}/2 \quad P_2\left(\epsilon^{(2)}_{j-1/2} - 3\,\epsilon^{(4)}_{j+1/2} + \epsilon^{(4)}_{j-1/2}\right)\right) \tag{27c}$$

$$D_j = P_2\,\epsilon^{(4)}_{j-1/2} \tag{27d}$$

$$G_j = P_2\,\epsilon^{(4)}_{j+1/2} \tag{27e}$$

$$P_2 = \Delta x/\Delta t \tag{27f}$$

$$\begin{aligned} RHS^n_j = {} & -1/4\left(\left(U^n_{j-1}\right)^2 - \left(U^n_{j-1}\right)^2\right) - P_2\Big\{\epsilon^{(2)}_{j+1/2}\left(U^n_{j-1} - U^n_j\right) \\ & - \epsilon^{(4)}_{j+1/2}\left(U^n_{j-2} - 3U^n_{j-1} - 3U^n_j - U^n_{j-1}\right) - \epsilon^{(2)}_{j+1/2}\left(U^n_j - U^n_{j-1}\right) \\ & - \epsilon^{(4)}_{j-1/2}\left(U^n_{j-1} - 3U^n_j - 3U^n_{j-1} - U^n_{j-2}\right)\Big\}. \end{aligned} \tag{27g}$$

Solve for ΔU^n_j and ΔU^n_{j-1}, for $j = 2, 4, 6, \cdots$.

The imposition of physical and numerical boundary conditions require the equations at $j = 2$ and $j = j\max - 1$ to be altered slightly, depending upon the numerical B.C.'s imposed. Our particular choices for numerical B.C.'s are the simple linear extrapolations.

$$\begin{aligned} U^n_0 &= 2U^n_1 - U^n_2 \\ U^n_{j\max+1} &= 2U^n_{j\max} - U^n_{j\max-1} \\ U_{j\max+2} &= 2U^n_{j\max+1} - U^n_{j\max}. \end{aligned} \tag{28}$$

We found that the scheme converged to steady state solutions most quickly when an under relaxation was applied. Which is exactly what our stability analysis suggested. Courant numbers of $C = 5$, 10 and 20 and relaxation factors of R 1, 0.8, 0.66, and 0.5 were tested. The best results were found when C 10 and R - 0.8. (see Figure 1)

VII. One-Point Scheme Application

The dissipation terms and related parameters for the one-point scheme are identical to those used in our two-point scheme. Using the Δ-form for our difference equation and writing this equation at j we have

$$A_j \Delta U_{j-1}^n + B_j \Delta U_j^n + C_j \Delta U_{j+1}^n = RHS_j^n - D_j \Delta U_{j-2}^n - G_j \Delta U_{j+2}^n. \tag{25}$$

where A_j, B_j, C_j, D_j, G_j and RHS_j^n are identical to (27). with exception to P. Here we define P according to our modified equation form,

$$P_1 = \Delta x \cdot \Delta t - \frac{C_j}{2} - 3\epsilon^{(4)} - \epsilon^{(2)} .$$

So now solve for ΔU_j^n at $j = 1, 2, 3, \cdots$.

Again the physical and numerical boundary conditions require some changes in defining ΔU_j^n at $j = 2$ and $j = j\max - 1$. The results obtained from our calculations with $C = 5$, 10, and 20 and $R = 1.0$, 0.8, and 0.5 were good. (see Figure 2)

However, the number of time steps before convergence to steady state solution is in contrast larger than that for the two-point scheme. So, we seek to improve the convergence rate of our one-point scheme.

The basic idea for improving the convergence rate is to iterate across a single time step in order to decrease the residual for that time step even further. The discretization is as follows.

First we have our basic equation,

$$A_j \Delta U_{j-1}^n + B_j \Delta U_j^n + C_j \Delta U_{j+1}^n + D_j \Delta U_{j-2}^n + G_j \Delta U_{j+2}^n = RHS_j^n. \tag{26}$$

We can write this in operator form as,

$$L_1(\Delta U_{j-2}^n, \Delta U_{j-1}^n) + B_j \Delta U_j^n + L_2(\Delta U_{j+1}^n, \Delta U_{j+2}^n) = RHS_j^n. \tag{27}$$

Now for the <u>inner iteration</u> let

$$\Delta U_j^{(m+1)} = \Delta U_j^{(m)} - \delta(\Delta U_j). \tag{28}$$

Set $\Delta U_j^{(m)} = 0$ initially.

$$L_1\left(\Delta U_{j-2}^{(m-1)}, \Delta U_{j-1}^{(m-1)}\right) - B_j\left(\Delta U_j^{(m)} - \delta(\Delta U_j)\right)$$

$$-L_2\left(\Delta U_{j-1}^{(m)}, \Delta U_{j-2}^{(m)}\right) - L_2\left(\delta(\Delta U_{j-1}), \delta(\Delta U_{j-2})\right) = RHS_j^n \tag{29}$$

$$B_j\delta(\Delta U_j) + C_j\delta(\Delta U_{j-1}) + G_j\delta(\Delta U_{j-2}) =$$

$$RHS_j^n - L_1\left(\Delta U_{j-2}^{(m-1)}, \Delta U_{j-1}^{(m-1)}\right) - B_j\Delta U_j^{(m)} - C_2\left(\Delta U_{j-1}^{(m)}, \Delta u_{j-2}^{(m)}\right). \tag{30}$$

We approximate the left-hand side of (30),

$$B_j\delta(\Delta U_j) + C_j\delta(\Delta U_{j-1}) + G_j\delta(\Delta U_{j-2}) \sim \bar{B}_j\delta(\Delta U_j)$$

and modify $\bar{B}_j$ in the following way.

$$\bar{B}_j = B_j - \frac{U}{2} \cdot 1/2\left(3\varepsilon_{j-1/2}^{(4)} - 3\varepsilon_{j-1/2}^{(2)} - 3\varepsilon_{j+1/2}^{(4)} - 3\varepsilon_{j+1/2}^{(2)}\right).$$

Now solve for $\delta(\Delta U_j)$ at $j = 1, 2, 3, \cdots$.

The imposition of boundary conditions will again require special treatment for $\delta(\Delta U_j)$ at $j = 2$ and $j = j\max - 1$.

Numerical experiments with $C = 5, 10$, and 20 and Relax = 1.0, 0.8, 0.6, 0.5 have shown good results for Relax = 1.0. (see Figure 3)

VIII. Conclusions and Recommendations

The two-point scheme with artificial viscosity was found to be unstable for certain Courant Numbers ($C = 5$, 10, and 20). However, applying a relaxation factor in the scheme stabilizes the method. The one point scheme appears unstable for certain Courant Numbers in its basic form. The one-point scheme is stable for Courant Numbers greater than zero in its modified form. However, a symmetric marching scheme will stabilize the method for all Courant Numbers. Both schemes appear to be suitable for aerodynamic problems since the results obtained from numerical experiments performed on Burgers' Equation are good.

The method has been successfully applied in solving the Euler equations about an airfoil by K. C. Reddy and Jim Jacocks, at the Arnold Engineering Development Center. A report on this work should be forthcoming. The method is also considered to have tremendous potential in providing a speed increase for Navier-Stokes solvers.

REFERENCES

1. Hoffman, Peter. "The Locally Implicit Method for Computational Aerodynamics." 1986 USAF-UES Summer Faculty Research Program Final Report, 1986.

2. Jameson, Antony. "Solution of the Euler Equations for Two Dimensional Transonic Flow by a Multigrid Method." Applied Mathematics and Computation, 13 (1983) 327-355.

(Figure 1)

BURGER'S EQUATION

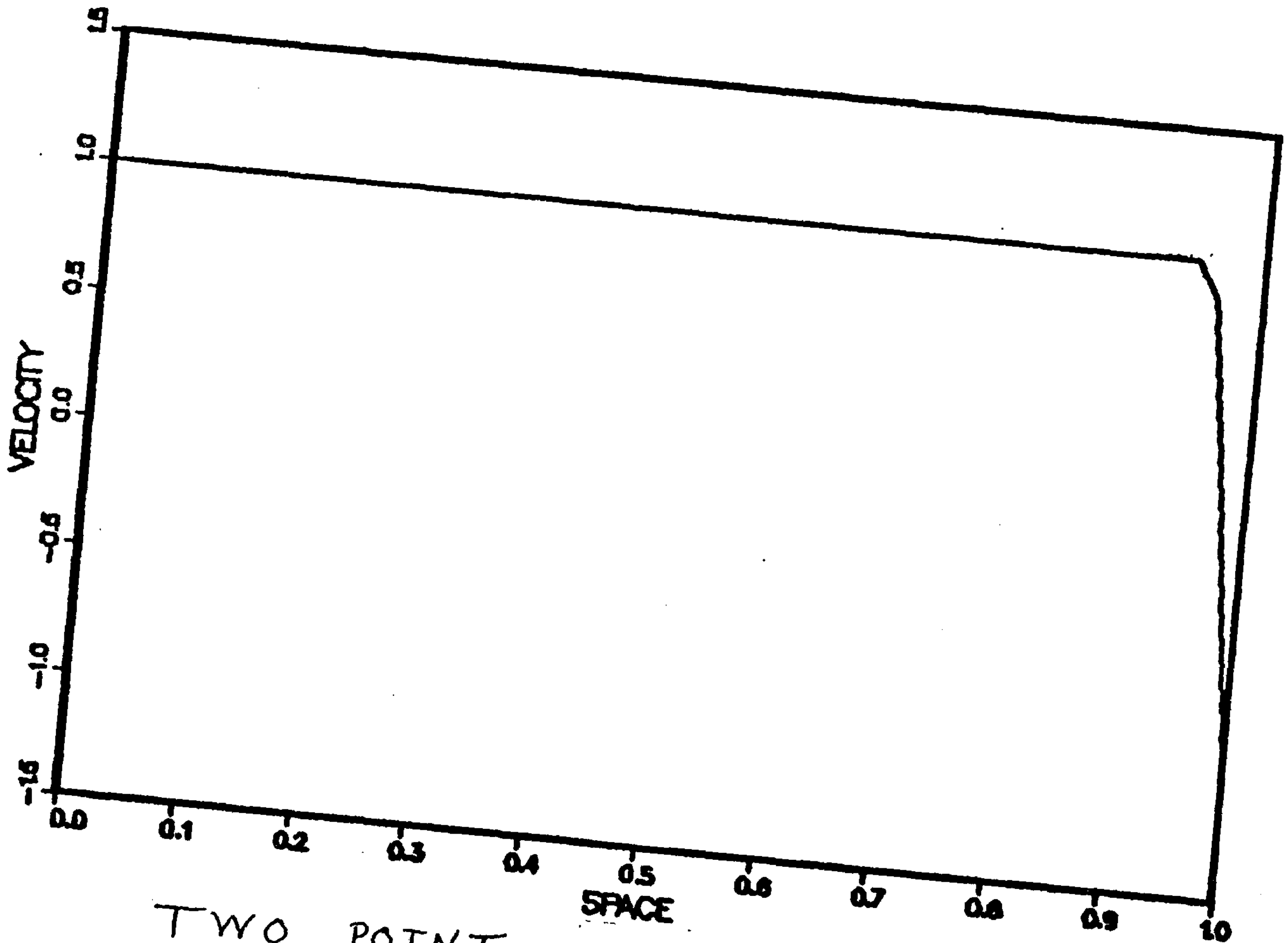

TWO POINT SCHEME

RELAX = 0.8

$K^{(2)} = 1.0$

$K^{(4)} = 0.03125$

CFL = 10

# of ITERATIONS = 47

(Figure 2)

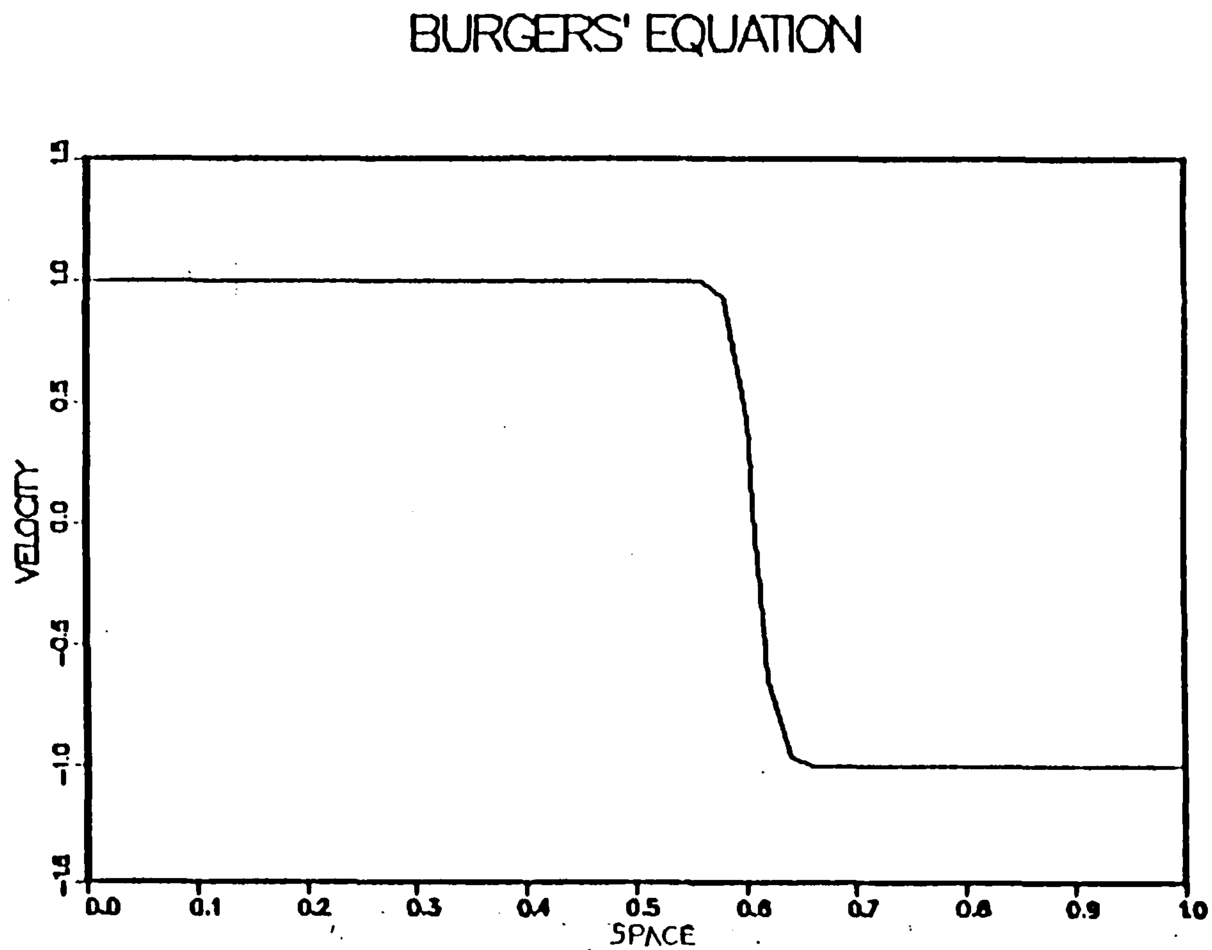

ONE POINT SCHEME (without inner iteration)

RELAX = 0.8 CFL = 10

$K^{(2)} = 1.0$ # of ITERATIONS = 60

$K^{(4)} = 0.03125$

(Figure 3)

BURGER'S EQUATION

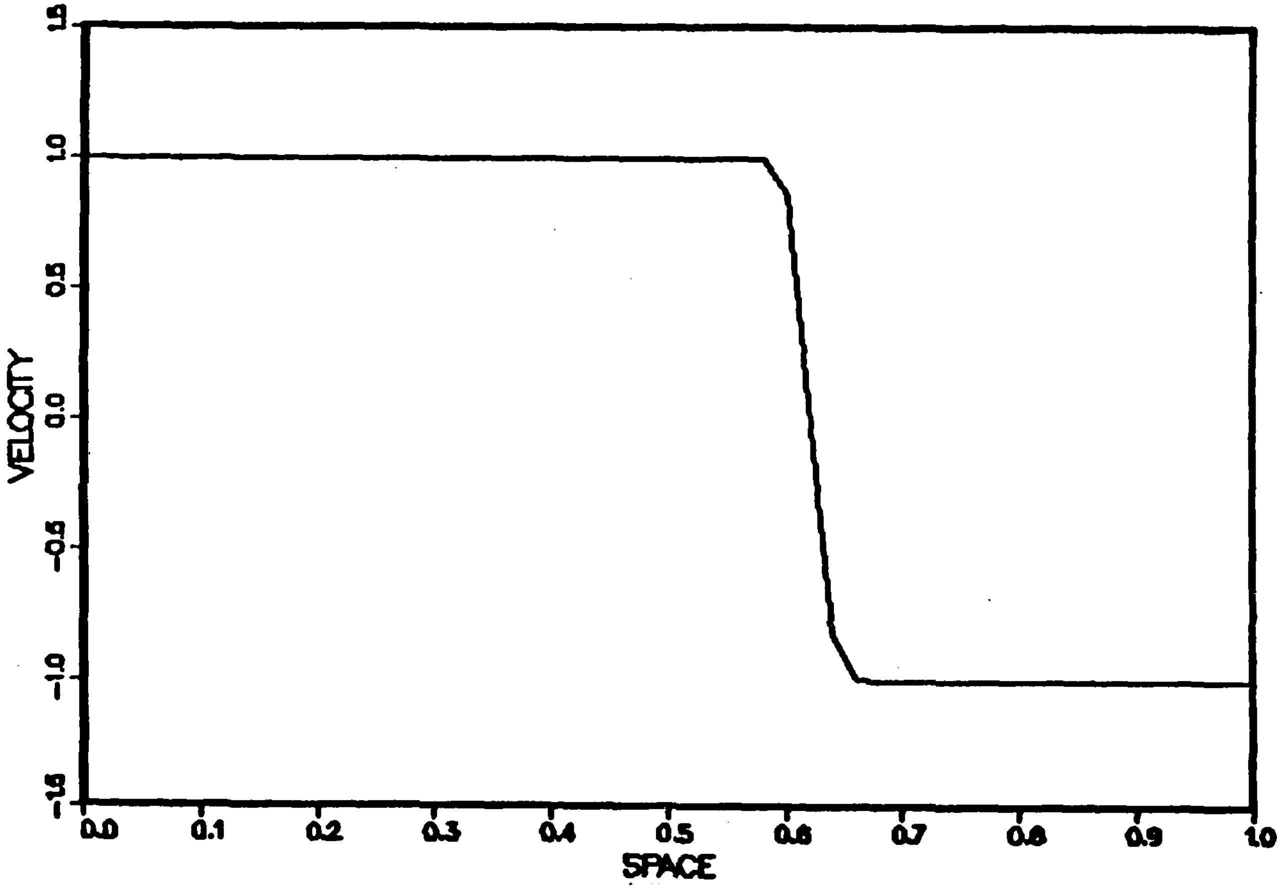

ONE POINT SCHEME (with inner iteration)

RELAX = 1.0 CFL = 10

$K^{(2)} = 1.0$ # of ITERATIONS = 20

$K^{(4)} = 0.03125$

1986 USAF-UES SUMMER FACULTY RESEARCH PROGRAM/

GRADUATE STUDENT SUMMER SUPPORT PROGRAM

Sponsored by the

AIR FORCE OFFICE OF SCIENTIFIC RESEARCH

Conducted by the

UNIVERSAL ENERGY SYSTEMS, INC.

FINAL REPORT

ADAPTIVE GRID GENERATION FOR VISCOUS FLOW PROBLEMS

Prepared by:	Christopher W. Reed
Academic Rank:	Graduate Student
Department:	Department of Engineering Sciences
University:	University of Florida
Research Location:	Armament Laboratory
	Eglin AFB
	DLC, Aerodynamics
	Branch, CFD Group
USAF Research:	Dr. Larry Lijweski
Date:	July 21, 1986
Contract No.:	F49620-85-C-0013

Adaptive Grid Generation for Viscous Flow Problems

By

Christopher W. Reed

ABSTRACT

An adaptive grid generation procedure is developed for viscous flow problems. The equations governing the adaptation are based on a variational statement resulting in a set of elliptic governing equations in which adaptation can occur independently in each coordinate direction. The method allows for explicit control of adaptation and orthogonality; however, smoothness of the grid is implicit in the equations. The adaptive grid generation equations respond properly to the control functions and are capable of providing the extremely refined mesh in the boundary layer regions. The grid generation equations are coupled with a thin layer Navier Stokes Code to solve a transonic axisymmetric projectile problem. A converged solution, however has not yet been obtained and it is necessary to investigate further the coupling procedure.

ACKNOWLEDGEMENTS

I wish to thank the Air Force Systems Command and the Air Force Office of Scientific Research for the support during the summer. I also wish to thank Mr. Steve Korn, Aerodynamics Branch Chief and Dr. Larry Lijewski, Air Force Armament Laboratory for the opportunity to work with the CFD group at Eglin AFB.

I. Introduction

The Air Force Armament Laboratory at Eglin Air Force Base is currently developing computational methods to determine the motion of stores released from aircraft traveling at transonic speeds. Critical to an accurate prediction of the store motion is an accurate calculation of the aerodynamic force acting on the store. For a standard projectile configuration, the aerodynamic force can be divided into three components: the surface pressure, the viscous drag and the base flow drag; the base flow drag can be as much as 50% of the total drag. It is, therefore, important to develop an accurate and efficient solution technique for the computation of viscous transonic projectile aerodynamics with base flow.

The current research and development effort of the laboratory is being centered on three-dimensional grid generation tecniques for use in Euler code. It is known that the coupling of an Euler code with a boundary-layer code can provide satisfactory pressure drag and viscous drag for a flow problem without separation. Also, research has been initiated on the application of a grid generation code and a thin-layer Navier-Stokes code which were installed during the 1984 AFOSR - SCEEE Summer Faculty Research Program [1]. The application of these codes to specific transonic projectile aerodynamics has been investigated by the U. S. Army Ballistic Research Laboratory and the results indicate that the thin-layer Navier-Stokes approximation can provide acceptably accurate solutions for complex transonic projectile flow problems [2].

In the application of a Navier-Stokes code or a combined Euler-boundary layer code to the transonic projectile flow problem, the intrinsic difficulty of the base flow problem is often avoided by modeling the base flow region with a sting; consequently, the important base flow drag cannot be computed. A computational technique for axisymmetric transonic projectile base flow

problems has recently been developed at the Army Ballistic Research Laboratory [3,4]. The planar grid used for the numerical computation was made up of two different grid systems, one covering the base flow region and the other covering the remaining flow region· consequently the thin-layer Navier-Stokes code was modified to take care of the flow field segmentation and patching.

The published results on the application of thin-layer Navier-Stokes codes clearly indicate that the thin-layer Navier-Stokes approximation can give acceptably accurate solutions for a projectile base flow at transonic speeds if a good grid network is provided for use in the solution algorithm. A good grid network is characterized by the smoothness of grids, the orthogonality of grids, and the grid resolution adaptive to the solution characteristics in the physical space. Enhancement of each of the grid characteristics has been shown to increase the accuracy of a numerical solution [5]. In fact the use of a grid not properly adaptive to the solution field can be detrimental to the convergence process of a solution algorithm. Also, for a complex transonic projectile flow problem, an extremely large number of grid points is often needed for the accuracy of the solution; however, the number of grid points which can be used in a solution algorithm is limited by the capacity of existing super computers. Therefore, it is important to develop and use adaptive grid generation techniques which can yield a good grid network with the limited number of grid points available.

II. Objectives

The primary objective of the summer research is to develop an adaptive grid generation scheme for use with viscous flow problems. Some critical features of the transonic viscous flow problem include shock regions, viscous sublayers and shear layer regions. Hence, a reliable adaptive grid generation

technique should be capable of generating fine grid resolution adapted to the pressure gradient and velocity gradient as well as providing extremely fine meshes in the viscous sublayer region for an accurate computation of the viscous drag force. In addition to these demands on the adaptation, the resulting grid should maintain to some degree both orthogonality and smoothness.

The specific steps necessary in accomplishing this objective include first the development of a set of equations to govern the grid node movement. The grid represented by these equations must respond to control functions reflecting the need for a refined mesh in the physical domain. Next, the proper definition of the control functions must be determined. In general, the control functions should be large when small grid spacing is desired, and small when no clustering is necessary. However the specific form of these functions, i.e. which variables to consider and which order derivatives to include, must be investigated. Finally, a means of coupling the adaptive grid generation procedure with the solution algorithm for the governing equations must be developed.

In order to evaluate the adaptive grid generation procedure, it has been applied to an axisymmetric transonic projectile problem with sting. The stipulation of axisymmetric flow reduces the physical domain to two independent spatial variables. Thus, the development of the adaptive grid generation procedure is presented for two dimensional grids, however, the method is readily extended to three dimensions. This flow problem includes the critical features of the transonic viscous flow problem and, thus, will provide a good test of the adaptive grid generation technique.

III. Adaptive Grid Generation

The generation of a computational mesh can be viewed as the development of a boundary fitted curvilinear coordinate system in which the intersection of the independent curvilinear coordinates define each grid node. For a two-dimensional problem there are two curvilinear coordinates ξ and η and their position in the physical domain are determined by the mapping

$$\begin{aligned} \xi &= \xi\,(x,y) \\ \eta &= \eta\,(x,y) \end{aligned} \tag{1}$$

The grid generation method, thus, becomes one of defining this mapping. The procedure developed here has its foundation in the calculus of variations. A functional for each grid characteristic can be defined such that the integral measures the deviation of the grid from those desired characteristics. Finding the solution (i.e. the curvilinear coordinates) which minimize these functionals will yield a grid network which contains the desired properties. The use of a variational approach in adaptive grid generation was first used by Brackbill and Saltzman and was successfully applied to a supersonic inviscid flow problem.[6,7] The functional used here is:

$$I_T = \int \frac{\nabla\xi\cdot\nabla\xi}{P}\,dxdy + \int \frac{\nabla\eta\cdot\nabla\eta}{Q}\,dxdy + \int (\nabla\xi\cdot\nabla\eta)^2\,dxdy \tag{2}$$

The first functional represents the adaptivity in the ξ coordinate direction. When the prescribed control function P is small the term $\nabla\xi\cdot\nabla\xi$ must also be small in order to minimize the integral. A small value of $\nabla\xi\cdot\nabla\xi$ corresponds to a large spacing of the curvilinear coordinates in the physical domain. Consequently, when P is large, the physical spacing will be small and, therefore, the inverse relationship between the control function and the

physical spacing is maintained. The second functional represents adaptation in the η coordinate direction where Q is the prescribed control function. The third functional is a measure of orthogonality defined such that an orthogonal grid will produce a minimum value for the integral. There is no explicit representation of smoothness, however, the resulting governing partial differential equations, as will be shown, are elliptic. The strong smoothing effect known to elliptic equations will provide the necessary smoothness provided the control functions are themselves smooth.

In order to find the solutions ξ and η which will minimize the total functional I_T the Euler-Lagrange equations in two dimensions are applied to the functional to yield two coupled partial differential equations. The solution to these equations, given below, represent the grid which minimizes the total functional I_T.

$$\frac{1}{P}(\xi_{xx} + \xi_{yy}) - \frac{\nabla P \cdot \nabla \xi}{P^2} + \eta_x^2 \xi_{xx} + 2\eta_x \eta_y \xi_{xy} + \eta_y^2 \xi_{yy} = 0 \tag{3}$$

$$\frac{1}{Q}(\eta_{xx} + \eta_{yy}) - \frac{\nabla Q \cdot \nabla \eta}{Q^2} + \xi_x^2 \eta_{xx} + 2\xi_x \xi_y \eta_{xy} + \xi_y^2 \eta_{yy} = 0 \tag{4}$$

Before proceeding to find the solution to these equations it will be beneficial to scale each functional so that the influence of adaptivity and orthogonality are of the same order of magnitude. A dimensional analysis shows the functional for adaptivity in the ξ direction to be of order (C/P), adaptivity in the η direction to be of order (C/Q) and orthogonality is of order (C^3/L^2) where C is the computational length scale and L the physical length scale. To provide consistent order throughout the resulting differential equations the following scaling was used.

$$P_L \int \frac{\nabla\xi \cdot \nabla\xi}{P}\, dxdy + Q_L \int \frac{\nabla\eta \cdot \nabla\eta}{Q}\, dxdy + \frac{\lambda}{J_L^{-1}} \int (\nabla\xi \cdot \nabla\eta)^2\, dxdy = 0 \tag{5}$$

where P_L, Q_L and J_L^{-1} are the local values of the two control functions and the Jacobian of the mapping respectively. These quantities are assumed constant during the application of the Euler-Lagrange equations. This violates the variational principle, however the resulting equations, properly scaled will yield better results. After including the scales the equations governing the grid are:

$$\xi_{xx} + \xi_{yy} - \frac{\nabla P \cdot \nabla\xi}{P} + \frac{\lambda}{J^{-1}} (\eta_x^2 \xi_{xx} + 2\eta_x \eta_y \xi_{xy} + \eta_y^2 \xi_{yy}) = 0 \tag{6}$$

$$\eta_{xx} + \eta_{yy} - \frac{\nabla Q \cdot \nabla\eta}{Q} + \frac{\lambda}{J^{-1}} (\xi_x^2 \eta_{xx} + 2\xi_x \xi_y \eta_{xy} + \xi_y^2 \eta_{yy}) = 0 \tag{7}$$

The parameter λ preceeding the portion of the equations governing orthogonality is a prescribed parameter which indicates the relative weighting of adaptivity to orthogonality that is desired in the grid network. The Laplacian operator is clear as the first two terms in each equation and equations will remain elliptic if the parameter λ is relatively small and the grid network remains relatively orthogonal. This emphasis on using elliptic equations to govern the grid generation is due to some desirable characteristics of such equations. In addition to the strong smoothing associated with these equations, elliptic equations also guarantee a one-to-one mapping between the cartesian and curvilinear coordinate systems. Furthermore, the elliptic equations represent a boundary value problem, thus, grid networks in fluid dynamics problems requiring the prescription of all boundaries can be

developed as well as for external flow problems in which the outer boundaries can be arbitrarily defined.

The grid generation governing equations are coupled, nonlinear and complex which implies the use of numerical techniques to find a solution. Again, the use of elliptic equations is beneficial in that a unique solution is known to exist and there are many proven numerical solution algorithms readily available. Before applying a finite difference algorithm however, it will be quite useful from a computational standpoint to invert the governing equations making x and y the dependent variables and ξ and η the independent variables. Obtaining a solution to the inverted equations corresponds to finding the inverse mapping

$$x = x\ (\xi,\ \eta) \qquad (8)$$
$$y = y\ (\xi,\ \eta)$$

The two governing equation for x and y in terms of ξ and η are:

$$a_1\, x_{\xi\xi} + a_2 x_{\xi\eta} + a_3 x_{\eta\eta} + b_1 y_{\xi\xi} + b_2 y_{\xi\eta} + b_3 y_{\eta\eta} = S_1$$

$$c_1 x_{\xi\xi} + c_2 x_{\xi\eta} + c_3 x_{\eta\eta} + d_1 y_{\xi\xi} + d_2 y_{\xi\eta} + d_3 y_{\eta\eta} = S_2$$

$$a_1 = -y_\eta(\alpha + \lambda'\beta^2) - 2\lambda' y_\xi \alpha\beta \qquad c_1 = y_\xi(\alpha + \lambda'\alpha^2) + 2\lambda' y_\eta \alpha\beta$$

$$a_2 = 2y_\eta(\beta + \lambda'\beta\gamma) + \lambda' y_\xi(4\beta^2 + J^2) \qquad c_2 = -2y_\xi(\beta + \lambda'\alpha\beta) - \lambda' y_\eta(4\beta^2 + J^2)$$

$$a_3 = -y_\eta(\gamma + \lambda'\gamma^2) - 2\lambda' y_\xi \alpha\beta \qquad c_3 = y_\xi(\gamma + \lambda'\beta^2) + 2\lambda' y_\eta \gamma\beta$$

$$b_1 = x_\eta(\alpha + \lambda'\beta^2) + 2\lambda' x_\xi \alpha\beta \qquad d_1 = -x_\xi(\alpha + \lambda'\alpha^2) - 2\lambda' x_\eta \alpha\beta$$

$$b_2 = -2x_\eta(\beta + \lambda'\beta\gamma) - \lambda' x_\xi(4\beta^2 + J^2) \qquad d_2 = 2x_\xi(\beta^2 + \lambda'\alpha\beta) + \lambda' x_\eta(4\beta^2 + J^2)$$

$$b_3 = x_\eta(\gamma + \lambda'\gamma^2) + 2\lambda' x_\xi \gamma\beta \qquad d_3 = -\, x_\xi(\gamma + \lambda'\beta^2) - 2\lambda' x_\eta \gamma\beta$$

$$\alpha = x_\eta^{\,2} + y_\eta^{\,2} \qquad \beta = x_\xi y_\xi + x_\eta y_\eta$$

$$\gamma = x_\xi^{\,2} + y_\xi^{\,2} \qquad J = x_\xi y_\eta - x_\eta y_\xi$$

$$S_1 = P_\xi(\alpha^2)/P \qquad S_2 = Q_\eta \gamma^2/Q \qquad \lambda' = \lambda/J$$

In the current research, second order finite difference expressions are used to represent the derivitives in the inverted governing equations and the Newton-Ryphson iterative procedure was used to solve the approximated equations.

Boundary Consistency

As the points in the interior of the domain move about during the iterative solution procedure to satisfy the finite difference equations it will be necessary to move grid points on the boundary coordinates along the coordinates to maintain consistency with the grid network in the interior. Direct application of the governing equations is not adequate since the grid nodes are constrained to move along the boundary, and it is therefore necessary to develop a separate procedure to apply to the boundary nodes. It is possible to write a non-dimensional functional for adaptivity along the boundary in terms of the arc length along the coordinate representing the

boundary, however, it is not possible to include orthogonality in this approach and it is therefore not developed.

The approach used instead is also based on a minimization, however, the equations governing the grid node movement are based on an energy analogy in which the potential energy stored in extensional and torsional springs placed between the grid nodes must be minimized. To represent the need for adaptivity, extensional springs with spring constants equal to the control function are assumed to exist between each node along the boundary. Such a system is shown in Figure 1, where ξ represents the boundary curvilinear coordinate of interest, S is the arc length along that boundary and P_i and P_{i+1} are the spring constants analogous to the control function in the 2-D adaptive grid generation equation. The total potential energy stored in the springs along the boundary is

$$E_A = \sum_i P_i(\Delta S_i)^2 \tag{9}$$

where $\Delta S_i = S_i - S_{i-1}$.

It is obvious then that for a large P_i, a small ΔS will be necessary to minimize the potential energy E_A thus maintaining a similar inverse relationship between the control function and the grid spacing as in the equations governing the grid in the domain. Without any regard to orthogonality the solutions S_i could be determined in eq.(9) so that E_A is minimized. In order to include a measure of orthononality, the orthogonality of the ξ and η coordinates at the boundary must be expressed in terms of the one-dimensional arc length S. A diagram showing an appropriate relationship is shown in Figure 2. First the arc length S between the node i is aproximated by the tangent vector $\underset{\sim}{t}$ between the two adjacent nodes. The x and y values of any point along the boundary in the locality of the i^{th} node can then be written in terms of S as

$$x(S_i) = S_{i-1} + x_\xi \cdot S_i$$

$$y(S_i) = y_{i-1} + y_\xi \cdot S_i$$

$$X_\xi = x_{i+1} - x_{i-1}$$

$$y_\xi = y_{i+1} - y_{i-1}$$

A measure of the orthogonality can then be made by calculating the scalar product of the tangent vector $\underset{\sim}{t}(x_\xi, y_\xi)$ with the vector $\underset{\sim}{r}$ which represents the direction of the η coordinate passing through the node of interest.

$$r_1 = x_0 - x(S_i)$$

$$r_2 = y_0 - y(S_i) \tag{10}$$

The expression for the scalar product D of the two vectors is

$$D(s_i) = x_\xi \cdot [x_0 - x(S_i)] + y_\xi \cdot [y_0 - y(S_i)] \tag{11}$$

which is equal to

$$|\underset{\sim}{r}||t|\cos\theta_i \tag{12}$$

where the angle θ_i is the angle between the ξ and η coordinates passing through the node of interest. The potential energy stored in a torsional spring measuring the skewness of the coordinates can be written as

$$E_0 = \sum_i \lambda\theta_i^2 \tag{13}$$

where λ is a torsional spring constant and plays the same roles as the parameter λ in the two dimensional grid generation equations. A consistent, but somewhat altered form of E_0 is used in which θ_i is replaced with $\cos\theta_i$. The resulting expression is a polynomial in S and therefore much simplified in form. After combining the expressions for extensional and torsional energy and applying a local scaling procedure similar to that used for the two dimensional governing equations a final total potential energy can be written as

$$E_T = \sum_i \left[\frac{P_i}{\hat{P}} (\Delta S_i)^2 + \frac{\lambda D^2(S_i)}{(\underset{\sim}{r_0} \cdot \underset{\sim}{r_0})}\right] \tag{14}$$

where $\hat{P}$ is the average of P_i and P_{i+1} and $\underset{\sim}{r}_0$ is the initial vector representing the direction of the η coordinate. In order to minimize the total energy E_T the derivative is set equal to zero:

$$\frac{\partial E_T}{\partial S_i} = 0 \text{ for } i = 1,2...N \tag{15}$$

resulting in a set of linear equations which can be solved for the arc length values at S_i for each node along the boundary. The position of the boundry nodes are coupled to the position of the interior nodes through the onthogonality and it is therefore necessary to update the boundary node locations continuously as the solution to the two-dimensional grid generation equations develops.

IV. Control Functions

During the development of the solution to the equations governing the fluid flow, i.e. the thin layer Navier Stokes equations, the dependent variables are going to experience large gradients. In transonic projectile problems, for instance, shocks and shear layer regions will develop, requiring refinement in the computational mesh to obtain an accurate solution. It is the control functions purpose to relay this information from the thin layer Navier Stokes solution to the equations governing the grid network adaptation. As described previously, the adaptive grid generation equations have been developed with an inverse relationship between the control function and the physical spacing of grid nodes, such that the control function is large in regions requiring mesh refinement.

The actual form of the control functions P and Q should reflect the magnitude of the trunction error in the finite difference approximations to the thin layer Navier Stokes equations. If, then, during the solution algorithm, a large truncation error developed, the resulting clustering as a response to the control functions would tend to reduce the error, maintaining therefore, a uniform value for the error throughout the domain. The expressions for the trunctation error, however, are quite complex and sometimes unknown making their calculation difficult or impossible. It is common, therefore, to use both experience and intuition to choose as the control functions a combination of the flow variable gradients which hopefully will reflect correctly the need for mesh refinement. For the transonic projectile problem both shocks and shear layers develop and the pressure and velocity are used to dictate the need for clustering. A general form for the central functions used presently is

$$P = \alpha_1 + \beta_1 \left|\frac{df_1}{ds}\right| + \gamma_1 \left|\frac{df_1}{ds^2}\right| + \ldots$$

$$Q = a_2 + \beta_2 \left|\frac{df_2}{dt}\right| + \gamma_2 \left|\frac{d^2 f_2}{dt^2}\right| + \ldots \tag{16}$$

where α_i, β_i, γ_i are prescribed coefficients, s is the arc length in the ξ dir, t the arc length in the η direction and f_i is the combinaion of variables used in the control function.

As part of the thin layer approximation, the velocity derivatives are not calculated in the streamwise direction. Assuming this to be the ξ direction the f_i become:

$$f_1 = p$$

$$f_2 = p + u$$

where p is the pressure and u is the fluid speed. Currently, the coefficients γ_i are set to zero and β_i are set to one. The two remaining coefficients α_1 and α_2 are set to a prescribed percentage of the maximum derivative of f_i.

$$\alpha_1 = \alpha_1' \left|\frac{df_1}{dS}\right|_{max}$$
$$\alpha_2 = \alpha_2' \left|\frac{df_2}{dt}\right|_{max} \tag{17}$$

Thus, the only required input are the two parameters, α_1' and α_2'. The influence of α_i' on the adaptive grid is to control the smoothness of the grid point spacing by controlling the relative magnitude of the control function along a coordinate direction. For instance, as α_i is increased, the ratio Pi/P_{i+1} for two points on a ξ coordinate will approach 1 and the spacing, therefore, will become equal. Eq. (16) is just one possible form of the control function and there will be a need to experiment with other possibilities in order to determine a correct form of the control functions.

V. Coupling

The next step in developing the adaptive grid generation procedure is to couple the adaptive grid generation equations with the solution algorithm for the thin layer Navier Stokes equations. The purpose of this coupling is to provide adaquate grid adaptation to the solution as it develops.

The use of the adaptive grid procedure will, of course, increase the necessary cpu time to obtain a solution and it is, thus, beneficial to adapt the grid as few times as possible. The number of timesteps between each grid adaption, however, must be determined and it will vary, depending on the number of timesteps required for convergence and the transient response of the

solution. After each grid adaptation it is necessary to interpolate the solution from the previous grid network onto the new grid network. This is requried to maintain the form of the solution as it is developing and to maintain accuracy in time for unsteady problems.

The adaptive grid generation procedure has been applied to an axi-symmetric transonic flow problem with a sting to eliminate the base flow region. The flow conditions include a Mach number of 0.96 and a Reynolds number of 750,000. The initial grid network, which also reveals the secant-ogive cylinder boattail (SOCBT) configuration of the projectile is shown in Figure 3. Ninety points are used in the streamwise coordinate direction and thirty five points are used in the coordinate direction normal to the projectile surface. The grid network was adapted at intervals of 25 time steps and the two control function parameters are $\alpha_1' = 0.01$ and $\alpha_2' = 5.0 \times 10^{-6}$.

The values of these parameters were chosen after some experimentation and they will depend on the physical length scale as well as the number of grid points used. The extremely small value of α_2 is to allow for the very fine mesh in the viscous sublayer region. Figures 4a and 4b show the calculated pressure coefficient along the projectile and the resulting adaptive grid network at 100 time steps (5 seconds, nondimensional time) and Figures 5a and 5b show the same at 200 time steps (10 seconds, nondimensional time).

The C_p plot of Figure 4a clearly shows that a large pressure gradient exists in the streamwise direction at the ogive-cylinder and cylinder-boattail junctures. The adaptive grid of Figure 4b shows the proper response to these gradients by clustering points in those regions. Also evident in this figure is the extremely fine resolution in the boundary layer region. The grid node

spacing at the projectile surface in this grid network is of order 10^{-5} which is suggested by Steger [2] for adequate resolution of the viscous sublayer.

The C_p plot at 10 seconds reveals that a shock just aft of the ogive-cylinder juncture has developed. This shock and a detached shock at the cylinder-boattail juncture are evident in the grid network of Figure 5b by the intense clustering at grid nodes in those regions. At this point it can be concluded that the adaptive grid generation equations are capable at responding well to the prescribed control functions. Unfortunately, when this solution procedure was carried further in time the solution failed to converge. The source of this failure needs to be investigated. Thus, more research is required before the adaptive grid generation procedure will be capable of yielding satisfactory results for the viscous projectile flow problem.

VI. Recommendations

At this point in the research, the adaptive grid generation equations have been shown to correctly respond in a predictable and reliable manner to the prescribed control functions. During an application to a steady transonic projectile flow problem, however, the coupled adaptive grid generation equations and the solution algorithm failed to produce a converged solution. To remedy this problem it will be necessary to conduct test to determine the effects of the control function parameters α_1' and α_2' on the adaptation procedure as well as investigate the coupling technique. Once suitable values for α_1' and α_2' are found and the coupling technique is improved, the adaptive grid generation procedure can be applied to the base flow problem.

References

1. Hsu, C. C., "On a Thin-Layer Navier-Stokes Code and Transonic Projectile Aerodynamics", Final Report, 1984 USAF-SCEEE Summer Faculty Research Program, August 1984.

2. Nietubicz, C. J., "Navier-Stokes Computations for Conventional and Hollow Projectile Shape at Transonic Velocities", AIAA-81-1262, 14th Fluid and Plasma Dynamics Conference, June 1981.

3. Sahu, J., Nietubicz, C. J., and Steger, J. L., "Navier-Stokes Computations of Projectile Base Flow at Transonic Speed with and without Base Injection", ARBRL-TR-02532, U. S. Army Ballistic Research Laboratory, November 1983.

4. Sahu, J, and Nietubicz, C. J., "Computational Modeling of the Base Region Flow for a Projectile with a Base Cavity", BRL-MR-3436, U. S. Army Ballistic Laboratory, April 1985.

5. Thompson, J. F., Numerical Grid Generation, Elsevier Science Publishing Co., New York, 1984.

6. Brackbill, J. U., "Coordinate System Control: Adaptive Meshes", in Numerical Grid Generation, edited by J. F. Thompson, North-Holland, 1982.

7. Saltzman, J., and Brackbill, J. U., "Application and Generalization of Variational Methods for Generating Adaptive Meshes", in Numerical Grid Generation, edited by J. F. Thompson, North-Holland, 1982.

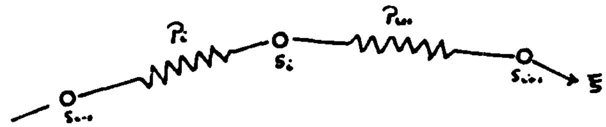

Figure 1. Extensional spring analogy

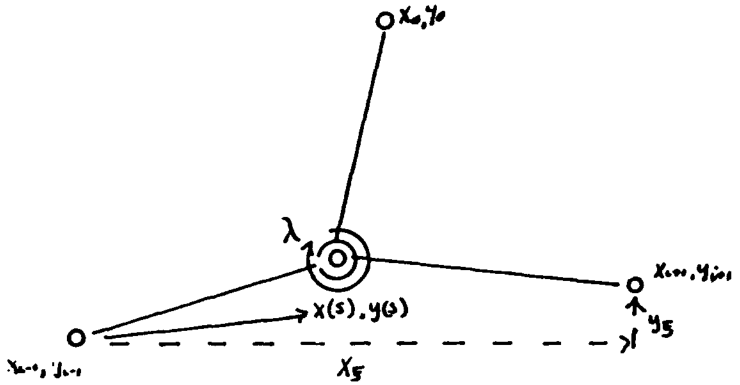

Figure 2. Torsional spring analogy

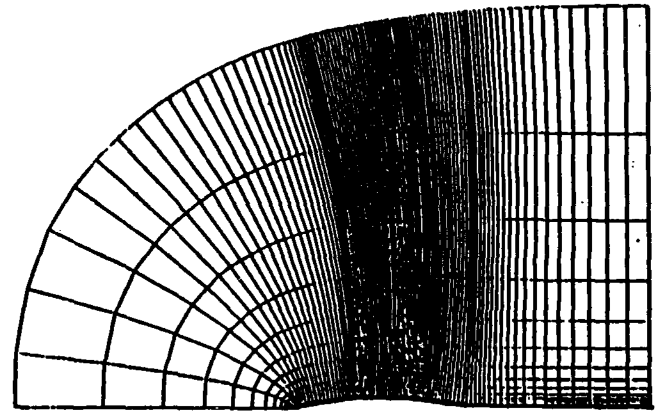

Figure 3. Initial grid configuration

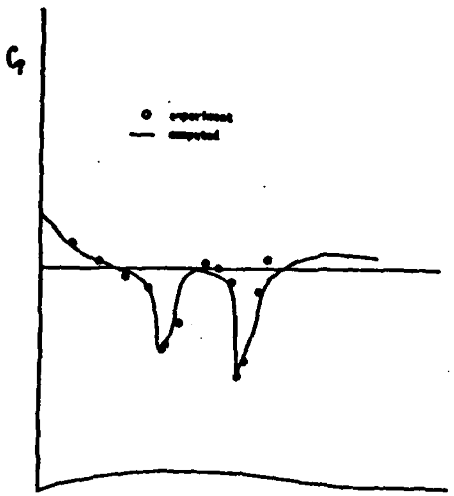

Figure 4a. Cp plot at 5 seconds

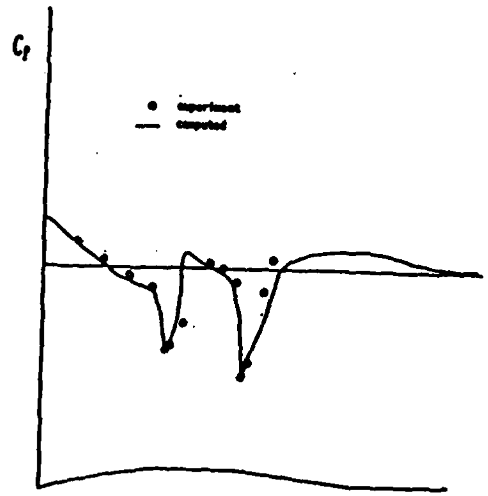

Figure 5a. Cp plot at 10 seconds

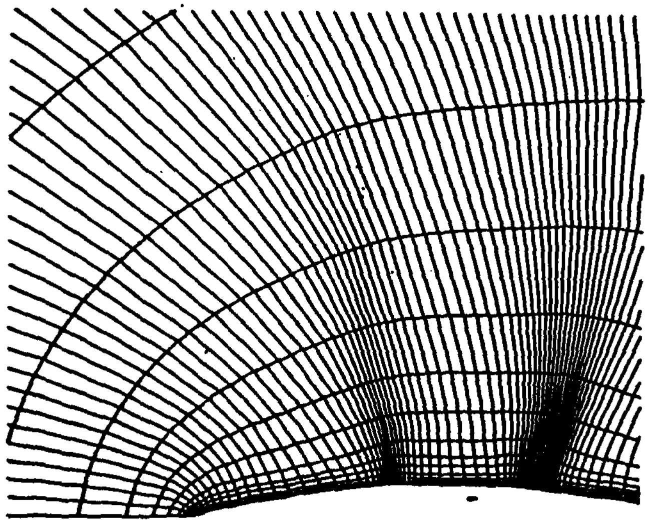

Figure 4b. Adapted grid at 5 seconds

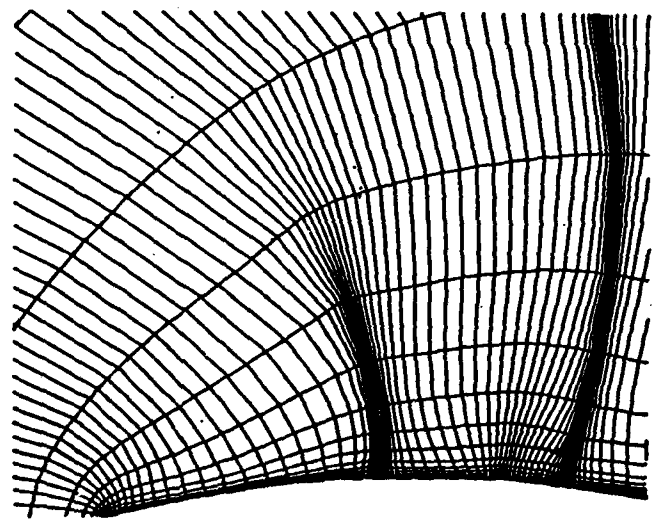

Figure 5b. Adapted grid at 10 seconds

1986 USAF-UES Summer Faculty Research Program/

Graduate Student Summer Support Program

Sponsored by the

Air Force Office of Scientific Research

Conducted by the

Universal Energy Systems, Inc.

Final Report

An Ultrastructural Study of Mossy Fiber Terminals Isolated from the Mammalian Brain

Prepared by: Brenda J. Claiborne, Greg Reger

Academic Rank: Assistant Professor

Department and University: Division of Life Sciences, University of Texas, San Antonio

Research Location: USAF School of Aerospace Medicine, Brooks Air Force Base

USAF Researcher: Dr. David Terrian

Date: September 20, 1986

Contract No. F49620-85-C-0013

An Ultrastructural Study of Mossy Fiber Terminals

Isolated from the Mammalian Brain

by

Brenda J. Claiborne

Greg Reger

ABSTRACT

A preparation of mossy fiber terminals isolated from the hippocampal formation of the rat brain was characterized at the ultrastructural level. Results indicated that the fraction was composed primarily of synaptic terminals, of which at least 31% contained zinc and were therefore terminals of the mossy fibers or their collaterals. All of the morphologically identifiable mossy fiber terminals contained zinc, showing that zinc is retained in the terminals during the isolation procedure. In addition, ultrastructural examination of the other fractions generated during the isolation procedure showed that each fraction was composed of the expected subcellular organelles.

Acknowledgements

I would like to thank the Air Force Systems Command and the Air Force Office of Scientific Research for sponsorship of my research. In addition, I would like to thank Dr. David Terrian, USAF School of Aerospace Medicine, Brooks Air Force Base, Texas, for the opportunity to work with him on an important problem in neurobiology. The project would not have been possible without the support of Dr. Davis who is in charge of the electron microscope facility at Brooks Air Force Base, and the assistance of Ms. W. Butcher and her staff in the electron microscope laboratory. Mr. Gregg Reger, a graduate student supported by the Air Force Office of Scientific Research for the summer, provided invaluable help with the technical aspects of the project. The prompt, courteous and efficient service of Universal Energy Systems was also greatly appreciated.

I. Introduction

One of research goals of the United States Air Force is to understand how neuronal excitability is regulated at the molecular level so that a rational approach may be developed for pharmacologically enhancing performance. As part of the research effort focused on this goal, Dr. David Terrian and his colleagues at Brooks Air Force Base have biochemically isolated a specific population of nerve terminals from the hippocampus of the rat brain. With this preparation they are examining biochemical and physiological aspects of neuronal excitability. The specific terminals they have isolated are from the mossy fibers, or axons, of the dentate granule cells; these terminals are of interest because they are thought to be involved in learning and memory.

For the past several years, part of my research interests have focused on these same axons. Using intracellular labeling techniques, the in vitro brain slice preparation and a computer-microscope system, I analyzed the morphology of the mossy fibers and the distribution of their terminals (Claiborne et al., 1986). Because of my previous experience in studying these terminals, I was assigned to Dr. David Terrian's laboratory at Brooks Air Force Base in San Antonio, Texas, for the 1986 USAF Summer Faculty Research Program.

II. Objectives of the Rese ~~h Effort

The overall objective of the research project was to characterize the mossy fiber terminal preparation at the ultrastructural level.

The specific goals were:

1. To examine the purity of the isolated mossy fiber preparation with the electron microscope.

2. To show whether or not zinc is retained in the mossy fiber terminals.

3. To characterize, at the ultrastructural level, the composition of the other fractions obtained during the isolation procedure.

4. To localize the sites of glutamate uptake in the isolated mossy fiber preparation.

III. Purity of the Mossy Fiber Preparation

To examine the purity of the isolated mossy fiber preparation at the ultrastructural level, samples of the fraction were fixed, dehydrated, embedded and sectioned for electron microscopy. These steps are summarized as follows:

The isolated mossy fiber fraction was prepared by Dr. David Terrian (Terrian et al., 1985) and an aliquot (approximately 0.5 cc) of the suspension was removed for electron microscopy. This aliquot was put into modified Karnovsky's fixative (1% paraformaldehyde, 1.25 % glutaraldehyde, 0.072 M cacodylate buffer, 0.045 M MgCl2 and 0.025% Al2Cl3). Samples were then pelleted into small

capillary tubes and left in the fixative for 1 hour. The pellets were removed and put into 0.1 M cacodylate buffer and washed in several changes of buffer over the course of 1 hour. Specimens were postfixed in 0.2 M osmium tetroxide for 1 hour, and then dehydrated through ascending concentrations of ethanol (50, 70, 85, 95, and 100%) for 15 minutes and 2 changes per step. They were embedded in epoxy and thin sections were cut on an ultramicrotome. Sections were routinely put onto mesh grids and stained with uranyl acetate followed by lead citrate. Sections were examined with a Hitachi microscope and micrographs taken at magnifications between 9,000 and 15,000. Both the sections and photographs were examined for mossy fiber terminals; the identification of mossy fiber terminals was based on published descriptions (Amaral and Dent, 1981).

Results showed that the fraction contained synaptic terminals, including some mossy fiber terminals, and nuclei, dendrites and axons. Although not quantified, the percentage of these latter three components was higher than would be expected for a "pure" mossy fiber terminal preparation. Additionally, the number of mossy fiber terminals of the appropriate size (4 um or greater in diameter) was lower than expected. Therefore, Dr. Terrian repeated the isolation, and we fixed and examined a sample from the first step of the procedure, the hippocampal homogenate. Although mossy fiber terminals were present, again they were not as large as expected. This result led

Dr. Terrian to modify the homogenization process. The biochemical procedures were repeated and the isolated mossy fiber terminal fraction was again examined with the electron microscope.

Qualitative results showed that the fraction contained primarily profiles of synaptic terminals. Other identifiable structures were seen only infrequently and included mitochondria, nuclei, dendrites and medullated fibers. Mossy fiber terminals were present in the isolated fraction. They were easily identified by their size (4 um or greater in diameter), their vesicle content, their irregular shape and the presence of two or more presynaptic densities. The other synaptic terminals in the fraction were morphologically similar to the mossy fiber terminals but were smaller.

In order to determine quantitatively the percentage of terminals that were mossy fiber terminals, a series of 20 random micrographs were taken from each of 4 different preparations. All of the presynaptic terminals in the micrographs were marked and Dr. D. Terrian and his technical staff calculated the perimeter and area of each profile. A profile was considered to be presynaptic if it contained vesicles and exhibited one or more presynaptic densities.

Results showed that, of a total of 1162 profiles, only 8.1% had an area greater than 1 um2, indicating that a relatively small proportion of the profiles could be

directly classified as mossy fiber terminals. It was possible, however, that some or all of the smaller profiles were 1) sections through mossy fiber terminals which only showed part of a terminal; 2) were sections through mossy fiber collateral terminals which have the same characteristics as the mossy fiber terminals, but are smaller; or 3) were other types of synaptic terminals present in the hippocampal formation. No ultrastructural methods were available to distinguish between possibilities 1 and 2, but experiments could be done to eliminate possibility number 3. These experiments were based on a unique property of the mossy fiber and collateral terminals -- they contain endogenous zinc, whereas other terminals in the hippocampus do not.

In order to determine if the smaller terminals contained zinc (and hence were either collateral or mossy fiber terminals), a series of random micrographs from the zinc-stained material prepared for the second set of experiments (see following section below) were taken. Results indicated that some, but not all, of the smaller terminals contained zinc: 21% of the terminals less than 1 um2 in area were positive for zinc, whereas 95% of the terminals 1 um2 in area or greater exhibited a positive zinc reaction. The total percentage of terminals of all sizes that were zinc-positive was 31%. This figure is probably an underestimate of the total number of zinc-containing profiles because the smaller terminals would be

statistically less likely to have dense precipitates than would the larger terminals.

The conclusions drawn from this set of experiments are that the fraction isolated by Dr. D. Terrian and his colleagues is composed primarily of synaptic terminals and that at least 31% of those terminals are zinc-containing and hence are profiles of terminals from the mossy fibers or their collaterals.

IV. Zinc Retention in Mossy Fiber Terminals

A unique property of the mossy fiber terminals in the mammalian hippocampus is their zinc content (Timm, 1958). It has been shown that the mossy fiber terminals both release and sequester zinc (Howell et al., 1984), and that chronic zinc deficiency 1)alters the function of the mossy fibers (Heese, 1979) and 2) is associated with learning deficiencies in children (Pfeiffer and Braverman, 1982). It is therefore possible that zinc may play an important role in neuronal excitability in the mammalian brain, and hence it was of interest to determine whether or not zinc is retained in the mossy fiber terminals during the isolation procedures. Techniques have been published for localizing zinc in brain tissue at both the light and electron microscopic levels using the so-called "Timm's stain" which involves treating the tissue of interest with sulphide. The sulphide complexes with the endogenous zinc and later reduces silver in the stain solution -- thereby forming a dark precipitate over the site of the original

zinc. Because there were no published reports of procedures for localizing zinc in biochemically isolated fractions of brain tissue, techniques used for this project were based on those for staining sections from mammalian brain (Haug, 1967; Danscher and Zimmer, 1978).

The isolated fractions were again prepared by Dr. David Terrian. Before the isolation procedure, half of the hippocampal tissue from the rat brains was incubated in a sodium sulphide solution (11.7 gm Na_2S, 11.9 gm NaH_2PO_4 in 1 liter of H_2O) for 5 minutes. Mossy fiber terminals were then isolated from both the sulphide-incubated and non-incubated tissue. (The non-incubated tissue served as a control for nonspecific tissue reactions.) When the final mossy fiber terminal fractions were obtained, aliquots of both were fixed using the same procedures described above and then divided into two groups. Some samples from the sulphide-treated tissue and some samples from the nontreated tissue were postfixed in osmium; the remaining samples were not osmicated. The non-osmicated samples served as controls for nonspecific reactions between osmium and sulphide -- if a nonspecific reaction occurred, electron-dense precipitates would form and would be mistakenly interpreted as a positive reaction for zinc. Aliquots of the isolated mitochondrial fraction (which would not be expected to contain zinc) were also treated in analogous fashion.

All samples were then dehydrated and embedded as described above. Thick sections (2 um) of each sample were cut for light microscopy and mounted on glass slides. The slides were immersed in the Timm's staining solution containing silver nitrate for 1 hour in the dark. (The composition of the Timm's stain solution was the same as that published by Danscher and Zimmer, 1978.) The sections were washed, stained with Toluidine blue, coverslipped and examined with the light microscope.

Results showed that all samples which were postfixed in osmium were covered with dense precipitate, even those which had not been incubated in the sodium sulphide solution. This indicated that a nonspecific reaction had occurred between the osmium and the Timm's stain. Those samples without either sodium sulphide or osmium treatment showed no reaction. Mossy fiber terminal fractions treated with sodium sulphide, but not osmicated, had discrete black deposits about 2 to 5 um in diameter scattered throughout the section, whereas the mitochondrial samples treated in the same fashion did not show any deposits. The deposits in the mossy fiber terminal fraction indicated that zinc was present.

Next I determined, at the ultrastructural level, if the zinc was located inside identifiable mossy fiber terminals. Some of the thick sections of the positively-stained sample (sulphide-treated, but without osmium) were reembedded and thin sections for electron microscopy were

cut. Results showed that electron-dense deposits indicative of zinc were present in all terminals which were identifiable as mossy fiber terminals -- that is, those that were greater than 4 um in diameter, were densely packed with vesicles and which had two or more presynatpic densities. Electron-dense precipitates were also present in some of the smaller terminals as discussed above.

The conclusion from these experiments is that zinc is retained in mossy fiber terminals during the isolation procedure.

V. Composition of Other Fractions

To characterize the composition of the other fractions obtained during the biochemical isolation of the mossy fiber terminals, aliquots of each fraction were fixed, dehydrated and embedded for electron microscopy as described above. Thin sections were cut, put onto mesh grids, and examined and photographed with the electron microscope. While examining the tissue with the microscope, notes were taken on the types of morphological structures seen in each fraction.

Results are as follows:

H: This fraction was very heterogeneous. It contained mitochondria, synaptic terminals, medullated fibers, nuclei, red blood cells and some mossy fiber terminals. The smaller profiles, including the synaptic terminals and mitochondria, were the predominate component.

P1: This subcellular fraction contained medullated fibers, small synaptic terminals and some nuclei. A relatively small percentage of the fraction consisted of mossy fiber terminals.

P2: This fraction consisted almost entirely of small profiles including synaptic terminals less than 1 um in diameter, mitochondria, and dendritic processes. There were also a few (less than 1% of the total) mossy fiber terminals.

P3: This fraction contained primarily synaptic terminals, with a number of very large (approximately 5 um in diameter) mossy fiber terminals. There were also some nuclei and medullated fibers.

M: At least 90% of this fraction was composed of medullated fibers. Only rarely were mossy fiber terminals seen.

N: This fraction was composed primarily (80 to 90%) of nuclei, with a few red blood cells, some small synaptic terminals and free mitochondria. No mossy fiber terminals were seen.

These ultrastructural results were in agreement with the predicted composition of the various fractions based on standard synaptosomal preparative procedures and Dr. D. Terrian's previous work on the cerebellum. The finding that the mossy fiber terminals were larger in the P3 fraction was of the most interest to Dr. D. Terrian and his

colleagues as this suggested that the terminals might be broken up during the last step in the isolation procedure.

VI. Glutamate Uptake Sites

This part of the project was not attempted because more time than we had predicted was spent on the first two objectives. I plan to continue to collaborate with Dr. D. Terrian on this aspect of the study.

VII. Recommendations

1. The characterization of the mossy fiber terminal fraction showed that most of the synaptic profiles which could be morphologically classified as mossy fiber terminals were smaller in diameter than intact mossy fiber terminals. This suggests that the mossy fiber terminals are breaking into smaller fragments during the isolation procedure, or that the fraction also contains some terminals of the mossy fiber collaterals. The role of the terminals of the mossy fiber collaterals is not yet known: a particularly interesting question is whether or not they participate in long-term potentiation as do the mossy fiber terminals themselves -- long-term potentiation is thought to be one of the cellular mechanisms underlying memory and learning. If the collateral terminals do participate in long-term potentiation, then the preparation developed by Dr. D. Terrian and his colleagues can be said to be functionally homogeneous. Hence, I am applying for a Minigrant to address the question of whether or not the

collateral terminals are involved in long-term potentiation.

2. Zinc is retained in the mossy fiber terminals during the isolation procedure. This result suggests that biochemical studies involving the role of zinc can now be done on the isolated mossy fiber terminals.

3. The other fractions generated during the isolation procedure contain the predicted subcellular components. The finding that the P3 fraction contains larger mossy fiber profiles than does the final fraction indicated that the conditions of the last step of the isolation procedure could be improved.

References

1. Amaral, D.G. and J. Dent, "Development of the Mossy Fibers of the Dentate Gyrus: 1. A Light and Electron Microscopic Study of the Mossy Fibers and Their Expansions," J. Comp. Neurol., 195 (1981) 51-86

2. Claiborne, B.J., Amaral, D.G. and W.M. Cowan, "A Light and Electron Microscopic Analysis of the Mossy Fibers of the Rat Dentate Gyrus," J. Comp. Neurol., 246 (1986) 435-458

3. Danscher, G. and J. Zimmer, "Light and Electron Microscopic Localization of Zinc in the Mossy Fibers of the Hippocampal Formation," Histochemie, 55 (1978) 27-40

4. Haug, F.-M., "Electron Microscopical Localization of the Zinc in Hippocampal Mossy Fiber Synapses by a Modified Sulfide Silver Procedure," Histochemie 8 (1967) 355-368

5. Heese, G.W., "Chronic Zinc Deficiency Alters Neuronal Function of Hippocampal Mossy Fibers," Science, 205 (1979) 1005-1007

6. Howell, G.A., Welch, M.G. amd C.J. Frederickson, "Simulation-induced Uptake and Release of Zinc in Hippocampal Slices," Nature, 308 (1984) 736-738

7. Pfeiffer, C.C. and E.R. Braverman, "Zinc, The Brain and Behavior," Biological Psychiatry, 17 (1982) 513-572

8. Terrian, D.M., Butcher, W.I., Wu, P.U. and D.L. Armstrong, "Isolation of Glomeruli from Areas of Bovine Cerebellum and Comparison of [^3H] Serotonin Uptake," Brain Res. Bull. 15 (1985) 469-475

9. Timm, F., "Zur Histochemie des Ammonshorngebietes," Z. Zellforsch. 46 (1958) 548

1986 USAF/UES Summer Faculty Research Program

Graduate Student Summer Support Program

Sponsored by the

Air Force Office of Research

Conducted by the

Universal Energy Systems, Inc.

FINAL REPORT

Response of Downslope and Florida Mesoscale Wind Systems to Physiographic Features

Prepared by: Anthony E. Restaino

Academic Rank: Graduate Student

Department and University: Department of Atmospheric Science, State University of New York at Albany

Research Location: Air Force Geophysics Laboratory, LYC
Hanscom Air Force Base Massachusetts

USAF Researcher: Dr. Robert M. Banta

Date: September 10, 1986

Contract No.: F49620-85-C-0013

Response of Downslope and Florida Mesoscale Wind System to Physiographic Features

by

Anthony E. Restaino

ABSTRACT

Numerical simulations of nocturnal slope flow were conducted using a 2-dimensional version of the Tripoli-Cotton CSU model. Variations of mountain height and soil moisture altered the intensity of downslope flows. And, Katabatic flow intensified with an increase in mountain height. Moreover, high soil moisture was found to suppress downslope flow. Significant perturbations developed in the katabatic layer after one hour of model run time. These perturbations excited gravity waves in the free atmosphere above the surface layer where potential temperature increased roughly 0.03 'C/Km.

A separate experiment for a Florida case study showed that soil moisture variations affected mesoscale wind fields, cloud formations, and precipitation.

Acknowledgments

I would like to thank the Air Force Systems Command, Air Force Office of Scientific Resarch, and the Cloud Physics Branch at the Air Force Geophysics Laboratory located at Hanscom AFB for sponsoring the GSSSP.

Special thanks goes to S.Sgt Charles Crouch, and Keeley Hanson for sharing their knowledge of computer system operations. Capt. Kim Pantley graciously supported me in data analysis. I also thank Barbara Main for preparing the figures shown in this paper.

I am very grateful to Dr. Robert Banta for spending much time with me in this research effort. His knowledge of atmospheric science and CRAY-IBM interaction made this project possible. I am indebted to Dr. Patrick Gannon who chose me to assist him this past summer. He's been a source of encouragement, support, and opportunity. I also thank Dr. Richard E. Orville and Kathy Stutsrim for allowing me to use the word processor at the Department of Atmospheric Science, SUNYA.

Finally, I would like to thank my parents for their unselfish assistance and generosity in supporting me during this ten week period.

I. Introduction

I am currently finishing a Master's Degree at the State University of New York at Albany. The thesis is a study of the seasonal variation of dynamics in tornado outbreaks. The emphasis is on how thermodynamics and hydrodynamics vary for outbreaks of tornadoes from winter to summer. My main interests are in synoptic meteorology, much of which I learned from Dr. Partrick Gannon when I attended Lyndon State College.

The research being conducted at AFGL/LYC regarding surface influences on mesoscale circulations was of interest to me since my area of research is on mesoscale phenomenon.

II. Objectives of the Research Effort

The overall objective of these two projects (downslope flow and Florida convection) is to determine the effects that specific surface conditions have on mesoscale circulations. The individual objectives were:

1. A study of observed cloud and precipitation patterns associated with soil moisture and physiographic features over south Florida.

2. Sensitivity studies of the response of nocturnal downslope wind systems to prescribed changes in terrain profiles, initial soil moisture.

3. A study of the steady state of the downslope flow.

4. A study of perturbations that develop in downslope flow.

III. Florida Meso-synoptic Systems[1]

McCumber and Pielke (6) developed a multi-level soil moisture flux model that was later modified by Tremback (9). We use this version to obtain soil moisture profiles for southern Florida during the period August 2-19, 1975. This is accomplished by using values of daily rainfall and evapotranspiration. We hope to see a relationship between surface relative humidity and cloud cover (upward motion).

Figure 1a shows the rainfall (cm) for central and southern Florida on August 12. Model derived surface relative humidity for the following morning is shown in Figure 1b. The letter 'D' marks the driest portions of the domain. As expected it corresponds quite well with Figure 1a. Cloud imagery at 1304 EDT is displayed in Figure 1c. Dashed lines represent the threshold at which cloud cover is detected by satellite. Solid contours indicate higher reflectivities of the cloud. It is apparent that clouds form on the edges of dry and moist boundaries of soil moisture. Of course, the shape of the peninsula, with its harbors, has a great deal to do with where clouds form, but clouds are noticeably absent from regions that are wet in Figure 1c.

---

[1] Additional discussion of project results is provided in the final report by Dr. Patrick Gannon, SFRP.

IV. Downslope Flow[2]

Four simulations of downslope flow were conducted with a numerical model developed by Tripoli and Cotton (10). Table 1 illustrates the experimental design for this paper. A critical bulk-Richardson number of 0.25 was chosen so diffusion of momentum from the surface layer to the free atmosphere would not be overly suppressed. This decision was based on work previously conducted by Petkovsek and Hocevar (8), Yamada (11), Bader (1), Garrett (4), and Manins and Sawford (5). The model is initialized with a mean wind of zero and a 5 'K inversion in the lowest 50 meters (the first model level above the surface for the low resolution model). The inversion is the same magnitude of degrees for the high resolution model except the first model level is at 25 meters above the surface. The inversion is much stronger for the high resolution simulations. Thus, comparisons cannot be made between high and low resolution experiments. The original purpose in using different resolutions was to examine the change in the depth of the katabatic layer since the layer itself is on the order of ten meters.

---

[2] Additional discussion of project results is provided in the final report by Dr. Patrick Gannon, SFRP.

TABLE 1

Simulation	Hill(Km)	Resolution	Run Time	Soil Moisture	T	X	Z
A	0.5	LOW	18000s	LOW	2s	200m	100m
B	0.5	LOW	7200s	HIGH	2s	200m	100m
C	0.5	HIGH	7200s	LOW	1s	100m	50m
D	1.0	HIGH	7200s	LOW	1s	100m	50m

The values of low soil moisture at the air-ground interface correspond to a relative humidity (RH) of 80%; the values of high soil moisture correspond to an RH of 100%. Up to 700mb the mixing ratio is 1 g/Kg in the ambient atmosphere.

Start time is 2100 solar time (sunset). The atmosphere above the surface layer is initialized with a dry adiabaitic lapse rate. Radiational cooling is the forcing mechanism in the model.

A. Steady State

Simulation A was run for 5 hours to show the types of perturbations that developed, and to examine steady state. This experiment will be later compared to Simulation B to examine the role that soil moisture plays in katabatic flow development.

Figure 2a shows the terms in the U-equation of motion for Simulation A. The terms in the figure are taken from a grid point 3.5Km to the right of the summit and 67 meters above the mountain surface. The expressions in Figure 2a shown at the right-hand side of the figure are negatives of

the following terms: UDU/DX and WDU/DZ are the horizontal and vertical advection of the U component of wind, DP/DX is the horizontal pressure force, DIFFUX and DIFFUZ are the horizontal and vertical transport of U (2). A, B, C, D, E in the figure are the terms respectively. We notice very little happening in the first 115 minutes. At this time pulsing (perturbations) become evident in the flow. It is apparent that as a bubble of lower pressure slides down the hill (DP/DX<0) horizontal and vertical advection of U increases. The vertical advection of U (B in the figure) is largest near 120 minutes then it becomes quite a bit smaller as time progresses. The horizontal advection of U (A in the diagram) slowly decreases, although in an oscillatory pattern as B, throughout the period. The same is true for the rest of the terms, but none seem to reach steady state. In Figure 2d the heat flux (WPTHP) and moisture flux (WPQTP) do not reach equilibrium at 5 hours of model run time. This diagram shows the downward transport of heat increasing until the second hour of run time. The same is true for the moisture flux. The high soil moisture heat and moisture fluxes (not shown) are much less pronounced because of less cooling and higher moisture at the air-ground interface.

A comparison between high soil moisture and low soil moisture simulations (Simulations A and B) can be seen in

Figures 2b and 2c. Figure 2b is the same experiment as Figure 2a but at a point on the mountain closer to the summit. In addition, Figures 2b and 2c have values plotted every 15 minutes, whereas Figure 2a has values plotted every 5 minutes. What is shown in comparing these figures is that the low soil moisture simulation has more active pulsing the first 100 minutes than the high soil moisture case. Nevertheless, the high soil moisture run becomes quite active at 2 hours. The reason for this is not well understood.

B. Variation in Mountain Height

Simulations C and D were run to examine the primary effects of mountain height. Earlier research by Fleagle (3), McNider (7) and Petkovesek and Hocevar (8) showed that the strength of drainage flows was inversely proportional to mountain slope. Their reasoning behind this is that compressional warming is much greater for a parcel sliding down a steep mountain than for a more gentle sloping mountain. This, however, is not the case when the stability of the air is neutral above the uniform surface layer inversion.

1. The One-half Kilometer Hill

Figure 3a shows 299 and 299.5 degree isentropes (lines of constant potential temperature) at initialization. Resolution is insufficient to see the 5° K inversion in the

lowest part of the domain. The waviness in isentropes is due to graphics interpolation. Note that the isentropes are parallel with the topography. This is very similar to the one kilometer hill (not shown). As a result, there is very little compressional warming for both hills initially. Maximum downward motion in the domain is plotted in Figure 3b (units are cm/s). The maximum value of -w is -2.6 m/s at about 95 minutes. Figure 3c is an illustration of the vertical time cross section of downward motion (cm/s). The abscissa is the time in minutes. Notice that maximum descent is 1300 m above z=0. Figures 3d, e and f show how the fields of vertical motion develop with time. Wind vectors are also shown in these figures. Isolines of vertical motion are in 25 cm/s increments. The circulation is evident in Figure 3d only 40 minutes after start time. Figure 3e is just 20 minutes later, yet perturbations in the wind field are evident. Figure 3f is at the end of the two hour simulation. The depth of the downslope flow is about 400 m with a strong return flow throughout the rest of the domain. Maximum descent, as expected, is directly above the summit.

2. The One Kilometer Hill

Figures 4a and 4b are the same as 3b and 3c respectively except we are now looking at the 1 Km hill results. Figure 4a shows that downward motion approaches -3 m/s. Yet, at two

hours the decent is less for the one Km hill than the half Km hill. Figure 4b illustrates the double maxima in negative vertical motion. This is considerably different than what we see in Figure 3c with the one-half Km hill. In Figure 4b it is seen that the strongest descent is at 1700 m above z=0, or it is almost a half kilometer higher than for the one-half kilometer hill.

The presence of gravity waves may be the reason for the double maxima and the decrease in the intensity of the sinking air at two hours run time. The half Km hill produced very small perturbations as a result of oscillations in the surface layer, but the one Km hill generated a very noticeable gravity wave. Figures 4c-f illustrate this. These figures show perturbation pressure (dynes/cm**2) with contours at every 10 dynes/cm**2. Figure 4c shows an interesting configuration of perturbation pressure (P') at the end of the first hour of model time. The minimum and maximum in the P' field are directly above the summit. Convergence aloft and divergence near the surface are coupled with minimum and maximum P' respectively. At this time there is not much of a return flow. Twenty minutes later, Figure 4d, the P' gradient is stronger. At this time the return flow becomes evident aloft. The important item is the wave in the P' field that has developed. The circulation is

centered about the trough axis of the wave. In Figure 4e, twenty minutes later, the wave has propagated away for the summit. The circulation about the trough axis has strengthened, and the wave has amplified. At the end of the two hour simulation Figure 4f shows that the wave has progressed further to the east, but amplitude has decreased. Neverthless, the circulation remains strong.

It would seem that this wave is in some way responsible for the double maxima of downward motion in Figure 4b. Also, the gravity wave seems to have a direct effect on the decrease of -w in Figure 4a as the second hour approaches. As the wave propagates eastward the region of compensating subsidence is increasing in size. Thus, from continuity, downward motion must eventually decrease with time. This can be seen in Figures 4d and 4e.

This wave propagated at approximately 1.2 m/s or at about the same phase speed as computed in Equation (1):

$$C = \pm \frac{1}{\mu}\left(\frac{g}{\bar{\theta}}\frac{\partial \bar{\theta}}{\partial z}\right)^{\frac{1}{2}} \qquad (1)$$

where, μ = horizontal wavelength
g = gravity
$\bar{\theta}$ = mean potential temperature
$\partial \bar{\theta}/\partial z$ = potential temperature lapse rate

The equation was applied to the ambient atmosphere at a height of about 1 Km where the wave was found. At this altitude the lapse rate of Theta was approximately 0.03' K/Km. Thus, buoyancy oscillations can exist in an atmosphere

that is nearly neutral in stabilty. Moreover, the perturbation pressure change associated with this gravity wave is smaller than many microbarographs can measure.

V. Recommendations

A. Downslope flows

1. Run a 3-D experiment to investigate the effects that a wet region on a hill side has on the evolution of katabatic flow. This is analogous to the situation when part of the mountain slope experienced rainfall from upslope convergence during the daylight hours.

2. Investigate the effects that a stable atmosphere has on the intensity of downslope flow.

3. Run a 2-D 24 hour simulation. This would show how upslope flow and downslope flow evolve over a day, and it would illustrate when steady state is reached.

4. Examine the effects that snow cover on the upper part of the mountain has on the development of katabatic wind systems.

B. Florida meso-synoptic systems

1. Run the same type of experiment again except for several cases when wind flow is from various directions. This will show how fields of vertical motion change for specified synoptic scale wind flows.

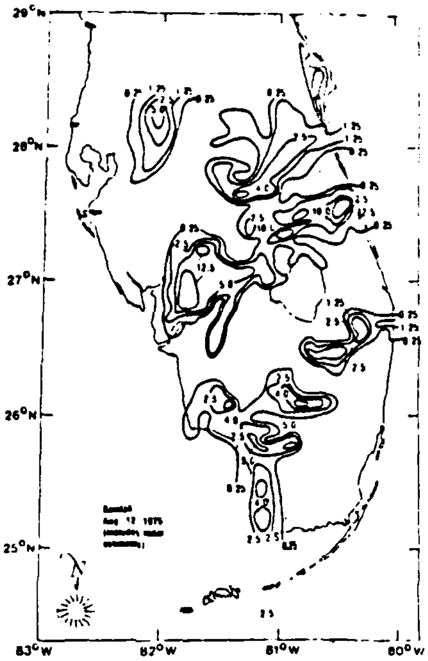

Figure 1a. Florida Rainfall (cm/s)

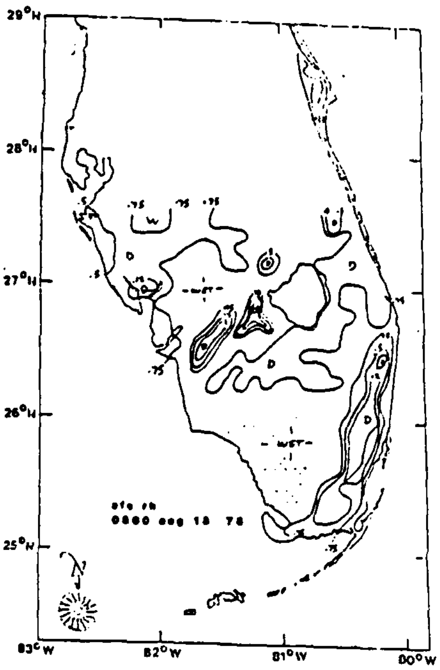

Figure 1b. Florida Relative Humidity (%/100)
'D' denotes dry regions.

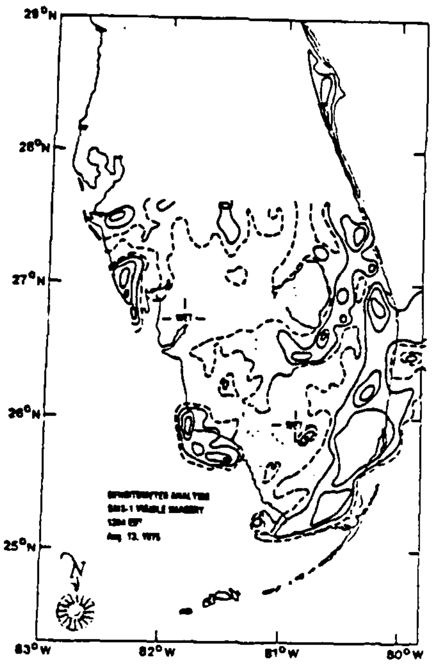

Figure 1c. Florida Cloud Cover Analysis. Dashed lines show where clouds are first detected. Solid lines indicate higher reflectivities of the cloud.

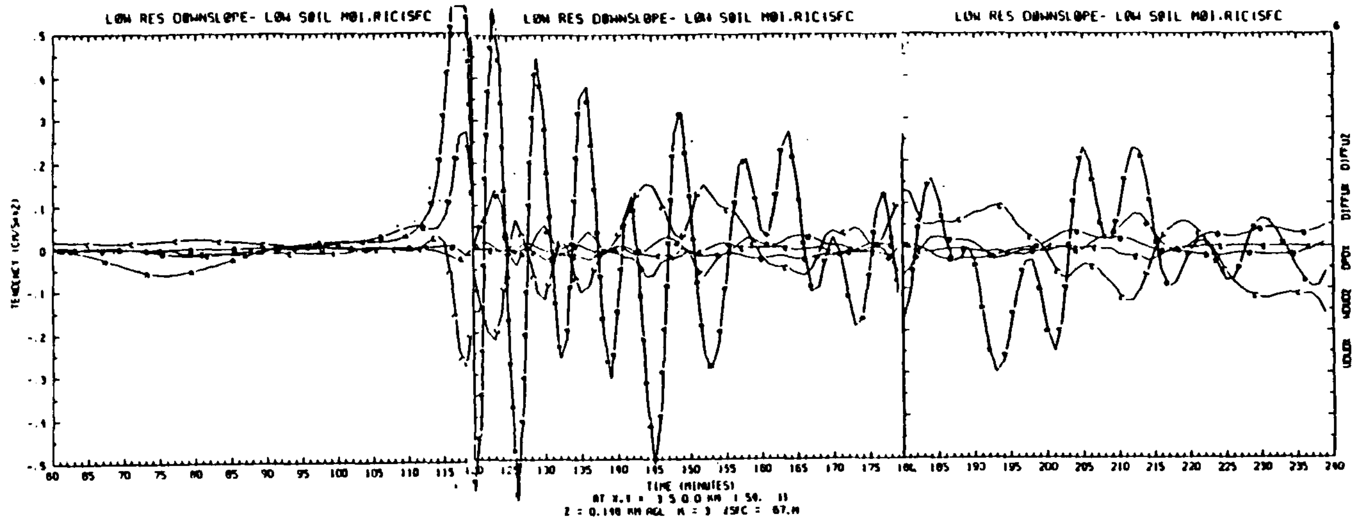

Figure 2a. TERMS IN THE U - EQUATION OF MOTION. This is for the one-half kilometer hill, low soil moisture at x=3.5 km.

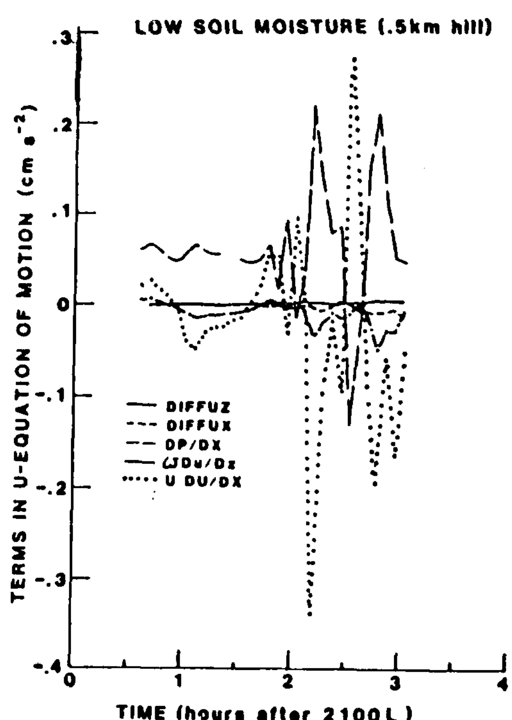

Figure 2b. Same as Fig. 2a except at x=2.3km

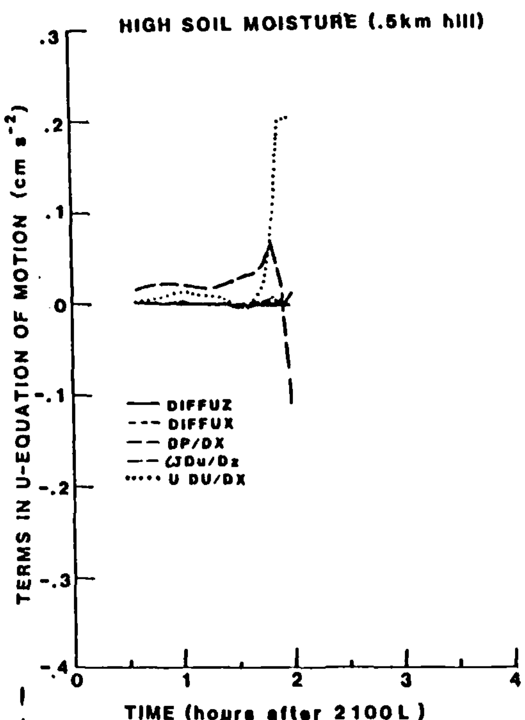

Figure 2c. Same as Fig. 2b except for high SM.

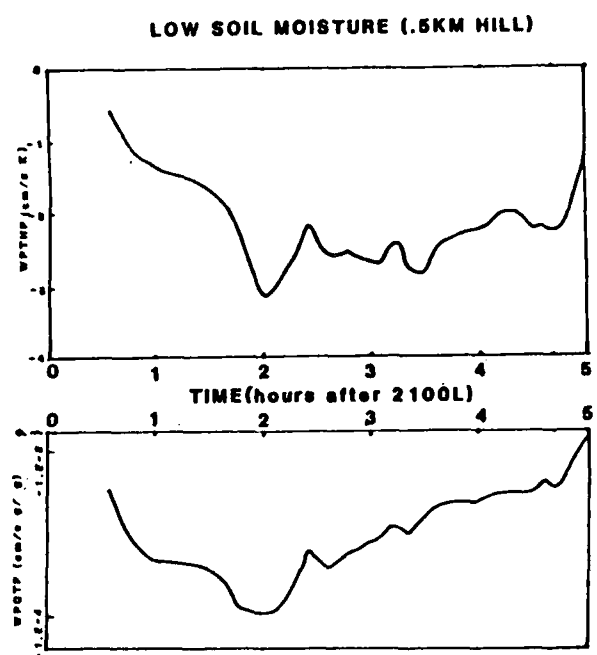

Figure 2d. Heat (WPTHP) and moisture (WPQTP fluxes for low SM at x=2.3 km.

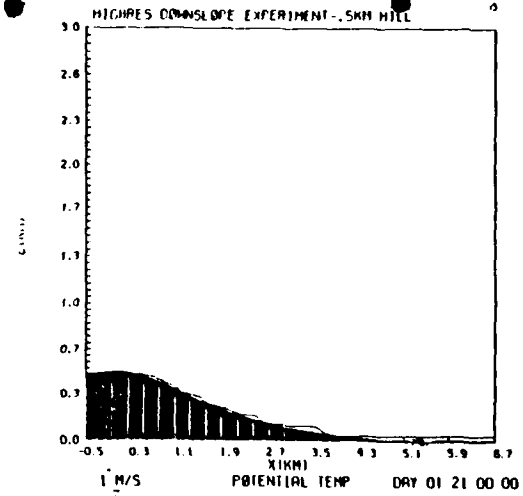

Figure 3a. Isentropes every 0.5 'K 0.5 km hill.

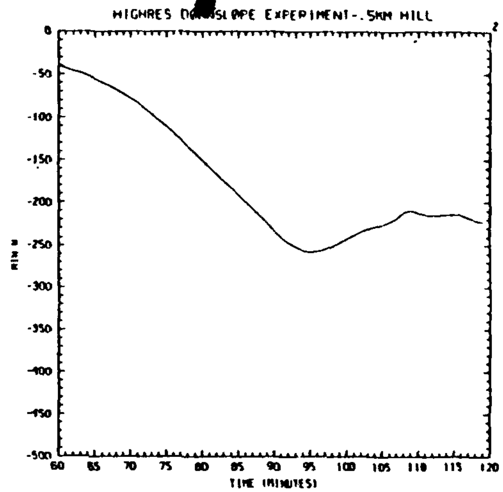

Figure 3b. Maximum downward motion (cm/s) in in domain as a function of time.

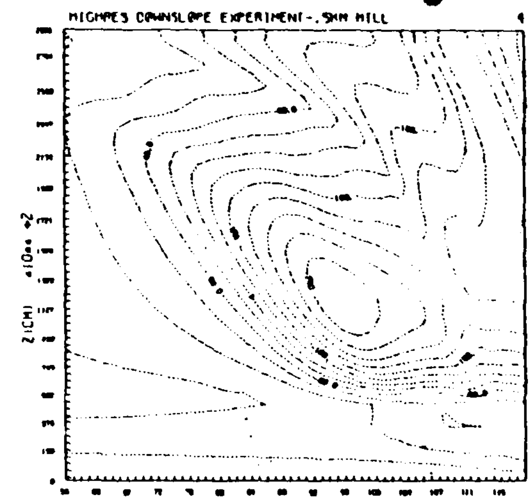

Figure 3c. Maximum downward motion (cm/s) in domain as a function of height and time (abscissa) in minutes.

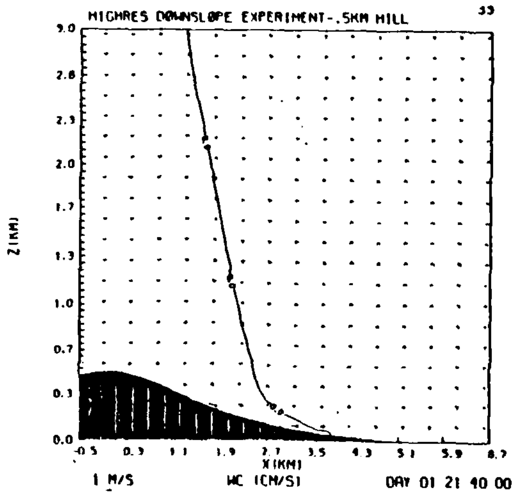

Figure 3d. Wind field 40 minutes after initialization. Vertical motion field contoured every 25 cm/s.

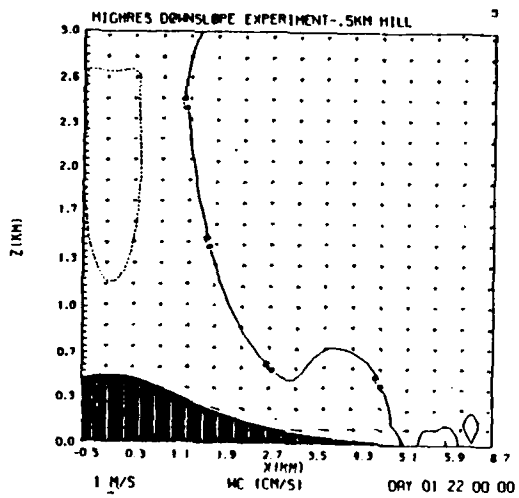

Figure 3e. Same as Fig. 3d except at one hour after initialization.

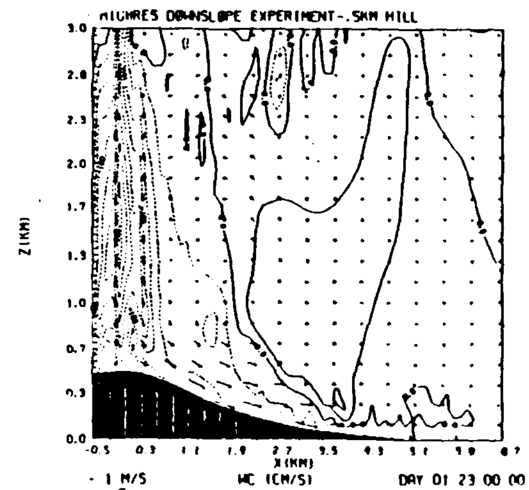

Figure 3f. Same as Fig. 3d except at two hours after initialization.

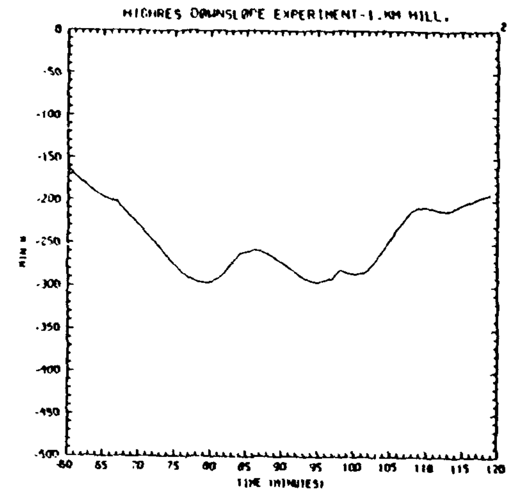

Figure 4a. Maximum downward motion (cm/s) in domain as a function of time for 1 km hill.

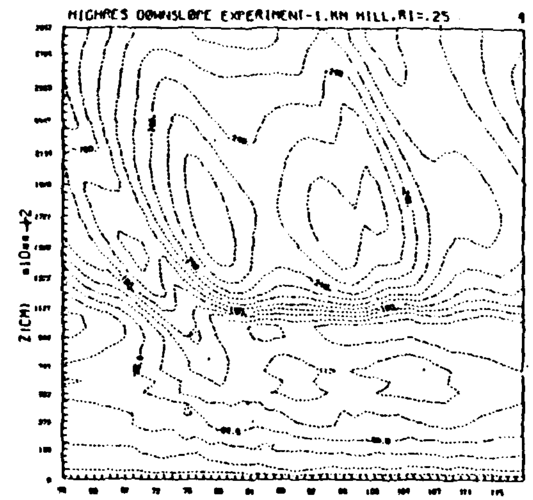

Figure 4b. Maximum downward motion (cm/s) in domain as a function of height and time (abscissa) in minutes.

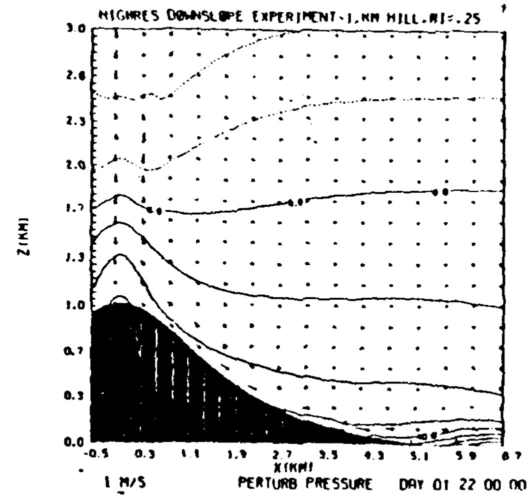

Figure 4c. P' 1 hour after initialization Increments are every 10 dynes/cm**2.

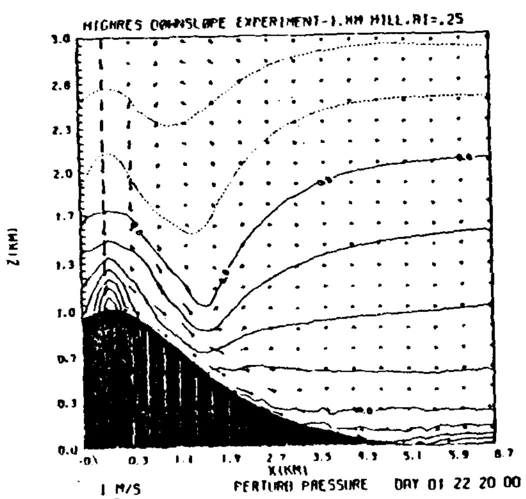

Figure 4d.

Same as Fig. 4c except 80 minutes after initialization.

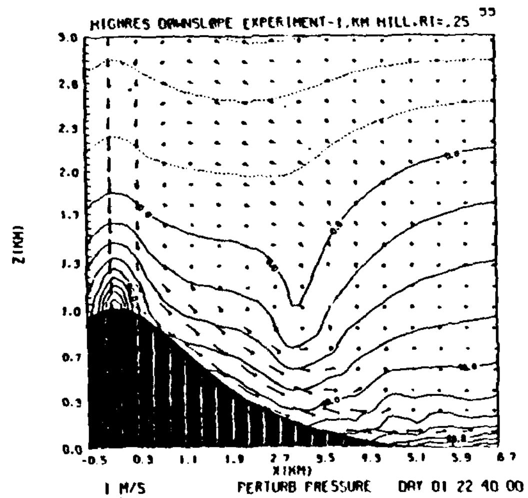

Figure 4e.

Same as Fig. 4c except 100 minutes after initialization.

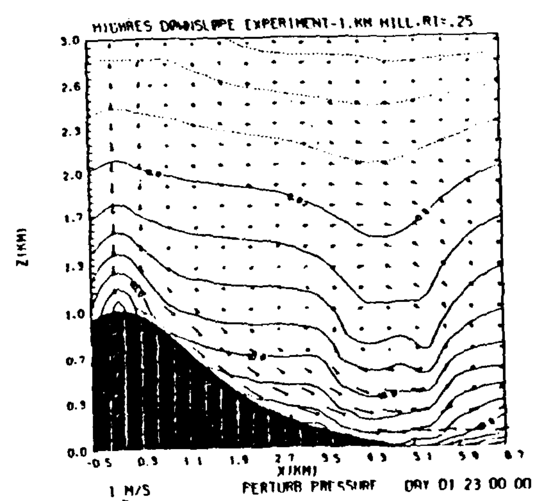

Figure 4f.

Same as Fig. 4c except 2 hours after initilization.

References

1. Bader, D. C., "Mesoscale Boundary Layer Development Over Mountainous Terrain," Ph.D. Dissertation, Atmos. Sci. Paper No. 396, Colorado State University, Fort Collins, Colorado 80523,(1985) 1-251.

2. Banta, R. M., "Daytime Boundary Layer Evolution over Mountainous Terrain. II. Numerical Studies of Upslope Flow Duration," Monthly Weather Review, 114 (1986) 1112-1130.

3. Fleagle, R. E., "A Theory of Air Drainage," Journal of Meteorology, 17 (1950) 227-232.

4. Garrett, A. J., "Drainage Flow Prediction with a One-Dimensional Model Including Canopy, Soil and Radiation Parameterizations," Journal of Climate and Applied Meteorology, 22 (1983) 79-91.

5. Manins, P. C. and B. L. Sawford, "Katabatic Winds : A Field Case Study," Quarterly Journal of the Royal Meteorological Society, 105 (1979) 1011-1025.

6. McCumber, M. C. and R. A. Pielke, "Simulation of the Effects of Surface Fluxes of Heat and Moisture in a Mesoscale Numerical Model. I. Soil Layer," Journal of Geophysical Research, 86 (1981) 9929-9938.

7. McNider, R. T., "A Note on Velocity Fluctuations in Drainage Flows," _Journal of the Atmospheric Sciences_, 39 (1982) 1658-1660.

8. Petkovsek, Z. and A. Hocevar, "Night Drainage Winds," _Archives for Meteorology, Geophysics and Bioclimatology_, 20 (1971) 353-360.

9. Tremback, C. J. and R. Kessler, "A Surface Temperature and Moisture Parameterization For Use in Mesoscale Numerical Models," _Preprints, Seventh Conference on Numerical Weather Prediction, Montreal, Quebec, Canada, American Meteorological Society_, (1985) 5 pp.

10. Tripoli, G. J. and W. R. Cotton, "The Colorado State University Three-Dimensional Cloud/Mesoscale Model - 1982. I. General Theoretical Framework and Sensitivity Experiments," _Journal De Recherches Atmospheriques_, 16 (1982) 185-219.

11. Yamada, T., "Numerical Simulations of the Night 2 Data of the 1980 ASCOT Experiments in the California Geysers Area," _Archives for Meteorology, Geophysics and Bioclimatology_, 34 (1985) 223-247.

1986 USAF-UES SUMMER FACULTY RESEARCH PROGRAM/

GRADUATE STUDENT SUMMER SUPPORT PROGRAM

Sponsored by the

AIR FORCE OFFICE OF SCIENTIFIC RESEARCH

Conducted by

Universal Energy Systems, Inc.

FINAL REPORT

Atmospheric Modeling for Operational Tactical Decision Aid

Prepared by:	Dennis W. Richardson
Academic Rank:	Ph.D. Candidate
Department and	Electrical Engineering
University:	Pennsylvania State University
Research Location:	Air Force Wright Aeronautical Laboratory
	Wright-Patterson Air Force Base, Ohio
USAF Researcher:	Roger L. Cranos
Date:	September 10, 1986
Contract Number:	F49620-85-C-0013

ATMOSPHERIC MODELING FOR OPERATIONAL TACTICAL DECISION AID

by

Dennis W. Richardson

ABSTRACT

The Tactical Decision Aid (TDA) is an integrated target/atmosphere/sensor model that is used to estimate target acquisition ranges for infrared sensors. It employs an extensive 8000 plus-line computer code, LOWTRAN, to evaluate the atmospheric extinction of infrared signals for various climatological conditions. The Operational TDA (OTDA) is a simplified version of the TDA housed on a hand-held computer. It is intended for field use. Since LOWTRAN is too voluminous to be employed for the OTDA, pre-computed extinction data tables are currently in use. The process of manual input of data from the tables to the OTDA is cumbersome and is prone to erroneous readings. Therefore, it is proposed to develop compact atmospheric extinction models which may be coded onto hand-held computers. Various types of atmospheric extinction, which are significant for the TDA application, were considered and simple models were developed based on the LOWTRAN computation.

Acknowledgements

I would like to express my gratitude to the Air Force Systems Command and the Air Force Office of Scientific Research for sponsoring my appointment as a Graduate Student Research Fellow. I would also like to acknowledge the Air Force Wright Aeronautical Laboratory (AFWAL), especially the Avionics Laboratory (AFWAL/AARI), for providing me with the opportunity to spend a summer at the laboratory. I would also like to thank members of the laboratory staff for their help in many ways; first and foremost, Roger L. Cranos for the guidance necessary for my work. I would also like to thank Jan Servaites for putting up with noisy office mates and the education on infrared sensors. Also, Jeff (J.D.) Sweet for his professional expertise concerning the computer system; Bill (Willie) Martin and Dan Zimmerman for introducing me to Skyline Chili, a splendid local cuisine, and Second Lieutenant Pat Marshall for sharing his enlightening thoughts. Here at Penn State, I would like to thank Steve Andre for his help in retrieving the data collected during the summer program. I would also like to especially thank Ken Tomiyama for allowing me the privilege to broaden my education while working under his guidance and for having patience when I made blunders.

I. Introduction

I graduated from Sharon Senior High School in Sharon, Pennsylvania in May of 1979. I immediately enrolled at The Pennsylvania State University where I received the Bachelor of Science degree in Electrical Engineering. Upon graduating in May of 1983, I applied to the Graduate School of Penn State where I am currently pursuing my Ph.D in Electrical Engineering and a Master of Arts degree in Mathematics. I am presently working under the supervision of Dr. Ken Tomiyama.

The combination of my academic system scientific background and my experience with numerical computation methods resulted in my selection by Dr. Tomiyama. My assignment was to utilize numerical optimization techniques to help develop compact models for atmospheric extinction for the OTDA.

II. Objectives of the Research Effort

The overall project at AFWAL/AARI-3 that I was involved with was the study of the Tactical Decision Aid (TDA) which evaluates target detection characteristics of infrared sensors, and is used in tactical decision making. It employs an extensive 8000 plus-line computer code, LOWTRAN, (Kneizys 1980, Kneizys 1983) to evaluate the atmospheric extinction of infrared signals for various climatological conditions. The operational TDA (OTDA) is a compact TDA, which is housed on a hand-held computer, and is intended for field use. There exists a need for compact analytical extinction models for use in the OTDA to replace the error-prone manual reading of the precomputed extinction tables. My individual objectives are to:

1. Arrive at a working knowledge of the computer code LOWTRAN, and to generate the necessary database which will aid in identifying various extinction mechanisms which are active in the spectral region of interest, 8 - 12 (μm), for the TDA application.
2. Develop the necessary optimization routines to produce compact analytical models for all active extinction mechanisms, based on the LOWTRAN computation.
3. Evaluate the accuracy of the developed models by coding error analysis routines.

III. Background

The Operational TDA (OTDA) cannot employ LOWTRAN for extinction computation due to its size. Instead, pre-computed extinction data tables are currently used. However, it is inconvenient to carry the printed tables the to field, and use of the tables is prone to erroneous readings. It is preferred to have an extinction computation program as a part of the OTDA. Thus, the development of such a program was proposed. As an initial step towards this goal, compact analytical models for various extinction mechanisms will be developed here based on the LOWTRAN computations.

It is noted that the quantity to be modeled is an average transmittance over 830 - 1250 (cm^{-1}), corresponding to 8 - 12 (μm) band, which is the primary band of sensitivity for infrared sensors. It was assumed that optical path between the

sensor and target can be considered horizontal and that the paths are located below 2 km altitude. It was decided to use the altitude of 300 (m), which is the altitude of the sensor test cite at AFWAL/AARI, as a representative altitude.

IV. Atmospheric Extinction Models

IV.1 Introduction

Infrared radiation passing through the atmosphere loses its intensity as a result of interactions with atmospheric constituents. This process is characterized by the extinction coefficient k, or the atmospheric transmittance t, which are defined as,

$$t = \exp\{-k\} = \frac{I(\text{emitted})}{I(\text{received})}, \qquad (1)$$

where I(emitted) and I(received) are the emitted and received intensities of electromagnetic wave, respectively.

The extinction coefficient k consists of contributions from many extinction mechanisms including; molecular resonant absorptions, molecular continuum absorptions, molecular scattering, aerosol (including fog) absorption and scattering, and rain absorption. The most recent version of LOWTRAN, LOWTRAN6, also includes cirrus cloud extinction.

LOWTRAN computes LOW resolution TRANsmittance, called band transmittance, which is basically an averaged transmittance over a small wavenumber interval. It adopts a basic assumption of the law of superposition, where the total extinction is the sum of individual contributions. This assumption enables us to

deal with each extinction mechanism separately.

As LOWTRAN suggests, some of the extinction mechanisms are inactive in the wavenumber region of interest, 830 - 1250 (cm^{-1}). Only the extinction due to the following need to be considered over this spectral region; water vapor, uniformly-mixed gasses, ozone, water vapor continuum, aerosol, and rain.

The OTDA requires the evaluation of the average transmittance over the 8-12 (μm) wavelength band. Therefore, the extinction models will be developed to represent the relationships between the average transmittance and various climatological conditions, including the optical path length.

IV.2 <u>Molecular Resonant absorptions</u>

In LOWTRAN, resonant absorptions due to the three gasses of concern are computed utilizing two intermediate quantities; called an absorber amount U and an equivalent absorber amount x, and two empirical transmittance models; one for ozone and another for both water vapor and uniformly-mixed gasses.

Transmittance profiles for the three absorbers over 830 - 1250 (cm^{-1}) band were generated, using LOWTRAN6, at 5 (cm^{-1}) intervals for various atmospheric conditions. Then the resulting profiles were averaged and stored together with the atmospheric conditions. Finally, analytical models were developed based on the LOWTRAN expressions and were curve-fitted, in an optimal manner, to the relationships of the average transmittances versus atmospheric conditions.

IV.2.1 <u>Water Vapor</u>

The transmittance expression used in LOWTRAN for a hori-

zontal path with homogeneous meteorological conditions of pressure P (mbar), temperature T (K), relative humidity RH (%), and path length R (km) at wavenumber v (cm^{-1}) is as follows.

$$t = f(x), \tag{2-a}$$

$$x = C(v)\ PN^{a}\ TN^{b}\ U, \tag{2-b}$$

$$PN = P/P_o, \qquad TN = T_o/T, \tag{2-c}$$

$$U = 0.1\ WH\ R, \qquad WH = 0.01\ RH\ F(T_o/T), \tag{2-d}$$

where f(.), C(v), a, b, PN, TN, P_o, T_o, WH, and F(.) are the empirical transmittance function, spectral parameter, absorber parameters (a = 0.9, b = 0.45), normalized pressure, normalized temperature, standard pressure (1013.25 mbar), standard temperature (273.15 K), water vapor density (g/m^3), and an empirical function for saturated water vapor density (g/m^3) at temperature T, respectively. The values of C(v) for each absorber, are stored in LOWTRAN at 5 (cm^{-1}) intervals over absorption bands where the absorption is non-trivial.

In earlier efforts to model the molecular resonant absorption (Gruenzel 1978, Pierluissi 1979), it was found that the following double exponential function agrees excellently with LOWTRAN empirical transmittance functions.

$$t = \exp\{-10^{a_o + a_1 x}\}, \tag{3-a}$$

$$x = \log C(v) + n \log(PN) + m \log(TN) + \log(U), \tag{3-b}$$

where a_o, a_1, n, and m are model parameters to be chosen.

This function was selected as our model since it agrees well with the band transmittance, which is a weighted average of transmittances. It is noted that the spectral parameter C(v) in this expression may be eliminated in our model since only an averaged transmittance is to be calculated. As a result, the model can be simplified to

$$t = \exp\{-10^{a_0 + a_1 \log(PN) + a_2 \log(TN) + a_3 \log(U)}\}, \quad (4)$$

or

$$t = \exp\{- A_0\, PN^{a_1}\, TN^{a_2}\, U^{a_3}\}, \quad (5)$$

where a_0, a_1, a_2, a_3, and A_0 = 10**a_0 are the model parameters.

For the optimal determination of the model parameters, we take the double logarithm of Eq. (4). This linearizes the model in terms of the unknown parameters as follows:

$$\log\{-\ln(t)\} = a_0 + a_1 \log(PN) + a_2 \log(TN) + a_3 \log(U). \quad (6)$$

Linear regression techniques may now be utilized to obtain the optimal parameter values.

IV.2.2 Uniformly-Mixed Gasses

The absorber in question here is a mixture of various atmospheric gaseous molecules whose density profiles are relatively unperturbed, except for the pressure and temperature dependencies. Therefore, the corresponding absorber amount U is a function of the pressure, temperature, and the path length only. The transmittance expression for this absorber is the same as that for the water vapor given in Eq. (2), except that

the pressure and temperature dependencies within the absorber amount U is integrated into those appearing in x. This leads to the following LOWTRAN model.

$$t = f(x), \tag{7-a}$$

$$x = C(v)\ PN^{a}\ TN^{b}\ U, \tag{7-b}$$

$$U = R, \tag{7-c}$$

where the absorber parameters a and b have values 1.75 and 1.375, respectively.

Thus, an appropriate model is again Eq. (4) or (5) with the expression for U being replaced by the path length R.

IV.2.3 Ozone

The transmittance expression for ozone is the same as that for the water vapor, except for the absorber parameter values, a = 0.4 and b = 0.2, and the expression for the absorber amount U. With the ozone density WO in g/m^3, U is given by

$$U = 46.667\ WO\ R. \tag{8}$$

Therefore, the appropriate model expression is again given by Eqs. (4) or (5) together with the absorber amount expression in Eq. (8).

IV.3 Water Vapor Continuum Absorption

The LOWTRAN6 expression for the water vapor continuum absorption consists of self and foreign components. The expression for a homogeneous path is given by,

$$t = \exp\{-v \tanh(hcv/2kT)\ [Rs\ Cs + Rf\ Cf]\ WH\ R\}, \tag{9}$$

where $hc/k = 1.43879$ (K/cm^{-1}), Rs and Rf are self (water vapor versus total air at standard condition) and foreign (all other molecular species versus total air) number density ratios, and Cs and Cf ($1/(cm^{-1}\ mol/cm^2)$) are wavenumber dependent parameters for self and foreign components, respectively.

The temperature dependence of the self component Cs is taken into account through a factor Kp defined by,

$$Kp = \begin{cases} 1, & T < 260, \\ (296 - T) / (296 - 260), & 260 < T < 296, \\ 0, & 296 < T, \end{cases} \tag{10}$$

as

$$Cs = (1 - Kp)\ Cs_1 + Kp\ Cs_2. \tag{11}$$

The parameters Cs_1, Cs_2, and Cf are stored in LOWTRAN at 10 (cm^{-1}) wavenumber intervals over regions where the water vapor continuum absorption is non-trivial.

It is noted that the number density ratio Rs is linearly dependent on the water vapor concentration WH. On the other hand, the sum of the two densities, water vapor and all others, is linearly dependent on the product PN*TN since it is the air density. Therefore, our model needs to 'arry linear dependencies on PN*TN and WH in an additive fashion. It is also noted that the wavenumber dependent coefficient in Eq. (9) can be imbedded into Cs and Cf. By combining all of these observations, we obtain the following expression:

$$t = e^{-[\{q(Cs_1'+Cf') + Kp(Cs_2'-Cs_1')\}\ WH + r\ Cf'PN*TN]\ WH\ R}, \tag{12}$$

where q and r are wavenumber independent constants, and Cs_1', Cs_2', and Cf' are scaled wavenumber dependent parameters.

For our model, the averages of Cs_1', Cs_2', and Cf' over 830 - 1250 (cm^{-1}) region are computed from the LOWTRAN data, and then those parameters in Eq. (12) are replaced with respective averages. Then the expression is simplified by combining the constants as,

$$t = \exp\{ -C_0 \, [PN\ TN + (C_1\ Kp + C_2)\ WH]\ WH\ R\}, \tag{13}$$

where C_0, C_1, and C_2 are the final model parameters.

IV.4 Aerosol Extinction

Aerosols are active over 830 - 1250 (cm^{-1}) region in both absorption and scattering. Since LOWTRAN has models for the extinction, we will consider the modeling of the extinction, instead of the absorption and scattering individually.

The transmittance due to aerosols is again given by an exponential law as,

$$t = \exp\{-X\ H\ R\}, \tag{14}$$

where X is the aerosol extinction profile which is dependent on the type of aerosol, the relative humidity RH and the wavelength . H is the aerosol density profile which represents the visibility and the height dependencies.

We first consider the aerosol extinction profile X. There are ten aerosol types used in LOWTRAN. Due to our assumption that applications of the OTDA is limited to horizontal paths below 2 km altitude, we only need to consider four humidity

dependent aerosols; RURAL, URBAN, MARITIME, TROPOSPHERE, and two humidity independent ones; FOG1 and FOG2. LOWTRAN stores four extinction profiles X( ) for each humidity dependent aerosol corresponding to the relative humidities of 0, 70, 80, and 99 (%), and one each for FOG1 and FOG2. These profiles are first averaged to eliminate wavelength dependence. Then the humidity dependencies in four aerosols are modeled using the following empirical relationship which is suggested in Shettle 1979, based on the observation by Hanel (Hanel 1976),

$$X = c_1 \, (1 - RH/100)^{c_2} , \qquad (15)$$

where c_1 and c_2 are model parameters. Noting that this relationship represents a straight line in log-log scale, optimal values for these parameters were obtained using the linear regression technique. The same model is also used for the two humidity independent models, FOG1 and FOG2, by setting c_2 to 0 to eliminate humidity dependence.

Next, the visibility dependent aerosol density profiles H(.) are studied. In the first 2 km height, H(.) is represented by three empirical functions of the visibility at 0, 1, and 2 (km) altitudes. These three profiles are fitted by the inverse relationship,

$$H(VIS) = d_1 \, VIS^{-1} + d_2, \qquad (16)$$

which is used in LOWTRAN for interpolation of H(.). Then, using the assumption that a typical altitude at which the OTDA is applied is 300 (m), the weighted average of the two profiles

at 0 and 1 (km) heights is adopted as our model.

Finally, Eqs. (14), (15) and (16) are combined to form the following aerosol model,

$$t = \exp\{-(VIS^{-1} + d_2')\, c_1'(1 - RH/100)^{c_2}\, R\}, \tag{17}$$

where d_1 is imbedded into c_1' by factoring it out to reduce the number of parameters. It is noted that d_2' is independent of the aerosol type.

IV.5 Rain Model

Because the rain extinction model used in LOWTRAN is a simple analytic function of the rain rate RR (mm/hr) and the range R (km), we can adopt it with a slight modification. After combining some constants to minimize the number of parameters, the model becomes as follows:

$$t = \exp\{-0.3647\ RR^{0.63}\ R\}. \tag{18}$$

V. Summary of Numerical Results

The model equations derived in the previous section are summarized in Table 1 together with the obtained optimum parameter values. The input variables are listed in Table 2 together with the default values for some of them. A simple FORTRAN program, called CTRAN, was coded to check the accuracy of the obtained model. Results of this preliminary error analysis are summarized in Table 3. Figure 1 illustrates relative humidity dependence of four aerosol extinctions and their models given in Eq. (15).

Table 1.

Extinction Models for the OTDA

(1) Molecular resonant absorption

$$t = \exp\{- A_o (P/P_o)^{a_1} (T_o/T)^{a_2} U^{a_3}\}$$

Water Vapor
$$\begin{bmatrix} A_o = 0.0850 & a_1 = 0.4981 \\ a_2 = 0.2989 & a_3 = 0.5582 \\ U = 0.1\ WH\ R & WH = 0.01\ RH\ F(T_o/T) \end{bmatrix}$$

Uniformly-mixed Gasses
$$\begin{bmatrix} A_o = 0.0118 & a_1 = 1.0792 \\ a_2 = 0.8488 & a_3 = 0.6178 \\ U = R & \end{bmatrix}$$

Ozone
$$\begin{bmatrix} A_o = 0.0076 & a_1 = 0.3091 \\ a_2 = 0.1541 & a_3 = 0.7498 \\ U = 46.667\ WO\ R & \end{bmatrix}$$

,where $F(s) = s \exp\{18.9766 - 14.9595\ s - 2.43882\ s^2\}$.

(2) Water Vapor Continuum Absorption

$$t = \exp\{ -C_o\ [(P/P_o)(T_o/T) + (C_1\ Kp + C_2)\ WH]\ WH\ U\}$$

$$Kp = \begin{cases} 1 & , \quad T < 260 \\ (296 - T)/(296 - 260), & 260 < T < 296 \\ 0 & , \quad 296 < T \end{cases}$$

$C_o = 1.655E-03 \quad C_1 = 0.5693 \quad C_2 = 0.5437$

(3) Aerosol Extinction

$$t = \exp\{-(VIS^{-1} - 0.005183)\ c_1'(1 - RH/100)^{c_2}\ R\}$$

#	Model	c_1'	c_2	Default VIS(km)
1	RURAL	0.3670	-0.02877	23
2	URBAN	0.3119	-0.08499	5
3	OCEAN	0.4013	-0.3417	23
4	TROPOSPHERIC	0.08054	-0.04621	50
5	FOG1	4.487	0	0.2
6	FOG2	1.309	0	0.5

(4) Rain Extinction

$$t = \exp\{-0.3647\ RR^{0.63}\ R\}$$

Table 2.

Input Variables for Extinction Models

Variable	Notation (Units)	Default
Pressure	P (mbar)	None
Temperature	T (°C)	None
Relative Humidity	RH (%)	None
Ozone Density	WO (G/m^3)	6.0E-05
Visibility	VIS (km)	*
Aerosol Model	I (integer)	0
Rain Rate	RR (mm/h)	0.0
Range	R (km)	None

* See Table 1 for model dependent default values.

Table 3.

Preliminary Error Analysis of Extinction Models

Model		R.M.S. Error
Water Vapor		0.0038
Uniformly-Mixed Gasses		0.0002
Ozone		0.0002
Water Vapor Continuum		0.0056
Aerosol	RURAL	0.0126
	URBAN	0.0427
	OCEAN	0.0172
	TROPOSPHERIC	0.0017
	FOG1	0.0011
	FOG2	0.0183

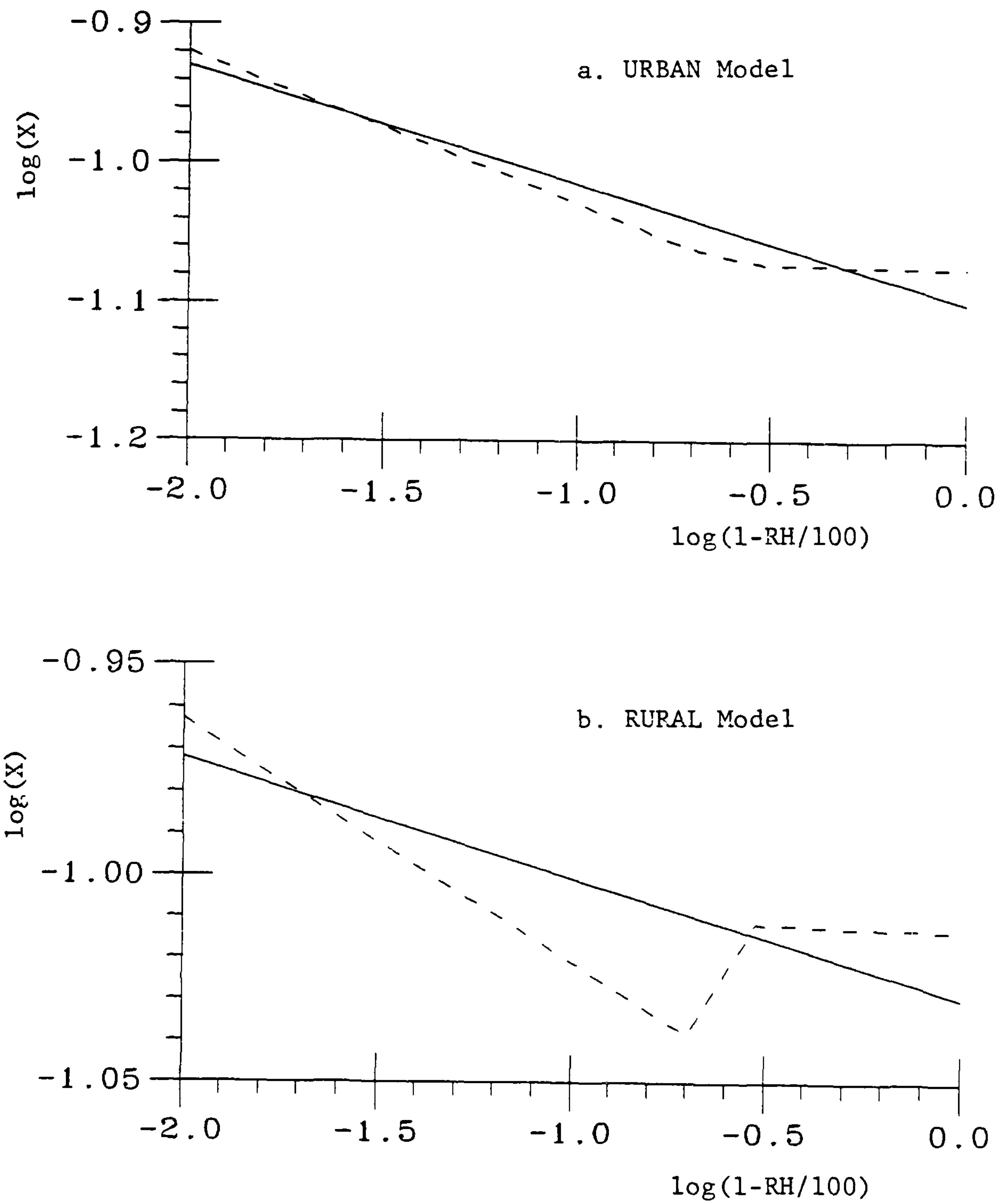

Figure 1. Relative humidity (RH) dependent aerosol extinction profile X. The dashed and solid lines are for the original model for LOWTRAN and the derived model for the OTDA, respectively.

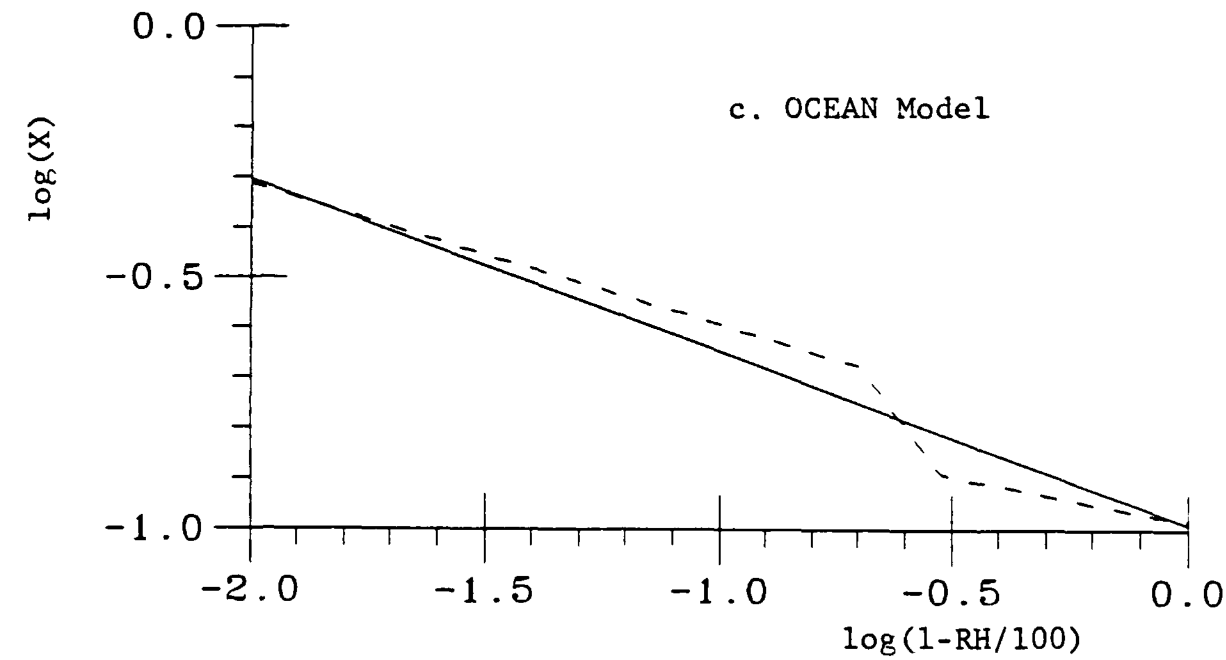

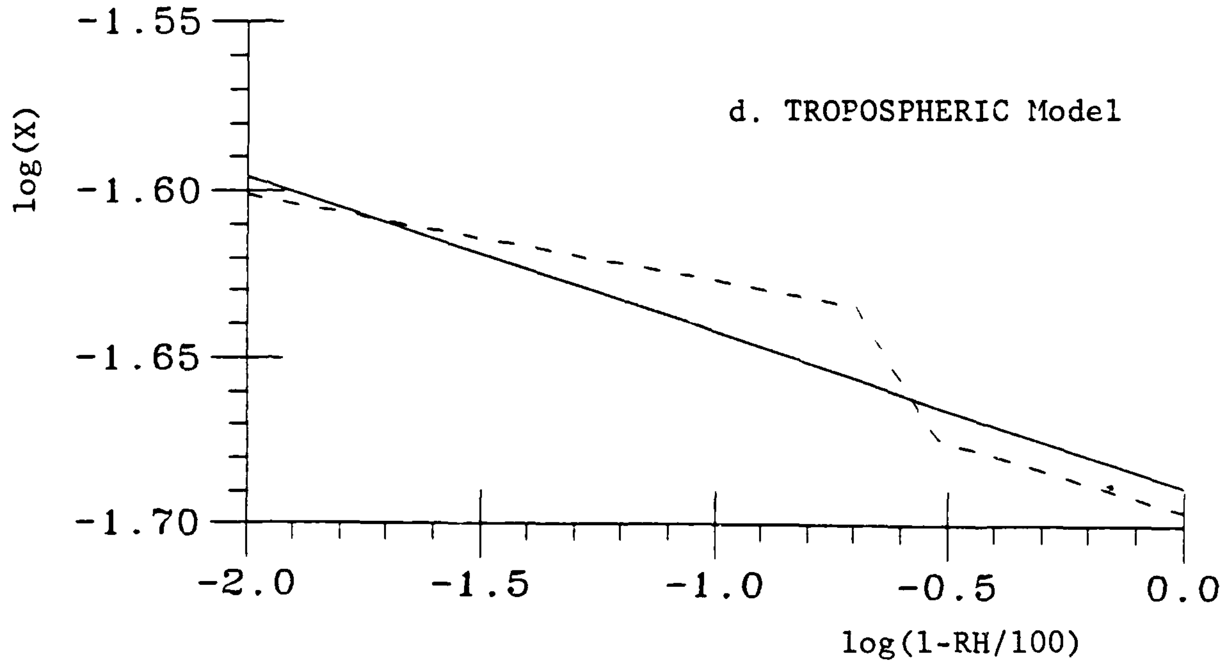

Figure 1. Continued.

VI. Conclusions

Simple models for atmospheric extinctions due to various atmospheric absorption mechanisms are developed for the use in the Operational Tactical Decision Aid. The developed models are; for three molecular resonant absorptions due to water vapor, uniformly-mixed gasses, and ozone; for water vapor continuum absorption; for aerosol extinction; and for rain extinction. All of those absorption mechanisms are active in the 8 - 12 (μm) band. Preliminary error analysis showed good overall accuracy and excellent accuracy for molecular resonant absorption models.

VII. Recommendations

1. Although the developed models generally agreed well with LOWTRAN computations, they need to be fully tested against all conceivable atmospheric conditions, including a range of possible optical path lengths. This may results in modifications of the obtained models.
2. After thorough testing, the developed models should be implemented on the OTDA to replace extinction data tables.
3. One of the perpetual question associated with the capability of a program like the TDA is the sensitivity of the output against the perturbation in the input variables. Regardless of the accuracy of the computation, the output will be in error if the input is disturbed. Therefore, in order for the TDA to be truly effective, it is highly recommended to perform a sensitivity analysis.

REFERENCES

Kneizys, F.X., E.P. Shettle, W.O.Gallery, J.H. Chetwynd, Jr., L.W. Abreu, J.E.A. Selby, R.W. Fenn, and R.A. McClatchey. (1980) "Atmospheric Transmittance/Radiance: Computer Code LOWTRAN 5," Report AFGL-TR-80-0067, Air Force Geophysics Laboratory, Hanscom Air Force Base, Mass.

Kneizys, F.X., E.P. Shettle, W.O.Gallery, J.H. Chetwynd, Jr., L.W. Abreu, J.E.A. Selby, S.A. Clough, and R.W. Fenn. (1983) "Atmospheric Transmittance/Radiance: Computer Code LOWTRAN 6," Report AFGL-TR-83-0187, Air Force Geophysics Laboratory, Hanscom Air Force Base, Mass.

Gruenzel, R.R. (1978) "Mathematical Expressions for Molecular Absorption in LOWTRAN 3B," Applied Optics, 17, 2591-2593.

Pierluissi, J.H., K. Tomiyama, and R.G. Gomez. (1979) "Analysis of LOWTRAN Transmission Functions," Applied Optics, 18, 1607-1612.

Shettle, E.P., and R.W. Fenn. (1979) "Models for the Aerosols of the Lower Atmosphere and the Effects of Humidity Variations on Their Optical Properties," Report AFGL-TR-79-0214, Air Force Geophysics Laboratory, Hanscom Air Force Base, Mass.

Hanel, G. (1976) "The Properties of Atmospheric Aerosol Particles as Functions of the Relative Humidity at Thermodynamic Equilibrium with the Surrounding Moist Air," Advances in Geophysics, Ed. by H.E. Landsberg and J. Van Mieghem, Academic Press, New York, 19, 73-188.

1986 USAF-UES SUMMER FACULTY RESEARCH PROGRAM /

GRADUATE STUDENT SUMMER SUPPORT PROGRAM

Sponsored by the

AIR FORCE OFFICE OF SCIENTIFIC RESEARCH

Conducted by the

Universal Energy Systems, Inc.

FINAL REPORT

AN EXPERIMENT TO CHARACTERIZE THE TURBULENT FLOW FIELD OF A CIRCULAR FREE JET OF HELIUM

Prepared by:	Kyle Ross
Academic Rank:	M.S. Graduate Student
Department and University:	Department of Mechanical Engineering The University of New Mexico
Research Location:	The Air Force Weapons Laboratory, Kirtland AFB, Albuquerque, NM.
USAF Researcher:	Dr. Bruce Masson

Date:	September 22, 1986
Contract No:	F49620-85-C-0013

AN EXPERIMENT TO CHARACTERIZE THE TURBULENT FLOW FIELD OF A CIRCULAR FREE JET OF HELIUM

by

Kyle Ross

ABSTRACT

An experiment designed to characterize the turbulent flow field of a circular free jet of helium is described. This experiment employs laser Doppler anemometry. Design of this experiment was part of the initial effort of research directed at relating certain velocity statistics of a basic flow to the laser beam transmision characteristics of the same flow. Of special interest is relating defects in laser beam quality to the existence of large scale coherent turbulent flow structures in the optical path. Work subsequent to the laser Doppler anemometry study will characterize the same jet flow by laser interferometry. Correlations between statistics described here and information resulting from the interferometry work are expected. Such correlations will relate the velocity statistics and laser beam transmission characteristics of the jet flow field.

The equipment configuration developed over the summer is described as are the methods used to extract various velocity statistics from the laser Doppler velocimetry data.

ACKNOWLEDGMENTS

I am grateful to the Air Force Systems Command, the Air Force Office of Scientific Research, and the Air Force Weapons Laboratory for sponsoring my summer appointment. I thank Dr. Bruce Masson for his support of my work and Captain Rich Charles for encouraging my involovement in his research. A special thanks to Captain Charles for his time spent and effort made in familiarizing me with his work. I also thank Professor Randall Truman for his guidance and willingness to give his time and effort. Dr. Trumans's help was invaluable.

I. INTRODUCTION:

I received my B.S.M.E. from the University of New Mexico in 1982. Prior to entering graduate school, I worked for 2 1/2 years at the High Energy Laser Test Facility, White Sands Missile Range, NM, where my tasks involved me with many different aspects of high energy laser facility support. My graduate course work has emphasized fluid mechanics.

II. OBJECTIVE OF THE RESEARCH EFFORT:

The objective of the summer effort was to design an experiment, employing laser Doppler anemometry, which could construct spatial distributions of the following for a free circular jet flow of helium:

1) mean velocity,
2) turbulent intensity,
3) Reynolds stress,
4) temporal correlation (autocorrelation) of velocity fluctuations,
5) integral time scale,
6) spatial correlation of velocity fluctuations,
7) integral length scale, and
8) power spectral density of velocity fluctuations.

Design of this experiment would necessarily include not only an equipment configuration, but also the development of data reduction schemes.

III. EQUIPMENT CONFIGURATION:

Figure 1 shows the equipment configuration developed over the summer. The acrylic cylindrical plenum in the foreground has a smooth convergent nozzle cut in its end piece which forms a 1/4" diameter

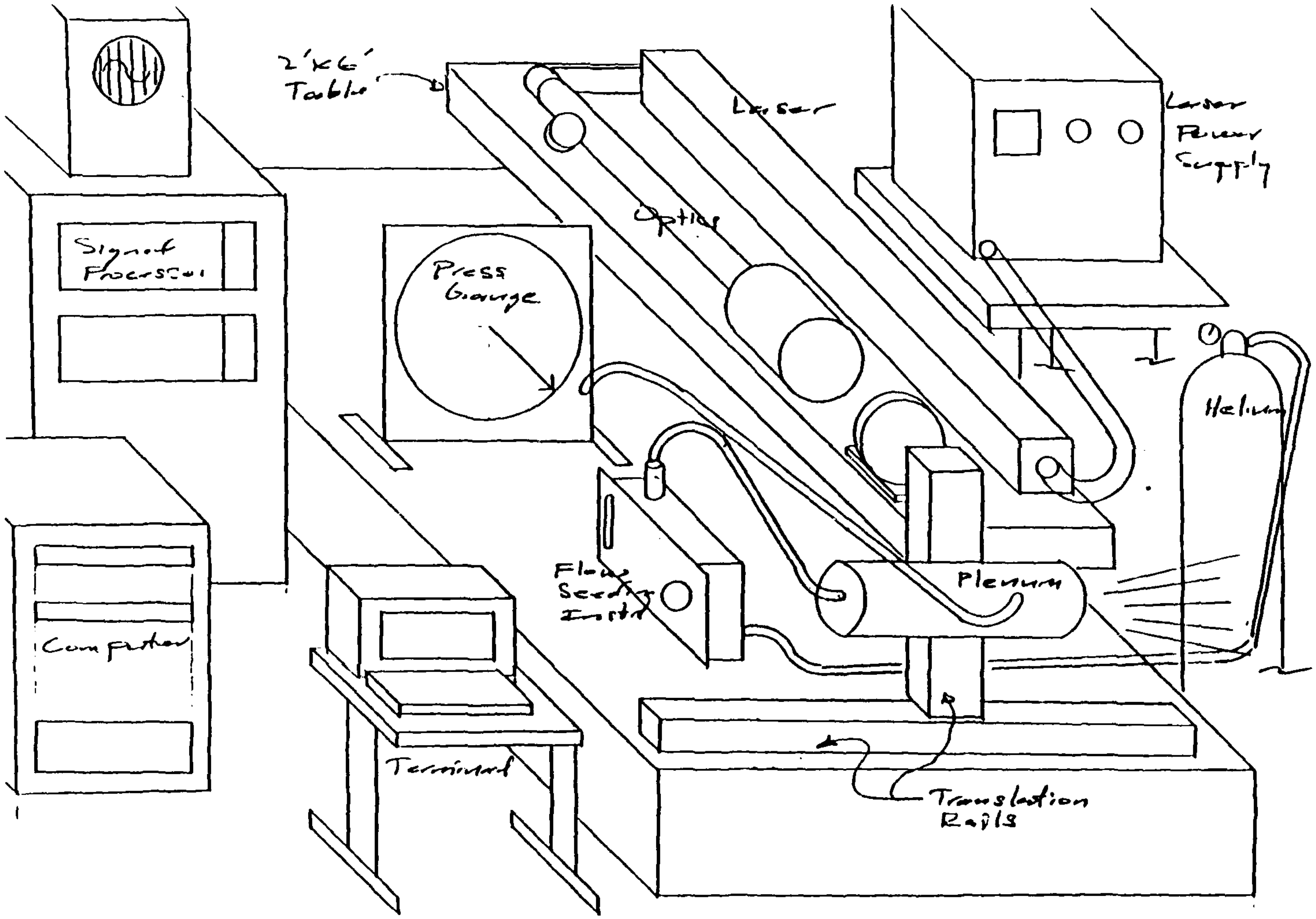

Fig. 1 Experimental Configuration

orifice at its outer face. This plenum is mounted on a translation mechanism built of two individual translation rails and secured to the large table. This mechanism allows motion of the plenum in a plane perpendicular to the axis of the laser Doppler velocimeter (LDV) optics. Helium is supplied by the K-bottle through a pressure regulator and flow seeding instrument to the plenum. A jet of helium exits from the orifice. Readings from a pressure gauge connected to a static pressure tap on the plenum wall indicate relative magnitudes of flow rate.

The argon-ion laser and LDV optical system are mounted on a 2'x 6' table elevated above and secured to the large table. This allows the plenum centerline, when raised to the level of the LDV optical axis, to be 12.75" above the surface of large table. This should largely diminish any influence from the table surface on the first several feet of the jet flow field downstream of the nozzle. The LDV system is a dual beam type having the convenience of on-axis back scatter operation.

The focusing lens located out in front of the beam expander is mounted on a translation stage allowing the lens, and hence the measurement volume, to be moved several inches along the axis of the LDV optics. Combined positioning of this lens with its single degree of freedom and the plenum with its two degrees of freedom allows the measurement volume to be readily positioned throughout the jet flow field.

The LDV signal processors in the equipment rack are counter types. Counter processors measure the duration of a predetermined number of signal cycles. The Doppler frequency is given by the number of cycles divided by the length of time taken for them to occur. A direct memory access (DMA) interface between the counters and the computer enables

direct transfer of data to the computer memory. This facilitates the storage of data taken at high rates.

The storage oscilloscope is used to view the filtered photomultiplier signal. Use of this oscilloscope is invaluable in the adjustment of such variables as high and low pass filters, gain settings, seeding concentration, number of signal cycles to be counted, and laser power. Correct setting of these variables is critical to obtaining a high signal to noise ratio, good clarity in the Doppler signal, and an acceptable data rate.

IV. DATA REDUCTION:

At the end of the summer work, the equipment configured to characterize the turbulent flow field of a free helium jet was working well. For a 1 psi difference between plenum and ambient pressures, software supplied by the LDV manufacturer (TSI incorporated) was giving mean velocities near the orifice several m/s less than those calculated for an ideal nozzel operating with the same pressure difference, as would be expected. With respect to producing the statistics of interest, the TSI software is somewhat limited. While it provides for mean velocity, turublent intensity, and Reynolds stress calculations, it has no routines to extract space and time correlations, integral scales, or power spectral density from velocity measurements. Figure 2 outlines a software development sequence expected to produce the desired statistics not addressed by TSI software. Starting at the top of this figure the first step in the sequence is to modify TSI data aquisition routines to create larger data sets (data taken over a longer period of time). The TSI data aquisition routines are structured to create continuous time records of 250 data points. At high data rates, a

Fig.2 Software Development Sequence

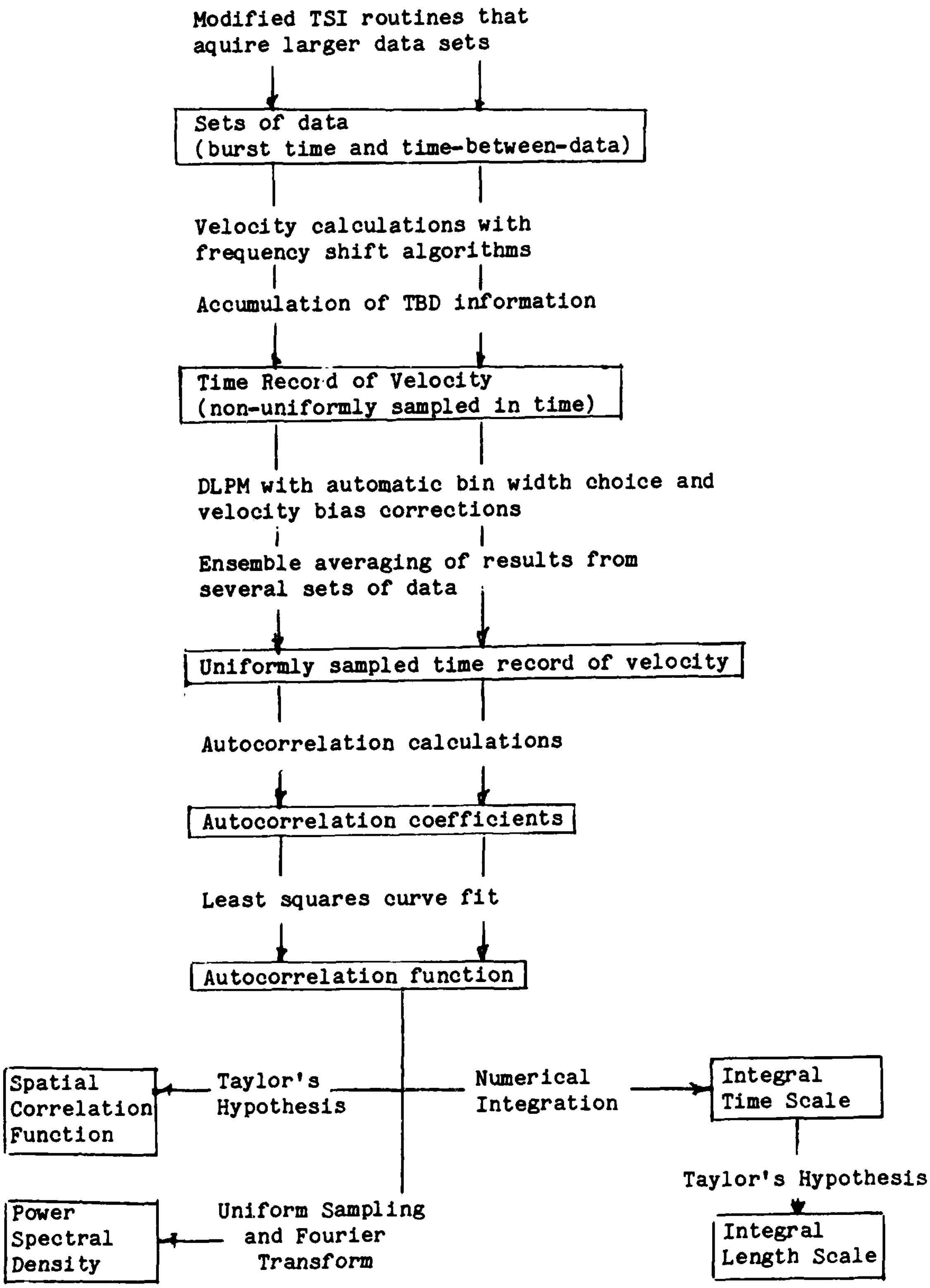

continuous time record of 250 data points is not long enough to show the maximum time separation that gives a significant correlation between velocity fluctuations. It is thus necessary to modify these routines to include more data points in a continuous record.

Next in the sequence is construction of a time record of velocity from the raw data. The LDV data is non-uniformly sampled in time because velocity data can only be taken when a scattering particle crosses the measurement volume. As a rule, particle crossings do not occur at regular intervals. Individual data records consist simply of burst time and time between data. The burst time is the time taken for 2^n cycles of Doppler signal to occur, where n (typically 3 or 4) is a selectable hardware setting on the signal processor. The time between data is the time elapsed between taking of the present measurement and taking of the one before it. Accumulation of the time between data values allows for a time record to be constructed. Velocity calculations would necessarily include algorithms to account for any frequency shifting used in the LDV setup. Figs. 3 and 4 show a typical time record of velocity and the relationship between particle velocity and Doppler signal, respectively.

The third step in the software development sequence is to calculate the many autocorrelation coefficients. Autocorrelation is a measure of the degree to which two measurements of a fluctuating velocity taken at different times (but at the same location) are correlated with one another. An autocorrelation coefficient is the autocorrelation for a particular time spacing (time lag) between measurements. Accumulating the many autocorrelation coefficients yields the autocorrelation function. This function represents the dependence of the degree of

Fig. 3 Typical LDV Velocity Time Record

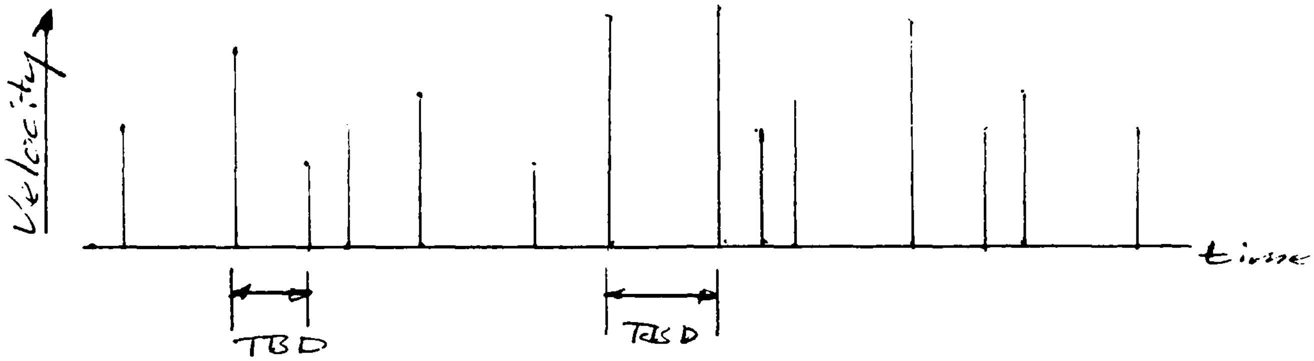

Fig. 4 Doppler Signal / Particle Velocity Relationship

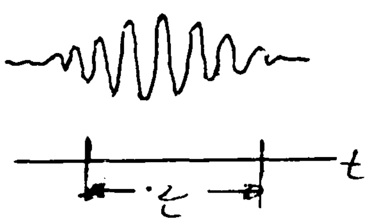

$$f_D = \frac{2^n}{\tau}$$

$$u = d_f f_D = \frac{\lambda}{2\sin k} f_D$$

τ = time for 2^n cycles

where

u = velocity

f_D = Doppler frequency

d_f = fringe spacing

λ = wavelength of laser light

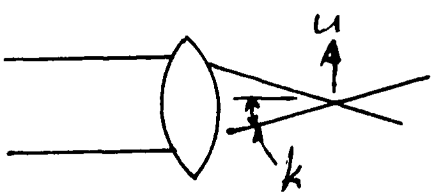

correlation on time spacing between measurements. Construction of the autocorrelation function is central to determining integral length and time scales as well as power spectral density of velocity fluctuations.

It is proposed that autocorrelation coefficients be determined using a method termed as the discretized lag product method (DLPM) [1]. With this method the time axis of the velocity record is divided into m bins of equal width, $\Delta\tau$, as shown in Figure 5. Velocity measurements are grouped into the bin in which their time of measurement falls. Once a velocity measurement has been assigned to a bin the time associated with that measurement is assumed to be that at the center of the assigned bin ($i\Delta\tau$). The autocorrelation coefficient for any given multiple of $\Delta\tau$ can then be determined by forming

$$R(j\Delta\tau) = \frac{\frac{1}{m-j}\sum_{i=1}^{m-j} u'(i\Delta\tau)\,u'(i\Delta\tau + j\Delta\tau)}{\frac{1}{m}\sum_{i=1}^{m} u'(i\Delta\tau)^2} .$$

where $u' = u - \bar{u}$ = instantaneous velocity - average velocity.

Numerical integration of the autocorrelation function yields the integral time scale. This scale gives a rough measure of the longest time which shows significant correlation in the turbulent behavior of the fluctuating velocity.

Through Taylor's hypothesis [2] the spatial correlation of velocity fluctuations can be related to the autocorrelation. The spatial correlation is a measure of the degree to which two measurements of a fluctuating velocity taken at different locations (but at the same time) are correlated with one another. By Taylor's hypothesis, if the turbulent velocity fluctuations are small compared with the mean velocity, eddies do not change appreciably in shape as they pass a given

Fig. 5 Division of Velocity Record Time Axis into Bins for Discretized Lag Product Method.

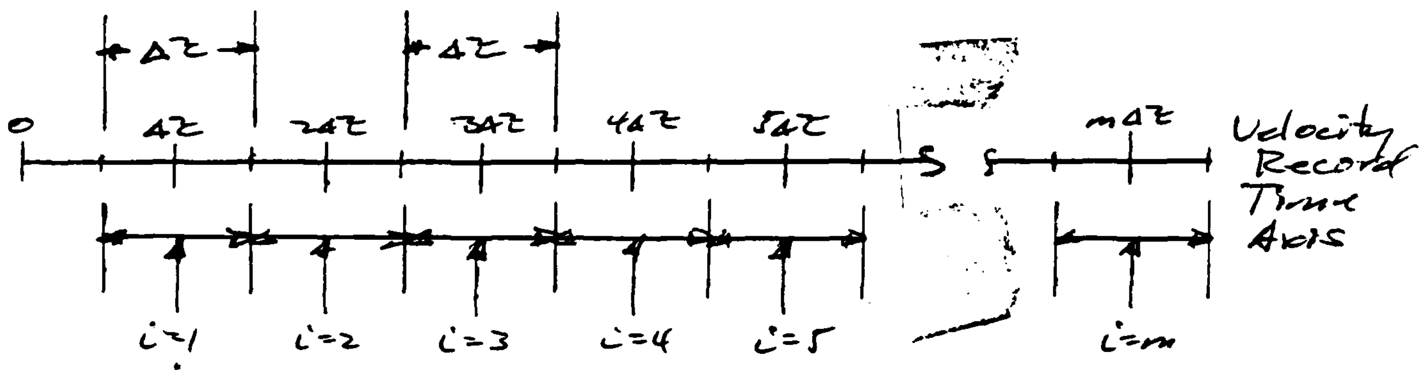

point. The autocorrelation with time delay τ then will be the same as the spatial correlation with separation $U_T\tau$, where U_T is the convection velocity used in Taylor's hypothesis. By this reasoning the integral length scale will be simply the product of the convection velocity and the integral time scale. The integral length scale is a rough measure of the size of the largest eddies that cause velocity fluctations. It is somewhat questionable as to how applicable the underlying assumption of Taylor's hypothesis is to the jet flow. Comparisons of length scale results using this hypothesis and results from actual two-point simultaneous measurements planned for the future should prove or disprove the validity of applying Taylor's hypothesis to the jet flow.

The remaining statistic in the software development sequence to be discussed is the power spectral density of velocity fluctuations. The power spectral density and the autocorrelation function are Fourier transforms of each other. Fourier transformation of the autocorrelation function will give the power spectral density.

V. RECOMMENDATIONS:

Major portions of the software development sequence outlined had been developed at the Air Force Weapons Laboratory prior to my becoming part of the research effort. Correlation routines were written based on the DLPM and on a linear interpolation scheme. From close study of a paper [1] comparing results using these two methods (and others), I suggest use of the DLPM in extracting autocorrelation information from the non-uniformly sampled velocity data because this approach seems to be the most viable. In building a routine to support DLPM, I suggest including logic to facilitate the automatic choice of an appropriate bin width. This might be done by considering statistics of the

time-between-data field. Additional suggestions are:

1) modify all time averaging operations to correct for any velocity biasing,

2) structure routines to enable ensemble averaging of several sets of data,

3) include algorithms to account for any frequency shifting used in the LDV setup,

4) install the additional LDV components necesssary to enable the two color, two component operation needed for Reynold's stress measurements, and

5) develop the outlined software development sequence in its entirety.

REFERENCES

1. Saxena, V., "Power Spectrum Estimation from Randomly Sampled Velocity Data", Symposium on Turbulence, 5th, University of Missouri-Rolla, 1977. Proceedings of the Fifth Bienneal Symposium on Turbulence, October 1977, pp. 209-219.

2. Panton, R. L., "Incompressible Flow," John Wiley and Sons, 1984, pp. 713-715.

1986 USAF-UES SUMMER FACULTY RESEARCH PROGRAM/

GRADUATE STUDENT SUMMER SUPPORT PROGRAM

Sponsored by the

AIR FORCE OFFICE OF SCIENTIFIC RESEARCH

Conducted by the

Universal Energy Systems, Inc.

FINAL REPORT

WEATHER ATTENUATION

Prepared by: Susan Ellen-Ann Sadofsky

Academic Rank: Master of Arts

Department and University: Mathematics Department, Boston University

Research Location: Cloud Physics Branch
Air Force Geophysics Laboratory
Hanscom Air Force Base
Bedford, MA 01731-5000

USAF Researcher: Dr. Arnold A. Barnes, Jr.

Date: August 13, 1986

Contract No.: F49620-85-C-0013

Weather Attenuation

by

Susan Ellen-Ann Sadofsky

ABSTRACT

38 GHz data from Lincoln Laboratory Experimental Satellite #8 (LES-8) taken during the AFGL Weather Attenuation Program (March - May 1986) was converted from raw counts to signal strength values. These values were plotted by hand in order to make comparisons and verify a computer program which converted the raw data and plotted the values.

ACKNOWLEDGEMENTS

I would like to thank the Air Force Systems Command and the Air Force Office of Scientific Research for sponsorship of my research. In particular I would like to thank the Cloud Physics Branch at the Air Force Geophysics Laboratory for allowing me to work for them for this summer as well as the past five summers. There are several individuals I would like to thank they include Arnold A. Barnes, Jr. for his direction in the project, Sgt. Charles C. Crouch III for his help with the computer, and Barbara A. Main for her help in obtaining this position.

Finally I would like to thank my father, Morris Sadofsky, for chauffeuring me to work for six summers and for his encouragement in my educational pursuits.

I. <u>INTRODUCTION:</u> I received my Master's degree from Boston University, Boston, Massachusetts. While at BU I studied Real Analysis, Numerical Analysis, and Applied Mathematics.

The research project at hand involved determining the effects of weather conditions on data transmitted to and from satellites.

II. <u>OBJECTIVES OF THE RESEARCH EFFECT:</u> The overall objective of the Weather Attenuation Project was to collect weather attenuation data and analyze the data to determine the effects of clouds, rain, and snow on EHF radio signals transmitted to and from satellites. The specific efforts were to compile an inventory of the data and to take the raw data from satellite LES-8, convert the raw data to signal strength values, plot the values, and investigate abnormalities in the data.

III. <u>RESEARCH EFFORT:</u> Prior to my arrival weather attenuation data was obtained from varying sources during March - May 1986. Upon my arrival I began to compile an inventory of this data. I then created a table which was later used to select those particular days of interest which were to be investigated in detail. A computer program was then devised to convert the raw data and list the signal stength values from satellite LES-8 in an organized manner. The values were then graphed both by hand and on the computer to assure that the computer program was operating correctly. Now that the program has been verified, it will be used to reduce the data from all eleven cases to be studied by the program.

IV. <u>RECOMMENDATIONS:</u> A number of anomalous points were noted in the reduced data, and the source of these should be determined. Since they appear in

the raw data, and show up for only one or two readings (taken one second apart) the data collecting and recording system would seem the most likely source. I would recommend that this be investigated so as to determine whether these points should be eliminated or smoothed in the future averaging which will be done. More comment statements should be included in the computer program to aid futher users as they modify the program for future use.

1986 USAF-UES SUMMER FACULTY RESEARCH /
GRADUATE STUDENT SUMMER SUPPORT PROGRAM

Sponsored by the

AIR FORCE OFFICE OF SCIENTIFIC RESEARCH

Conducted by the

UNIVERSAL ENERGY SYSTEMS , INC.

FINAL REPORT

MBTI PSYCHOMETRIC STUDY OF UNITED STATES AIR FORCE AIRCREW PERSONNEL

Prepared by	:	John Yolman Salinas Eric V. Morris Moussa Pierre Tamer
Academic Rank	:	M.D. Students
Department and University	:	Meharry Medical College School of Medicine
Research Location	:	Department of NeuroPsychiatry School of Aerospace Medicine Brookes Air Force Base
USAF Research	:	Dr. Timothy Strongin
Date	:	August 18th , 1986
Contract No.	:	F49620-85-C-0013

MBTI Psychometric Study of United States
Air Force Aircrew Personnel

Yolman J. Salinas

ABSTRACT

A retrospective study of MBTI scores of thirty-four aircrewmen from Air Force files were analyzed and integrated to yield information of personality structure and patterns among the group. Comparisons with other sample populations were made, as well as with a previous study from the School of Aerospace Medicine.

ACKNOWLEDGEMENTS

The writers would like to thank the Department of Neuropsychiatry in the School of Aerospace Medicine for their valuable support , assistance , and guidance throughout this project. It was a pleasure to be able to contribute to this ongoing study.

We would also like to acnowledge our appreciation to Dr. Timothy Strongin , Capt. , for his generous guidance and indispensible collaboration in allowing us to contribute with this project.

The writers would also like to acknowledge our appreciation to Dr. Bryce Hartman , Dr. D.R. Jones , and Dr. J.C. Patterson for their valuable presence and feedback during our stay at the School of Aerospace Medicine.

Thanks are also due to Air Force personnel Gary Schofield , Skip Holden , Janet Ross , and Tom Eckhoff for their assistance with all the details.

We would like to acnowledge sponsorship of the Air Force Systems Command , Air Force Office of Scientific Research , and the Schoool of Aerospace Medicine who made all this possible.

OBJECTIVES OF THE RESEARCH

U.S Air Force Aircrew members are a unique population. The present research describes personality traits in an elaboration and update of work initiated by Fine and Hartman (1967). Specifically MBTI scores were analyzed from samples of Air Force Pilots, Navigators, and finalists for MSE (space shuttle) duties . Parametric statistics were applied to a retrospective analysis of these MBTI (Myers Brigg Type Inventory) scores obtained from Air Force Aircrew members. This study will explore the possible existence of a type model as established by Fine and Hartman for this population with regards to the MBTI. It is hoped that these findings will contribute to an empirical understanding of psychometric norms or patterns which might be useful in balanced clinical evaluations and organizational consultations regarding Air Force Aircrew members.

INTRODUCTION

The MBTI (Myers-Briggs Type Indicator) is a test that uses the concept of psychological types, described by C.G. Jung (1921), and attempts to specify random variation in behavior as actually being quite orderly and consistent, being due to basic differences in the way individuals prefer to use their perception and judgement. It is a self-report inventory developed to measure personality preferences. The merit of the theory underlying the MBTI is that it enables us to expect specific differences in specific people and to use this information to more constructively understand human behavior. Specifically in this instance, the theory of the MBTI is to be implemented and tested on U.S. Air Force flyers to possibly delineate them as being a unique population. Their unique responses on standard personality tests as revealed by Fine and Hartman (1967) will be further tested with regards to the MBTI, which was not previously examined in the original battery of tests.

Military pilots represent a specific segment of of modern American society. They have enough personality characteristics in common to justify model analysis. It was found that there is a personality pattern common to successful professional flyers, with strengths and weaknesses so balanced that they adapted well to their particular lifestyle. In particular , emotional life, coping skills, current life adjustment, personal information, physical findings, career, and childhood were found to bias the personality types most common among the group, as stated by Hartman. The study allowed construction of a model personality picture since results were both reliable and internally consistent. What deviance existed, particularly on the projective tests, was discussed as a trend in personality balance. For the most part , however, these men had a personality pattern in common. The typical personality is characterized by an alloplastic approach to the world, matter of fact, terse direct ways of coping, strong needs for personal achievement, and high regard for responsibilities and family life. This conceptualization was arrived through formulation established by White and his theories regarding motivation as applied by Hartman.

The typical personality pattern described by Hartman suits these men to adapt to military flying insomuch as the pilots seemed to fit a Piagin model, a continuous series of assimilation-accomodation transactions with the environment in which previous experiences structure the individual's relationship to and incorporation of a new experience. Furthermore, flying is consistent with these men's typical identification with a lower middle class blue collar worker father and with a background emphasis on orderliness, respect, sports, and health as was also discovered by Hartman. With this general personality pattern that was described by Hartman , it was the intention of this research project to incorporate and evaluate the use of the Myers-Briggs Type Indicator to further understand the military flyer's typical , common personality traits , and adaptations which can hopefully be applied by psychiatrists toward evaluation of individual prognosis, management, and suitability for special tasks . In support of this goal, it was found that psychiatric problems of pilots seen at aerospace referral centers were consistent with the modal pattern described by Hartman.

The value of implementing the Myers-Briggs Type Indicator is in its particular efficiency as a potential

screening tool. Also it offers a new method to analyze personality patterns with a basic underlying theory that stresses dichotomies. The MBTI contains four separate dichotomous indices - extroversion/introversion , sensing/intuition , thinking/feeling , judgement/ perception . As stated , each index reflects one of four basic preferences which under Jung's theory , direct the use of perception and judgement. The preferences affect what people attend to and also how they draw conclusions about what they perceive. By design, each of the four indices expresses one dominant pole , so that the four indices yield sixteen possible combinations called personality types. The intent of the theory is to reflect a habitual choice between rival alternatives within each index. Each type , therefore, is a reflection of an acquired personality pattern with its unique approaches to handling the environment. The MBTI is concerned with individual differences in basic functions and attitudes. It is this quality that proves useful in such areas as career guidance and counseling where use of a preferred mode of perception and judgement can provide valuable information to the type of functioning of an individual. The MBTI , therefore can provide information about individuals and about trends within individuals in certain professions where specific modes of functioning are preferred. Studies have been

performed crossexamining such unique patterns within as well as between certain professions.

With regards to Air Force Aircrew members, it was found that not only were certain personality patterns more common but that there were certain similarities and differences between other professions which further helped to define and compare the model proposed by Hartman. Specifically comparisons were made with models described by Korchin and Ruff of Mercury astronauts as discussed by Hartman. On a more general basis, studies using the MBTI have indicated a difference between the personality type interactions of scales of those samples versus this study. Such studies include those by Thomas , Hicks, and Kerin and Slocum. which will be presented later. The value of the MBTI in allowing psychometric analysis of the various type indices for interaction permits cross-comparison between similar studies of other sample populations.

CHARACTERISTICS FREQUENTLY ASSOCIATED WITH EACH TYPE

	SENSING TYPES WITH THINKING	SENSING TYPES WITH FEELING	INTUITIVES WITH FEELING	INTUITIVES WITH THINKING
INTROVERTS JUDGING	**ISTJ** Serious, quiet, earn success by concentration and thoroughness. Practical, orderly, matter-of-fact, logical, realistic and dependable. See to it that everything is well organized. Take responsibility. Make up their own minds as to what should be accomplished and work toward it steadily, regardless of protests or distractions. Live their outer life more with thinking, inner more with sensing.	**ISFJ** Quiet, friendly, responsible and conscientious. Work devotedly to meet their obligations. Lend stability to any project or group. Thorough, painstaking, accurate. May need time to master technical subjects, as their interests are not often technical. Patient with detail and routine. Loyal, considerate, concerned with how other people feel. Live their outer life more with feeling, inner more with sensing.	**INFJ** Succeed by perseverance, originality and desire to do whatever is needed or wanted. Put their best efforts into their work. Quietly forceful, conscientious, concerned for others. Respected for their firm principles. Likely to be honored and followed for their clear convictions as to how best to serve the common good. Live their outer life more with feeling, inner more with intuition.	**INTJ** Have original minds and great drive which they use only for their own purposes. In fields that appeal to them they have a fine power to organize a job and carry it through with or without help. Skeptical, critical, independent, determined, often stubborn. Must learn to yield less important points in order to win the most important. Live their outer life more with thinking, inner more with intuition.
INTROVERTS PERCEPTIVE	**ISTP** Cool onlookers, quiet, reserved, observing and analyzing life with detached curiosity and unexpected flashes of original humor. Usually interested in impersonal principles, cause and effect, or how and why mechanical things work. Exert themselves no more than they think necessary, because any waste of energy would be inefficient. Live their outer life more with sensing, inner more with thinking.	**ISFP** Retiring, quietly friendly, sensitive, modest about their abilities. Shun disagreements, do not force their opinions or values on others. Usually do not care to lead but are often loyal followers. May be rather relaxed about assignments or getting things done, because they enjoy the present moment and do not want to spoil it by undue haste or exertion. Live their outer life more with sensing, inner more with feeling.	**INFP** Full of enthusiasms and loyalties, but seldom talk of these until they know you well. Care about learning, ideas, language, and independent projects of their own. Apt to be on yearbook staff, perhaps as editor. Tend to undertake too much, then somehow get it done. Friendly, but often too absorbed in what they are doing to be sociable or notice much. Live their outer life more with intuition, inner more with feeling.	**INTP** Quiet, reserved, impersonal. Enjoy especially theoretical or scientific subjects. Logical to the point of hair splitting. Interested mainly in ideas, with little liking for parties or small talk. Tend to have very sharply defined interests. Need to choose careers where some strong interest of theirs can be used and useful. Live their outer life more with intuition, inner more with thinking.
EXTRAVERTS PERCEPTIVE	**ESTP** Matter-of-fact, do not worry or hurry, enjoy whatever comes along. Tend to like mechanical things and sports, with friends on the side. May be a bit blunt or insensitive. Adaptable, tolerant, generally conservative in values. Dislike long explanations. Are best with real things that can be worked, handled, taken apart or put back together. Live their outer life more with sensing, inner more with thinking.	**ESFP** Outgoing, easygoing, accepting, friendly, fond of a good time. Like sports and making things. Know what's going on and join in eagerly. Find remembering facts easier than mastering theories. Are best in situations that need sound common sense and practical ability with people as well as with things. Live their outer life more with sensing, inner more with feeling.	**ENFP** Warmly enthusiastic, high spirited, ingenious, imaginative. Able to do almost anything that interests them. Quick with a solution for any difficulty and ready to help anyone with a problem. Often rely on their ability to improvise instead of preparing in advance. Can always find compelling reasons for whatever they want. Live their outer life more with intuition, inner more with feeling.	**ENTP** Quick, ingenious, good at many things. Stimulating company, alert and outspoken, argue for fun on either side of a question. Resourceful in solving new and challenging problems, but may neglect routine assignments. Turn to one new interest after another. Can always find logical reasons for whatever they want. Live their outer life more with intuition, inner more with thinking.
EXTRAVERTS JUDGING	**ESTJ** Practical realists, matter-of-fact, with a natural head for business or mechanics. Not interested in subjects they see no use for, but can apply themselves when necessary. Like to organize and run activities. Tend to run things well, especially if they remember to consider other people's feelings and points of view when making their decisions. Live their outer life more with thinking, inner more with sensing.	**ESFJ** Warm-hearted, talkative, popular, conscientious, born cooperators, active committee members. Always doing something nice for someone. Work best with plenty of encouragement and praise. Little interest in abstract thinking or technical subjects. Main interest is in things that directly and visibly affect people's lives. Live their outer life more with feeling, inner more with sensing.	**ENFJ** Responsive and responsible. Feel real concern for what others think and want, and try to handle things with due regard for other people's feelings. Can present a proposal or lead a group discussion with ease and tact. Sociable, popular, sympathetic. Responsive to praise and criticism. Live their outer life more with feeling, inner more with intuition.	**ENTJ** Hearty, frank, decisive, leaders in activities. Usually good in anything that requires reasoning and intelligent talk, such as public speaking. Are well informed and keep adding to their fund of knowledge. May sometimes be more positive and confident than their experience in an area warrants. Live their outer life more with thinking, inner more with intuition.

METHODS

A retrospective analysis of Myers-Briggs Type Inventory scores for 34 Aircrew personnel will be performed from information derived from United States Air Force files. The data will be graphically analyzed in this study. Parametric statistical studies will be performed in an upcoming study. The study was conducted at the USAF School of Aerospace Medicine, a consultation service for Air Force operations. The 34 Aircrew members selected for this study represent a cross-section of Air Force flying officers. These men were in residence at the school when the test was administered. A tabulation of their MBTI scores and status is shown below in figure one. The sample included 33 male and one female ranging in age from 20 - 41. Their Air Personnel position varied from MSE (Manned Space Engineer) to Pilot to Navigator.

The study being reported here was designed to explore the hypothesis of whether a specific personality type pattern predominated with regards to the MBTI , and whether specific interactions among the various scales were apparent for comparison with other studies of different populations.

[illegible]	[illegible]	PERSONALITY TYPE (1)	AIR PER. POSIT (2)	ARISI DX	ARISII DX	TRAITS (3)	AGE	SEX (4)	STATUS (5)	RACE (6)
[illegible]	[illegible]	1000	11	030070	107109	030140	25	1	1	0
[illegible]	[illegible]	0000	10	107109	107109	107109	25	1	0	1
[illegible]	[illegible]	1101	10	107109	107109	107109	31	1	0	0
[illegible]	[illegible]	0110	10	030000	106110	107109	28	1	2	0
[illegible]	[illegible]	1000	13	030700	107109	107109	23	1	0	0
[illegible]	[illegible]	1000	12	107109	107109	107109	41	1	1	0
[illegible]	[illegible]	0001	10	107109	107109	107109	39	1	1	0
[illegible]	[illegible]	0000	10	107109	107109	107109	24	1	1	0
[illegible]	[illegible]	1010	14	031600	107109	030181	25	1	0	0
[illegible]	[illegible]	0000	12	107109	107107	107109	34	1	2	0
[illegible]	[illegible]	0001	10	107109	107109	107109	24	1	0	0
[illegible]	[illegible]	1000	12	107109	107109	107109	39	1	1	0
[illegible]	[illegible]	0000	12	031600	107109	030140	39	1	1	0
[illegible]	[illegible]	0000	10	107109	107109	107109	20	1	0	0
[illegible]	[illegible]	1111	11	107109	107109	107109	32	1	1	0
[illegible]	[illegible]	1100	00	107109	107109	107109	31	1	0	0
[illegible]	[illegible]	1000	00	107109	107109	107109	29	1	1	0
[illegible]	[illegible]	0000	00	107109	107109	107109	29	1	1	0
[illegible]	[illegible]	1100	00	107109	107109	107109	28	1	0	0
[illegible]	[illegible]	0100	00	107109	107109	107109	29	1	1	0
[illegible]	[illegible]	0000	00	107109	107109	107109	30	1	0	0
[illegible]	[illegible]	0100	00	107109	107109	107109	29	1	1	0
[illegible]	[illegible]	0110	00	107109	107109	107109	27	1	1	0
[illegible]	[illegible]	0100	00	107109	107109	107109	31	1	0	0
[illegible]	[illegible]	1000	00	107109	107109	107109	31	1	1	0
[illegible]	[illegible]	1110	00	107109	107109	107109	31	1	1	0
[illegible]	[illegible]	0100	00	107109	107109	107109	30	1	1	0
[illegible]	[illegible]	0101	00	107109	107109	107109	29	1	1	0
[illegible]	[illegible]	0000	00	107109	107109	107109	31	1	1	0
[illegible]	[illegible]	0100	00	107109	107109	107109	29	1	1	0
[illegible]	[illegible]	0000	00	107109	107109	107109	31	1	1	0
[illegible]	[illegible]	1000	00	107109	107109	107109	30	1	1	0
[illegible]	[illegible]	1000	00	107109	107109	107109	25	0	0	0
[illegible]	[illegible]	0100	00	107109	107109	107109	30	1	1	0

NOTES:
(1) PERSONALITY TYPES:
E=0 I=1
S=0 N=1
T=0 F=1
J=0 P=1
(EXAMPLE: 1000 = ISTJ)
(2) AIR PERSONNEL POSITION
00 = N/A
10 = STUDENT PILOT
11 = INSTRUCTOR PILOT
12 = COMMANDER
13 = CO-PILOT
14 = NAVIGATOR
(3) TRAITS:
1 = NO TRAIT
0 = TRAIT
(4) SEX:
0 = FEMALE
1 = MALE
(5) MARITAL STATUS:
0 = SINGLE
1 = MARRIED
2 = DIVORCED
(6) RACE:
0 = WHITE
1 = BLACK

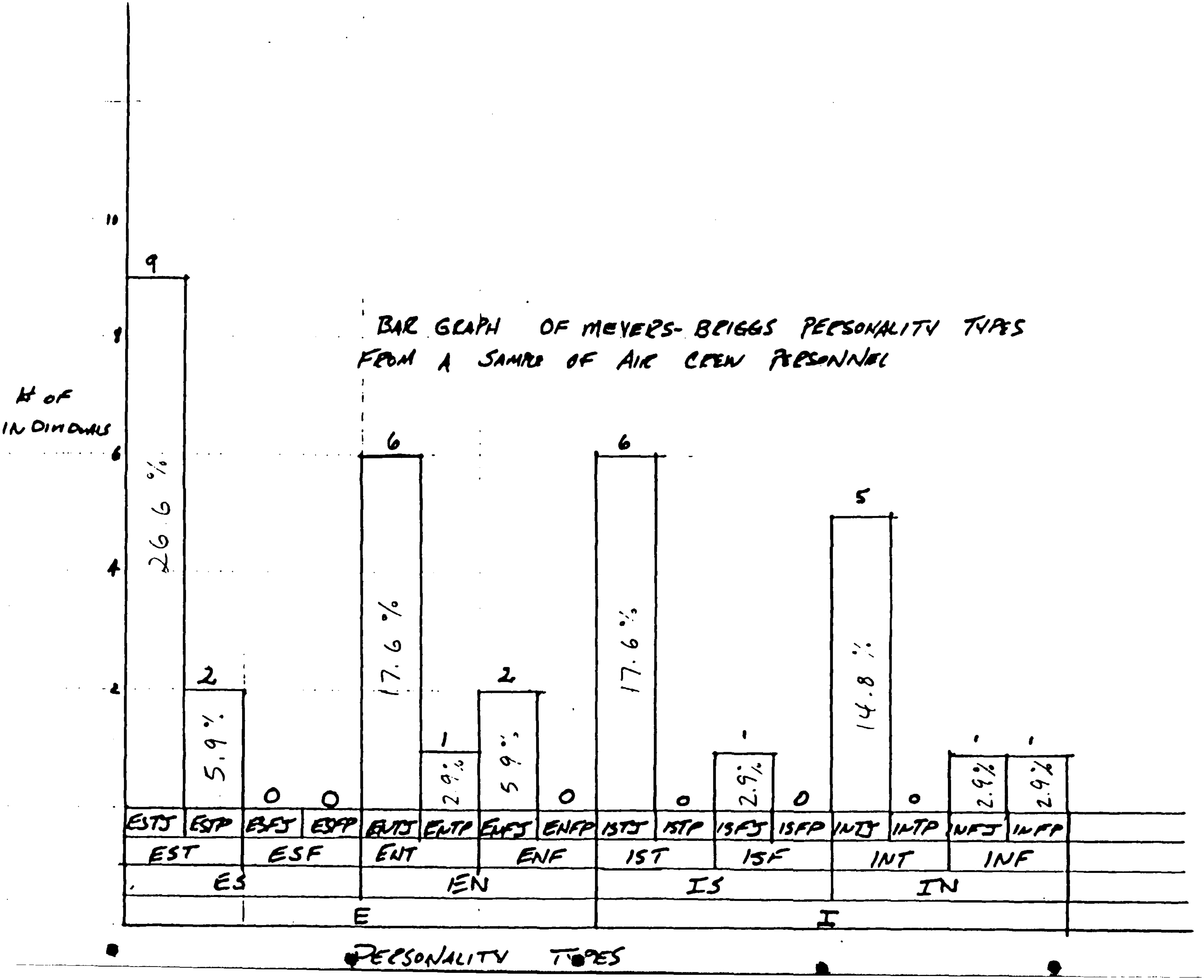
BAR GRAPH OF MEYERS-BRIGGS PERSONALITY TYPES
FROM A SAMPLE OF AIR CREW PERSONNEL
OF INDIVIDUALS
10
8
6
4
2
9
26.6 %
2
5.9%
0
0
6
17.6 %
1
2.9%
2
5.9%
0
6
17.6%
0
1
2.9%
0
5
14.8%
0
1
2.9%
1
2.9%
ESTJ
ESTP
ESFJ
ESFP
ENTJ
ENTP
ENFJ
ENFP
ISTJ
ISTP
ISFJ
ISFP
INTJ
INTP
INFJ
INFP
EST
ESF
ENT
ENF
IST
ISF
INT
INF
ES
EN
IS
IN
E
I
PERSONALITY TYPES

BAR GRAPH OF MEYERS-BRIGGS PERSONALITY TYPES FROM A SAMPLE OF EMPLOYEES OF A RURAL PUBLIC SCHOOL SYSTEM

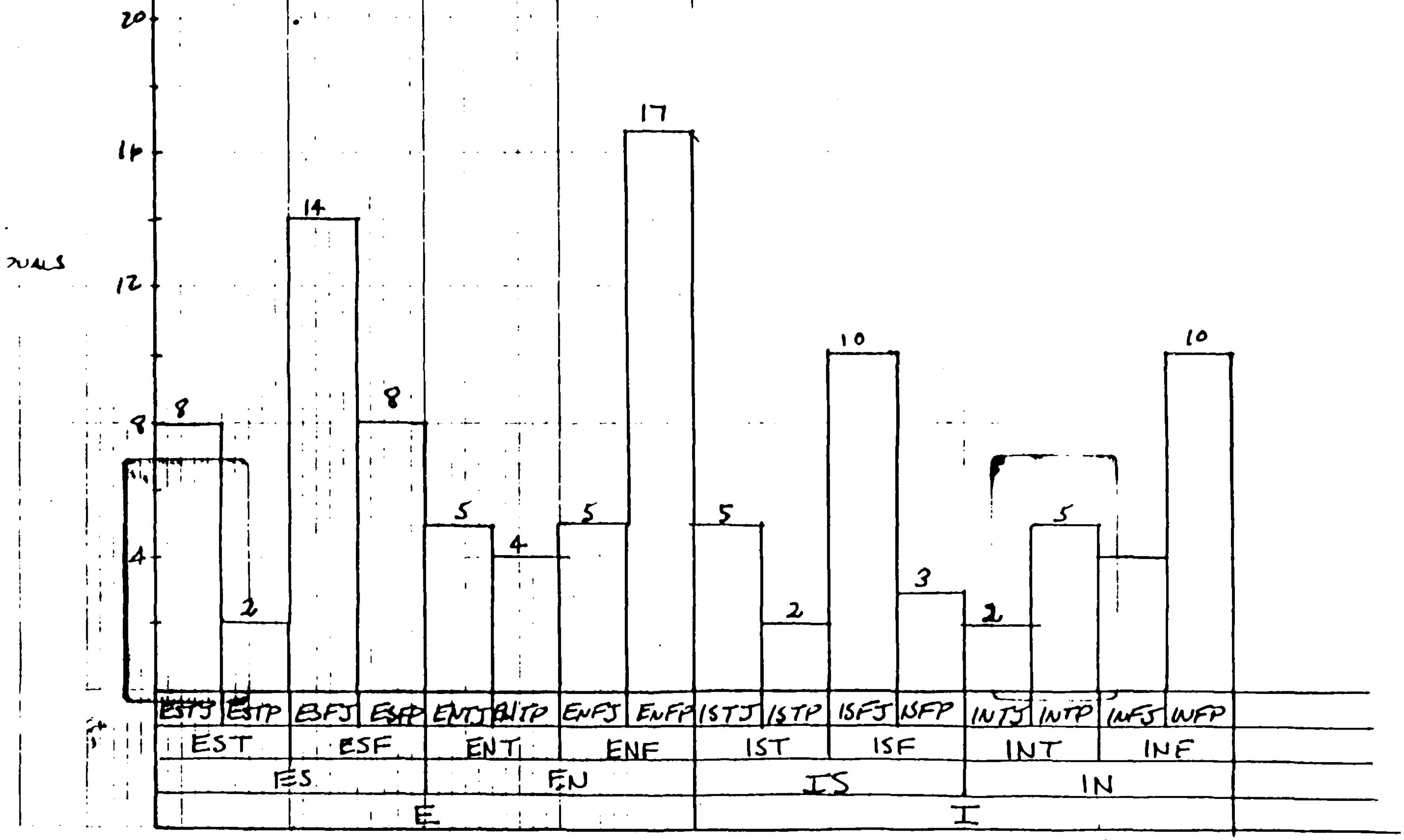

FREQUENCY GRAPH OF FLYERS

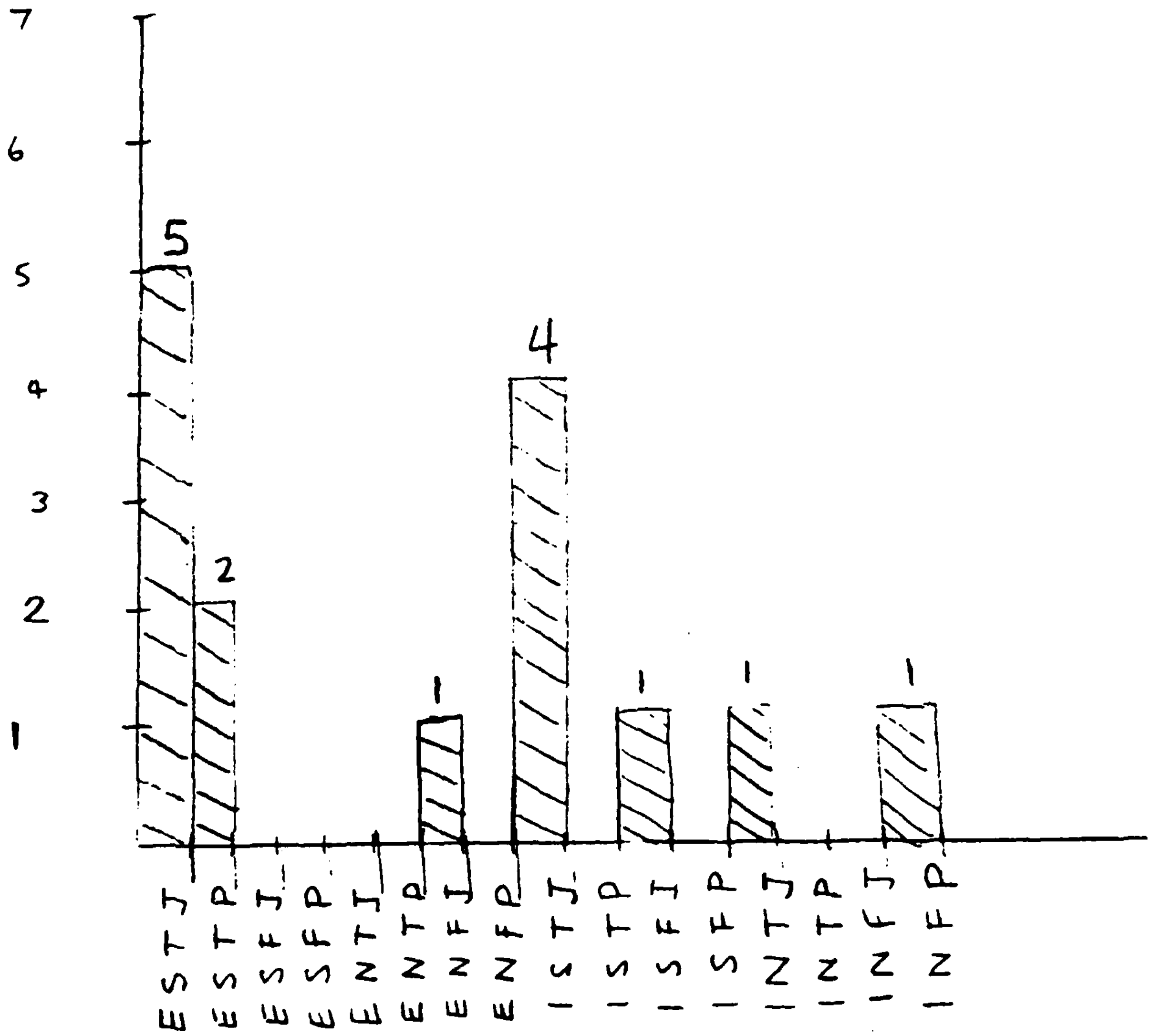

FREQUENCY GRAPH
OF
MSEs

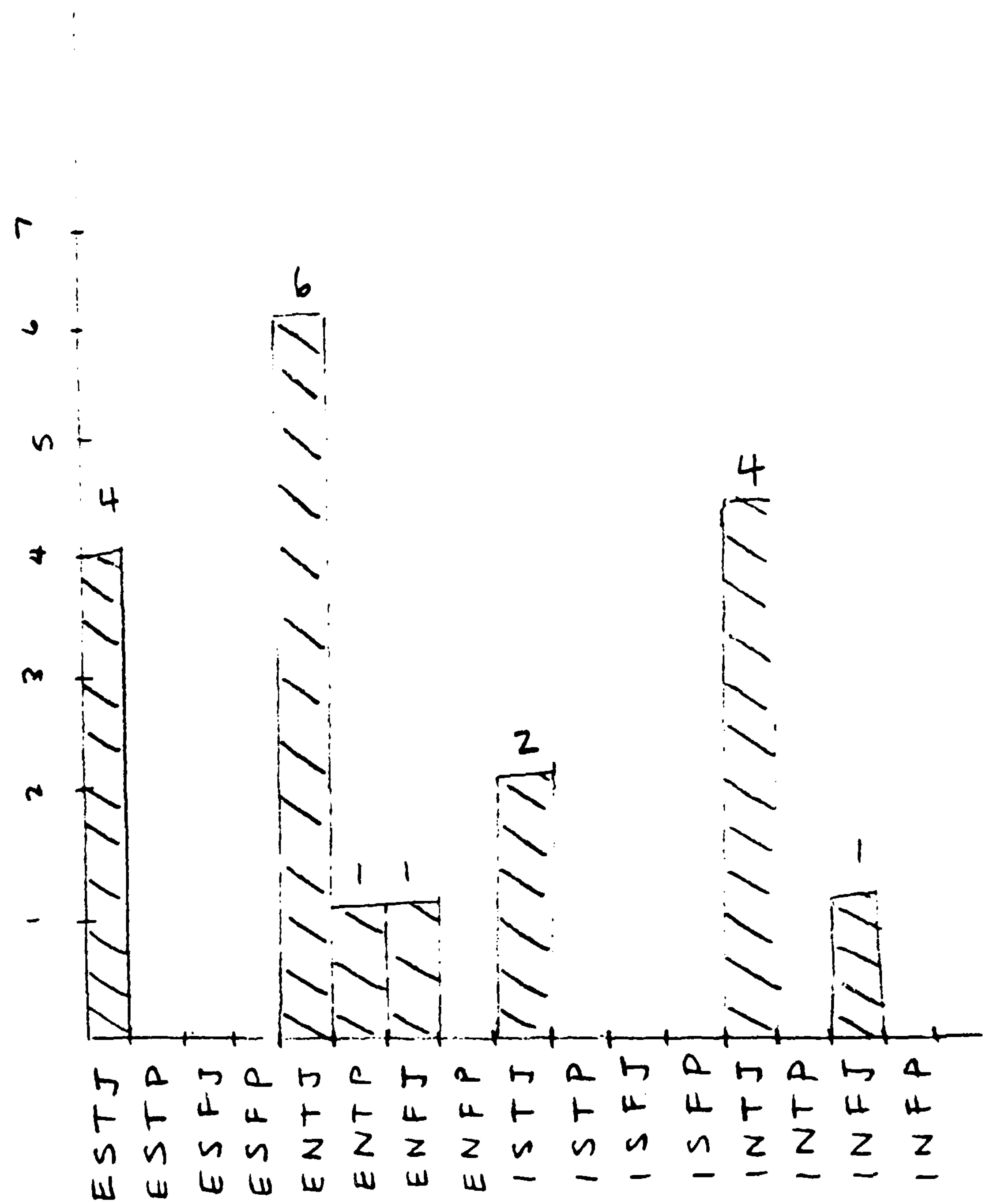

RESULTS and DISCUSSION

Upon initial collection of the data, an effort to categorize the 34 Aircrew members according to MBTI types was graphed, figure 2. This data can be further analyzed and compared. When figure 2 is compared to figure 3 , different sample's distribution,(Hicks 1984) , the raw data seems to be quite distinct with some minor overlaps. Although sample number might be significant, the data was percentage-wise quite unique in many ways lending support to the belief that different professions would tend to reflect differently with regards to the MBTI of personality.

Nevertheless, when aircrew members are analyzed as a group, they can be further broken down by position. Representation of the type breakdown for each is shown in figures 4 and 5 for MSE (Manned Space Engineers) and Flyers respectively. Even before this data is analyzed, it might be more useful and worthwhile to note that not so initially obvious, a pattern was uncovered in figure 2. Specifically, there was an unusually large population of aircrew personnel who shared to particular scales, namely T-J , Thinking and Judgement versus Feeling and

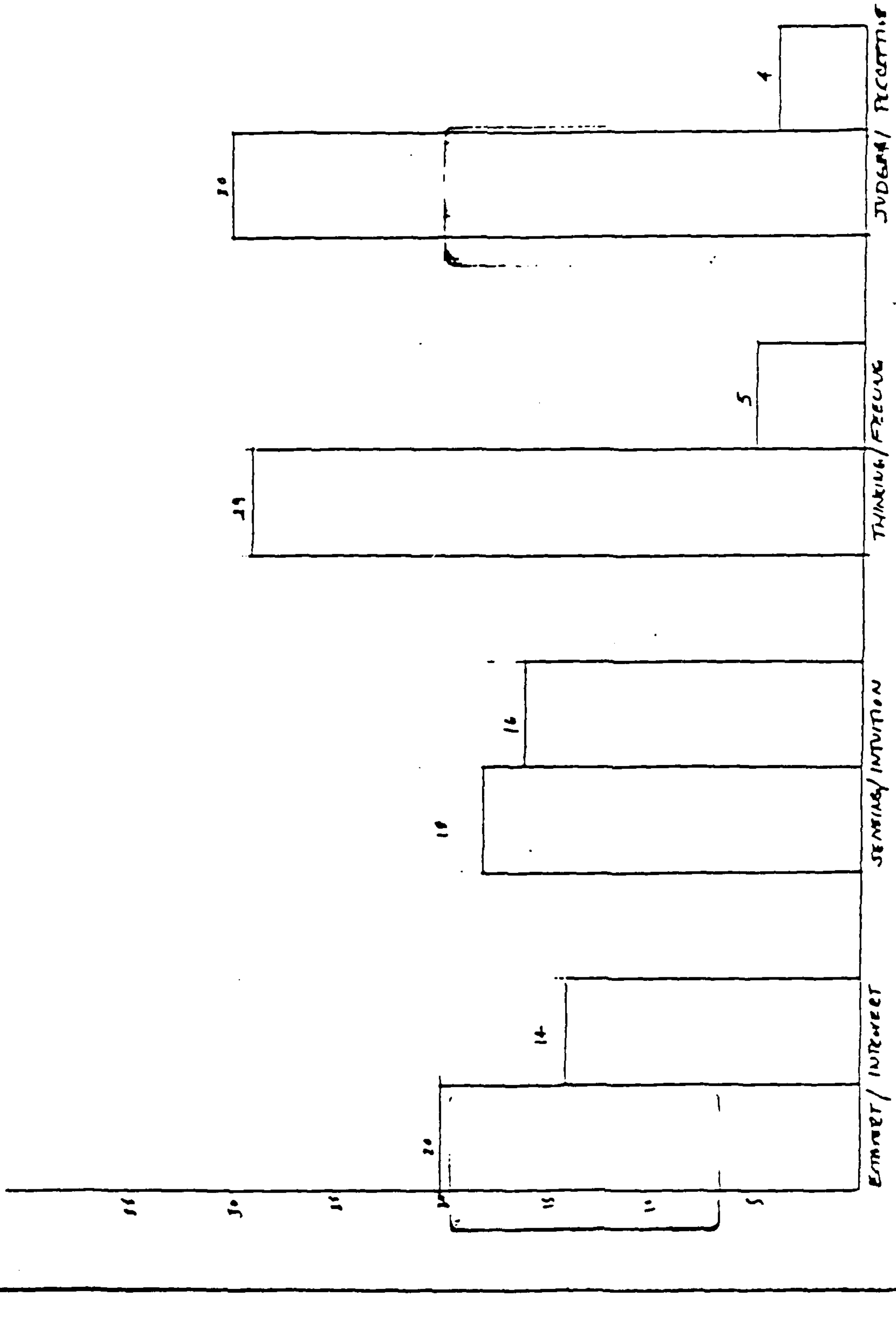

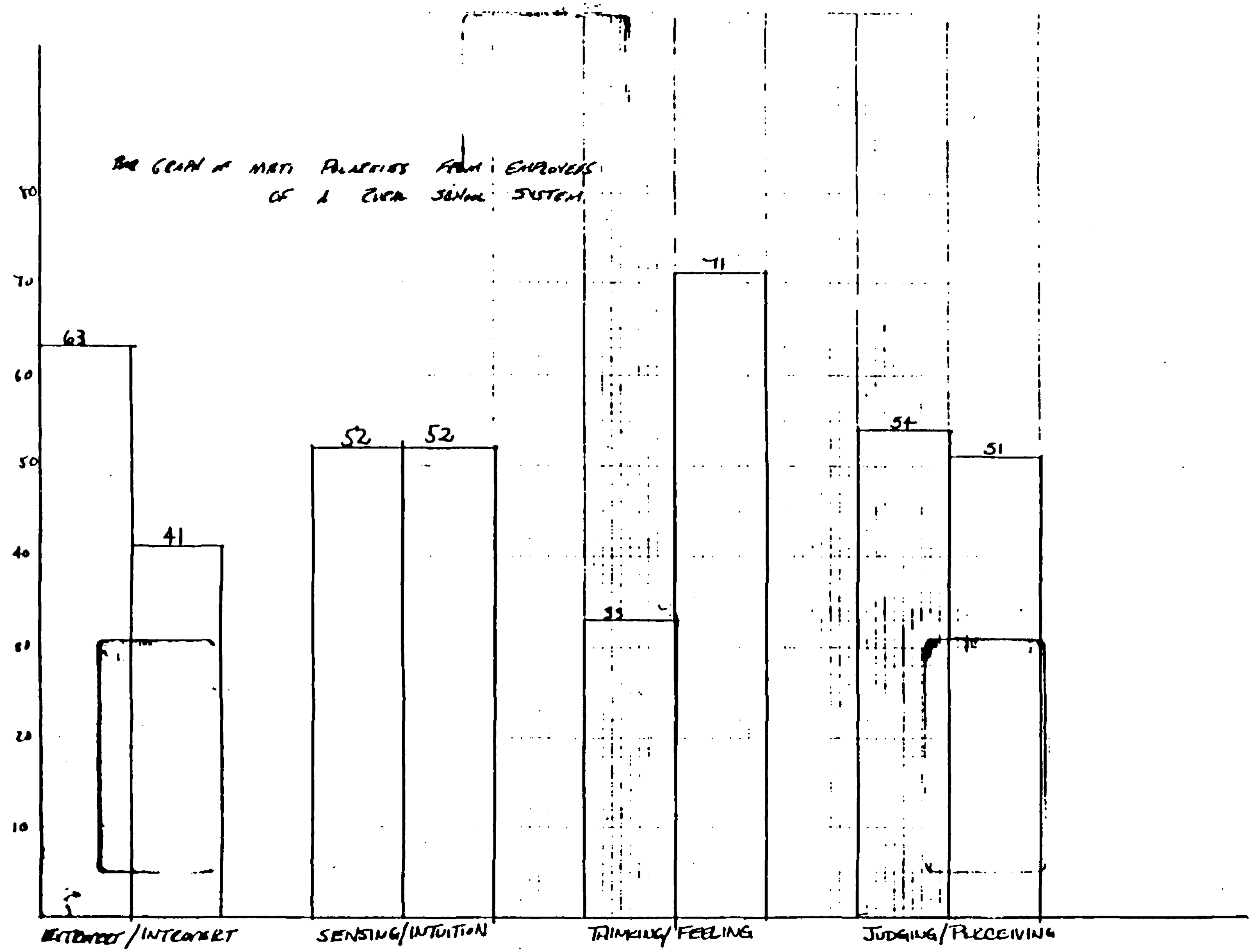
BAR GRAPH OF MBTI PROPERTIES FROM EMPLOYEES
OF A RURAL SCHOOL SYSTEM
80
70
60
50
40
30
20
10
63
41
52
52
33
71
54
51
EXTROVERT/INTROVERT
SENSING/INTUITION
THINKING/FEELING
JUDGING/PERCEIVING

Perception. Of the 34 Aircrew, 26 demonstrated this similarity 76.6%. This topic of interaction between scales was not so dramatically evident between any other two scales, something which could be statistically testable. Even after breaking this sample of Aircrew to determine whether there was some underlying factor regarding position, it was noticed that all of the ENTJ were MSEs. The MSEs also dominated the INTJ type, but the flyers retaliated by dominating the ISTJ to account for the overall predominant TJ subclass. The ESTJ nevertheless prevailed in both Flyers and MSEs.

When the data was further broken down into individual scales, to detect further patterns, figure 6 , of polar dominance among the scales, it was again apparent that the T & J , Thinking and Judgement dominated their respective scale. This was not the case in the study by Hicks , figure 7. In this instance, the employees of a rural public school system showed completely different results with regards to the thinking/ feeling and judgement/perception scales. This again provided some distinction among the Aircrew members when compared to another profession , school administrators.

A more detailed analysis of a particular scale with regards to its score breakdown, continuous data, yielded

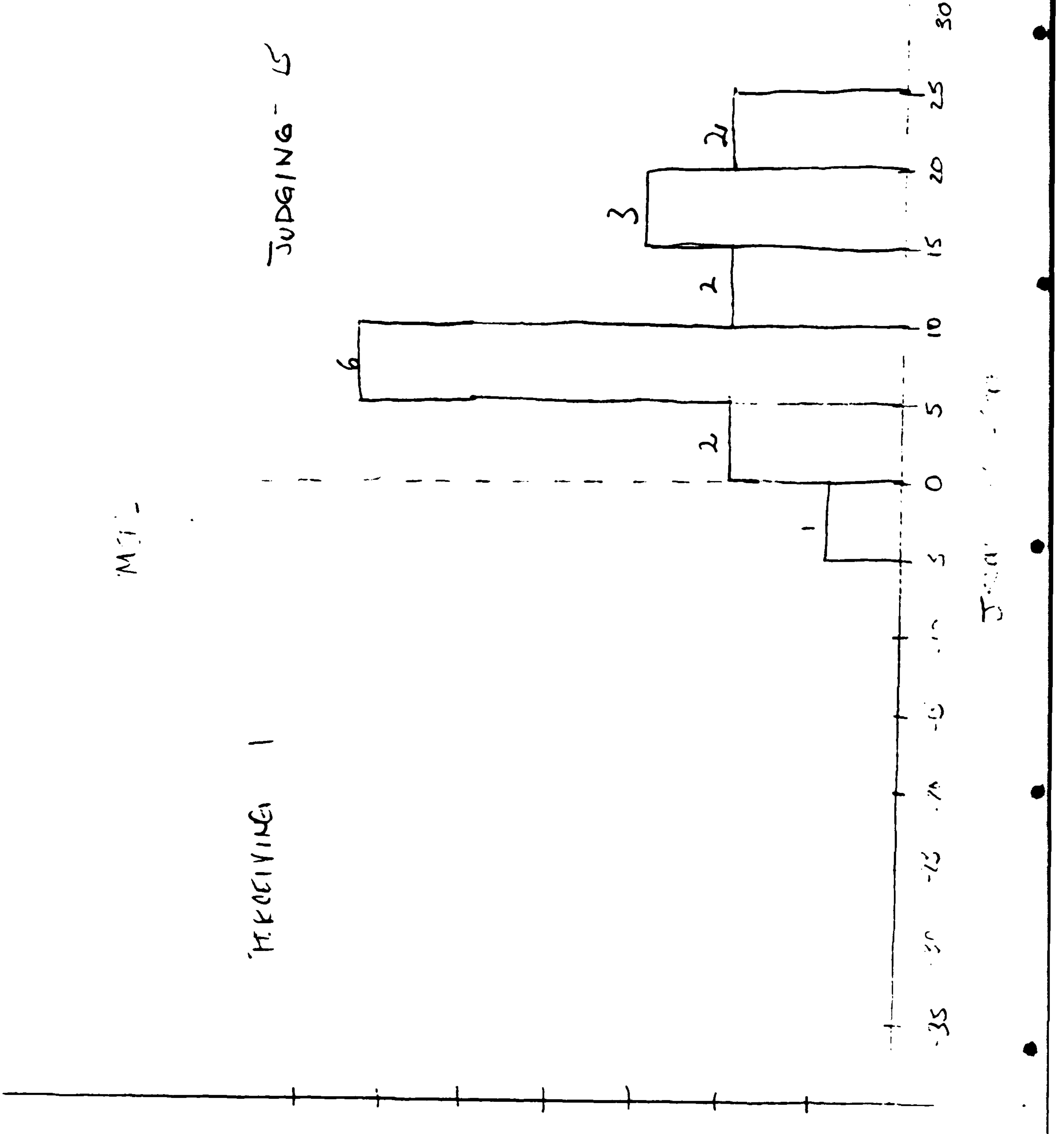
JUDGING
6
3
2
2
2
1
0
5
10
15
20
25
30
-35

+16	-9
+10	-1
+10	-3
+26	-8
+5	-7
+10	-12
+15	-21
	-16
	-11

EXTRAVERSION VS INTRAVERSION
FREQUENCY CHART

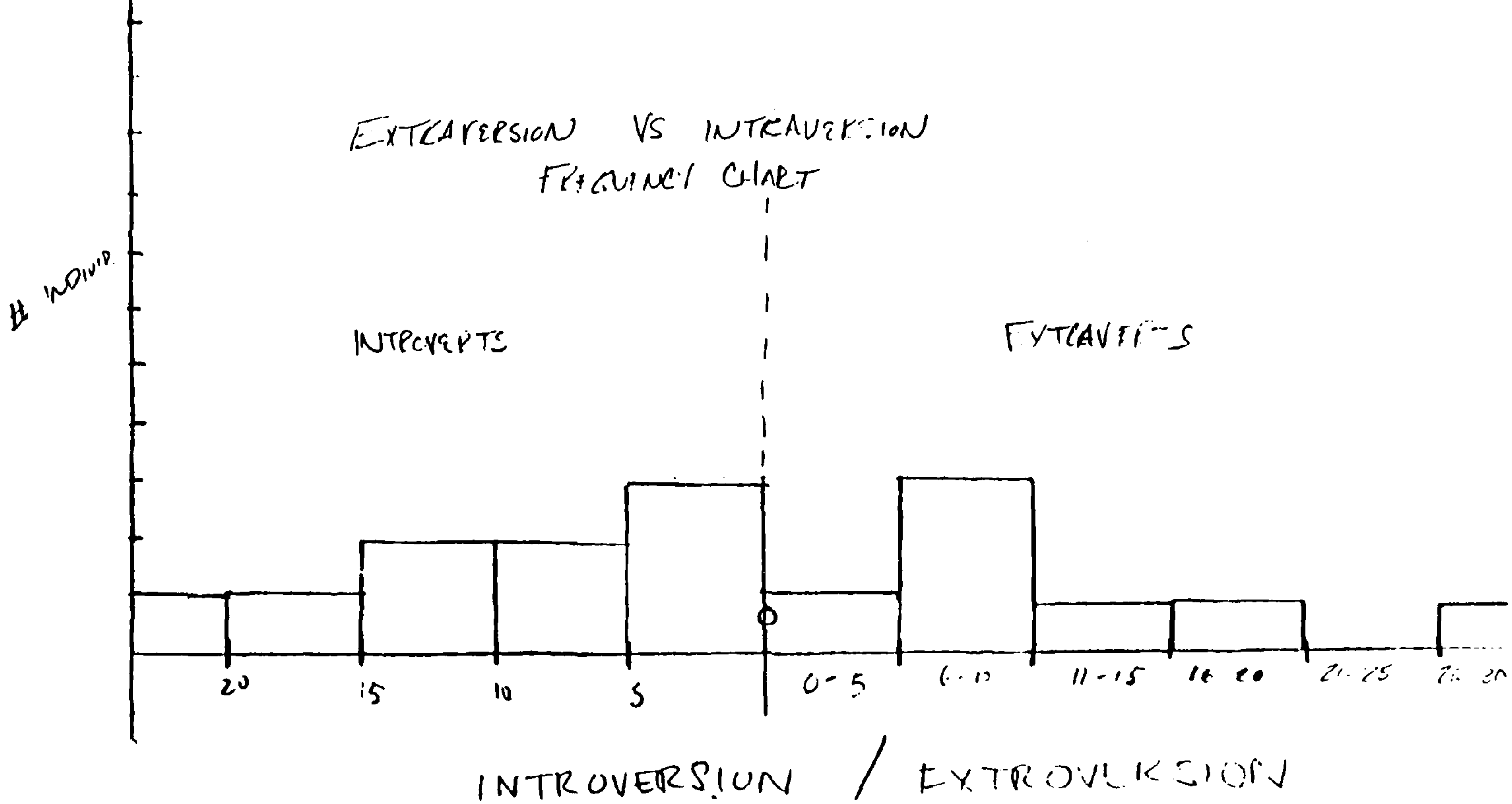

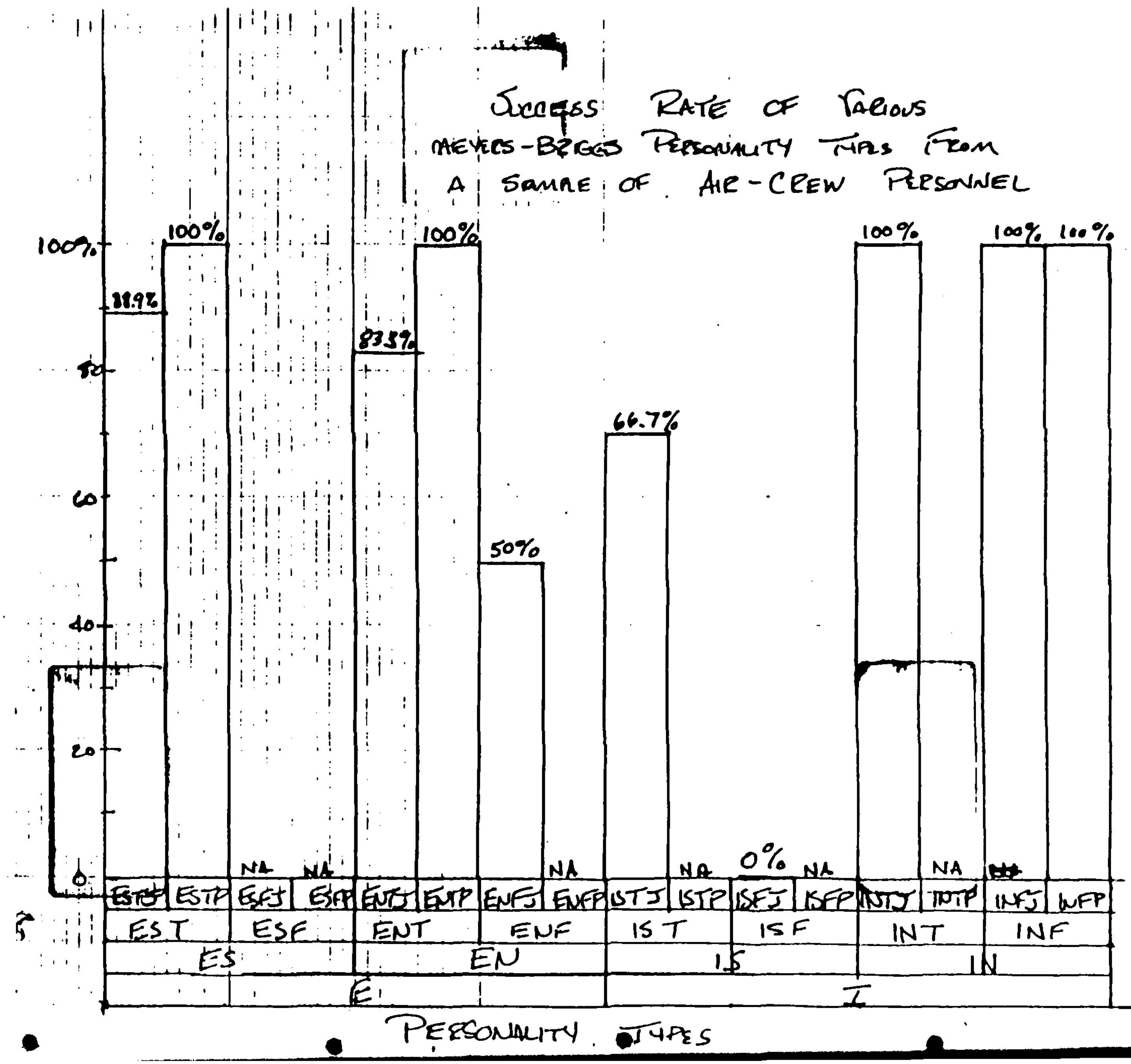
SUCCESS RATE OF VARIOUS
MEYERS-BRIGGS PERSONALITY TYPES FROM
A SAMPLE OF AIR-CREW PERSONNEL
100%
80
60
40
20
0
88.9%
100%
NA
NA
83.3%
100%
50%
NA
66.7%
NA
0%
NA
100%
NA
100%
100%
ESTJ
ESTP
ESFJ
ESFP
ENTJ
ENTP
ENFJ
ENFP
ISTJ
ISTP
ISFJ
ISFP
INTJ
INTP
INFJ
INFP
EST
ESF
ENT
ENF
IST
ISF
INT
INF
ES
EN
IS
IN
E
I
PERSONALITY TYPES

other interesting results. Specifically, the judgement/perception scale was chosen, which happens to be the central scale in Jungian theory. When the scores of the MSEs was distributed, not only was the polar dominance of the (Figure 8) judging index evident, but a particular modal score dominated as well for 6 of the 16 MSEs. This particular statistic could be useful if the continuous data was statistically analyzed parametrically, which will be done in an upcoming study. The same chart was performed for a more evenly distributed scale for MSEs, the (Figure 9) extroversion/introversion scale. Upon observing the data, no apparent pattern was evident, something which could be statistically verified.

The value of analyzing the data in this retrospective study, is that performance could be tracked according to the personality type on file for the Aircrew member to determine any patterns. It is possible that certain personality types might be more successful than others at handling the demands of the job. On the other hand, this might not necessarily be true, but nonetheless the data is open for scrutiny. In Figure 10, just this representation was made, where success rate of a sample of Aircrew personnel was categorized against MBTI type. It was found that success rate greater than 80% was pretty evenly distributed among types with the exception of 3 types , ENFJ , ISFJ , ISTJ .

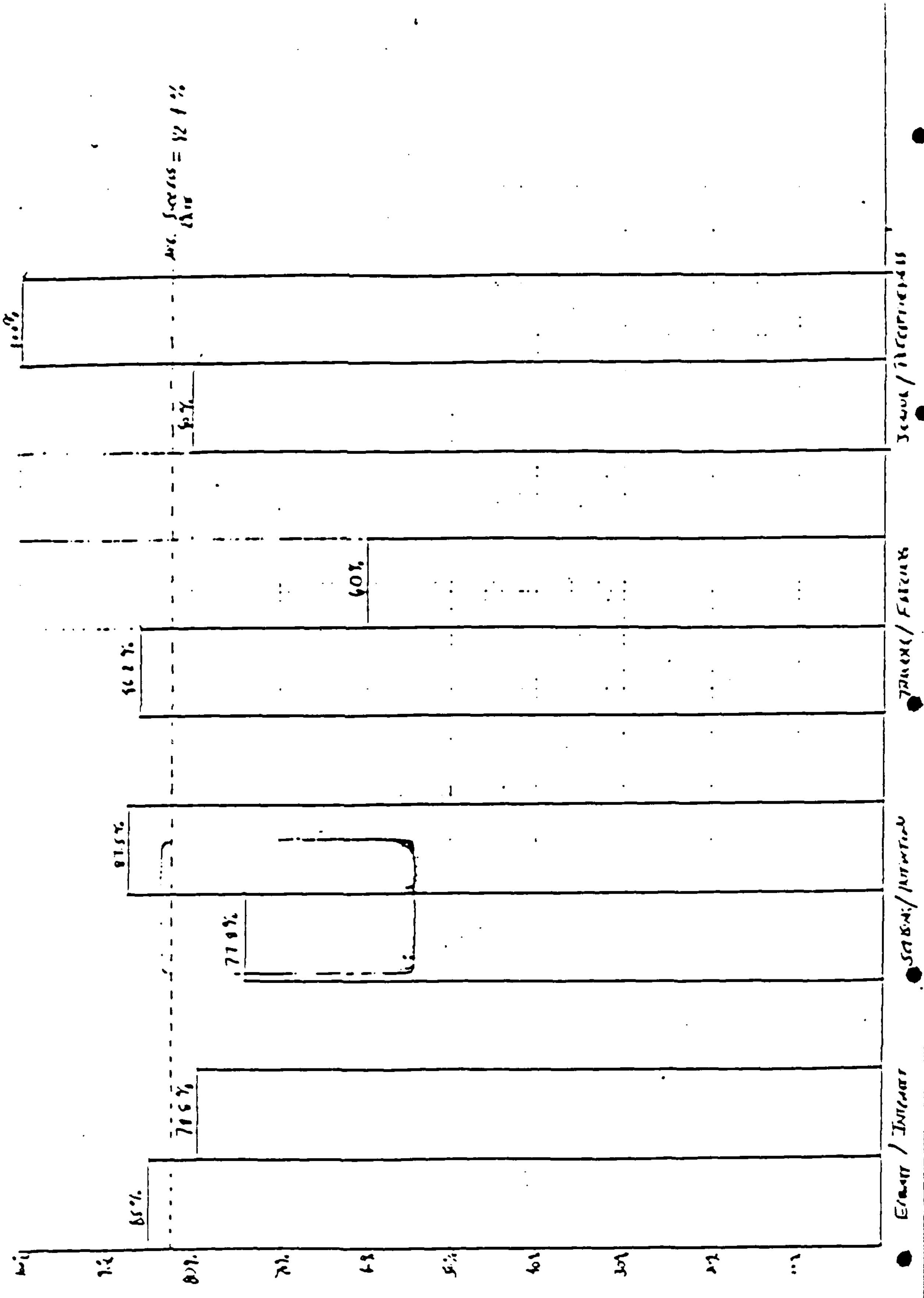

At first glance this statistic might be misleading, if one fails to look at specific sample and group N number, which would make this finding statistically invalid until a larger sample number was available. Another interesting representation, Figure 11, analyzes success rate with respect to particular scale. If one remembers that the T/F scale , Thinking/Feeling was dominated by Thinkers overwhelmingly, then the low Feeling percentage would also have to be said to be statistically not reliable until a larger sample pool was available. Nevertheless, the possibilities of uses of the MBTI are worthwhile, if one considers the relative efficiency of the test. Studies involving the use of the MBTI for assessing occupational choice, performance , and the like have been done, with particular citation of a study by Carlyn (1977).

When comparisons are made with other studies , the results displayed for the aircrew members tends to seem unique to this population. Specifically, in a study by Thomas (1984) of mechanical engineer students , it was found a correlation between the the J/P dimension and the S/N and T/F dimensions. In our case , a correlation was only evident between the J/P and T/F. In a study by Kerin and Slocum (1981) of graduate marketing subjects with one year experience of business it was found that NFs differed

with NTs in their preference for more objective , quantitative data. This was something which was found in the original Hartman paper for the prototype aircrew member, and which could lead the MBTI as a valuable tool in informational data retrieval from the different personality types of aircrew. Another different study by Bruhn , Bunce and Greaser tested physician assistants and nurse practitioners with the hopes of finding correlations among the scales of the MBTI and also to determine predictors of success from personality characteristics, something very similar to this study. Correlations were indeed found between the SN and JP scales, which was once again quite distinct from our study observations. A TF and JP interaction similar to ours was found but only for a sub-sample of their population and it was inversely related to ours in any case with an FP rather than Tj dominance.

Significantly the Myers Briggs Type Indicator has found many uses in vocational counseling, in screening and selecting applicants, and in predicting academic success. In our case , it is hoped that the Indicator has served a purpose in further typifying the personality patterns of existing successful Aircrew, which can subsequently be used in the capacities mentioned above.

REFERENCES

1. Fine , Paul M. , Hartman , Bryce O. , " Psychiatric Strengths and Weaknesses of Typical Air Force Pilots ", Air Force Publication SAM TR 68 121 , USAF School of Aerospace Medicine Texas , November 1968

2. Hicks , Lou E. , " Conceptual and Empirical Analysis of Some Assumptions of an Explicitely Typological Theory " Journal of Personality and Social Psychology , 1984 Vol 46, No. 5 , 1118-1131

3. Bruhne, J.G. , Bunce, H. , Greaser, R.C. , " Correlations of the Myers-Briggs Type Indicator with Other Personality and Achievement Variables ", Psychological Reports 1978 Vol 43 , 771-776

4. Kerin, R.A. , Slocum, J.W. , " Decision-Making Style and Acquisition of Information : Further Exploration of the Myers Briggs Type Indicator " , Psychological Reports 1981 , Vol. 49 , 132-134

5. Thomas, Charles R.," Regression of Myers Briggs Type Scales " Psychological Reports , 1984 , 55,568

6. Carlyn, M. , " An Assessment of the Myers Briggs Type Indicator ", Journal of Personality Assessment , 1977 Vol 41 , 3

7. Myers, I.B. , The Myers Briggs Type Indicator Manual , Princeton , New Jersey , Consulting Psychologists Press , 1985

8. Lynch , Anne Q., " The Myer Briggs Type Indicator : A Tool for Appreciating Employee and Client Diversity ", Journal of Employment Counseling , September 1985 , 105

9. Pinkney, J.W. , " The Myers-Briggs Type Indicator as an Alternative in Career Counseling ", The Personnel and Guidance Journal , November 1983 , 173

10. Carlson, J.G. , " Recent Assessments of the Myers Briggs Type Indicator ", Journal of Personality Assessment , 1985 , Vol. 49 , 356

11. Carskadon , T.G. , " Test-Retest Reliabilities of Continuous Scores on the Myers Briggs Type Indicator " Psychological Reports , 1977 Vol 41, 1011-1012

1986 USAF-UES SUMMER FACULTY RESEARCH PROGRAM/

GRADUATE STUDENT SUMMER SUPPORT PROGRAM

Sponsored by the

AIR FORCE OFFICE OF SCIENTIFIC RESEARCH

Conducted by the

Universal Energy Systems. Inc.

FINAL REPORT

Analytical Computer Modeling of the NPN BICFET Device

Prepared by:	Dennis Whitson and W. David Schmidt
Academic Rank:	Full Professor / Graduate Student
Department and	Physics Department
University:	Indiana University of Pennsylvania
Research Location:	Avionics, Electronics Technology Division,
	Electronics Research Branch, Device Research Group
USAF Researcher:	Gary McCoy and Chern Huang
Date:	Septemper 24, 1986
Contract No.:	F49620-85-C-0013

Analytical Computer Modeling of the NPN BICFET Device

by

Dennis Whitson and W. David Schmidt

ABSTRACT

A computer program was written for an analytical model of the NPN Bipolar Inversion Channel Field Effect Transistor (BICFET) device. From this analysis a number of conclusions can be drawn: (1) Type of metal used is extremely important; (2) The "Fermi Factor" which determines the electron population in the spike layer could be crucial and the spike layer may have to be grown in the semi-insulator rather than the semiconductor; (3) Collector stretch may be negligible at realistic current density values; (4) For the GaAs/AℓGaAs system a functioning NPN device may be easier to fabricate than a PNP device; (5) There are two independent gain factors: (a) the exponential argument which depends on ψ_{ms} and (b) p_o which depends only on the density of the spike layer dopant.

ACKNOWLEDGMENTS

We would like to thank the Air Force Systems Command and the Air Force Office of Scientific Research for sponsorship of our research. The Avionics Laboratory of Wright Patterson Air Force Base has an environment quite conducive to scientific research. Everyone we interacted with over the summer was extremely helpful and friendly. The general attitude shown at the labs makes for a productive, interesting, and amiable atmosphere. Special thanks go to Gary McCoy amd Chern Huang for giving us the opportunity and the guidance necessary for the research. Also, we would like to thank the members of the computer support team for all their help.

Finally Dennis Whitson would like to thank his wife, Sandy, for her loving support and impressive patience in putting up with our seperation during the summer.

I. Introduction

Recent research interests of Dennis Whitson have been in the area of semiconductor device physics. During the summers of 1981, 82, 83, and 84, he worked at Westinghouse Research & Development labs. Dr. Whitson also worked there one day a week during the school year and spent a sabbatical year (1984-85) at the labs. During this time he was involved mainly with double injection silicon power devices with both injection and MOS gates. The summer of 1985, Dr. Whitson was at GTE labs working with isolation techniques in power intergrated circuits. At that time he decided that he wished to become involved with compound semiconductors and hetereojunction devices. This is an area that avionics/AADR is pursuing and it fit very nicely into his plans.

W. David Schmidt was a M.S. graduate student at Indiana University of Pennsylvania and is now in the Ph.D. graduate program at Dartmouth.

II. Objectives of the Research Effort

The objective of the ten week research effort was to make significant progress in the modeling of two GaAs/AℓGaAs devices: the BICFET (bipolar inversion channel field effect transistor) and the DOES (double heterostructure optoelectronic switch).

The three layers of material (e.g. AℓGaAs(p)/GaAs(n^+)/GaAs(p)) that form the BICFET (1,2) are also the first three layers of the DOES device (3). It is hoped that both the DOES device and the BICFET can be processed on the same substrate. This would allow both optical switching and electronic signal processing with the same integrated circuit.

The BICFET device (1,2) by itself offers intriguing possibilities:

1. High current gain ($\sim 10^5$),
2. High current operation ($\sim 10^6$ A/cm^2),
3. High frequency operation (~ 400 GH$_z$). and
4. Different scaling laws than bipolar or MOSFET with no punchthrough.

III. COMPUTER PROGRAM OPTIONS

Since Taylor and Simmons(1) modeled a silicon NPN device we decided to duplicate their work first and then to proceed to modeling GaAs/AlGaAs devices. In the process we also checked a number of their approximations. The computer program therefore has a number of options in it.

Two of the options that can be used or not are "Collector Stretch" and "Fermi Factor". These two options affect the equation used for charge balance, i.e.

$$Qe + Qi + Qc = 0 \tag{1}$$

where Qe = emitter charge, Qi = spike layer charge, and Qc = collector charge. Using the "Fermi Factor" results in

$$Q_i = \frac{-q N_i}{1 + 4 e^{(\epsilon_p - \Delta E_i)/KT}} \tag{2}$$

where Ni is the charge density per cm^2 of the spike layer, ϵ_p is the acceptor level energy above the valence band in the spike layer, and ΔE_i is calculated from the density of the inversion layer at the interface (semiconductor/spike layer), p_o, using the equation:

$$p_o = N_V e^{-\Delta E_i/KT} \tag{3}$$

If the "Fermi Factor" is not used then the denominator in equation(2) is equal to one. When "Collector Stretch" is used we have

$$Q_c = \left(\frac{2 q \epsilon_s}{\beta}\right)^{\frac{1}{2}} \left[p_o + \beta \phi_s \left(N_d - \frac{J_c}{q V_s}\right)\right]^{\frac{1}{2}} \tag{4}$$

When "Collector Stretch" is not used $J_c = 0$ in this equation. The inclusion of J_c (Collector current density) in this equation causes the collector depletion area to increase, i.e. to "stretch", whenever the device is conducting current.

Other options include the choice of either calculating certain parameters or using default values. The effective velocities can be calculated

$$V_n = \frac{V_{tn}}{1 + d/\ell_n} \quad ; \quad V_p = \frac{V_{tp}}{1 + d/\ell_p} \tag{5}$$

where d is the thickness of the semi-insulator; V_{tn} and V_{tp} are the thermal velocities in the semi-insulator for electrons and holes, respectively, and

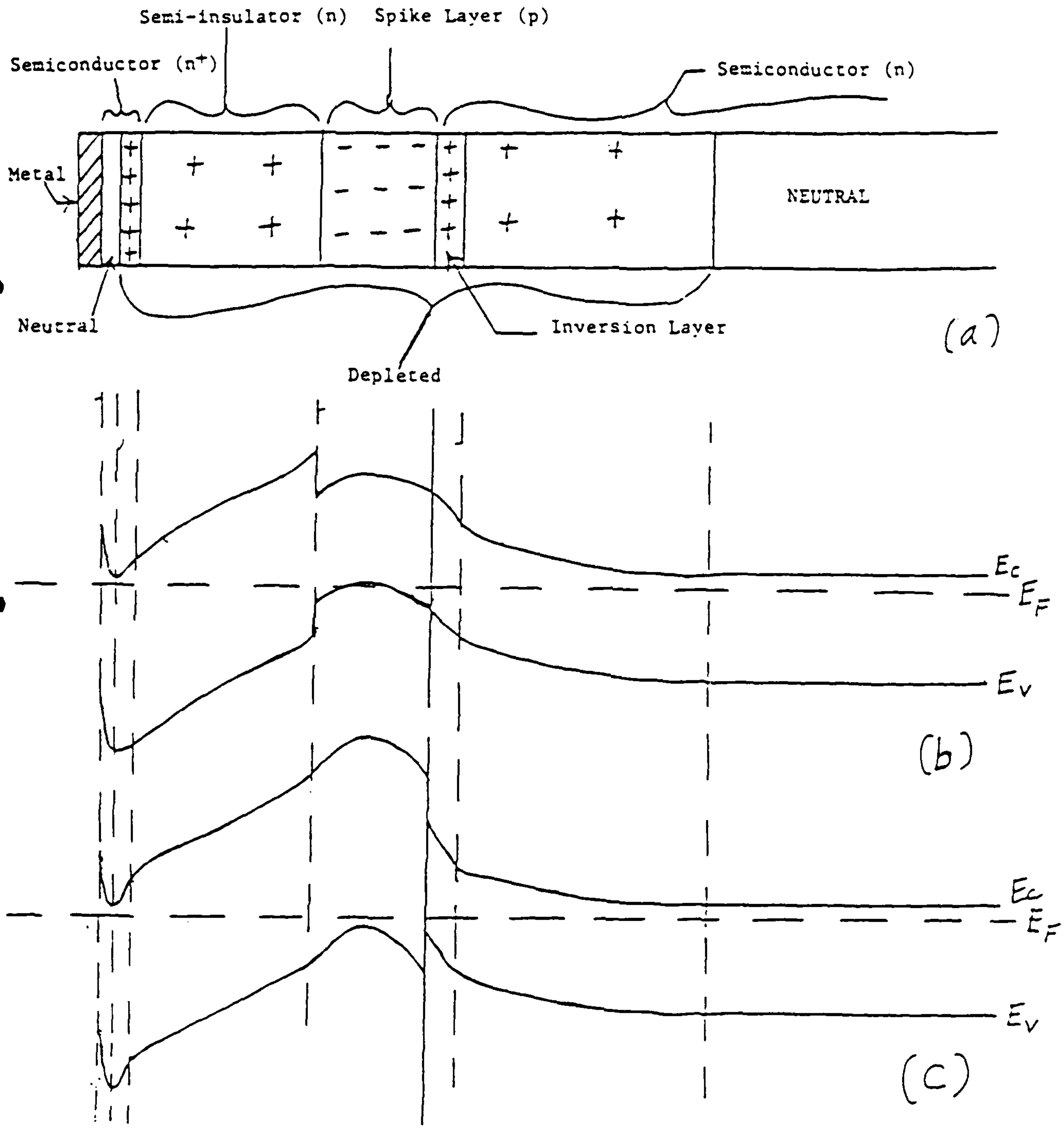

Figure 1. (a) Cross-section of a NPN BICFET. The semi-insulator region is about 200 Å wide and the spike layer is about 20 Å, (b) Equilibrium band diagram with the spike layer in the semiconductor. (c) Spike layer in the semi-insulator.

$$\ell_n = \frac{D_n}{V_{tn}} \quad ; \qquad \ell_p = \frac{D_p}{V_{tp}} \tag{6}$$

where D_n and D_p are the diffusion constants in the semi-insulator for electrons and holes, respectively. The default values are:

$$V_n = V_p = V_{tn} = V_{tp} = 10^7 \ \mathrm{cm/sec} \tag{7}$$

If Φ_n is calculated we use

$$\Phi_n = KT \, \ell n\left(\frac{N_c}{N_d}\right) + \Delta E_c + \Psi_{ms} \tag{8}$$

where N_c is the effective density of states of the conduction band, N_d is the donor concentration in the semiconductor, ΔE_c is the difference in conduction bands between the semi-insulator (wide-band gap semiconductor) and the semiconductor, and ψ_{ms} is the difference between the work functions of the metal and the semiconductor. The default value is:

$$\Phi_n = 0.02 \text{ eV} \tag{9}$$

When choosing to calculate ψ_{ms} you also have a choice of the type of metal:

$$\begin{aligned} \text{A}\ell : \ \psi_{ms} &= 0.026 \ \ell n N_d - 1.218 \\ n^{+}\text{Poly}: \ \psi_{ms} &= 0.026 \ \ell n N_d - 1.348 \\ \text{Au}: \ \psi_{ms} &= 0.026 \ \ell n N_d - 0.308 \end{aligned} \tag{10}$$

These values were taken from experimental results(4). The default value for ψ_{ms} is:

$$\psi_{ms} = -.32 \tag{11}$$

One can also calculate a consistent set of equilibrium values or use the default values:

$$V_1^{*} = -1.2, \quad \phi_s^{*} = 0.88 \tag{12}$$

These variables are defined in Figure 2. If the default values are used instead of calculating these values, equation (1) is not satisfied in equilibrium.

Other parameters that must be specified each time the program is run are the spike layer concentration, the semiconductor donor concentration, N_d, the range and number of steps of the collector to emitter voltage, V_{ce}, and the range and number of steps of the source current, J_s. For each value of J_s the full range of values of V_{ce} are stepped through.

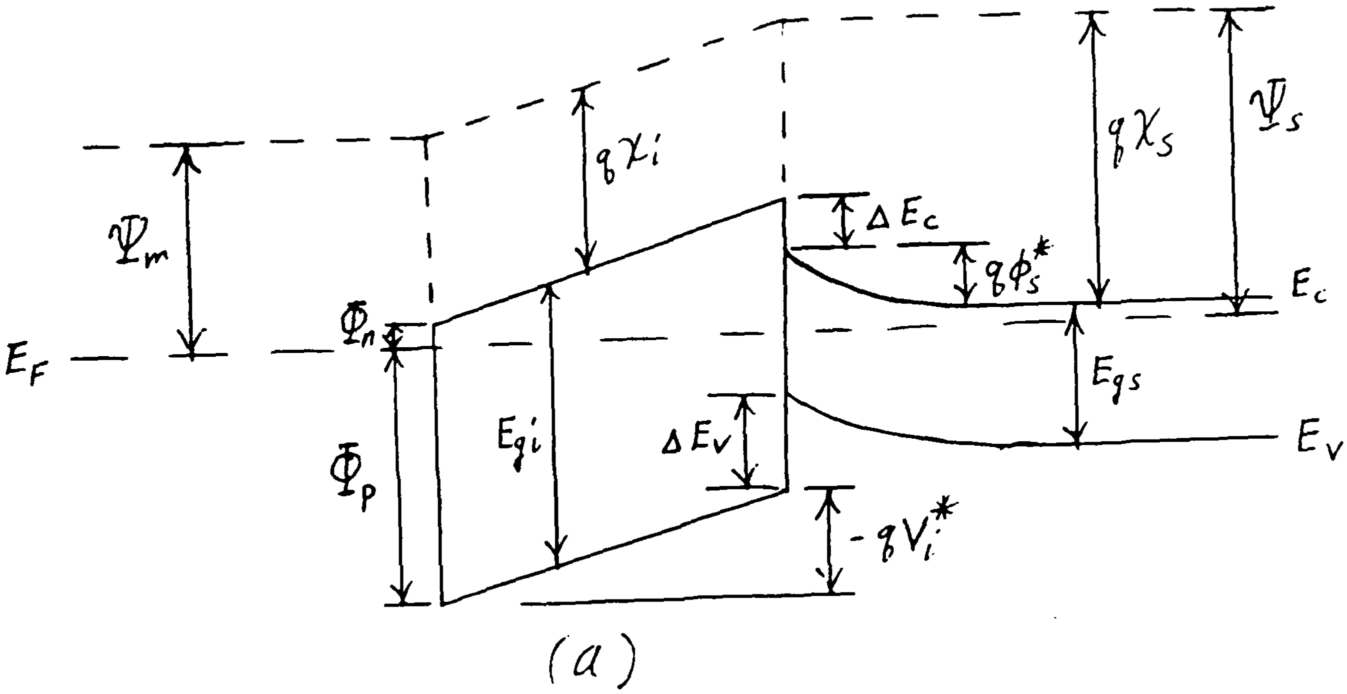

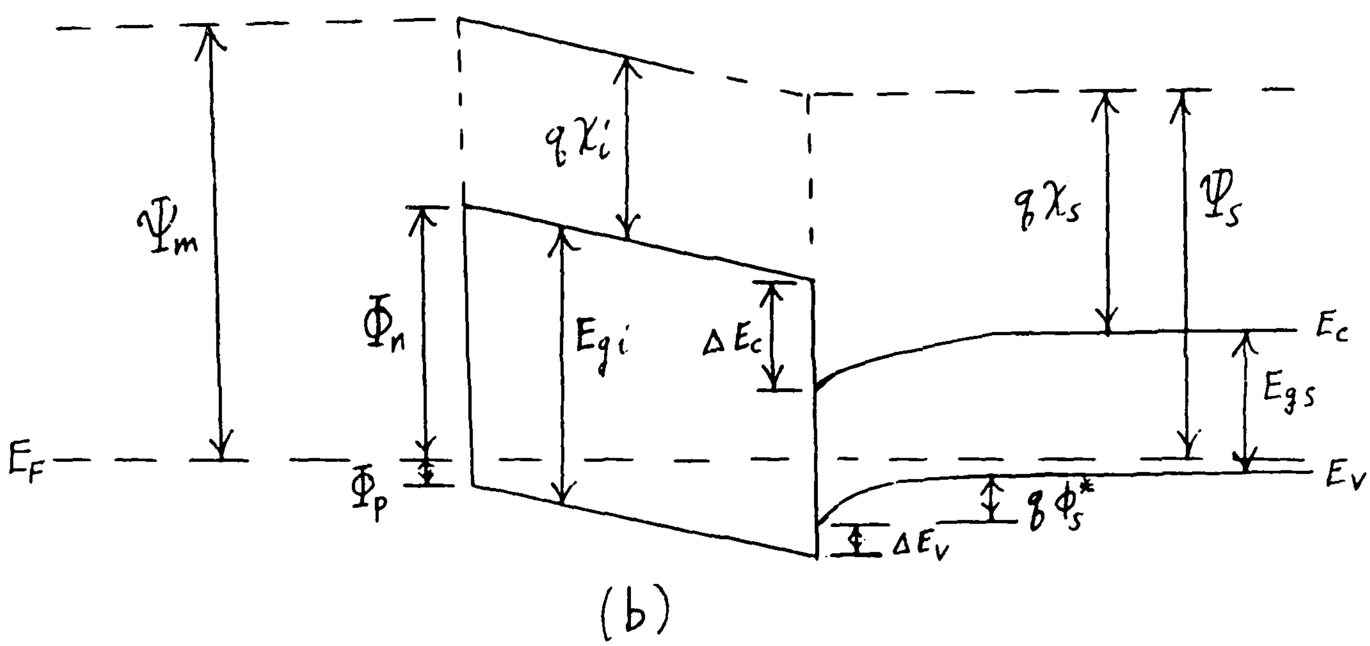

Figure 2: Equilibrium band diagrams assuming that the spike layer is infinitesimal (a) Diagram for NPN device (Figure 1(a)). (b) Diagram for PNP device.

IV APPROXIMATIONS IN THE PHYSICAL MODEL

Certain approximations cannot be checked within the present model. Among these are: (1) treatment of the wide-band gap material as an insulator; (2) assumption that the semi-insulator and the spike layer are totally depleted; (3) neglect of the band shape of the spike layer; and (4) neglect of carrier-carrier scattering and Auger recombination.

Other approximations can be and were checked using the present model: (1) neglect of "collector stretch"; (2) neglect of "Fermi factor"; (3) thermionic emission vs. diffusion; (4) using default value of 0.02 for Φ_n; (5) using default value of -0.32 for ψ_{ms}; (6) assuming that $\Delta E_c = q(\chi_s - \chi_i)$; and (7) using default value of -1.2 for V_i^*.

The treatment of the wide-band gap material as an insulator, i.e., assuming that:

$$V_i = \frac{Q_e}{C_i} \quad ; \quad C_i = \frac{\epsilon_i}{d} \tag{13}$$

does not allow the model to determine whether the semi-insulator is always depleted or not. If the semi-insulator is not totally depleted then there would be a neutral area whose size would change with the applied voltage. This could change the emitter efficiency.

Neglecting the band shape of the spike layer (see Figure 1) could have two effects. If the electric field didn't cross the x-axis at the mid-point of the spike layer then the band shape may be asymmetrical and the effective ΔE_c and ΔE_v could change with semiconductor and semi-insulator donor concentration. Also the curvature as shown in Figure 1(b) would put most of the valence band above the quasi-Fermi level and most of the acceptors would not be occupied by an electron. This would reduce the effective charge in the spike layer and the semi-insulator would probably not be fully depleted.

It is found[5] with p-i-n diodes that carrier-carrier scattering and Auger recombination profoundly reduce the current carrying capacity of the diode. Anything much above 2,000 A/cm^2 is very difficult to attain. Effects of this sort may not allow currents on the order of 10^6 A/cm^2 as hoped for with the BICFET. However, the BICFET has a current path on the order of 300-400 A as opposed to 10-400μm for the p-i-n diode. Thus, with the BICFET these effects may not be as important, but they probably should be considered.

V RESULTS FROM THE COMPUTER MODEL OF THE BICFET

All results of the computer program reported here are for the silicon NPN BICFET. The gain equation for the PNP device is, however, discussed later on. The I-V curve for a device with all the approximations (no collector stretch, no Fermi factor) and all the default values (including spike layer concentration = 1.6 x 10^{19}) has a response similar to that in Figure 3 except that Jc is constant for larger values of V_{ce} (> 0.5V). Collector stretch is an important factor when:

$$N_d \lesssim \frac{J_c}{q V_s} \tag{14}$$

As seen in Figure 4, the collector stretch causes a negative slope but that the lines become more horizontal as J_c (and J_s) decrease. For the case of collector stretch the results for $N_d = 10^{15}$ are essentially the same as for $N_d = 10^{17}$. For the case of no collector stretch the curves for $N_d = 10^{17}$ show a definite positive slope as seen in Figure 3. However, if J_c is decreased, the curves for collector stretch and no collector stretch are identical for N_d of any value. Thus, if $J_c \leq 10^4$ A/cm^2 collector stretch is probably negligible.

Introducing the Fermi factor into the set of equations that were solved iteratively caused the I-V curves to be distorted as shown in Figure 5. The Fermi factor reduces the effective spike layer charge by a factor of 100. For the equations with collector stretch this produces:

$$J_c \cong \frac{q V_s}{\beta \phi_s} p_o \tag{15}$$

where $$\phi_s = V_{ce} - V_i + \psi_{ms} \tag{16}$$

For this situation the values of p_o (inversion layer concentration at the interface), V_i and ψ_{ms} are constant. Thus J_c increases as ϕ_s decreases with V_{ce}. However, for the case of no collector stretch the curves are flat for $N_i \geq 5.0 \times 10^{18}$. For $N_i = 5 \times 10^{17}$ (on the order of 100 times less than $N_i = 1.6 \times 10^{19}$) the slope is positive and not negative as it was in the case of collector stretch with the Fermi factor. For the case of no collector stretch the gain increases as N_i is reduced. As shown in Equation (17) the gain increases with a

$$G = \frac{v_n}{v_p} \frac{N_c}{p_o} e^{(\Delta E_v - \Phi_n)/kT} \tag{17}$$

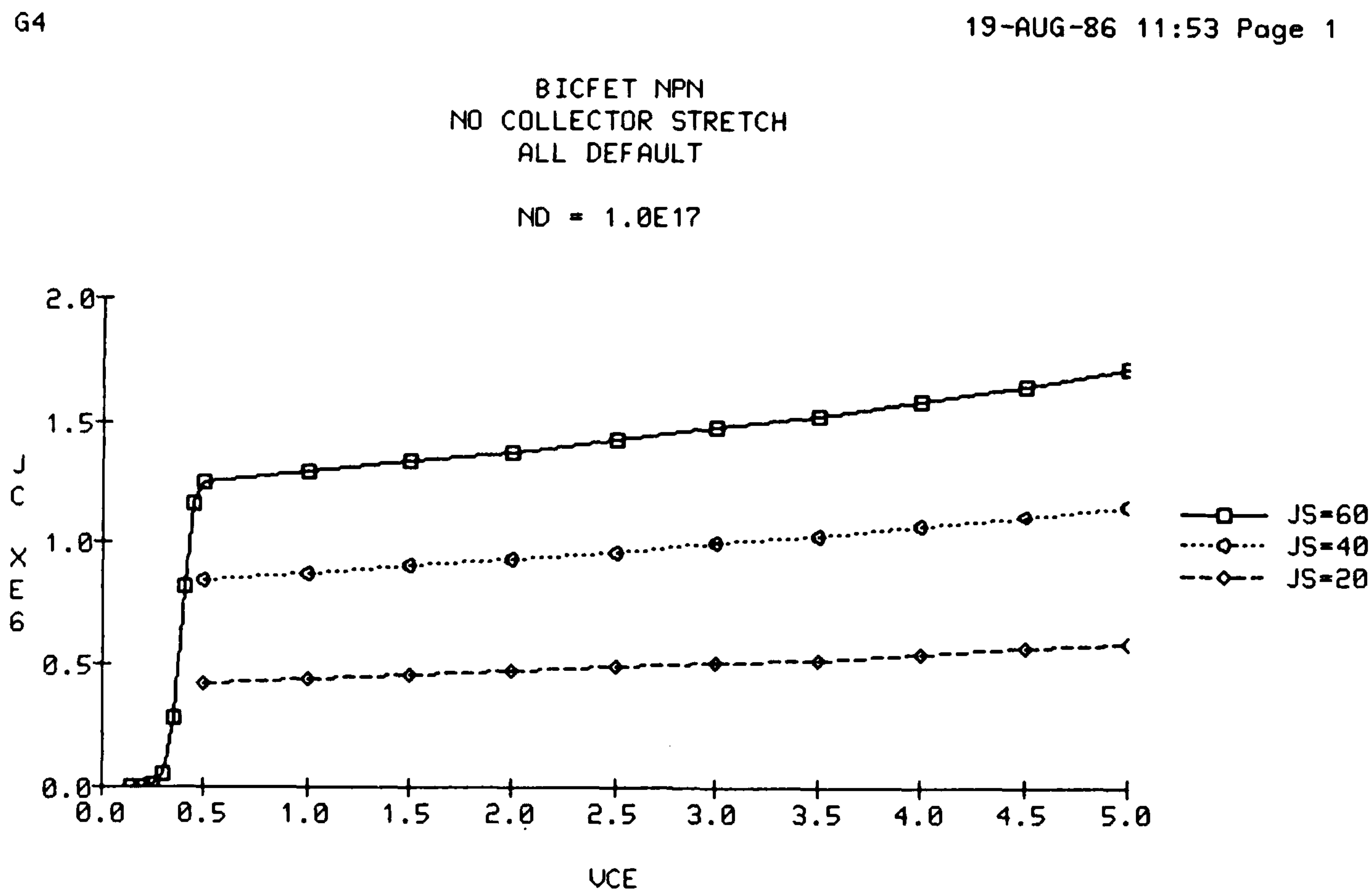

Figure 3: Characteristic curves for a NPN BICFET device with $N_d = 10^{17}$ cm^{-3} and no collector stretch. All default values were used including $N_i = 1.6 \times 10^{19}$ cm^{-3}. The collector current, J_c, has units of 10^6 A/cm^2 while the source current, J_s, is in A/cm^2.

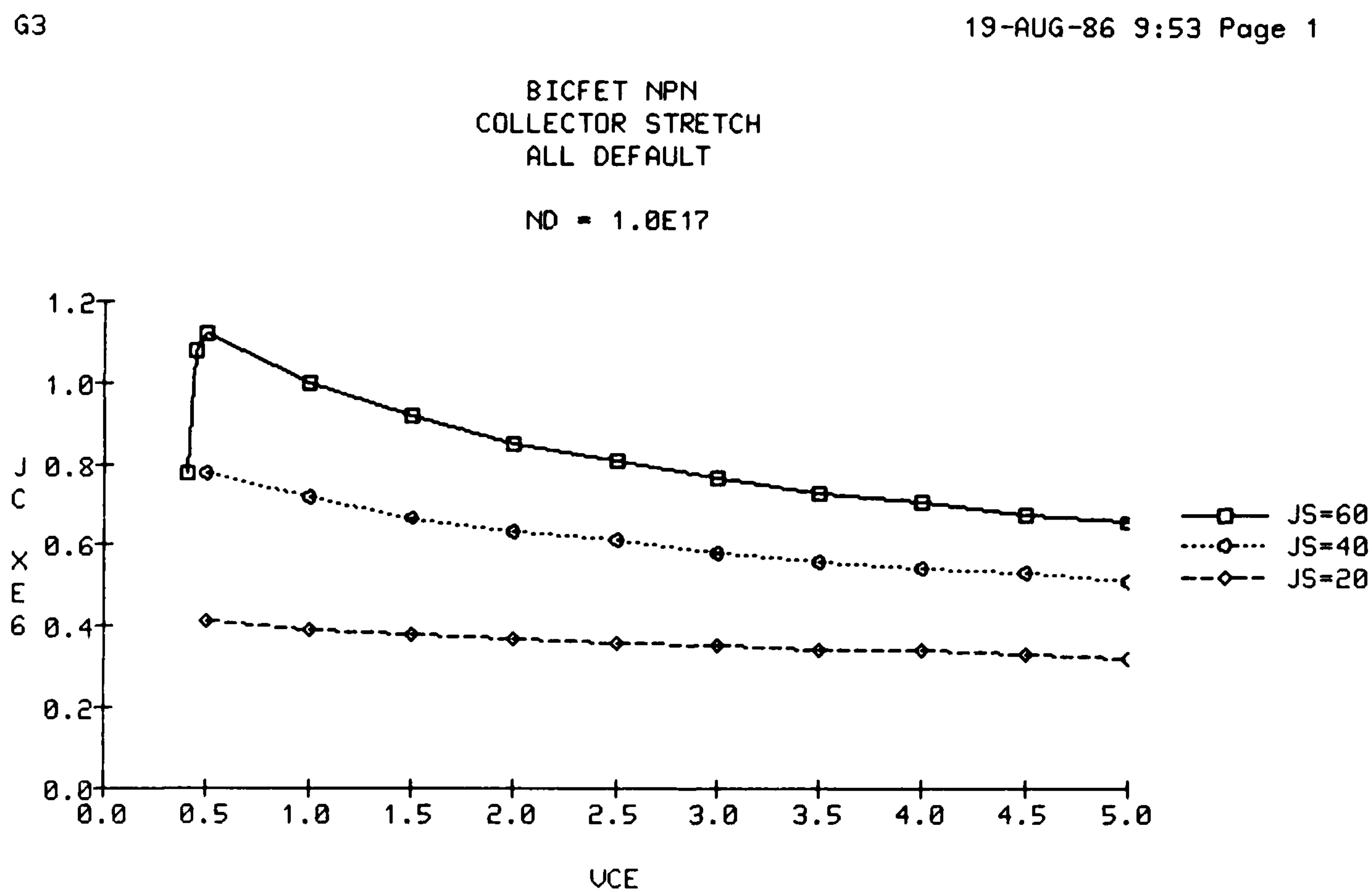

Figure 4: Characteristic curves for a NPN BICFET device with $N_d = 10^{17}$ cm^{-3} and collector stretch. All default values were used including $N_i = 1.6 \times 10^{19}$ cm^{-3}. The collector current, J_c, has units of 10^6 A/cm^2 while the source current, J_s, is in A/cm^2.

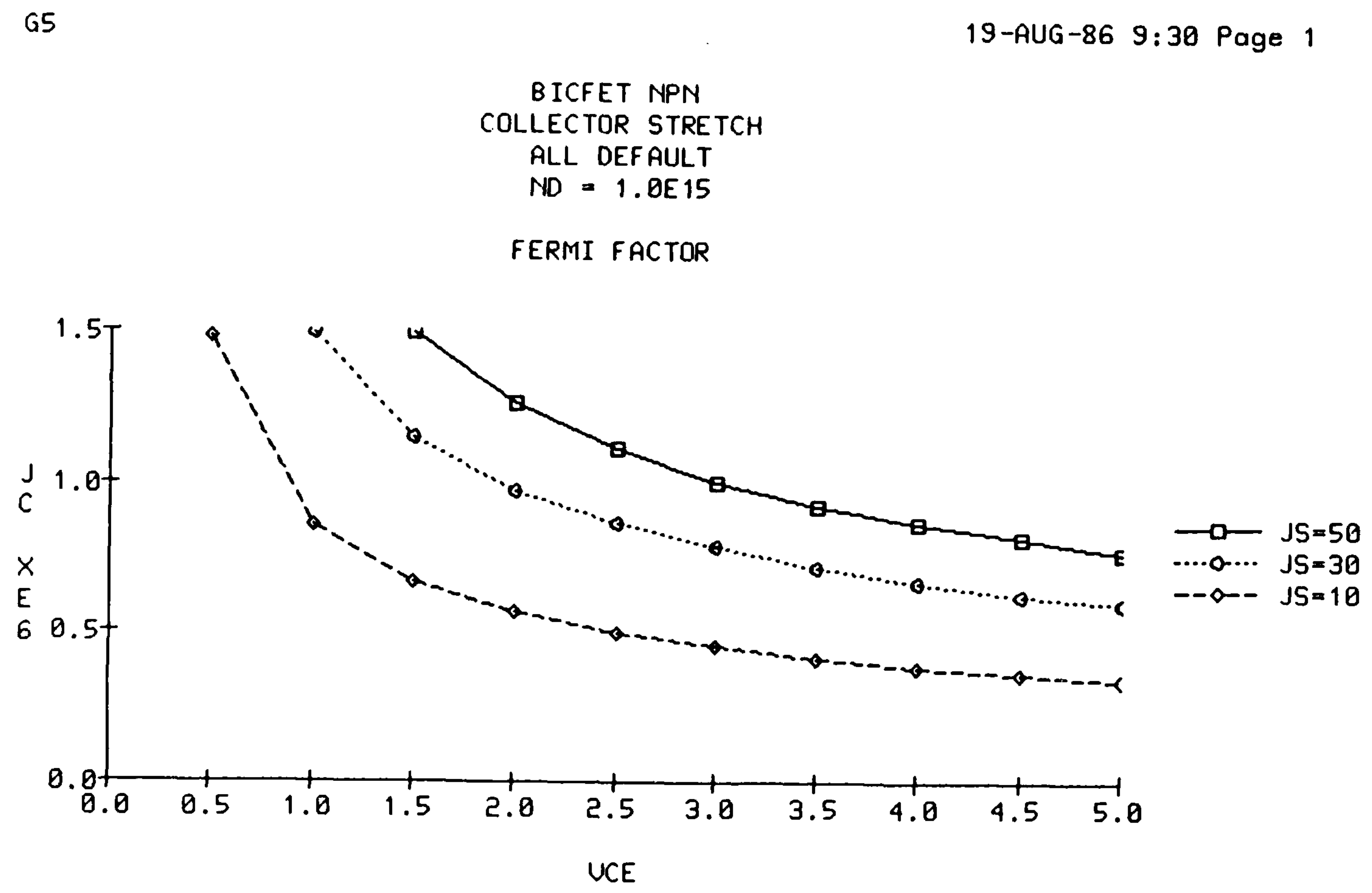

Figure 5: Characteristic curves for a NPN BICFET device with $N_d = 10^{15}$ cm^{-3}, collector stretch and Fermi Factor. All default values were used including $N_i = 1.6 \times 10^{19}$ cm^{-3}. The collector current, J_c, has units of 10^6 A/cm^2 while the source current, J_s, is in A/cm^2.

decrease in p_o. Because of charge balance, the positive inversion charge, p_o, will decrease as the negative spike layer charge ($-qN_i$) decreases. Table I shows this clearly. Note that the product, p_o G, remains constant. This indicates that changing N_i affects only p_o and not the exponential factor.

N_i	p_o	G
5.0×10^{19}	64×10^{19}	0.21×10^4
3.0	23	0.58
1.6	6.4	2.1
1.0	2.5	5.4
0.5	0.62	21
0.1	0.038	350
.05	0.017	800

$p_o\, G = 1.3 \times 10^{24}$

TABLE I No Collector Stretch, All Defaults, N_d=10^{15}, V_{ce}=1.0, J_s=40

For large values of J_c there will be some distortion due to collector stretch as shown in Figure 5, however, where J_c is low enough (and collector stretch is negligible) substantial gain can be achieved by lowering N_i. There is a limit to the reduction of N_i. The value of N_i must be large enough to deplete the emitter region (the semi-insulator) and to reduce the recombination due to interface states.

When gain is found as a function of J_s, collector stretch is seen to be an important factor for $J_s \geq 20$ A/cm^2, while the Fermi factor gives a dramatically different result for all values of J_s.

The question of thermionic emission vs diffusion in the semi-insulator comes down to one of whether the ratio of effective velocities (V_n/V_p) in the gain equation (Equation 17) is much different than one. For typical silicon values this ratio is about 1.8. This effect is small compared to changes caused by other parameters.

For the discussion of the next three approximations it is useful to consider both NPN and PNP deivces. These approximations are : Φ_n = constant, ψ_{ms} = constant and $\Delta E_c = q(\chi_s - \chi_i)$ where χ_s and χ_i are the electron affinities for the semiconductor and semi-insulator, respectively.

The gain equations are:

$$\text{NPN:} \quad G = \frac{N_c}{p_o} e^{(\Delta E_v - \Phi_n)/KT}$$

$$\text{PNP:} \quad G = \frac{N_V}{n_o} e^{(\Delta E_c - \Phi_p)/KT} \tag{18}$$

where

$$\text{NPN:} \quad \Phi_n = KT \ln \frac{N_c}{N_{ds}} + \Psi_{ms} + q(\chi_s - \chi_i)$$

$$\text{PNP:} \quad \Phi_p = KT \ln \frac{N_V}{N_{As}} - \Psi_{ms} + \Delta E_v + \Delta E_c - q(\chi_s - \chi_i) \tag{19}$$

where

$$E_c - E_F = KT \ln \frac{N_c}{N_{ds}}$$

$$E_F - E_V = KT \ln \frac{N_V}{N_{AS}} \tag{20}$$

where N_V is the effective density of states for the valence band, n_o is the inversion electron concentration at the interface, N_{ds} is the semiconductor donor concentration, N_{AS} is the semiconductor acceptor concentration, and the gain equation for PNP is written down by analogy to that of the NPN.

If we assume that

$$\Delta E_c = q(X_s - X_i) \tag{21}$$

then

$$\text{NPN:} \quad G = \frac{N_{ds}}{p_o} e^{(\Delta E_v - \Delta E_c)/KT} \; e^{-\Psi_{ms}/KT}$$

$$\text{PNP:} \quad G = \frac{N_{As}}{n_o} e^{(\Delta E_c - \Delta E_v)/KT} \; e^{\Psi_{ms}/KT} \tag{22}$$

For the NPN silicon device modeled in the computer program it was found that certain parameters did not change when ψ_{ms} and N_d were varied. In fact it was found that $p_o \cong 6 \times 10^{19}$, $V_{ce,cut\text{-}in} \cong 0.15$, $V_i \cong -0.08$,

$N_e \cong .12 \times 10^{12}\ cm^{-2}$, $N_{cc} \cong 4.68 \times 10^{12}\ cm^{-2}$ where $N_i = N_e + N_{cc} = 4.8 \times 10^{12}\ cm^{-2}$. N_i, N_e and N_{cc} are the charge densities for the spike layer, the emitter and the collector, respectively and V_{ce}, cut-in is the voltage where J_c goes thru zero as V_{ce} is lowered (see Figure 3). However, certain parameters changed dramatically (see Table II) with a change in ψ_{ms}. These results along with those in Table I indicate that the gain for an NPN device can be regarded as having two independent parts: ${p_o}^{-1}$ and the exponential

Metal	ψ_{ms}	Φ_n	Gain	J_c
Default	-.32	.02	2.1×10^4	$.83 \times 10^6$
Aℓ	-.32	.047	7.5×10^3	$.30 \times 10^6$
n^+Poly	-.45	-.084	1.1×10^6	44×10^6
Au	.59	.96	4.8×10^{-12}	2.3×10^{-10}

Table II $N_{ds} = 10^{15}\ cm^{-3}$

factor. In Table I it is seen that p_o changes with N_i but that the exponential factor does not. In the above it is seen that as ψ_{ms} changes the exponential factor changes but that p_o does not.

In order to more clearly define this property the gain equation can be rewritten by taking:

$$\psi_{ms} = 0.026 \ln N_{ds} - B \tag{23}$$

where[4], experimentally:

$$\begin{aligned} A\ell:&\quad B = 1.218 \\ n^+poly:&\quad B = 1.348 \\ Au:&\quad B = 0.308 \end{aligned} \tag{24}$$

Thus, for a NPN device:

$$G = \frac{1}{p_o} e^{(\Delta E_v - \Delta E_c)/KT} e^{B/KT} \tag{25}$$

where, theoretically:

$$B = kT \ln N_c + qX_s - \psi_m \tag{26}$$

Now, if we assume:

$$\Delta E_c \neq q(X_s - X_i) \tag{27}$$

we have:

$$\begin{aligned} NPN: \quad & G = \frac{N_c}{p_o} e^{(\Delta E_v - \Psi_m + q\chi_i)/KT} \\ PNP: \quad & G = \frac{N_v}{n_o} e^{(\Psi_m - \Delta E_v - E_{gs} - q\chi_i)/KT} \end{aligned} \tag{28}$$

where

$$\Psi_{ms} = \Psi_m - \Psi_s = \Psi_m - (qX_s + E_c - E_F) \tag{29}$$

and equations (20) have been used. For the case of the GaAs/AℓGaAs (semiconductor/semi-insulator) system we will take $qX_i \cong 4.5$ *e*V. Since we could not find any published values of X_i (electron affinity) for AℓGaAs we have taken an average value (see, e.g., reference 6) for some compound semiconductors. From equations (28) it is obvious that one should minimize Ψ_m (metal work function) for a NPN device, but maximize Ψ_m for a PNP device; while ΔE_v and X_i should be maximum (minimum) for a NPN (PNP) device. Also, for a PNP device it would be good to pick a semiconductor with a smaller E_{gs} (energy gap).

For the NPN device let us choose x=0.4 ($Al_x\, Ga_{1-x}As$ where [7] $\Delta E_v = 0.436X$). Then

$$\Delta E_v + qX_i - \Psi_m \cong 4.67 - \Psi_m \tag{30}$$

and since there are many metals[8] (e.g. Ti: $\Psi_m = 3.92$, Sn: $\Psi_m = 4.51$) with work functions less than 4.67 the NPN has a good chance of being realized. For a PNP device with x=0.2 we have

$$\Psi_m - \Delta E_v - E_{gs} - qX_i \cong \Psi_m - 6.01 \tag{31}$$

Since there are very few metals (Pt: $\Psi_m \cong 6.37$) with a work function larger than 6.0 it would seem that it might be difficult to fabricate a successful PNP device. Thus, it appears that for the GaAs/AℓGaAs system the NPN device has a better chance of working than the PNP device.

The final approximation ($V_i^* = -1.2$ and $\phi_s^* = 0.88$ where $\Psi_{ms} = \phi_s^* + V_i^*$) does not affect a conducting device but does affect the equilibrium (superscript asterick indicates equilibrium values) values of the emitter charge density, N_e^*, and the collector charge density,

$N_{cc}{}^*$. If the equilibrium values are calculated using a self-consistent (i.e. $N_i = N_e{}^* + N_{cc}{}^*$, etc.) iteration loop then $p_o{}^*$, $N_e{}^*$, and $N_{cc}{}^*$ are not a function of N_d. (They do change values with the metalization chosen). However, if the default values are used the value of $p_o{}^*$ is inversly proportional to N_d.

	Po^*	$N_e{}^*$	$N_{cc}{}^*$
Aℓ	-2.5×10^{19}	1.77×10^{12}	3.03×10^{12}
n^+ Poly	-2.2×10^{19}	1.96×10^{12}	2.84×10^{12}
Au	-5.3×10^{19}	0.45×10^{12}	4.35×10^{12}

(a) Self consistent equilibrium values for $N_d = 10^{15}$, 10^{16}, and 10^{17}.

$N_d = 10^{15}$	2.75×10^{19}	1.77×10^{12}	3.08×10^{12}
$N_d = 10^{16}$	2.75×10^{18}	1.77×10^{12}	1.03×10^{12}
$N_d = 10^{17}$	2.75×10^{17}	1.77×10^{12}	1.12×10^{12}

(b) Default values used.

TABLE III Equilibrium values under various conditions

IV CONCLUSIONS

There are some conclusions that can be drawn from the analysis using this particular model.

1. Type of metal used is extremely important.
2. Experimental values of the electron affinity, X_i, of $A\ell_x Ga_{1-x}A_s$ are needed as a function of x.
3. The "Fermi factor" may be extremely important.
4. If the "Fermi factor" is important then it may be useful to put the spike layer in the semi-insulator rather than the semiconductor.
5. Collector stretch may be negligible at realistic current density values.
6. For the GaAs/AℓGaAs system a functioning NPN device may be easier to fabricate than a PNP device.
7. There are two independent gain factor: the exponential agrument which depends on Ψ_{ms} and p_o which depends only on N_i.

8. The question as to whether the conduction process in the semi-insulator is analogous to thermionic conduction or diffusion is a relatively small factor.

VII RECOMMENDATIONS

1. Write program for GaAs/AℓGaAs system.
2. Write program for "diodes", i.e. $J_s = 0$ for NPN and PNP devices.
3. Build diodes and compare the experimental results with the above.
4. Measure values of the electron affinity, X_i, for $A\ell_x Ga_{1-x}As$ as a function of x.
5. Investigate the possibility of experimentally achieving the spike layer in AℓGaAs.
6. Experimentally investigate the ohmic contact to AℓGaAs for both p and n type.
7. Pursue the "Fermi Factor" problem.
8. Build fully functional devices.
9. Investigate the temperature dependence of the BICFET both theoretically and experimentally.
10. Begin both experimental work and theoretical work on the DOES device.

REFERENCES

1. Taylor, G.W. and J. G. Simmons, "The Bipolar Inversion Channel Field-Effect Transistor (BICFET) - A new Field-Effect Solid-State Device: Theory and Structures", IEEE Transactions on Electron Devices, ED-32, 2345-67, Nov. 1985.
2. Taylor, G.W. and J.G. Simmons, "Small Signal Performance of the BICFET", IEEE Transactions on Electron Devices, ED-32, 2368-77, Nov. 1985.
3. Taylor, G.W. J.G. Simmons, A.Y. Cho and R.S. Mand, "A New Double Heterostructure Optoelectronic Switching Device Using Molecular Beam Epitaxy", J. Appl. Phys. 59(2), pp. 596-600, Jan. 15, 1986.
4. Deal, B.E., E.H. Snow, and C.A. Mead, "Barrier Energies in Metal-Silicon Dioxide-Silicon Structures", J. Phys. Chem. Solids, 27, pp. 1873-79, 1966.
5. Sze, S.M. Physics of Semiconductor Devices, 2nd Ed., pg. 122, Wiley-Interscience, 1981.
6. M.P. Shaw, "Properties of Junctions and Barriers", pg.5, Vol. 1, Ed. by William Paul, "Band Theory and Transport Properties", Series Ed. T.S. Moss, "Handbook on Semiconductors".
7. A.J. Hill and P.H. Ladbrooke, Electronics Letters, 22 (#4), 218 (1986).
8. A.F. Ioffe, "Physics of Semiconductors", pg. 230, Academic Press (1960).

1986 USAF-UES SUMMER FACULTY RESEARCH PROGRAM/

GRADUATE STUDENT SUMMER SUPPORT PROGRAM

Sponsored by the

AIR FORCE OFFICE OF SCIENTIFIC RESEARCH

Conducted by the

Universal Energy Systems, Inc.

FINAL REPORT

JET DIFFUSION FLAME

Prepared by:	James P. Seaba
Academic Rank:	BSME
Department and	Department of Mechanical Eng.
University:	University of Iowa
Research Location:	Fuels Branch, Aeropropulsion
	lab, Wright Aeronautical labs
USAF Researcher	W. M. Roquemore
Date	August 28, 1986
Contract No.	F49620-85-C-0013

JET DIFFUSION FLAME

by

James P. Seaba

ABSTRACT

Three different gases, and nozzles were used at various flow rates in a jet diffusion flame. The flame was seeded with TiO2 particles and laser sheets were used for flow visualizations of the flame. The visualizations were recorded by both still photographs and motion pictures. Two different phenomenia were being evaluated, flame lift which occured at high flow rates, and structure movement which could only be visualized at low flow rates.

The outer structure and flame bulge of the flame were digitized using the motion pictures. Therefore the velocity of the structures were determined at various flow rates for different gases and nozzle sizes.

Acknowledgments

I would like to thank the Air Force Systems Command and the Air Force Office of Scientific Research for sponsorship of my research. I would like to thank several members of the Wright Aeromautical labs in the fuel branch, W. M. Roquemore, Cindy Obringer, Teri Boos, and special thanks to Curtis Reeves who helped me through the unfriendly world of MODCOMP.

I. Introduction

I am currently working on my MSME at the University of Iowa. The area of study is combustion. My advisor, L. D. Chen is continuing his research at Wright Patterson Air Force Base with respect to diffusion flames. I assisted my advisor in this area, gaining experience with flow visualization techniques, and familarizing myself with the facilities available to me.

II. Objectives of the Research Effort

The overall objective of the research consisted of two different types of phenomenia of a jet diffusion flame. First, at high flow rates the combusting flame will lift off the nozzle at a certain distance. This distance varies with flow rate, nozzle size, and type of gas used.

Secondly, vortex structures are formed on the outer (air side) and inner (fuel side) locations of the jet flame. A flame bulge (stoichometric condition) appears in the flame. All of these structures move away from the nozzle (z-direction) at different rates of speed relative to each other. The velocity of each structure varies with flow rate, nozzle size, and type of gas used.

I was primarily analyzing the second phenomenia. My objective was to determine the velocity of the outer structure and flame bulge of various gases and nozzle sizes, at different flow rates.

III Experimental Setup

A vertical jet diffusion flame was seeded with TiO2 particles. A laser was pulsed at the camera speed (1000 frames per second) to capture the desired structures. The TiO2 particles were created by adding TiCl4 to the fuel and air side of the test apparatus. TiCl4 reacts with water vapor, which is formed in the products of the combustion process, to form TiO2 particles. The Stoichometric reaction is:

$$TiCl_4 + 2\,H_2O \rightarrow TiO_2 + 4\,HCl$$

The test matrix used consisted of three gases and nozzle sizes. The gases used were ethylene, propane, and methane. The nozzle sizes were 10, 11, and 22.5 millimeters. The flow rates varied over a wide range of reynold numbers.

IV Data Acquisition

The film was used to determine the velocity of the outer structures and flame bulge. This was accomplished with a digitizer, MODCOMP computer system, and software designed specifically for this purpose. A projector was placed behind the digitizer to display the flame on the digitizer screen. A coordinate system and a real length scale (centimeters) were setup by the user. The length scale was referenced from the nozzle diameter.

Seven points of interest were recorded every other frame, until one period was complete. The seven points are illustrated below:

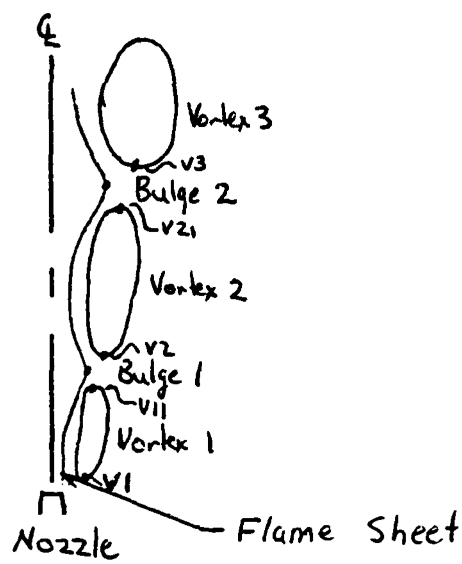

The definition of period is when the flame bulge and/or outer vortex reappears as recorded in the first frame. After a period was digitized, the computer displayed the average velocity of the structure over the entire period. The average velocity was calculated by least square method

(LSM). Standard deviation, and the regression coefficient was also recorded.

The distance from the nozzle verses time were stored for each structure. Each structure was graphed over one period, an example is attached on the following page. The compiled velocity and statistics were also stored. At least four periods were recorded for each condition digitized. Twenty four conditions were recorded over the entire summer.

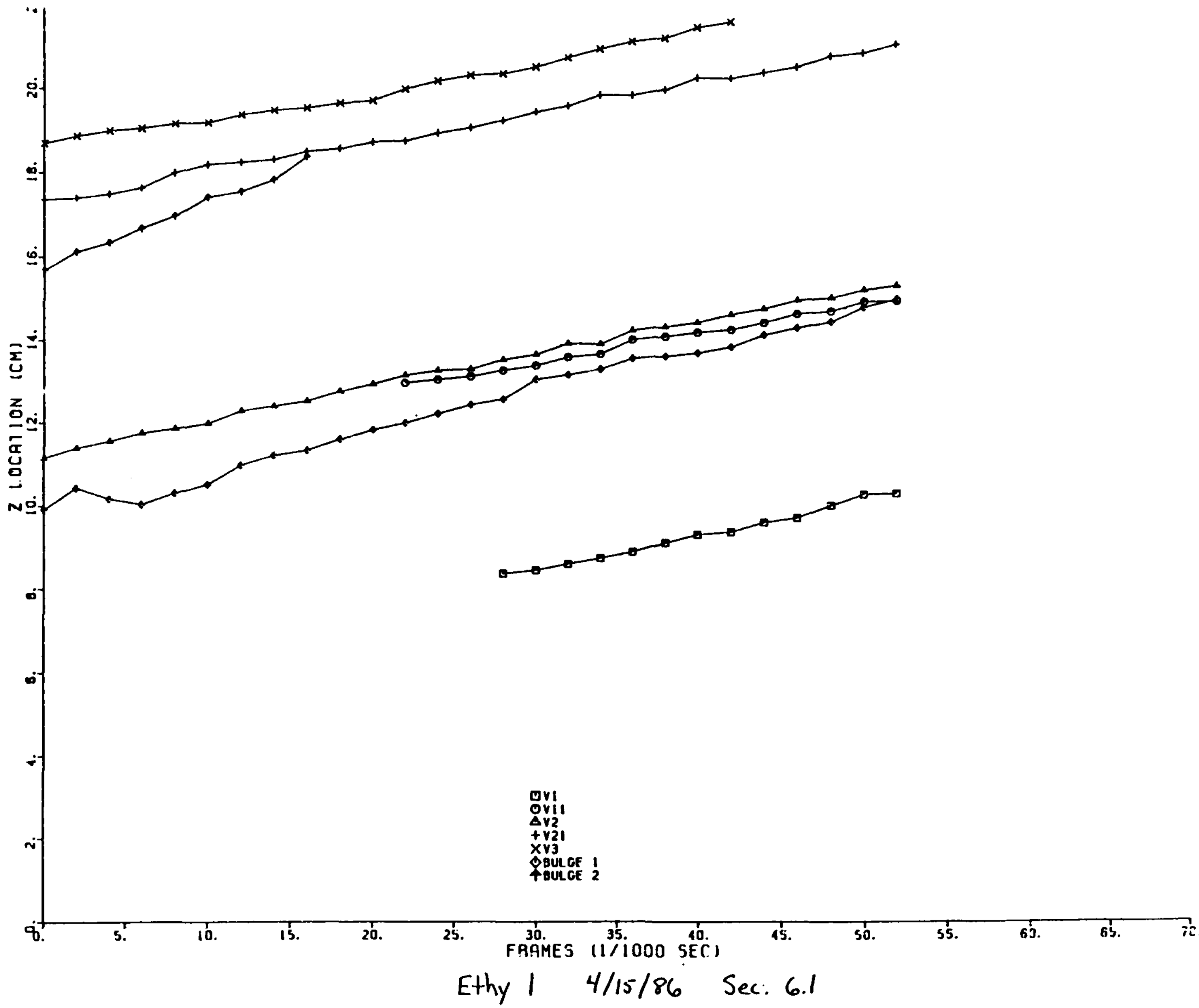
Z LOCATION (CM)
FRAMES (1/1000 SEC)
V1
V11
V2
V21
V3
BULGE 1
BULGE 2
Ethy 1 4/15/86 Sec. 6.1

V Results

The data was plotted as distance from nozzle verses time for all of the periods. It was shown from the plots as well as the regression coefficient that the LSM was an adequate assumption to determine the average velocity over one period.

The repeatability was very good at most conditions. Further analysis of the data will be carried out during the rest of the year at the University of Iowa.

VI. Recommendations

Expansion of the data base is desired. Films currently exist that have desired conditions for digitizing. The exact conditions desired will not be known until the present data has been analyzed.

Flow visualizations of the jet diffusion flame is desired in the horizontal direction. This experiment would determine if the outer structures are buoyancy induced.

1986 USAF-UES SUMMER RESEARCH PROGRAM/

GRADUATE STUDENT SUMMER SUPPORT PROGRAM

Sponsored by the

AIR FORCE OFFICE OF SCIENTIFIC RESEARCH

Conducted by the

UNIVERSAL ENERGY SYSTEMS, INC.

FINAL REPORT

MECHANISMS OF CHROMATIC CONTRAST

Prepared by:	Laura Sewall
Academic Rank:	Graduate Student
Department and	Psychology
University:	Brown University
Research Location:	Human Resources Laboratory
	Williams Air Force Base
USAF Researcher:	Dr. George Geri
Date:	October 20, 1986
Contract No.	F49620-85-C-0013

MECHANISMS OF CHROMATIC CONTRAST

by

Laura Sewall

ABSTRACT

The question of whether chromatic contrast is recurrent or non-recurrent was explored using psychophysical procedures. Stimuli were presented to four observers by a three-channel maxwellian view optical system. The target consisted of a four-element bulls-eye pattern. The central spot was varied in wavelength in order to determine each subject's unique yellow using a variety of color conditions for the several annuli. The basic experimental question was whether or not the contrast effect of a region of the visual field is influenced when its appearance is altered by contrast with another region of the visual field. Although more research is required, we tentatively conclude that contrast-induced color appearance has no effect on adjacent regions of the visual scene. Thus, chromatic contrast seems to behave like a non-recurrent network.

ACKNOWLEDGEMENTS

This report constitutes a summary of research conducted in the summer of 1986 at the Human Resources Laboratory, Williams AFB, Arizona. The author gratefully acknowledges support as a Summer Graduate Fellow sponsored by the U.S.A.F. Systems Command, Air Force Office of Scientific Research. In particular, I wish to thank my focal point, Dr. Liz Martin, for providing consistent practical and personal support. In addition, I wish to thank Dr. George Geri for his patience, feedback, and technical assistance.

I. INTRODUCTION:

I am currently a graduate student at Brown University. My general area of interest is visual science. I wish to explore the limits and mechanisms of human visual performance, using psychophysical methods. In particular, I have done research on lightness constancy, and wish to further study color vision.

The USAF is interested in all aspects of vision because of its obvious importance in pilot performance. At the Williams Air Force Base, where the primary interest is pilot training, a major effort is the development and refinement of flight simulators. A primary concern is accurate and realistic visual displays. Many issues remain unsolved concerning light levels, range of colors, stability of light sources, scattered light, etc. Several researchers at the HRL are working on various aspects, both applied and basic, of these questions. My background and interests overlap and supplement those of the HRL staff.

II. OBJECTIVES OF THE RESEARCH EFFORT:

Many factors in addition to the spectral composition of a light determine hue. Intensity, duration, image size, retinal location, and adaptation state all contribute. One of the most important parameters is the color of adjacent regions in the visual field. If, for example, a white circular test spot is surrounded by a red annulus it will appear tinged with green. This effect is termed simultaneous chromatic contrast or chromatic induction. Since Chevreul's pioneering study, published in 1838(1), considerable work has been focussed on the phenomenon. In recent years neurophysiological techniques have supplemented the traditional psychophysical procedures.

On an empirical level, many basic aspects of the phenomenon have been explored. It is known that the induced hue is roughly complementary to the inducing hue, e.g., red induces green, yellow induces blue, red-blue induces green-yellow, etc. It is known that maximal chromatic induction occurs with minimal brightness differences. It is known that induction decreases sharply as the fields are separated; a 10 minute gap reduces the amount of induction by approximately 90 percent(2). It is known that the amount of induction increases as the inducing field is made larger.

Despite the long history of research on simultaneous chromatic contrast, the basic mechanisms are still poorly understood. It is clear that the perceptual effects are a manifestation of lateral interactions in the visual nervous system. The nature and level of these interactions, however, remain speculative. It is the goal of our research to explore certain perceptual aspects of chromatic indution that relate directly to the nature of the underlying neural processes. Specifically, we set out to see if chromatic contrast exhibits a phenomenon analogous to an effect termed "disinhibition," which is found in some neural networks. The existence of disinhibition, or the lack of it, has important implications concerning the basic organization and mechanisms that underly any lateral information processing system.

Disinhibition in the visual system was first demonstrated electrophysiologically by Hartline and Ratliff using the eye of the horseshoe crab, *Limulus*(3). They recorded from single optic nerve fibers while stimulating the retina with small spots of light. It was well known that activity from a given retinal region, call it A, could be inhibited by stimulating a neighboring retinal region, call it B. Hartline and Ratliff showed that if a third retinal region (C), adjacent to B, was stimulated two effects could be observed: activity from B decreased, as expected, and activity from A *increased*. This latter effect is the

phenomenon of disinhibition. The explanation is simply that the lateral inhibition of B onto A was decreased via C's lateral inhibition onto B. Similar effects can be observed in the considerably more complex vertebrate retina.

The importance of the demonstration of disinhibition lies not in the phenomenon itself, but in what it implies for the underlying neural substate. Figure 1, adapted from Ratliff, Hartline, and Miller(4), illustrates two fundamentally different kinds of lateral inhibitory systems. The recurrent type, shown on the left, is consistent with disinhibition. Notice that the lateral inhibition from each unit feeds onto its neighbors at or before the site X where impulses are generated. Thus, the inhibitory output of unit B depends upon its ultimate response, rather than just on the stimulus to it. The net effect is that if B is inhibited by a third unit, C, its inhibition onto A is decreased and A's activity is increased. Ratliff calls this recurrent or response-dependent inhibition and it clearly can account for the disinhibition effect. The non-recurrent type of inhibitory organization, shown on the right, is not consistent with disinhibition. Notice that the lateral inhibition from each unit feeds onto its neighbors *after* the site X where impulses are generated. In this scheme, the inhibitory output of unit B does not depend upon its ultimate response. Rather, it depends only upon the stimulus to it, i.e., the inhibition is non-recurrent or stimulus-dependent. Thus, if B is inhibited by a third unit, C, its inhibition onto A is unaffected and A's activity is unchanged. It is clear that this kind of non-recurrent inhibitory organization would not predict the disinhibition effect.

Ratliff summarizes why it is critical that a lateral inhibitory system be characterized as either recurrent or non-recurrent(5):

> The difference between these two forms of inhibition is important. ...in the recurrent system influences are not only exerted on neighbors, but also

> indirectly on others by way of those affected directly. The inhibition that one receptor exerts on another may thus be diminished by the activity of still other receptors that are in a position to inhibit the first. (from *Mech Bands*,, p. 131)

The non-recurrent system is quite different in that the inhibition that one receptor exerts on another is *not* diminished by other receptors.

The concept of recurrent versus non-recurrent systems, worked out so beautifully in the *Limulus* retina, can also be applied to the perceptual phenomenon of simultaneous chromatic contrast. The underlying physiology is, of course, immensely more complex involving many levels and huge numbers of neurones. Color appearance, however, is obviously in part determined by lateral interactions in the nervous system and the question of recurrent versus non-recurrent organization is thus a valid and important issue. Before any general model of color perception can hope to account for complex visual scenes, chromatic induction must be understood. And befor chromatic induction can be understood, lateral effects must be characterized as either recurrent or non-recurrent. Our purpose was to explore how chromatic induction might be shown to be recurrent or non-recurrent.

III. APPROACH:

In terms of color perception, our basic experimental goal can be phrased as followed: Is the chromatic induction of a region B of the visual scent onto adjacent region A affected when region B's hue is altered by induction from its neighboring region C? If the answer is "yes," chromatic induction can be considered to reflect an underlying recurrent organization. If the answer is "no," chromatic induction can be considered to reflect an underlying non-recurent organization.

Our approach can best be understood by considering a schematic of the actual stimulus arrangement as shown in Figure 2. It consists of a bullseye pattern where A is a circular test spot, B is an annulus surrounding A, and C is an annulus surrounding C. In principle, we first determine the wavelength that produces unique (or pure) yellow for A when seen alone. We then surround A with a B that induces a change in A, say a greenish B that causes A to be tinged with red. We then re-determine the wavelength that again produces a unique-yellow A, now with the B surround. This is our measure of the standard chromatic induction effect. Next we surround B with a C that induces a change in B, say a reddish C that makes B even greener due to chromatic induction. Then we again determine the wavelength for A that is required for unique yellow, now surrounded by B which is in turn surrounded by C. If induction is recurrent, surrounding B with C should have an effect upon A, i.e., B's change in appearance via induction should in tern affect A's appearance. If induction is non-recurrent, B's altered appearance should have no effect on A's appearance. Our response measure is the wavelength that is required for a unique-yellow A in the latter two conditions.

The apparatus used to generate the stimuli was a standard three-channel, maxwellian-view optical system that was constructed at the HRL during the summer of 1985. The details were given in last year's project report. Necessary modifications and calibrations required for the chromatic induction experiments were made in June and July of this year. Considerable effort was required to achieve photographic apertures that allowed the precise registration of the bullseye's components. The outside diameters of fields A, B, and C were determined to be 1.04, 2.37, and 4.0 degrees of visual angle. The three fields were always flashed simultaneously for 0.5 sec every 15 sec. Retinal iluminance of the stimulus was 100 trolands.

The wavelength required to produce unique yellow for the various conditions was determined by a method of constant stimuli. Wavelengths were presented in quasi-random order and the subjects were required to respond either "red" or "green." For each session the wavelength spanned a region from clearly reddish yellow to clearly greenish yellow. With repeated presentations it was possible to generate enough responses at each wavelength so that a smooth curve could be drawn through the data to accurately estimate the 50 percent red-50 percent green point. That wavelength was defined as the one giving unique yellow.

IV. RESULTS:

The results for three subjects are shown in Figure 3. The number entered for each subject in each condition is the wavelength required for unique yellow. It is the mean of four determinations, each done on a different day. The number in parenthesis is the standard deviation. Means are based on eye-ball fits to the data. We are now in the process of re-determining these values based upon a computerized procedure. Preliminary results indicate that the informal fits are extremely accurate. We are also in the process of determining statistical significance based upon t-tests. Our conclusions at this point must be viewed as tentative, but it seems likely that the t-tests will confirm our judgment based upon the means and standard deviations. At the left of the figure the relevant stimulus arrangements are diagrammed. Although incompletely analyzed at this point and not presented, complete data from a fourth subject confirms our tentative conclusions.

A series of steps was necessary to build up to the full bullseye condition shown in figure 2. First, the unique-yellow wavelength for each subject was determined for A alone. The values for subjects SU, LI, and LA are shown in the row labelled "a," which refers to the stimulus condition. The values are fully consistent with those found in the literature

for these conditions. The small standard deviation (0.8 to 1.8 nm) attest to the precision of the method. Condition "b" shows the result when unique-yellow was determined for the B field alone. As expected, they do not differ significantly from the "a" condition. The next condition, labelled "c," is the crucial one. We determined unique yellow for A with a unique-yellow B (from b condition) and a red C of 640 nm. The red C field did in fact induce green into the B field, a standard indiction effect. The unique-yellow wavelengths for A in the c condition are shown in the c row. Upon comparing them with the a condition, it is seen that the differences are small but consistent: in every case the c condition gives a *longer* wavelength for unique yellow. This would indicate that the red C field causes the A field to look slightly greener. Thus, to counter this the yellow locus is shifted slightly in the long-wave (red) direction. Note that this is in the wrong direction from what is expected if induction is recurrent. A recurrent system would require that the greenish (from induction) B field would induce redness and thus result in a shift in the short-wave (green) direction. A non-recurrent system would require, of course, no shift at all from the a result. (Control experiements d and e, not shown, demonstrated that the change in appearance of B in the c condition was sufficient to have caused a significant recurrent-type shift in the unique-yellow wavelength of A.)

The results from conditions a-e were totally unexpected and revealed that some aspect of our assumptions about the underlying mechansisms must be wrong. Ths most likely problem seemed to be our assumption that in the full bulleye stimulus, the c condition, C would have no direct effect upon A. This seemed reasonable in advance of our study since it is well known that even a small gap between two fields wipes out almost all of an induction effect. The visual angel separating A and C in our stimulus is 46 minutes, extremely large in this context. In addition, it is filled with component B that we expected to also stop induction from C directly onto A. Walroven has shown, however, that some

induction is transmitted across large gaps. This raises the possibility that these may be two contrast effects: a large one between contiguous fields and a small, but not trivial, one between even remote fields. For the sake of brevity, we refer to the former as the near-contrast-effect (NCE) and the latter as the far-contrast effect (FCE). Given this possibility our c results could be interpreted as follows: near contrast (NC) is non-recurrent, thus the green B field does not induce redness into A; far contrast (FC) from the red C field not only induces greeness into B, but also into A. Another view is, however, also equally plausible: NC is recurrent, but the induced redness from the green B is off-set by the slightly greater FC induction of greeness from the red C field.

From the point-of-view of deciding whether NC is recurrent or non-recurrent, it must be admitted that experiment c is ambiguous. The confounding influence of a possible FCE must be either eliminated or controlled. As a step towards sorting these factors apart, we decided to first determine whether or not the FCE is in fact a significant influence in our conditions. To do this we simply set up a condition where the B field was blocked leaving A and C with a gap between them. The results for this condition are shown in Figure 3 and labelled "f." Comparing the f results with the c results, it is seen that the directions of the shift are the same, i.e., the remote red C field does in fact induce greeness into A across a 46 min gap. In fact for two of the subjects the shift is larger in f than in c. The magnitude of shifts in the two conditions is difficult to interpret, but it is clear that in our conditions FC is potent and cannot be ignored.

We conclude from experiment f that the FCE complicates the meaning of experiment c. Thus far, we have not separated the effects of FC and NC. Thus, we cannot decide whether NC is recurrent or non-recurrent. Further experiments are required to settle this issue.

V. RECOMMENDATIONS:

Our experiments of last summer we regard as fruitful, but incomplete. They certainly helped us to focus on the nature of recurrent versus non-recurrent systems and they revealed the complicating factor of FC. In the time available we feel that we accomplished a great deal. A number of important aspects of the research, however, was left undone at the summer's end. We recommended a series of new studies that are needed to resolve the basic issues.

Improvements on old experiments

A number of things need to be either completed or extended from the work outlined above:

1.) The data from the fourth subject will be analyzed.

2.) The entire body of data will be analyzed using computer curve fitting and statistical analysis.

3.) The experiments were all done at one luminance level. It would be of great interest to vary the luminance of field C over as large a range as possible. The point is that this might give larger induction effects and therefore be easier to establish significant differences.

New Experiments

The major problem not addressed by last summer's work was the apparent confounding of NC and FC effects. Specifically, the results of c could be interpreted as resulting from either a non-recurrent NCE in conjunction with a small FCE or a recurrent NCE slightly out-weighed by a sizeable FCE. It is critical that these two choices be evaluated by experiment. This seems possible if we could set up a condition that would

retain the size of the effect of FC on A, but eliminate any possible recurrent induction of B onto A. If the small long-wave shift observed in c is entirely from FC, i.e., NC is non-recurrent, then the new results should be the same as c. If, on the other hand, the c results originate from a balance between a recurreent NC (short-wave shift) and a slightly stronger FC (long-wave shift), then the new results (with NC eliminated) should show a much larger long-wave shift compared with c. It may not be possible to perfectly achieve this new condition but it can be closely approximated by creating a new field D that surrounds C and blocking C itself. This would create a gap between D and B which would almost totally destroy any recurrent NC by eliminating the green formerly induced from C onto B. FC would, however, be unaffected since a Walraven conclusively showed FC is unaffected by even relatively large gaps. Thus, one could test the predictions from the two possible interpretations just outlined. In this way, one should be able to settle the original issue of recurrent versus non-recurrent organization.

Other experiments could be done to further explore the mechanisms of contrast. Of particular interest would be conditions designed to examine the properties of the FCE. Very little work has been done on this topic beyond Walraven's initial study. For example, the effects of FC and NC need to be carefully compared in order to explore whether they are fundamentally different mechanisms or merely one mechanism expressed to different degrees. It is important to establish, for example, that the FCE is not merely an artifact of chromatic adaptation from the scattered light.

The recommended experiments refer only to the red-green apparent system. It would also be interesting to explore the yellow-blue system by measuring the unique-green locus. We know that the two systems do not always behave in the same fashion. Thus, any general model of color perception must include characteristics of both systems. It would

also be possible and worthwhile to examine the black-white mechanism from the same perspective of recurrent versus non-recurrent organization.

REFERENCES

1.) Chevruel, M. (1838). *The principles of harmony and contrast of colours and their applications to the arts.* (Originally published in 1838. Translation by C. Martel, 1899, 3rd edn.) Bell, London.

2.) Walraven, J. (1973). Spatial characteristics of chromatic induction. *Vision Res. 13,* 1737-1753.

3.) Hartline, K and F. Ratliff (1957). Inhibitory interaction of receptor units in the eye of *Limulus. J. Gen. Physiol. 40,* 357-376.

4.) Ratliff, F., K. Hartline, and W. Miller (1963). Spatial and temporal aspects of retinal inhibitory interaction. *J. Opt. Soc. Am. 53,* 110-120.

5.) Ratliff, F. (1965). *Mach bands,* Holden-Day, San Francisco.

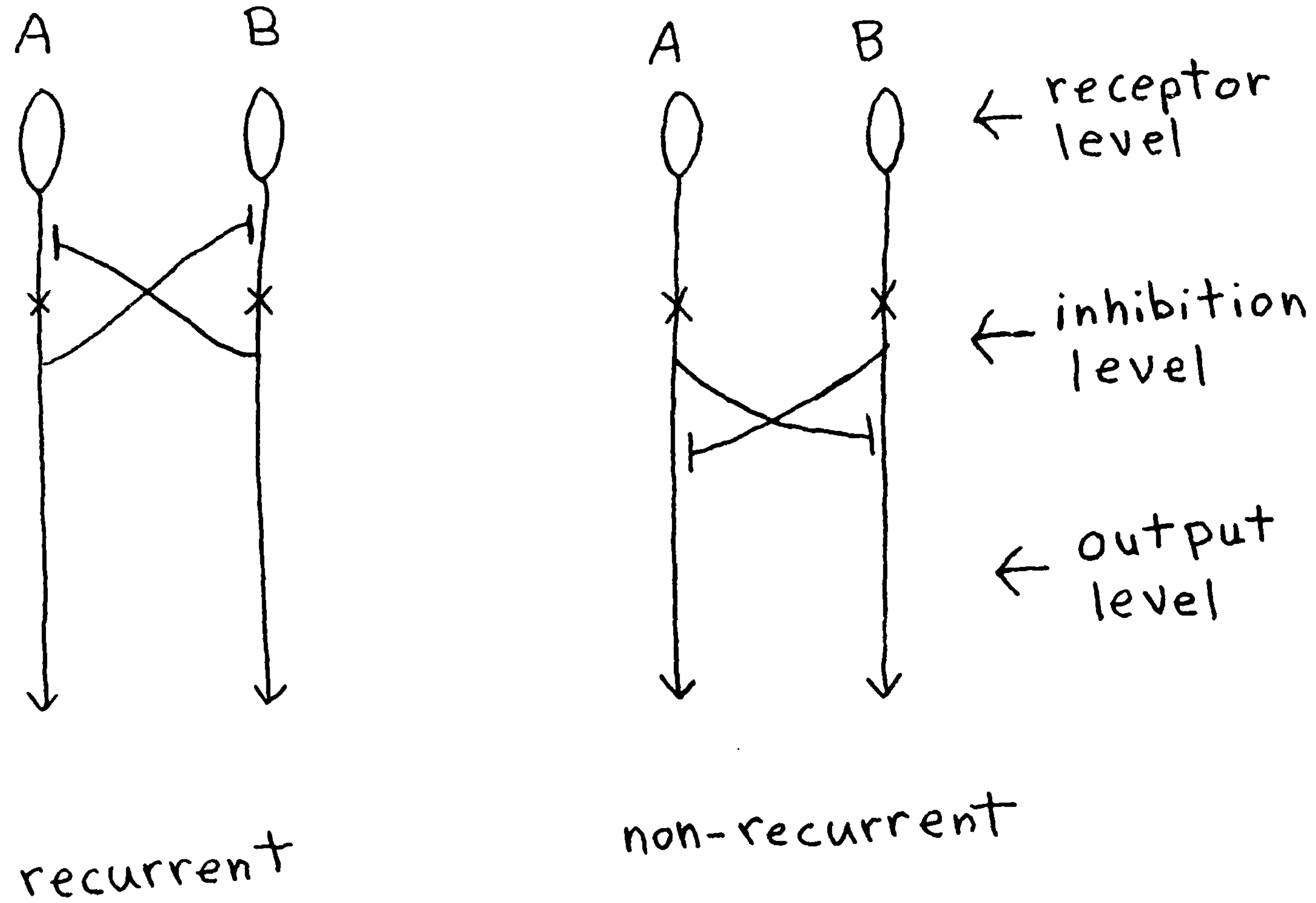

Fig. 1 see text for details

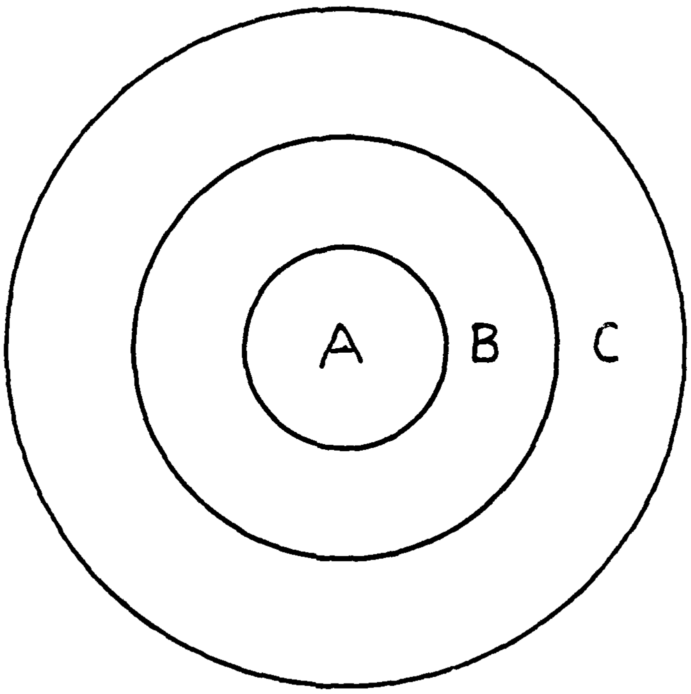

Fig. 2 see text for details

	Stimulus	SU	LI	LA
a.		574.5 (1.8)	578.9 (1.27)	579.3 (.84)
b.	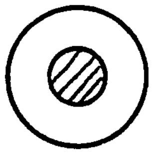	576.0 (2.04)	580.6 (1.49)	579.2 (.70)
c.	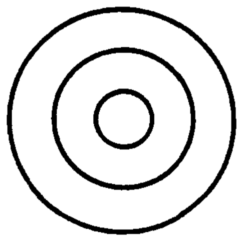	575.5 (1.69)	581.8 (1.02)	581.8 (2.27)
f.	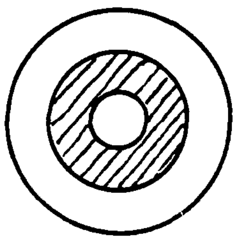	582.0 (1.26)	581.1 (1.85)	584.9 (.92)

Fig. 3 see text for details

1986 USAF-UES SUMMER FACULTY RESEARCH PROGRAM/

GRADUATE STUDENT SUMMER SUPPORT PROGRAM

Sponsored by the

AIR FORCE OFFICE OF SCIENTIFIC RESEARCH

Conducted by the

Universal Energy Systems, Inc.

FINAL REPORT

Computer Simulation of Physical Phenomena

Prepared by:	L. Taylor Simpson
Academic Rank:	Graduate Student
Department and University:	Computer Studies North Carolina State University
Research Location:	AFGL/LSI
USAF Researcher:	Steven M. Miller
Date:	August 21, 1986
Contract No:	F49620-85-C-0013

<u>Computer Simulation of Physical Phenomena</u>

by

L. Taylor Simpson

<u>ABSTRACT</u>

NO Relaxation by NO and by Argon can be modeled using a set of three coupled differential equations. The computer was used to numerically approximate the solution to these equations. The computer was then used to compare the relaxation curves obtained using different values for the relaxation rates.

Another program was written to match phenomena observed from the heat pipe oven with a transition within the cesium atom. The program was used to successfully identify several of the emission wavelengths observed by Dr. Christian.

ACKNOWLEDGEMENTS

I would like to acknowledge the Air Force Systems Command and the Air Force Office of Scientific Research for their sponsorship of this research project. Also, I would like to thank the researchers at the Cochise Facility at the Air Force Geophysics Laboratory for their patience, support and inspiration. They are Dr. Steven M. Miller, Dr. C. Mark Phillips, Dale Sinclair, and Henry Murphy.

Most of all, I would like to thank Dr. Wolfgang Christian not only for the opportunity to work with him again, but also for the friendship and guidance that he has given me in the three years I have known him.

I. Introduction

I received a B.S. from Davidson College in May of 1986. In the fall I will begin graduate study at North Carolina State University in the computer studies department.

During the summer of 1984 I worked with Dr. Wolfgang Christian as a research assistant in laser spectroscopy. During this time I wrote several data analysis programs which are still being used by Dr. Christian. Because of my familiarity with his work and my interest in programming, Dr. Christian asked me to assist him in the building of a cesium heat pipe oven at the Air Force Geophysics Laboratory.

II. Objectives of the Research Effort

The primary goal of the research project was to build a cesium heat pipe oven. Once the device had been built, we wanted to look at spectra of the multiphoton ionization and of the emission in both the visible and the infrared regions. The heat pipe oven can also be used as a source of infrared radiation to excite the v=2 vibrational state in NO.

III. Heat Pipe Spectra Analysis

The spectra of the multiphoton ionization and of the emission taken from the heat pipe oven identified several transitions within the cesium atom. The computer can quickly and easily check all possible transitions and choose the one which is the closest match to the wavelength from the lab data.

The first step in the solution to the problem is to calculate the energy contained in each energy level inside the cesium atom. Several of these values were obtained from Atomic Transition Probabilities Volume III by Charlotte E. Moore; others were calculated using formulae found in an article in Zeitschrift fur Physik A Atoms and Nuclei called "Precise Quantum Defects of nS, nP, and nD

Levels in CsI" by C. J. Lorenzen and K. Niemax, and the values for the F, G, and H levels were calculated based on the Rydberg states.

There are three programs based on these calculations. The first matches a one photon reaction with a transition with delta j equal to +1 or -1. The second matches a one or two photon reaction with a transition with delta j equal to 0, +2 or -2. The final program matches a one or two photon reaction with a transition with any delta j. This last program is used as a last resort to find a match when either the first or the second program fails.

The algorithm used by the three program is simple. It identifies a possible pair of energy levels and calculates the difference in energy between them. These energy differences are kept in a linked list sorted by the distance from the desired amount of energy as calculated from the wavelength input by the user. Once all possible transitions have been considered the list is scanned to display the desired number of matches.

IV. NO Relaxation Model

The purpose of computer modeling of NO relaxation is to predict how the photoacoustic and infrared signals depend on the molecular relaxation rates. There are two models that were programmed. They are NO relaxation by Argon and NO relaxation by NO. This discussion will concentrate only on the latter since the two models are similar. The four reactions that are modeled are:

$$NO(1) + NO(0) \xrightarrow{k_1} NO(0) + NO(0) + \Delta E_1$$

$$NO(2) + NO(0) \xrightarrow{k_2} NO(1) + NO(1) + \delta E$$

$$\xrightarrow{k_3} NO(0) + NO(0) + \Delta E_2$$

$$\xrightarrow{k_4} NO(1) + NO(0) + \Delta E_{21}$$

These four reactions dictate that a model with three states be used. Call these states n1, n2, and q. They represent the number of molecules in the v=1 vibrational state, the number in the v=2 state, and the amount of translational energy, respectively. The reactions are represented in the following diagram:

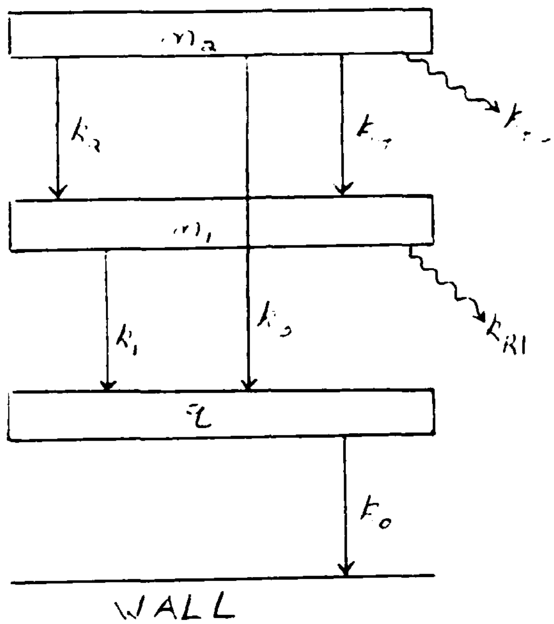

At this point, it is very straightforward to write down the set of coupled differential equations for this system:

$$\frac{dn_2}{dt} = (-k_2 - k_3 - k_4 - k_{R2})n_2$$

$$\frac{dn_1}{dt} = (2k_2 + k_4)n_2 - (k_1 + k_{R1})n_1$$

$$\frac{dq}{dt} = (k_2\delta E + k_3\Delta E_2 + k_4\Delta E_{21})n_2 + k_1\Delta E_1 n_1 - k_0 q$$

The equations written in matrix form would be:

$$\frac{d}{dt}\begin{bmatrix} n_1 \\ n_2 \\ q \end{bmatrix} = \begin{bmatrix} & & \\ & & \\ & & \end{bmatrix}\begin{bmatrix} n_1 \\ n_2 \\ q \end{bmatrix}$$

If x is the three state vector and A is the coefficient matrix, then the matrix equation would be:

$$\frac{dx}{dt} = Ax$$

This equation looks like the differential equation whose solution is the exponential function:

$$x = x_0 e^{At} \qquad\qquad x_0 = \begin{bmatrix} 1 \\ 0 \\ 0 \end{bmatrix}$$

The value of x_0 is used because all the molecules are assumed to be placed in the v=2 vibrational state by the laser pulse.

The exponential function cannot be generalized to take a matrix as the argument, but the operations of multiplication and addition can. Therefore the Taylor series determines the value of the exponential function:

$$e^{At} = 1 + At + (At)^2/2 + \ldots + (At)^n/n! + \ldots = \sum_{i=0}^{\infty}(At)i/i!$$

which can be quickly expanded by the computer for any coefficient matrix A.

The program generates a table of values based on the parameters input by the user. The columns in the table correspond to the values of time, n_1, n_2,

and q respectively. This information is then input into the spreadsheet program for further consideration.

V. Spreadsheet Program

The spreadsheet program was initially obtained from public domain. I had explored its uses before the start of the project and discussed them with Dr. Christian. I had also made some changes in the program for home use such as allowing for simple editing of text and formulas and enlarging the sheet itself. Since I was already familiar with the source code, I was able to make the additional changes necessary to make the program serve for laboratory use. The features added include graphing of data, the combining of data files, and the manipulation of large portions of data at once.

VI. Results

Experimentally, the reaction rate k_1 can be determined by exciting the v=1 vibrational state, but the distinction between the rates k_2, k_3, and k_4 is difficult to determine based on the infrared signal alone because the resulting curves vary only by an amplification factor. However, a look at the photoacoustic signal reveals that the curves actually change shape as one of the parameters varies (see figure 1).

VII. Recommendations

The next step in understanding the relaxation mechanism would be to excite the v=2 vibrational state inside a photoacoustic cell and record the molecular relaxation. Then a curve fitting program could be used to vary the rates k_2, k_3, and k_4 to fit the experimental data and thus determine the values of the rates in question.

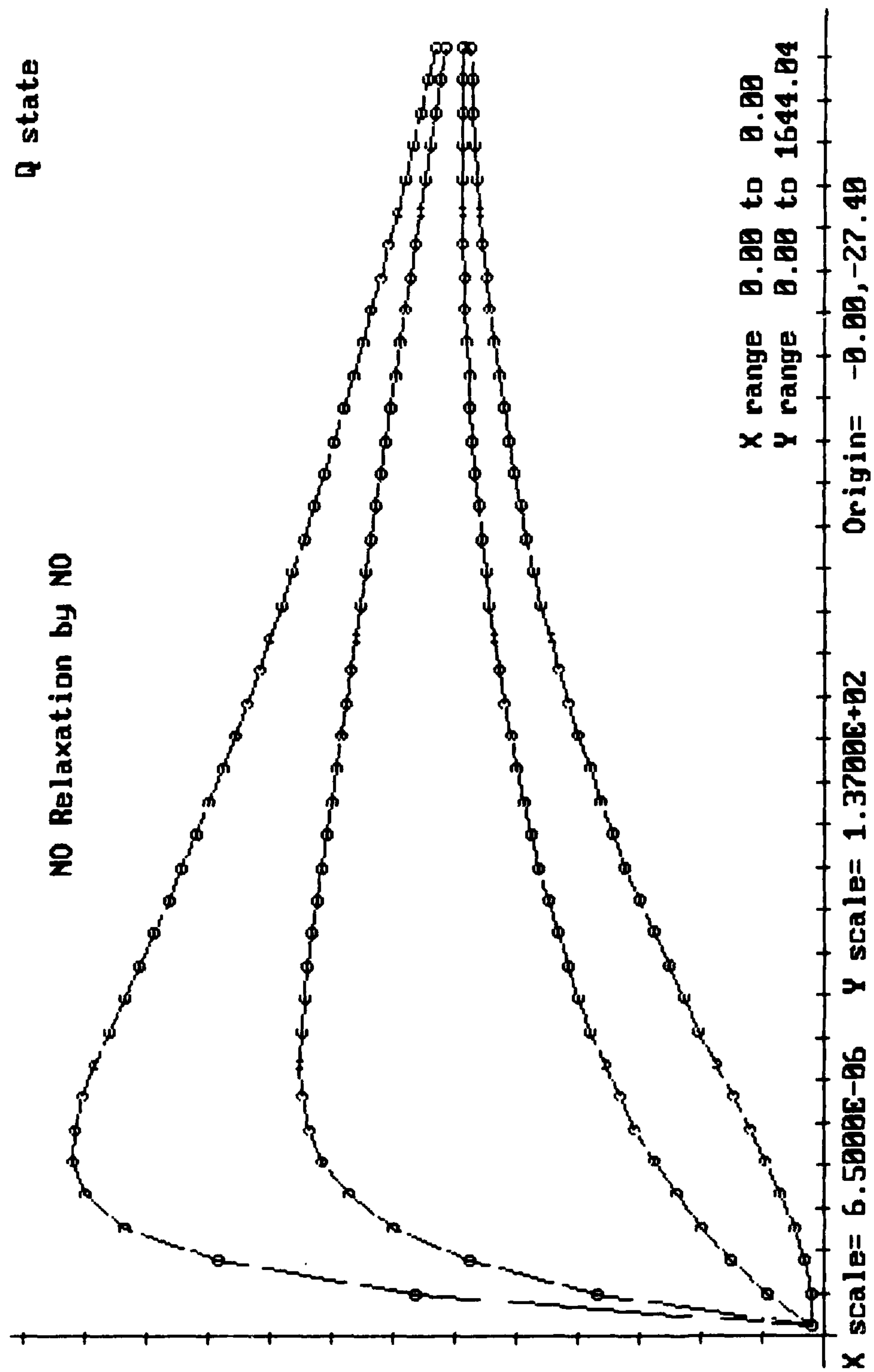
Q state
NO Relaxation by NO
X range 0.00 to 0.00
Y range 0.00 to 1644.04
X scale= 6.5000E-06 Y scale= 1.3700E+02 Origin= -0.00,-27.40

REFERENCES

1. Lorenzen, C. J. and K. Niemax, "Precise Quantum Defects of nS, nP, and nD Levels in CsI," Zeitschrift fur Physik A Atoms and Nuclei, Springer-Veriag, Volume 315, No. 2 (1984), pp. 127-133.

2. Moore, Charlotte E., Atomic Transition Probabilities Volume III, Washington, United States Department of Commerce, 1966, pp. 124-127.

```
program MATCH2;
       { matches an emission wavelength with a one or two photon energy
         level transition in the CsI atom }
       { written by Taylor Simpson -- Last Update 8/6/86 }
       { NOTE: The calculations are based on an article in
         Atoms and Nuclei by C. J. Loremzen and K. Niemax:
         "Precise Quantum Defects of nS, nP, and nD levels in CsI" }
       { NOTE: The other values are taken from
         ATOMIC ENERGY LEVELS by Charlotte E. Moore  }

type  position = (S1,P1,P3,D3,D5,F,G,H);
const Ei   : array[position] of real =
             (31406.4710,   31406.4698,   31406.4702,   31406.4710,
              31406.4710,   0.0,          0.0,          0.0);
      a    : array[position] of real =
             (4.0493527,    3.5914856,    3.5589599,    2.4754562,
              2.4663091,    0.0,          0.0,          0.0);
      b    : array[position] of real =
             (0.238100,     0.380223,     0.392469,     0.009320,
              0.014964,     0.0,          0.0,          0.0);
      c    : array[position] of real =
             (0.24688,      -0.64771,     -0.67431,     -0.43498,
              -0.45828,     0.0,          0.0,          0.0);
      d    : array[position] of real =
             (0.06785,      20.9538,      22.3531,      -0.76358,
              -0.25489,     0.0,          0.0,          0.0);
      e    : array[position] of real =
             (0.1135,       -84.108,      -92.289,      -18.0061,
              -19.6900,     0.0,          0.0,          0.0);
      Rcs = 109736.86;
type  transition = record
                     n1,n2         : integer;
                     pos1,pos2     : position;
                     energy,diff   : real
                   end;
      cellptr    = ^cell;
      cell       = record
                     elmt : transition;
                     next : cellptr
                   end;
var   wavelength, wavenum      : real;
      photons                  : integer;
      maxlevel, matches        : integer;
      matchlist, pos           : cellptr;
      trans                    : transition;
      i, j                     : integer;
      ch                       : char;
{-----------------------------------------------------------------------}
function Z(n: integer; j: position): real;
var temp, sum : real;
begin
  sum := n-a[j]; temp := SQR(n-a[j]);
  sum := sum - b[j]/temp; temp := SQR(temp);
  sum := sum - c[j]/temp; temp := temp*SQR((n-a[j]));
  sum := sum - d[j]/temp; temp := temp*SQR((n-a[j]));
  sum := sum - e[j]/temp;
  Z := sum
end;
{-----------------------------------------------------------------------}
function Ecalc(n: integer; j: position): real;
begin
```

```
      if (n=7) AND (j=P1) then Ecalc := 21765.65
   else if (n=8) AND (j=P1) then Ecalc := 25709.14
   else if (n=7) AND (j=P3) then Ecalc := 21946.66
   else if (n=8) AND (j=P3) then Ecalc := 25791.78
   else if (n=7) AND (j=D3) then Ecalc := 26047.86
   else if (n=7) AND (j=D5) then Ecalc := 26068.83
   else if (n)=6) AND (j in [S1..D5]) then Ecalc := Ei[j] - Rcs/SQR(Z(n,j))
   else if n=4 then
     Case j of
       F  : Ecalc := 24472.3;
       else Ecalc := 999999.0                        {marks undefined value}
     end
   else if n=5 then
     Case j of
       D3 : Ecalc := 14499.490;
       D5 : Ecalc := 14597.08;
       F  : Ecalc := 26971.415;
       G  : Ecalc := 27010.0;
       else Ecalc := 999999.0                        {marks undefined value}
     end
   else if j=F then
     Case n of
       1..3 : Ecalc := 999999.0;                     {marks undefined value}
       6    : Ecalc := 28329.7;
       7    : Ecalc := 29148.17;
       8    : Ecalc := 29678.94;
       9    : Ecalc := 30042.52;
       10   : Ecalc := 30302.38;
       11   : Ecalc := 30494.6;
       12   : Ecalc := 30640.9;
       else   Ecalc := Ei[S1] - Rcs/SQR(n)
     end
   else if j=G then
     Case n of
       1..3 : Ecalc := 999999.0;                     {marks undefined value}
       6    : Ecalc := 28347.0;
       else   Ecalc := Ei[S1] - Rcs/SQR(n)
     end
   else if j=H then
     Case n of
       1..3 : Ecalc := 999999.0;                     {marks undefined value}
       6    : Ecalc := 28356.0;
       else   Ecalc := Ei[S1] - Rcs/SQR(n)
     end
   else Ecalc := 999999.0                            {marks undefined value}
end;
{------------------------------------------------------------------------}
procedure Insert(t: transition; l: cellptr);
         { inserts the transition t into list l based on the
           diff field of the transition }
var pos,temp : cellptr;
    i        : integer;
begin
  pos := l; i := 1;
  while (pos^.next<>nil) AND (pos^.next^.elmt.diff<t.diff)
         AND (i<=matches) do
    begin
      pos := pos^.next;
      i := i + 1
    end;
  if i<=matches then begin
    new(temp);
    temp^.elmt := t;
    temp^.next := pos^.next;
    pos^.next := temp
  end
```

```
end;
{-----------------------------------------------------------------------}
procedure writepos(p: position);
begin
  Case p of
    S1 : write('S1/2');
    P1 : write('P1/2');
    P3 : write('P3/2');
    D3 : write('D3/2');
    D5 : write('D5/2');
    F  : write('F   ');
    G  : write('G   ');
    H  : write('H   ')
  end
end;
{-----------------------------------------------------------------------}
begin
  repeat
    ClrScr;  GotoXY(1,5);
    write('      Enter Maximum Level: ');  readln(maxlevel);
    write('      Enter Wavelength in Angstroms: ');      readln(wavelength);
    write('      How many photons? '); readln(photons);
    wavelength := wavelength/photons;
    wavenum := 1.0E8/wavelength;
    write('      How many matches? ');     readln(matches);
    writeln;
    new(matchlist);
    matchlist^.next := nil;
    for i := 4 to maxlevel do
      for j := 4 to maxlevel do
        with trans do
          begin
            n1 := i;
            n2 := j;

            pos1 := S1;
            pos2 := S1;
            energy := Ecalc(j,S1) - Ecalc(i,S1);
            diff := ABS(energy-wavenum);
            if energy>0 then Insert(trans,matchlist);

            pos1 := P1;
            pos2 := P1;
            energy := Ecalc(j,P1) - Ecalc(i,P1);
            diff := ABS(energy-wavenum);
            if energy>0 then Insert(trans,matchlist);

            pos1 := P3;
            pos2 := P3;
            energy := Ecalc(j,P3) - Ecalc(i,P3);
            diff := ABS(energy-wavenum);
            if energy>0 then Insert(trans,matchlist);

            pos1 := P1;
            pos2 := P3;
            energy := Ecalc(j,P3) - Ecalc(i,P1);
            diff := ABS(energy-wavenum);
            if energy>0 then Insert(trans,matchlist);

            pos1 := P3;
            pos2 := P1;
            energy := Ecalc(j,P1) - Ecalc(i,P3);
            diff := ABS(energy-wavenum);
            if energy>0 then Insert(trans,matchlist);

            pos1 := D3;
```

```
pos2 := D3;
energy := Ecalc(j,D3) - Ecalc(i,D3);
diff := ABS(energy-wavenum);
if energy>0 then Insert(trans,matchlist);

pos1 := D5;
pos2 := D5;
energy := Ecalc(j,D5) - Ecalc(i,D5);
diff := ABS(energy-wavenum);
if energy>0 then Insert(trans,matchlist);

pos1 := D5;
pos2 := D3;
energy := Ecalc(j,D3) - Ecalc(i,D5);
diff := ABS(energy-wavenum);
if energy>0 then Insert(trans,matchlist);

pos1 := D3;
pos2 := D5;
energy := Ecalc(j,D5) - Ecalc(i,D3);
diff := ABS(energy-wavenum);
if energy>0 then Insert(trans,matchlist);

pos1 := F;
pos2 := F;
energy := Ecalc(j,F) - Ecalc(i,F);
diff := ABS(energy-wavenum);
if energy>0 then Insert(trans,matchlist);

pos1 := G;
pos2 := G;
energy := Ecalc(j,G) - Ecalc(i,G);
diff := ABS(energy-wavenum);
if energy>0 then Insert(trans,matchlist);

pos1 := H;
pos2 := H;
energy := Ecalc(j,H) - Ecalc(i,H);
diff := ABS(energy-wavenum);
if energy>0 then Insert(trans,matchlist);

pos1 := S1;
pos2 := D3;
energy := Ecalc(j,D3) - Ecalc(i,S1);
diff := ABS(energy-wavenum);
if energy>0 then Insert(trans,matchlist);

pos1 := D3;
pos2 := S1;
energy := Ecalc(j,S1) - Ecalc(i,D3);
diff := ABS(energy-wavenum);
if energy>0 then Insert(trans,matchlist);

pos1 := S1;
pos2 := D5;
energy := Ecalc(j,D5) - Ecalc(i,S1);
diff := ABS(energy-wavenum);
if energy>0 then Insert(trans,matchlist);

pos1 := D5;
pos2 := S1;
energy := Ecalc(j,S1) - Ecalc(i,D5);
diff := ABS(energy-wavenum);
if energy>0 then Insert(trans,matchlist);

pos1 := P1;
```

```
        pos2 := F;
        energy := Ecalc(j,F) - Ecalc(i,P1);
        diff := ABS(energy-wavenum);
        if energy>0 then Insert(trans,matchlist);

        pos1 := F;
        pos2 := P1;
        energy := Ecalc(j,P1) - Ecalc(i,F);
        diff := ABS(energy-wavenum);
        if energy>0 then Insert(trans,matchlist);

        pos1 := P3;
        pos2 := F;
        energy := Ecalc(j,F) - Ecalc(i,P3);
        diff := ABS(energy-wavenum);
        if energy>0 then Insert(trans,matchlist);

        pos1 := F;
        pos2 := P3;
        energy := Ecalc(j,P3) - Ecalc(i,F);
        diff := ABS(energy-wavenum);
        if energy>0 then Insert(trans,matchlist);

        pos1 := D3;
        pos2 := G;
        energy := Ecalc(j,G) - Ecalc(i,D3);
        diff := ABS(energy-wavenum);
        if energy>0 then Insert(trans,matchlist);

        pos1 := G;
        pos2 := D3;
        energy := Ecalc(j,D3) - Ecalc(i,G);
        diff := ABS(energy-wavenum);
        if energy>0 then Insert(trans,matchlist);

        pos1 := D5;
        pos2 := G;
        energy := Ecalc(j,G) - Ecalc(i,D5);
        diff := ABS(energy-wavenum);
        if energy>0 then Insert(trans,matchlist);

        pos1 := G;
        pos2 := D5;
        energy := Ecalc(j,D5) - Ecalc(i,G);
        diff := ABS(energy-wavenum);
        if energy>0 then Insert(trans,matchlist);

        pos1 := F;
        pos2 := H;
        energy := Ecalc(j,H) - Ecalc(i,F);
        diff := ABS(energy-wavenum);
        if energy>0 then Insert(trans,matchlist);

        pos1 := H;
        pos2 := F;
        energy := Ecalc(j,F) - Ecalc(i,H);
        diff := ABS(energy-wavenum);
        if energy>0 then Insert(trans,matchlist)
      end;
writeln('         Transition      Energy          Wavelength(A)');
i := 1; pos := matchlist^.next;
while (pos<>nil) AND (i<=matches) do
  begin
    with pos^.elmt do
      begin
        write('     ',n2:2); writepos(pos2);
```

```
            write(' -> ',n1:2);  writepos(pos1);
            writeln('    ',energy:10:4,'      ',photons*1.0E8/energy:8:2)
          end;
        i := i + 1;
        pos := pos^.next
      end;
    writeln;
    write('Another wavelength? (Y/N) ');
    repeat
      read(KBD,ch);
      ch := UPCASE(ch)
    until ch in ['Y','N']
  until ch='N'
end.
```

```
PROGRAM SOLN;
       { solve a system of differential equations }
       { based on the molecular model of NO relaxing by NO }

const      sertrms   =  12;           {number of terms in series expansion}
           numpts    =  40;
           E2        =  3752;
           E1        =  1876;
           E21       =  1876;
           dE        =  -28.0;
type       index     =  1..250;
           vector    =  array[1..3] of real;
           matrix    =  array[1..3,1..3] of real;
var        k0,k1,k2,
           k3,k4,kR1,kR2  : real;
           dt,p           : real;
           soln           : vector;              {N2,N1,q}
           TMAT,CMAT,EMAT : matrix;
           i,j,k          : index;
           fname          : string[8];
           outfile        : text;
{--------------------------------------------------------------------}
procedure readnum(var number: real; default: real);
          {reads a number.
           if the user types an empty string then the default
           value is assigned}
var st    : string[15];
    X,Y   : integer;
    ch    : char;
    i     : integer;
    error : integer;
begin
  X := WhereX; Y := WhereY;
  repeat
    GotoXY(X,Y); write('              ');
    GotoXY(X,Y); i := 0; st := '';
    repeat
      read(KBD,ch);
      if (ch=^H) {backspace} AND (length(st)>0) then begin
        write(ch,' ',ch);
        Delete(st,length(st),1)
      end else if ch<>^M then begin
        st := st + ch;
        write(ch);
        i := i + 1
      end else writeln
    until ch=^M;
    if st='' then begin
      GotoXY(X,Y); writeln(default:8);
      number := default;
      error := 0
    end else Val(st,number,error)
  until error=0
end;
{----------------------------------------------------------------}
procedure mult(var T,C : matrix; f : real);
          {multiply two matricies and a constant. result returned in T}
var   i,j,k     :  index;
      sum       :  real;
      temp      :  matrix;
begin
  for i := 1 to 3 do
```

```
    for j := 1 to 3 do
      begin
        sum:=0.0;
        for k := 1 to 3 do sum:=sum+T[i,k]*C[k,j];
        temp[i,j]:=sum*f
      end;
  for i := 1 to 3 do
    for j := 1 to 3 do
      T[i,j]:=temp[i,j]
end;
{---------------------------------------------------------------------------}
procedure add(var E,T : matrix);
         {add two matricies together. result returned in E}
var   i,j : index;
begin
  for i := 1 to 3 do
    for j := 1 to 3 do
      E[i,j]:=E[i,j]+T[i,j]
end;
{------------------------------------------------------------------------------}
procedure vmult(var E : matrix;var S : vector);
         {multiply a vector by a matrix. result returned in S}

var i,j       :  index;
    temp      :  vector;
    sum       :  real;
begin
  for i := 1 to 3 do
    begin
      sum:=0.0;
      for j := 1 to 3 do sum:=sum+E[i,j]*S[j];
      temp[i]:=sum;
    end;
  for i := 1 to 3 do S[i]:=temp[i]
end;
{----------------------------------------------------------------------------}
begin                                                 {main procedure-SOLUTION}
  ClrScr;
  writeln; writeln;
  write('Enter the name of the output file: '); readln(fname);
  assign(outfile,fname + '.DAT'); rewrite(outfile);
  writeln(outfile); writeln(outfile);
  writeln('For the following parameters type ENTER to use the default value');
  write('   enter k0:  '); readnum(k0,10.0);
  write('   enter k1:  '); readnum(k1,2.16E6);
  write('   enter k2:  '); readnum(k2,4.97E7);
  write('   enter k3:  '); readnum(k3,0.0);
  write('   enter k4:  '); readnum(k4,0.0);
  write('   enter kR2: '); readnum(kR2,30.0);
  write('   enter kR1: '); readnum(kR1,15.0);
  write('   enter Time Interval: '); readnum(dt,1E-6);
  write('   enter Pressure (in atm): '); readnum(p,0.01);
  k0 := k0/p;  k1 := k1*p;  k2 := k2*p;  k3 := k3*p;  k4 := k4*p;
  CMAT[1,1]:= -k2 -k3 -k4 -kR2;
  CMAT[1,2]:= 0.0;
  CMAT[1,3]:= 0.0;
  CMAT[2,1]:= 2*k2 + k4;
  CMAT[2,2]:= - k1 - kR1;
  CMAT[2,3]:= 0.0;
  CMAT[3,1]:= k2*dE + k3*E2 + k4*E21;
  CMAT[3,2]:= k1*E1;
  CMAT[3,3]:= - k0;

  {INITIAL CONDITIONS AFTER PASSAGE OF THE LASER PULSE}
  soln[1] := 1.0 {N2};  soln[2] := 0.0 {N1};  soln[3] := 0.0 {q};
  for i := 1 to 3 do      {compute exponent matrix (ut) at 1/20 of the }
```

```
    for j := 1 to 3 do                                       {time interval}
      begin
        CMAT[i,j] := CMAT[i,j]*(dt/20.0);
        if (i=j) then TMAT[i,j]:=1.0        {sets TMAT and EMAT equal to the}
          else TMAT[i,j]:=0.0;                          {identity matrix}
        if (i=j) then EMAT[i,j]:=1.0
          else EMAT[i,j]:=0.0;
      end;
  for i := 1 to sertrms do                {computes the power series expansion}
    begin
      mult(TMAT,CMAT,1/i);
      add(EMAT,TMAT)
    end;
  for i := 1 to numpts do
    begin
      writeln(outfile,(i-1)*dt:8,'      ',
                      soln[1],'      ',soln[2],'      ',soln[3]);
      for j := 1 to 20 do vmult(EMAT,soln)      {computes next data value}
    end;
  close(outfile)
end.
```

1986 USAF-UES SUMMER FACULTY RESEARCH PROGRAM/

GRADUATE STUDENT SUMMER SUPPORT PROGRAM

Sponsored by the

AIR FORCE OFFICE OF SCIENTIFIC RESEARCH

Conducted by the

UNIVERSAL ENERGY SYSTEMS, INC.

FINAL REPORT

A DISCUSSION OF BOUNDARY ELEMENT METHODS

Prepared by:	Jim Sirkis
Academic Rank:	Doctoral Candidate
Department and University:	Department of Engineering Sciences, University of Florida
Research location:	Armanents Laboratory, DWW
USAF Researcher:	Josef Smith
Date:	9/9/86
Contract No.:	F49620-85-C-0013

A DISCUSSION OF BOUNDARY ELEMENT METHODS

by

Jim Sirkis

The boundary element solution to transient potential problems is presented. In doing so, steady potential problems are also discussed. Analytical and implementation difficulties associated with boundary element methods are exposed through four increasingly more difficult example problems. The first example discussed is heat conduction through an infinite square prism. Each example thereafter examines more complex governing equations and boundary conditions. The potential discussion culminates with the boundary element solution to transient heat conduction through an infinite circular cylinder with heat conduction through its surface. Finally, the extension of boundary element methods from scalar to tensor problems is described.

ACKNOWLEDGEMENTS

The author would like to acknowledge the support of the Air Force Systems Command and AFOSR for their support in this effort. The author would also like to thank AFATL for extending the use of their facilities. The invaluable assistance from Mr. M. E. Gunger and Lt. D. L. May is also gratefully acknowledged.

I. INTRODUCTION: As an undergraduate and graduate student at the University of Florida, I pursued an educational background strong in engineering mechanics, electronics and optics. My specific area of interest is experimental stress analysis. I am, therefore, familiar with photoelasticity, holographic interferometry, moiré interferometry, fiber optic strain sensors, resistance strain sensors, as well as, digital methods of strain measurement.

The Clusters and Warheads Branch (MNW) at the Airforce Armament Laboratory (AFATL) is primarily interested in high strain rate mechanical behavior. Hence, a hybrid numerical-experimental technique to study high strain rate deformation is of interest to the Clusters and Warheads Branch at Eglin AFB.

II. OBJECTIVES OF RESEARCH EFFORT: The preliminary goals for the summer research period were to first develop a transient scalar boundary element code; to then explore its capabilities and limitations. The indications being favorable, a transient tensor boundary element code would then be developed. Due to time limitations only the steady tensor code was completed.

III. THE BOUNDARY ELEMENT METHOD: A two-dimensional linear differential operator will be used to introduce the concepts behind the boundary element method. There is no loss of generality in specifying a two-dimensional operator since the three-dimensional development is identical.

$$L(u) = \phi \tag{1}$$

and

$$u = f \quad \text{on} \quad \Gamma_1 \tag{2)a}$$

$$\frac{\partial u}{\partial n} = g \quad \text{on} \quad \Gamma_2 \tag{2)b}$$

where $\Gamma = \Gamma_1 + \Gamma_2$ is the bounding curve of surface B (Figure 1). If the idea that there is a fundamental solution associated equation (1) is accepted, then the boundary element method can be developed following Rizzo [1], the solution to equation (1) can be written as

$$u(p) = - \int_{\Gamma_2} u(Q)\frac{\partial G}{\partial n}(p,Q)d\ell + \int_{\Gamma_1} G(p,Q)\frac{\partial u}{\partial n}(Q)d\ell - \int_B \phi(p,Q)G(p,Q)d\sigma + W(p) \quad (3)$$

where

$$W(p) = - \int_{\Gamma_1} f(Q)\frac{\partial G}{\partial n}(p,Q)d\ell + \int_{\Gamma_2} g(Q)G(p,Q)d\ell.$$

Here, p is any point in B, Q is any point on Γ, $d\ell$ is a differential arclength element and $d\sigma$ is a differential surface element. An integral equation for the unknown $u(Q)$ and $\frac{\partial u}{\partial n}(Q)$ can be obtained through the limiting process $\lim_{p \to P} u(p)$ where P is any point on the bounding curve. This process yields

$$cu(P) = - \int_{\Gamma_2} u(Q)\frac{\partial G}{\partial n}(P,Q)d\ell + \int_{\Gamma_1} G(P,Q)\frac{\partial u}{\partial n}(Q)d\ell - \int_B \phi(P,Q)G(P,Q)d\sigma + W(P) \quad (4)$$

with

$$W(P) = - \int_{\Gamma_1} f(Q)\frac{\partial G}{\partial n}(P,Q)d\ell + \int_{\Gamma_2} g(Q)G(P,Q)d\ell.$$

where c depends on the surface roughness and the singularity contained in G. It is now possible to find the unknown functions $u(Q)$ and $\frac{\partial u}{\partial n}(Q)$. The substitution of these functions into equation (3) gives the solution to $L(u) = \phi$ in B. Therefore, only knowledge of the function on the boundary is necessary to find the functional value at any interior point.

The numerical solution to equation (4), and subsequently equation (3), can be effected by first descretizing the boundary curve into N segments, i.e. Γ_i, i=1,2,3...N. Next, the functions u(Q) and $\frac{\partial u}{\partial n}(Q)$ are approximated by suitable polynomials over each segment. In this report u(Q) and $\frac{\partial u}{\partial n}(Q)$ are approximated by zero order polynomials, that is, u(Q) and $\frac{\partial u}{\partial n}(Q)$ are assumed constant over each boundary segment. The development for higher order polynomials is similar and is given by Brebbia [2]. Based on the aforementioned assumptions equation (4) can be written as

$$-cu(P) - \sum_{i=1}^{N_1} u(Q_i) \int_{\Gamma_2} \frac{\partial G}{\partial n}(P,Q_i)\,d\ell_i + \sum_{i=1}^{N_2} \frac{\partial u}{\partial n}(Q_i) \int_{\Gamma_1} (P,Q_i)\,d\ell_i = Y(P) \tag{5}$$

with

$$Y(P) = + \sum_{i=1}^{N_2} f(Q_i) \int_{\Gamma_1} \frac{\partial G}{\partial n}(P,Q_i)\,d\ell_i - \sum_{i=1}^{N_1} g(Q_i) \int_{\Gamma_2} G(P,Q_i)\,d\ell_i$$

$$+ \sum_{i=1}^{N} \int_{B} \phi(P,Q_i) G(P,Q_i)\,d\sigma_1$$

and, therefore can be reduced to

$$[A - IC]\{u\} + [M]\{\frac{du}{dn}\} = \{Y\} \tag{6}$$

where

$$\{u\} = \begin{bmatrix} 0 \\ 0 \\ \cdot \\ \cdot \\ \cdot \\ u_{N-2} \\ u_{N-1} \\ u_N \\ \\ \end{bmatrix} \qquad \{g\} = \begin{bmatrix} \frac{\partial u}{\partial n_1} \\ \frac{\partial u}{\partial n_2} \\ \frac{\partial u}{\partial n_3} \\ \cdot \\ \cdot \\ \cdot \\ 0 \\ 0 \\ 0 \end{bmatrix}$$

$$A_{ij} = \int_{\Gamma_1} \frac{\partial G}{\partial n}(P_j,Q_i)d\ell_i \text{ and } M_{ij} = \int_{\Gamma_2} G(P_j,Q_i)d\ell_i;$$

where I is the identity matrix, N_1 and N_2 are the number of nodes where $\frac{\partial u}{\partial n}$ and u are unknown, respectively. Since {u} has zero elements in the positions where $\{\frac{\partial u}{\partial n}\}$ has non-zero elements and vice versa, equation (6) can be reduced to

$$[N - IC + M]\{x\} = \{y\}, \tag{7}$$

with

$$\{x\} = \begin{bmatrix} \frac{\partial u}{\partial n_1} \\ \frac{\partial u}{\partial n_2} \\ \cdot \\ \cdot \\ \cdot \\ \frac{\partial u}{\partial n_{N-d}} \\ un_{N-d+1} \\ \cdot \\ \cdot \\ \cdot \\ u_N \end{bmatrix}$$

Equation (7) represents a system of N equation for N unknowns. Upon solving for x equation (3) can be used to find u(p) at any interior point. A four point Gauss-Legrendre numerical quadrature was successfully used to evaluate the off diagonal elements of A and M. This integration scheme was also used to find the solution at interior points.

The chief difficulty encountered when implementing this numerical scheme is integrating over the singularity contained in G (diagonal elements of A). In an effort to keep the boundary element code as general as possible, this integration is carried out numerically. The numerical procedure used follows the approach suggested by Hornbeck [3]. The interval containing the singularity is broken into the two intervals shown in Figure 2; in this figure the singularity is located at X_1. A 24 point Gauss-Legendre numerical quadrature is used in the interval X_1 to $X_1 + .001$ and a four point Gauss-Legendre quadrature is used from $X_1 + .001$ to X_2. Since the zeroes of the Legendre polynomials are clustered near the ends of the interval, subdividing the interval of interest places the maximum number of integration points near the singularity. This approach proved very accurate in evaluating the diagonal elements of A.

IV. TRANSIENT HEAT CONDUCTION THROUGH AN INFINITE PRISM OF CONSTANT CROSS-SECTION: The problems discussed hereafter fall under the modified Helmoltz operator class via the Laplace transform. The fundamental solution to this governing equation is given by Rizzo [4] as $G = 1/2\pi\, K_0(kr)$. In this section, the Laplace transform approach to boundary element methods is introduced. First, the heat conduction through circular and rectangular prisms (both with unit temperature on the boundary) is discussed. Then, the problem of constant heat production in an infinite cylinder is discussed.

Finally, the problem of heat conduction from an infinite circular prism with heat radiated from its surface is discussed. All the numerical solutions are compared to the analytic solutions given by Carslaw and Jaeger [5].

Before proceeding with numerical examples, the corresponding transform domain system must be developed. The general heat conduction equation is stated as

$$\nabla^2 T = \frac{\partial T}{\partial t} \tag{8a}$$

and

$$C_1 T + C_2 \frac{\partial T}{\partial n} = \theta \tag{8b}$$

where C_1 and C_2 are constants, and is a function of position and time. Following Rizzo and Shippy [8], the Laplace transform of equation (8a) and boundary conditions (8b) yields

$$k\nabla^2 \overline{T} - s\overline{T} = 0 \tag{9a}$$

and

$$C_1 \overline{T} + C_2 \frac{\partial \overline{T}}{\partial n} = \overline{\theta} \tag{9b}$$

where $\overline{T}$ signifies the Laplace transform of T and s is the Laplace transform parameter. In equation (9), it is assumed $T(0,\underset{\sim}{r}) = 0$. The time domain solution can be retrieved through the inverse Laplace transform. In each of the following cases, the least square method of Schapery [6] is used to perform the inverse Laplace transform. Rizzo and Shippy [8] also give a complete discussion of this method. In their paper, Rizzo and Shippy use conditions on the frequency response for large frequency and on the time response for small time to find the steady state constants. The accuracy of

this method seems to be better when the steady state constants are found numerically.

V. HEAT CONDUCTION THROUGH INFINITE PRISMS OF UNIFORM CROSS-SECTION WITH UNIT SURFACE TEMPERATURE: The solution to transient heat conduction through an infinite square prism is given. In the time domain the surface temperature is unity, this transforms to 1/S. The frequency domain problem statement is

$$\nabla^2\bar{T} - s\bar{T} = 0 \tag{10a}$$

and

$$\bar{T} = 1/s \text{ on } \Gamma. \tag{10b}$$

An evenly spaced twenty point grid is used in the solution of this problem. Figure 3 gives the time responses found with equation (9).

Next, the solution to heat conduction through an infinite circular prism with unit surface temperature is presented. Equations (10) also govern this problem, in this case however, an evenly spaced 24 point grid was used. Figure 4 presents the time response for a representative point in the domain. The accuracy for all other points is comparable.

VI. HEAT CONDUCTION THROUGH AN INFINITE CIRCULAR CYLINDER WITH CONSTANT HEAT PRODUCTION: The next step in complexity is produced by the addition of constant heat production. Here, the initial and surface temperatures are zero; heat is produced at a unit rate per unit volume. The frequency domain governing equation is

$$\nabla^2\bar{T} - s\bar{T} = -1$$

with

$$\bar{T} = 0 \text{ on } r = 1$$

This example shows the B.E.M. can accurately give the solution to frequency domain, non-homogeneous modified Helmholtz equation and hence also give the time response. The same domain and 24 point grid is used in this solution. Figure 5 gives the time response.

VII. HEAT CONDUCTION THROUGH AN INFINITE CIRCULAR CYLINDER WITH RADIATION AT THE SURFACE: This final example discusses the heat conduction produced in a cylinder when heat is radiated from its surface. This example is different in that functional values for the boundary conditions are not explicit, rather a relationship between the temperature and its normal derivative is given.

$$\nabla^2\bar{T} - s\bar{T} = 0 \tag{11)a}$$

and

$$\frac{\partial\bar{T}}{\partial n} + \bar{T} = \frac{1}{s} \tag{11)b}$$

Substituting boundary conditions (11b) into integral equation (4) gives a boundary element equation in the form of

$$\frac{1}{2}\bar{T} = \bar{T} \int_\Gamma \left(\frac{\partial G}{\partial n} + G\right) d\ell - \frac{1}{s} \int_\Gamma G\, d\ell$$

Equivalently, the fundamental solution, its normal derivative and the boundary conditions can be redefined as

$$\frac{\partial G^*}{\partial n} \equiv \frac{\partial G}{\partial n} + G \,, \qquad G^* = G$$

and

$$\frac{\partial \bar{T}}{\partial n} = \frac{1}{s} \quad \text{on } \Gamma$$

where G is the fundamental solution to the modified Helmholtz equation. This reformulation precipitates the use of the boundary element method. Again, the same domain and grid were used in the solution to this problem. The time response is given in Figure 6.

VIII. TWO DIMENSIONAL TENSOR BOUNDARY ELEMENT METHODS: Boundary element methods can easily be extended to handle quantities governed by the laws of tensor transformation. In the case of two dimensional problems, there are in general four unknown quantities. For isotropic elasticity the unknown quantities might be displacements and their normal derivatives.

The tensor B.E.M. will be introduced following Figure 7, where the normal derivative of the displacement components are known on Γ. The fundamental solution to this type of problem is in tensor form and given by Rizzo [7]. In order to find a unique solution, it is necessary to integrate around the boundary twice. Integrating twice and taking the limit to the boundary, gives the following system of equations for the unknown boundary displacements.

$$\frac{1}{2}\left[\begin{array}{c} U_1 \\ \hline U_2 \end{array}\right] + \left[\begin{array}{c|c} A_{11} & A_{12} \\ \hline A_{21} & A_{32} \end{array}\right]\left[\begin{array}{c} U_1 \\ \hline U_2 \end{array}\right] = \left[\begin{array}{c|c} M_{11} & M_{12} \\ \hline M_{21} & M_{22} \end{array}\right]\left[\begin{array}{c} G_1 \\ \hline G_2 \end{array}\right] ; \qquad (12)$$

where the dashed lines signify partitioned matrices and vectors. If there are N nodes, then system (12) represents 2N equations for 2N unknowns. The solution method for interior points is identical to that described in Section III.

IX. RECOMMENDATIONS: As seen in the previous examples, the accuracy of the constant element-boundary element method is excellent for transient problems. However, this approach gives poor and sometimes spurious results for complex geometries. As shown by Cruse [8], the accuracy of the B.E.M. can be dramatically increased by employing linear elements. For simple geometries the small improvement in accuracy produced by linear elements does not justify the increase in computer time.

In general, for a given accuracy level the B.E.M. solutions are much more efficient than finite difference or finite elements solutions [9]; however, the surface integral introduced by non-homogeneous governing equations can greatly increase the run time of a boundary integral solution. To combat this problem, it is important to take advantage of symmetry when ever possible. The run time of the example presented in Section VI was reduced up to 85% when symmetry considerations were invoked.

The chief purpose of this report is to explore the boundary element solution to transient problems. Hence, it is important to note that the time dependent solutions consistently breakdown for large time. This is exemplified by the solution to heat conducting through an infinite square prism for large time (Figure 8). Rizzo and Cruse [10] point out that this behavior is attributable to the inverse Laplace transform. Bellman et. al. [11] shows that numerical inverse Laplace transforms inherently grow unstable for large time. For short duration events, such as elastic or plastic wave propagation, the instability does not present a problem [12]. In the case of long duration events, such as creep, a time dependent fundamental solution can be derived [13]. This approach is not as desirable as it might seem since the B.E.M. solution must be evaluated at each time step, hence, greatly increasing computer time.

REFERENCES

1. Rizzo, F. J., "The Boundary-Integral Equation Method: A Modern Computational Procedure in Applied Mechanics", Boundary-Integral Equation Method: Computational Applications in Applied Mechanics, ed. T. A. Cruse and F. J. Rizzo, ASME, N.Y., 1975.

2. Brebbia, C. A., The Boundary Element Method for Engineers, John Wiley and Sons, Inc., N.Y., 1978.

3. Hornbeck, R. W., Numerical Methods, Prentice-Hall, Inc., N.J., 1975.

4. Rizzo, F. J. and Shippy, D. J. "A Method of Solution for Certain Problems of Transient Heat Conduction," AIAA Jou., Vol. 8, No. 11, pp. 2004-2009, 1970.

5. Carslaw,. S. and Jaeger, J. C., Conduction of Heat in Solids, Oxford Press, London, 1959.

6. Schapery, R. A., "Approximate Methods of Transofrm Inversion for Viscoelastic Stress Analysis," Proceedings of the Fourth U. S. National Congress on Applied Mechanics, Vol. 2, pp. 1075-1085, 1962.

7. Rizzo, F. J., "An Integral Equation Approach to Boundary Value Problems of Classical Elastostatics," Quart. Appl. Math., Vol. 25, No. pp. 83-95, 1967.

8. Cruse, T. A., "Two-Dimensional BIE Fracture Mechanics Analysis," Appl. Math. Modelling, Vol. 2, pp. 287-293, 1978.

9. Fenner, R. T., "The Boundary Integral Equation (Boundary Element) Method in Engineering Stress Analysis," The Boundary Integral Equation Method in Stress Analysis, Mechanical Engineering Publications Ltd., London, 1983.

10. Rizzo, F. J. and Cruse, T. A., "A Direct Formulation and Numerical Solution of the General Transient Elastodynamic Problem I," Jou. of Math. Anal. and Appl., Vol. 22, pp. 244-259, 1968.

11. Bellman, R. E., Kalaba, R. E. and Lockett, J., Numerical Inversion of the Laplace Transform, American Elsevier, N.Y., 1966.

12. Cruse, T. A., "Direct Formulation and Numerical Solutin of the General Transient Elastodynamic Problem II," Jou. of Mau. Anal. and Appl., Vol. 22, pp. 341-355, 1968.

13. Brebbia, C., Progress in Boundary Element Methods, John Wiley and Sons, N.Y., 1981.

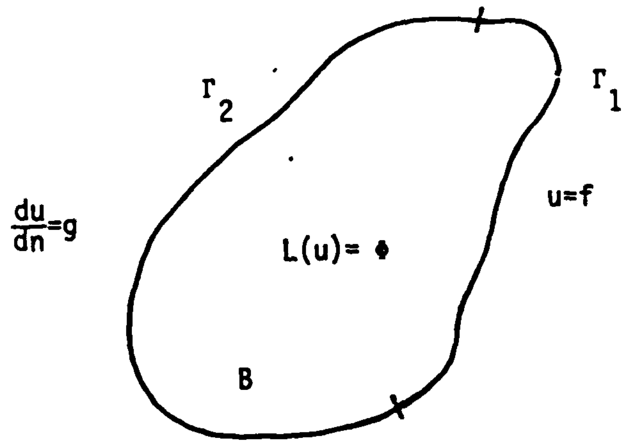

Figure 1. - General Two-Dimensional Domain

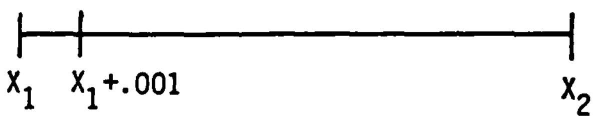

Figure 2. - Division of the Integration Interval to Facilitate Accurate Intregration Around a Singularity

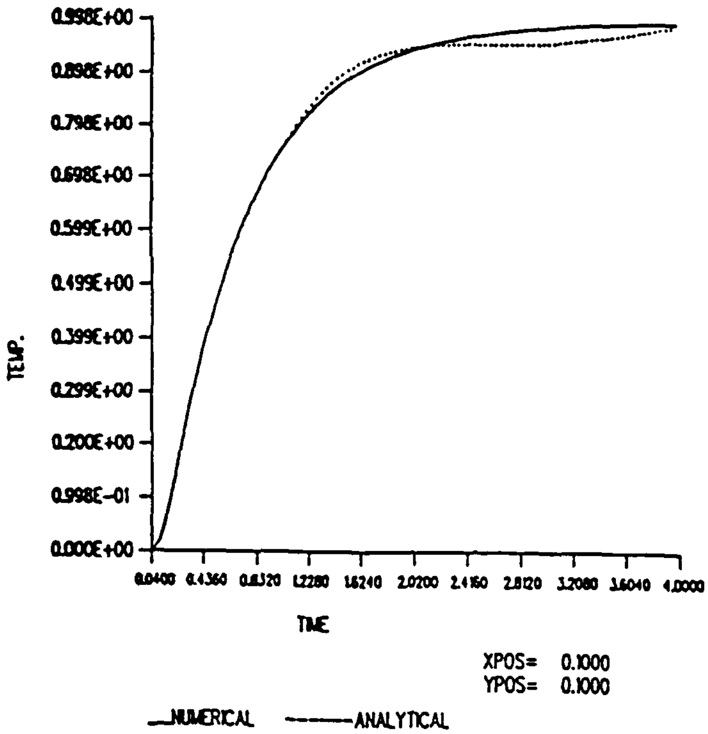

FIGURE 3. Time Response in a Square With Uniform Temperature on the Surface

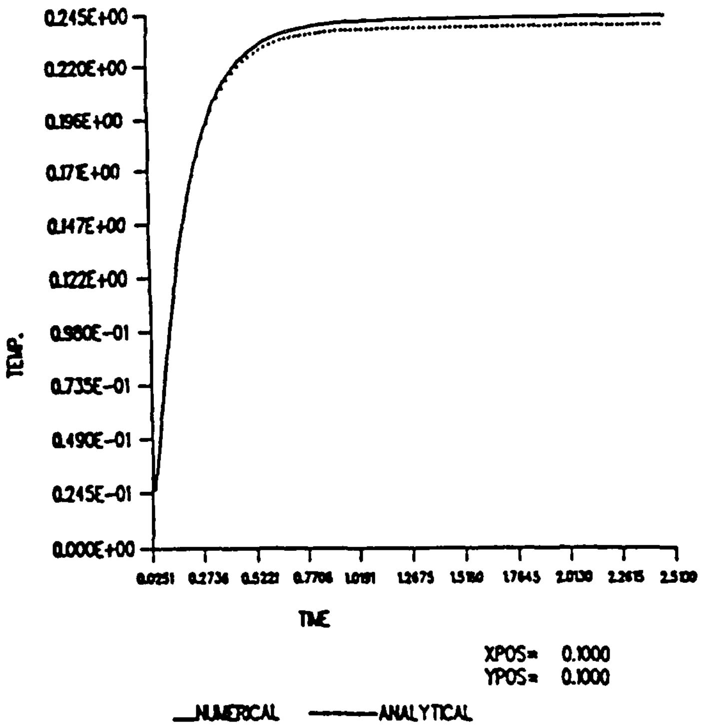

FIGURE 4. Time response in a Circle With Uniform Temperature on the Surface

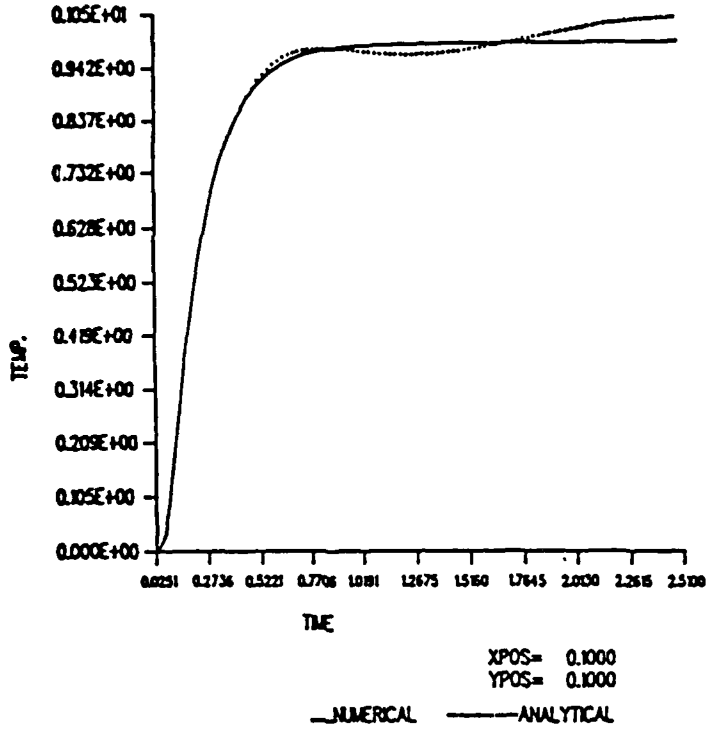

FIGURE 5. Time Response in a Circle With Constant Heat Production

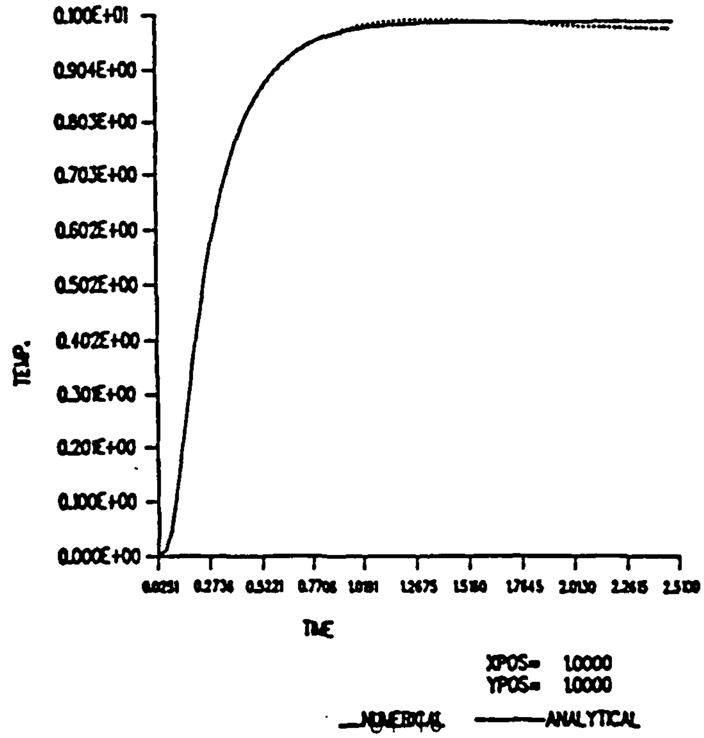

FIGURE 6. Time Respnse in a Circle With Radiation at its Surface

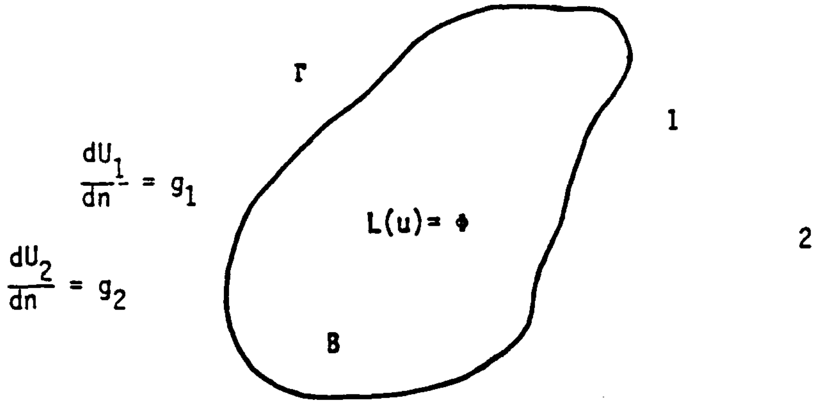

FIGURE 7. General Two Dimensional Domain (Tensor)

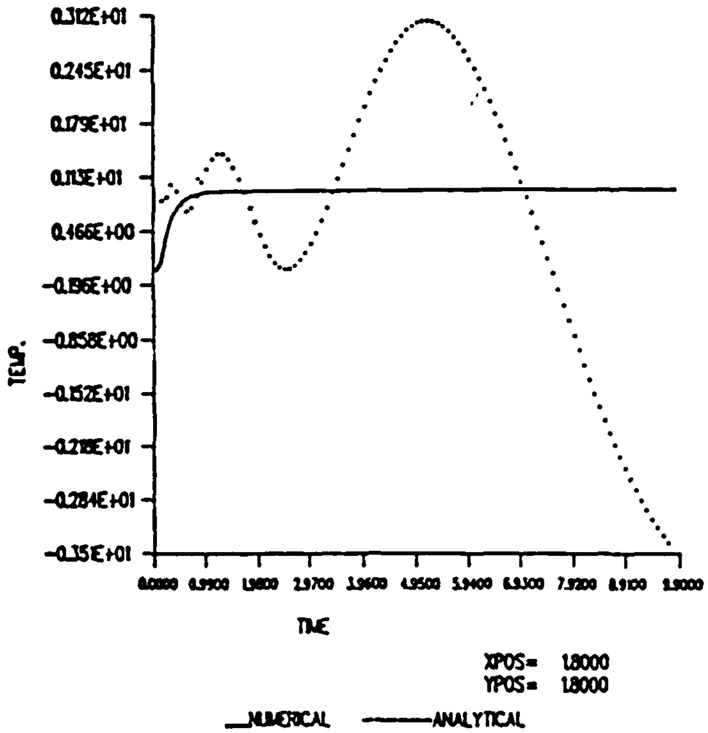

FIGURE 8. Time Response of a Circle With Unit Temperature on its Surface (For Large Time)

1985 USAF-UES Summer Faculty Research Program/

Graduate Student Summer Support Program

Sponsored by the

Air Force Office of Scientific Research

Conducted by the

Universal Energy Systems, Inc.

Final Report

Automatic Program Generation from Specifications

Prepared by: Michael J. Slifker

Academic Rank: 2nd Year Graduate Student

Department and University: Department of Computer Science, Cornell University

Research Location: Air Force Weapons Laboratory, Kirtland Air Force Base

USAF Research: Captain Robert Millar

Date: September 15, 1986

Contract No.: F49620-85-C-0013

1985 USAF-UES Summer Faculty Research Program/

Graduate Student Summer Support Program

Sponsored by the

Air Force Office of Scientific Research

Conducted by the

Universal Energy Systems, Inc.

<u>Final Report</u>

Automatic Program Generation from Specifications

Prepared by:	Michael J. Slifker
Academic Rank:	2nd Year Graduate Student
Department and	Department of Computer Science
University:	Cornell University
Research Location:	Air Force Weapons Laboratory,
	Kirtland Air Force Base
USAF Research:	Captain Robert Millar

Date:	September 15, 1986
Contract No.:	F49620-85-C-0013

Automatic Program Generation from Specifications

by

Michael J. Slifker

ABSTRACT

A skeletal system for generating correct Prolog programs from specifications was developed. We have limited ourselves to the subclass of problems which are equivalent to reduction to normal forms with respect to a set of rewrite rules. The system takes, as input, a set of declarations and type definitions of the basic elements of the specification, along with equational descriptions of a set of transformations and predicates. A Prolog program is produced which, given input of the proper type, generates a consistent sequence of transformations on the input, ultimately resulting in an output object of the same type satisfying a distinguished output predicate.

Acknowledgements

I would like to thank the Air Force Systems Command and the Air Force Office of Scientific Research for the sponsorship of my research this summer, and Dr. Alex Pelin for providing me with an interesting and challenging project. The Air Force Weapons Laboratory at Kirtland Air Force Base provided me with a pleasant and stimulating atmosphere which served to make my work quite enjoyable as well as interesting. I would like to thank Captain Robert Millar, Captain Mike Tebo, and Brian Kennedy for giving me guidance and assistance in my research, and in familiarizing me with the exciting opportunities afforded by the state of New Mexico.

Finally, I would like to thank Michelle Friedman for her patience, encouragement and unfailing support throughout the summer.

I. Introduction

I received my Bachelor of Science degree from the University of Pennsylvania, and am currently a second-year graduate student in the Department of Computer Science at Cornell University. At this early stage in my graduate career, I have been interested primarily in programming logics and the semantics of programming languages.

The project at the Weapons Laboratory originated with an idea of Dr. Alex Pelin of Florida International University. A method for computing normal forms developed by Pelin and Gallier [2,3] is the basis for the program.

II. Objective of the Research Effort

Our goal was to explore the possibility of developing a viable system for generating programs automatically from specifications, at least for a limited category of problems. It has often been stated that such software tends to be highly reliable and easy to maintain, and these advantages can hardly be overestimated given the current level of productivity in the software industry.

III. Overview

Our system takes as input the following elements:

1. A description of the input data type;
2. A description of the output data type;
3. A description of the input/output relation;
4. A set of transformations;
5. A set of tests.

Based on this data, the system tries to generate a program **P** which takes as input an item **i** of the input data type and produces an item **o** of the output data type such that the input/output relation holds between **i** and **o**. The program **P** is constructed by using only the tests and the transformations given in the input specification.

We have limited ourself to the category of problems in which the output item **o** is of the same type as the input item **i**. This class consists of those problems which can be solved by computing normal forms with respect to a set of rewrite rules, and we apply a version of the methodology developed by Pelin and Gallier [2,3]. Details of this methodology may be found in their papers, as well as in Dr. Pelin's final report.

The system takes specifications from a file and produces a set of Prolog clauses which are asserted into the current Prolog database as

well as being written to an output file. The system is broken up into four basic parts: initialization, input processing, type checking, and generation of the main predicates. The initialization consists of copying a set of "header" clauses to the output file. This is information which must be present in all generated programs. In the second phase, each line in the specification file is examined and converted into an appropriate set of clauses (some type checking is also done along the way). In the type checking stage, some simple type checking and consistency checking is done. It is ensured that the user has provided enough information for the system to work with.

The final stage is the generation of clauses for the main predicate. The predicates produced are best illustrated by an example:

If the program name has been declared as 'sort1' and the output predicate has been declared as 'sorted', with type 'array -> bool', then the program would produce, among others, the following clauses:

```
sort1(A,A) :- array(A), sorted(A), !.
sort1(A,B) :- array(A), rewrite(A,C), !, sort1(C,B).
sort1(A,_) :- run_time_error(A,' not of proper type').
```

These clauses have the same form regardless of the specification. The notion of reduction is captured in the clauses for the 'rewrite' predicate, and it is the strategy for producing these clauses that forms the heart of the program generation problem. The 'rewrite' predicate is

supposed to represent a one-step reduction which results in an object which is "closer" to the normal form. A rewrite rule consists of either a top-level application of one of the transformations supplied with the specifications, or of a recursive call to the main predicate on a subterm of an object.

The strategy which is used at this point is rather primitive. The system considers all rules of the form **C** -> **R**(t)=false, where **R** is the output predicate, **C** is a conjunction of tests, and **t** is a term of the appropriate type (i.e. all definitions of the output predicate which describe conditions forcing the output predicate to be false). A rewrite clause is produced for each such definition. If at any time during a reduction a form is found which can be unified with **t**, and for which **C** is true, then this clause will try to find a transformation which makes **C** false without going into another such case. Otherwise, a recursive call of the main predicate is made on the highest level subterm which is of the proper type.

IV. <u>Syntax and rules for giving specifications:</u>

All lines in the specification file must be terminated by a period. The reason is that, although they are disguised slightly, each line must be a valid Prolog term. For the same reason, all types, distinguished elements, type constructors, transformations, tests, and program names must begin with a lower case letter, or with a number. In short, they must be valid Prolog atoms. Also, in the definitions of transformations and tests, variables will generally be used, and as such must begin with a capital letter or an underscore character ('_').

Elements of a specification:

1. There are several declaration predicates. All objects must be declared before they can be used. The predicates are:

   - basetype(<data type>).

     - this declares <data type> as one of the data types defined in the specifications. The system has the declaration 'basetype(bool)' already built in.

   - type_constructor(x).

     - this declares x to be a type constructor. An example is the successor function on natural numbers.

   - test(x).

     - this declares x to be one of the tests used by the system.

- transformation(x).

  - this declares x to be one of the allowable transformations to be applied to the data objects.

- outpred(x).

  - this declares x to be the predicate satisfied by the desired output of the program.

- progname(x).

  - this declares x to be the name of the 'main' predicate in the generated program.

2. Syntax of type declarations:

<declaration> --> <object> ':' <type> '.'
<type> --> <basetype>
<type> --> <basetype> '->' <type>

where <basetype> has been previously declared with the 'basetype' predicate, and <object> is one of the following: a distinguished element of a certain data type (e.g. 'zero:nat.'); a type constructor, test, or transformation previously declared with the appropriate predicate (e.g. 'succ:nat -> nat.', 'less_than:nat -> nat -> bool.'); the name of the main predicate in the target program, after it has been declared by 'progname' (e.g. 'sort_array:array -> array'). Note that some of this information is redundant at this point. For example, if we know that the output predicate is 'sorted', and that its domain is 'array', we know already the type of the predicate 'sort_array'. This

redundancy may ultimately be dispensed with. In addition, the definition 'subtype(<type$_1$>,<type$_2$>).' is allowed, where <type$_1$> has been previously defined.

3. Transformation definitions:

Transformations are defined using arbitrary arithmetic operations and primitive recursive equations. This is best shown by some examples:

- inv:array -> array (switches the last two elements of an array):

```
                inv(lambda) = lambda.
         inv(add(lambda,N)) = add(lambda,N).
  inv(add(add(Array,M),N)) = add(add(Array,N),M).
```

- fac:nat -> nat (factorial function on natural numbers)

```
           fac(0) = succ(0).
     fac(succ(N)) = times(succ(N),fac(N)).

       times(0,N) = 0.
times(succ(M),N) = plus(N,times(M,N)).

        plus(0,N) = N.
  plus(succ(M),N) = succ(plus(M,N)).
```

4. Test definitions:

The general form of a test definition is as follows:

Unconditional:

pred(<args>) = true.

pred(<args>) = false.

pred(<args>) = B(pred$_1$(<args$_1$>),...,pred$_n$(<args$_n$>)).

(where B is an arbitrary Boolean expression over $\wedge$, $\vee$, and ~ (conjunction, disjunction and negation, respectively), which may use '=' for logical equality).

Conditional:

The most general form of a conditional rule is:

Cond => pred(<args>) = Expression.

Here, Expression is 'true', 'false', or an arbitrary Boolean expression as in the unconditional case. Cond is also an arbitrary Boolean expression.

5. Comments may be included by enclosing them between '/*' and '*/'.

Example: specification file for sorting arrays

```
---------------------------------------------------

/* base types: */

basetype(nat).
basetype(array).
type_constructor(s).
type_constructor(add).

      0:nat.
      s:nat -> nat.
lambda:array.
    add:array -> nat -> array.

/* transformations: */

transformation(inv).
```

```
inv:array -> array.

        inv(lambda) = lambda.
  inv(add(lambda,N)) = add(lambda,N).
inv(add(add(A,M),N)) = add(add(A,N),M).

/* tests: */

test(le).
test(sorted).

outpred(sorted).

     le:nat -> nat -> bool.
sorted:array -> bool.

le(N,N) = true.
le(N,M) = true => le(N,s(M)) = true.

sorted(lambda) = true.
sorted(add(lambda,N)) = true.
le(M,N) = true => sorted(add(add(A,M),N)) = sorted(add(A,M)).
le(M,N) = false => sorted(add(add(A,M),N)) = false.

progname(sort1).

sort1:array -> array.

--------------------------------------------------
```

V. Recommendations:

The bulk of future work on this project is required in the final phase: the generation of the rewrite clauses. At this point, only a single strategy is implemented, and that is a fairly simple one. There are several possibilities which should be followed up: The development of a system for proving theorems by induction (this would be very useful in finding which transformations should be applied at various stages during the reduction); the introduction of complexity functions in order to move toward termination; the installation of a number of search techniques which can be tried individually (it is highly unlikely that any single strategy will work universally for such a general problem).

In the other phases of the system, various improvements suggest themselves. Parametrized data types could be introduced; general type constructors, such as cartesian products and disjoint sums, could be incorporated directly into the system; a library of data types could be built, so that inexperienced users would not be required to specify the entire specifications.

References

1. W. Clocksin and C. Mellish: Programming in Prolog, Springer-Verlag, 1984.

2. J. Gallier and A. Pelin: Exact Computation Seuences, Proceedings of CAAP '86, Springer-Verlag Leçture Notes in Computer Science, Vol 214, 1986, pp. 45-59.

3. A. Pelin and J. Gallier: Building Exact Computation Sequences, to appear in Theoretical Computer Science.

1986 USAF-UES SUMMER RESEARCH PROGRAM/

GRADUATE STUDENT SUMMER SUPPORT PROGRAM

Sponsered by the

AIR FORCE OFFICE OF SCIENTIFIC RESEARCH

Conducted by the

Universal Energy Systems, Inc.

FINAL REPORT

VOID AND BOUNDRY LAYER EFFECT ON THE STRESS DISTRIBUTION NEAR CYLINDRICAL INCLUSIONS

Prepared by:	Gregory L. Walker
Academic Rank:	Graduate Student
Department and University:	Dept of Engineering Mechanics, University of Wisconsin-Madison
Research Location:	Edwards Air Force Base, Rocket Propulsion Laboratory MKPB Division
USAF Researcher:	Dr. Chi-Tsieh Liu
Date:	September 21, 1986
Contract No:	F49620-85-C-0013

VOID AND BOUNDRY LAYER EFFECTS ON THE STRESS DISTRIBUTION NEAR CYLINDRICAL INCLUSIONS

by

Gregory L. Walker

ABSTRACT

A finite element analysis of two closely spaced, solid cylindrical inclusions in a soft surrounding matrix was undertaken. Both materials were assumed to be isotropic and incompressible. The region between the inclusions is a zone of stress concentration and is in a tri-axial stress state. Void formation due to tearing, peeling, de-wetting, or other simular phenomenom has been modeled by assuming a very low Youngs modulus in those regions; the resulting stress re-distrubition and stress concentration reductions are then viewed and tabulated. The size and location of voids and the modulus of two thin boundry layers which seperate the inclusion from the matrix are varied to gain insight on the inter-relationships between these effects and the resulting stress pattern.

ACKNOWLEDGMENTS

My deepest thank-you to those people involved in the Air Force Office of Scientic Research and the Air Force Systems Command for allowing me the opportunity to use my skills in a meaningful manner this summer. The Edwards Air Force Base Rocket Propulsion Laboratory provided me with the opportunity to test and develop these skills, and to those both directly and indirectly responsible I give my deepest appreciation.

A special thank-you is due to Dr. Chi-Tsieh (Jimmy) Liu for the opportunity to assist him in his work, to Russell Leighton and Joe Hildreth for their unending patience, and to all the wonderful men and women at the Rocket Propulsion Laboratory.

Allow me also to express my gratitude towards Ken and Vikki DeHart, for without whom I may never have had such a comfortable and enjoyable time.

I. Introduction

As a continuing graduate student in the Engineering Mechanics Department at the University of Wisconsin-Madison I have been exposed to, and involved with, material testing and analysis for some time. I have had limited experience using a device called SPATE (Stress Pattern Analysis by Thermographic Emissions) in an attempt to develop a method for seperating elastic from plastic stress in materials. In addition I am currently studying finite element modeling techniques and their applications to composite and anisotropic materials.

The research conducted at the Edwards Air Force Rocket Propulsion Laboratory addressed such problems as the strain-augmented burning rate of solid rocket propellent, and the interactions between solid rocket fuel and such things as walls, insulation, and the surrounding matrix.

I am thankful to be assigned to a problem which so closely parallels my interests and future plans as an engineer.

II. Objectives of the Research Effort

The intent of my research period at the Rocket Propulsion Laboratory was to investigate and record the stress pattern in the vicinity of two solid, cylindrical inclusions. The particles are imbedded in a soft matrix and subjected to an axial load coincident with a line joining the centers. This effort was accomplished by using a finite element approach to model of actual, idealized specimen. Specifically, our goals are to determine:

1. The relationships between the stress magnitude and its location, both near and far from the particle.
2. The effects of voids and void size on the stress concentration and the change in stress concentration location.
3. The effect of the modulus gradient in the boundry layers next to the particle on the stress concentrations in the vicitinty of the particle.
4. The effect of Poission's ratio.

III. Problem Description

To a degree, solid rocket propellent can be considered to be a very hard cylinder or sphere perfectly bonded to a soft, elastic material. Both materials are assumed to be homogeneous, linear elastic, isotropic, and incompressible; i.e. Poisson's ratio = 0.5. Tears, voids, and de-bonding/de-wetting phenomena can be represented by a similar material, but with a very low value of Young's modulus.

The specific problem addressed (Fig. 1) was that of two closely spaced, identical cylinders, radii of 1, in an elastic plate. The plates measures 8 X 6 X 0.5, and the cylinders have their axes of rotation normal to the plate surface. The axial load is a tensile,

distributed load of magnitude 1 and is applied coincident with a line joining the centers of the cylinders. In this way all stresses as seen in figures 2 - 6 represent the stress concentration or stress raiser at a particular point.

The spacing between particles is such that d/r < 0.1, where d is half the distance between inclusions and r is the radius of the cylinder. Due to mechanical, thermal, and inertia loadings the propellent may experience both a normal tensile and a shearing load, which leads to stress concentrations in the region between two closely spaced particles. The close spacing of the solid particles should lead us to expect a three dimensional stress state in the region between the particles, these results will show that a tri-axial stress state also exists on the diametrically opposing side.

Surrounding each cylindrical inclusion are two very thin (2um.), concentric layers of material. The modulus in these layers is allowed to vary so that investigations can be made on the influence of the boundry layer modulus gradient on the stress near the particle. Moving radially outwards, say for the case of a hard-soft boundry layer, we find the solid (E=100) is wrapped be a hard thin layer (E=40), which in turn is surrounded by a softer layer (E=16). Finally the soft matrix (E=10) is reached.

Studies conducted on inclusions in elastomers have shown "that adhesion is not the determining factor of bond failure" (3), but rather the formation of onion shaped holes close to the surface of the solid particle resulting in a cohesive faliure. An effort has been made to simulate these types of defects and the influence of a modulus gradient in the boundry layer surrounding the inclusion through a finite element analysis which was performed on the Prime computer system using a software package named Patran.

TABLE 1

	Actual	Relative
Dimensions		
radius	250um.	1
height	2000um.	8
width	1500um.	6
Young's Modulus		
cylinder	5000psi.	100
matrix	500psi.	10
voids	0.00001psi.	0
hard/soft	2000/800psi.	40/16
soft/hard	100/300psi.	2/6
Loads		
normal	1.03MPa.	1
shear	138kPa.	0.138
Poission's ratio*	$\mu = 0.5$	

FIGURE 1

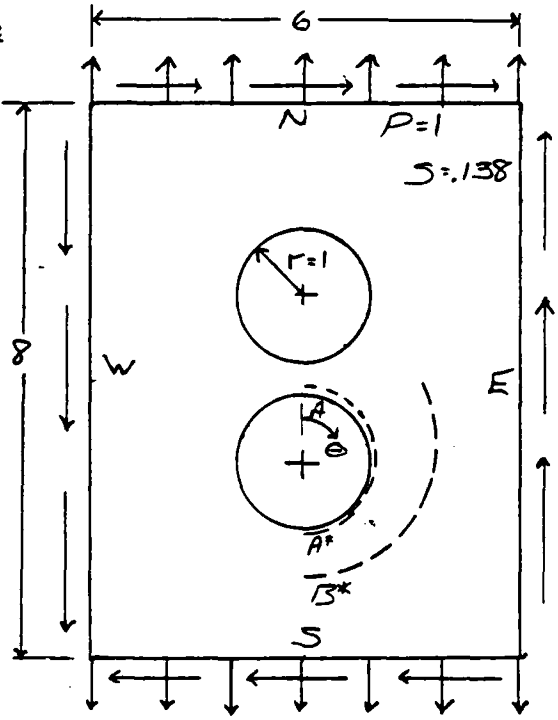

IV. Basic Stress Distribution With No Voids or Boundry Layers

The initial case under consideration is that of a solid rocket propellent particle whose modulus is ten times greater than that of the surrounding matrix to which it is perfectly bonded. An axial stress of magnitude 1 is applied and the resulting stress pattern for the principal stress sigma 1 is seen in figures 2 and 3. The maximum stress is approximately 3.5 times that of the applied load and is located in the small region between the inclusions. This position is what I have termed the "northern location". Diametrically opposite is the "southern location" and here a stress riser of about 1.8 is present, about half as large as the northern location. Of interest is the region of stress at +/- 60 degrees from the "north". In this region we find an area whose stress is actually less than that of the applied load. This low stress region is also depicted in figure 2 where it appears in the shape of a rough oval.

The computer generated plots provide a good impression of the general stress field and can produce some very pretty pictures as evidenced in figures 5 and 7, but to tell the whole story plots of stress along the circumference of the cylinder are also necessary. For this reason we shall consider both near and far field plots along cuts A-A* and B-B*. The data is compiled using an average stress value of adjacent elements along the inner boundry layer, cut A-A*, and along the outermost arc, cut B-B*, from north to south.

In figure 8 a near field plot of the stresses sigma 1 and sigma z has been constructed which contains a number of interesting characteristics. Most prominent is that the maximum value of the principal stress sigma 1 is much greater than the 3.5 we saw earlier on the computer generated stress field pattern. However, the gross results are essentially the same. That is, the northern location is the region of highest stress and is approximately twice that of the southern location.

The three dimensional effects, shown by the out-of-plane stress sigma z are not trivial. At the northern location its value is almost half that of the principal stress and the tri-axial stress state extends to about 30 degrees east and west of north. A tri-axial stress state is found at the southern location location as well.

Refering to figure 9 we see that the stress in the y direction - the direction of loading - is similar in magnitude and shape to the principal stress. More interesting is the perpendicular stress sigma x. For sigma x we note that the stress concentration in the northern location is also non-trivial and reaffirms our prediction of a tri-axial stress state between the voids. I believe this stress, at right angles to the applied load, contributes towards initiating the de-wetting or peeling process. As with sigma z , this stress drops to nearly zero in the vicinity of the eastern location. At the far field location (figure 10), sigma 1 and sigma y are very nearly equal and are within 40% of the applied load which is shown as a dashed line. At this far field location sigma x and sigma z are essentially zero, again showing how the zone of three dimensional stress is confined to a small region.

V. Boundry Layer Influence

The thin layers of material surrounding the solid rocket propellent grain can have its modulus adjusted to demonstrate what effect a modulus gradient has on the overall stress distribution and the areas of high stress concentration. For the cas e with no voids present some dramatic results are found. A modulus gradient, be it an increasing or a decreasing gradient, will significantly reduce the principal stress concentration in zones of tri-axial stress and in fact will cause a reduction in the near field stress at all locations around the circumference of the inclusion. Figure 11 shows this marked drop near station 1 and 2 and again near the southern location.

The out of plane stress tends to violate this principal. Although the hard-soft boundry layer has a lower stress value than the case with no boundry layers, it appears that the soft-hard boundry layer model has the opposite effect. I believe this effect can be explained by realizing that for the soft-hard case the modulus of the boundry layers are both less than that of the surrounding matrix. In essence this is the same as using an even softer matrix with the same hard inclusion and with no boundry layers present.

VI. Void Influence

A single northern void is created by letting one element on each side of north have a very low value for Young's modulus. Symmetry is still preserved but the magnitude and direction of the high stress region has changed. Figures 4, and 5 show the resulting stress pattern for the case with no boundry layers present. In comparing figures 2 and 4 we note that the maximum value has decreased from 3.5 to 2.6 and now occurs to each side of north.

A double void at the northern location has also been developed to further our understanding of the de-wetting phenomena. Figures 13 and 14 compare the principal stress for hard-soft and soft-hard boundry layers for a single and a double void at the northern location. Although the maximum stress will continue to shift towards the east, the gross pattern of stress is still essentially the same.

VII. Poission's Ratio Effect

The result of changing Poission's ratio does not seem to result in much change for the stress distribution. Figure 15 demonstrates contains the resulting stress pattern along section A-A* for the specific case of a single northern void with no boundry layers present. Between the northern and eastern locations the stress of an incompressible material is only slightly lower than of a compressible medium. Near the southern location however the results have flipped, the incompressible material exhibits a higher stress. The difference in stress due to the change in Poission's ratio is not small near the southern location, but I fail to understand the reason or implications of this result.

TABLE 2

NEAR FIELD STRESS (SECTION A-A*)

NO VOIDS PRESENT

Station	No Boundry Layers				H-S Layers		S-H Layers	
	Sigma 1	Sigma X	Sigma Y	Sigma Z	Sigma 1	Sigma Z	Sigma 1	SigmaZ
1	4.50	2.40	3.60	2.05	2.40	0.59	2.69	2.63
2	3.05	1.15	2.70	1.15	1.90	0.18	2.28	1.71
3	1.65	0.15	1.55	0.50	1.32	0.17	1.37	0.79
4	0.95	0.05	0.85	0.20	0.91	0.10	0.60	0.21
5	0.40	0.10	0.35	0.05	1.20	0.02	0.18	0.01
E 6	0.30	0.15	0.20	0.02	0.56	-0.02	0.01	-0.20
7	0.70	0.05	0.50	0.05	0.82	0.00	0.38	-0.01
8	1.25	-0.05	1.05	0.25	1.10	0.05	0.93	0.29
9	1.70	0.10	1.60	0.50	1.29	0.15	1.45	0.81
10	2.05	0.65	1.85	0.80	1.10	-0.18	1.58	1.07
S 11	2.15	1.05	1.80	0.95	0.99	-0.19	1.52	1.28

TABLE 3

FAR FIELD STRESS (SECTION B-B*)

NO VOIDS PRESENT

TABLE 4

NEAR FIELD STRESS (SECTION A-A*)

SINGLE NORTHERN VOID

Station	Table 3: No Boundry Layers	Table 4: No Boundry Layers	Table 4: H-S Layers	Table 4: S-H Layers
	Sigma 1	Sigma 1	Sigma 1	Sigma 1
N 1	---	---	---	---
2	---	---	3.90	3.50
3	---	2.10	2.50	2.57
4	0.61	1.10	1.05	1.19
5	0.71	0.45	0.58	0.17
E6	0.80	0.30	0.43	-0.34
7	0.83	0.55	0.87	0.41
8	0.85	1.15	1.13	0.90
9	0.92	1.70	1.23	1.33
10	1.11	2.05	1.14	1.60
S 11	1.21	2.10	1.02	1.55

TABLE 5

NEAR FIELD STRESS (SECTION A-A*)

Station	DOUBLE NORTHERN VOID H-S Layers	DOUBLE NORTHERN VOID S-H Layers	POISSION'S EFFECT No Boundry Layers
	Sigma 1	Sigma 1	Sigma 1
N 1	0.05	0.06	0.00
2	-0.01	-0.01	3.34
3	3.64	3.64	2.26
4	1.90	2.09	1.17
5	2.43	1.38	0.55
E 6	0.56	-0.21	0.18
7	0.44	-0.36	0.54
8	0.91	0.28	0.92
9	1.07	0.70	1.20
10	1.12	1.53	1.32
S 11	0.96	1.46	1.27

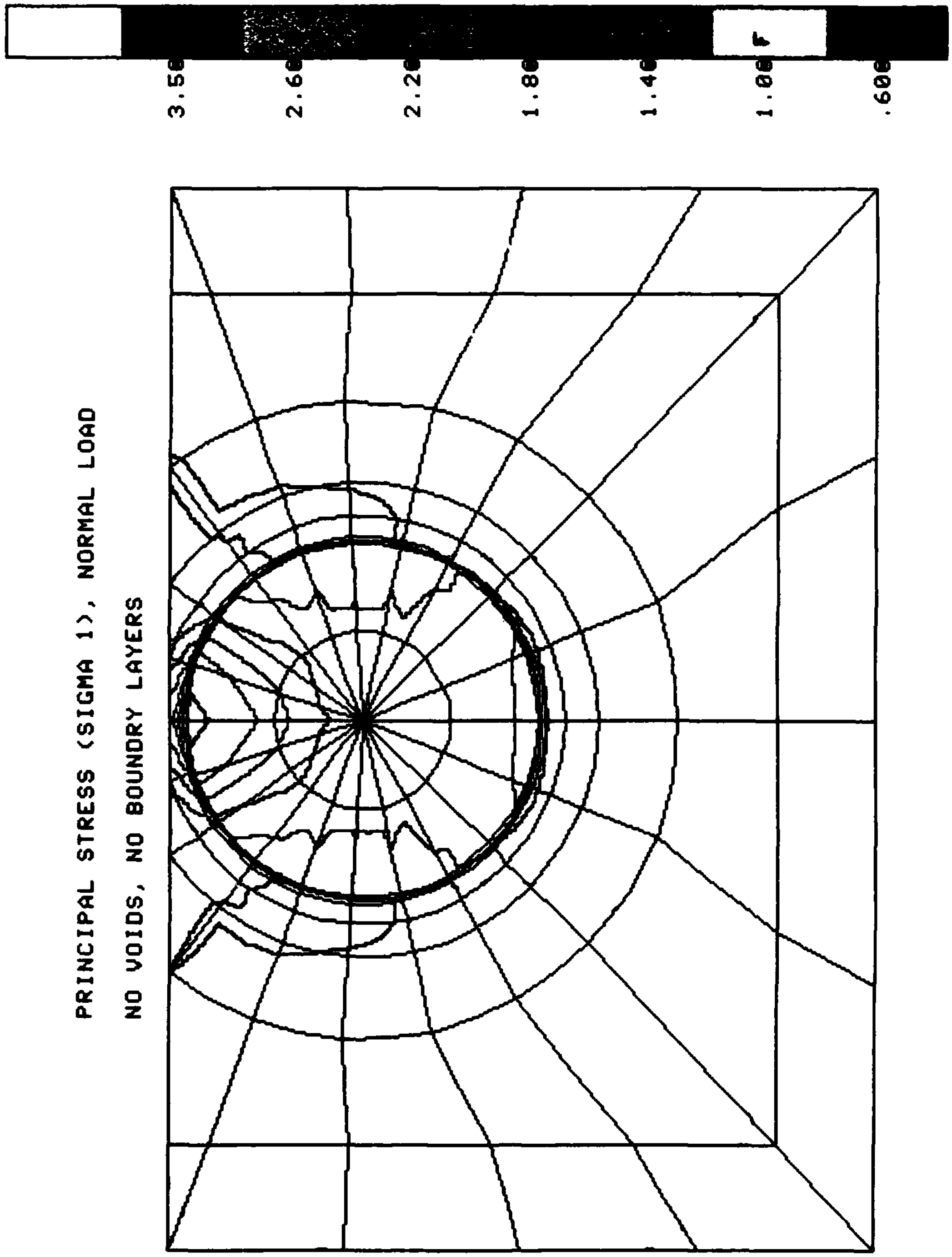

PRINCIPAL STRESS (SIGMA 1), NORMAL LOAD
NO VOIDS, NO BOUNDRY LAYERS

PRINCIPAL STRESS (SIGMA 1), NORMAL LOAD

NO VOIDS, SOFT-HARD BOUNDRY LAYERS

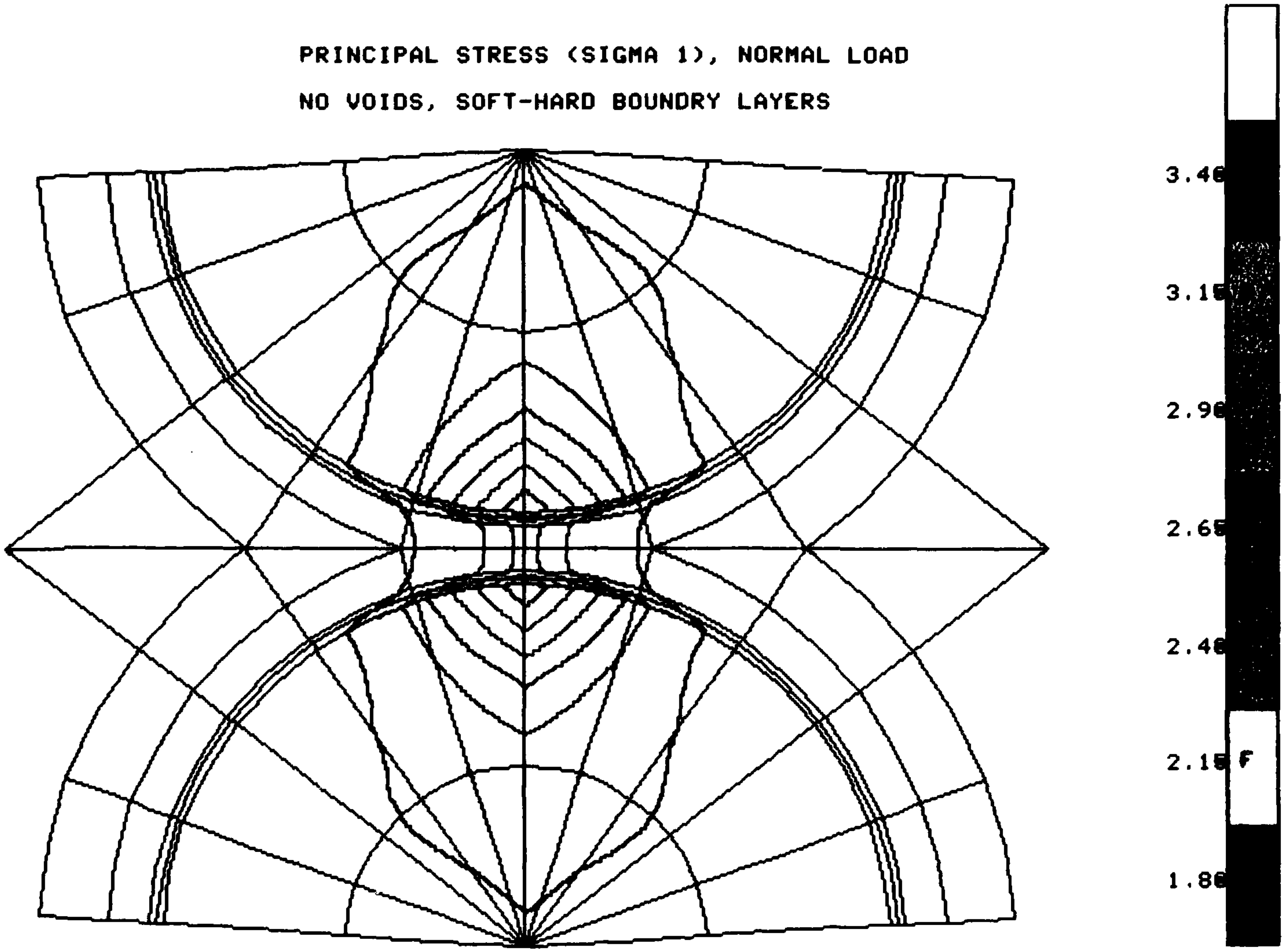

PRINCIPAL STRESS (SIGMA 1), NORMAL LOAD

SINGLE NORTHERN VOID, NO BOUNDRY LAYERS

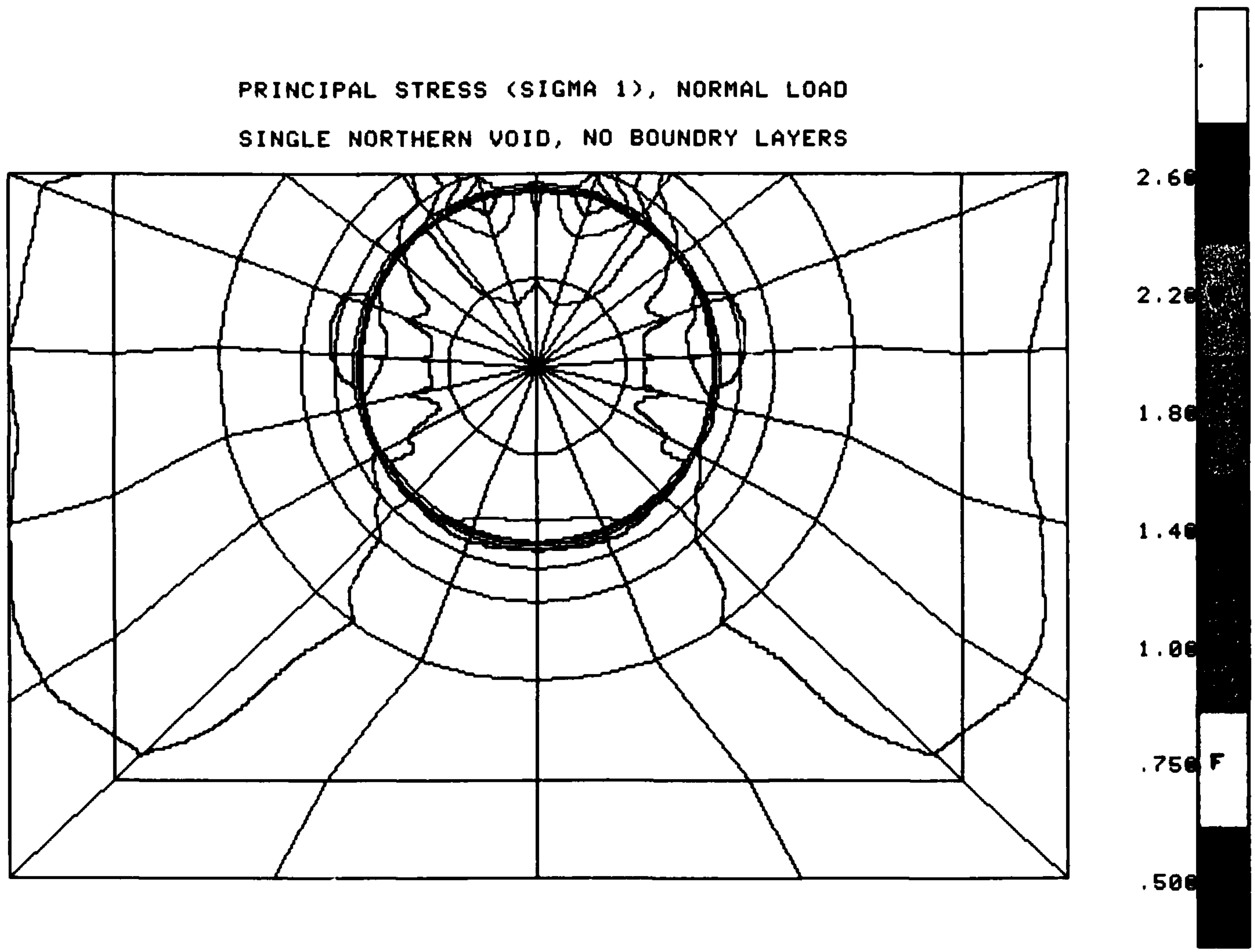

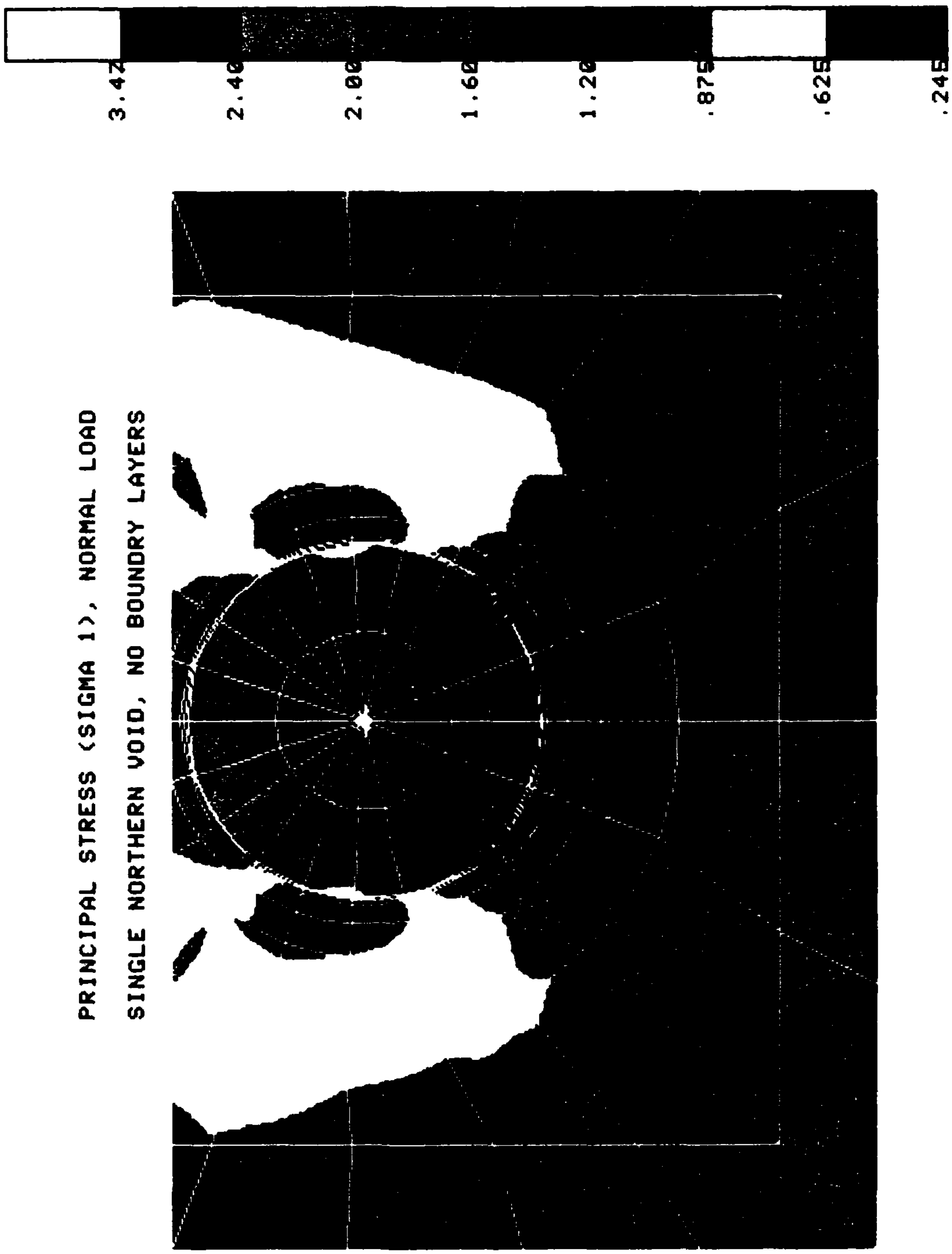

PRINCIPAL STRESS (SIGMA 1), NORMAL LOAD
SINGLE NORTHERN VOID, NO BOUNDRY LAYERS

PRINCIPAL STRESS (SIGMA 1), NORMAL LOAD

DOUBLE NORTHERN VOID, NO BOUNDRY LAYERS

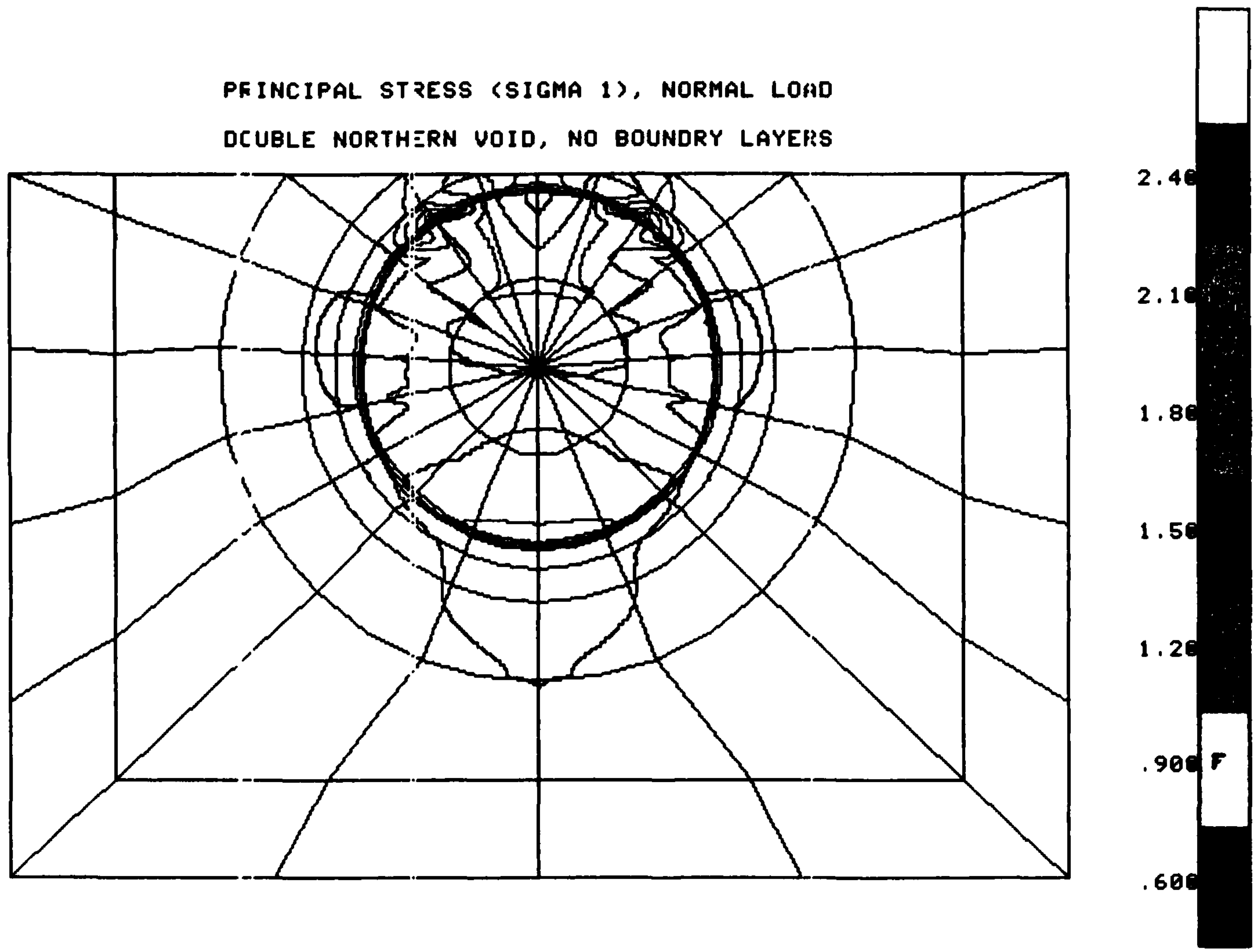

PRINCIPAL STRESS (SIGMA 1), SHEAR LOAD

NO VOIDS, SOFT-HARD BOUNDRY LAYERS

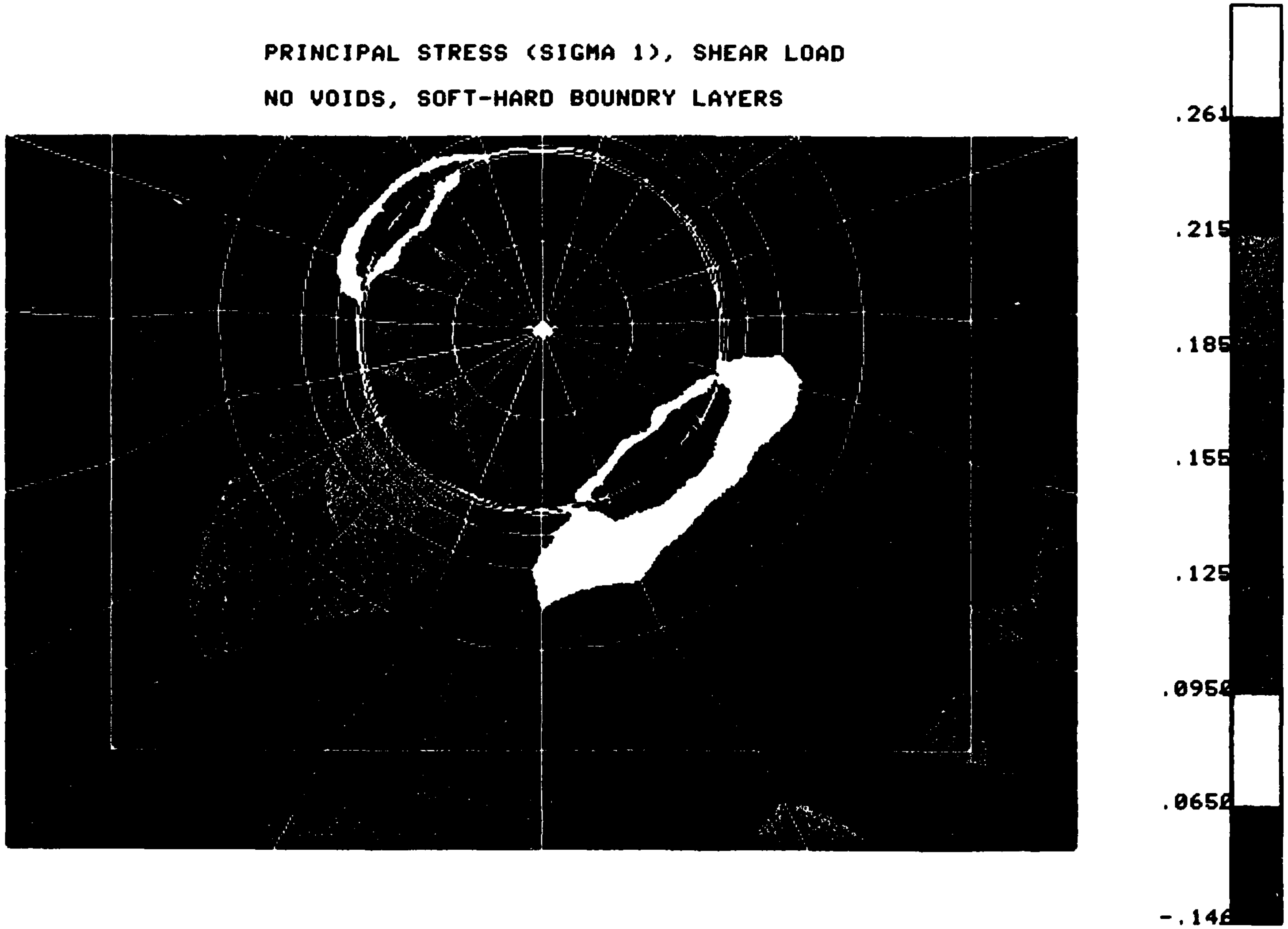

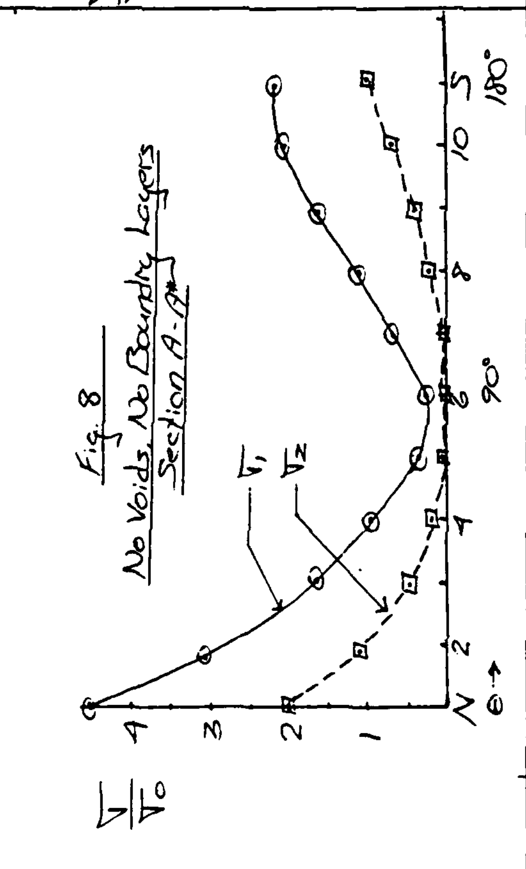
Fig 8
No Voids, No Boundry Layers
Section A-A*
σ1
σ2
σ/σo
θ→
90°
180°

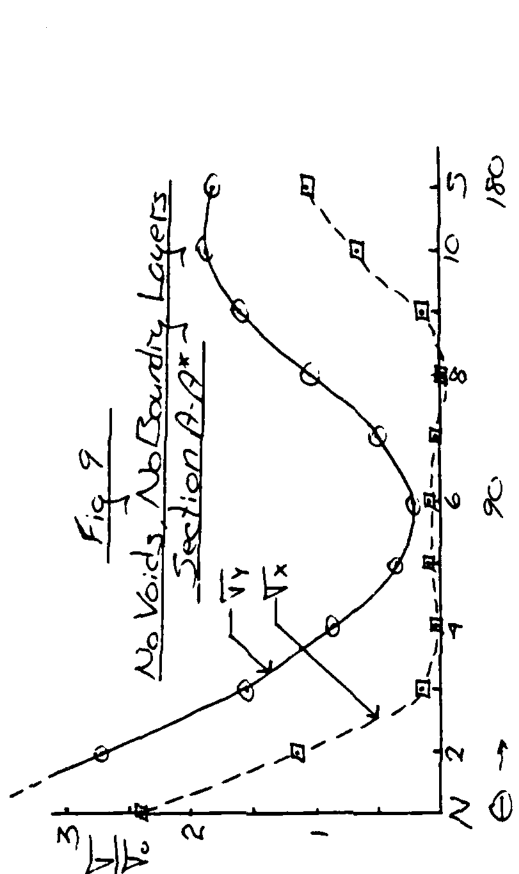
Fig 9
No Voids, No Boundry Layers
Section A-A*
σy
σx
σ/σo
θ→
90
180

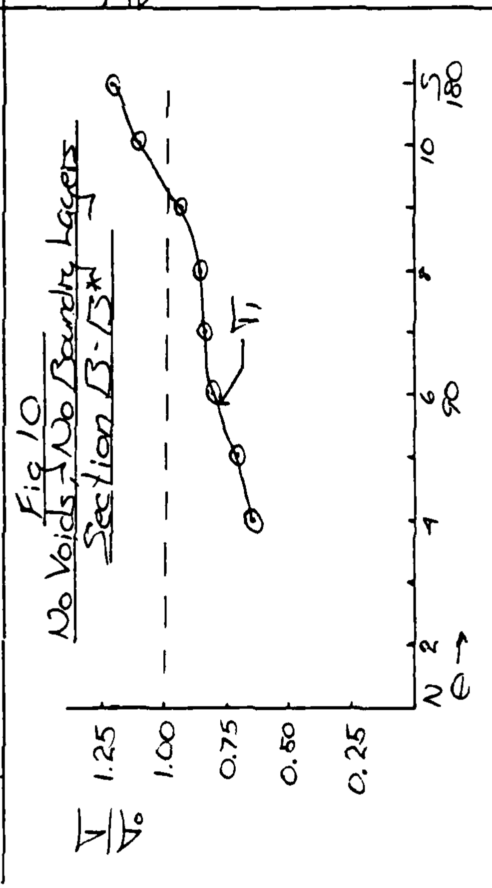
Fig 10
No Voids, No Boundry Layers
Section B-B*
σ1
σ/σo
1.25
1.00
0.75
0.50
0.25
θ→
90
180

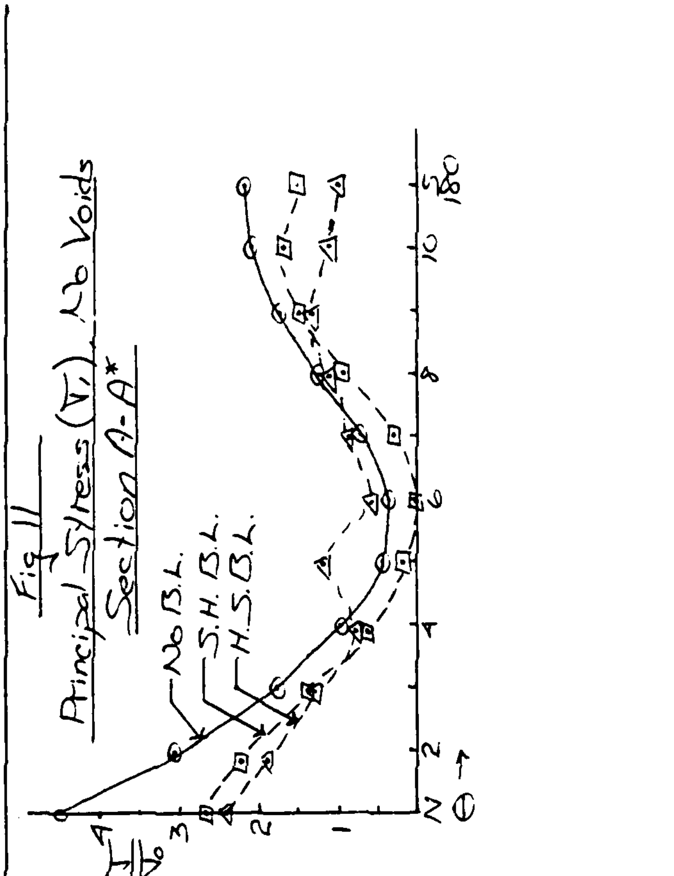
Fig 11
Principal Stress (σ1) No Voids
Section A-A*
No B.L.
S.H.B.L.
H.S.B.L.
σ/σo
θ→
180

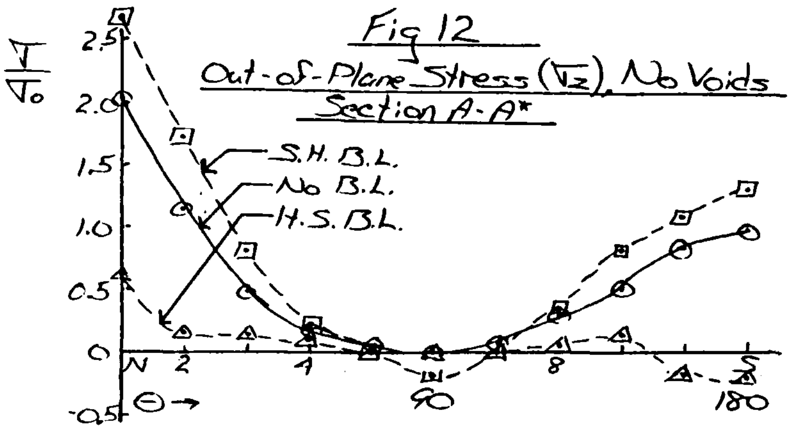

Fig 12
Out-of-Plane Stress (σ_z), No Voids
Section A-A*

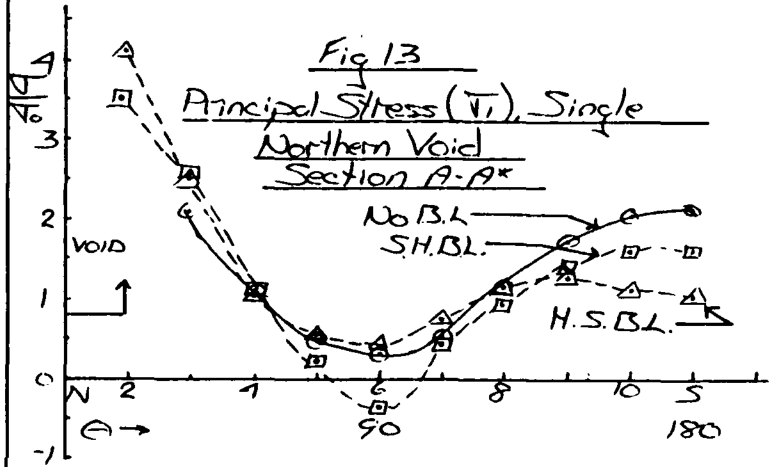

Fig 13
Principal Stress (σ_1), Single
Northern Void
Section A-A*

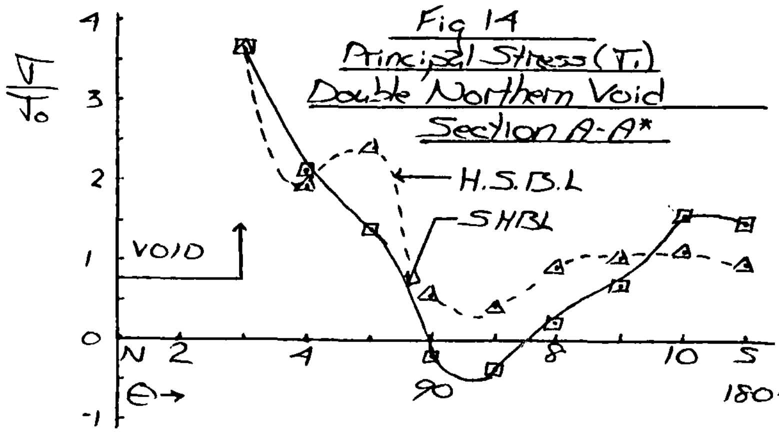

Fig 14
Principal Stress (σ_1)
Double Northern Void
Section A-A*

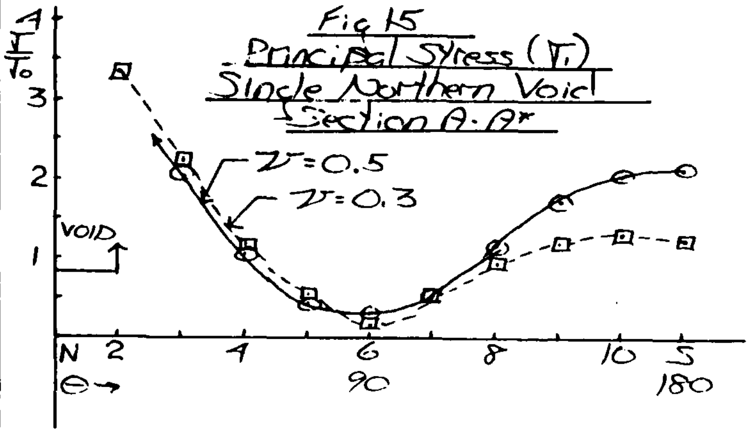

Fig 15
Principal Stress (σ_1)
Single Northern Void
Section A-A*

VIII. Recommendations

Graphic information of the stress distributions near a solid cylindrical particle in a soft elastic matrix has been presented. This information may be used for the determination of the maximum stress intensity, location, and its distribution near and around the particle. To develop this area further I suggest the following areas of possible continued research.

1. Applying a load in the direction perpendicular to the line connecting the centers.
2. A combination of shear and axial loads will yield results pertaining to the non-linearity of the stress field in the vicinity of the particles.
3. Continued experimentation so as to determine the optimum modulus gradient, or conversely to predict the effect of adverse modulus gradients on tearing and de-wetting of the binder.
4. Effects of voids at an arbitrary location on the stress intensity in the zone between the particles.

REFERENCES

1. Tsuchida, E., Nakahara, I.,
"Stress Interference Between Two Spherical Cavities In An Elastic Solid"
Publisher unknown, pp. 267-272.

2. Knauss, W.,G., Mueller, H.,K., DuPont de Nemours and Co., E.,I.,
"Polymer Reinforcement From The Viewpoint of Fracture Mechanics"
Air Force Office Of Scientific Research
Contract # F49620-77-C-0051, pp. 203-220

3. Oberth, A.,E., Bruenner, R.,S.,
"Tear Phenomena Around Solid Inclusions In Castable Elastomers"
Trans. Soc. Rheol., Vol 9, Part 2, (1965), pp. 165-185

1986 USAF-UES SUMMER FACULTY RESEARCH PROGRAM/

GRADUATE STUDENT SUMMER SUPPORT PROGRAM

Sponsored by the

AIR FORCE OFFICE OF SCIENTIFIC RESEARCH

Conducted by the

Universal Energy Systems, Inc.

FINAL REPORT

Experimental Studies on Heat Pipe Coupling and Condensation Rates in Packed Beds of Spheres

Prepared by:	Mark M. Weislogel
Academic Rank:	Masters Candidate
Department and University:	Dept. of Mechanical Engineering Washington State University

Research Location:	Aero-Propulsion Laboratory, Aerospace Power Division, Power Technology Branch, Nuclear/Thermal Technology Group
USAF Researcher:	Elliot Kennel, Engineer, APL
Date:	July 30, 1986
Contract No.:	F49620-85-C-0013

Mark Weislogel

ABSTRACT

Coupled Heat Pipes

A steady state model using an electrical circuit analogy was developed to estimate the proportions of heat transferred through the coupled system given a certain condenser heat input to one of the pipes. It was found that the higher the condenser heat input to the Target pipe, the larger the proportion of heat is transferred through the couplings to be dissipated by the Rescue pipe is in comparison to that "dumped" into the central evaporator. Also, the greater the ratio of the coupling length to the evaporator length, the higher the heat dissipated by the Rescue pipe.

The experimental portion of the research was not completed, but the procedure and apparatus concepts were fully developed.

Packed Bed Study

An experimental research program was developed and proposed concerning the condensation phenomenon in packed beds of spheres. A load cell approach will be used to monitor the condensate and vapor fronts as they propagate across the bed upon its charging. Little research has been done in this area and, though the work proposed is fundamental in nature, it has direct application in energy storage system design and performance.

ACKNOWLEDGEMENTS

I would like to thank the Air Force Systems Command and the Air Force Office of Scientific Research for sponsoring my study this summer. Particulary I would like to thank those of the Aero-Propulsion Lab, Nuclear/Thermal Technology group, whose input was both helpful and educational.

I would like also to acknowledge my advising professor, Mr. Jacob Chung of Washington State University, for introducing me to this program and for helping to focus my ideas.

I. Introduction

I received a B.S. degree in Mechanical Engineering from Washington State University in May, 1986. During the latter portion of my undergraduate studies I began to show particular interest in Fluid Dynamics and Heat Transfer. When I heard of the subject matter in which Jacob Chung (Ph.D., W.S.U.) proposed to investigate at Wright-Patterson this summer, I applied to come along as one of his graduate student assistants.

The initial plan was that I would do an experimental study on the energy storage capabilities of a packed bed of spheres containing a phase change material. Two weeks into my summer session, however, I was re-directed. Since this topic was being looked into by other Summer Faculty, I opted to perform a summer experiment involving heat pipes and, simultaneously, to devise an experimental method and apparatus to investigate condensation (2-phase flow) in packed beds as a thesis topic for the coming year. This change in schedule was encouraged by Mr. Elliot Kennel, an Engineer at APL, and was much to my approval. Both new research assignments are experimental in nature in which I am most interested and most qualified to perform.

II. Objectives of Research Effort

Two subjects have been investigated in my research, the objectives of each to be treated separately.

1. Concerning the summer heat pipe experiment:

The primary objective of this study is to couple two identical heat pipes in a fashion that may improve a system's response to a

condenser heat input. More specifically, the transient response of a coupled heat pipe configuration with condenser heat input (at one of the pipe's condenser) was to be analyzed and compared with the results of a previous test where a single pipe was exposed to similar conditions [1].

2. Concerning condensation in a packed bed:

The overall objective here is to experimentally determine the rate of condensation in a packed bed of spheres--a phenomenon not addressed, to my knowledge, in the literature. My specific objectives are:

A) To develop a system to operate repeatably with step load inlet conditions with and without the presence of a noncondensable gas.

B) To monitor and quantify the condensation-, energy storage-, and vapor-fronts in the bed with time.

C) To establish a relation for the time dependence of the bed porosity, proportional to the pressure drop across the bed, which is functionally dependent on the condensation rate.

III. Heat Pipe Coupling

Though some experimental equipment was already available for this study, the bulk portion needed to be fabricated, which includes namely; 3 Copper-Water heat pipes, a specially designed wrapping tool, a central evaporator coupling device, thermal conduction links, and a calorimetric section (see Figures 1 and 2). This process took nearly the entire 10-week session to complete.

PROCEDURE ACCOMPLISHED. Once the heat pipe wrapping tool was completed, the heat pipes were cleaned, wrapped, filled, and welded

HEAT PIPE COUPLING

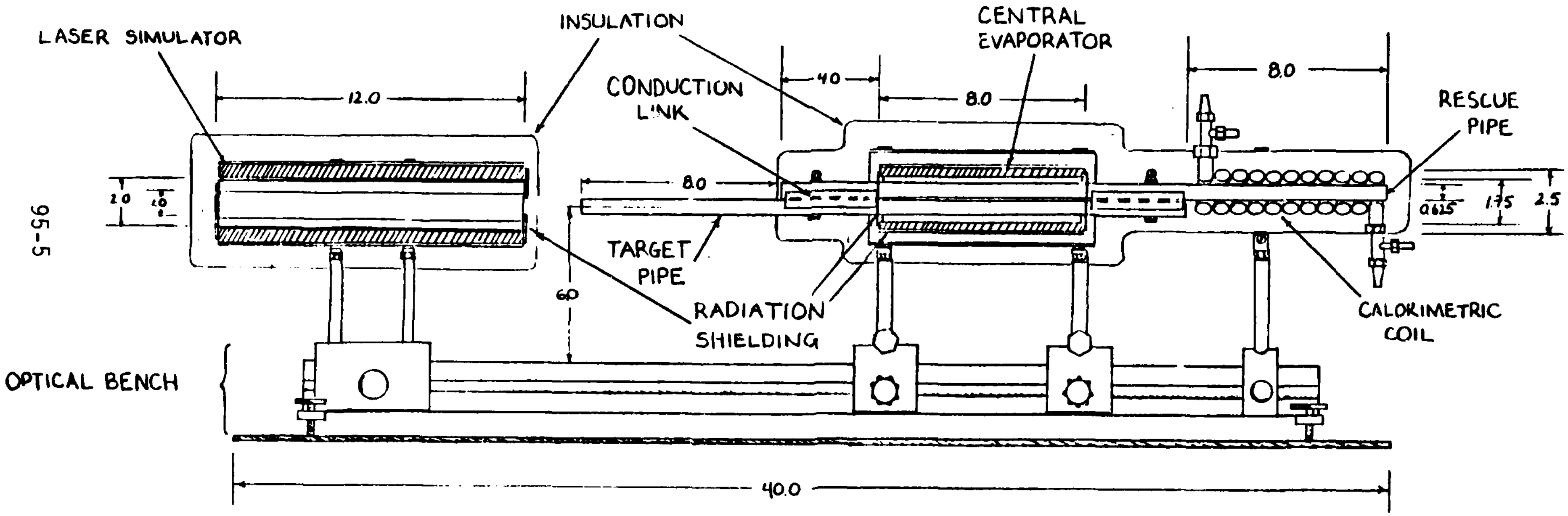

FIGURE 1. DETAILED SCHEMATIC FOR HEAT PIPE EXPERIMENT

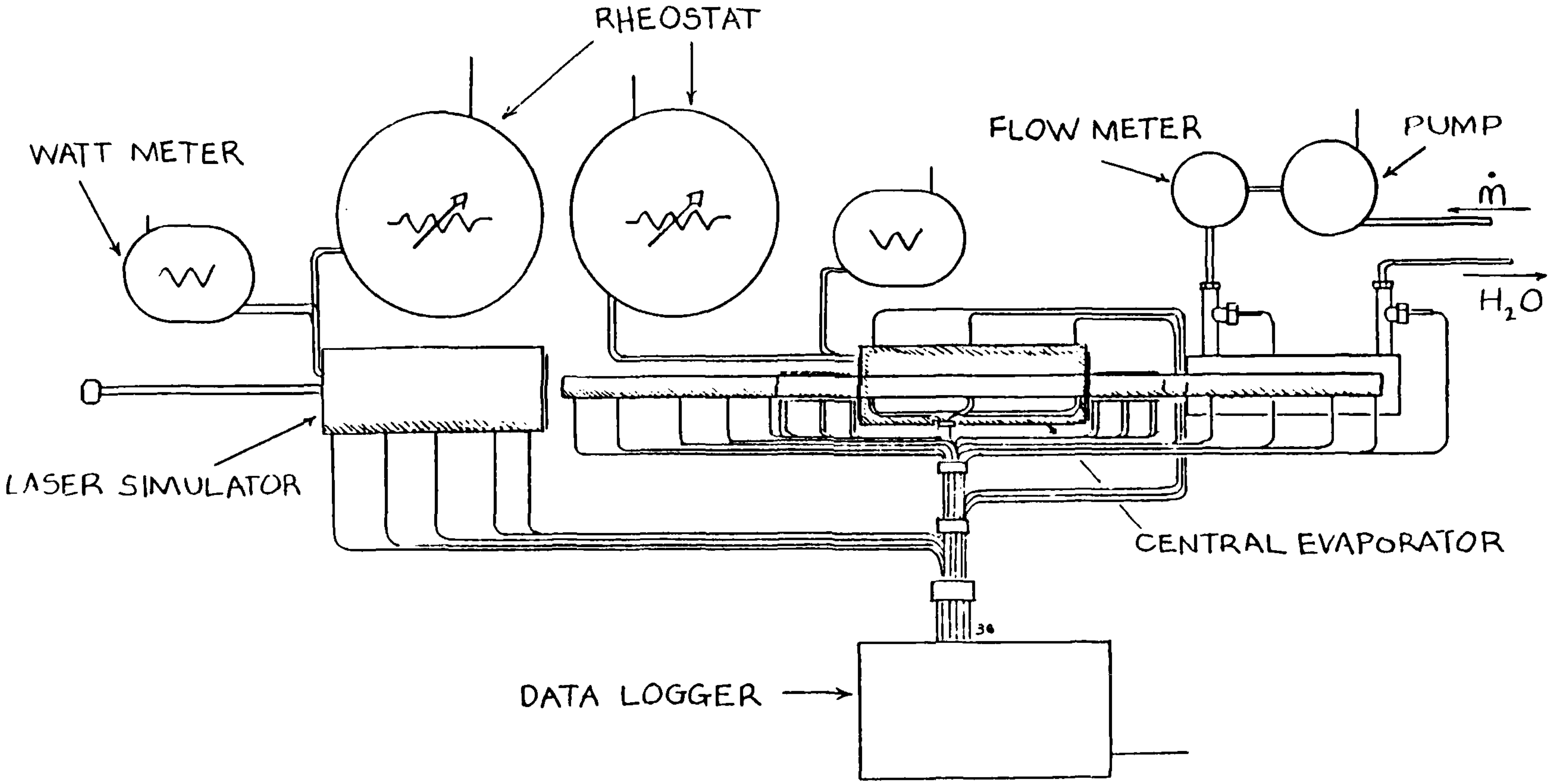

FIGURE 2. GENERAL SCHEMATIC OF EXPERIMENTAL APPARATUS

and ready to be instrumented to determine their transient properties vital to the eventual coupled test. They will also be tested for identical behavior. The flow meter for the test was calibrated and loss data for the system components was taken. The apparatus was almost completed by the end of the 10th week. Don Reinmuller, Technician in charge of building the system, estimated that the apparatus would be finished and assembled within 3 weeks after my Summer Session.

EXPERIMENTAL PROCEDURE. An energy balance for the system yields the following:

$$ql + qce - qout = qstt + qstr + qsts + qloss \quad \text{(E1)}$$

Where; ql = Heat input from the laser

qce = Heat input from the central evaporator

qout = Heat rejected by Rescue pipe condenser

qloss = Heat loss to surroundings,

qstt = Heat stored in Target pipe for time interval

qstr = Heat stored in Rescue pipe for time interval

qsts = Heat stored in coupling components for time interval

Known from equipment readings are ql, qce, and qout. From preliminary tests qloss, qstt, and qstr as funtions of pipe, or system, temperature may be determined, thus leaving qsts as a function of time to be solved for using equation E1. The heat transfer from the Target pipe to the Rescue pipe may be determined by an equation using a ratio of temperature drop across one

conduction link to the other. The test is quite controlled and all desired quantities may be determined directly or by straight forward calculations.

SIMPLIFIED ANALYSIS. While the designs for the system were in the shop the following preliminary analysis was carried out, presented here in an abbreviated form:

The main purpose of this analysis was to get an idea of the heat transported through the various components of the system (conduction links, central evaporator, etc.) as a function of the coupling dimensions and materials.

An analogous electrical circuit was developed to simulate the actual system. A number of assumptions were made in order to use this approach: 1) The system operates at steady-state conditions (no heat storage). 2) There is no resistance to heat transfer in the pipes. And 3) each pipe is uniform in temperature. It is apparent from previous transient heat pipe experiments [1, 2] that none of these assumptions are justified. However, a rough idea of the heat flow paths through the system may be obtainable from this sort of study. This may, in turn, reveal the advantages and/or disadvantages of a coupled heat pipe configuration.

The heat pipe system and its reasonably analogous simplified counterpart are shown in Figure 3. The case that is of interest is that created when the switch, S in Figure 3b, is switched to position 2. For this condition, rearranging the circuit results in Figure 3c. Where;

Where; Re = Resistance to radiative heat input
R = Resistance to heat flow across conduction links
Ri = Internal resistance between central

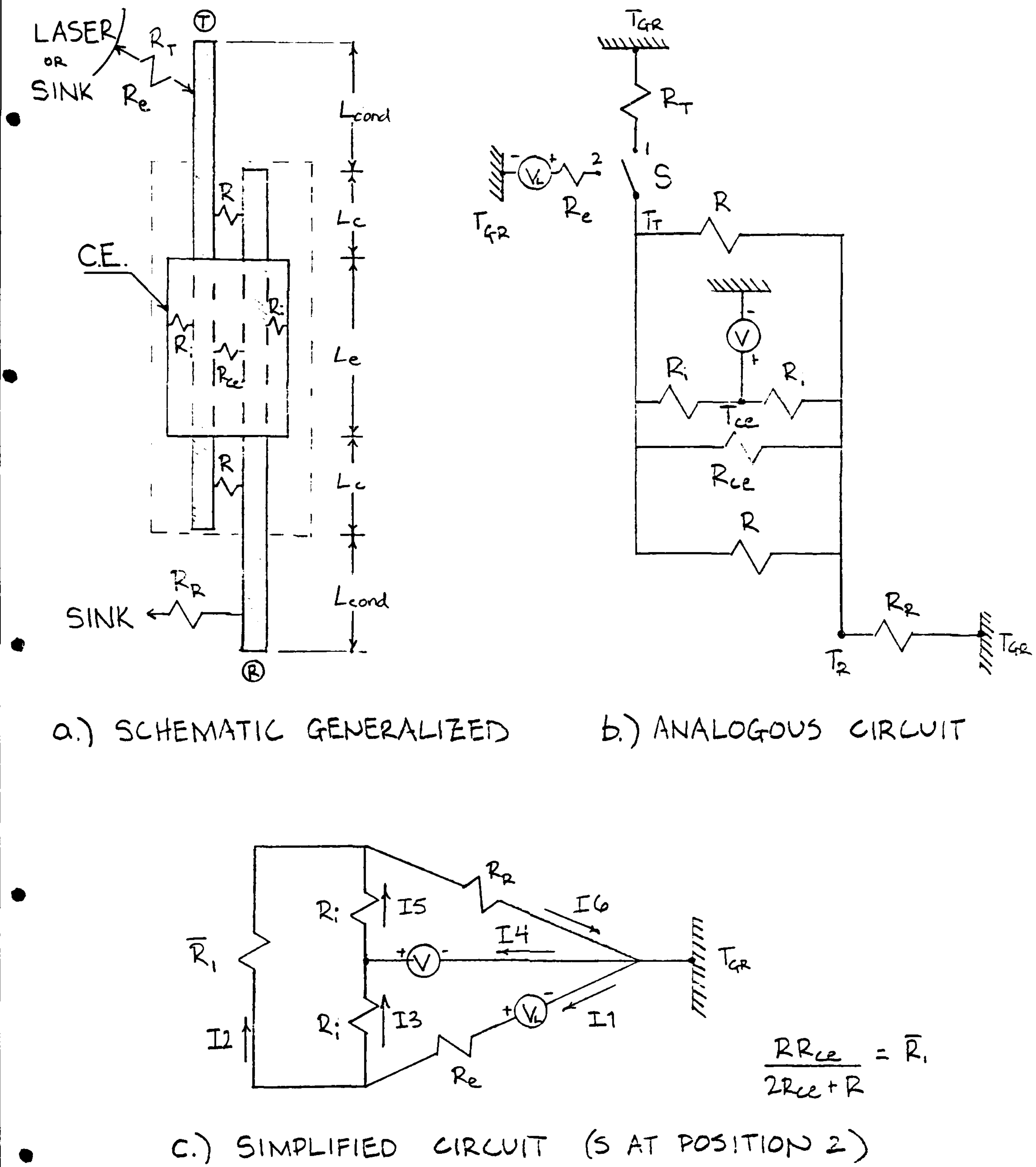

FIGURE 3. COUPLED PIPE CIRCUIT ANALOGY

evaporator (C.E.) and heatpipes
Rce = Resistance to heat exchange between pipes in C.E.
Rr = Resistance to Rescue pipe condenser heat rejection
V = Heat flux source for node Tce in (C.E.)
Vl = Heat flux source for node Tl upon laser heat input
Tt = Temperature of Target pipe
Tr = Temperature of Rescue pipe
Tgr = Ground temperature

For the situation of Figure 3c, equations, using Kirchoff's laws, can be solved simultaneously for the currents (heat fluxes) drawn in the circuit in terms of the system voltages and resistances. A 6X7 matrix was solved to find these relationships and the results are provided in the appendix. For any given voltages (temperature sources) the currents may be determined if the resistances are known.

The resistances themselves may be expressed in terms of the system's component materials and dimensions. For instance,

$R = t_c/(k_c A_c)$ $\quad$ $Rce = t_e/(k_e A_e)$ $\quad$ $Ri = t_i/(k_e A_i)$

and for my case,

$Rr = 1/UA_{cond}$ $\quad$ ($= Rr \cong Re$)

Where; tc = Effective thickness of couple
te = Effective thickness of mat'l between pipes in evaporator
ti = Effective thickness of mat'l between pipes and evaporator walls
kc = Conductivity of couple mat'l
ke = Conductivity of mat'l in evaporator
Ac,e,i = Effective heat flux areas between the pipes at the couple points, C.E., and between the evaporator walls and the pipes respectively

$Ac \propto Dp(Lc)$	Lc = Length of couple
$Ae \propto Dp(Le)$	Le = Length of evaporator
$Ai \propto Me(Le)$	Dp = O.D. of pipe
	Me = Eff. width for C.E.

U = Overall heat transfer coeff. at Rescue pipe condenser

For my case (experimental geometry and properties) the resistances are relatively easy to determine and are listed in the Appendix. These values when plugged into the equations resulting from the matrix operations yield the results presented in Table 1 expressed in terms of V. To varify this solution, observation of Figure 3 shows that for V1=0 and Rr=Re, I1 should equal -I6, as should I2=0, I3=-I5, and I4=I6-I1. Considering the directions of the currents drawn in Figure 3, it is seen that each one of these conditions is met.

An interesting conclusion from the results tabulated above is the fact that I2 is not a function of V, the C.E. heat input.

The heat transport (flux) represented by I2 is that occuring at the coupling locations. In other words, it is the heat transferred from the Target pipe to the Rescue pipe via resistance $\bar{R}1$. $\bar{R}1$ is really divided-up into three resistances connected in parallel, two R's and one Rce, as illustrated in Figure 3b. These resistances are of primary interest as it is hoped to have substantial heat transport capabilities at these locations, especially across R, implying that these values be small by comparison to the other resistances of the system.

After some manipulation the current flow through R and Rce is found to be

$$I_r = \frac{R_{ce}(I2)}{R + 2R_{ce}}$$

(note: 2Ir + Ice = I2)

Expressed in terms of the system dimensions and properties, and recalling that te=tc, and ke=kc,

$$I_r = \frac{L_c(I2)}{L_c + 2L_e} \qquad \text{(E2)}$$

Similarly,

$$I_{ce} = \frac{2L_e(I2)}{L_c + 2L_e} \qquad \text{(E3)}$$

Because I2 is a function of the voltages and resistances of the system, the equations E1 and E2 must be combined with another result to be helpful.

An idea of the percentage of heat transported through a given resistance can be obtained by taking a ratio of the current through that particular resistance to the maximum current flowing in the circuit. This ratio is termed the transport ratio, TR. The maximum current is the total current generated by the voltage sources. Depending upon the voltage values, the maximum current (Imax) may vary. From the values in Table 1 transport ratios for the $\overline{R1}$ resistors have been determined based on Imax and are listed in Table 2.

From Table 2, for the conditions given, it is apparent that the greater C is in magnitude, the more heat will be transferred across the couplings. In general, for given voltages,

$$TR = 2L_c(I2)/(I_{max}(L_c + L_e))$$

For instances of V less than V1 the system behaves desirably - best at V1 much greater than V - yielding higher transport ratios, say X%. This implies that the Rescue pipe will receive X% of the laser heat input. The other 100-X% will be "dumped" in to the central evaporator.

From this development it is possible to estimate the

proportions of heat being transferred through the system. Due to the assumptions made in order to use this resistor/current analysis, the results are strictly qualitative in nature.

To optimize the system a better understanding of the effective dimensions mentioned above (te, tc, etc.) is necessary as is a model accounting for the thermal storage of the system. The results of Table 2 indicate then for a given system with fixed resistances, the greater the laser heat input (V1) the more heat will be transferred through the conduction couplings (I2 through R1 will increase) in proportion to that transferred through other channels. Also, for given laser and central evaporator heat inputs (V1 and V), the greater the length of the coupling to the length of the evaporator, again, the greater the heat transfer through the conduction couplings.

IV. Condensation in Packed Beds

To meet the small temperature change criterion for high heat transfer heat exchangers, system designers are forced to consider change of phase, a constant temperature process, in which to remove or add heat from a working fluid. For use in general energy storage applications, packed beds of spheres containing a phase change material (PCM) have been proposed and constructed in the past with a single-phase fluid circulating through the bed.

In this portion of my research I worked to devise an approach to investigate the possibiliy of heat transfer in packed beds with change of phase of the working fluid as well as that of the PCM encapsulated in the spheres. An experimental method to study the fundamental aspects of this phenomenon will be described below. A brief proposal for support for fabrication and completion of the experiment is provided in the recommendations section.

DESCRIPTION OF APARATUS

A schematic of the proposed experimental aparatus is provided in Figure 4. It consists mainly of a constant inlet pressure and temperature system and a packed bed section with a condensate collection device. The bed can be oriented vertically or horizontally and may accommodate a wide range of sphere sizes. A closed loop system was selected to make available a larger selection of working fluids, most of which are toxic to some degree. A more detailed schematic of the bed is provided in Figure 5. As seen from this figure, the bed is to be broken-up into several packages each representing a psuedo-differential volume of the bed along its axis.

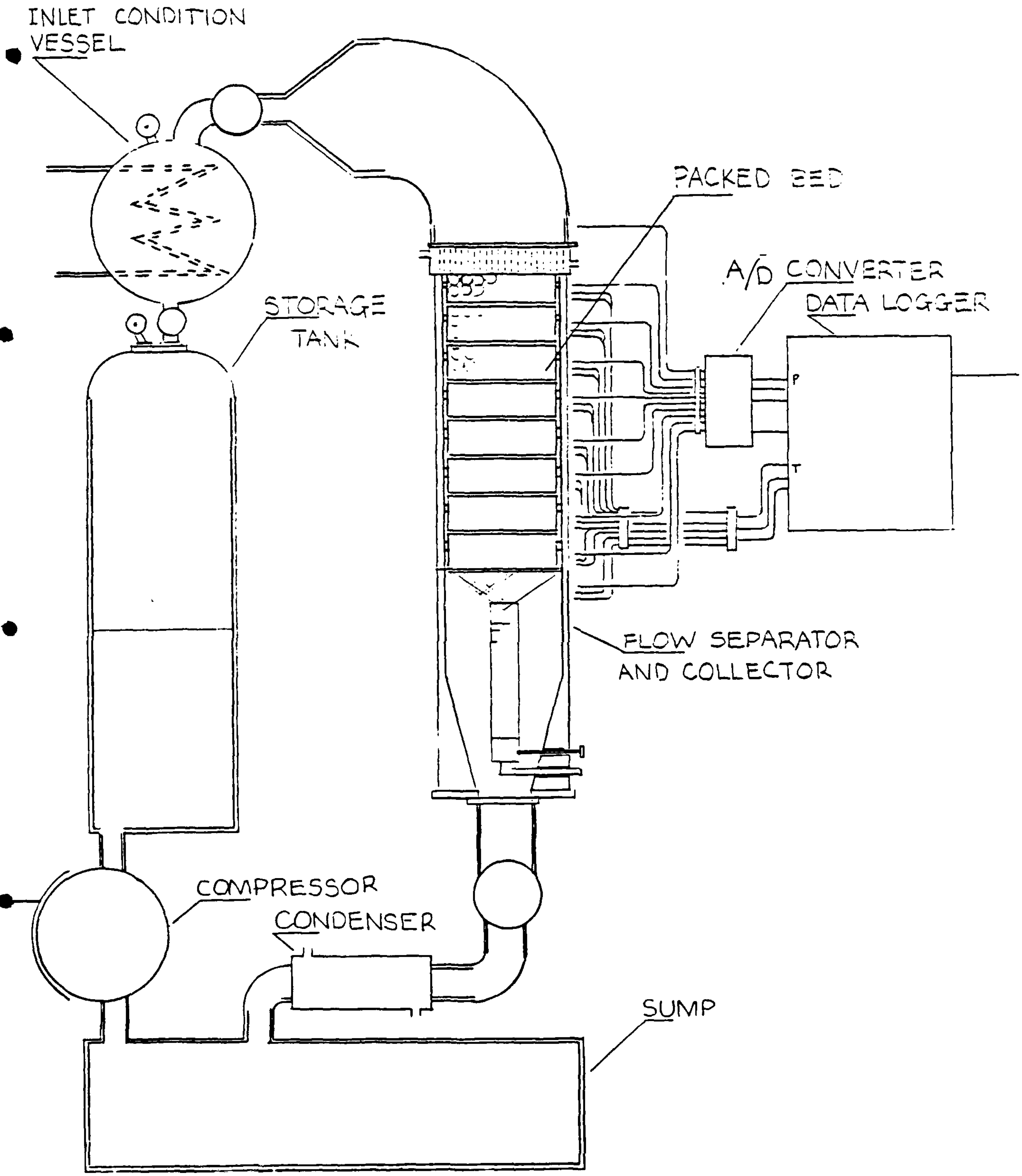

FIGURE 4. SCHEMATIC OF EXPERIMENTAL APPARATUS

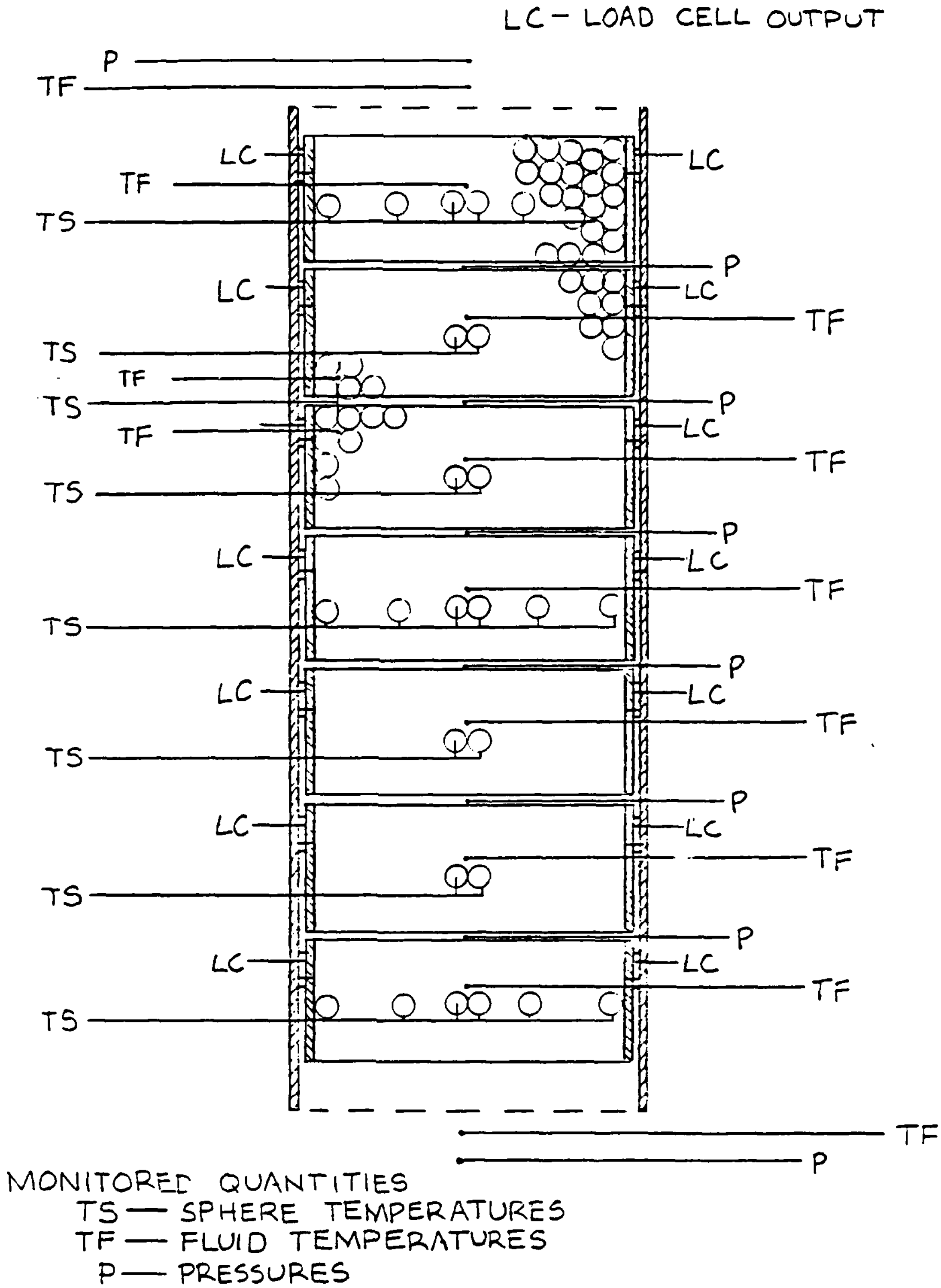

FIGURE 5 DETAIL OF PACKED BED COLUMN

DATA ACQUISITION

CONDENSATION RATE MEASUREMENT. Each package is to be spaced just far enough from the adjacent packages to allow capillary contact of the condensing fluid, but inhibit the spheres of one package to touch the spheres of another. In this way, load cells can be used to accurately measure the amount of condensate in each package with time.

Drip rates out of and/or into the packages can be obtained from the load cell data and the mass balances for the system. Located at the end of the bed is 2-phase flow seperation device for use in the vertical orientation. For the horizontal orientation, grooves milled into the package walls will remove the condensate from the vapor.

TEMPERATURE MEASUREMENTS. The transient energy storage of the bed can be monitored by inserting sensitive thermocouples at the center and wall positions of certain spheres in the bed. If the PCM is different than the encapsulating material, the thermocouples would be attached to both inside and outside walls of the sphere shell. Measured with time, this energy storage data can be used to compute an ideal condensation rate because the energy storage rate is directly proportional to the vapor condensation rate (assuming complete unsensible heat exchange). This value can then be compared with the measured condensation rates.

Temperature measurements will be made axially as shown in Figure 5. Lateral bed temperatures will be monitored as well as local fluid temperatures. Sphere temperature behavior near the package interfaces will be studied to check the effect of the break

in continuity of the bed at these locations.

PRESSURE MEASUREMENTS. Pressure data from the bed is vital for mass and momentum balance equations and are necessary for correcting the bulk values output by the load cells. Probe-type transducers are proposed for these measurements. If 2-phase flow measurement becomes a problem, flow-through manometers may be necessary [3]. The pressure drops expected may be as low as 0.02 ATM, so the instruments will need to be sensitive.

PRELIMINARY WORK ACCOMPLISHED

In addition to design calculations and materials considerations, a small simulatory experiment was conducted using steam and nylon sheres (0.125" mean diam.). Constant pressure inlet conditions were attained by poking a hole in a sealed flask of boiling water. Upon initiation of the vapor flow into the cylindrical bed (0.75" diam., 12" long), vapor-, condensate-, and energy storage-fronts were seen to propagate, at a rate dependent upon the inlet pressure, along the length of the bed. The inlet pressure remained constant (note; condensation is also a constant pressure process) until enough condensate accumulated in the bed to inhibit vapor flow. For the case of condensation in beds of particles, the porosity of the bed is a function of the vapor condensation rate and effective particle diameter.

For small pressure drops across the bed, the three fronts mentioned above practically coincide with each other. For this condition, the downstream side of the front remains at its initial temperature, while the upstream side remains at the inlet temperature of the vapor. This condition was photographed with a

high speed video camera to better visualize the condensation phenomena.

TABLE 1 RESULTING CURRENTS (FCN(V))

CURRENT	$V=.5V_L$	$V=V_L$	$V=2V_L$
$I6 = 16V + .1V_L$	16V	16V	16V
$I5 = 16V - 7V_L$	2.4V	9V	14V
$I4 = 32V - 16V_L$	0	16V	24V
$I3 = 9V_L - 16V$	2.2V	-7V	-11.5V
$I2 = 7V_L$	14V	7V	3.4V
$I1 = 16V_L - 16V$	16V	0	-8V

TABLE 2 TRANSPORT RATIOS

CONDITION	IMAX	TR(RI)*	TR(R)#
$V=.5V_L$	16V	0.85	0.86c
$V=V_L$	16V	0.43	1.70c
$V=2V_L$	24V	0.14	0.28c

* BASED ON CURRENT I2/IMAX

\# $TR(R) = 2L_c(I2)/(L_c+2L_e) = 0.4\,I2$

$C = L_c/(L_c+2L_e)$

V. Recommendations Concerning Heat Pipe Coupling

Time was not available to perform the coupled pipe testing. Due to the predicted enhanced response of the system to condenser heat input the investigation is worth completing.

It is most advisable that if the electrical analogy system evaluation technique be used, the solution listed in the Appendix needs to be reduced. This could be accomplished easily by an order of magnitude method ($Re \gg R1$, etc.), or by analytical methods. Sufficient time was not available for this reduction.

It is also recommended that a transient model be developed since, unfortunately for me, the phenomenon of condenser heat input will be practically entirely transient.

No prediction of system failure is provide by the eletrical analogy. System failure, mainly dryout of the pipes, may be estimated if both heat fluxes (V1 and V) into the coupled system and respective pipe temperatures are known. From the pipe temperatures, limiting heat transport values may be calculated and if found to be less than the heat input to the system dryout of one or both pipes is likely.

Before any experimental work is done for the coupled system, it is mandatory that the transient properties for the pipes be determined (see [2]).

VI. Recommendations Concerning Packed Bed

An energy storage system utilizing a phase change of the working fluid in addition to encapsulated PCM in the bed is appealing in that low changes in bed and fluid temperatures are to

be expected. The increased heat transfer rate associated with a change in phase of the inlet vapor is also an added attraction. In order to implement such a system in practice, a more fundamental understanding must be acquired of condensation in packed beds. There is no apparent literature addressing the subject.

I propose to investigate this topic as my Masters Thesis topic during the 1986-87 academic year. My objectives would be to measure the condensation rate in a packed bed of spheres using a constant pressure step input condition for the entering vapor and to develop a better understanding of the characteristic fronts associated with the condensing flow process. Changes in bed porosity due to condensate accumulating in the bed will also be investigated.

A list of components necessary to carry out the proposed research is provided in the appendix. Included also are their likely costs and a rough total of the expected funding needed to complete the study.

This work, if undertaken, will be unique in that it addresses a fundamental problem, condensation in packed beds, yet is still very directed towards application in the energy storage fields.

FOR BREVITY
* THE APPENDIX IS SAVED FOR THE LAB COPY REPORT

REFERENCES

1. Tilton, D., Johnson, J., Gottschlich, J., Iden, S., "Transient Response of a Liquid Metal Heat Pipe", A Technical Report. AFWAL-TR-86-2031, Aug., 1985.

2. Ambrose, J.H., Chow, L.C., Beam, J.E. "Transient Heat Pipe Response and Rewetting Behavior", AIAA/ASME 4th Joint Thermophysics and Heat Transfer Conference, AIAA-86-1359, June, 1986.

3. Hewitt and Hall-Taylor, Annular Two-Phase Flow, Edinburgh, Scotland,1970, pp. 274-6.

APPENDIX

RESULTS OF MATRIX OPERATIONS

CURRENTS IN TERMS OF SOURCE VOLTAGES AND SYSTEM RESISTANCES

$$I6 = \frac{V_L(R_e + R_i) + R_e(V - V_L) - V_L R_i\left[\dfrac{\bar{R}_1 R_e + \bar{R}_1 R_i + R_i R_e}{\bar{R}_1 R_i + 2R_e R_i + R_e \bar{R}_1}\right]}{\left[\dfrac{R_e^2\left[2R_R R_i + R_R \bar{R}_1 + R_i^2 + R_i \bar{R}_1\right] + R_i^2 R_e\left[R_R + \bar{R}_1\right] + R_R R_i R_e \bar{R}_1}{\left[\bar{R}_1 R_i + 2R_e R_i + R_e \bar{R}_1\right]}\right]}$$

$$I5 = \frac{I6(R_i R_R + R_i R_e + R_i \bar{R}_1 + \bar{R}_1 R_e) - V_L R_i}{\bar{R}_1 R_i + 2R_e R_i + R_e \bar{R}_1}$$

$$I4 = \frac{I6(R_R + R_e + \bar{R}_1) - V_L - \bar{R}_1 I5}{R_e}$$

$$I3 = I5 - I4$$

$$I2 = I6 - I5$$

$$I1 = I2 + I3$$

APPENDIX (CON'T)

RESISTANCE VALUES AND INFO.

$k_c = k_e$ = Copper = 401 W/mK

$A_c = \frac{1}{2}\pi D_p L_c = 0.0025 m^2$

$A_e = \pi D_p L_e = 0.0101 m^2$

$A_i = \frac{1}{2}\pi D_p L_e = 0.0050 m^2$

A_{cond} = RESCUE PIPE CONDENSER AREA = $0.0101 m^2$

U_{1} MEASURED $\cong$ 1600 W/m^2K

$L_e = 2L_c = 0.00159 m$

<u>RESULTS</u>

R = 0.00158 K/W

R_{ce} = 0.000392 K/W

R_i = 0.000784 K/W

R_R = 0.0619 K/W

R_e = 0.0619 K/W

$\bar{R}_1$ = 0.000262 K/W

EXTRA DETAIL FOR TABLE 2

$TR(\bar{R}_1)$ = TRANSFER RATIO OF CURRENT ACROSS $\bar{R}_1$

$TR(R)$ = TRANSFER RATIO ACROSS COUPLINGS ⇒ R RESISTOR

1986 USAF-UES Summer Faculty Research Program/
Graduate Student Summer Support Program

Sponsored by the
Air Force Office of Scientific Research
Conducted by
Universal Energy Systems, Inc.

Final Report

An Investigation of Prospective Media for Thin Film Fabrication of III-V Semiconductors

Prepared by: Steven P. Wicelinski

Academic Rank: Graduate Student

Department and University: Department of Chemistry, Louisiana State University

Research Location: Frank J. Seiler Research Laboratory,
USAF Academy
Colorado Springs, CO 80840-6528

USAF Researcher: Dr. John S. Wilkes

Date: August 24, 1986

Contract No.: F49620-85-C-0013

An Investigation of Prospective Media for Thin Film Fabrication of III-V Semiconductors

by

Steven P. Wicelinski

Abstract

Investigations have been performed to determine the prospects of electrochemically forming layers of the III-V semiconductor gallium arsenide from an $AlCl_3$:1-methyl-3-ethylimidazolium chloride room temperature molten salt. Basic electrochemical studies of gallium and arsenic species in 1-methyl-3-ethylimidazolium chloroaluminate molten salts have been carried out. In addition, electrodeposition experiments under potentiostatic conditions were performed to determine if GaAs films could be produced by codeposition in the $AlCl_3$-MEIC molten salt system. Characterization of novel low temperature melts based on gallium chloride was begun involving differential scanning calorimetry, electrochemical and nuclear magnetic resonance studies.

Acknowledgements

I wish to thank the Air Force Systems Command and the Air Force Office of Scientific Research for sponsorship of my research. In addition, I would like to thank two members of the Frank J. Seiler Research Laboratory staff, Lt Col Chester J. Dymek, Jr. and Dr. John S. Wilkes, for providing me with the assistance and guidance necessary for productive research.

I. Introduction

Currently, I am pursuing a PhD in Chemistry at Louisiana State University. My research involves the prospects of gallium arsenide film formation from room temperature molten salts. Included in this work is the investigation of media suitable for thin film fabrication of III-V semiconductor materials.

One area of research currently being pursued at the Frank J. Seiler Research Laboratory is the Physical Chemistry and Electrochemistry of Room Temperature Molten Salt Systems. The research being carried out at Seiler broadly encompasses the methods and means by which my research is performed. Thus, due to the similarity in molten salt chemistry and equipment availability, I was provided with the opportunity to perform research at the Seiler Lab.

II. Obectives of the Research Effort

The objective of the first project area involved investigating the prospects of electrochemically forming layers of gallium arsenide from a room temperature $AlCl_3$:MEIC melt. This effort involved:

1. The study of the electrochemistry of gallium and arsenic species in the $AlCl_3$:MEIC molten salt system.
2. Performing electrodeposition experiments under potentiostatic conditions to determine if GaAs films could be produced by codeposition in the $AlCl_3$-MEIC molten salt system.

Characterization of low temperature chlorogallate molten salts systems was the objective of the second project area of my research. This research involved:

1. The study of the electrochemistry of $GaCl_3$-BPC and $GaCl_3$-MEIC molten salt systems.
2. Performing preliminary physical characterizations of the chlorogallate melts.

III. Prospects for GaAs Film Formation

All electrochemical experiments were performed in a drybox with a purified helium atmosphere. The procedure used for the purification of $AlCl_3$ was similar to that described by Gale and Osteryoung (1). Procedures used for the synthesis and purification of 1-methyl-3-ethylimidazolium chloride were similar to those described by Wilkes et al. (2). Working electrodes used for voltammetry were a platinum button electrode sealed in glass (area = 0.810 mm^2) and a tungsten electrode (area = 7.06 mm^2). Molybdenum foil served as the counter electrode and the reference electrode consisted of a high purity, coiled Al wire immersed in a N=0.6 $AlCl_3$-MEIC melt contained within a glass fritted tube. Arsenic trichloride (Alfa, 99.999%) and gallium trichloride (Aesar, 99.999%) were used as received. Voltammetric investigations were made with a PAR Model 175 Universal Programmer and a PAR Model 173 Potentiostat/Galvanostat.

Cyclic voltammetric studies have been performed in the $AlCl_3$-MEIC melts at various melt compositions containing Ga(III). Ga(III), added

as $GaCl_3$ to the $AlCl_3$-MEIC melts, exhibits similar behavior as when added to $AlCl_3$-BPC melts (3). Two poorly defined reduction waves, Ga(III) to Ga(I) reduction followed by Ga(I) to Ga(0) reduction, occur in the neutral to acidic regime. However, an oxidation peak at approximately +1.35V vs Al (N=0.6) reference which occurs in the acidic $AlCl_3$-MEIC melts is sharper than the oxidation peak in the corresponding $AlCl_3$-BPC melts. Glassy carbon, tungsten and platinum working electrodes were employed with the best response being exhibited by platinum.

Next, As(III) added to the chloroaluminate melt as $AsCl_3$ was investigated by voltammetry in the chloroaluminate melt. In the acidic regime ($N > .5$), a broad but well resolved reduction peak occurs at approximately +0.5V vs Al/Al(III) reference. On the reverse scan, a peak at approximately +1.7V can be seen and is presumably the arsenic stripping peak. The electrochemistry of arsenic becomes more distinctive with increasing basicity. At $N \sim 0.5$ $AlCl_3$-MEIC three oxidation waves occur at ~0.7V, ~1.3V, and ~1.6V. On the reverse scan, three well resolved reduction waves occur at ~1.5V, ~0.4V, and ~-0.25V. Preliminary evidence indicates that the chlorocomplexes of the intermediate valence states of arsenic are stable in the neutral region.

Prior to electrolysis of As(III) and Ga(III) mixtures, the electrochemistry of these species was examined by cyclic voltammetry. In view of the slow kinetics for Ga(III) reduction relative to As(III) reduction, a five to ten-fold excess of $GaCl_3$ over $AsCl_3$ was used. Most studies involved investigating the mixture of As(III) and Ga(III)

in neutral $AlCl_3$-MEIC melts. The cyclic voltammograms obtained from these studies are quite complex. Before proper conclusions may be drawn, it appears that other electrochemical methods such as normal pulse polarography, coulometry, and rotating disc electrode studies will be required. Electrodeposition experiments were performed under potentiostatic conditions at room temperature in neutral $AlCl_3$-MEIC melts. Several films were grown on Pt foils at various potentials with current densities ranging from 1 - 10mA/cm^2. These codeposition experiments were performed in melts containing 20 to 40 microliters of $AsCl_3$ with the Ga(III) concentration being at least five times greater than the As(III) concentration. It is felt that the increased electrochemical window of neutral $AlCl_3$-MEIC melts will minimize any possible Al contamination problems. Characterization of these electrodeposits using various analytical methods such as X-ray fluorescence and X-ray diffraction is currently in progress. Potentiostatically controlled reduction of mixtures of As(III) and Ga(III) appears promising, but a comment on the results is dependent on the ongoing analyses.

IV. Low Temperature Chlorogallate Molten Salt Systems

During research to find media suitable for thin film fabrication of III-V semiconductors (3), some mixtures of gallium trichloride and 1-butylpyridinium chloride (BPC) or 1-methyl-3-ethylimidazolium chloride (MEIC) have been found to be liquid at room temperature (4). Chlorogallate melts were prepared in a helium filled dry box with a total air and water content of less than 15 ppm. Slow gradual addition

of gallium trichloride to either BPC or MEIC, recommended to avoid melt decomposition, produces melts that are clear colorless liquids.

The compositions of these melts may be expressed as the mole fraction, N, of $GaCl_3$. $GaCl_3$-MEIC melts in the composition range of N~0.3 to N~0.8 are liquid at room temperature. Within the composition range $0.3 < N < 0.7$, several $GaCl_3$-BPC melt compositions in the acidic regime ($N > 0.5$) and some in the basic regime ($N < 0.5$) are liquid at room temperature. However, certain melt compositions near the neutral region (N~0.5) are not liquid until approximately 45°C.

Differential Scanning Calorimetry studies, employing a Perkin Elmer DSC-7, were performed on several compositions of the two chlorogallate melt systems. $GaCl_3$-MEIC melt composition from N~0.28 to N~0.84 and $GaCl_3$-BPC melt compositions from N~0.32 to N~0.68 were analyzed by DSC. Samples of various melt compositions were placed into stainless steel pans, weighed (10-40 mg sample quantities) and sealed in the dry box. DSC scans were usually performed at rates of 5°C/min and 10°C/min from -65°C to +125°C. Except in a few cases, the DSC investigations yielded information concerning a glass transition or a melting point for the various samples. Selected melting point data are provided in Table 1 for the two chlorogallate melt systems. In addition, the DSC studies have shown the melts to be stable, exhibiting no sign of decomposition, up to at least 125°C.

TABLE 1

Melting and Glass Transition Temperatures

Melt System	N	t, °C
$GaCl_3$-BPC	0.30	30.7
$GaCl_3$-BPC	0.40	30.5
$GaCl_3$-BPC	0.50	46.4
$GaCl_3$-BPC	0.60	-1.5
$GaCl_3$-BPC	0.68	5.7*
$GaCl_3$-MEIC	0.30	21.4
$GaCl_3$-MEIC	0.40	5.5
$GaCl_3$-MEIC	0.50	14.5
$GaCl_3$-MEIC	0.60	-15.7*
$GaCl_3$-MEIC	0.70	< -50
$GaCl_3$-MEIC	0.80	20.7*

*Glass Transition

Preliminary electrochemical work has been performed on the chlorogallate molten salt systems. Voltammetric investigations were made with a PAR Model 175 Universal Programmer and a PAR Model 173 Potentiostat/Galvanostat. The electrochemical windows have been obtained by cyclic voltammetry for the $GaCl_3$-BPC melts and the $GaCl_3$-MEIC melts. In the acidic regime of these melts, it is reasonable to state that the anodic limits correspond to chlorine evolution while the cathodic limits correspond to gallium deposition. However, in the basic regime of these melts, the anodic limit appears to correspond to the electrooxidation of chloride ions, while the cathodic limit appears to correspond to the electroreduction of the respective organic cation. Similar to neutral $GaCl_3$-RCl melts also exhibit wide electrochemical windows (~3.7V for N=0.5 $GaCl_3$-BPC and ~4.0V for N=0.5 $GaCl_3$-MEIC melts respectively).

Nuclear magnetic resonance studies utilizing ^{69}Ga and ^{71}Ga NMR have begun on these melts. Though in the early stages, the gallium NMR should provide valuable information about the chemical species present in the various melt compositions. Since only preliminary NMR results of these melts are available, it wouid be inappropriate to draw any conclusions at this time.

V. Recommendations

1. The electrochemistry of gallium is fairly straight-forward in chloroaluminate melts. However, the electrochemistry of arsenic species in the chloroaluminate melts can be very complex. This in part

explains the complexity of the electrochemistry of mixtures of As(III) and Ga(III) in the chloroaluminate melts. To complete an analysis of the electrochemistry of these species, coulometry, normal pulse polarography and rotating disc electrodes studies should be performed.

2. Suggestions concerning the electrodeposition experiments depend on the forth-coming results of the film analyses. Once a suitable potential and melt composition are determined, optimization of film quality may be addressed. It may be necessary to perform the electrodeposition experiments at a higher temperature while employing some innovative pulsing sequences during the process. Film analysis employing several surface analytical techniques is recommended, though not always available.

3. More work to determine the usefulness of the chlorogallate melts as solvents for electrochemical and spectroscopic studies is required. Various studies need to be performed to determine their suitability for thin film fabrication of III-V semiconductor materials.

Determination of the density and viscosity of the various melt compositions of the chlorogallate melts systems is strongly recommended.

The $GaCl_3$-MEIC molten salt system requires some additional melting point/glass transition investigation around the N~.35 and N~.65 melt compositions to complete the phase diagram for the system. Similarly, the $GaCl_3$-BPC system requires further investigation, particularly more visual confirmation to complete its phase diagram.

4. Continuation of the NMR studies of the chlorogallate melts is also recommended. In order to better understand the melt structure, it is advisable to examine the anion and cation interactions by NMR. Valuable information concerning these chlorogallate melts can be obtained from ^{1}H, ^{69}Ga and ^{71}Ga NMR experiments.

References

1. R. J. Gale and R. A. Osteryoung, "Molten Salt Techniques," Vol. 1, R. J. Gale and D. G. Lovering (eds.), Plenum Press, New York (1983), p. 55.

2. J. S. Wilkes, J. A. Levisky, R. A. Wilson, and C. L. Hussey, Inorg. Chem., 21, 1263 (1982).

3. S. P. Wicelinski and R. J. Gale, "GaAs Film Formation from Low Temperature Chloroaluminate Melts," Proc. 5th Int. Symp. on Molten Salts, Vol. 86-1, The Electrochemical Society, Inc. (1986), p. 144.

4. S. P. Wicelinski, R. J. Gale, and J. S. Wilkes, J. Electrochem. Soc., submitted for publication.

5. M. Lipstajn and R. A. Osteryoung, J. Electrochem. Soc., 130, 1968 (1983).

1986 USAF-UES SUMMER FACULTY RESEARCH PROGRAM/
GRADUATE STUDENT SUMMER SUPPORT PROGRAM

Sponsored by the

AIR FORCE OFFICE OF SCIENTIFIC RESEARCH

Conducted by

Universal Energy Systems, Inc.

FINAL REPORT

Study of Oxygen-Related Defects in Electron-Irradiated, Boron-doped Silicon

Prepared by: Celeste Benay Williams

Academic Rank: Graduate Research Assistant

Department and University: Dept. of Electrical Engineering, Auburn University

Research location: Rome Air Development Center, Solid State Sciences Division/ Radiation Harden Electronic Technology Branch, RADC/ESR

USAF Researcher: Dr. Peter J. Drevinsky

Date: September 5, 1986.

Contract No: F49620-85-C-0013

Study of Oxygen-Related Defects in Electron-Irradiated, Boron-doped Silicon

by

Celeste Benay Williams

ABSTRACT

Radiation-induced defects in electron-irradiated, boron-doped silicon have been studied by means of a capacitance transient technique. The technique is known as Deep Level Transient Spectroscopy, DLTS. The DLTS spectra for the sample were obtained and analyzed to find the energy levels and concentrations of deep defects introduced into the energy gap region of a semiconductor. Samples were fabricated by ion implantation tecniques to determine the role of oxygen concentration in defect formation in boron-doped silicon.

I. Introduction

My graduate work, at Auburn University, involves a study of silicon light emitters and the role of process-induced crystal defects on luminescence. Hence, my assignment to the Radiation Harden Electronic Technolog branch, RADC/ESR, which investigated the effects and formation of induced defects, was quite advantageous.

II. Objectives of the Research Effort

The overall objective of the investigative research involves the study of the effects and nature of radiation-induced crystal defects in semiconductor devices. The detection and study of defects, due to displacement damage, is carried out by using capacitance transient techniques, specifically by Deep Level Transient Spectroscopy (DLTS) [1-5]. With this method, an investigation into the role of oxygen in the formation of radiation-induced defects is studied.

III. History

It is important to notice that defect states process- or radiation-induced, can have deep energy levels in the energy gap region of a semiconductor and play an important role in device performance [6-7]. At such levels, carrier recombination or generation and trapping are dominating processes (see Fig. 1). For example, such defects can greatly alter the reverse I-V characteristics of a diode by increasing the reverse saturation current or the defect can degrade the

luminescence of light emitting diodes by increasing the minority carrier times through carrier trapping. Hence, the study of the nature of such defects is very helpful in the selection of growth and fabrication processes in order to optimize device characteristics. Most importantly, the devices used in space technology are exposed to radiation which can produce performance-altering defects.

Defect levels in the space charge or depletion region of a junction, may be detected by their influence on either the junction current (TSC) or the capacitance (DLTS). A modulating reverse bias that opens and closes the depletion region produces a capacitance transient. As the reverse bias is suddenly turned off and immediately reapplied, the transient is produced when the defect levels in the depletion region emit charge carriers. This transient can be readily detected, see Fig. 2. As the bias opens the depletion region, the carrier traps, which are filled when the region collapsed, will empty at a rate dependent on the temperature and the energy level [1-2]. This rate is the carrier emission rate, e_n or e_p. Hence, the exponential capacitance decays can be detected.

The DLTS method is a useful technique to display the time constant of the decaying capacitance signal by the introduction of a rate window concept [1],[8]. The idea of the rate window is that if the capacitance transient

produces a maximum signal at a selected decay rate, then a DLTS maximum signal is obtained when the decay rate passes through the selected window rate. By a slow scan of the sample temperature (i.e., a change in the thermal carrier emission rate from a level) the capacitance decay rate is varied and a DLTS peak signal obtained when the decay rate is within range of the window rate. There are a variety of ways for implementing a rate window. However, the one used involved a lock-in amplifier. For this technique, a maximum DLTS output is obtained when the reciprocal of the capacitance decay time constant approximates the lock-in frequency of the amplifier [1],[8]. That is, the rate window is determined by the choice of the lock-in operating frequency. The DLTS spectra are capable of providing information about the energy level, concentration, and capture cross section of the defects (see Appendix). Also, it can distinguish between minority and majority carrier levels. A spectrum signal in the +y direction represents a majority carrier trap, which is found by a reverse bias. A forward bias injects minority carriers (as well as majority carriers) into the collapsed depletion region. Thus, minority carrier emission is observed from minority traps. The DLTS signal is then in the -y direction [3]. The DLTS sensitivity typically allows one to detect concentrations of about 10^{-4} times the dopant concentration.

The typical DLTS spectrum for 1-MeV, electron-irradiated boron doped silicon using n+ - p junctions is given in Figs. 3a-c, taken from Refs. 5,9, and 10. The p side is the lighter doped side so that the depletion region extends mostly into the p region. Hence, the observed defects are in the boron doped region. The various induced defects involve: point defects, boron (a principal dopant), carbon and oxygen (both unintentional impurity contaminants), and the interactions of these particles. The identifying labels for the DLTS spectra peaks may differ for various authors, but all the peaks are in agreement. The nomenclature followed is that given in Ref. 5, where the majority carrier traps are H1, H2, and H3. E1 represents a minority carrier trapping defect. Kimerling [9-10] and others [5],[11-12] have provided identifications of the defect states derived from EPR and IR studies. The H1 state is the divacancy (V-V) defect, H2 is a carbon interstitial defect (Ci), and H3 is described also as a carbon-related defect, given as either a carbon interstitial and substitutional complex (Ci-Cs) [10] or a carbon-oxygen-vacancy (C-O-V) structure [12]. Ref. 5 observes that in low oxygen content samples (i.e., float zone), the H3 defect is not present. Hence, one proposed structure is C-O-V because of the dependency on oxygen. Kimerling [9], however, observed no involvement of an O-V component in the formation of H3. See Fig. 4.

"CsCi [H(0.36)]. ... the constancy of E(0.13)(C-V) in the annealing data [in Fig. 4] shows clearly that this state is not a product of a Ci + (V-O) reaction. The activation energy (0.71) and frequency factor ...of [data] are consistent with Ci diffusion to Cs. The CiCs assignment remains favourable.... " Ref. 9.

Thus, Kimerling's studies lead to the support of the Ci-Cs structure.

The E1 structure is of special interest as an induced defect because it is a minority carrier trap. It is observed to be dependent on a major dopant and contaminant impurities, and it is possibly related to reverse anneal effects [4-5],[10-13].

Annealing studies of 1-MeV electron-irradiated silicon samples show that the E1 defect anneals out at about 200C [4],[10]. However, at the same time, a majority carrier trap (H4) appears (see Fig. 5, taken from Refs. 4 and 5). Mooney and co-workers [12] observed identical activation energies for the anneal out and the grow in of E1 and H4, respectively. It has been found that H4 always appears in samples that exhibited E1 [5] and Mooney et al observed that H4 does not appear in samples in which E1 is not observed. Drevinsky and DeAngelis [4-5] observed that the H4 defect formation is independent of oxygen concentration in annealing studies in which the H4 defect is observed, both in float-zone (oxygen-lean) and Czochralski (oxygen rich) samples. Also, Drevinsky and DeAngelis observed that the production of the H4 majority trap is independent of E1

in the float zone samples. However, they did observe H4 whenever E1 appeared.

The E1 structure is reported to be a boron-related defect that forms according to the proposed mechanism diagram used in Fig. 6 [5]. The structure results from an interaction of boron and oxygen interstitials (Bi-Oi) [5],[12]. A study of the role of boron in the production of the E1 minority trap revealed a linear dependence of E1 formation rate with the boron concentration [5],[1...]. (See Ref. 5). In observing the dependence of E1 with boron, Drevinsky and DeAngelis noticed a dependence of E1 on the oxygen concentration as well [5]. The E1 production rate was seen to increase in Czochralski (oxygen-rich) samples, and to sharply decrease as the oxygen concentration was reduced. From the comparison of E1 introduction rates in float-zone, modified (i.e., oxygen-introduced) float-zone, and Czochralski samples, a clear indication of the oxygen involvement in the E1 structure was observed [5].

An investigation of the dependence of E1 on oxygen concentration is to be carried out using silicon samples fabricated with varying oxygen content.

IV. Experimental Procedures

Several types of p-type , boron-doped silicon samples with controlled oxygen concentrations were used for DLTS studies: (1) float-zone, (2) Czochralski, and (3) magnetically-grown Czochralski (MCZ). Sample TYPE 1

was used as such for low-oxygen content (about $10^{16}/cm^3$). Some of these were in-diffused with ^{18}O to increase the intrinsic oxygen content. ^{18}O was used, instead of ^{16}O, to permit a SIMS analysis in order to obtain the oxygen content and profiles (i.e., concentration per depth). Also, ^{18}O could be readily identified from the background concentration of naturally-occurring oxygen. Sample TYPE 2 contained high oxygen concentrations ($^{18}O/cm^3$ range) in as-grown silicon. Sample TYPE 3 involved magnetically grown crystals which contained a radial oxygen gradient in the ingot, with higher concentrations in the center and lower toward the edge. With this combination of samples, oxygen content ranged from about 10^{16} to $10^{18}/cm^3$.

The p-type material, of 15 mils thickness, had a front ion implantation of $^{31}P^+$ and a back implant of $^{11}B^+$ to create the n^+-p-p^+ junction. A photolithography technique was used to control diode fabrication and geometry. Mesa areas of about 7.5×10^{-3} cm^2 were formed. Photolithography forms masking patterns that open or block openings to the silicon surface. The metallization mask provided a gold dot contact on the mesa and a Ti-Pd-Ag contact to the back p+ layer. The implanting method allowed no oxidation steps that could alter the oxygen content. The implants were annealed in a nitrogen ambient.

The wafers with mesas were diced into square chips of 0.25 cm on edge, with each chip containing a single diode. The chips were affixed to TO-5 headers using an electrically-conductive silver epoxy, Epo-Tek H31 (Epoxy Technology, Inc., Billerica, Ma.), which was cured at 80C for 90 minutes. The contacts were bonded ultrasonically with 1-mil aluminum wire, with two wires to the mesa contact for redundancy. Thus, the mounted DLTS samples consisted of three leads, two to the n+ layer and the grounded lead to the p+ contact.

The samples are irradiated under ambient conditions with 1-MeV electrons to fluences of 2*1015 - $1*10^{16}$ electrons/cm^2 on the Dynamitron accelerator. The samples are kept in dry-ice until ready for DLTS measurements, to prevent unwanted annealing.

V. Results/Discussion

Typical DLTS runs on electron- irradiated, Boron-doped samples are shown in Figs. 7-8. The H1 and H3 defects are clearly seen (Fig. 7). The rate window (lock-in amplifier frequency) is set at 5 Hz with a detector sensitivity of 5 mV. The E1 defect is clearly observed in Fig. 8 in a sample where H2 has been annealed out in order to remove the influence of H2 on the amplitude of E1. Using the equations shown in the Appendix, one obtains the data given in Table 1 from the DLTS peaks. The carrier trap energy levels given in the table are in good agreement with those found in the

literature. To obtain better values, Arrhenius plots, in which the rate window is varied resulting in a shift of the signal peaks to give several data points, could be plotted [1]. However, the lineshape calculations [15] give good approximations as long as the shape of the peak is clean and distinct. Note, however, that the lineshape equations may be modified to include slightly distorted peaks. See Appendix.

The DLTS spectra are obtained with an x-y chart recorder with the temperature x-axis zeroed at a specific baseline point. This direction was given a sensitivity of 0.25 mV per cm. The temperature is recorded by a copper-constantan thermocouple setup so that the mV readings can be translated into temperature, using a standard thermocouple chart. The sample was cooled down to about 88K and slowly warmed up by a cartridge heater to room temperature. The baselines for both scans are pretty much level. However, there is a baseline drift for the E1 peak. This drift alters the height of the DLTS signal. However, since the height of the signal gives the trap concentration (see Appendix and Table 1), there is only a difference of about 5 to 10% in the concentration for typical drifts. This particular drift introduces an error of less than 5% in the E1 concentration.

To obtain the E1 signal, the junction was biased from -3.5 to +0.75 volts (note the depletion widths,

given in Table 2). The slight forward bias caused the injection of electron minority carriers into the p region of the collapsed depletion region. The carriers were trapped by the defect and then emitted during the reverse bias phase of the pulse. In order to obtain the majority carrier defects, the junction was biased from -3.5 to -0.5 volts. In order to determine the uniformity of the defect throughout the p region examined, several scans can be made with the reverse bias being increased, step-wised, just below the diode breakdown voltage to widen the depletion width. A pulse width of 100 usec was used throughout and was found to be sufficient to allow carrier trapping.

VI. Summary/Recommendations

Participation in the study has provided insight into the usefulness of DLTS in detecting defects in semiconductor materials and devices. The initial experiments on the role of oxygen in samples containing typical oxygen concentrations of float-zone and Czochralski-grown silicon, have been completed. The investigation is continuing at RADC/ESR (Solid State Sciences Division) with a more detailed examination of additional DLTS samples containing known concentrations of oxygen.

REFERENCES

1. Miller, G.L., Lang, D.V., and L.C. Kimerling, "Capacitance Transient Spectroscopy," Ann. Rev. Mater. Sci., (1977) 377-448.

2. Lang, D.V., "Space-Charge Spectroscopy in Semiconductors," J. Appl. Phys. 45, (1974) 3023-30.

3. Drevinsky, P.J., Schott, J.T., and H.M. DeAngelis, "Detection of Processing and Radiation Induced Defects in Solar Cells by Transient Capacitance Spectroscopy," 13th IEEE Photovoltaic Specialists Conf., (1978) 1232-37.

4. Drevinsky, P.J., and H.M. DeAngelis, "Defect Behavior in Electron-Irradiated Boron- and Gallium-Doped Silicon," NASA Conf. Publ. 2256, (1982) 145-56.

5. Drevinsky, P.J., and H.M. DeAngelis, "Interactions of Interstitial Silicon with (B_s) and (O_i) in Electron-Iraddiated Silicon," Proceedings of 13th International Conf. Defects on Semiconductors, Coronado, CA., (1984) 807-13.

6. Oldham, W.G., and S.S. Naik, "Admittance of P-N Junctions Containing Traps," Sol. State Elect., 15, (1972) 1085-96.

7. Corbett, J.W., and G.D. Watkins, Radiation Effects in Semiconductors, New York, Gordon and Breach Science Publ., 1971.

8. Chupa, K.L., and S.R. Das, Thin Film Solar Cells, New York, Plenum Press, 1983.

9. Kimerling, L.C., Blood, P., and W.M. Gibson, "Defect

States in Proton-Bombarded Silicon at T<300K," *Inst. Phys. Conf. Ser. 46* chap. 3, (1979) 273-80.

10. Kimerling, L.C., "Defect States in Electron-Bombarded Silicon Capacitance Transient Analysis," *Conf. Ser. 31* Chap.2, (1977) 221-30.

11. Lee, Y., Cheng, J., Mooney, P.M., and J.W. Corbett, "Carbon Interstitial in Electron-Irradiated Silicon," *Sol. State. Comm.* 21, (1977) 109-11.

12. Mooney, P.M., Cheng, J., Suli, M., Gerson, J.D., and J.W. Corbett, "Defect Energy Levels in Boron-Doped Silicon Irradiated with 1-MeV Electrons," *Phys. Rev. B* 15, (1977) 3836-43.

13. Aleksandrov, L.N., Zotov, M., Stras, V., and B. Surin, "Investigation of Radiation Defects in Neutron Irradiated Silicon," *Sov. Phys. Semi.* 18, (1984) 42-44.

14. Kimerling, L.C., "On the Role of Defects Charge State in the Stability of Point Defects in Silicon," *Sol. State Comm.* 16, (1975) 171-74.

15. Schott, J.P., "Lineshape Analysis for Capacitance Transient Spectra," Rome Air Development Center, Solid State Sciences Division, Hanscom AFB, MA. Report #RADC-TR-79-258, September 1979.

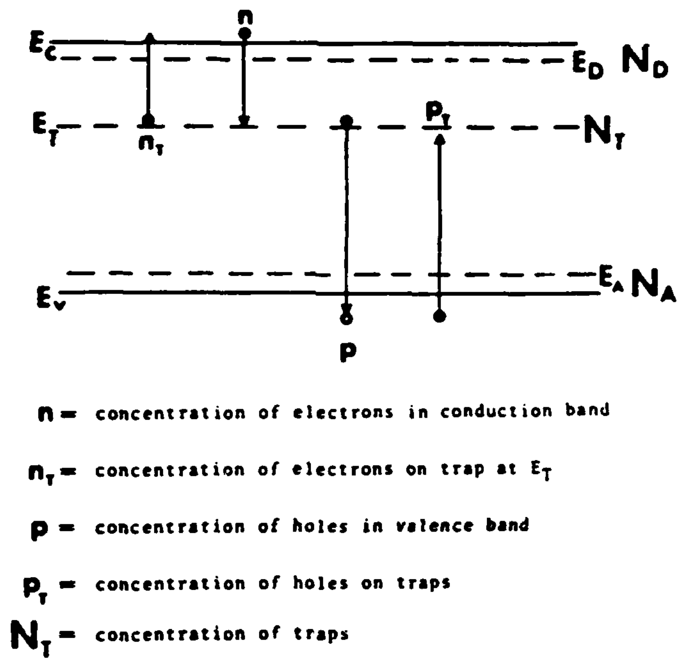

Fig. 1. Carrier capture and emission processes at defect level.

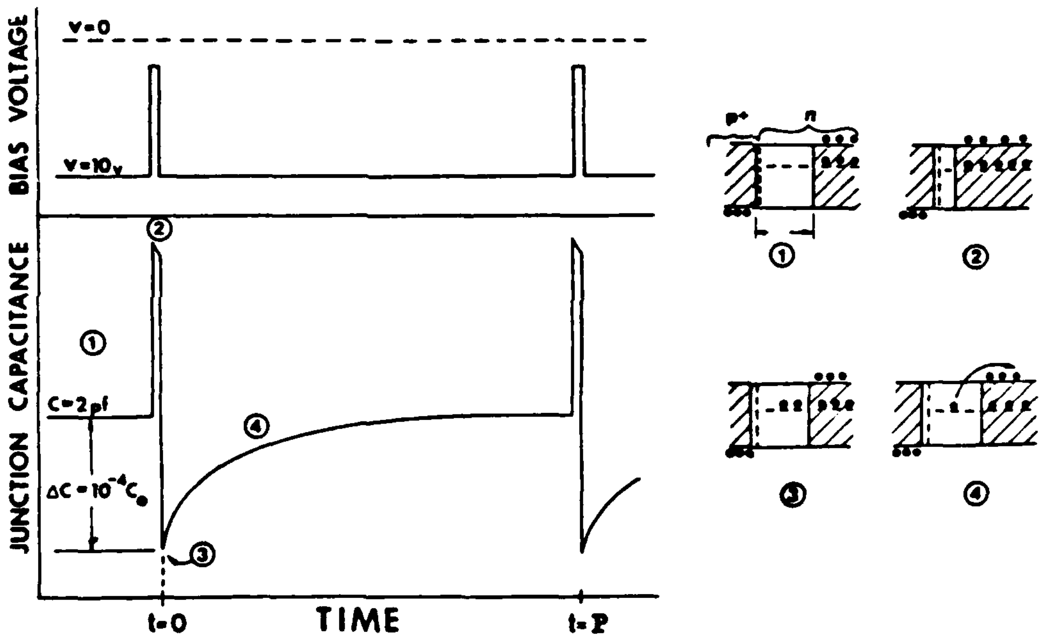

Fig. 2. Diode bias and capacitance transient as function of time.

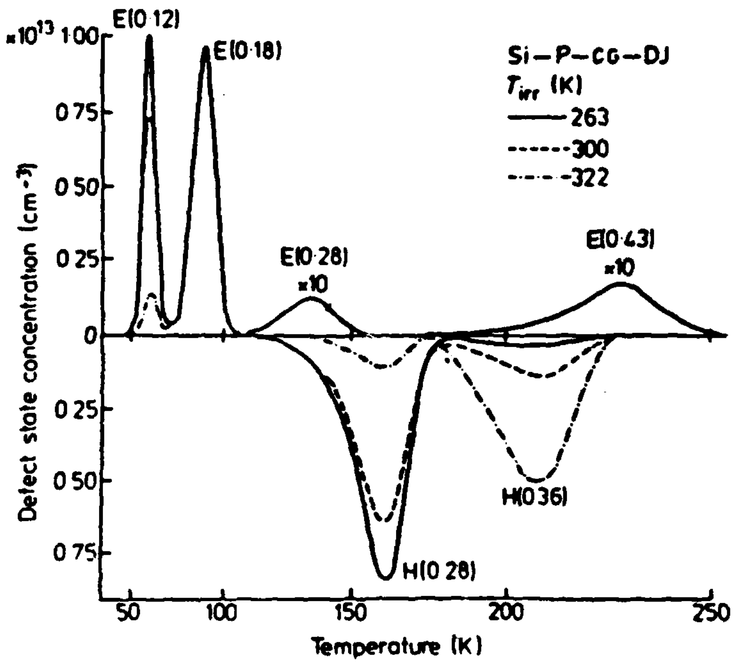

Fig. 4. Anneal of DLTS spectra of another irradiated sample taken from Ref. 9.

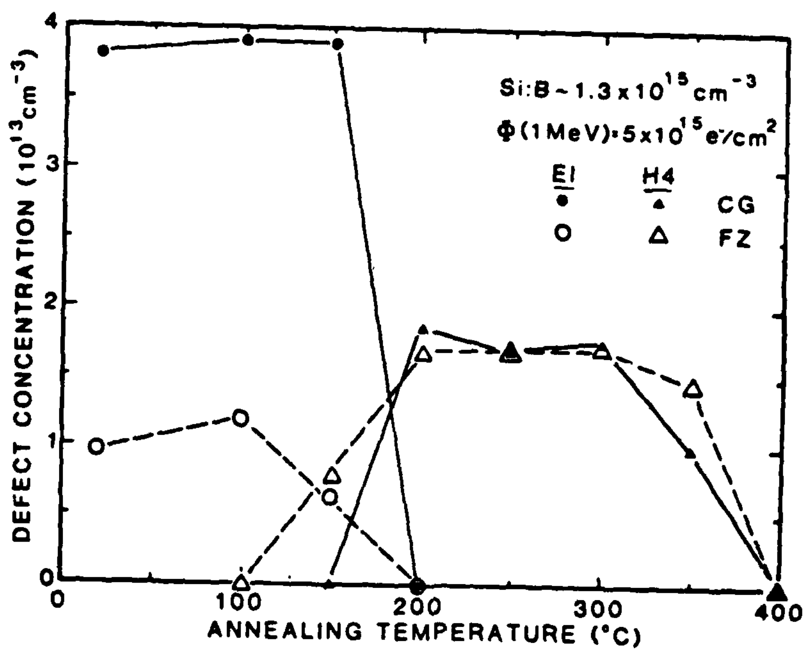

Fig. 5. Typical isochronal anneal of E1 and grow-in of H4 of electron-irradiated float zone and crucible-grown silicon [Refs. 4-5].

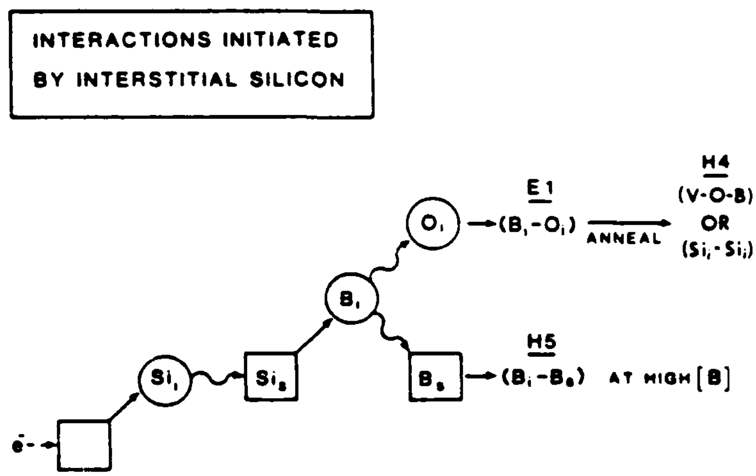

Fig. 6. Proposed interactions initiated by interstitial silicon [Ref.5].

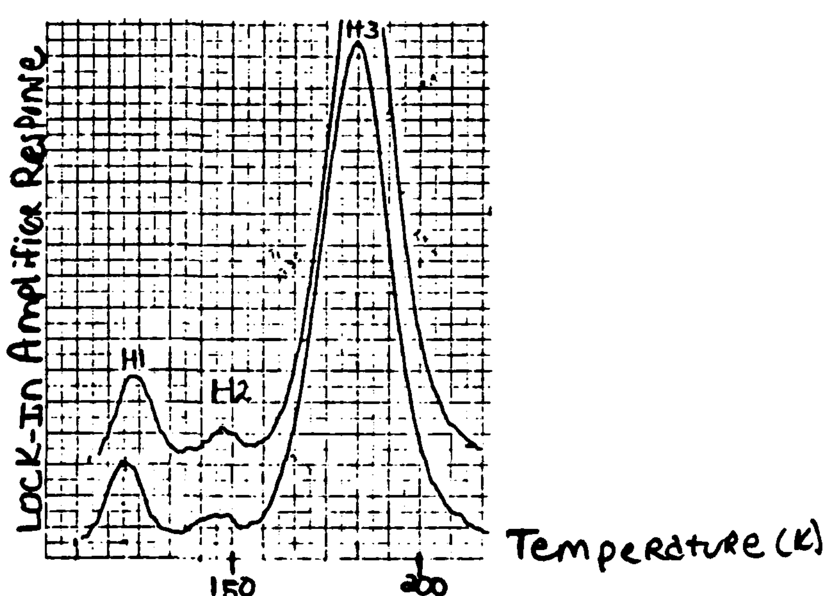

Fig. 7. DLTS spectra of electron-irradiated silicon showing majority carrier traps H1, H2, and H3.

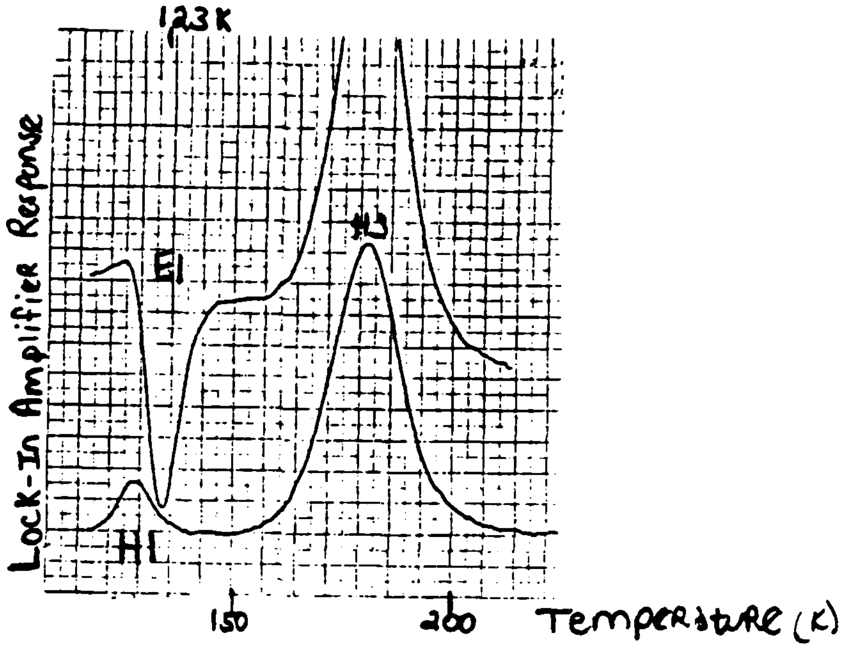

Fig. 8. DLTS spectra of electron-irradiated silicon, showing minority carrier trap, E1.

TABLE 1. Defect Energy Levels and Concentrations.

	Energy (eV)	Trap concentration cm^{-3}
H1	0.16	1.0×10^{14}
H2	0.28	5.0×10^{12}
H3	0.35	9.0×10^{13}
E1	0.29	1.1×10^{13}

TABLE 2. Depletion Widths o Typical Bias Setting (Boron Concentration of $10^{15}/cm^{3}$)

Applied Bias (volts)	Depletion Width (uM)
-3.5 -> -0.5	2.37 -> 1.30
-3.5 -> +0.5	2.37 -> 0.65
-3.5 -> +0.75	2.37 -> 0.36

APPENDIX

1. Analysis of DLTS spectra peaks: (SEE Ref. 15)

   a. ΔE(eV) from lineshape of peaks:

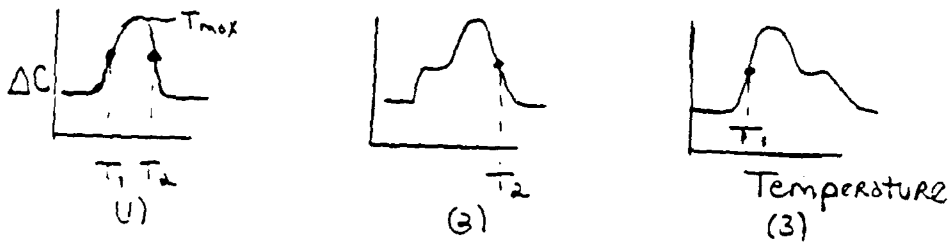

$$\Delta E = \left[k \ln \frac{\alpha_2}{\alpha_1} \Big/ \frac{1}{T_1} - \frac{1}{T_2}\right] - 2kT_{max} \qquad (1.)$$

$$\Delta E = \left[k \ln \alpha_m/\alpha_1 \Big/ \frac{1}{T_{max}} - \frac{1}{T_2}\right] - 2kT_{max} \qquad (2.)$$

$$\Delta E = \left[k \ln \alpha_2/\alpha_m \Big/ \frac{1}{T_1} - \frac{1}{T_{max}}\right] - 2kT_{max} \qquad (3.)$$

$k = 8.62 \times 10^{-5}$ eV/°K

Ratio ($\ln \alpha_2/\alpha_1$) depends on the lineshape

$\ln \frac{\alpha_2}{\alpha_1} = 2.833$ $\qquad \ln \frac{\alpha_m}{\alpha_1} = 1.283$ $\qquad \ln \frac{\alpha_2}{\alpha_m} = 1.551$

b. Trap Concentration, N_T:

$$\frac{N_T}{N_I} = \frac{(2)(0.26)\left(\text{Lock-in Amp Sensitivity-Volts}\right)\left(\text{Capacitance pf}\right)\left(\text{Peak (cm) Amplitude}\right)\left(\frac{\Delta W}{W}\right)^{-1}}{C\,(\text{pf, measured})} \qquad (4)$$

N_I = intrinsic (background) concentration $= 10^{14}/cm^3$

$\Delta W/W$ is a correction ratio due to the varying portions of the depletion widths (W) being examined with a modulating bias at different forward biases.

Bias	$\left(\frac{\Delta W}{W}\right)^{-1}$
−3.5 — −.5 V	2.37
−3.5 — +.5 V	1.50
−3.5 — +.75 V	1.30

1986 USAF-UES Summer Faculty Research Program/
Graduate Student Summer Support Program

Sponsored by the
Air Force Office of Scientific Research

Conducted by the
Universal Energy System, Inc.
Final Report

A Study of the Finite Element Method in Limited Area Weather Prediction Modeling

Prepared by:	Cornell L. Wooten
Academic Rank:	Graduate Student
Department and University:	Department of Mathematics Texas Southern University
Research Location:	Air Force Geophysics Laboratory/LYP Hanscom, Massachusetts
USAF Research:	Dr. Sammuel Yee
Date:	September 20, 1986
Contract No:	F49620-85-C-0013

A Study of Finite Element Method in Limited Area Weather Prediction Modeling

by

Cornell L. Wooten

ABSTRACT

A preliminary study of the use of finite element techniques in limited area atmospheric models was performed. This included a survey and summarization of the basic theory and programming procedures employed in finite element approximations. Attention was then focused on the fully operational Canadian model, particularly on the development of the finite element grid scheme. A key component of this is a 2-dimensional nonuniform rectangular grid which contains a subregion of high resolution. An alternative grid, consisting of a combination of rectangular and trapezoidal elements, was developed. This grid contains fewer elements in the overall domain while maintaining the same high resolution over the area of interest. A finite element program to solve a Poisson equation using a simplied version of either grid scheme was written. Runs were made with both grid types and the results were compared at the grid points within the high resolution region. The error at most of these point were smaller for the new grid. More extensive tests should be conducted; however, these results indicate that further investigation of the new grid scheme is warranted.

Acknowledgments

I would to thank the Air Force Systems Command and the Air Force Office of Scientific Research for sponsorship of my research. Dr. Donald Chisholm, of the Air Force Geophysics Laboratory, provided encouragement and access to the excellent Geophysics Reasearch Library. Furthermore, whenever I had a question, there was always someone available to answer it. With that kind of assistance and cooperation, one can only be stimulated to think and work harder.

Dr. Sammuel Yee, my focal point, was one of those available people. Dr. Yee regularly met with me and my supervising professor; in fact, it was durning one of those meetings that we thought of the idea that will be presented in this paper. Finally, I would like to thank Dr. Robert Nehs, my supervising professor, for giving me the opportunity to apply for this research position.

I. Introduction

Durning my undergraduate school years, I pursued two degrees. That does not sound unusual; however, I earned both degrees from two different schools while attending them simultaniously. One degree was in mathematics, and I earned it from Texas Southern University. The other was in mechanical engineering, and I earned it from Rice University.

The mechanical engineering degree provided a varied exposure to many numerical techniques, and the mathematics degree provided a solid background and means to analyze the various techniques. However, after finishing college, I felt that I had learned only a small portion of what is available in the field of numerical analysis. So, I decided to go to graduate school. Thus, I am currently pursuing an advanced degree in applied mathematics from Texas Southern University.

At the geophysics laboratory, my supervising professor and I attempted to examined the feasibility of using the finite element technique for limited area weather modeling. Our efforts are presented in this paper.

II. Objectives of the Research Effort

The overall objective of our research project was to make a preliminary examination of the practicability of using the finite element method in a limited area atmospheric model.

Our individual goals were:

1. to study the basic theory of finite element approximations,
2. to survey current applications of the finite element method in local weather prediction models, and
3. to develop a preliminary finite element program.

III. The Finite Element Method

In order to study the finite element method (FEM), we began with a survey of some of the literature in this area ([1],[2],[3],[4],[5],[6],[7]). The following is a very brief synopsis of the FEM.

The FEM has developed rapidly over the past thirty years as a technic for solving a wide variety of problems in engineering, physics, and mathematics. The first step of the process consists pf covering the domain of the problem with a grid, formed by partitioning the region into small non-overlapping pieces called elements. Local approximations (shape functions) of the solution are formed over each element and these are patched together to from global approximating functions (basis functions). The basis functions $T_1, T_2,$ and, T_n are generally piecewise polnomials which are zero over most of the elements.

The next step is to determine the coefficients in the expression

$$V = \Sigma d_i T_i \tag{3.1}$$

so that the function V is, in some sense, the best approximation to the solution. In problems this leads to a matrix equation

$$S \cdot D = C, \tag{3.2}$$

where S is an n x n-matrix, D and C are n x 1-vectors. The unknown coefficients $d_1, d_2, \ldots, d_n$ in 3.1 form the vector D. The terms of the other arrays in 3.2 involve integrals of expressions containing basis function or their derivatives. Integrations are performed over individual elements and usually require numeric procedures. After the arrays S and C are determined, the system 3.2 is solved for $d_1, d_2, \ldots, d_n$.

For one dimensional problems in which the domain R is an interval, elements are formed by a partition of R into subintervals. The Simplest shape Functions, piecewise linear functions having the value 1 at one subinterval endpoint and 0 at the rest of the end points.

The rectangles and triangles are popular elements for two dimensional problems. A rectangular domain R may be subdivided by lines parallel to the sides of R into a grid consisting of rectangles. The corresponding shape functions are often products of pairs of one dimensional shape functions.

For example, prouducts of roof functions produces the bilinear shape functions $a+bx+cy+dxy$.

Triangular element are useful in the approximation of boundaries of irregular domains. More complex elements, including those with curved sides, are formed by isometric tranformations. This technic involves non-singular mappings of some standard element, such as a rectangle or triangle, into the domain R.

The main advantage of the FEM is the flexibility in the choice of elements and shape functions. Furthermore, the resulting algebraic system will often involve a positive definite symmetric matrix containing a large number of zeros. The disadvantages generally arise from the complexity of the method. The programming problem usually requires a large storage capability and numerous calculations. Moreover, questions concerning the accuracy and stability associated with a particular finite element scheme cannot be answered easily.

In recent years there has been a lively debate as to the relative merits of the FEM and the older finite difference method among the supporters of each. The situation is complicated by the fact that comparisons of results depend upon many factors, including the type of problem, the grid used for the domain, the numeric procedures employed in the program, the design of the computer and the criteria used in evaluating the results. Similar difficulities arise when different finite element schemes are compared. Generally, the use of more complex element or shape functions of a higher order will increase the rate of convergence of the method at the cost of increased computer requirements. The question of which is the best scheme, or even a satisfactory one, for a particular problem is one that requires further research and experimentation.

IV. History of Limited Area Weather Modeling

In order to gain a perspective about finite element modeling of meteorological phenomena, a study of the Canadian limited area finite element model was attempted. Several paper were examined, and the following is a summary of our readings.

Limited area modeling did not immediately come into existence; it was a culmination of years of study and the piecing together of parts into an overall model. Many have made contributions to the study; however, since we were mainly interested in the grid or mesh solution type, we studied the works of only a few individuals.

Our interest were then concentrated on the configuration of the mesh that the model was solve with. Staniforth and Mitchell[8] studied the efficiency of using the finite element method to solve the shallow- water equations, which was a barotropic model. They used vorticity and divergence as predictive variables rather than the velocity components, and they used a semi-implicit time discretization. The shape function known as roof functions, were used for interpolation. The equations were solved on a uniform rectangular grid. Later, Staniforth and Mitchell[10] generalized the above model to a variable resolution rectangular mesh. Meaning, the mesh had one area of particularly fine resolution, and the rest of the mesh had course resolution. Methods were given for approximating the elliptic boundary-value problems; however, we were mainly interested in the mesh itself. Experiments were performed using several mesh configurations, and all had uniform high-resolution everywhere. They found that, " the forecast produced on uniformly high resolution mesh can be essentially reproduced for a limited time over the specific area of interest by a variable -mesh configuration at a fraction of the computational cost."[12] Noise problems were elimated by smoothly varying the resolution away from the area of interest.

They therefore concluded that the above was a workable strategy for the limited-area/time numerical weather prediction problem. Meanwhile, Staniforth and Daley[9] were formulating a baroclinic model for the vertical discretization of the sigma coordinate system. They wanted to combine the baroclinic model model with the barotropic model[10] in order to create a three-dimensional limited area model. Finally, the three-dimensional liminted area model was created by Staniforth and Daley[11], and it had the adddition of the moisture

equation to enhance the overall accuracy.

V. A Finite Element Model

At the suggestion of our research colleague, we considered possible alternatives to the variable rectangular grid described in the previous section. We felt that the flexibility of the finite element method has not been fully utilized in such limited area models Figure 1 displays a simple version of a grid scheme that we developed. Square ABCD represents the higher resolution area which is covered by a uniform rectangular mesh. The rest of the domain is partitioned by two layers of trapezoidal elements. Square EFGH was placed so that $A_2/A_1 = A_3/A_2$, where A_1, A_2, A_3 are the areas of elements in different layers (see Figure 1).

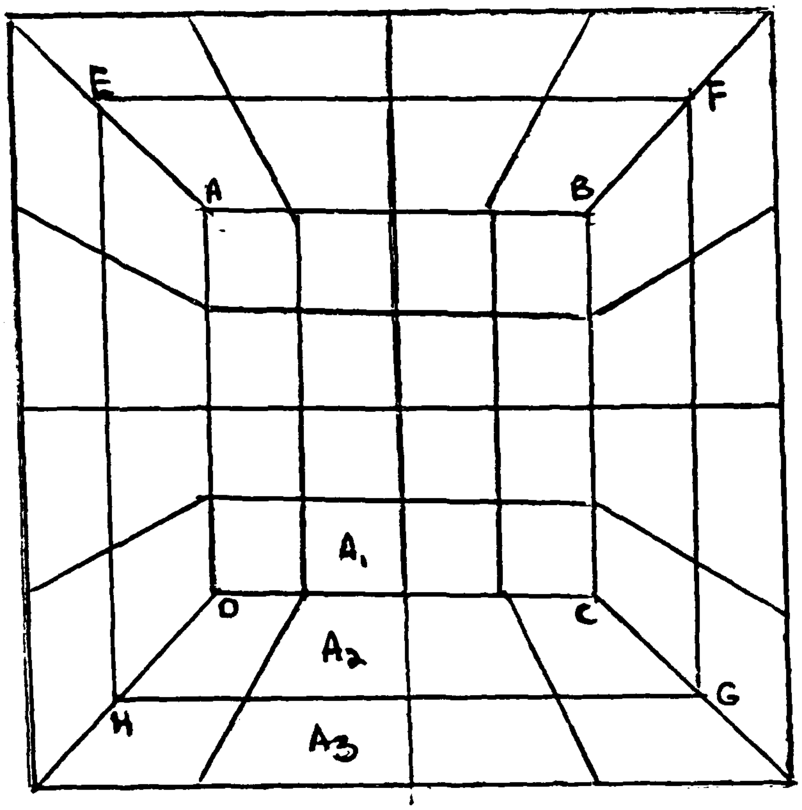

Figure 1 Square domain of a finite element model

Next we wanted to compare this configuration with an analogous nonuniform rectangular grid in which ABCD is cover by the same high resolution grid. Our grid contains fewer elements and, therefore, will require less storage and fewer computations. In order to test the accuracy, a **finite** element program was written in which either grid could be employed with bilinear shape functions. A simple time independent problem was choosen for the program;

$$u_{xx} + u_{yy} = f(x), \text{ and} \quad (5.1)$$

$$u = g(x) \quad \text{on the domain boundary.}$$

We ran the program with both grids using $f(x) = \sin\pi x$ and $g(x) = 0$ in (5.1). Utilizing the analytic solution to (5.1), the results for both grids were compared at the grid points within the high resolution area ABCD. The rectangular grid gave rather uniform results; the percent error at all grid points ranged from 1.25% to 1.36%. The results from the new grid were not as good at the corner points A, B, C and D but were better at interior points. (The percent error at each corner was 2.8%; however, at the rest of the boundary points, it ranged from .2% to 1.5% and at the interior points it ranged from .5% to .7%.) These initial results are encouraging, but time did not permit a more extensive series of tests. However, we feel that further investigation of the new grid scheme is justified.

Many of the components of our program are modifications of procedures found in Akin[1]. The program employes a subroutine which generates the initial mesh data for the rectangular grid. However, the corresponding data for the new grid must be supplied as input.

References

1. Akin, J. E., Application and Implementation of Finite Element Methods, New York, Academic Press (1980).

2. Chari, M. V. K. and P. P. Silvester, Finite Elements in Electrical and Magnetic Field Problems, New York, John Wiley and Sons, Inc., (1980).

3. Davis, A. J., The Finite Element Method, A First Approach, Clarendon Press Oxford (1980).

4. Huebner, K, H., The Finite Element Method for Engineers, New York, John Wiley and Sons, Inc., (1975).

5. Lapidus, L. and G. F. Pinder, Numerical Solutions of Partial Differential Equations in Science and Engineering, New York, John Wiley and Sons, Inc., (1982).

6. Strang, G. and G. J. Fix, An Analysis of the Finite Element Method, New York, Prentice-Hall (1973).

7. Wait, R. and A. R. Mitchell, Finite Element Analysis and Applications, New York, John Wiley and Sons, Inc., (1985).

8. Staniforth, A. N. and H. L. Mitchell, "A Semi-Implicit Finite Element Barotropic Model," Mon. Wea. Rev., 105, 154-169, (1977).

9. Staniforth, A. N. and Roger W. Daley, "A finite Element Formulation for the Vertical Discretization of Sigma-Coordinate Primitive Equation Models," Mon. Wea. Rev., 105, 1108-1118, (1977).

VI. Recommendations

1. In order to facilitate further study, a subroutine should be developed which would generate the intial mesh data for this type of grid.

2. There should be further testing of this particular grid, including runs with different functions f and g in (5.1). Also, the question of where the intermediate square EFGH should be placed needs to be examined further. It would be important to determine, if possible , which location produces the best (in some sense) results.

3. The next step would be the investigation of a similiar grid which has a higher resolution. This would involve a finer mesh (more squares) over ABCD and probably additional trapezoidal layers (i.e.-more intermediate squares of the type EFGH).

4. The use of this grid scheme for time dependent problems should then be stuied extensively. This will introduce questions of stability and numeric time discretization procedures. The work would begin with a simple initial value problem but should eventually lead to more complex dynamic systems; for example, the shallow-water problem.

5. We also feel that comparisons should be made with models based upon finite difference techniques only.

10. Staniforth, A. N. and H. L. Mitchell, "A Variable-Resolution Finite Element Technique, for Regional Forecasting with the Pritive Equations," Mon. Wea. Rev., 106, 439-477, (1978).

11. Staniforth, A. N. and Roger W. Daley, "A Baroclinic Finite Element Model for Regional Forecasting with the Primitive Equations," Mon. Wea. Rev., 107, 107-121, (1979).

12. Staniforth, A. N., "The Application of the Finite Element Method to Meteorological Simulations--A Review," International Journal For Numerical Mehtods in Fluids, 4, 1-12, (1984).

1986 USAF-UES SUMMER FACULTY RESEARCH PROGRAM/

GRADUATE STUDENT SUMMER SUPPORT PROGRAM

Sponsored by the

AIR FORCE OFFICE OF SCIENTIFIC RESEARCH

Conducted by the

Universal Energy Systems, Inc.

FINAL REPORT

Synthesis and Polymerization of Dinitropropyl Vinyl Ether

Prepared by: John S Wroblewski

Academic Rank: Graduate student, Masters of Science program

Department and University: Chemistry Dept. at the University of Southwestern Louisiana

Research Location: Rocket Propulsion Laboratory EAFB, Liquids ,Chemistry and Materials/LKLA

USAF Researcher: Mostafa Talukder

Contract No: F49620-85-C-0013

ABSTRACT

Energetic polymers are recently being investigated because of their use as binders in solid rocket propellants. For this reason, the synthesis of dinitropropyl vinyl ether (DNPVE) and its energetic prepolymer has been undertaken. The polymerization of DNPVE was carried out with a p-dicumyl chloride/AgSbF6 catalyst system at -88^{o}C. The catalyst, p-dicumyl chloride, is a bifunctional catalyst and will be incorporated within the polymer. The polymer chain was terminated with ethanolamine which results in a hydroxyl group at both ends of each polymer chain. By changing the monomer catalyst ratio, the molecular weight of the polymer was controlled. A polymer with molecular weight of 1600 to 1700, gave the best splitting patterns in the NMR spectra. Further work is needed on the physical properties of the polymer for complete evaluation as binder for solid rocket propellants.

Acknowledgements

I would like to thank the Air Force System Command for allowing this learning experience to take place at the Rocket Propulsion Laboratory, Edwards Air Force Base, California. I would also like to acknowledge the Universal Energy System, Inc. for chosing me as a 1986 summer fellow as well as Susan K. Espy and Rodney C. Darrah for their continuous help throughout the summer program.

At the rocket lab, I would like to thank those in my group whom I worked with: Lt. John Andreshak and Dr Robert Chapman and those who provided moral support: Bill Robbs, John Marshall, Ismail Ismail, Mel Abrego, Ronnie Porter, Marietta Krissak, and Wayne Roe. I am also very grateful to Mostafa Talukder, whom I worked closest with, for his unselfish giving of his knowledge, advice, and support.

Finally, I would like to thank the faculty at the University of Southwestern Louisiana for their support in my temporary relocation and especially my advisor, Dr. August Gallo, for his continual support.

I. Introduction

The purpose of this project was to synthesize large amount of monomer, dinitropropyl vinyl ether(DNPVE) and its polymer poly-DNPVE. The physical properties of the polymer will be studied in order to evaluate the polymer as binder for solid rocket propellants.

The polymerization was unique in two ways: first, the incorporation of the catalyst within the polymer and second, the termination of the polymer with ethanolamine which results in a hydroxy-terminated polymer.

The catalyst, para-dicumyl chloride (p-DCC), is a bifunctional catalyst which means that the monomer will polymerize from two sites on the catalyst. Therefore, the catalyst is incorporated into the polymer rather than at the end of the polymer chain. This is advantageous from the polymer chemists' point of view because the molecular weight can be approximated due to the incorporation of the p-DCC within each polymer chain by nuclear magnetic resonance (NMR). For example, the p-DCC will give a single peak at 7.5-7.6ppm which integrates to four hydrogen atoms. Among other peaks, there is a characteristic peak at 4.4ppm which should be for the two hydrogen atoms per monomer unit. Therefore, if the actual peak at 4.4ppm integrates to 16 hydrogen atoms, then there are four monomer units per p-DCC unit. Knowing the weights of monomer (DNPVE) , p-DCC, and ethanolamine, the total molecular weight of the polymer can be approximated. The molecular weight was compared to the calculated value found from the mole ratio of reactants. Agreement was good for weight range between 1500 and 1700, however, NMR results for molecular weights outside of that range were difficult to obtain due to poor spectra resolution.

Other uses of the catalyst, p-DCC, are for the synthesis of bifunctional polymers and as an initiation-transfer catalyst (INIFER). Since p-DCC polymerizes from two sites, the functional group of the compound used to terminate the polymerization will appear at each end of the polymer chain. Catalysts which cause polymerization at only one site results in a monofunctional polymer leaving the unreactive catalyst at one end of the polymer. A bifunctional polymer can be used in a variety of reactions such as extended copolymerization or synthesis of a polyurethane. Para-dicumyl chloride can also be used, along with boron triachloride, as a INItiator and transFER (hence: INIFER) catalyst. The boron triachloride removes a chlorine from the catalyst forming a carbocation (positive carbon). This cation initiates the polymerization which forms the active polymer in-situ. The catalyst can then transfer a chlorine to the active polymer, terminating the polymer and regenerating the carbocation of p-DCC.

Ethanolamine is used to terminate the active polymer with a primary hydroxyl group. Hydroxy-terminated polymers are termed "prepolymers" because of their reactions with diisocyanates to form a polyurethane. Polyurethanes are currently being used as binders for solid rocket propellants. The use of poly-DNPVE as an energetic prepolymer is proposed to increase the burning speed and efficiency of the solid rocket fuel.

II. Goals and Objectives

It is the goal of the researcher to synthesize and polymerize dinitropropyl vinyl ether (DNPVE). Since the percent yield of pure DNPVE is low using previous procedures (1), a large amount must be synthesized for further polymerization. Some factors of this synthesis will be altered in order to maximize the yield of

DNPVE. Poly-DNPVE will be catalyzed by p-DCC and silver hexafluoroantimonate and terminated with ethanolamine. The molecular weight of the polymer will be varied between 600 and 10,000 by changing the ratio of p-DCC to DNPVE. A 90 MHz JOEL FT-NMR will be used to determine the purity of the reactants and products and to approximate the molecular weight of the polymer.

III. Synthesis

Dinitropropyl vinyl ether was synthesized by refluxing dinitropropanol (DNP) and divinyl ether (DVE) in dichloroethane (DCE) (scheme 1). The ratio of DNP to DVE (1:1) used in a previous method (1) was changed to 1:2 because of the high volatility of DVE. The reaction was catalyzed by mercury oxide (HgO) and trifluoroacetic acid (TFA). The best workup procedure consisted of washing the crude monomer with a solution of 0.1% NaOH which was saturated with NaCl. After extraction, the DCE layer was dried with magnesium sulfate and gravity filtered through a course sintered glass funnel. The resulting yellow solution was evaporated under reduced pressure to give a 100-120% crude yield. If one washed the organic extract with dilute HCl or neglected to wash altogether, a lower overall yield was obtained. The yellow-orange solution was further purified by column chromatography by using alumina as the absorbent and CCl_4 as the eluting solvent. The column was 2.5in x 7in and 100g of alumina per gram of sample was used. Fractions with similar NMR spectra were combined and evaporated to give a 22-26% yield. DNPVE was vacuum distilled at 55-56^{o}C (0.7mmHg); NMR($CDCl_3$) (dd,6.4ppm,1H), (s,4.5ppm,2H), (m,4.2ppm,2H), (s,2.2ppm,3H).

The polymerization of dinitropropyl vinyl ether was catalyzed by para dicumyl chloride (p-DCC) as shown in scheme 2. A 100ml flask was charged with 35ml of

freshly distilled dichloromethane (DCM) and p-DCC under N_2 atmosphere. When the solution was at -88°C, silver hexafluoroantimonate ($AGSbF_6$) in 10ml of fresh DCM was added. After allowing 10 min for generation of the carbocation (scheme 3), freshly distilled monomer was added. The amounts of p-DCC and monomer were varied according to the molecular weight of the polymer desired. Immediately after monomer addition, the polymer was terminated with ethanolamine. Schemes 4 and 5 show the p-DCC functioning as a bifunctional catalyst as well as the termination step with ethanolamine (EA).

The product was decanted into methanol. The yellow ppt. was washed with methanol/NH_4OH and filtered. The off-white solid was dissolved in acetone and re-precipitated with methanol. The methanol was evaporated and the white powder was dried under vacuum; NMR, (s,7.4ppm,4H), (m,5.1ppm,2H), (s,4.5ppm,2nH), (b,2.6ppm,2nH), (S,2.3ppm,3nH), (s,2.0ppm,12H), (d,1.7ppm,2nH) where n is the number of monomer units per molecule, impurities appear at 1.2 and 1.3ppm.

IV. Discussion and Recommendations

In order to use the prepolymer, poly-DNPVE, as a solid rocket binder, there are several areas which need further investigation. The poor yield of DNPVE may be due to several factors. It is recommended that the washing procedure be improved such that the product solution in DCE becomes a light yellow solution. It is also very possible that the monomer is polymerizing during concentration because the solution becomes orange-yellow and viscous. If these ideas are correct, the monomer may be purified by vacuum distillation without the previous use of liquid chromatography (LC). Avoiding the use of LC may increase the yield by a factor of 2x.

Since the polymerization process is water sensitive, it is recommended that the reaction be done in a dry box. In this case, all the reactants can be purified, dried, and de-aired in the box. It is difficult to remove all of the AgCl from the polymer so other solvents should be investigated for product purification. The polymer with a molecular weight of about 1500 seemed to give the best NMR spectrum, however, polymers with molecular weights lower and higher than 1500 also need to be further analyzed.

Since ethanolamine ($H_2NCH_2CH_2OH$) contains an active site at the nitrogen and at the oxygen, it is possible for the polymer to be terminated with $-NH_2$ rather than the desired group, -OH. By protecting the hydroxyl(-OH) group of the EA with a trimethylsilyl group, the only active site with a high electron density would be nitrogen. This process will ensure a hydroxyl terminated polymer. The resulting polymer can be compared to a previously synthesized polymer having a similar molecular weight from the unprotected method. If the spectra of both compounds match, than it can be assumed that protection of the hydroxyl group is not necessary; therefore, the original procedure provides a convenient one pot synthesis of the prepolymer, poly-DNPVE.

The final goal should be to test the physical properties of the polymer; therefore, large amounts will need to be synthesized and tested. Since it is the goal of this project to synthesize a more efficient and effective solid rocket binder, more time is needed to optimize the entire synthesis as well as the synthesis of the polyurethane binder from the poly-DNPVE. Finally, p-DCC can be used as a powerful synthetic catalyst. Further studies of this catalyst should be undertaken in order to show its full potential as a bifunctional catalyst or as a possible INIFER catalyst.

References

(1) Shackelford, S. A., McGuire, R. R., and Cochoy, R. E., US Patent No. 4,426,540 (1984)

** Research sponsored by the Air Force Office of Scientific Research/AFSC, United States Air Force, under Contract F49620-85-C-0013. The United States Government is authorized to reproduce and distribute reprints for governmental purposes notwithstanding any copyright notation hereon.

Schemes

1.DNPVE

$HOCH_2CH3$ + $CH2CH\text{-}O\text{-}CH{=}CH2$ ----------------
DNP DVE

$CH_2CH\text{-}O\text{-}CH2C\text{-}CH3$

2. p-DCC

$$\begin{array}{ccc} CH_3 & & CH3 \\ \vdots & & \vdots \\ CL\text{-}C\text{-} & & \text{-}C\text{-}Cl \\ \vdots & & \vdots \\ CH_3 & & CH3 \end{array}$$

3. Carbocation

$CL(CH_3)2C\text{-}$ $\quad$ $\text{-}C(CH3)2CL$ + 2AgSbF6 -------

$(CH3)2$ C- $\quad$ $C\text{-}(CH3)2 + 2SbF_6^- + 2AgCl$

4. Incorporation
p-DCC + I ---------

5. Termination
$\text{- - -}CH_2\text{-}\overset{}{\underset{+}{CH}}$ + $H2NCH2CH2OH$ $\longrightarrow$

$\text{- - -}CH_2\text{-}CH\text{-}NH\text{-}CH_2\text{-}CH_2OH$

1986 USAF-UES SUMMER FACULTY RESEARCH PROGRAM/

GRADUATE STUDENT SUMMER SUPPORT PROGRAM

Sponsored by the

AIR FORCE OFFICE OF SCIENTIFIC RESEARCH

Conducted by the

Universal Energy Systems, Inc.

FINAL REPORT

Development of a High Speed Infrared Detection and Recording System with Resident Image Processing and Graphic Data Display for Support of Remote Defense Nuclear Agency High-Powered Pulsed Microwave Source Measurements

Prepared by:	Jon D. Zobel Jr.
Academic Rank:	Graduate Student
Department and University:	Department of Electrical Engineering University of Colorado at Colorado Springs
Research Location:	The Frank J. Seiler Research Laboratory, NH, United States Air Force Academy, CO
USAF Researcher:	Captain Dan Fredal

Date:	11 August 1986
Contract No.:	F49620-85-C-0013

Development of a High Speed Infrared Detection and Recording System with Resident Image Processing and Graphic Data Display for Support of Remote Defense Nuclear Agency High-Powered Pulsed Microwave Source Measurements

by

Jon D. Zobel Jr.

ABSTRACT

Infrared detection and measurement of electromagnetic field strengths is used at the University of Colorado at Colorado Springs (UCCS). In each experiment, the measurements are of steady-state, continuous wave (CW) conditions. However, Seiler Labs was asked to support the test of a pulsed microwave source to be conducted by the Defense Nuclear Agency (DNA) at the Air Force Weapons Lab (AFWL) in late July or early August, 1986, and the AGA Thermovision 780 system that is used at UCCS is not suited for such tests. Subsequent investigation revealed that an appropriate and affordable system could not be obtained for the test. At that point, a means of adapting the present system at UCCS to support the test was pursued. The resulting system consists of the AGA system, and a modified IBM PC/AT to store the data and do all of the necessary data/image processing at the remote test site. The effort was a three phase group effort. It included hardware development, software development, and detection material acquisition. This report covers the hardware portion of the project.

Acknowledgments

I would like to thank the Air Force Systems Command and the Air Force Office of Scientific Research for sponsoring my work. In addition, I woula like to thank Major Ronald Lisowski and the Department of Astronautics at the Air Force Academy for providing us space in their lab to work, and all the members of the staff at the Frank J. Seiler Research Laboratory, USAFA, who provided valuable help and assistance in our efforts.

I. Introduction

I received my Bachelor of Science degree in electrical engineering from the University of Colorado at Colorado Springs with an emphasis in applied electromagnetics, and am presently working on my Master of Science in electrical engineering at UCCS with the same emphasis. During my undergraduate studies, I worked in the electromagnetics lab/anechoic chamber facilities at UCCS supporting experiments in IR CW measurements.

II. Objectives of the Research Effort

The goal at Seiler was to come up with a means of recording the field strength of a high-powered pulsed microwave source. The duration of the experiment was to be approximately two (2) seconds, with the pulse-width of the source being on the order of nanoseconds. Therefore, the measurements would be of transiate field strengths as opposed to the CW, steady-state nature of the experiments conducted at UCCS. The OSCAR (Off-line System for Computer Access and Recording) recording unit has a magnetic tape drive associated with it. The tape unit has a one (1) second write time in order to record the data on tape, which is not acceptable for the DNA test. Therefore, a faster method of recording the data was needed. Since an appropriate and affordable IR system could not be found, it was decided to modify the one in use at UCCS.

The following items needed to be accomplished in order

to meet our objective of modifying the present system in order to do the transient field measurements:

1. Understand the internal operation of the OSCAR unit. See if it is capable of providing significantly more than one image per second, and, if so, what temporary modifications were needed to record all of the images.

2. Find a means of storing all of the data as fast as or faster than the OSCAR unit is capable of generating it.

3. Be able to do all of the data processing necessary at the test site.

4. Find or develop a material that could be used as a detection screen in order to be able to map the field pattern.

The scope of this paper will include items 1 and 2. The other two will be covered in more detail in reports by my two colleagues on this project, Paul Bussey and Bob Littleton. The faculty member on this project was Dr. Ron Sega, also from UCCS.

III. The OSCAR Unit

This piece of equipment was the crucial component of our proposed system. If the number of "images" that it was capable of generating was not sufficient for our image processing techniques, the goals of the overall summer

research would not have been met.

After discussions with Jan Eklund, President of Eklund Infrared Systems (the manufacturer of the AGA 780 and OSCAR systems), it was known that the system generates 25 "fields" each second, numbered sequentially from one (1) to four (4), and that two fields are interlaced in order to produce an image. With the OSCAR unit, it writes only fields 1 and 3 to tape, and does nothing with fields 2 and 4. Fields 1 and 3 are interlaced to produce an image for display. If there was a way to also get the information for the even-numbered fields, the field rate of 25 per second would yield 12.5 images during a two (2) second test (the expected duration of the tests to be conducted in August at AFWL). Our scheme would be to interlace fields 1 and 3 to get one image, and then interlace fields 2 and 4 for another.

The technical reference manual for the OSCAR provided all of the schematics for the system. Analysis of the system-level schematic and the schematic for the Input Controller 2 card (INC2) revealed that the data for fields 2 and 4 was being processed by the A/D converter, but that it was prohibited from being placed on OSCAR's data bus. This was done by some gating logic located on the INC2 card, where the D/A, A/D, and resident-memory control signals are generated. After achieving a thorough understanding of the function of the INC2 card, the data for fields 2 and 4 was made available to OSCAR's bus by modifying three (3) IC's on the INC2 card. All of the modifications had to be of a temporary nature so that OSCAR could still be used at other

times in its designed configuration. This was accomplished by unsoldering the 3 IC's from the board, and installing DIP sockets in their place. Then the IC's themselves (IC8, IC12, and IC29) were modified by having certain pins pulled up and soldered to others. In this fashion, OSCAR could essentially be changed from one mode of operation to another simply by replacing 3 IC's. These modifications are listed in Table 1.

IC No.	Part No.	Modification
8	74LS00	Pull up pin 9 and solder to pin 10.
12	74LS20	Pull up pins 4 and 5, and solder to pin 2.
29	74LS367	Pull up pin 10 and solder to pin 8 (ground).

Table 1
INC2 Card Modifications

These modifications alone would have been enough to allow us to use OSCAR as we wished. However, as an added measure, the buttons on the front panel of OSCAR were disabled by unplugging them from the circuit cards they connected to, and the two memory cards within OSCAR are removed from the card cage. These were done to prevent any part of OSCAR's original operating mode from interfering with our intended mode of operation.

A list of the actual steps for the mode change is

contained in the appendix of this paper.

To insure that the data lines from OSCAR are not loaded by the interface cable running to the AT, and by the AT itself, a buffer circuit has been designed and implemented. It plugs into the back of OSCAR in the Remote Controller 1 connecter. A schematic of the buffer card can be found in the appendix.

IV. Data Storage System

Some of the criteria for our system dictated that it must be a stand-alone system capable of collecting the IR data, storing it, processing it, and displaying it while still at the test site. It also had to be easily transportable. In order to meet these requirements we decided to use an IBM PC/AT for both our data storage and image-processing/graphic-display needs. The AT was equipped with an extended graphics adapter (EGA) card and monitor, a memory expansion board with an additional 0.5 Mbyte of RAM, and an AT TurboSwitch II capable of increasing the CPU clock to 12 MHz. In addition to all this, an additional circuit card had to be designed and installed in order to decode the data from OSCAR and control the direct memory access (DMA) chip in the AT, causing it to store the image data from OSCAR in a manner that would permit it to be processed by our image processing code. The general layout of this card, its corresponding schematic, and the overall system configuration can be found in the appendix.

The test of the DMA controller card involved several steps. First, it required the construction and implementation of a simple data generation scheme. This was very useful in checking out and debugging the card while having it do the transfer of just a single byte of data, and eventually a full 64K of data. It consisted of eleven on/off type switches, of which three were debounced. These three were used to simulate the three control signals that will eventually be coming from OSCAR due to the IC modifications that were made to it. The other eight switches, used as data switches, were not debounced because during the initial tests we were not going to change the data during the transfer. This initial set up proved quite effective in identifying most of the operating problems with the DMA control card and the associated software. The test circuit and the software generated to perform the transfers are located in the appendix.

The next test circuit replaced the data switches with two cascaded synchronous 4-bit binary counters (74163), and the switch representing the strobe control line from OSCAR with a frequency generator (HP 3312A). This allowed us to attempted to push the DMA card toward the 400 Kbyte transfer rate that OSCAR generates. This test also utilized the AT TurboSwitch, which we had set at 9.5 MHz. This was the fastest speed that the AT was capable of operating at, as determined by starting the system at different clock rates until an error was detected during power-up. The DMA control system checked out fine until the frequency of the strobe was increased to 270 kHz, at which point some of the sequential data values were lost. This loss of data became worst as the

frequency was increased to 400 kHz, and meant that our proposed scheme would not work using a PC prototyping card. A copy of the schematic for the test circuit is located in the appendix.

The only alternative was to implement the design using an AT prototyping board. By using the AT instead of the PC board, we could do 16-bit transfers using a 16-bit DMA channel instead of 8-bit transfers. This in turn would reduce the needed data transfer rate from 400 kHz to 200 kHz, which would work since previous testing indicated that the design would work for frequencies up to 270 kHz. However, the graduate fellowship ended before this could be done, and the success of this work is not known.

V. Recommendations

The fellowship was completed before the scheduled test at AFWL; therefore, a complete system operation was not performed, and any problems arising from it are not known.

It is greatly recommended that the DMA controller circuit be placed on an AT prototyping card instead of one for the IBM PC. This will reduce the speed at which the AT has to perform the transfers from 400 kbyte to 200 kbyte, since it would be doing two word-transfers utilizing a 16-bit DMA channel instead of one word at a time, and eliminate the problems that have been encountered with the original circuit card. The circuit needs to be rebuilt anyway, because with all of the design changes that were made by the Air Force

researcher in his original design, and subsequent wiring changes that were needed to implement these changes, the wiring is not as close to the ground plane as it should be, and thus the circuit is more sensitive to noise than it could be.

VI. References

1. IBM Technical Reference Personal Computer AT, No. 1502243.

2. Lancaster, Don, TTL Cookbook, Howard W. Sams & Co., Inc., 1974.

3. Norton, Peter, Programmer's Guide to the IBM PC, Microsoft Press, 1985.

APPENDIX

OSCAR MODE CONVERSION

AGA TO IBM PC/AT

The following are the steps that must be done in order to use OSCAR with the IBM PC/AT as the data storage unit.

1. Open OSCAR's front panel. Pull out the two (2) memory cards (M1 and M2).
2. Pull out the control card (INC2). Replace IC8 (74LS00), IC12 (74LS20), and IC29 (74LS367) with the customized equivalent chip. Return the card to its slot in OSCAR's card cage.
3. Pull the plugs that connect to the front panel switches. Disconnect them where they attach to the circuit cards in the card cage. Most of them are accessible from the front; the back may have to be removed in order to unplug one of the cables. Secure the front and back panels.
4. Plug the buffer card assembly into the Remote Controller 1 connecter (DB37) in the back of the Oscar unit.
5. Plug the interface cable into the male DB25 connecters on the buffer board and the IBM PC/AT.

These steps must be reversed in order to restore OSCAR to its normal operating mode.

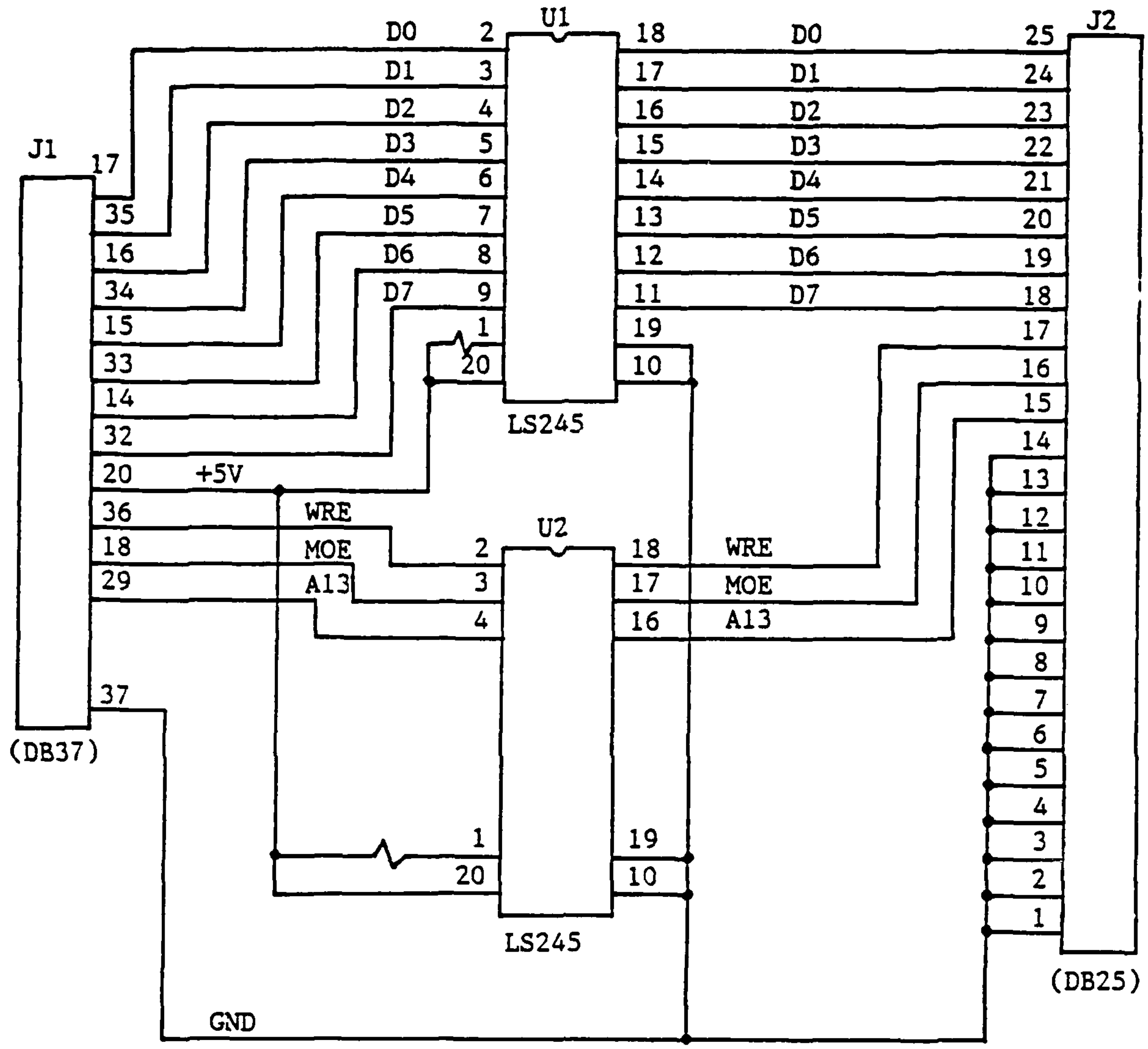

Note: All resistors are 10kΩ.

Buffer Board Schematic

PC Board : Vector Plugboard 4613-2

IC NO.	Part No.
U1	74LS245
U2	74LS367
U3	74LS367
U4	74LS374
U5	74LS74
U6	74LS138
U7	74S74
U8	74LS244
U9	74LS02
U10	74S00
U11	74LS21
U12	74LS273
U13	74LS04
U14	74S32
U15	74LS02

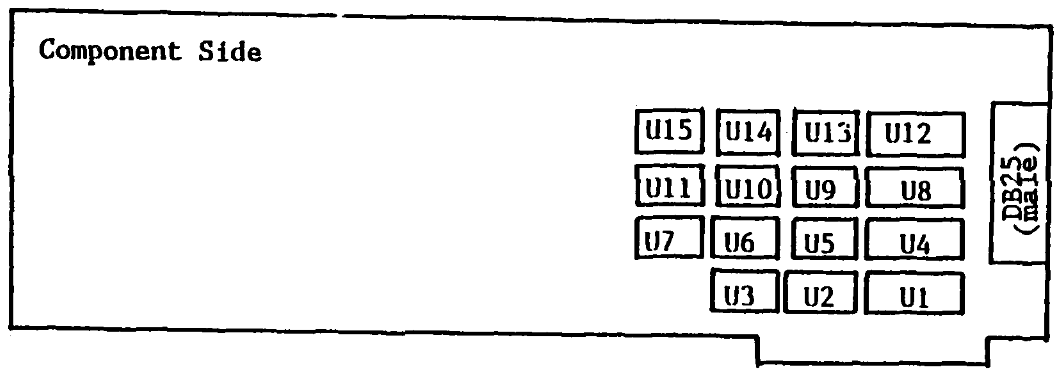

DMA Control Card Layout

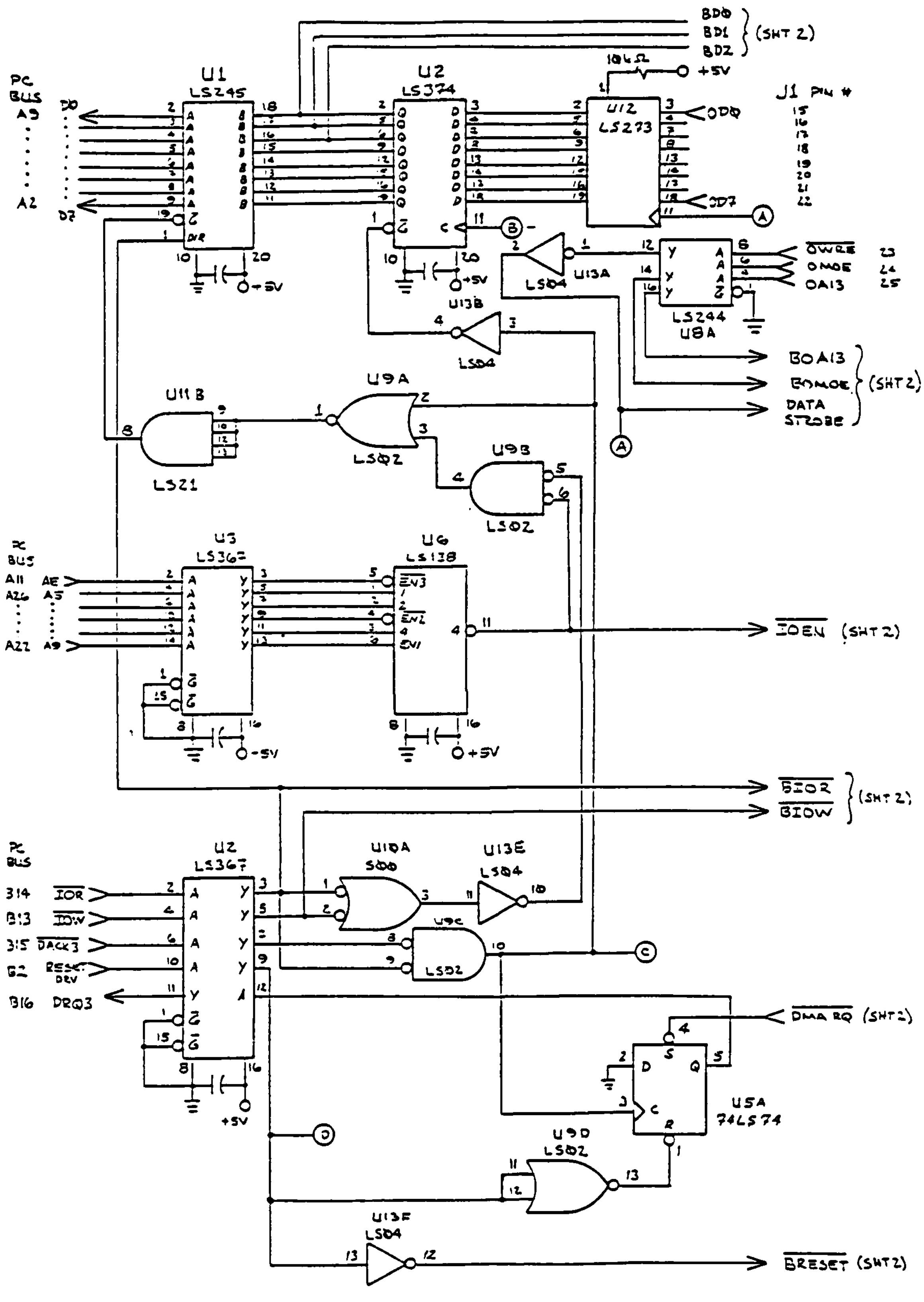

DMA Control Card Schematic (page 1 of 2)

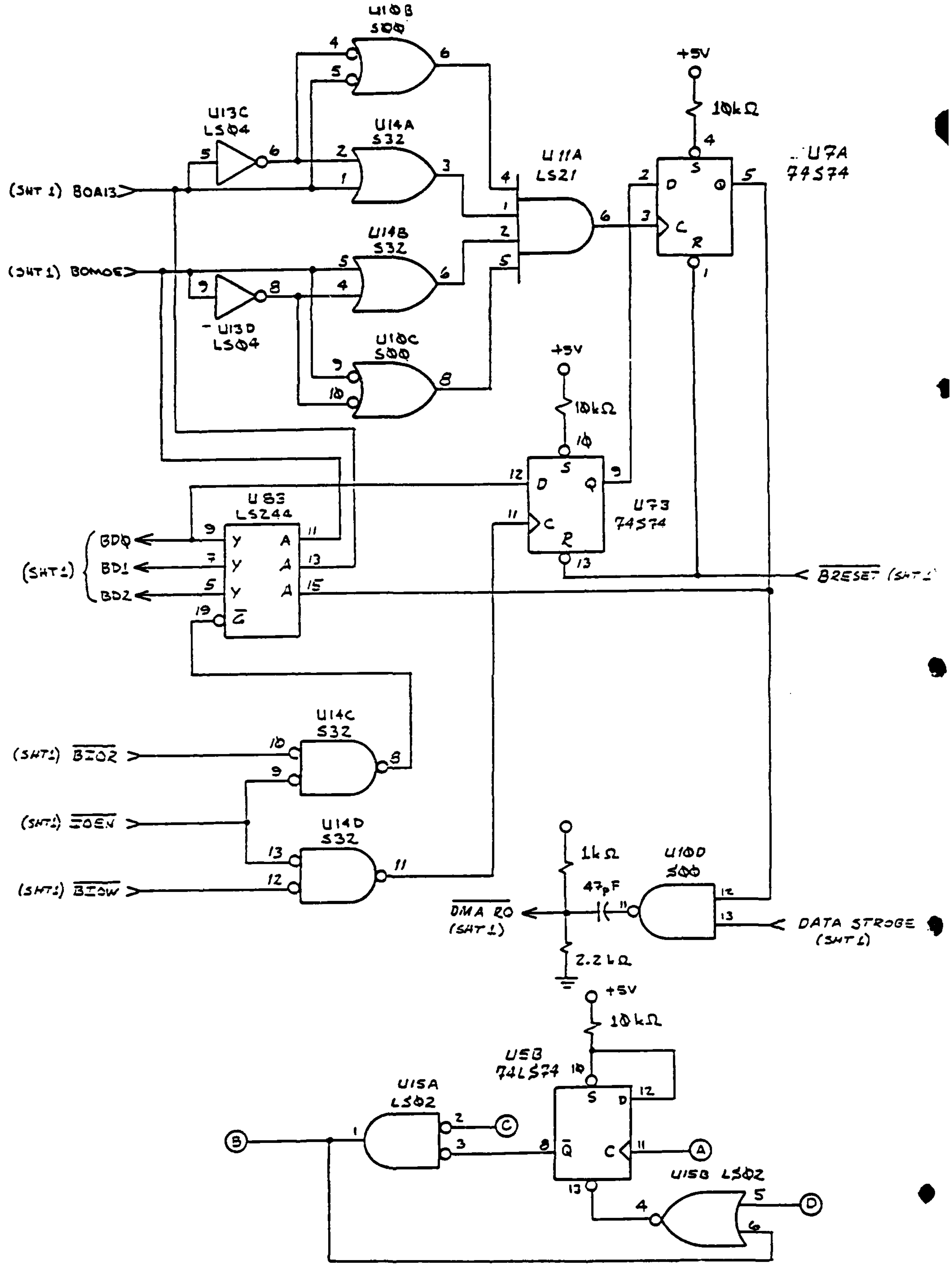

DMA Control Card Schematic (Page 2 of 2)

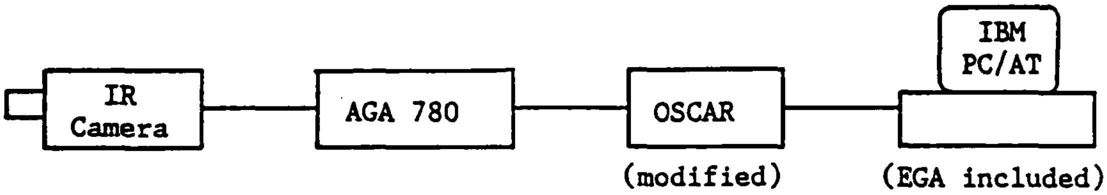

IR Detection System Configuration

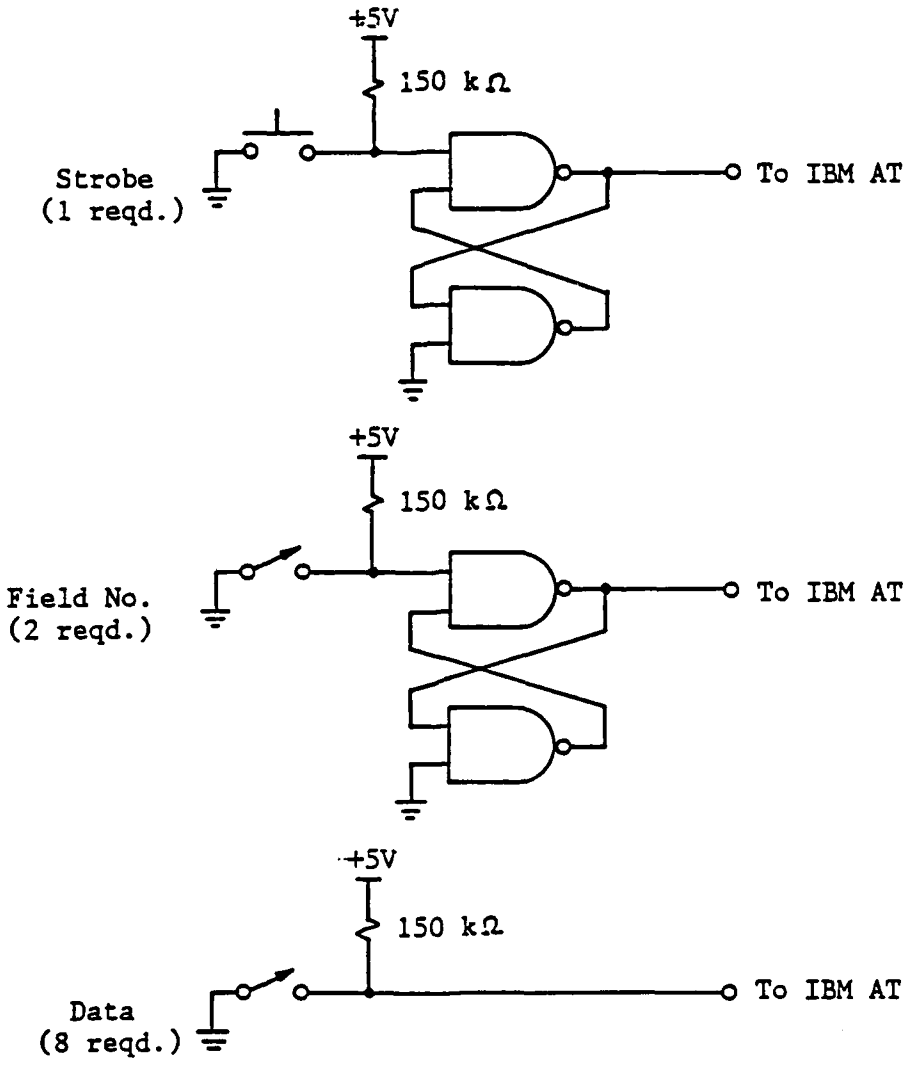

1st Test Circuit

```
1     REM  DMA TEST PROGRAM
2     REM  CREATED 17 JUL 86
50    REM
51    REM  SET PAGE REGISTER FOR CHANNEL 3 TO 006
52   OUT &H82,&H6
90    REM
91    REM  INITIALIZE PORT 300 WITH ALL 1's
92   OUT &H300,&HFF
100   REM
101   REM  CLEAR FLIP FLOP
102  OUT &HC,&H17
200   REM
201   REM  SET MODE REGISTER
202  OUT &HB,&H57
300   REM
301   REM  LOWER ADDRESS BYTE
302  OUT &H6,&H0
400   REM
401   REM  UPPER ADDRESS BYTE
402  CUT &H6,&H0
600   REM
601   REM  LOWER BYTE WORD COUNT
602  OUT &H7,&H20
700   REM
701   REM  UPPER BYTE WORD COUNT
702  OUT &H7,&H0
800   REM
801   REM  SET MASK REGISTER
802  OUT &HA,&H3
9999 END
```

Software for 1st Test Circuit

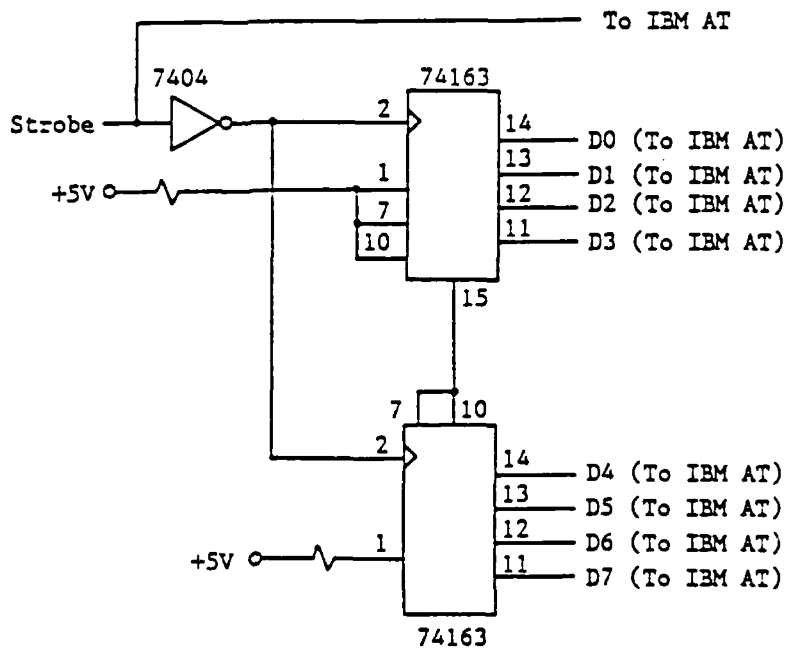

2nd Test Circuit

```
Program Test_Dma ;

{***********************************************************}

  Procedure Initialize;

    Const
      mask_reg            = $0A;
      xfer_latch          = $300; {I/O port, DMA control board}
      mode_reg            = $0B;
      dma_ch3_disable     = $07;
      xfer_ff_disable     = $00;
      dma_ch3_demand_mode = $07;

    Begin
      Port[mask_reg] := dma_ch3_disable;
      Port[xfer_latch] := xfer_ff_disable;
      Port[mode_reg] := dma_ch3_demand_mode;
    End; {Initialize}

{***********************************************************}

  Procedure Transfer(Start_Page_Addr, Start_Offset_Addr,
                     Page_Count                  : Integer;
                     Var Start_field             : Integer;
                     Var Error                   : Boolean;

    Const
   (* DMA #1 registers *)
      dma_ff               = $0C; {Internal flip-flop}
      mode_reg             = $0B;
      start_addr_reg       = $06;
      word_cnt_reg         = $07;
      mask_reg             = $0A;
      status_reg           = $08;
      page_reg             = $82; {page register, DMA #1, ch 3}

   (* DMA control board registers *)
      xfer_latch           = $300; {I/O port, DMA control board}
      xfer_status          = $300; {          "               }
      xfer_ff_disable      = $00;
      xfer_ff_enable       = $01;

   (* Masks *)
      Xfer_Status_Mask     = $03;
      Xfer_Enable_Mask     = $04;
      Ch3_TC_Mask          = $08;

   (* Misc constants *)
      clear_ff             = $17;
      dma_ch3_demand_mode  = $07;
      dma_ch3_enable       = $03;
      Full_Page_Start_Addr = $0000;
      Full_Page_Count      = $FFFF;

    Var
      Word_Count, Count             : Integer;
      Xfer_Field_Status, DMA_Status : Byte;
```

```
Begin
  If (Hi(Start_Offset_Addr) in [$00, $20, $40, $60, $80,
     $A0, $C0, $E0]) and (Lo(Start_Offset_Addr) = $00)
    Then
      Begin
        Error := False;

     (* Transfer first page *)
        Port[page_reg] := Start_Page_Addr;

        Port[dma_ff] := clear_ff;
        Port[start_addr_reg] := Lo(Start_Offset_Addr);
        Port[start_addr_reg] := Hi(Start_Offset_Addr);

        Word_count := $FFFF - Start_Offset_Addr;
        Port[word_cnt_reg] := Lo(Word_Count);
        Port[word_cnt_reg] := Hi(Word_Count);

     (* Make sure xfer flip flop is disabled *)
        Port[xfer_latch] := xfer_ff_disable;
        Repeat {Until field number changes}
          Xfer_Field_Status := Port[Xfer_Status]
        Until (Xfer_Enable_Mask and Xfer_Field_Status) = 0;

     (* Start DMA transfer *)
        Port[mask_reg] := dma_ch3_enable;

        Port[xfer_latch] := xfer_ff_enable;
        Repeat {Until field change enables DMA}
          Xfer_Field_Status := Port[Xfer_Status]
        Until (Xfer_Enable_Mask and Xfer_Field_Status) <> 0;

        Sound(600);
        Delay(50);
        NoSound;

     (* Get the starting field number *)
        Start_Field := (Xfer_Status_Mask and Xfer_Field_Status);

        Repeat {Until terminal count, DMA done}
          DMA_Status := Port[status_reg]
        Until (Ch3_TC_Mask and DMA_Status) <> 0;

        Count := 1; (* one page transfered *)

     (* continue DMA transfers *)
        While Count < Page_Count Do
          Begin
         (* Set up for full page transfers *)
            Port[dma_ff] := clear_ff;
            Port[start_addr_reg] := Lo(Full_Page_Start_Addr);
            Port[start_addr_reg] := Hi(Full_Page_Start_Addr);

            Port[word_cnt_reg] := Lo(Full_Page_Count);
            Port[word_cnt_reg] := Hi(Full_Page_Count);

            Port[page_reg] := Start_Page_Addr + Count;

            Port[mask_reg] := dma_ch3_enable;
```

Software for 2nd Test Circuit (Page 2 of 5)

```
                Repeat {Until terminal count}
                  DMA_Status := Port[status_reg]
                Until (Ch3_TC_Mask and DMA_Status) <> 0;

                Count := Count + 1;
              End; {While}
          End {Then}
        Else
          Error := True;
      End; {Transfer}

{**********************************************************}
{                        MAIN PROGRAM                      }
{**********************************************************}
  Label TA;

  Const
    starting_location_1 = $4000;
    starting_location_2 = $5000;

  Var
    Page_start, adr_strt, lb_addr_start, ub_addr_start,
    Pg_count, First_Field, value_in_memory,
    expected_val_in_mem, i                    : integer;
    Bad_Addr, Bad_Data                        : boolean;

  Begin (* main program *)
    ClrScr;
    Page_start := $04;
    Writeln('The initial page register setting is ',Page_start);
    adr_strt := $0000;
    Writeln;
    Writeln('The start address within that page is ',adr_strt);
    Pg_count := 2;
    Writeln;
    Writeln('The number of pages of data being transfered is ',
             Pg_count);
    Writeln;
    Writeln;
    Writeln('Toggle one of the field switches now.');
    Initialize;
TA: Bad_Addr := false;
    Transfer(Page_Start, Adr_strt, Pg_count, First_Field, Bad_Addr);
    If Bad_Addr Then
      Begin
        Writeln('The start address was not on an even
                 64k boundary.');
        Writeln;
        Write('What is the start address ($XXXX)? ');
        Readln(adr_strt);
        Writeln;
      End;
    If Bad_Addr Then GOTO TA;
    Sound(600);
    Delay(50);
    NoSound;

    Bad_Data := False;
    value_in_memory := Mem[starting_location_1:$0000];
    expected_val_in_mem := value_in_memory;
```

Software for 2nd Test Circuit (Page 3 of 5)

```
i := $0;

Repeat
  value_in_memory := Mem[starting_location_1:i];
  If (value_in_memory = expected_val_in_mem)
    Then
      If expected_val_in_mem < 255
        Then
          expected_val_in_mem := expected_val_in_mem + $01
        Else
          expected_val_in_mem := expected_val_in_mem - 255
    Else
      Begin
        Writeln('Data error in page 4 at ',i);
        expected_val_in_mem := value_in_memory + $01;
        Bad_Data := True
      End;
  i := i + 1;
Until i = $FFFF;

value_in_memory := Mem[starting_location_1:i];
If (value_in_memory = expected_val_in_mem)
  Then
    If expected_val_in_mem < 255
      Then
        expected_val_in_mem := expected_val_in_mem + $01
      Else
        expected_val_in_mem := expected_val_in_mem - 255
  Else
    Begin
      Writeln('Data error in page 4 at ',i);
      expected_val_in_mem := value_in_memory + $01;
      Bad_Data := True
    End;

i := 0;

Repeat
  value_in_memory := Mem[starting_location_2:i];
  If (value_in_memory = expected_val_in_mem)
    Then
      If expected_val_in_mem < 255
        Then
          expected_val_in_mem := expected_val_in_mem + $01
        Else
          expected_val_in_mem := expected_val_in_mem - 255
    Else
      Begin
        Writeln('Data error in page 5 at ',i);
        expected_val_in_mem := value_in_memory + $01;
        Bad_Data := True
      End;
  i := i + 1;
Until i = $FFFF;

value_in_memory := Mem[starting_location_2:i];
```

```
  If (value_in_memory = expected_val_in_mem)
    Then
      If expected_val_in_mem < 255
        Then
          expected_val_in_mem := expected_val_in_mem + $01
        Else
          expected_val_in_mem := expected_val_in_mem - 255
    Else
      Begin
        Writeln('Data error in page 5 at ',i);
        expected_val_in_mem := value_in_memory + $01;
        Bad_Data := True
      End;

  Writeln('It is ',Bad_Data,' that there was a data error.');
End. {main program}
```

Software for 2nd Test Circuit (Page 5 of 5)

```
Program clear_memory ;

  Const
    starting_location_1 = $4000;
    starting_location_2 = $5000;

  Var
    i     : integer;

  Begin
    i := 0;
    Repeat
      Mem[starting_location_1:i] := 0;
      i := i + 1;
    Until i = $FFFF;

    Mem[starting_location_1:i] :=0;

    i := 0;

    Repeat
      Mem[starting_location_2:i] := 0;
      i := i + 1;
    Until i = $FFFF;

    Mem[starting_location_2:i] := 0;
  End.
```

Memory Clearing Program - Test Circuit 2